Relationships and fire feedbacks in the Earth system over medium and long timescales in the deep past

Submitted by Sarah Jane Baker to the University of Exeter
as a thesis for the degree of
Doctor of Philosophy in Geography (Physical)
In July 2017

I certify that all material in this thesis which is not my own work has been identified and that no material has previously been submitted and approved for the award of a degree by this or any other University.

Signature: ……..

Abstract

Fire is a natural process that has existed on our planet for more than ~350 million years, and is a process that continues to influence our everyday lives. On Earth, a relationship exists between the process of combustion and the natural functioning of the Earth system. Here, the process of combustion has been implicated in playing an essential role for life on Earth, where natural Earth system processes have been shown to influence ignition probability, fire spread and fire behaviour, and where fire can provide a variety of feedbacks, to the Earth system over different timescales.

Over medium timescales of decades to hundreds of thousands of years, the likelihood and behaviour of fires are controlled by regional climate changes and vegetation type, whilst the occurrence of fire can play a crucial role in influencing biome persistence and development. Over long timescales (hundreds of thousands to multi-million year), the components influencing the probability of fire and fire behaviour not only involve processes occurring over local and regional spatial scales, and over short and medium timescales, but also long term processes occurring globally, such as changes in atmospheric oxygen concentration and the evolution of vegetation. Across these timescales in Earth's past, combustion has been shown to impact global ecosystems, climate and the carbon cycle by generating feedbacks that influence Earth's biogeochemical cycles. However, it is clear that our understanding of the role that fire plays in the Earth system, although improving is still developing.

This thesis provides an analysis of these Earth system - fire relationships and feedbacks across medium and long timescales in deep time, in order to understand the role that fire may have played and what the record of fire can tell us about the functioning and re-equilibrating of the Earth system during and after significant carbon-cycle perturbation events occurring in Earth's deep past.

The results presented in this thesis contribute what is believed to be the first fossil evidence that rising atmospheric oxygen and fire feedbacks may have aided in the termination of a significant carbon-cycle perturbation event, termed the 'Toarcian oceanic anoxic event' that occurred ~183 million years ago during the Jurassic period, and the return of the Earth system towards 'background functioning'.

This thesis also provides an analysis of the record of wildfire in the form of fossil charcoal across the initiation of an anoxic event that occurred ~93 million years ago, during the Cretaceous period. The results illustrate that CO_2 - climate driven changes in wildfire activity can be observed across medium timescales even during times of significant carbon-cycle perturbations, and modelled high atmospheric oxygen concentrations. These results illustrate how hypothesized changes in the hydrological cycle, and likely moisture content of fuel, appear to be the dominant control on wildfire activity during this period.

Finally, this thesis provides an analysis of charcoal abundance variations occurring across natural, orbitally forced cycles, termed the Milankovitch cycles. The results presented illustrate that natural variations in charcoal abundance are possible over intermediate timescales within the geological record. This thesis therefore illustrates a need to take into consideration and incorporate 'natural background' fluctuations in fire activity occurring over medium timescales, when analysing and predicting past and future climate change patterns.

Acknowledgements

Firstly, I would like to thank Professor Claire Belcher, Professor Stephen Hesselbo and Professor Timothy Lenton for their assistance and guidance throughout the research.

I would like to thank Claire Belcher for her continued support, encouragement and enthusiasm throughout. Claire has been a role model for me on both a personal and professional level, and I extend my gratitude towards her.

My appreciations and gratitude to Stephen Hesselbo and Timothy Lenton for their advice and knowledge, and for Stephen Hesselbo also for his assistance in the collection of samples from the Peniche section and from the Mochras core.

I would also like to thank the Natural Environment Research Council (NERC) for funding this project through a studentship grant NE/L501669/1.

With thanks to Luís Duarte for his assistance in collecting samples in Peniche, and for his advice not only of the local geology, but also of the best local restaurants and dishes in Portugal. I would also like to thank Jim Riding and the British Geological Society for the assistance with accessing the Mochras core, and collection of samples. Thank you also to Micha Ruhl, Weimu Xu and Marisa Strom from the University of Oxford for their assistance in collecting samples from the Mochras core, and the helpful scientific discussions.

A special thank you to all of my friends from the wildFIRE Lab research group as well as others from within the Geography and Earth System Science department. In particular, I would like to thank Vicky Hudspith, Mark Grosvenor, Stacey New, Nick Walding, Chris Boulton, Jessica Thorn, Alastair Crawford, Rebecca Dewhirst and Freya Garry (to name just a few) who have made my time at the University one of the most enjoyable. Thank you for the provision of regular Costa coffees, our scientific (and not so scientific) discussions, my post-it notes of encouragement in the final days of writing up, and for all of the fun we've had over the last few years.

Appreciations to the technical staff at the university who have enabled me to conduct all of the lab work required for this research. Thank you to Luke Mander for your assistance in the lab and invaluable advice on how to make a palynology slide.

A special thanks to Mark Grosvenor for his commitment and unfaltering enthusiasm for the seemingly endless hours spent processing samples.
Finally, I would like to thank my family and friends for their love and support. My grandparents who are forever enthusiastic about my research, and have always wanted to learn about and be a part of the work that I do. My parents, for not only their financial support throughout my studies, but also their continued support and encouragement to always do the best I can.
Amir Abbasi, thank you for always believing in me, and being by side throughout.

Contents

Chapter 8. Thesis Discussion and Synthesis

List of Figures

2. Chapter 2

3. Chapter 3

8. Chapter 8

List of Tables

Chapter 3

List of Equations

List of Abbreviations

C: Carbon

Ca: Calcium

C_{org}: Organic Carbon

CH_4: Methane

CIE: Carbon Isotope Excursion

C-OAE/OAE 2: Cretaceous Oceanic Anoxic Event/Oceanic Anoxic Event 2

CO_2: Carbon dioxide

C-T: Cenomanian - Turonian

$\delta^{13}C$: Isotopic signature for carbon. Ratio between isotopes ^{12}C and ^{13}C

Fe: Iron

H_2S: Hydrogen sulphide

Li: Lithium

Ma: Number of millions of years ago

Myr: Millions of years

N: Nitrogen

OAE: Oceanic Anoxic Event

Os: Osmium

O_2: Oxygen

P: Phosphorus

PO_4: Phosphate

PAL: Present Atmospheric Level

Pb: Lead

PCE: Plenus Cold Event

***p*O_2:** Atmospheric Oxygen

***p*CO_2:** Atmospheric CO_2

SEM: Scanning Electron Microscope

SST: Sea Surface Temperature

TOC: Total Organic Carbon

TOM: Total Organic Matter

T-OAE: Toarcian Oceanic Anoxic Event

1. Drivers of fire and fire feedbacks to the Earth system through time

1.1 Introduction

The process of combustion has become an integral part of human life, described as “the most important reaction for the human race” (Rein, 2013, p.15). Yet the relationship between humans and fire is changeable, as fire can also lead to destruction and devastation, threatening ecosystems, human life and well-being (Mortiz et al. 2012), and may result in significant economic costs (Bowman et al., 2009; Forest Service, 2015).

Over the past couple of decades, a persistent rise in the number of ‘uncontrolled fires’ across the globe (Bowman et al., 2009; Forest Service, 2015), has led to a growing scientific interest in the relationship between fire, climate and the environment (Pechony and Shindell, 2010; Mortiz et al., 2012; Woillez et al., 2014). Hence, recently many studies have focused around predicting and mitigating future fire threats (e.g. Flannigan et al., 2009; Gibbons et al., 2012; Mortiz et al., 2012; Stephens et al., 2013; Levis and Ward, 2013; Wang et al., 2017). However this ‘worldwide phenomena’ has existed in the natural world for more than ~350 million years (Myrs), arising shortly after the first appearance of land vegetation (Belcher, 2013), and furthermore, plays “an essential role for life on Earth” (Rein, 2013, p.15). Within the Earth system, combustion is an important process (Li et al., 2014), influencing global ecosystems, climate, and the carbon (C) cycle by generating feedbacks that influence Earth’s biogeochemical cycles (e.g. Kump, 1988; Lenton and Watson, 2000a,b; Handoh and Lenton, 2003; Bowman et al., 2009; Belcher, 2013; Levis and Ward, 2013). However, it is clear that our understanding of the role that fire plays in the Earth system, although improving (e.g. Belcher 2013; Scott et al., 2014) is still developing (Glasspool et al., 2015).

1.2 Fire Fundamentals

Fire, or combustion, is a rapid chemical, exothermic, oxidative reaction that relies on the presence of three main components, heat, oxygen (O_2), and fuel (Jones and Chaloner, 1991; Torero, 2013; Glasspool et al., 2015). These three fire fundamentals form the fire triangle (Figure 1.1).

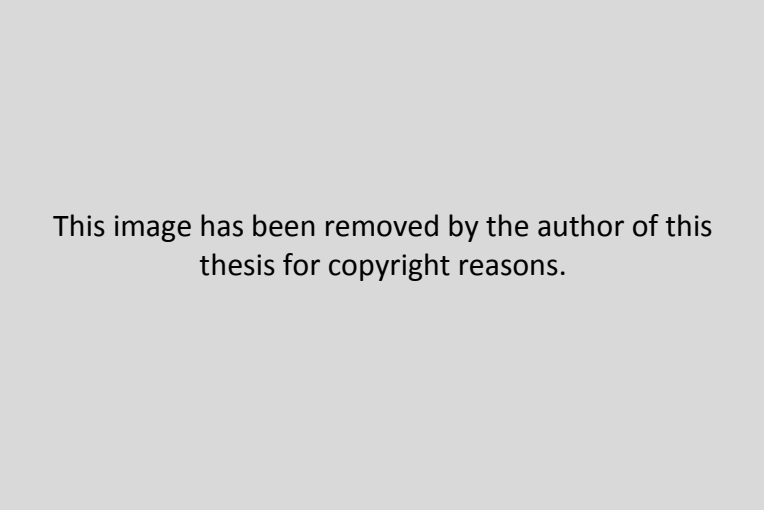

Figure 1.1 The fire triangle (taken from Spruce, 2016).

In order for a fire to start and spread, four phases need to occur (Scott, 2000). These are pre-ignition, ignition, combustion and extinction (Torero, 2013). During the pre-ignition phase, a sufficient heat energy source is required (Scott et al., 2014). Once heat energy is applied to organic materials, an endothermic reaction in which the temperature of the fuel increases, causing water to evaporate and volatiles to be released (Scott, 2000). The volatile gases are produced from organic compounds such as lignin and cellulose contained within plants (Scott, 2000; Scott et al., 2014). Cellulose makes up ~70% of wood cell walls and remains stable up until ~250°C (Scott, 2000). High temperatures beyond 250°C from an ignition source, cause the breakdown of the cellulose molecules, producing flammable gases including carbon dioxide (CO_2), ammonia and methane (CH_4), which mix with the O_2 in the air (Scott et al., 2014). In doing so a rapid exothermic reaction takes place, completing the ignition phase (Scott, 2000). In the presence of O_2, this rapid increase in heat enables the reaction to continue, enabling combustion to occur and a fire to start and spread (Scott,

2000; Scott et al., 2014). Finally, once all of the fuel has been exhausted, or there is a decrease in heat, the fire is extinguished (Scott, 2000).

Whilst Figure 1.1 indicates the fundamentals; a fuel source, sufficient O_2 supply, a heat source and continued generation of heat to allow the fuel to carry a fire, there are many other processes that operate spatially and over time that can influence a fire. For example, on a local scale and short timescale (minutes to years), weather, fuel type and topography are important in determining both the likelihood and behaviour of fires. Whilst at the other end of the spectrum for palaeo-fire studies conducted in deep time over long multi-million year timescales, the evolution of vegetation and changes in the abundance of oxygen in Earth's atmosphere also become important. Understanding the relationship between fire and each of these components provides key pieces of information that can be utilized to aid our understanding of the natural world and how our planet has changed and adapted throughout its history.

1.3 Relationships and fire feedbacks over short timescales

Over short timescales (minutes to years), the components influencing the likelihood of and behaviour of fires tend to be local, and include fuel type, weather and local topography (Figure 1.2).

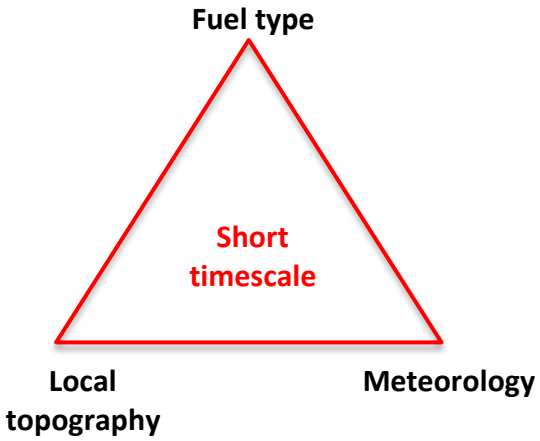

Figure 1.2 Key fire influences over short timescales

1.3.1 Fuel Type

Changes in fuel are capable of influencing ignition, prorogation and fire behaviours (Scott, 2000; Planas and Pastor, 2013). These can vary depending on extrinsic fuel properties (e.g. fuel load, shape and size, arrangement of fuel and bulk density); intrinsic properties of the fuel (e.g. chemical composition, conductivity, heat capacity and heat of combustion), as well as the fuel's state (e.g. moisture content and living vs. dead ratio) (Planas and Pastor, 2013; Abatzoglou et al., 2016; Belcher and Hudspith, 2017).

1.3.1.1 Intrinsic Fuel Properties

Heat Transfer and heat capacity – In order for a fire to spread, three of the four phases of combustion need to occur (pre-ignition heating, ignition and combustion) before extinction is reached (Cochrane and Ryan, 2009). Therefore fuels surrounding a fire must be adequately heated in order to allow ignition to occur and a fire to spread. The transfer of heat to surrounding vegetation can occur through conduction, radiation and/or convection (Figure 1.3) (Cochrane and Ryan, 2009). "Conduction is the direct transfer of heat energy from one molecule to another", and is expressed as being the "primary manner of heat transfer at the very beginning of a fire as ignition occurs" (Cochrane and Ryan, 2009, p. 28). As different soil and fuel types have different volumetric heat capacities (amount of energy required to change a unit temperature of a unit

volume), some fuels may require less energy to heat and ignite than others. An example of this can be seen in fuels with varying densities, where high density fuels tend to have higher heat capacities when compared with lower density fuels (Cochrane and Ryan, 2009). These types of fuel therefore require more heat to raise their temperature before ignition occurs (Cochrane and Ryan, 2009).

Convection of heat from a fire occurs via the atmosphere where air is heated, expands and then rises carrying the heat with it (Cochrane and Ryan, 2009). This allows fires to pre-heat tree canopies and any other vegetation existing above the fire. Heat radiation is defined by Cochrane and Ryan (2009, p. 29) as the "main form of heat transfer responsible for preheating fuels". Fires are able to radiate heat through electromagnetic waves that travel in a straight line from the fire (Cochrane and Ryan, 2009). Therefore radiative heat transfer is highest when fuels are perpendicular to the radiating heat transfer (Cochrane and Ryan, 2009). However, the energy flux per unit area from radiated heat decreases with distance away from the fire, expressed as "at a rate equal to the inverse of the distance squared" (Cochrane and Ryan, 2009, p. 29). Therefore distance and location of fuel with respect to the fire can significantly alter the amount of radiative energy received by vegetation, and thus the ability of a fire to pre-heat and ignite fuels to spread (Cochrane and Ryan, 2009).

Figure 1.3 Illustration of the different heat transfer processes occurring in a wildfire. Taken from Cochrane and Ryan (2009, p. 28)

Chemical Composition and heat of combustion – Wild-land fuels (e.g. wood, grasses, fine leaf litter, shrubs etc.) consist predominantly of cellulose, lignin and hemicellulose, as well as a smaller quantity of components such as terpenes, resins and minerals (Sullivan and Ball, 2012).

Terpenes have been shown to present "an elevated flammability" due to their "high heating value, relatively low flash point and Low Flammability Limit (LFL)" (Ormeño et al., 2009, p. 471). The low flash point (point at which volatiles released into the air and are ignited - these airborne particles and gases, once they become hot enough, are capable of radiating "their own light" thus producing what we observe as a flame (Rein, 2013, p. 17)) of ~43°C and LFL (the lower concentration for which airborne particles and gas can be ignited, producing a flame - below this concentration, a flame will not propagate (Ormeño et al., 2009)) of ~0.7%, means that the existence of terpenes increases the probability of wildfires due to their high flammability (Núñez-Regueira et al., 2005; Ormeño et al., 2009). Furthermore, vegetation with higher quantities of terpenes and resins (such as conifers) have the potential to produce a larger heat release during combustion, which can aid fire propagation by heating and drying fuels ahead of the fire (Zhao et al., 2012; Belcher, 2013; Simpson et al., 2016). Vegetation with higher quantities of minerals however has the opposite effect, as "minerals act as catalysts for the pyrolysis of cellulose, favouring carbon formation and reducing the emission of flammable volatile compounds" (Planas and Pastor 2013, p. 54). These fuel types therefore tend to produce smaller flames and do not burn as well (Planas and Pastor, 2013).

1.3.1.2 Extrinsic properties

Fuel shape and size - Certain types of vegetation can promote flammability and fire spread. These tend to be smaller particles that have a high surface-to-volume ratio (Planas and Pastor, 2013). High surface-to-volume ratios tend to have a higher "rate of energy and mass exchange with the gaseous phase" (Fernandes and Rego, 1998, p. 121). This enables the delay to ignition time to be reduced as proximal fuels are heated more quickly, increasing the rate of combustion and allowing rapid ignition and fire spread (Fernandes and Rego, 1998; Simpson et al., 2016). Furthermore fuels with a high surface-to-volume ratio are capable of drying faster than fuels with a low surface-to-volume making them more fire prone (Belcher, 2013). A key example of this can be found in grass vegetation, which

has been shown to enhance flammability due to its high surface-to-volume ratio and lightly packed fuel beds (Bond, 2008; Hoffmann et al., 2012), and has thus been found to be the primary cause of high flammability within the tropical savanna (Hoffmann et al., 2012). Certain vegetation types however, for example deciduous woodland, do not burn so easily and can even act as natural fire breaks (Alberta Government, 2012).

Biomass and bulk density - Biomass/bulk density relates to the "mass of biomass per unit volume of fuel bed" (Simpson et al., 2016, p. 104). Bulk densities can aid in fire propagation and spread rates by enhancing fuel connectivity (Simpson et al., 2016). However this only occurs up until a certain threshold (Rothermel, 1972; Simpson et al., 2016), beyond which the bulk density of a fuel bed can have a negative impact on fire propagation. This is because high bulk densities hinder air entrainment, which would otherwise aid in the drying of fuels, making them less susceptible to burning (Tachajapong et al., 2008; Planas and Pastor, 2013).

Arrangement of Fuel – A layer of 'horizontal' fuels such as dead woody materials and litter, if fairly uniform and continuous, can help fire to propagate more quickly (Planas and Pastor, 2013; Simpson et al., 2016). This compares to 'vertical' fuels, such as grasses, shrubs and trees, which can allow a fire to pass upwards from the understory to the canopy (Planas and Pastor, 2013). Low lying branches can also enable fire to spread from the floor to the canopy (Alberta Government, 2012). Within these vertical versus horizontal groups, certain types of vegetation can further enhance fire propagation. For example conifer trees tend to grow closer together allowing fire to spread more easily between them, as well as the dead branches and needles accumulating on the forest floor providing more fuel for a surface wildfire (Alberta Government, 2012). Furthermore, Belcher and Hudspith (2017) found that as fireline intensity (also determined as rate of fire spread) increases, the probability of a fire transitioning from a surface fire to a crown fire also increases. This is because fireline intensity can influence flame height, and therefore the ability of the flames to heat canopy fuels from the surface increases with increasing fireline intensity (Belcher and Hudspith, 2017).

1.3.1.3 Fuel State

Moisture content – The moisture content of fuel can determine how susceptible a fuel bed is in enabling a fire to spread (Belcher, 2013). This is because vegetation with high water content requires more energy to dry and heat during the pre-ignition phase, in order for ignition temperatures to be reached (Cochrane and Ryan, 2009). The point at which a bed of fuel cannot support a "spreading flame" is termed the "moisture of extinction (M_{ex})" (Watson and Lovelock, 2013, p. 276), which currently, in present atmospheric O_2 levels (21%), is estimated at ~39% moisture content (Belcher and Hudspith, 2017). Fuels with moisture contents beyond the moisture of extinction percentage will not ignite, and therefore often act to suppress a fire by preventing its spread.

Living vs dead ratio – Dead fuels denote any non-living remains as well as detritus from living vegetation (Cochrane and Ryan, 2009). The moisture content of dead fuels is highly susceptible to weather, whereby changes in precipitation, wind and sun exposure can change the moisture content of the dead fuels (Cochrane and Ryan, 2009). This is because dead fuels can exchange moisture from their surroundings. For example, dead fuels exposed to increased humidity and precipitation can absorb moisture and increase their moisture content not only from direct exposure to rain, but also from the ground (Cochrane and Ryan, 2009). However, they can also lose moisture through evaporation. Living vegetation however, is able to take up water as and when required and therefore can remain fairly moist even in higher temperature conditions where dead fuels would quickly dry out (Belcher, 2013). The moisture content of live fuel is therefore predominantly controlled by internal mechanisms of water uptake etc. and can be calculated by dividing moisture by the dry fuel weight, whereby moisture is equal the moist fuel weight minus the dry fuel weight (Cochrane and Ryan, 2009).

Hence the ratio of living fuel to dead fuel can determine how quickly and easily ignition and fire spread can occur.

1.3.2 Meteorology

Weather is defined as the atmospheric condition at a particular time and place that can change over the short term, from minutes through to months (NASA, 2005). This includes, wind, temperature and humidity, precipitation, solar radiation, storminess and atmospheric stability (NASA, 2005; Belcher, 2013). Each of these factors can influence ignition probability and fire spread differently.

Storminess - Natural sources of wildfire ignition come from lightning strikes, volcanic events, spontaneous combustion, meteor strikes or sparks created from falling rocks (Scott, 2000; Glasspool et al., 2015). Under current atmospheric conditions, more than eight million lightning strikes occur each day across the globe (Scott, 2000), making lightning strikes the most common natural source of ignition (Belcher et al., 2010). Studies have shown that the occurrence of "cloud-to-ground lightning strikes" have "a significant and positive influence on the probability of ignition in most areas" (Wotton and Martell, 2005, p. 1389), therefore an increase in storminess and lightning strikes can increase the probability of ignition of a fire. This is often termed the 'lightning ignition efficiency' (Abatzoglou et al., 2016). However, other conditions such as fuel moisture are capable of controlling the probability that a lightning strike would lead to a sustainable ignition (Wotton and Martell, 2005) (see also Fuquay et al., 1979; Flannigan and Wotton, 1990; and Abatzoglou et al., 2016). This is because lightning strikes only last for an instant and thus a fire must be able to be ignited and quickly become self-sustaining in order to survive and spread (Belcher et al., 2010).

Solar radiation, temperature, precipitation and humidity – Humid conditions and episodes of persistent rainfall enable fuels to become and remain moist. Their high moisture contents mean that more energy is required to heat and dry fuels before they can be ignited, and therefore the probability of ignition and fire spread is reduced (Cochrane and Ryan, 2009). In contrast, high temperatures and increased solar radiation can lead to warming and drying of fuels, making them more susceptible to burning as their moisture content is decreased (Grissino-Mayer and Swetnam, 2000; Hély et al., 2001; Flannigan and Wotton, 2001; Pausas, 2004; Flannigan et al., 2000; 2009). An example of this can be seen in Pausas' (2004) study where analysis of inter-annual fire, precipitation and

temperature records in the Eastern Iberian Peninsula (Mediterranean Basin) over the last three decades illustrated a strong correlation between area burned and decline in summer rainfall. Here, the inter-annual variability in burned area illustrated that during wet summers, fire activity was lower compared with dry summers where burned area increased (Pausas, 2004). A similar scenario can also be seen in Cwynar (1987) and Grissino-Mayer and Swetnam's (2000) study. Here, Grissino-Mayer and Swetnam (2000) found that currently fire frequency is found to be highest during arid periods, just before the summer monsoon. In contrast during late-winter/early-spring, higher soil and fuel moisture levels were hypothesized to have led to low fire activity (Grissino-Mayer and Swetnam, 2000). Whilst, Cwynar's (1987) linked increases in solar radiation and air temperature during summer months which were hypothesized to have led to drier, warmer conditions, with increased probability of wildfire ignition and spread through the heating and drying fuels (Viegas et al., 1992; Collins et al., 2006). In contrast during winter months increases in relative humidity were thought to have increased the moisture content of fuels, decreasing the probability of ignition and fire propagation (Collins et al., 2006).

Atmospheric Stability and Wind

Wind has been shown to significantly influence wildfire intensity and behaviour, affecting its direction of propagation; combustion reaction, heat transfer mechanisms, gas and fire-brand transportation in the convective column and flame geometry, as well as having links with unusual and/or extreme fire behaviours (Planas and Pastor, 2013). During high winds, flames are tilted closer towards un-burnt fuel (Morandini et al., 2001). This increases the heat radiation on the un-burnt fuel, causing heating and drying of fuels ahead of the fire and can thus aid in fire spread (Beer, 1991; Cochrane and Ryan, 2009). A key example of this can be found in Anderson et al.'s (2010) study, which focused on the influence of heat transfer from a progressing fire front. Here, Anderson et al. (2010) found that with wind, temperatures close to the "fuel bed surface decay exponentially with distance from the fire front" in contrast to no wind where "the temperature decreases rapidly within a very short distance of the flame front" (Anderson et al., 2010, p. 284). Furthermore during high winds, small particles such as embers can get lofted by the fire's plume and distributed varying distances depending on the wind (e.g. Anthenien et al., 2006). As these embers

can start new fires through the process of ‘spotting’, wind direction and strength can play a significant role in the development and spread of the fire (Porterie et al., 2007; Cochrane and Ryan, 2009). Examples of this can be found in studies by Beer (1991) and Taylor et al. (2004), where Beer (1991) found that fire fronts spread up to 50% faster during winds of between 2 metres per second (m/s) to 6 m/s, under unstable atmospheric conditions, and Taylor et al. (2004) concluded that areas with higher rates of flame spread coincided with periods of wind gusts. Atmospheric stability has also been shown to influence fire behaviour by affecting convection plumes produced during a wildfire (Heilman and Bian, 2010; Planas and Pastor, 2013). An example of this is given by Heilman and Bian’s (2010), whose study into atmospheric boundary-layer turbulence/wind gustiness concluded that areas with increased atmospheric instability or high turbulence coincided with periods of some of the largest wildfires recorded. The atmospheric boundary layer defines the “part of the atmosphere that directly feels the effect of the Earth’s surface” (Met office, 2015). Turbulence in this layer is created as the wind blows over the land surface, but also by changes in thermals, for example rising air that is heated from the sun etc. (Met office, 2015). Therefore increased turbulence within the boundary layer can aid fire propagation by assisting in the transfer of heat upwards towards overlying canopy fuels above the fire, as well as dictate the direction of fire propagation, thus often promoting erratic fire behaviour (Heilman and Bian, 2010).

1.3.3 Landscape and local topography

Local topography can influence fire behaviour in a very similar way to that of wind by altering the heat transfer process (Morandini et al., 2001). In areas where there is a slope, flames can tilt up-slope radiating heat onto un-burnt vegetation, pre-heating it and enabling the fire to spread more easily (Morandini et al., 2001; Cochrane and Ryan, 2009). This is much like if there was an up-slope wind.

Changes in topography can also influence general weather patterns creating localized weather conditions affecting fuel type and their moisture content (Belcher, 2013). For example, areas with particularly high hills/mountains receive more precipitation, and exposure to prevailing winds compared with lower elevations where fuels tend to dry out quicker. The direction of the slope can further influence how much solar radiation the vegetation is receiving during the day (Swanson, 1981). For example, south-west facing slopes receive higher

amounts of solar radiation, thus creating warmer and drier conditions. North facing slopes tend to be cooler and more shaded, thus maintaining higher moisture contents and delaying drying well into the fire seasons, meaning a decreased likelihood of a fire occurring (Stringer, 2009). Other landscape features such as large rock outcrops, snow avalanches, landslides and/or streams can act as natural fire-breaks, and can therefore prevent fires spreading (Swanson, 1981).

1.3.4 Fire feedbacks and interactions over short-timescales

Weather is considered as the largest driver for regionally burned areas over short-timescales, where temperature, humidity, wind and precipitation control fire spread rates and ignition tendencies (Jolly et al., 2015). Inter-annual changes in weather produce conditions conducive for burning at certain times of the year, where warm, dry, windy conditions often result in “the most severe fires” (Jolly et al., 2015, p. 2). These periods during which wild fires are likely to occur, spread and affect resources are often referred to as the ‘fire seasons’ (Voiland, 2015). On micro-scales, the re-occurrence of fires can affect species competition and compositions, soil structure and plant nutrition (Lhermitte et al., 2011) where fire disturbances on species competition and composition can initiate a small-scale positive feedback (Reilly et al., 2006). This is due to the promotion of co-existence of species by fire, through limiting the development and thus dominance of strong competitive species, enabling the development of the less competitive species (Reilly et al., 2006) (e.g. Walker and Peet, 1984; Brockway and Lewis, 1997; Peterson and Reich, 2008).

Without fire occurrence, competitive species would not only suppress the less competitive species, but may also drive them to local extinction (Peterson and Reich, 2008). An example of this can be seen in savannah environments within North America (e.g. Walker and Peet, 1984; Peterson and Reich, 2008) whereby annual to biennial (occurring every two years) fire occurrence is hypothesized to enable the development of grasses by limiting shrub and tree growth (e.g. Peterson and Reich, 2008). In areas experiencing low fire frequency, species richness was found to be low, hypothesized to be primarily due to a decline in grassland species associated with high tree canopy cover and understory shrub and tree cover competitively excluding the less competitive grass species (Peterson and Reich, 2008).

Once a fire has occurred, a small positive feedback can be initiated. Examples of this can be seen in areas of Amazonia, where once an area of forest becomes susceptible to a fire, for example through drought, and a fire occurs, the probability of future fires occurring in that area are greatly increased (Nepstad et al., 2001). This is due to a reduction in canopy foliage following a fire enabling more solar radiation to reach forest floors (Nepstad et al., 2001; 2004). Here not only does this cause drying of finer fuels at the forest floor, but can also promote soil and leaf moisture loss causing some trees to shed leaves by increasing air temperatures, increasing flammability (Nepstad et al., 2001; 2004). Additionally, dead trees killed by the fire begin to decompose and fall to the forest floor, aiding the reduction in canopy thickness and increasing forest flammability (Nepstad et al., 2004). Furthermore, an increase in species diversity such as grasslands within once tree-dominated areas promoted by the previous fire occurrence, can further aid a future fire due to their high surface-to-volume ratio, making them quicker and easier to dry out, and thus more flammable than the previous tree and shrub dominated vegetation. A probability of a second fire is greatly increased, and likely to “burn more intensely because of the additional fuels and drying. Larger trees with thicker bark may be killed during the second burn, further increasing forest flammability” (Nepstad et al., 2001, p. 399). This process can create a positive feedback loop (Figure 1.4).

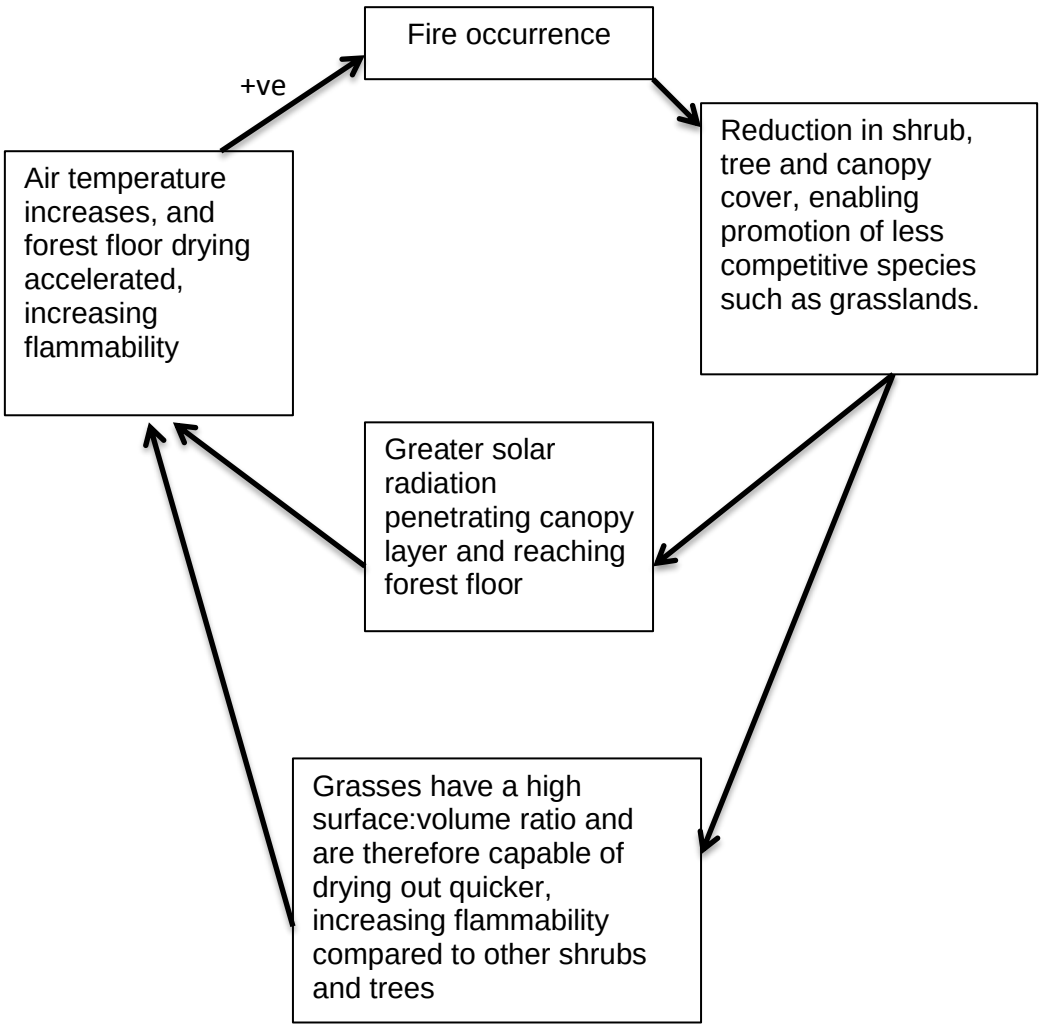

Figure 1.4 Positive short-term feedback loop created by fire occurrence on local and short timescales

Another feedback hypothesized over short timescales relates to the aerosols released during a wildfire and their interaction with the atmosphere. Aerosols have a short lifespan of up to one week (Ramanathan et al., 2001), and can consist of carbonaceous aerosols such as black carbon and organic carbon (Ramanathan et al., 2001). Here, the small particles (predominantly organic and black carbon) produced within the fire's emissions, for example large quantities of smoke released into the atmosphere, that can inhibit the amount of rainfall received and amount of sunlight reaching the ground within a region (Nepstad et al., 2001; Turquety, 2013). These small particles act as cloud condensation nuclei, enabling water vapour to condense on them forming droplets (Novakov and Penner, 1993). These particles can saturate the atmosphere with enough "condensation nuclei that cloud water droplets do not become heavy enough to

fall to the earth" (Nepstad et al., 2001, p. 401). This can cause a decline in the amount of rainfall received, thus promoting drier conditions conducive for the ignition and spread of future fires (Turquety, 2013).

Furthermore, aerosols produced in smoke plumes can absorb solar radiation, causing a decrease in the amount of sunlight received at the Earth's surface (Ramanathan et al., 2001). This can further aid in the reduction of precipitation due to a decline in evaporation (Turquety, 2013). However, a negative feedback also exists, as increased aerosol emissions can lead to an increase in a cloud's albedo (reflectivity of solar energy from the Earth back out to space) (Turquety, 2013). Although this aids in the reduction of precipitation, creating drier conditions at the surface and thus promoting fire spread, the reduction in precipitation also increases the lifetime of the cloud (Turquety, 2013). This could lead to a prolonged reduction in sunlight reaching the Earth's surface that would otherwise aid in the drying of fuels and re-growth of vegetation, and can therefore be attributed to a short-term negative feedback on fire as well as a short-term cooling (Figure 1.5).

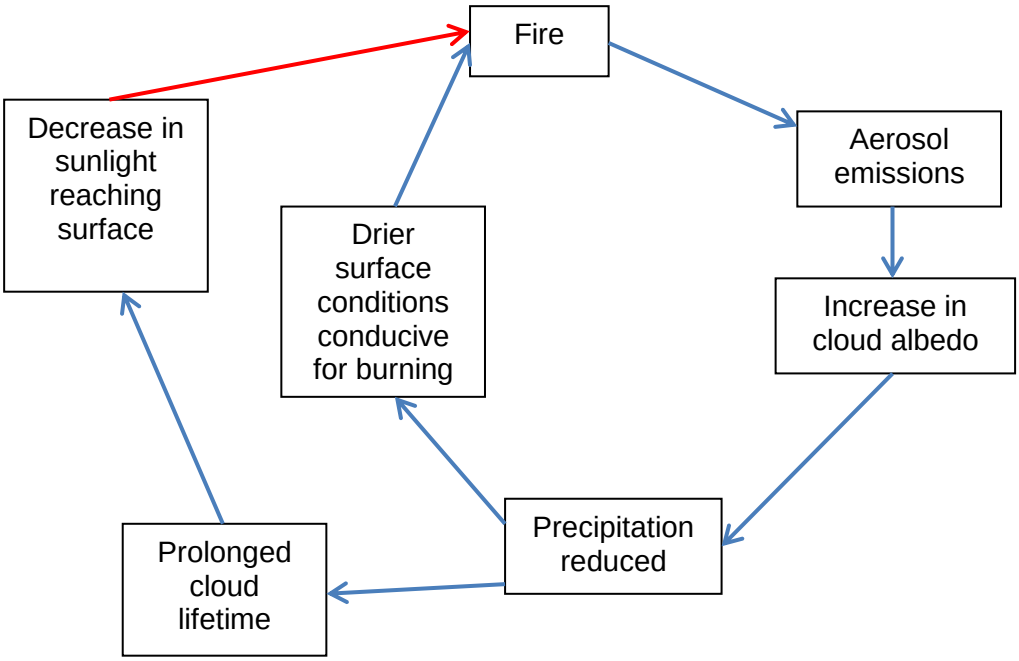

Figure 1.5 Feedbacks created by fire occurrence on regional climate. Blue arrows denote positive feedbacks, red arrow denotes a negative feedback.

1.4 Relationships and fire feedbacks over medium timescales

Over medium timescales (decades to hundreds of thousands of years), the components influencing fire behaviour and likelihood can become more regional, where short timescale fire influences are still occurring, but longer and larger scale factors also play a significant role in influencing fire. For example, studies conducted over hundreds of years consider changes in climate that tend to override the importance of any small-scale annual/day-to-day weather driven fire influences. These influences are defined in Figure 1.6.

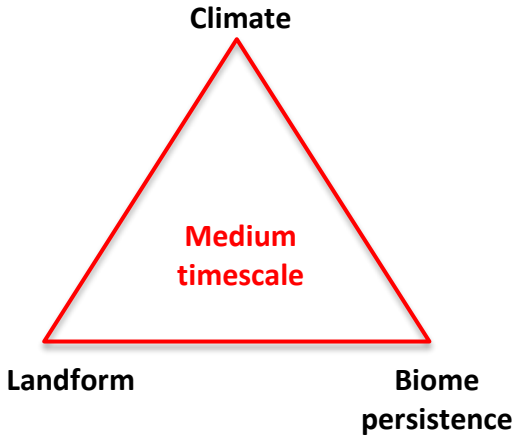

Figure 1.6 Key fire influences over medium timescales

1.4.1 Climate

In contrast to weather, climate refers to a region's 'long-term' (more than 30 years) weather pattern (NASA, 2005; Met Office, 2015), and thus relates to 30+ year averages of precipitation, temperature, humidity etc. occurring across a region (NASA, 2005). Analyses of fire and climate records indicate that climate is a fundamental driver for fire spread (Bowman et al., 2009), where climate variability is key to promoting fire activity over medium timescales (Haberle and Ledru, 2001). Here, wetter periods enable fuel build up, and drier periods increase fuel susceptibility (Bowman et al., 2009). In contrast, long periods of persistent climate conditions can often be detrimental to fire activity, where persistent dry/wet conditions can indirectly influence fire through fuel availability (Mooney et al., 2011; Thonicke et al., 2013). Therefore, unlike weather, linking fire records with climate drivers can often be complicated as changes in climate can both directly and indirectly influence fire activity (Planas and Pastor, 2013).

Direct climate influences on fire are similar to those discussed in the 'weather' section, whereby changes in the frequency of ignition (e.g. storm activity and thus lightning strikes), and the probability that a fire will spread (e.g. through the moisture content of fuel) for example, can have a direct impact on whether a region experiences increased or decreased fire activity (Planas and Pastor, 2013). If fuel is available, warm, dry climate periods can often be linked with increased fire activity, whilst cooler, wetter climates can be associated with lower fire activity. This is through the same principles as those discussed in the weather section whereby increased precipitation can increase live and dead fuel

moistures, making them harder to ignite and support a spreading flame (Cochrane and Ryan, 2009). An example of this can be seen in Greisman and Gaillard's (2009) study of Holocene burning between 8600 and 6000 BC in Sweden. Here, high fire activity, represented by high charcoal abundances in the sedimentary record, were associated with warm dry climate periods occurring at ~8550, 7600, 5500 to 5100 and 4500 BC (Greisman and Gaillard, 2009), whilst cooler, wetter periods occurring between 6500 to 6000 BC and 4750 BC likely supressed fire activity in the region, resulting in the low charcoal abundances found (Greisman and Gaillard, 2009).

However, if fuel is not always available within a region, the relationship between climate and fire activity can become more complicated. This is because climate can also indirectly influence fire activity by driving changes in fuel availability that can often lead to unexpected changes in biomass burning depending on the state of the vegetation (Mooney et al., 2011).

A prime example of this can be seen in studies where periods of increased precipitation are found to coincide with increased fire activity (e.g. van der Werf et al., 2008; Daniau et al., 2007; Daniau et al., 2013). This is because although drier climate periods can heat and dry fuels making them more susceptible to ignition, prolonged dry climate periods can also often limit terrestrial vegetation due to hydrological stresses, and thus diminish fuel loads (van der Werf et al., 2008; Mooney et al., 2011). This relationship can be seen in van der Werf et al.'s (2008) study of fire activity in modern day Australia, where northern areas of Australia were found to experience higher fire activity compared to central parts of Australia, despite central Australia experiencing less rainfall. In contrast, the northern study sites were found to experience higher fire activity under a wetter climate, hypothesized as being due to an increase in ecosystem productivity driven by the higher precipitation rates, providing fires with a larger fuel source (van der Werf et al., 2008).

Climate driven fuel changes influencing fire activity can also be seen in the geological record (e.g. Daniau et al., 2007; 2013). An example of this can be seen in a study by Daniau et al. (2013), where climate, vegetation and fire history from a South African core covering the last ~170,000 years (from present day), was analysed.

Within the core Daniau et al. (2013) found that throughout the 170 kyr period, there were six 'fire cycles' illustrating high and low charcoal abundances. Variations in charcoal abundances, taken to represent changes in fire activity, were found to correspond to orbital precessional forcing. Orbital precessional forcing exerts a control on the amount of solar radiation reaching the Earth's surface in each hemisphere (see Chapter 6 for more information), and is thus thought to cause north-south shifts in the Inter-tropical Convergence Zone (ITCZ) (a zone close to the equator where northern and southern air masses meet and converge, often producing low pressure) (Daniau et al., 2013). During maximum precession, high solar radiation in the southern hemisphere summer is hypothesized to have occurred, causing reinforcement of "the convection associated with the ITCZ, which in turn causes higher summer rainfall over southern Africa" (Daniau et al., 2013, p. 5070). During these periods of high summer rainfall, high charcoal abundances were observed, whilst during the periods of decreased summer rainfall associated with precession minima causing the northward migration of the ITCZ away from the study area, lower charcoal abundances were observed (Daniau et al., 2013).

Daniau et al. (2013) suggest that higher charcoal abundances, and thus wildfire activity, can be attributed to an increase in biomass, where the increased summer rainfall in South Africa during precession maxima enabled increased grassland productivity and/or a shift in grassland extent. This is suggested to be due to the notion that "rainfall can strongly affect grass biomass at one spot" where changes in rainfall of ~200 mm could easily double grass productivity (Daniau et al., 2013, p. 5071), and further supported by the morphology of the charcoal particles, that illustrate a higher proportion of elongate particles, which can be attributed to grass char (Daniau et al., 2013, and references therein). The high charcoal abundances found consistently every ~23 kyrs during precession maxima in south-Africa, were therefore hypothesized to have been indirectly influenced by the changes in rainfall, caused by the south-ward shift of the ITCZ, driving a rise in grassland biomass (Daniau et al., 2013).

1.4.2 Biome persistence/species dominance

Biomes represent “broad-scale ecological regions defined by vegetation structure and climatic conditions” (Gallagher et al., 2010, p. 2). Shifts in biomes and species dominance can significantly influence fire activity within a region, where, for example, development of more flammable vegetation types (e.g. vegetation with high surface-to-volume ratios and low moisture contents) can result in higher/more frequent wildfire activity when compared to the development and/or dominance of less flammable vegetation types (e.g. broad leaves and high moisture contents) (Hoffmann et al., 2012; Belcher, 2013). This means that a shift in biomes and/or the expansion of vegetation types can control the flammability of regions according to the type of vegetation dominating a biome (Belcher, 2013).

A key example of this can be seen in Hudspith et al.’s (2015) study (conducted from sediments preserved in Screaming Lynx Lake, interior Alaska), of variations in calculated charring temperatures (pyrolysis intensities) over the last ~11 kyrs, which were found to coincide with changes in dominant vegetation type and ecosystem shifts. Within the study, Hudspith et al. (2015) found that pyrolysis intensities (calculated from reflectance measurements of macroscopic charcoal particles), over the last 11 kyrs were generally high, except for one period of low pyrolysis intensities observed between 10-11 kyrs. This period was found to coincide with an interval of birch shrub tundra (Hudspith et al., 2015). As modern tundra fires are expressed as being typical of “low-to moderate-intensity” and “expressing low charcoal reflectance values (corresponding to charring temperatures <500°C)” (Hudspith et al., 2015, p. 8), Hudspith et al. (2015) hypothesize that this period of low pyrolysis intensities are likely due to the presence of the birch shrub tundra vegetation.

Subsequent to this interval, pyrolysis intensities suddenly increased up until ~9 kyrs ago, and remained high until present day (Hudspith et al., 2015). The marked increase in pyrolysis intensity between 9-10 kyrs was found to be coincident with an increase in ‘arboreal pollen’, inferred as being indicative of “the establishment of trees on the landscape” (Hudspith et al., 2015, p. 8) and where aspen trees dominated the vegetation composition. Although aspen is defined as having a “low flammability due to high inherent moisture content of the fine fuels” as well as a “reduced surface load fuel due to relatively rapid decomposition” when compared with other vegetation types such as spruce, this ‘broadleaved’ species

can enable a build-up of “low bulk density surface litter” (Hudspith et al., 2015, p. 8). Surface litter with a low bulk density enables higher heat diffusion (Hudspith et al., 2015), and thus propagation of surface fires once ignited. Hudspith et al. (2015) therefore conclude that it is likely that the shift from birch tundra to an aspen dominated vegetation composition drove the sudden increase in pyrolysis intensities observed between 9-10 kyrs ago.

1.4.3 Landform

Large landform features can also influence fire behaviour, providing natural fire breaks and/or enhancing fire spread (Swanson, 1981). For example, sharp mountain ridges can act as effective fire breaks preventing a fire from crossing, regardless of available fuel (Swanson, 1981), whilst large canyons that can funnel wind through often increase the wind speed, and can therefore intensify fires. Other features such as large rivers, lakes, wetlands and scarps can also act as effective fire-breaks (Swanson, 1981). Thus considering geomorphological changes could be important across medium timescales.

1.4.4 Fire feedbacks and interactions over medium-timescales

Over medium timescales, the effects of fire on the atmosphere, meteorology and vegetation experienced over short timescales combine, where a new positive feedback is initiated, which is capable not only of promoting a shift in biome but can also sustain the new biome (Staver et al., 2011; Hirota et al., 2011; Hoffmann et al., 2012). An example of this can be seen in Staver et al.’s (2011) study which shows that although globally, climate is considered the main control on biome distribution and tree cover, in areas where climate conditions are milder (e.g. mild seasonality and ‘intermediate mean annual rainfall’ levels of between 1000 to 2500 mm), fire becomes the dominant control. Within these ‘milder climate’ regions, Staver et al. (2011) find that the occurrence of fire and the positive feedback between fire and the development of grasslands (e.g. Figure 1.4), governs whether an area becomes and/or remains a certain biome such as a forest or a savanna, and can even enable the expansion of biomes (e.g. savanna) into regions where climate would otherwise promote a dominancy of a different biome (e.g. forests).

Globally, biome development is dependent on climate conditions (Staver et al., 2011). An example of this can be seen in areas of Africa which experience high mean annual rainfall, found to promote forest growth – here, tree cover was found to increase with increasing rainfall up until ~1000 mm mean annual precipitation. Beyond 1000 mm, savanna and forested areas co-exist until ~2500 mm (termed 'intermediate' stage of rainfall by Staver et al. (2011)), beyond 2500 mm rainfall per year, savannas were not found to persist, yet forested areas thrived (Staver et al., 2011). When considering rainfall seasonality, Staver et al. (2011) found that globally (across Africa, South America and Australia), forested areas only occurred where the dry season lasted <7 months of the year, and where annual rainfall was >1000mm, indicating that long, dry periods are detrimental to forest persistence. Yet, the length of the dry season did not constrain savanna persistence, as savannas were found to occur in areas experiencing up to 2500 mm annual rainfall, in both areas studied, experiencing just a two month period of dry conditions as well as a dry season lasting beyond 7 months (Staver et al., 2011). This means that in areas where conditions are particularly wet (>2500 mm per year), with a short dry season (<7 months), climate conditions favour the existence of forested areas over savanna. In areas that are much drier (<1000 mm rainfall) and experience a longer dry season (>7months), climate conditions favour the existence of savanna (Staver et al., 2011). This creates two distinct 'stable states' of vegetation across the globe (Staver et al., 2011; Hirota et al., 2011) Hirota et al. (2011) also note another 'stable state' beyond savanna termed the 'tree-less' state). These 'stable states' mean that it is unlikely that the biome will shift.

Within the savanna biome, fire occurrence was found to be generally higher when compared to forested regions across all continents studied (South America, African and Australia) (Staver et al., 2011). The occurrence of fire within the savanna biome is suggested to aid in the persistence of this biome through a positive feedback (Figure 1.4 and 1.7). This has also been found with "savannas occurring in areas now wet enough to support forest that were probably established during drier periods in Earth's history, in line with the idea that fire feedbacks promote the persistence of historical biome distribution" (Staver et al., 2011, p. 232). Furthermore, this maintenance of savanna biomes due to the positive feedback with fire, could further lead to the expansion of savanna beyond

regions where the influence of climate would directly limit tree cover, and promote savanna (e.g. drier climates) (Figure 1.7) (Staver et al., 2011). This expansion is hypothesized to have likely also led to the development of 'bimodel' areas of savanna and forests, where climate conditions allow for either forest and/or savanna to exist (annual rainfall sits between 1000 mm and 2500 mm, and where seasonality is fairly mild (<7months dry/wet season)) (Staver et al., 2011). Thus within these 'intermediate'/'unstable' state (Staver et al., 2011; Hirota et al., 2011) areas, fire is considered the dominant control on the existence and persistence of savanna vs. forest/tree cover (Staver et al., 2011; Hirota et al., 2011).

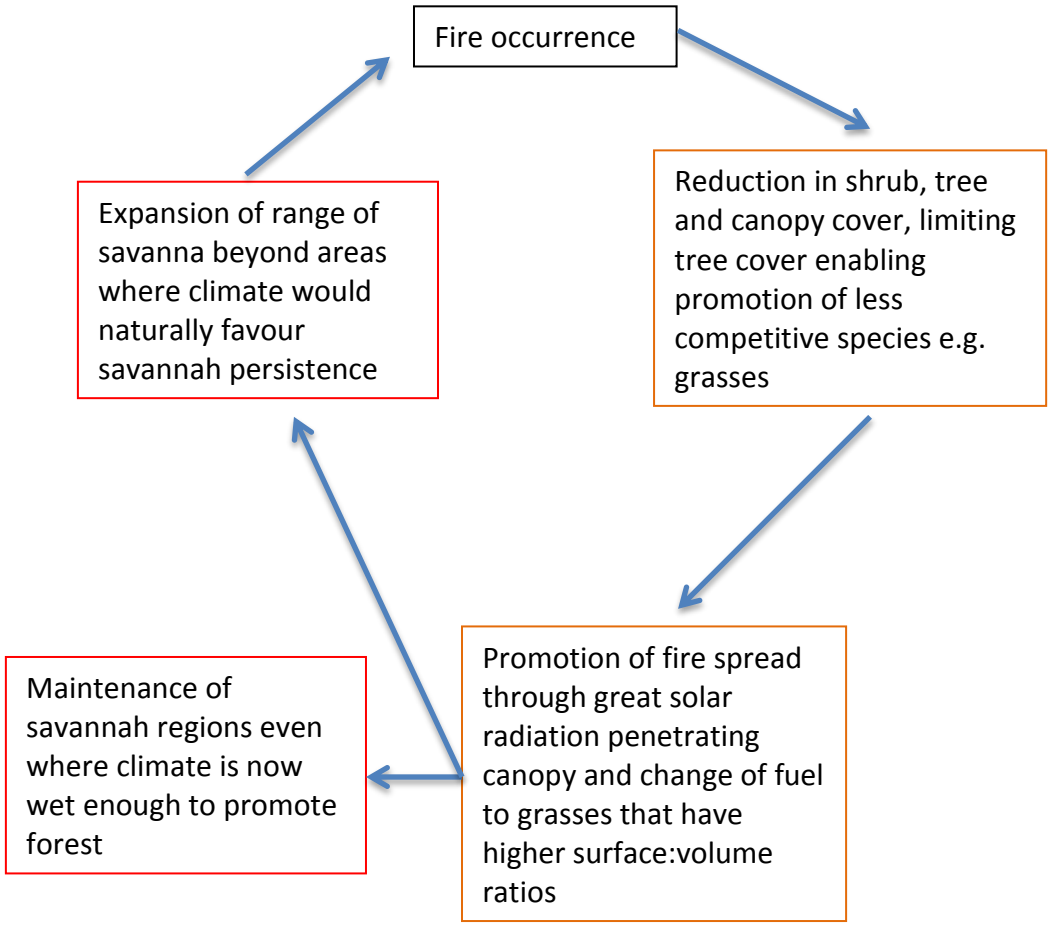

Figure 1.7 Positive feedback over medium timescales where fire can lead to the expansion of savanna into areas where climate would otherwise promote the distribution of forested areas. Red boxes indicate medium timescale events whilst orange boxed denote short timescale events.

Another feedback hypothesized across medium timescales in the form of decades, relates to the CO_2 and other greenhouse gases, such as methane (CH_4) and nitrous oxides (N_2O) released from fires, that unlike aerosols, have a longer, decadal lifespan (Randerson et al., 2006). An example of this can be seen in Randerson et al.'s (2006) study where following the Donnelly Flats forest fire, which burned ~7600 ha between the 11th and 18th June, 1999 in Alaska, post-fire surface albedo and greenhouse gases were found to continue to influence radiative forcing for up to 55 years. Radiative forcing is described as "a measure of the influence a factor has in altering the balance of incoming and outgoing energy in the Earth-atmosphere system and is an index of the importance of the factor as a potential climate change mechanism" (Solomon et al., 2007, p. 21). Here, greenhouse gases absorb infrared radiation, emitting it back towards the Earth's surface rather than allowing it to be reflected back out into space - this causes a 'positive radiative forcing'. Therefore, although the pulse of greenhouse gases from the fire is predicted to have gradually decreased over the 55 years due to oxidation (CH_4) and uptake (CO_2), Randerson et al. (2006, p. 1131) hypothesize that "the greenhouse gases will contribute to a positive radiative forcing" for up to 55 years following a fire.

1.5 Relationships and fire feedbacks over long timescales

Over long timescales (hundreds of thousands to multi-million year), the components influencing probability of fire and fire behaviour not only involve processes occurring over local and regional spatial scales, and over short and medium timescales, but also long term processes occurring globally, such as atmospheric oxygen concentration changes and the evolution of vegetation events (Figure 1.8).

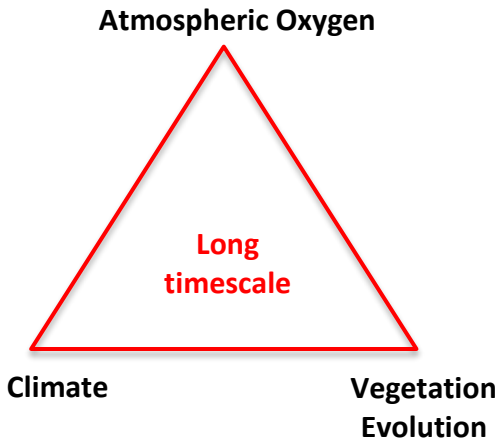

Figure 1.8 Key fire influences over long timescales

1.5.1 CO_2 driven climate change and vegetation evolution

Over long-timescales, significant geological events such as a large volcanic/Large igneous province (LIP) eruption must be considered as potential drivers of fire, where, for example, increased concentrations of CO_2 can drive in significant climate and thus vegetation and wildfire activity changes that can occur over long timescales.

A key example of this can be seen in Belcher et al.'s (2010) study of charcoal and paleontological data across the Triassic-Jurassic boundary (~201.6 million years ago (Ma) (Schootbrugge et al., 2009)). Here, Belcher et al. (2010) found a five-fold increase in charcoal abundances during the early Jurassic. During this time, a rise in global temperatures is estimated, likely driven by increased CO_2 concentrations (Belcher et al., 2010). This CO_2 driven climatic warming is hypothesized to have led to a dominance of narrow-leaved species, as larger broad-leaved species' photosynthetic function may have been impaired, ultimately resulting in their extinction (Belcher et al., 2010). As narrow leaved species are more flammable compared with broad-leaved species due to their high-surface-to-volume ratio, Belcher et al. (2010) postulate that the change to a dominant narrow-leaved species, driven by CO_2 driven climate change may have aided the rise in inferred fire activity across the Triassic-Jurassic boundary.

Another influence on fire activity over long timescales is the evolution of vegetation species and their respective flammability. One example of this is the Pinaceae that has been shown to develop a “fire-resistant trait” back in the Cretaceous period (Belcher and Hudspith, 2017, p. 1528). Here, a thickening of the bark has been found ~126 Ma in Pinaceae, hypothesized to have developed to protect against localized heating from low-intensity surface fires, and later ~89 Ma thicker bark and branch shredding (He et al., 2012), yet the evolution of the Pinaceae dates back to ~240 Ma (He et al., 2012). The development of these ‘fire-resistant traits’ are speculated to be linked with fire, where increasing planet flammability (suggested as due to elevated atmospheric O_2 concentrations during the Cretaceous (He et al., 2012)) and the development of “more intensive crown fires ~89 Ma” is hypothesized to have driven certain species to evolve and develop these traits in order to survive (He et al., 2012; Belcher et al., 2013).

1.5.2 Atmospheric oxygen

Controlled laboratory experiments conducted by Watson (1978) illustrated that the relative volume of O_2 in the atmosphere could significantly influence fire activity (Watson and Lovelock, 2013).

The experiments tested the lowest required volume of atmospheric O_2 that would enable combustion to occur for a consistent fuel type (paper) exhibiting different moisture contents. From these experiments it was concluded that below 17% vol. of O_2, combustion was not possible even for ‘oven dry fuel’ which had a moisture content of 0, and therefore at least 17% vol. of O_2 is required in the atmosphere to enable combustion to occur in the natural world (Watson, 1978; Watson et al., 1978; Watson and Lovelock, 2013). As oxygen rises, fuel of increasing moisture contents were also found to become more susceptible to ignition (Watson, 1978; Watson and Lovelock, 2013). To define this relationship between O_2 and fuel moisture, the point at which a bed of fuel cannot support a “spreading flame” was termed the “moisture of extinction (M_{ex})” (Watson and Lovelock, 2013, p. 276). The moisture of extinction was found to have a linear relationship with O_2 concentrations up until ~28% vol. (Figure 1.9), thus even fuel with high moisture content could support a spreading flame if O_2 levels were high enough.

Figure 1.9 – Watson's (1978) findings illustrating the relationship between fuel moisture and atmospheric O_2. Points refer to the lowest moisture content of fuel required to suppress flame spread at varying atmospheric O_2 concentrations for regular ignition and high ignition. M_{ex} refers to the 'moisture of extinction' and is measured in "percent of dry weight" *Ox* refers to the "oxygen percent concentration" (i.e. present day this is ~21%) (taken from Watson and Lovelock, 2013, p 276-277).

Subsequent to Watson's (1978) study, authors have argued for lower atmospheric O_2 limits that would enable combustion to occur. Cope and Chaloner (1980) (citing Coward and Jones, 1952) suggested that methane (CH_4) and carbon monoxide could burn in a mixed atmosphere with just 7% O_2, and thus argued that fire could also occur in atmospheres with similar O_2 concentrations. Clark and Russell (1981) suggested that if already ignited, woody material could burn in just 13% O_2, and Wildman et al. (2004) suggested that a minimum of just 12% O_2 was required to burn dry pine dowels. However, Belcher and McElwain (2008) indicate that ignition for Wildman et al.'s (2004) experiment was conducted through a 'window' into the controlled O_2 atmosphere, and thus O_2 may have seeped through. Furthermore the type of material used in Wildman et al.'s (2004) study had a moisture content of just 0.2%, and was thus deemed unrealistic for natural vegetation (Belcher and McElwain, 2008). Instead, recent fire experiments argue for higher O_2 concentrations that below which combustion of natural material cannot occur, producing similar percentages to that found by Watson (1978) (e.g. Belcher and McElwain, 2008; Belcher et al., 2010). For example, Belcher and McElwain (2008) suggest a lower limit of 15% vol. atmospheric O_2, after finding that combustion of a range of materials (including matches, candles, paper and *Pinus caribeae*) was not possible below 15%, and

only limited combustion occurred between 15-17% vol. O_2. In support of Watson's (1978) findings, Belcher and McElwain (2008) concluded that only at 17% could combustion readily occur.

Furthermore, in order for a fire to occur and spread within the environment, not only is an ignition required but a fire must also be self-sustaining to allow it to spread (Belcher et al. 2010). Laboratory experiments demonstrated that at 15% O_2, combustion could not be sustained even when the most flammable material type (dry peat) was used (Belcher et al., 2010). At 17%, high temperatures were sustained in the fuel after the ignition source had been switched off, and a "self-sustaining smoldering front" (which requires lower ignition energy than flaming combustion) was maintained, moving away from the original ignition source (Belcher et al., 2010, p. 22449). This led Belcher et al. (2010) to conclude that self-sustaining combustion could not occur in atmospheres with less than 17% O_2.

Beyond partial pressures of ~17% vol. O_2, fire becomes very sensitive to small changes in O_2 (Belcher et al., 2010). Using parameter inputs of 'probability of fire spread' and 'probability of local fire extinction' Belcher et al. (2010) were able to plot burn probability across varying O_2 concentrations using their FIREOX model (Figure 1.10). This model illustrated that between atmospheric O_2 volumes 19% to 21% a small rise in O_2 can result in a large rise in burn probability, and thus wildfire activity (Belcher et al., 2010).

Figure 1.10 – Estimated burn probabilities as a function of atmospheric oxygen concentration according to the FIREOX model (taken from Belcher et al., 2013, p 232).

These experiments illustrate the sensitive nature of the relationship between fire and O_2, indicating the need for a minimum of ~17% O_2 in order for combustion to occur and become self-sustaining. This relationship can be utilized to provide key information on past atmospheric O_2 concentrations and changes throughout Earth's history.

The notion that the record of wildfire could be used to provide information on changes in palaeo-atmospheric O_2 concentrations was first suggested by Chaloner (1989) who stated that based on the findings of Watson (1978), Cope and Chaloner (1980) and Clark and Russell (1981), "wildfire required adequate O_2 for the combustion of plant fuel" and that "fossil charcoal from the Devonian onwards suggest that the oxygen level in the atmosphere has not fallen below 13% in this interval" (Chaloner, 1989, p. 171).

The first record of land vegetation dates back to the Silurian period (~443 – 418 Ma) (Scott, 2000), suggesting that from this time, suitable fuel for fires existed (Belcher, 2013). However, although the first record of charcoal also dates back to the Silurian (~410 Ma) in the form of charred rhyniophytoid remains (Glasspool

et al., 2004; Scott and Glasspool, 2006) (described as a “small leafless plant” (Belcher, 2013, p. 235)), the first evidence of charred wood in the fossil record does not appear until the Middle-Late Devonian (~380 Ma) (Scott, 2000; Belcher, 2013). Scott and Glasspool (2006) indicate that the likely restricted nature of the fuel load during the Silurian means that fires were unlikely to have been widespread. Instead, as Belcher et al. (2013, p. 235) indicate, the “evolution of wood represents the emergence of the first large fuel load able to sustain and carry a fire for a significant period” and therefore “until the evolution of woody shrubs and trees it is unlikely that fire would have ever been widespread”. Evidence for a spread in forest vegetation comes from Late Devonian coals, where *Archaeopteris* (the first, large wooded tree) evolved and rapidly spread (Scott and Glasspool, 2006). Yet, it is not until ~20 Ma later that the record of charcoal from the Late Devonian suggests the development of extensive wildfires (Scott and Glasspool, 2006; Belcher, 2013). Evidence for the presence of land vegetation (fuel) and the likelihood of lightning strikes (ignition source) indicates that the occurrence of widespread fires was most likely influenced by atmospheric O_2 concentrations, which are thought to have increased gradually as land vegetation evolved until the required concentration was reached to support significant fires (Scott and Glasspool, 2006; Belcher et al., 2013). From this point, evidence of wildfire in the form of fossil charcoal can be found throughout the geological record preserved within a variety of volcanic rocks as well as marine and terrestrial sediments, including near-shore clastic sediments and coal deposits (Scott, 2000).

However it was not until relatively recently that the presence of charcoal throughout the geological record was used to aid the debate on past variations in Earth’s atmospheric O_2 (e.g. Scott and Glasspool, 2006; Belcher and McElwain, 2008) (Watson and Lovelock, 2013). Research has indicated that fossil charcoal abundances in sediments track numerical model predictions of atmospheric O_2 (e.g. Scott and Glasspool, 2006; Belcher and McElwain, 2008; Belcher et al., 2010). For example, using the defined lower percentages of O_2 proposed for fire ignition, Scott and Glasspool, (2006) hypothesized that below 13% O_2, except under exceptional circumstances, wildfires would not ignite or spread irrespective of moisture content. Between 13-16% fires would be rare, and only vegetation growing in areas liable to drying would burn. Between 18-23% O_2 (including present atmospheric level (PAL) of ~21%), plant matter must have a low moisture

content to burn. Beyond 25% fires would be widespread even in wetter climates and beyond 30%, fire activity would be globally distributed with vegetation burning irrespective of its moisture content. Using this criteria, Scott and Glasspool's (2006) investigation into changes in charcoal content between the Silurian and the Permian lead to a prediction that an increase from 2% charcoal content to 43% found in sediments during the Pennsylvanian Carboniferous period (320-290 Ma) could indicate a palaeo-atmospheric O_2 content of >25%, due to the high percentage of flora preserved as charcoal. This was then compared to earlier sediments of Late Devonian age (385-359 Ma) where there was little evidence of fossil charcoal, and modelled O_2 levels were predicted to have been lower than PAL (Scott and Glasspool, 2006) (Figure 1.11).

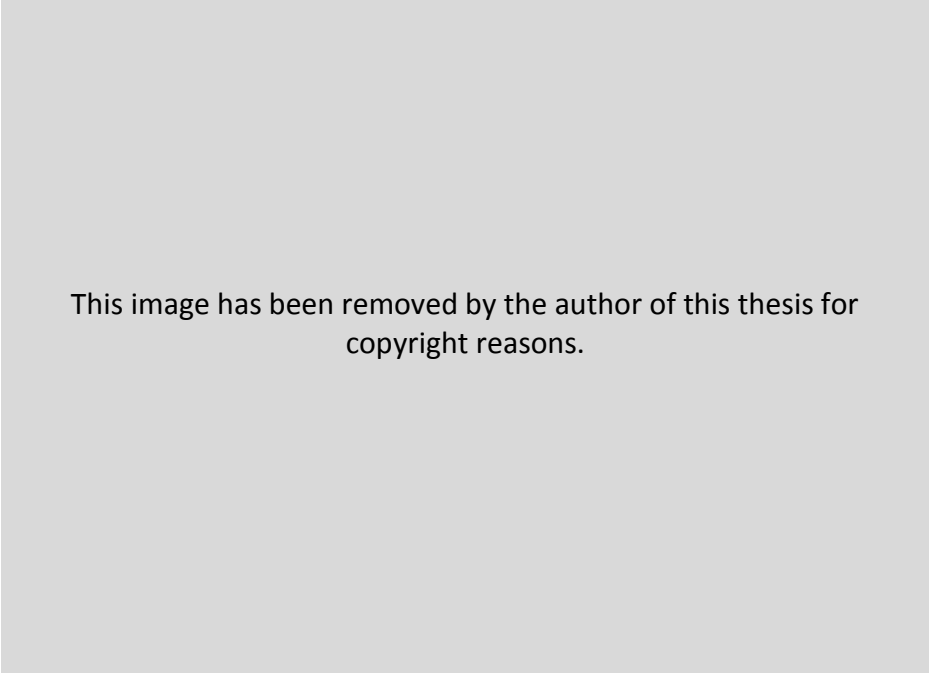

Figure 1.11 - Illustration of modelled fluctuations in atmospheric O_2 concentration from the Silurian to the Permian, coupled with the trends in wildfire occurrence predicted from the abundance of fossil charcoal (taken from Scott and Glasspool, 2006, p 10862). Shaded area indicates the fire window. Black squares indicate modelled O_2 concentrations from Berner (2006), whilst white squares are from Berner et al. (2003).

From their study, it was clear that changes in the abundance of charcoal within sediments over million year timescales, could be attributed to periods in Earth's history that are thought to have experienced higher atmospheric O_2 concentrations, compared with periods where little/no charcoal was found and periods of low atmospheric O_2 concentrations were estimated.

The record of wildfire has also been used to test the precision of numerical O_2 models. Belcher and McElwain (2008) collated data on the record of past wildfires throughout the Mesozoic (taken from published records of wildfire derived charcoal, inertinite and polycyclic aromatic hydrocarbons (PAH's)) and plotted their occurrence against modelled O_2 from three O_2 models; the GEOCARBSULF model (Berner 2006), Falkowski et al.'s model (2005), and the COPSE model (Bergman et al., 2004) (Figure 1.12). Belcher and McElwain (2008) used their novel combustion experiments undertaken in a range of atmospheres, to reveal that the presence of wildfire activity indicate that oxygen cannot have been lower than 17% within the Triassic, Jurassic and Cretaceous periods, and thus indicate that atmospheric O_2 levels cannot have been as low as some of the models had suggested (e.g. Falkowski et al., 2005; Berner, 2006). Furthermore, the relationship between rising O_2 and rising ignition and burn probability (Belcher et al., 2010) suggests that atmospheric O_2 concentrations are unlikely to have exceeded 30 - 35% vol. (Watson and Lovelock, 2013). This is because beyond 30% O_2, the probability of ignition even for fuels with a high moisture content would be so high that fire frequency would be such that the regeneration of forests would soon be prevented (Lenton and Watson, 2000a). The fossil record indicates that there has been a continued persistence of land vegetation from ~440 Ma (Scott, 2000). Therefore O_2 concentrations above 30 – 35% would be deemed incompatible with fossil evidence for the existence of land vegetation. These upper and lower O_2 limits for combustion indicate that past O_2 concentrations have likely remained between ~17% to ~30% over the last ~350 Myrs, forming what has been termed the 'fire window' (Watson and Lovelock, 2013).

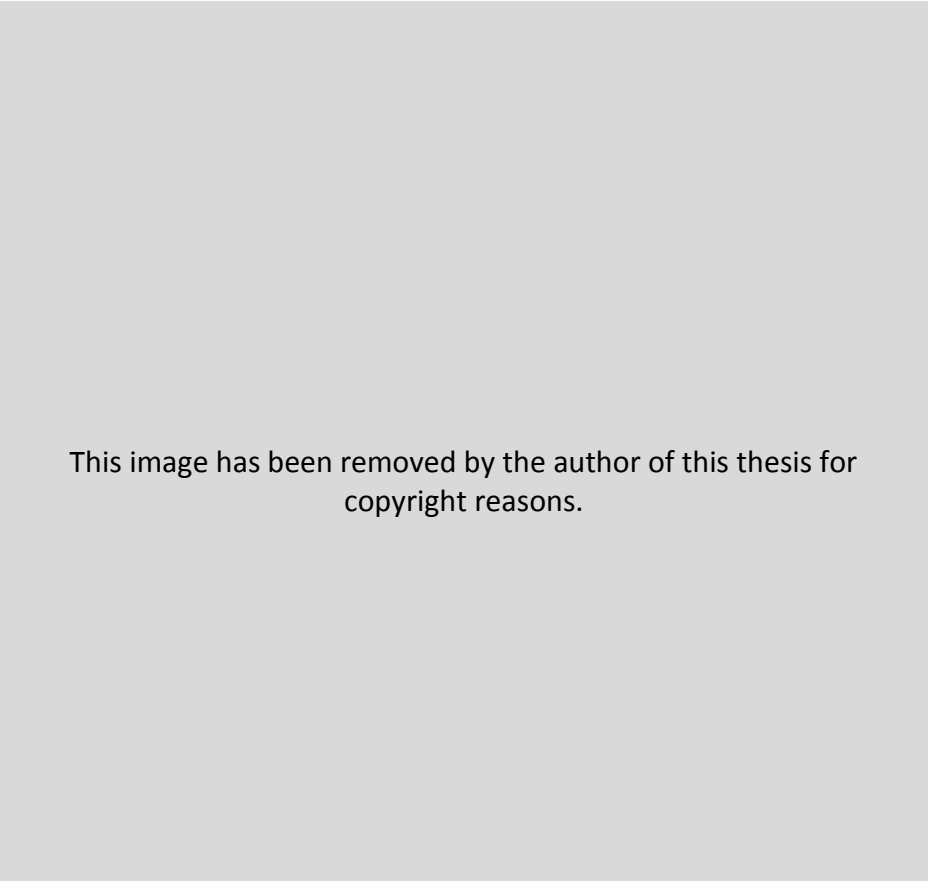

Figure 1.12 - Modelled O_2 curves plotted against the record of wildfires throughout the Mesozoic. 'Vertical black lines represent known occurrences in fires in the fossil record.' (Belcher and McElwain, 2008, p 1199). Black vertical lines indicate published known occurrences of fire in the fossil record.

The relationship between fire, fuel moisture and atmospheric oxygen indicates that O_2 changes are likely the main driver of fire changes across multi-million year timescales, unlike medium timescales where climate is speculated to be the main driver.

1.5.3 Fire feedbacks and interactions over long-timescales

One role that fire has been suggested to act as an essential feedback mechanism is in stabilizing atmospheric O_2 concentrations and maintaining concentrations within habitable bounds. Here changes in wildfire activity are found to influence the weathering and distribution of limiting nutrients, which in turn affects the C-cycle and the most important O_2 source for the planet.

As previously discussed, the process of combustion can tell us a lot about past atmospheric O_2 concentrations. The requirement for at least ~17% vol. O_2 to

allow combustion to occur has aided numerical biogeochemical model estimations, constraining their predictions to sit within the 'fire window' (refer to chapter 3 for more information on numerical modeling of atmospheric O_2). The ability for the Earth's atmospheric O_2 concentrations to remain within the 'fire window' over the last ~370 Myrs, indicates that O_2 has remained fairly stable, and thus there must be natural feedback mechanisms that exist to prevent O_2 from rising beyond ~30% and declining below ~16-17% (Watson and Lovelock, 2013; Lenton, 2013).

Photosynthesizing primary producers provide the main source of O_2 to our atmosphere, which is reflected in the geological record by the burial of organic carbon (C_{org}) (Figure 1.13). To stabilize atmospheric O_2 either the source of O_2 (C_{org} and pyrite burial) or the sink (oxidative weathering) must be influenced as levels rise/fall (Lenton, 2013). Chemical weathering reactions are assumed to be near complete at PALs (Holland, 1984), making oxidative weathering a weak negative feedback on rising concentrations (Lasaga and Ohmoto, 2002). Oxidative weathering therefore cannot act sufficiently to remove high O_2 and prevent it sky rocketing even higher (Lenton, 2013), leaving the source of O_2, C_{org} burial, as the ultimate regulating force on atmospheric O_2 (Lenton, 2013).

Hence, the modulation of C_{org} burial has formed the main component of all of the proposed O_2 regulation feedback (Watson and Lovelock, 2013).

C_{org} burial is controlled by the availability of bio-limiting nutrient phosphorus (P) (Lenton and Watson, 2000a), sourced from the continental weathering of rocks (Föllmi, 1996; Kump et al., 2014). Once weathered the soluble P accumulates in soils where it is made available to the terrestrial biota. P is often released during organic matter decomposition (DeBano, 1990) where via rivers, run-off, and groundwater flow both across the soil surface and subsurface, it is mobilized and transported to the oceans (Föllmi, 1996; Randall et al., 2001; Kump et al., 2014). Variations in the delivery of P to the marine realm can therefore exert a significant control on the burial of C_{org} buried on the ocean floor, and thus the leak of O_2 to the atmosphere.

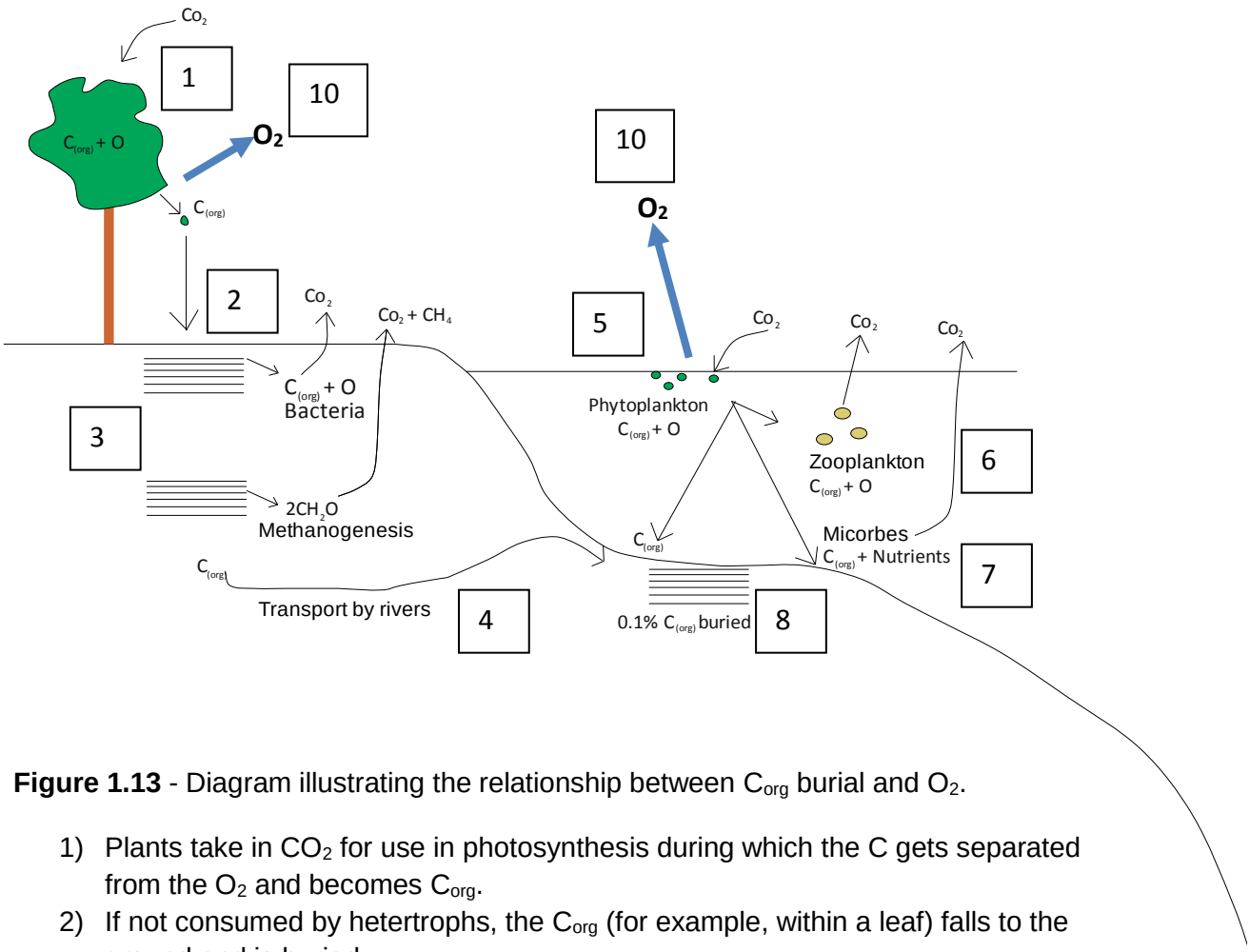

Figure 1.13 - Diagram illustrating the relationship between C_{org} burial and O_2.

1) Plants take in CO_2 for use in photosynthesis during which the C gets separated from the O_2 and becomes C_{org}.
2) If not consumed by hetertrophs, the C_{org} (for example, within a leaf) falls to the ground and is buried.
3) The C_{org}, now part of the soil can remain here for up to 50 years (Kump et al., 2014) if not used in chemical reactions by bacteria or fungi, such as methanogenesis.
4) Every ~1000 years 5cm of soil is transported by rivers to the oceans (Kump et al., 2014).
5) A similar process occurs with the phytoplankton within photic zone which during photosynthesis, separates C_{org} and O_2 from the CO_2.
6) The majority of the C_{org} is consumed by zooplankton.
7) Some is consumed by microbes near the seafloor that also produce nutrients.
8) At present day, ~0.1% C_{org} produced in surface waters reaches the sea floor to be buried in the sediments alongside the terrestrial $C_{org.}$
9) The C_{org} becomes buried and lithified into sedimentary/metamorphic rock, locking the C_{org} away from consumers
10) The C_{org} locked up in these organic rich sediments can be associated with a release of O_2 as the C_{org} has not undergone consumption, therefore its O_2 atom that was liberated during photosynthesis has not been consumed by respiration/used in methane oxidation. This represents a present day leak of ~0.1% of O_2 to the oceans and atmosphere (Lenton, 2001).

The responsiveness of wildfire to variations in atmospheric O_2 (Watson, 1978; Belcher et al., 2010) has been considered to provide a key feedback in regulating

O_2 concentrations through its influence on the delivery and availability of P (e.g. Kump, 1988; Lenton and Watson, 2000a; Lenton, 2001; Handoh and Lenton, 2003).

Here, two feedback mechanisms (Kump, 1988; Lenton and Watson, 2000a) have been proposed, that apply the relationship between O_2, fire and primary productivity to act as a stabilizing factor for atmospheric O_2 concentrations in the Earth system.

Feedback Hypothesis 1 (Kump, 1988)

Kump (1988) was one of the first to suggest a biological feedback mechanism that acts to stabilize atmospheric O_2 across geological timescales. Kump's (1988) feedback involves the relationship between wildfire and O_2, and the effect of wildfire on the redistribution of the limiting nutrient P (Lenton and Watson, 2000a; Lenton, 2013). Here, Kump (1988) suggests that the regulation of atmospheric O_2 relies on negative feedbacks involving the main source of O_2, (C_{org} burial), and in the model, uses the supply of P and its ratio with C within organic matter as the main control on the amount of O_2 liberated to the atmosphere.

In the terrestrial system, both nitrogen (N) and P are limiting nutrients, required for primary productivity and thus C_{org} burial. Nitrates can be fixed from the N in the atmosphere according to demand. P however, can only be obtained through the weathering of silicate minerals in rocks (Föllmi, 1996), therefore making weathering the ultimate control of C_{org} burial on land. In the marine system, C_{org} burial is dependent on the sedimentation rate and burial flux from primary producers in the surface waters. Here, although N is the ultimate limiting nutrient for these primary producers, its availability tracks that of the P content, therefore making P the ultimate limiting nutrient for primary producers in the photic zone and thus C_{org} burial in the marine system (Lenton, 2001).

Using Redfield's (1958) ratios of C:P Kump (1988) exclaims that the C:P ratio of terrestrial organic matter is roughly equal to 1000:1 compared with marine organic matter that has a C:P ratio of 105:1. The burial of terrestrial organic matter has therefore removed less P per C unit than the equivalent amount required for marine organic matter (Kump et al., 2014). Using this theory, Kump (1988) predicts that with increased atmospheric O_2, there would be an increased

likelihood of fires (Watson, 1978), which would cause an 'ecological disturbance' and reduce the amount of terrestrial vegetation and biomass. The P utilized by the previous terrestrial vegetation would now go directly into rivers and wash into the marine environment. This is due to "enhanced soil erosion as a result of the loss of ground cover, the atmospheric transport of ash (generated from the P-rich leaves and stems of plants), and the prevention of 'climax' communities that would be nutrient-efficient and prevent the loss of P from the land system" (Kump, 1988, p. 153).

In Kump's (1988) biogeochemical feedback, more P redistributed to the oceans compared with the land, should cause an overall decline in the amount of C_{org} buried, as marine C:P burial ratios are ~100:1, compared with terrestrial C:P burial ratios anticipated at ~2000:1. The subsequent burial of the marine organic matter would therefore liberate less O_2 than what would have otherwise been liberated by the terrestrial organic matter (Kump et al., 2014). The decrease in O_2 production levels would result in a decrease in atmospheric O_2 levels, and thus provide a negative feedback on rising atmospheric O_2 (Figure 1.14).

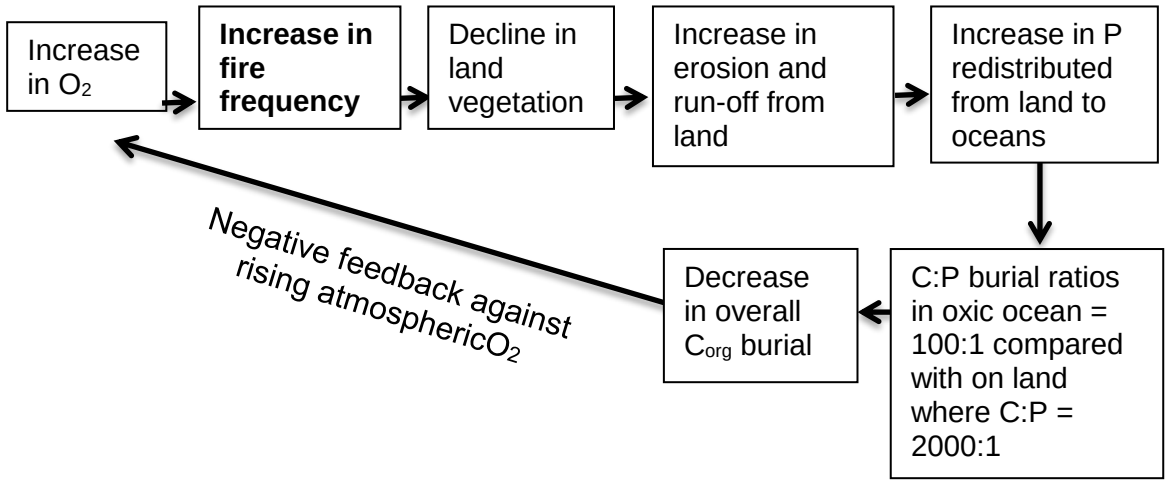

Figure 1.14 Kump's (1988) and Kump et al.'s (2014) atmospheric O_2 regulation feedback against rising atmospheric O_2 using the relationship of fire activity with O_2

Feedback Hypothesis 2 (Lenton and Watson, 2000a)

The weathering flux of P "provides the ultimate control of organic matter accumulation in terrestrial ecosystems and net loss from them" (Lenton, 2001, p. 616). The flux of P to marine surface waters (controlling primary productivity and thus the burial flux of C_{org}), is determined by the balance between riverine input and P burial in ocean sediments (Lenton, 2001). Within this feedback, the riverine input of P to surface waters is ultimately controlled by the amount of weathering on land e.g. through the chemical weathering of continental rock (Lenton and Watson, 2000a; Lenton, 2001).

Vegetation type and cover have been shown to influence the weathering of P from rocks where increased production of vascular plants may amplify weathering rates (Föllmi, 1996; Lenton, 2001), the factor of which is anticipated to be "at least of similar magnitude to that for the bulk weathering of rock" (Lenton and Watson, 2000, p. 260). This is conducted through a number of mechanisms including the enhancement of the hydrological cycle (Bets, 1999) and thus precipitation and weathering rates (Lenton, 2001); acidification of soil water through root and heterotrophic respiration of plant litter, generating increased pCO_2; secretion of organic acids by mycorrhizal fungi, increasing rock porosity and dissolving minerals; and physical weathering caused by tree roots splitting rocks (Lenton, 2001).

It has therefore been hypothesized that a decline in vegetation biomass, for example as a result of wildfires, would have a detrimental effect on the weathering of P. As continental weathering provides the ultimate control on P sourced to the marine system via rivers, a decline in P to surface waters following a fire is anticipated. This occurs not only due to a decline in biomass but also by the likely replacement of forested areas with faster, regenerating ecosystems, whose roots are much shallower and thus not capable of exerting as larger weathering effect as the larger roots from trees (Lenton, 2001). The decline in P weathering caused by a decrease in land biomass from fires, therefore provides a negative feedback against the burial of C_{org} and the leak of O_2 to the atmosphere (Lenton, 2013) (Figure 1.15).

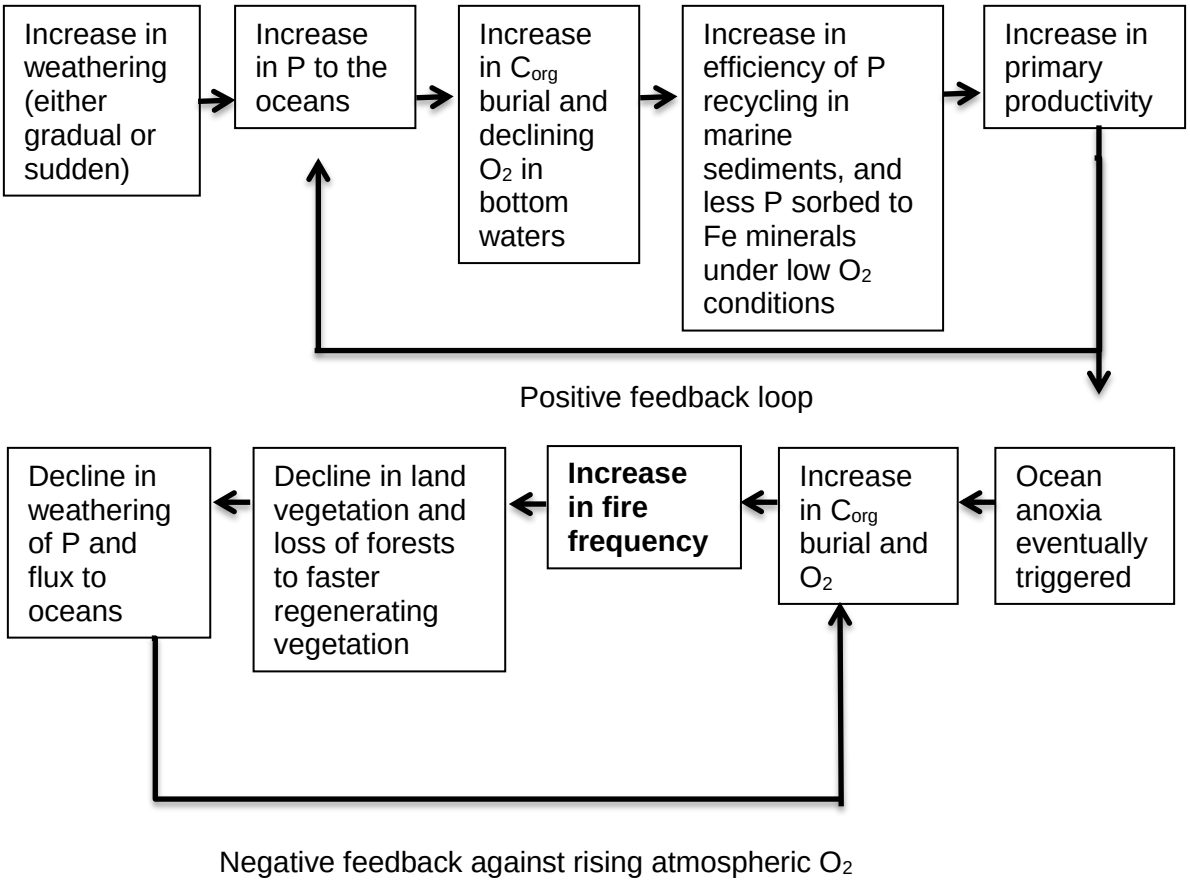

Fig.1.15 Feedback against rising atmospheric O_2 if fires decrease the weathering of P and thus supply to ocean sediments

Both Kump (1988) and Lenton and Watson's (2000a) feedback mechanisms are capable of regulating atmospheric O_2 concentrations within the 'fire window', but only if the effects of fire on vegetation and the distribution of P to the marine environment is incorporated (Watson and Lovelock, 2013). This illustrates the significant importance of fire as a feedback mechanisms in the natural world.

The effects of fire in regulating C_{org} burial and atmospheric O_2 have been tested using numerical models. Although these are discussed in more depth in Chapter 3, it is clear that without the presence of fire and its influence on C_{org} burial, atmospheric O_2 concentrations would not have been capable of stabilizing between ~17% and 30% throughout the last ~370 Myrs (Watson and Lovelock, 2013; Lenton, 2013). Fire is therefore a key process in the Earth system, required to maintain our atmospheric O_2 concentrations at the PAL and within habitable bounds.

1.4 Thesis Summary and Aims

It appears that the process of combustion may play an essential role for life on Earth, where natural Earth system processes influence ignition probability, fire spread and fire behaviours, and where fire can provide a variety of feedbacks, to the Earth system over different timescales.

This thesis aims to analyse these Earth system - fire relationships and feedbacks across medium and long timescales in deep time, in order to understand the role that fire may have played and what the record of fire can tell us about the functioning and re-equilibrating of the Earth system during and after significant C-cycle perturbation events occurring in Earth's deep past.

This thesis will:

1) Firstly look at the role of fire as a crucial feedback process in ending significant, global C-cycle perturbation events over long timescales. These events are termed Oceanic Anoxic Events (OAEs), and are classed as periods of major environmental change occurring in Earth's history, where much of the world's oceans became depleted in oxygen and marine mass extinctions occurred. During an OAE, there is evidence for an increase in C_{org} burial. As C_{org} burial can be related to a leak in O_2 to the atmosphere, Handoh and Lenton (2003) hypothesize that the C_{org} buried during the OAE caused O_2 to gradually rise, terminating ocean anoxia approximately one million years after the event had begun.

   Fire is sensitive to changes in atmospheric oxygen that occur over long timescales. Part one of this thesis therefore aims to test the hypothesis that OAEs were terminated due to a rise in atmospheric O_2. To do this, the record of fire in the form of fossil charcoal preserved in sediments deposited before, during and after the Jurassic OAE (Toarcian OAE, occurring ~183 million years ago) are analysed.

   As the Toarcian-OAE occurred during a time where atmospheric O_2 concentrations are predicted to be ~20% vol., O_2 concentrations therefore sit within the 'rapid increase in fire probability' window (Belcher, 2013), thus fire should be sensitive to any change in O_2 during this time interval. Analysis of charcoal across the Toarcian OAE will provide the first fossil

based evidence to test whether Handoh and Lenton's (2003) hypothesis that OAEs are terminated by a rise in atmospheric O_2 is true as well as analyse the role that fire may have played (if any) in ending ocean anoxia.

2) The second part of this thesis will look more closely at the changes in fire occurrence and what the record of fire can tell us over medium timescales, across these significant global events. To do this, the record of fire is analysed across the initiation of Cretaceous OAE 2, which occurred ~93.5 million years ago, during a time where atmospheric O_2 is predicted to have been between 23% vol. and 27% vol. Between these O_2 concentrations, laboratory experiments show that the probability of ignition and fire spread is much less sensitive to changes in O_2. Therefore any changes in O_2 are likely to be much less important in terms of driving major changes in fire. This therefore allows for the assessment of medium-timescale climate responses and climate driven fire changes to Earth system perturbations.

3) Thirdly after analysing the record of fire across both long and medium timescales within the deep past across significant Earth system perturbations, this thesis will look at the 'natural background' signal of wildfire across medium timescales. There are currently few studies that have analysed fire trends occurring over medium timescales of tens to hundreds of thousands of years within the geological record, yet these medium timescale trends in wildfire activity are important in enabling the disentangling of the charcoal record across time. This will be conducted by looking at the record of wildfire across naturally occurring orbital cycles termed the Milankovitch cycles, which occur over tens to hundreds of thousands of years.

2. Introduction to Oceanic Anoxic Events

2.1 Introduction

Oceanic anoxic events (OAEs) represent periods in Earth's history that experienced significant environmental change, with disturbances to the global C-cycle; environmental conditions and terrestrial and marine biotas (Schlanger and Jenkyns, 1978; Jenkyns, 1980; Jenkyns, 2010). OAEs are represented in the rock record by widely traceable organic rich horizons and large positive excursions in both the organic and carbonate C isotope records ($\delta^{13}C_{org}$ and $\delta^{13}C_{carb}$ respectively) (Schlanger and Jenkyns, 1978; Jenkyns, 1980; 2010). During these events, enhanced C_{org} production, burial and preservation occurred, where bottom seawaters became depleted in O_2 across a wide geographic range (Schlanger and Jenkyns, 1976; Handoh and Lenton, 2001; Jenkyns, 2010; Caswell and Coe, 2012).

Initial identification of these events was based on the presence of organic-rich horizons (e.g. Figure 2.1) that were locally high in total organic carbon (TOC) (e.g. Moberly and Larson, 1975). The occurrence of the organic rich beds indicated that deposition is likely to have occurred during times of regular "supply of organic matter and conditions conducive for preservation of that organic material including depletion of dissolved O_2 in waters overlying the sediment/water interface" (Arthur and Sageman, 1994, p. 500).

Figure 2.1 – Photograph of a Cretaceous OAE (Livello Bonarelli event), black shale, deposits amongst white and pink limestone of the Scaglia Bianca Formation (Late Albian-Cenomanian age). For scale, person is ~1.8 m tall. (Robinson et al., 2017).

Later, in 1980, Scholle and Arthur (1980) identified a positive C isotope excursion in bulk rock $\delta^{13}C_{carbonate}$ (Equation 2.1), which appeared coeval with OAE's at the Cenomanian-Turonian boundary and at the Aptian-Albian boundary. The discovery of a C isotope excursion, according to Jenkyns (2010, p. 6), "conformed perfectly to expectations" due to the association of these events with anomalously high burial rates of marine C_{org}, leading to the recognition of many more anoxic events. The total number of OAE occurrences now sits at approximately eleven events, with nine occurring in the last 200 Ma (Figure 2.2) (Erbacher et al., 1996; 1998; Leckie et al., 2002).

Equation 2.1 - $\delta^{13}C$ Isotope Equation

$$\delta^{13}C=[(^{13}C/^{12}C)_{sample} / (^{13}C/^{12}C)_{standard} – 1] \times 1000$$

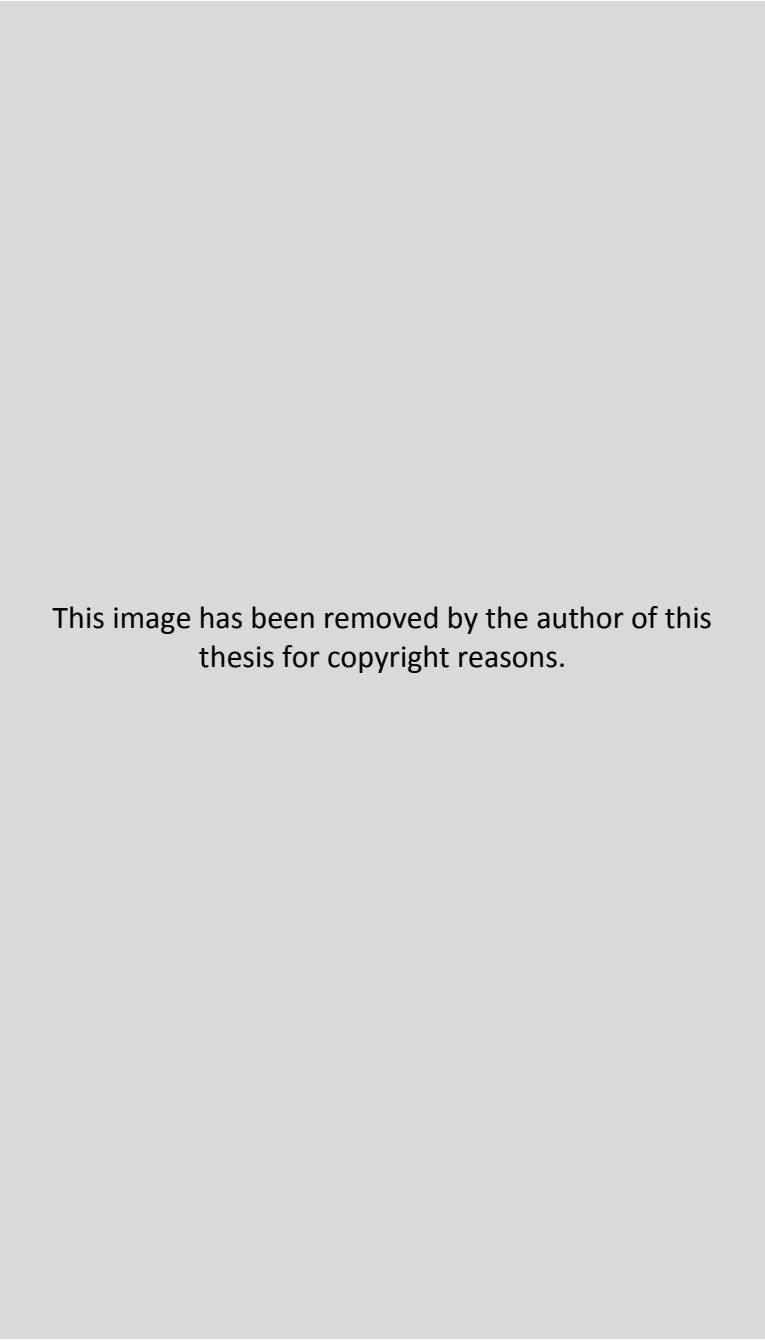

Figure 2.2 – Diagram illustrating the occurrence of Oceanic anoxic events throughout the last 200 Ma. (Adapted from Jenkyns, 2010).

The positive isotope excursion is achieved by the preferential assimilation of ^{12}C by primary producers during photosynthesis (van der Velde et al., 2014). Although CO_2 is composed of both ^{12}C and ^{13}C isotopes, during photosynthesis the 'lighter' ^{12}C isotope reacts more rapidly, and is therefore preferentially assimilated during C fixation to produce organic matter (Gu and Alexander, 1996; Ferrio et al., 2003). An increase in primary production can therefore leave an

excess of ^{13}C within the global C reservoir whilst the ^{12}C is locked away in the organic matter produced (Schouten et al., 2000; Petsch, 2003) (Figure 2.3).

Ocean plankton and other shelled organisms use bicarbonate and carbonate ions to make their shells (the formation of bicarbonate and carbonate itself involves a reaction with CO_2 and therefore carries the isotopic signature of the C-isotope ratio present at the time within the C reservoir (Hayes, 1993; Kump et al., 2014)). With an excess of ^{13}C isotopes left, the ocean calcifying marine organisms assimilate a heavier $\delta^{13}C_{Dissolved\ Inorganic\ Carbon}$ (commonly measured as $\delta^{13}C_{carbonate}$) signal into their shells/tests, which translates as heavier isotopic signatures within the $\delta^{13}C_{carbonate}$ formed (Figure 2.3) (Kump and Arthur, 1999; Brice et al., 2002). The heavier the $\delta^{13}C_{carbonate}$ signature produced, the faster the rate and the larger the amount of C_{org} is hypothesized to have been buried (Guo et al., 2013).

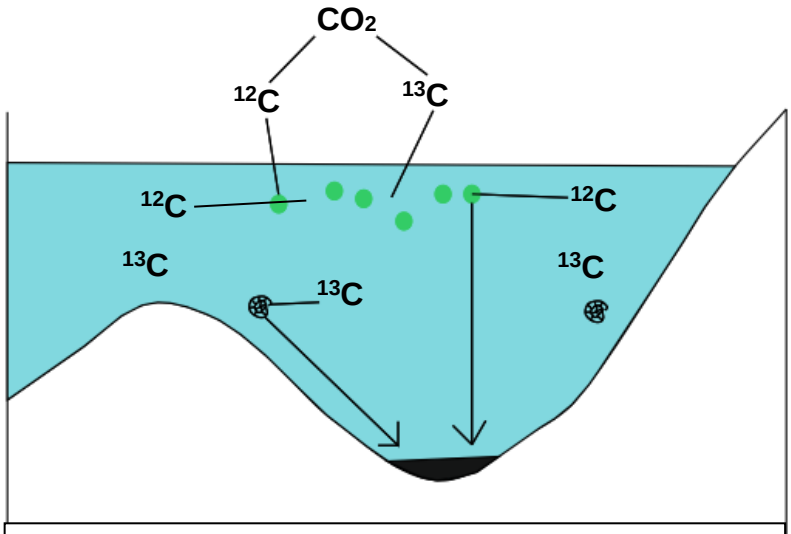

Increased assimilation of ^{12}C by the increase in primary producers leaves an excess of ^{13}C within the atmosphere-ocean system. Carbonate producing organisms then use the left over, available ^{13}C to incorporate into their shells, which eventually becomes buried, carrying with it the heavier ^{13}C rich $\delta^{13}C_{carbonate}$ isotopic signature. This produces a heavier signal than previously deposited carbonate sediments that were able to incorporate more of the then available ^{12}C into their shells, thus producing a positive C isotope excursion

Figure 2.3 – Diagram illustrating how an increase in primary productivity within the photic zone can lead to a positive $\delta^{13}C_{carbonate}$ isotope excursion within the rock record.

An enrichment of the heavier $^{13}C_{cabonate}$ recorded within sedimentary rock produces a positive $\delta^{13}C_{carbonate}$ excursion, commonly up to +5‰ above background values (Weissert et al., 1985; Arthur et al., 1985; Vincent and Berger, 1985; Schlanger et al., 1987; Jenkyns and Clayton, 1986; Weissert and Channel, 1989; Weissert and Bréhéret, 1991; Gale et al., 1993; Algeo et al., 1995; Bartolini et al., 1996; Schouten et al., 2000; van Breugel, 2006). An example of this can be observed within Middle to Late Aptian sediments where there is a shift from a background of ~+1‰ $\delta^{13}C_{carbonate}$ to a $\delta^{13}C_{carbonate}$ value of up to +5‰ (Weissert et al., 1985).

The isotopic signature of C_{org} typically varies accordingly with the signature of marine carbonates due to the relationship between dissolved C_{Inorg} (e.g. dissolved CO_2 within the ocean reservoir) and its fixation by autotrophs producing the C_{org} (Guo et al., 2013). Due to this relationship coupled with the preferential assimilation of ^{12}C by primary producers, (Gu and Alexander, 1996; Ferrio et al.,

2003) the C_{org} signal produced is isotopically lighter when compared to C_{carb} values, commonly between -22‰ and -34‰ (Kump and Arthur, 1999; Kah et al., 1999). The relationship between the C_{org} and C_{carb} therefore enables the $\delta^{13}C_{carbonate}$ values to reflect the isotopic composition of the atmosphere/ocean after assimilation. $\delta^{13}C_{organic}$ values reflect the photosynthetically assimilated C signature (^{12}C), although the isotopic composition can also be influenced by the metabolic behavior of the organic community, the input from marine vs. terrestrial sources of organic matter, the degradation of particulate C_{org} below the sediment water interface, and the remineralization of dissolved C_{org}/other C byproducts within the water column (Guo et al., 2013, p.).

2.2 Triggering an OAE

Although the concept of OAEs was first introduced in the 1970's (e.g. Schlanger and Jenkyns, 1976), the triggering mechanisms behind these significant events is still debated (Jenkyns, 2010). This is because OAEs can often display varying characteristics (see Figure 2.12), from the presence of organic rich beds and a positive C-isotope excursion (e.g. OAE 2), to a positive C-isotope excursion disrupted by a negative C-isotope shift and (locally) a lack of organic C-rich strata (e.g. within the Toarcian OAE). This has led to proposition of different triggering mechanisms, some of which attempt to account for the positive excursions observed in $\delta^{13}C$ records, whilst others focus on understanding the varying percentages of organic content and widespread anoxia. The models postulated to account for the deposition of organic rich strata and ocean anoxia include a barred basin, ocean stagnation, and global transgression.

2.2.1 Barred Basin Model

Early studies (e.g. Woolnough, 1937) suggested that a common depositional setting for black shale could be within a barred (silled) basin, where the presence of the bar would reduce O_2 flow to deeper waters within the basin, resulting in poor circulation and vertical mixing. Over time, this enables the formation of anoxic conditions as fresh, oxygenated waters are not able to replace the stagnant O_2 poor bottom waters in the basin. Any organic matter deposited within this setting is then preserved under the anoxic/low O_2 conditions due to reduced

oxidation and decomposition (Demaison and Moore, 1980; Pratt, 1984; Canfield, 1994).

This hypothesis was initially favorable with early studies (Arthur and Sageman, 1994), although Tourtelot (1979) indicated that within a bared basin setting, “sediments deposited beneath the area of high productivity could be rich in organic matter and form black shales without necessarily there being an anoxic event” (Tourtelot, 1979, p. 317). The barred basin model is commonly associated with the present day Black Sea where waters are anoxic between 100m to 200m depth (Murray et al., 2005).

2.2.2 Stagnant Ocean Model

The stagnant ocean model suggests that an OAE can be triggered by sluggish global ocean circulation, where bottom ocean waters become stagnant enabling the O_2 minimum zone to expand (Arthur and Schlanger, 1979; Hotinski et al., 2001). However, the depth required before bottom waters can become depleted in O_2 is debated, as Twenhofel (1915; 1939) and Moore (1949) suggest a need for very shallow water environments. In comparison to Pompeckj (1901); Schuchert (1910), and Rich (1951) who suggest anoxia could occur in a deeper water environment of up to several thousand feet (Hallam, 1967; Arthur and Sageman, 1994).

The ocean stagnation model has been suggested as a likely trigger during periods when the Earth had an equable climate devoid of polar ice caps, e.g. the late Mesozoic Era (Selley, 1990). At present day, deep water circulation is driven by cold, oxygenated bottom waters originating from the poles that flow beneath warmer, low latitude waters (Selley, 1990). However, during the Mid to Late Cretaceous, global land configuration around the Atlantic and Indian oceans may have been restricted enough to allow only limited access to deep, oxygenated waters of the world’s oceans (Jenkyns, 1980). This may, therefore, have enabled stagnation throughout much of the water column, aided by a high salinity stratification reducing vertical mixing. Records indicated that many OAEs appear to occur close to the equator (Jenkyns, 1980), where increased primary productivity in the photic zone in these regions likely fueled C_{org} burial, aiding in the creation of an O_2 deficient intermediate/deep water layer (Figure 2.4).

Due to increased productivity within the photic zone of tropical areas, this model can account for the positive excursion of $\delta^{13}C_{carbonate}$ recorded across OAE

deposits within palaeo-equatorial regions, as well as the physical signature of the organic rich shales. However, Hotinski et al. (2001) and Pedersen and Calvert (1990), expressed concerns with the sluggish circulation model, stating that recently published 'coupled ocean-atmosphere models' confounded the idea that sluggish circulation during the Cretaceous caused the occurrence of OAEs (Pedersen and Calvert, 1990, p. 454).

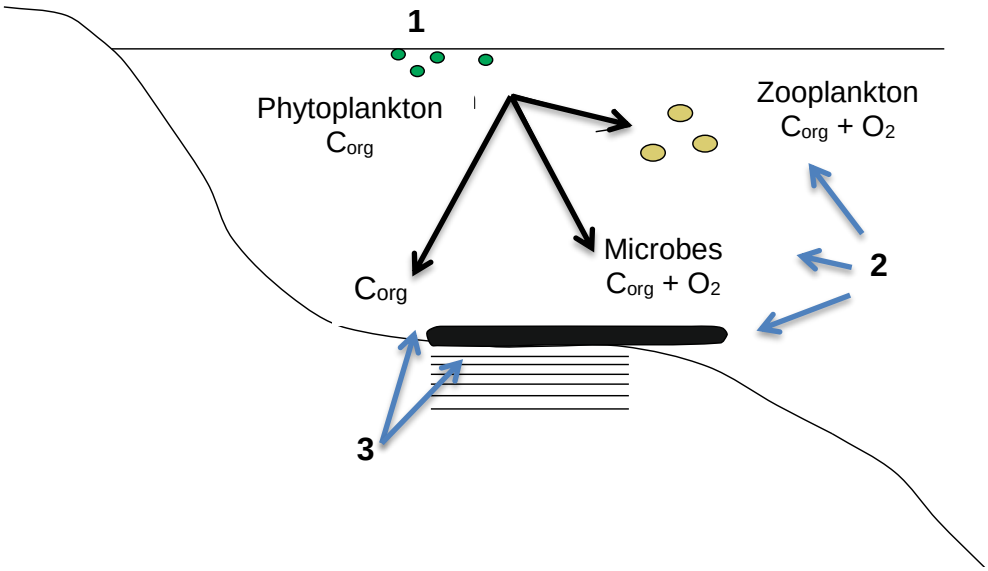

Figure 2.4 – Diagram illustrating how increased primary productivity within the photic zone can lead to increased C burial and the expansion of the O_2 minimum zone.

1) Increased primary productivity within the photic zone produces more organic matter, resulting in increased C_{org} burial
2) Bacteria and zooplankton consume some of the organic matter produced by the phytoplankton, using O_2, and expanding the O_2 minimum zone. This creates an anoxic layer.
3) Any organic matter not consumed by the bacteria together with zooplankton, is buried in the sediments as an organic rich layer. Due to the increase in productivity, an increase in the amount of organic matter and C_{org} not consumed by bacteria/zooplankton will therefore result in an increase in the amount of organic matter and C buried.

2.2.3 Transgression Model

The transgression model was first proposed in 1976 by Schlanger and Jenkyns (1976), who noted that the occurrence of the then two known OAEs (Cenomanian-Turonian (C-T) boundary and the Aptian-Albian boundary (OAE1a)), coincided with two major transgressive phases during the Cretaceous (Figure 2.5).

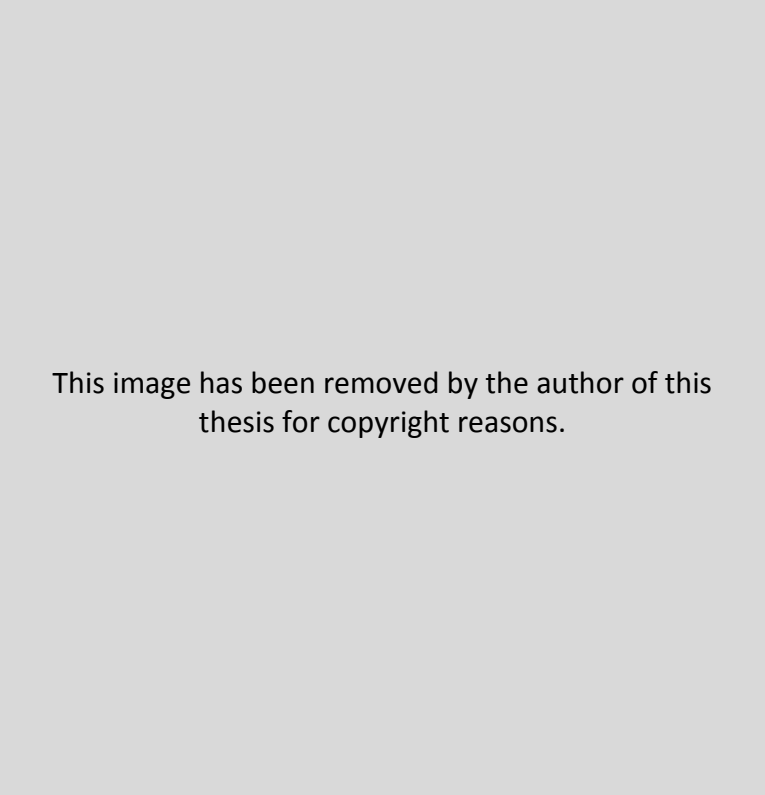

Figure 2.5 – Diagram illustrating the occurrence of the two known OAEs and their coincidence with major transgressive phases (taken from Schlanger and Jenkyns, 1976).

During relative sea level rise, the flooding of land surfaces increases the amount of terrestrial organic matter and leaching of key limiting nutrients such as nitrogen (N) and phosphorous (P) into the marine environment (Erbacher et al., 1996), stimulating increased primary productivity within the photic zone. The increase in marine productivity, coupled with the influx of terrestrially derived organic matter, enables increased bacterial consumption (denitrifying, sulphate-reducing and CH_4 producing) of the organic matter, (Jørgensen, 1982). The bacteria oxidize the sinking planktonic organic matter causing a depletion of O_2 in the water column (e.g. Froelich et al., 1979; Jørgensen, 1982; Westrich and Berner, 1984),

therefore enhancing and expanding the O_2 minimum zone, forming anoxic conditions (Figure 2.6) (Jenkyns, 1980). The increase in terrestrial organic matter and organic matter produced by primary producers, coupled with anoxic bottom waters is anticipated to have led to increased burial and preservation of organic matter producing organic rich, laminated sediments. Another common physical signature associated with the transgression model is the presence of extinction events, particularly of planktonic protozoa (Erbacher et al., 1996). The increase in primary productivity during a transgressive phase is hypothesized to have led to an increase in the assimilation of ^{12}C isotopes (Gu and Alexander, 1996; Ferrio et al., 2003), leaving an excess of ^{13}C within the ocean, to be incorporated into carbonates. Hence, this hypothesis accounts for a positive excursion in $\delta^{13}C_{carbonate}$, coupled with the burial and preservation of organic rich strata. This mechanism was later used by Jenkyns (1980) to express a common link between the then known three Cretaceous OAEs (occurring during the late Barremian-Aptian-Albian; at the C-T boundary, and during the Coniacian-Santonian), that appeared to coincide with suspected global rises in sea level.

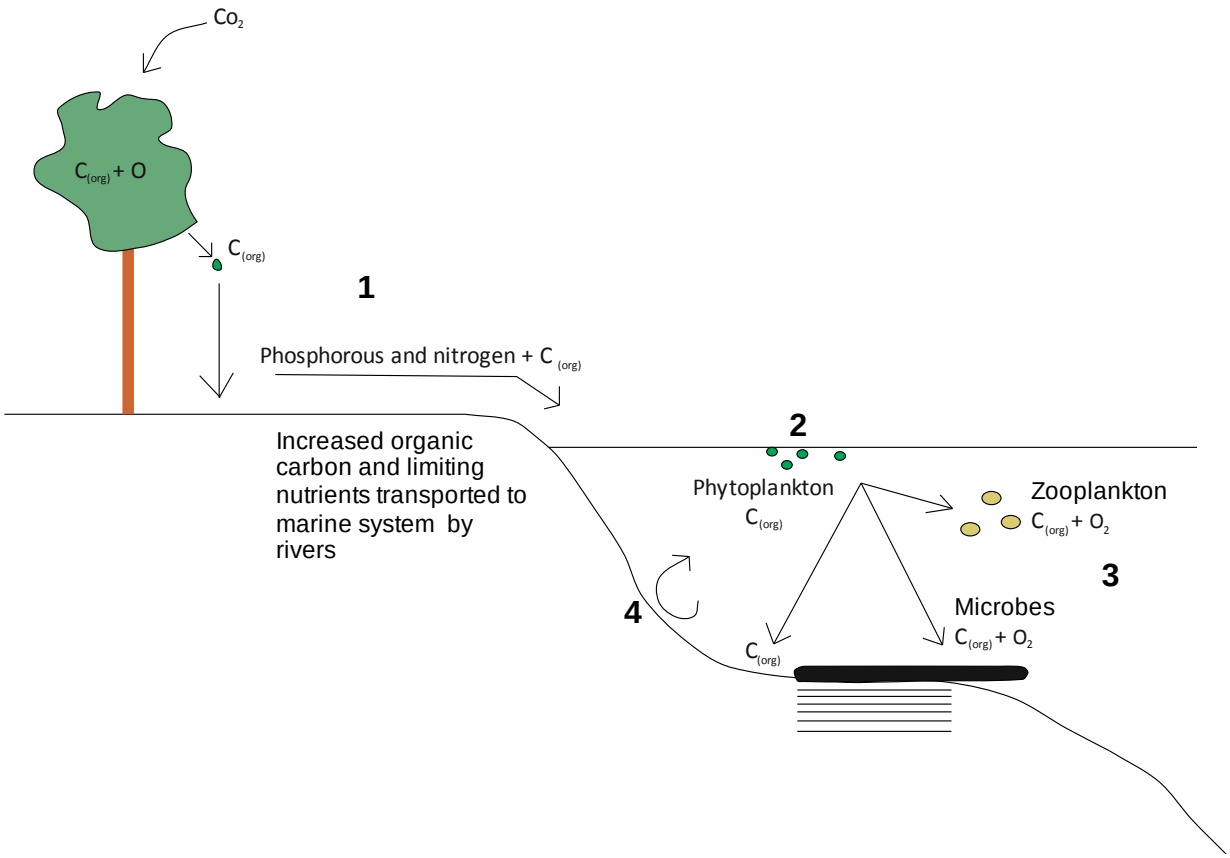

1) Flooding of land surfaces causes increased leaching of limiting nutrients and C_{org} into the marine system
2) This leads to increased primary productivity within the photic zone in the oceans, and assimilation of ^{12}C. This also increases the amount of organic matter reaching bottom waters
3) Bacteria and other microbes consume the organic matter, using O_2 in the process. This creates a tongue of anoxia (represented by the black oval), enabling the burial and preservation of C_{org}.
4) Vertical mixing caused by wind and tides enable efficient recycling of nutrients to sustain productivity

Figure 2.6 – Diagram illustrating how increased leaching from the land during a transgression can lead to increased C_{org} burial and the expansion of the O_2 minimum zone. (Adapted from Jenkyns, 1980).

It was later hypothesized that following a transgression, a regression could further aid in the preservation of the organic rich beds produced under anoxic conditions (Hallam and Cohen, 1989; Erbacher et al., 1996). During a regressive phase it was postulated that there would be an increase in sedimentation rates within an ocean basin that had a ‘continental hinterland’. The increase in land surface area caused by the sea level fall would increase the area of potential surface run-off,

resulting in a high input of organic matter, thus enabling the preservation of black shales by quickly burying earlier deposits (Erbacher et al., 1996) (Figure 2.7).

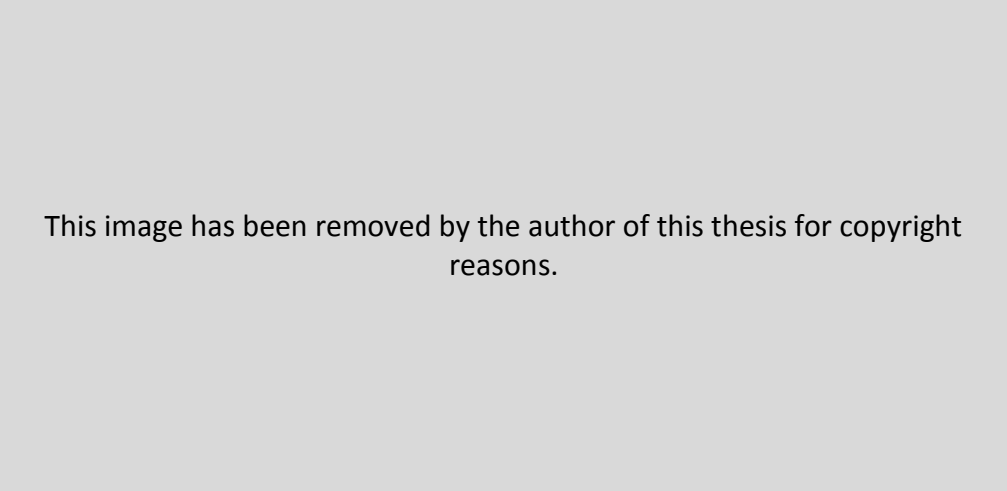

Figure 2.7 – Diagram illustrating how increased sedimentation rates during a relative sea level lowstand could enhance black shale preservation (Taken from Erbacher et al., 1996).

However, many OAEs also display negative C isotope excursions (CIEs) within both C_{org} and C_{carb} isotope records, often separating the overall positive $\delta^{13}C$ excursion associated with these events (e.g. Erbacher, 1994; Weissert and Mohr, 1996; Weissert et al., 1996; Jenkyns and Clayton, 1986; 1997; Menegatti et al., 1998; Schouten et al., 2000; Jenkyns, 2003; Herrle et al., 2004; Hesselbo et al., 2007; Jenkyns, 2010).

Negative excursions in $\delta^{13}C_{carbonate}$ and $\delta^{13}C_{organic}$ record can be observed prior to the Early Aptian OAE; (Leckie et al., 2002; van Breugal et al., 2007); the Early Albian OAE; (Herrle et al., 2004) during the Toarcian OAE, (Hesselbo et al., 2007) and preceding OAE 2 (Barclay et al., 2010). The presence of these negative excursions, originally thought to be of diagenetic origin (Jenkyns and Clayton, 1997), have now been shown to be due to a likely influx of isotopically light C (^{12}C) that must have been present during the time of deposition (Jenkyns, 2010). An influx of ^{12}C would increase the amount and availability of ^{12}C within the atmosphere (represented by light $\delta^{13}C$ values recorded in terrestrial wood isotopes) and the ocean system (represented by light $\delta^{13}C$ values within marine carbonates and C_{org}) enabling a 'lighter' $\delta^{13}C$ signal to be recorded (Dickens et

al., 1995; Hesselbo et al., 2000; Beerling et al., 2002; Brice, 2002; Jahren, 2002; Kemp et al., 2005; van Breugal, 2006; Higgins and Schrag, 2006; Cohen et al., 2007; Kuroda et al., 2007; Svensen et al., 2007; Turgeon and Creaser, 2008; Bralower, 2008; Wignall et al., 2009; Zeebe et al., 2009; Adams et al., 2010; Jenkyns, 2010; Cui et al., 2011; Flögel et al., 2011).

The drivers behind the release of isotopically light C into the ocean-atmosphere system, although still debated, are thought to most likely stem from either; large volcanic events (e.g. Mahoney et al., 1993; Storey et al., 1995; Tejada et al., 1996; Sinton and Duncan, 1997; Torsvik et al., 1998; Kerr, 1998; Larson and Erba, 1999; Tejada et al., 2002; Snow et al., 2005; Wignall 2005); CH_4 hydrate release (Dickens et al., 1995; 1997; 2000; Gröcke et al., 1999; Hesselbo et al., 2000; Jahren et al., 2001; Kemp et al., 2005; Pearce et al., 2008; Zeebe et al., 2009); intrusion of mantle derived melts into C-rich strata (e.g. Svensen et al., 2004; McElwain et al., 2005; Svensen et al., 2007; Retallack and Jahren, 2008; Ganino and Arndt, 2009; Flögel et al., 2011), or a combination of the above (e.g. Jahren, 2002; Svensen et al., 2004; Wignall, 2005; Kuroda et al., 2007; Cohen et al., 2007). More recently, studies have postulated that extensive biomass burning (Finkelstein et al., 2006), and release of CH_4 and CO_2 from terrestrial sources may have further aided in the movement towards negative $\delta^{13}C$ values (e.g. Pieńkowski et al., 2016; Them et al., 2017).

2.3 Producing a negative C-isotope excursion

2.3.1 Volcanic Events

Advances in radiometric dating have enabled increasingly accurate dating of the occurrence of major volcanic events, leading to the coupling of volcanic events with major extinction events and OAEs (Arthur et al., 1985; Kerr, 1998; Wignall, 2005; Kuroda et al., 2007; Turgeon and Creaser, 2008; Schaltegger et al., 2008). This has been illustrated for OAE1a; OAE2; the Palaeocene-Eocene boundary and the Weissert OAE (Figure 2.8), (as illustrated by Mahoney et al., 1993; Tejada et al., 1996; Larson and Erba, 1999, Tejada et al., 2002; Turgeon and Creaser, 2008; Storey et al., 1995; Torsvik et al., 1998, Snow et al., 2005 and

Wignall, 2005), with Wignall (2005) concluding it can therefore be implied that there is a strong association between volcanic eruptions, LIPs, and the development of widespread O_2 poor conditions within the world's oceans.

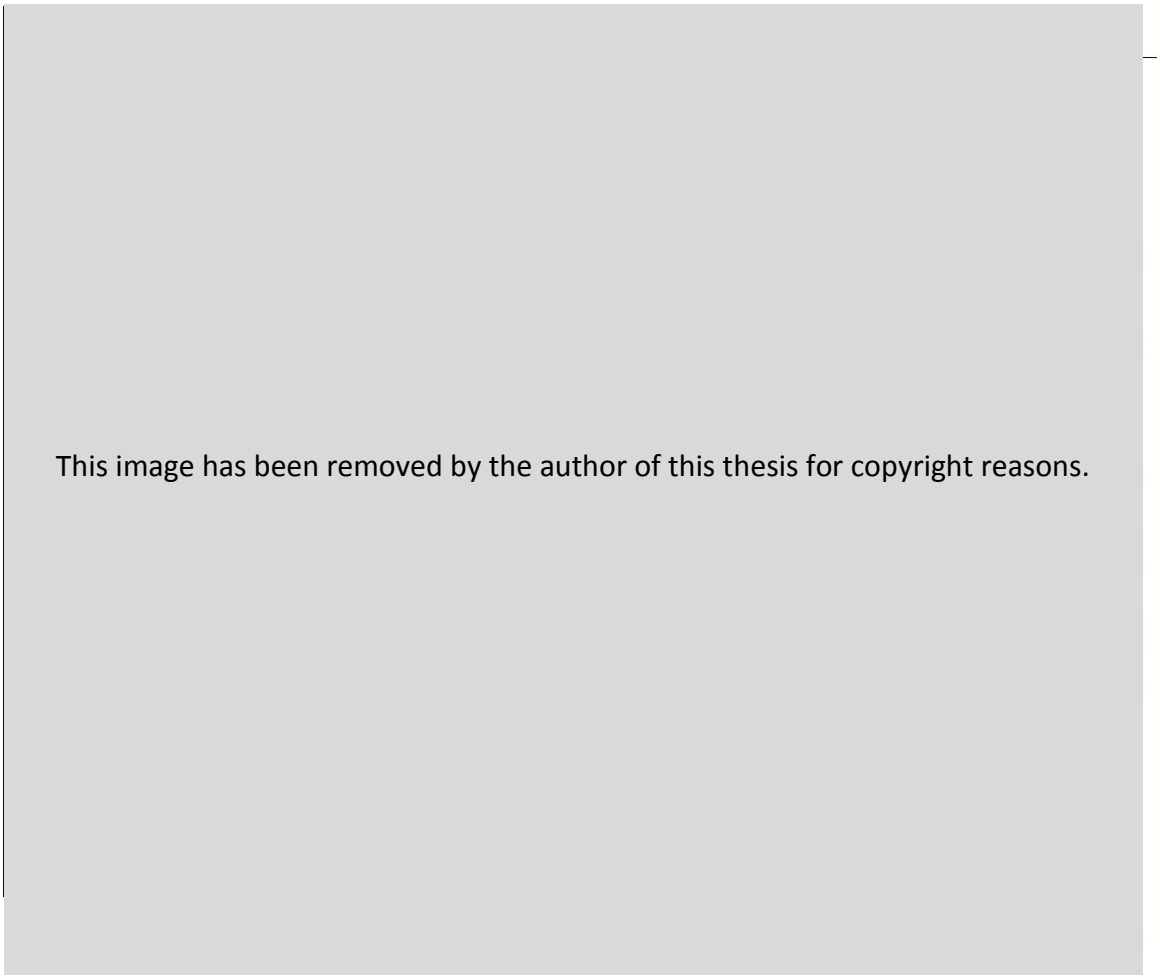

Figure 2.8 – Diagram illustrating the occurrence of OAEs alongside the occurrence and emplacement of LIPs (Taken from Brice et al., 2002).

Volcanic CO_2 has a unique isotopic signature with a higher percentage of ^{12}C present, making it isotopically light ($\delta^{13}C$ value of approximately -6‰ (Mayorga et al., 2005)). Degassing during a large eruption could therefore be capable of changing the isotopic composition recorded in sediments by increasing the relative proportion of ^{12}C in the ocean-atmosphere system.

The release of CO_2 from a LIP eruption has also been hypothesized as a potential trigger for an OAE, leading to significant climate disruptions over medium timescales, and marine extinction events due to increases in dissolved CO_2 concentrations within surface waters (due to atmosphere-ocean interaction) (e.g. Wignall, 2005).

Firstly, the increase in dissolved CO_2 is anticipated to cause a decline in the pH of the oceans (due to the process of carbonate and bicarbonate ion production through carbonic acid dissociation (Equation 2.2)). A decline in pH can cause problems for carbonate-secreting organisms as it reduces carbonate ion concentration, making calcium carbonate structures vulnerable to dissolution (Fabry et al., 2008; Barker and Ridgwell, 2012).

Equation 2.2 Process of Ocean acidification caused by increased CO_2 levels within the atmosphere:

1. Carbon dioxide dissolves in seawater to produce carbonic acid and hydrogen ions

$$CO_2 + H_2O \leftrightarrow H_2CO_3$$

2. Carbonic acid dissociates to produce bicarbonate ions and hydrogen ions

$$H_2CO_3 \leftrightarrow HCO_3^- + H^+$$

3. Bicarbonate can dissociate to form carbonate ions and hydrogen ions

$$HCO_3^- \leftrightarrow CO_3^{2-} + H^+$$

Secondly, the release of large quantities of volcanic CO_2 is hypothesized to have led to an increase in global temperatures, leading to an enhanced hydrological cycle where increases in evaporation, continental weathering, precipitation and run-off occur (Cohen et al., 2007; Steinthorsdottir et al., 2012). The increase in continental weathering and run-off, documented by a shift in osmium isotopes (Cohen et al., 2007; Percival et al., 2016) is suggested to have enhanced the supply of nutrients from the land to the oceans, driving marine productivity up. The increase in marine productivity would therefore increase the amount of organic matter reaching the sea floor and also enhance O_2 deficiency within bottom waters, as the organic material is consumed by oxidizing bacteria, initiating an anoxic event (Figure 2.9). Furthermore the warming of ocean temperatures has been shown to alter the supply of O_2 to bottom ocean waters, as O_2 does not dissolve as readily within warmer waters (Wignall, 2005). Additionally an alteration in the ocean's circulation could be initiated, as warmer

polar waters will not be able to drive the deep-water circulation due to a decrease in the temperature gradient between the equator and the poles (Wignall, 2005). This would cause a decline in the amount of cool, oxygenated bottom waters reaching the deeper oceans.

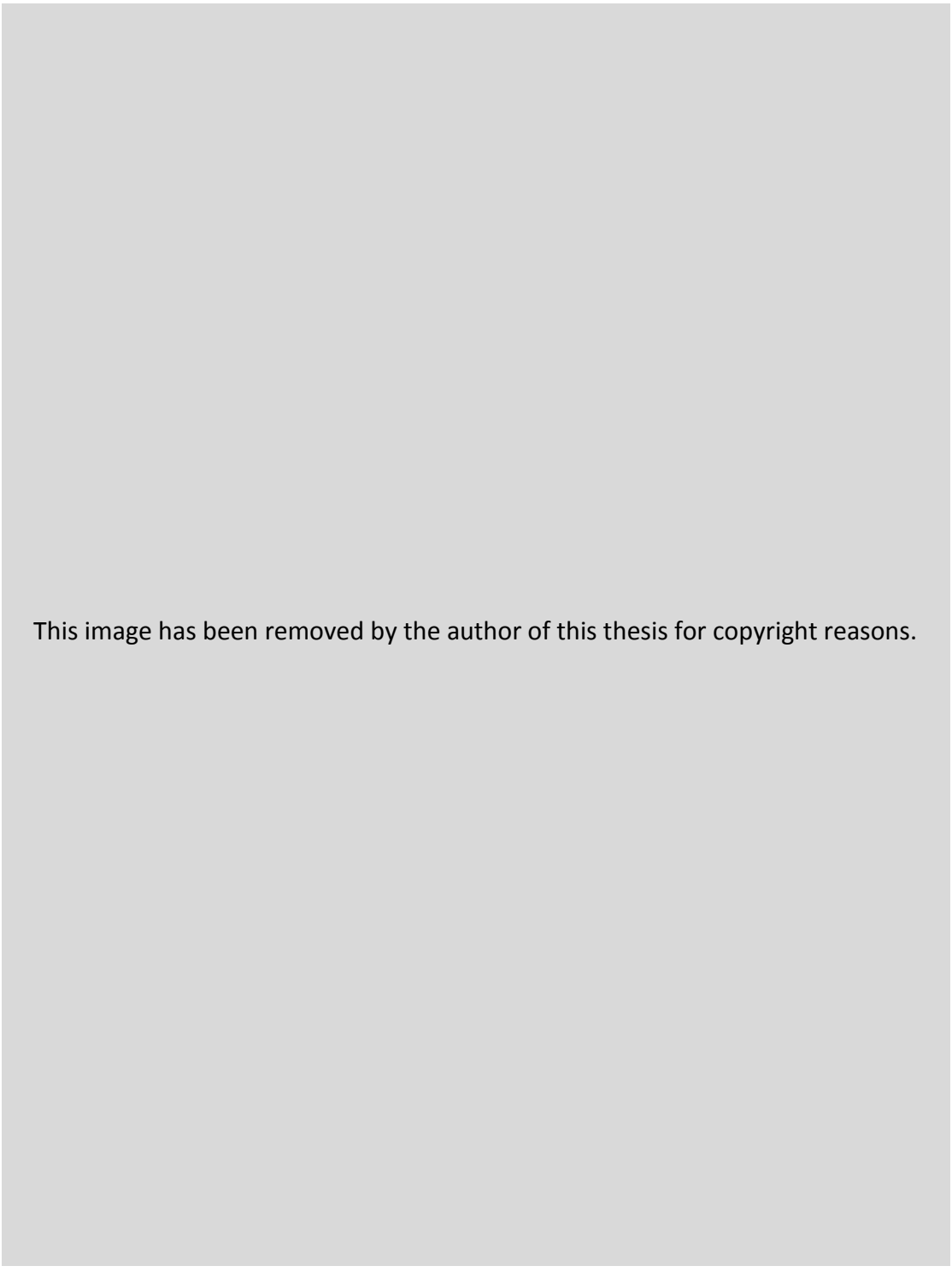

Figure 2.9 – Flow diagram illustrating the feedback mechanisms involved with increased CO_2 produced by a major volcanic eruption and the creation of LIPs. (Modified from Wignall, 2005).

Authors have therefore suggested that degassing during major volcanic eruptions could not only account for the production of O_2 deficient waters and therefore an OAE, but also the negative CIE observed within some OAE sediments. The volcanism hypothesis has, however, come under scrutiny as many authors suggest that even the largest LIP eruption may not have produced enough CO_2 to account for the negative excursion observed within some OAE sediments (e.g. Hesselbo et al., 2000; Wignall, 2004; Weissert and Erba, 2004; Zeebe et al., 2009). For example, Kump and Arthur (1999) and Weissert and Erba (2004) indicate that the effect that volcanic CO_2 could have on the marine C isotope signature is less than 0.5‰ (for both $\delta^{13}C_{carbonate}$ and $\delta^{13}C_{organic}$), and is therefore unlikely to have altered the isotopic signal sufficiently.

In 1995, Dickens et al. (1995) identified that the model hypothesis for the Paleocene-Eocene Thermal Maximum (PETM) produced an inadequate negative excursion, and suggested that a release of CH_4 through the destabilization of CH_4 hydrates could better account for the scale of the negative CIE observed. CH_4 has a $\delta^{13}C$ value of ~ -60‰ (Kennett et al., 2000; Hesselbo et al., 2000; Jahren, 2002; Tyler et al., 2012), making it significantly isotopically lighter than volcanic CO_2. Dickens et al. (1995) therefore suggested that a release of 1100 to 2100 Gt of CH_4 caused by a destabilization of CH_4 hydrates below the sea floor, could rapidly oxidize to produce ^{12}C enriched CO_2, which could account for a decline in $\delta^{13}C$ values of as much as -2 to -3 ‰. This hypothesis was later tested by Dickens et al. (1997) using a numerical simulator. A scenario of a 1.12 x 1018 g of CH_4 release within the 'present day C cycle' illustrated that the deep and shallow oceans and atmosphere would experience a decrease of -2.3 ‰ in $\delta^{13}C$ over a 104 year period, before returning to pre-excursion values over a ~2 x 10^5 year period. This result alongside an estimated increase in global surface temperatures of ~2°C over the 104 year period, suggested that "significant CH_4 release from oceanic hydrates is a plausible explanation for observed carbon cycle perturbations" (Dickens et al., 1997, p. 259). This hypothesis was later supported by Bains et al. (1999) and Jahren et al. (2001), whose mass balance equations (taken from Dickens et al., 1997) estimated a total release of CH_4 of 1500 Gt. The release of 1500 Gt of CH_4 was postulated to have been released during 'forcing episodes' during the Late Paleocene, causing multiple injections of biogenic CH_4. Speculations for the CH_4 hydrate hypothesis were further

supported by Kemp et al. (2005), Cohen et al. (2007), and also Zeebe et al. (2009), stating that “the magnitude of the carbon isotope excursion then requires the isotopic composition of the carbon input to be lighter than -50 ppt, consistent with a highly ^{13}C depleted source such as biogenic methane” (Zeebe et al., 2009, p. 578).

Since, CH_4 hydrate dissociation has been postulated to have occurred during the Early Aptian (Gröcke et al., 1999; Jahren et al., 2001) and the Early Toarcian (Hesselbo et al., 2000; Beerling et al., 2002), where the release and subsequent oxidation of CH_4 hydrates in large quantities could have reduced oceanic O_2 levels, promoting C_{org} burial and ocean anoxia without requiring a change in the productivity levels (Hesselbo et al., 2000).

However, the triggering of CH_4 hydrate dissociation would require either warming of bottom ocean waters; slope failure, a super plume, astronomical forcing or the thermal metamorphism of coals.

2.3.2 Methane (CH_4) hydrate release

CH_4 hydrates form under specific physical, chemical and geological conditions with high water pressures, low temperatures, and in areas where there is sufficient CH_4 produced by organic matter degradation on the sea floor (World Ocean Review 1, 2010). These conditions enable the encapsulation of the gas within a matrix/cage of water molecules called a clathrate (Figure 2.10). The term ‘hydrate’ is commonly used when discussing accumulations of clathrates, which refer to the molecular structure of the CH_4 hydrate (Lonero, 2008).

Figure 2.10 – Molecular structure of a methane hydrate/clathrate, where the methane gas is enclosed within a cage of water molecules. (Taken from World Ocean Review 1 (2010)).

A warming of bottom waters by even a few degrees could cause the CH_4 hydrate to dissociate, releasing the encapsulated gas (Dickens et al., 1995).

Using a numerical ocean model, Brice (2002) demonstrated that a sudden switch of deep-water formation from southern to northern high latitudes could cause a mid-depth and deep-ocean warming of between 3°C and 5°C, supporting the Dickens et al. (1995) model. However, many authors have scrutinized the numerical model (Brice, 2002) labeling it 'inconsistent with recent findings' (e.g. Thomas et al., 2002; Zachos et al., 2003; Higgins and Schrag, 2006), and thus proposing other hypotheses for its release (e.g. Cohen et al., 2007), such as slope failure, the presence of a 'super plume', astronomical forcing and the thermal metamorphism of coals.

2.3.2.1 Slope failure and CH_4 release

Continental slope failure, for example caused by tectonic activity, could have the ability to destabilize gas hydrates located within slope sediments, allowing the release of hydrates within the underlying sediments (e.g. Dickens, 1995; Katz et al., 2001; Nixon and Grozic, 2007). However, Higgins and Schrag (2006) criticize the suggestion for any tectonic activity causing slope failure stating that the CH_4 release proposed by Dickens (1995) would require the unlikely destabilization of >10% of global continental slopes assuming that CH_4 hydrates occupied an average 1 vol.% of pore space.

2.2.5.2 Super plumes and CH_4 release

It has been postulated that uplift caused by a super plume could have liberated "hundreds of Gt of carbon from CH_4 clathrates on timescales of tens to hundreds of millions of years" (Jahren, 2002, p. 177). One example given is the eruption of the Ontong Java flood basalt. Jahren (2002) hypothesize that the eruption of the flood basalt could have destabilized hundreds of Gt of C from CH_4 hydrates during the Aptian-Albian (OAE 1a), the oxidation of which may have promoted ocean anoxia (Jahren, 2002; Tejada et al., 2009). Super plumes have also been suggested to have led to the restriction of ocean currents by warming and elevating the seafloor, creating oceanic plateaus (e.g. Condie, 2004), and promoting anoxia during supercontinent breakup due to restricted circulation (e.g. Condie et al., 2001). A super plume could also initiate anoxia due to the subsequent stratification of the seafloor caused by warming of bottom waters (Condie, 2004). Although Tejada et al. (2009) indicated that previous studies lacked 'direct evidence,' the Tejada et al. (2009) study of osmium isotopes across OAE 1a provided evidence in support of a large magmatic episode, consistent with the eruption of the Ontong Java Plateau, coinciding with the deposition of OAE 1a sediments.

2.3.2.2 Astronomical Forcing and CH_4 release

In 2005, Kemp et al. identified three abrupt negative 'steps' occurring at regular intervals within the large negative CIE of the Toarcian (Jurassic) OAE. Kemp et al. (2005) hypothesize that these steps are related to pulses of CH_4 release occurring on the timescale of Milankovitch precession cycles (~21 kyrs) (Kemp et al., 2005; Hesselbo and Pieńkowski, 2011, Hermoso et al., 2012) (refer to chapter 6 for details on Milankovitch cyclicity). Kemp et al. (2005) therefore suggested that a combination of Karoo-Ferrar volcanic activity coupled with changes in solar insolation controlled by Milankovitch precession cycles, could "trigger the thermal dissociation of methane through the steepening of geothermal gradients in continental shelf sediments" (Kemp et al., 2005, p. 398), which would led to the destabilization of CH_4 hydrates.

2.3.2.3 Thermal metamorphism of coals and CH_4 release

The intrusion of dykes into C-rich sedimentary strata, particularly coal bearing, is hypothesized to have enabled the release of large quantities of CH_4, larger than that of a CH_4 hydrate source (Svensen et al., 2004). The intrusion of hot mantle-derived melts (for example, during the emplacement of the Karoo-Ferrar LIP) is proposed to have converted some of the C_{org} to CH_4, as it is heated between 100°C to 200°C (Hunt, 1979; Svensen et al., 2004). The thermogenic CH_4 produced has a $\delta^{13}C$ value of between -35‰ and -50‰ making it isotopically light and capable of producing large negative excursions within the $\delta^{13}C$ record (Svensen et al., 2004). The subsequent oxidation of the explosive release of CH_4 (that commonly occur in hydrothermal vents) (Figure 2.11) may have contributed to ocean anoxia, increasing pCO_2 levels, global temperatures, and enhancing primary productivity (Dickens, 2000; Hesselbo et al., 2000).

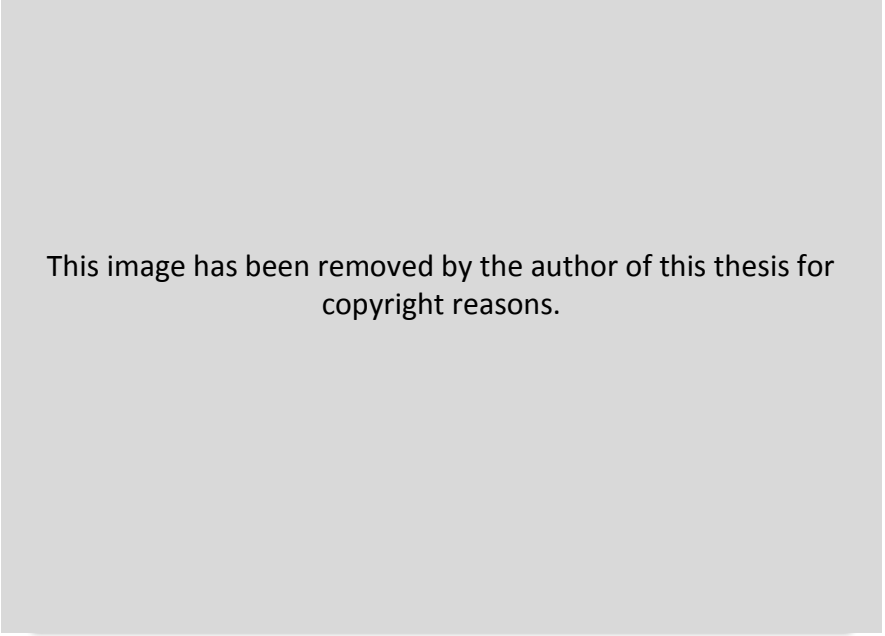

Figure 2.11 – Cross sectional diagram of a volcanic basin. The intrusion of sills (coloured red) into organic rich sedimentary strata (grey) metamorphose the organic material into CH_4 which is later released explosively through hydrothermal vents (Taken from Svensen and Planke, 2008).

2.3.3 Extensive biomass burning

The isotopic signature of peat, organic matter, vegetation and soil are isotopically lighter than that of current CO_2 values (Finkelstein et al., 2006). Finkelstein et al. (2006) illustrated that significant peat combustion, if sustained over 1000 years, was capable of nearly doubling atmospheric CO_2 concentrations from PAL of ~2.4‰ to 4.6‰ yielding a "pronounced negative $\delta^{13}C$ excursion in the atmosphere (up to ~-2.4‰), vegetation (~-2.4‰) and the surface ocean (~-1.2‰)" (Finkelstein et al., 2006, p. 501).

A previous boreal forest fire experiment had demonstrated that the CO_2, produced from what was then classed as a medium-to-high severity fire consuming ~60% of the vegetation available to burn, held an isotopic $\delta^{13}C$ value of -26.97°/◦◦ (Schuur et al., 2003). Together with the knowledge that CH_4 produced by smoldering fires may produce lower $\delta^{13}C$ values than that produced by flaming fires (Chanton et al., 2000), led to the hypothesis that peat combustion could be a plausible mechanism behind negative CIEs often observed in rock records during times of high CO_2 (Finkelstein et al., 2006). Based on this Finkelstein et al. (2006) hypothesizes that the release of CO_2 from biomass burning, could initiate "a short-term warming of the atmosphere (up to 14.4°C, with a duration of 1628 yr), which is consistent with the magnitude and length of an observed Toarcian excursion event" (Finkelstein et al., 2006, p. 501).

2.3.4 Other terrestrial sources of CO_2 and CH_4

Peińkowski et al. (2016) suggest that a positive feedback loop may have existed during the Toarcian (T-OAE), in which increased temperature and humidity associated with the OAE could have aided in the decomposition of plant litter. The decomposition of the plant litter is postulated to have assisted the movement towards negative $\delta^{13}C$ values and exacerbated the greenhouse climate by releasing CO_2 and CH_4 into the atmosphere. Pieńkowski et al. (2016, p. 8) suggest that this is evidenced by changes in the frequency of fungal spores during the T-OAE, indicating a "climate-driven enhanced decomposition of wood and rapid destruction of terrestrial carbon pool".

From this, it is hypothesized that thermogenic CH_4 release possibly from the intrusion into Gondwanan coals, could have triggered global warming leading up to the 'peak' in the negative CIE. This warming may have then enabled the rapid

decomposition in the terrestrial realm, mobilizing the terrestrial C reservoir, which would have had the potential to contribute to the negative CIE.

Them et al. (2017) also postulate that the astronomically timed pulses of greenhouse gas release during the T-OAE may have resulted from terrestrial environments. Within the study, Them et al. (2017) hypothesize that the influx of CH_4 may have originated from terrestrial environments such as wetlands, lakes and soils. As wetlands "represent the dominant non-anthropogenic source of atmospheric methane today" (Them et al., 2017, p. 124), Them et al. (2017) suggest that during warm, greenhouse periods such as occurred during the Jurassic (Korte et al., 2015), these environments may have become more extensive. Therefore a positive feedback is suggested involving global warming and an enhanced hydrological cycle from the emplacement of LIP Karoo-Ferrar, leading to increased CO_2 and CH_4 release from terrestrial environments (Them et al., 2017). The small scale astronomically paced excursions within the broader negative CIE curve, are also postulated to have forced changes in climate leading to the release of CH_4 from terrestrial environments (Them et al., 2017).

2.3.5 Releases of isotopically light C and climate change during an OAE

Releases of large quantities of isotopically light C (e.g. from large volcanic events and/or CH_4 release) have been linked with marked warming events and significant shifts in climate (Svenson et al., 2007; Barclay et al., 2010). These climatic changes caused by the release of "several thousand gigatons of isotopically light carbon as greenhouse gases" are often recorded in sedimentary rocks where chemical proxy data (e.g. $\delta^{18}O$ and TEX_{86}) illustrates warming events of between 5-10°C lasting on the order of a few hundred thousand years, and often accompanied by widespread ocean anoxia (Svensen et al., 2007, p. 555), as well as evidence of an enhancement of the hydrological cycle (Steinthorsdottir et al., 2012). Examples of this can be seen during the initiation of the Jurassic Toarcian OAE and Cretaceous OAE 2.

During the Jurassic OAE, pulses of isotopically light C were released (hypothesized as likely from volcanic CO_2 outgassing from LIP Karoo-Ferrar (Kemp et al., 2005; McElwain et al., 2005), and/or CH_4 hydrate release (Hesselbo et al., 2000; Kemp et al., 2011)),, the largest of which (estimated at ~1200 ppmv of increased atmospheric CO_2 concentrations (based on variations in stomatal abundances from cuticles preserved in Jurassic OAE sediments (McElwain et al., 2005)), coincides with an increase in estimated surface temperatures of ~6.5°C (McElwain et al., 2005). Coeval also, is a hypothesized increase in continental weathering rates of between 400 - 800%, documented by a positive excursion in $^{187}Os/^{188}Os$ within the Jurassic Jet Rock beds of Yorkshire (Cohen et al., 2007; Percival et al., 2016).

Similarly, the onset of OAE 2 has been linked to significant climatic shifts occurring across medium timescales of tens to hundreds of thousands of years (e.g. Jarvis et al., 2011). OAE 2 is hypothesized to have been triggered by an influx of volcanically derived CO_2 beginning up to ~500 kyrs prior to the initiation of the OAE (Turgeon and Creaser, 2008; Barclay et al., 2010; Du Vivier et al., 2014; 2015; Jenkyns et al., 2017), driving increases in global temperatures, enhancing the hydrological cycle and increasing continental weathering rates (Du Vivier et al., 2015; Jenkyns et al., 2017). Periods of rapid CO_2 drawdown during the OAE (hypothesized as being due to increased primary production, and capable of occurring within 10-100 kyrs (Barclay et al., 2010)) are hypothesized to have initiated a rapid cooling of global temperatures, evidenced by sea surface temperature (SST) estimates using TEX_{86} which show a rapid decline in temperatures of up to ~2.5°C (Jarvis et al., 2011, van Helmond et al., 2013) coeval with the declining CO_2 estimates (Barclay et al., 2010).

2.4 Summary

OAEs record periods in Earth's past, when major disturbances in the global C-cycle and significant changes in environmental conditions and climate occurred. Although initial studies attempted to find a common triggering mechanism between the anoxic events (e.g. Jenkyns, 1980), OAEs are since often treated individually, hence, the triggering mechanisms for ocean anoxia and C-cycle

perturbations can also be treated separately. However, what are common to every OAE, are the influx of limiting nutrients and increased burial of C_{org}.
Due to the re-occurrence of these events throughout Earth's history, and the hypothesis that many of the events were triggered during globally warm periods and after large influxes of CO_2, the re-occurrence of another OAE in the near future is thought to be becoming increasingly likely (Lenton and Watson, 2000b; Watson, 2016).

The predicted duration of many OAEs has been enabled by advances in dating techniques and cyclostratigraphy (e.g. Kuhnt et al., 2005; Suan et al., 2008a; Huang and Hesselbo, 2014 Eldrett et al., 2015b) indicating that OAEs occurred over varying timescales, and often displayed individual characteristics.
Anoxic events are often treated as individual events due to their occurrence over varying timescales, from medium to long, and the display of varying characteristics (Handoh and Lenton, 2003). This has resulted in several trigger mechanisms being proposed, where the effects of the trigger mechanism and the anoxic event can be observed over both medium (e.g. thousand to hundreds of thousands of years climate change) and long timescales.
In the following three chapters I consider drivers of long-timescale fire feedbacks during OAEs, and then consider shifts in fire across one long-duration OAE – the T-OAE, and a relatively short lived OAE – OAE 2.

3. C_{org} burial, atmospheric O_2, ocean anoxia, and fire feedbacks over long-timescales

3.1 Introduction

During an OAE, increased burial and preservation of C_{org} burial is recorded in the rock record. Photosynthesizing primary producers provide the main source of O_2 to our atmosphere, reflected in the geological record by the burial of C_{org} (Figure 1.13). Changes in the amount of C_{org} burial, in conjunction with oxidative weathering estimates, can and have been used in numerical biogeochemical models, to estimate past atmospheric O_2 concentrations (pO_2), (Berner et al., 2003). Here, many attempts have been made at estimating past pO_2 concentrations for the last ~420 million years (Myrs) of Earth's history, ranging from the construction of biogeochemical and geochemical models (e.g. Berner and Canfield, 1989; Lenton and Watson, 2000a,b; Berner, 2003; Bergman et al., 2004; Falkowski et al., 2005; Berner, 2006) to the use of proxy data such as the presence of fossil charcoal (Glasspool and Scott, 2010); stable isotopes in plant resins and ambers, and trapped air bubbles in ice cores (e.g. Tappert et al., 2013; Stopler et al., 2016).

3.2 Predicting palaeo-atmospheric O_2

3.2.1 Proxy Methods

Estimating changes in atmospheric O_2 within the geological past can be challenging due to a lack of reliable proxy methods (Tappert et al., 2013). Current proxies are restricted to O_2/N_2 ratios (e.g. Stolper et al., 2016); stable isotopes in plant resins, ambers (e.g. Tappert et al., 2013), and the presence/absence of fossil charcoal (e.g. Glasspool and Scott, 2010).

Variations in O_2/N_2 ratios are anticipated to reflect changes in the partial pressures of O_2 (Keeling and Shertz, 1992; Kozlova et al., 2008; Scripps O_2 Programme, 2016). As N_2 concentrations have been shown to vary very little compared to O_2, the ratios are thought to predominantly reflect atmospheric O_2

fluctuations (Keeling and Shertz, 1992). O_2/N_2 ratios provide present day O_2 estimates, enabling the identification of small scale oscillations in O_2 of just 0.02% (Kozlova et al., 2008; Scripps O_2 Programme, 2016) that occur over a yearly basis (Scripps O_2 Programme, 2016). However, this proxy requires the presence of air samples to test, and would therefore require the presence of ancient air to test geological atmospheric O_2 variations. Thus far, this method has been able to test up to 800 kyr old air that was trapped in polar ice (Stolper et al., 2016).

In 2013 Tappert et al. (2013) developed a new technique for estimating O_2 changes in the geological record using the $\delta^{13}C$ composition of plant resins, as plant resins are expressed as enabling almost "pristine" preservation of "$\delta^{13}C$ signatures over geological time" (Tappert et al., 2013, p. 240). However O_2 estimates produced, particularly for the Late Cretaceous period of between ~11-12% O_2, appear to contradict both model (Berner, 2006) and other proxy method (Glasspool and Scott, 2010) estimates of high atmospheric O_2, of between ~21% (Berner, 2006) and 25% (Glasspool and Scott, 2010). The production of such low estimates coupled with a "high uncertainty in quantifying the plant $\delta^{13}C$ response to global pO_2 and CO_2 variations" (Mills et al., 2016, p. 1023), has thus led to reservations with the reliability of this method (e.g. Mills et al., 2016).

The third proxy method relies on the presence and abundance of fossil charcoal in the geological record. The use of charcoal as a potential O_2 proxy has been widely used for the reconstruction of atmospheric O_2 variations for throughout Earth's deep past (e.g. Lenton and Watson, 2000b; Glasspool and Scott, 2006; Belcher and McElwain, 2008), due to its high resistance to degradation (Matthewman et al., 2012) and near continuous presence throughout the geological record (Glasspool and Scott, 2006; Belcher and McElwain, 2008).

Previous lab experiments illustrate the sensitive nature of the relationship between fire and O_2 and the need for at least ~17% O_2 in order for combustion to occur, and for the fire to be self-sustaining (e.g. Watson, 1978; Belcher et al., 2010). This has enabled the presence of fossil charcoals to document the existence of an atmosphere with a content of at least 17% O_2 during different periods of Earth's history, aiding in the precision of numerical O_2 models that may otherwise predict lower O_2 concentrations (Belcher and McElwain, 2008).

Changes in the abundance of fossil charcoal over million year timescales, has also been used as a proxy to indicate periods that may have experienced

higher/lower atmospheric O_2 concentrations, where periods (over millions of years) of sustained high charcoal abundances are taken to illustrate times in Earth's history that may have experienced higher atmospheric O_2 concentrations (such as during the Cretaceous) (e.g. Glasspool and Scott, 2006). Charcoal's high resistance to degradation, its near continuous presence in the geological record dating back over 400 million years (Glasspool et al., 2004; Glasspool and Scott, 2006) and the notion that ignition sources (lightning strikes) and fuel (land vegetation) have been available throughout the last ~400 million years of Earth's history (first appearance of land vegetation dating back to ~443-418 Ma (Scott 2000)), enable the record of fossil charcoal to provide a good proxy for changes in atmospheric O_2 in the geological past, that unlike Tappert et al.'s (2013) plant resin estimates, appear to well track numerical O_2 model predictions, and unlike the O_2/N_2 ratios are capable of documenting changes in geological history that extend beyond 800 kyrs ago.

3.2.2. Modelling palaeo-atmospheric O_2

O_2 within the ocean-atmosphere system is dictated by the large reservoir of O_2 in the atmosphere ~ 3.7×10^{19} mol, divided by the small flux of O_2 from C_{org} burial ~18×10^{12} mol O_2 yr^{-1} (Catling and Claire, 2005) (and coupled removal by oxidative weathering), producing a long residence time of O_2 within the ocean-atmosphere system (Handoh and Lenton, 2003, Catling and Claire, 2005). Therefore variations in atmospheric O_2 are anticipated to occur over million year timescales (Lenton and Watson, 2000b, Catlin and Claire, 2005, Lenton, 2013). Over these timescales, the source of O_2 is balanced by O_2 sinks such as the oxidative weathering of C_{org}, pyrite and organic sulphur (Lenton and Watson, 2000b; Berner et al., 2003) (Equation 3.1).

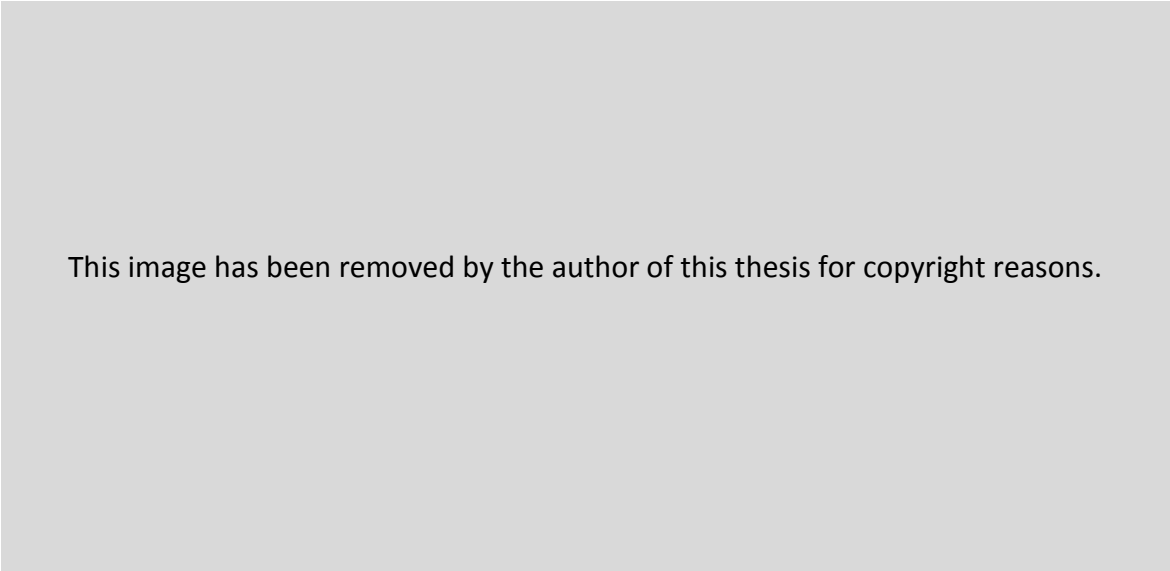

Using this information, the balance between burial and weathering has formed the foundations for many numerical biogeochemical and geochemical models that are able to predict O_2 fluctuations over the last ~420 Myrs of Earth's history (e.g. Berner and Canfield, 1989; Lenton and Watson, 2000b; Bergman et al., 2004; Berner, 2006).

The Rock Abundance Method (Berner and Canfield, 1989)

Berner and Canfield (1989) developed one of the first models to predict past atmospheric O_2 changes using a rock abundance method. The model works by assigning three different rock types with varying contents of C and pyrite sulphur. These include marine sediments; coal basin sediments and other non-marine sediments (e.g. arkoses and redbeds). The abundance of each of these three rock types is recorded from data taken from Ronov (1976), across the Phanerozoic, assuming that when one rock type depletes, the sediment is redistributed to another rock type. The relative abundances (%) of each of these rock types is then related to variations in the O_2 content of the atmosphere using calculations of relative burial and weathering fluxes over time.

To do this, the model assumes is that if oxidized redbeds were being weathered and eroded away whilst organic rich beds were being deposited, there would be a net leak of O_2 to the atmosphere. If however there was net weathering and erosion of sediments containing a good proportion of organic rich/pyrite rich shales, followed by the sedimentation of redbeds which contain no organic matter or pyrite (therefore no C_{org} burial and no leak of O_2 to the atmosphere), it would result in the net decrease of O_2. Due to these fluvial redbeds also containing a lot

of iron (Fe), which is easily oxidized, the redbeds also act as an O_2 sink. This oxidation of Fe produces the redbeds distinctive orange colouration (Belcher, 2014).

To stabilize the predicted palaeo-atmospheric O_2 concentrations, the model uses a negative feedback called 'rapid recycling'. This assumes that younger sediments will be weathered first, prior to underlying older sediments. Therefore if there is a period of increased burial of C_{org} causing increasing O_2, Berner and Canfield (1987) hypothesize that this would soon be subjected to weathering, thus preventing O_2 rising too high.

To simulate this, Berner and Canfield (1989) increased the weathering rates of the younger sediments compared to older sediments. The results of this model can be seen in Figure 3.1, whereby increases in predicted O_2 are times where organic-rich beds are deposited, which were then later replaced by more continental redbeds, bringing the atmospheric O_2 concentration down.

Figure 3.1 – Plot of predicted atmospheric O_2 concentrations over the last 600 Myrs, using estimates from the rock abundance model (Berner and Canfield, 1989). The upper and lower continuous lines represent the error margins from the model (taken from Berner et al., 2003, p. 108).

Lenton and Watson's (2000) model - Redfield Revisited

Lenton and Watson's (2000a,b) model 'M8' was produced to better constrain Berner and Canfield's (1989) rock abundance model that predicted that past atmospheric O_2 concentrations had varied between <15% and 35% (Figure 3.1). These upper and lower O_2 limits predicted by Berner and Canfield (1989) were deemed "incompatible with both upper and lower bounds on O_2 suggested from combustion experiments" (Lenton and Watson, 2000b, p. 205). Lenton and Watson (2000b) therefore suggested that more negative feedbacks were required to better constrain the O_2 estimates and thus a new 'dynamic model' of coupled biogeochemical cycles of P, N, C and O_2, was produced.

Lenton and Watson (2000b) began with a 'simplified' ocean model 'M1' (Figure 3.2) where the effects of continental uplift (the main forcing mechanism), was determined only within the ocean-atmosphere system. This model was then used as a basis for a range of other variables that could contribute to changes in the O_2 content. These effects include; the effects of iron-phosphate (Fe-P) on phosphate burial and C_{org} burial (model M5); amount of 'oxygen exposure time' (model M6); and the effect of biological amplifications and the combined biogeochemical effects (model M8). Each model with the new variants was then tested using the forcing parameter 'uplift', producing varying O_2 concentration outputs for an increase in uplift rates by 50% and a decrease in uplift rates by 50%. Increased uplift rates were anticipated to increase C burial at a faster rate compared to weathering, thus driving O_2 concentrations up (Lenton and Watson, 2000b). Decreased rates of uplift were expected to increase weathering at a faster rate than C_{org} burial and thus are associated with causing a decrease in the leak of O_2 to the atmosphere (Lenton and Watson, 2000b). Each model is described briefly below.

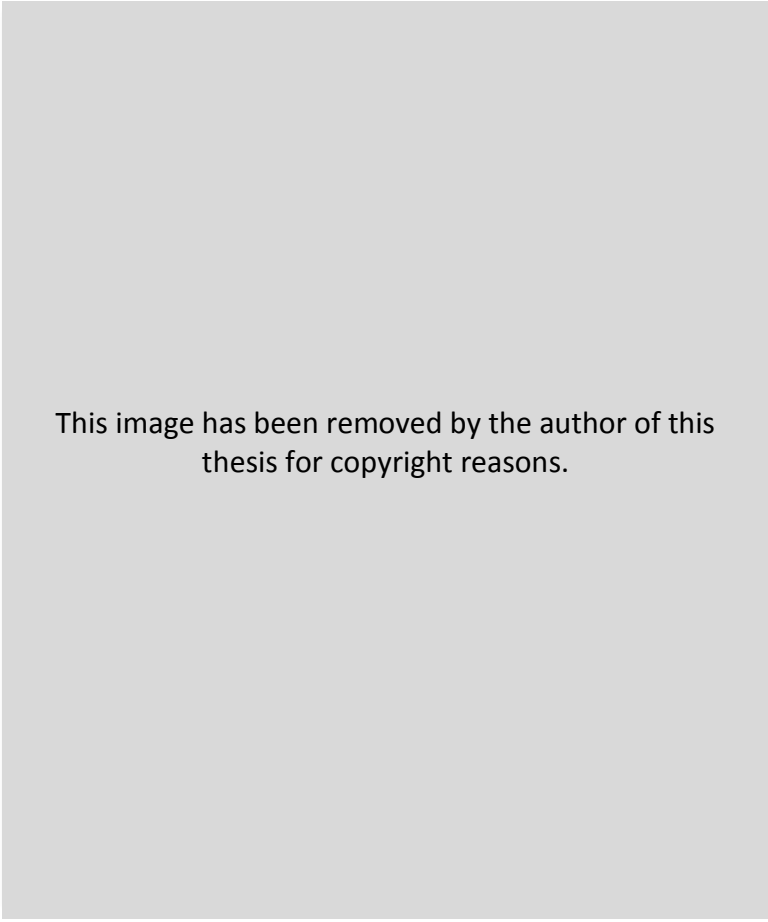

Figure 3.2 – The 'Basic Ocean Model (M1)'. Ovals indicate the three main reservoirs, dependent variables are indicated by circles and 'Uplift' represents the single forcing/input parameter. Solid arrows indicate a direct relationship between components, whilst dashed arrows indicate an inverse relationship (e.g. if starting component increases, the second component decreases) (taken from Lenton and Watson, 2000b, p. 251). Letters are discussed in the text below.

Basic Ocean Model (M1)

The basic ocean model uses three reservoirs; deep ocean phosphate, deep ocean nitrate and pO_2. The pO_2 is expressed as "the concentration dissolved in high-latitude surface waters that ventilate the deep ocean, which is directly proportional to the atmospheric partial pressure of O_2 (Henry's Law) assuming that the temperature and salinity of these waters remains constant" (Lenton and Watson, 2000b, p. 251). Throughout the models Lenton and Watson (2000b) use Redfield's ratios for the composition of the organic matter and relative quantities/stoichiometry of respiration ($P:N:C:O_2$ = 1:16:117:170). Like Kump's (1988) model, Lenton and Watson (2000b) use limiting nutrients N and P to control C_{org} burial and pO_2. Within the model, Lenton and Watson (2000b) use

the forcing parameter 'uplift' as it controls the weathering flux of limiting nutrients P and N, thus controlling C burial and the main source of O_2, as well as limiting the amount of oxidation of continental rocks, controlling the main sink of pO_2. A brief description of the relationships between the components of M1 is outlined below.

Parameter relationships used in each model (Figure 3.2):

A – Output of O_2 determined by weathering of reduced materials in continental rocks, assuming that all reduced material exposed will become oxidised. Therefore the rate of uplift directly influences the rate of oxidative weathering.

B – New production determines the O_2 demand. Anoxic fraction = O_2 supply – O_2 demand. Therefore new production directly affects the anoxic fraction.

C – Assumes that the limiting nutrient phosphate is completely used up during new production.

D – New production determines the concentration of C_{org} produced.

E – Rate of uplift determines weathering flux of P derived from rocks.

F – The amount of nitrate with respect to its Redfield ratio with P, linearly determines the "selective advantage of N fixation and the resultant flux into the reservoir of available nitrogen" (Lenton and Watson, 2000b, p. 252). Therefore if nitrate levels decrease relative to phosphate, then certain organisms obtain their N from the atmosphere. When these organisms are eaten and decompose, the N obtained by them returns to nitrate in the water, increasing nitrate levels (Tyrell, 1999).

G – Water column dentrification varies linearly with the anoxic fraction - whenever O_2 falls significantly low (low anoxic fraction), nitrate is the first 'electron acceptor used in place of oxygen' (Bianucci et al., 2012) during the decomposition of organic matter. This is due to its high energy yield, second to that of O_2 (Bianucci et al., 2012). Therefore as the anoxic fraction decreases, water column denitrification decreases.

H – Organic nitrate burial is a function of C_{org} burial flux and the C:N burial ratios. Organic matter of 'high quality can increase N mineralization rates' (Stelzer et al., 2014, p. 388) and increase organic nitrate burial.

(For the relevant equations for each of these parameters used in 'M1' see Lenton and Watson, 2000b, p. 252).

Variable parameters used:

I – Organic phosphorous (Org-P) is assumed to be linearly dependent on C_{org} buried. More organic matter buried enables higher P retention so more organic P can be buried (Mort et al., 2008).

J – P sorbed to iron hydroxides (Fe-P) is assumed to vary inversely with bottom water anoxia (therefore is proportional to the anoxic fraction) as less P is sorbed to Fe-P in low O_2 environments (Barber, 2002).

K – P bound in calcium minerals (Ca-P) is assumed to be proportional to the supply of P to sediments in organic matter.

Within the M1 model, the main negative feedback is the dependence of Fe-P burial on anoxia. The effects of dentrification create a positive feedback between nitrate content and pO_2 levels:

Negative feedback - Lenton and Watson (2000b, p. 254) suggest that 'under anoxic conditions P tends to be buried with C_{org}, but under oxic conditions there is a shift in favour of its burial by absorption and reaction with iron hydroxides. Therefore increases in pO_2 may cause less C to be buried per unit of P and less O_2 to be released to the atmosphere'.

Positive feedback - Due to the relationship between denitrification and O_2, lower O_2 concentrations leads to an increase in anoxia and denitrification of nitrate, leaving the ocean system low in the limiting nutrient nitrate. This therefore decreases productivity and the resulting C burial.

The use of these feedbacks within the model however, produced a weak net negative feedback against rising pO_2 concentrations. Thus when the uplift forcing is increased by 50%, increasing O_2, the feedback system leaves pO_2 rising as the system 'switches off' after being unable to prevent anoxia disappearing. This therefore indicates a need for further stronger feedbacks to stabilize pO_2 content between the combustion parameters.

Model ‘M5’

This model has an additional negative feedback dependent on the organic P burial being suppressed by anoxia. During times of low O_2 there is a decrease in the amount of organic P buried. This is because in anoxic conditions, there is a decrease in sediment P retention, thus less organic P can be buried (Mort et al., 2008). With a decrease in organic P burial, there is an increase in the amount of dissolved inorganic P (acting as a limiting nutrient), and thus fuels production and C_{org} burial (Lenton and Watson, 2000b).

By adding these feedbacks to the original ‘M1’ model, the new ‘M5’ model is able to better stabilize the system when uplift rates are increased and decreased by 50%, retaining O_2 concentrations between 26.5% and 12.7% respectively. However the lower value of 12.7% is still outside the lower combustion parameter of 17% O_2 (Watson, 1978) indicating a need for further constraints.

Model ‘M6’

‘M6’ incorporates another negative feedback determined through the enhancement of C_{org} buried during anoxic periods, using ‘oxygen exposure time’. ‘Oxygen exposure time’ is a function of C_{org} sedimentation rate and the O_2 concentration of bottom waters. The feedback works by increased sedimentation, and/or decreased bottom water oxygenation reducing the amount of time for which organic matter is exposed to high O_2 (oxic) conditions. This enhances C_{org} burial by increasing preservation and decreasing the probability of decomposition of the sediments. This feedback enabled O_2 concentrations to be stabilized between 22.8% and 15.1% pO_2 for increased uplift of 50% and decreased uplift of 50% respectively.

However each of the above feedback models briefly described above, rely on the presence of anoxia, and do not include the effects of the land on the system. Therefore, Lenton and Watson (2000b) produced a new model ‘M8’ within which biological amplifications on P weathering were incorporated.

Model ‘M8’

Effects on the land can severely alter the feedbacks involved in regulating the pO_2 content. In testing Kump’s (1988) feedback (refer to Chapter 1, section 1.5.3 and Figure 1.14 herein), both Inghall and Jahnke (1994) and Lenton and Watson (2000b) found the feedbacks to be too weak in stabilizing pO_2 (Lenton, 2001). Furthermore, Lenton (2001) argues that there is a lack of evidence in continental shelf sediments for increases in C:P burial ratios towards the shore, where according to Kump’s (1988) theory, terrestrial material and therefore larger C:P ratios should be more common. Lenton and Watson (2000b) and Lenton (2001) therefore proposed new feedbacks involving P, in which a new relationship between fire and P was hypothesized.

Using a ~20% moisture content as a representative of land-based vegetation, and Watson’s (1978) relationship between the probability of ignition and pO_2 concentrations, Lenton and Watson (2000b), like Kump (1988), suggest that during increased pO_2, fire frequency will increase. However the increase in fire frequency in Lenton and Watson’s (2000b) model is predicted to decrease the amount of biomass and trigger a shift from forest-dominated vegetation to faster, regenerating herbaceous vegetation (Lenton, 2001). The type of vegetation can have a profound effect on the amount of weathering occurring on continental rocks, controlling the amount of the limiting nutrient P that enters the marine system. This is due to effects such as tree roots enhancing weathering by splitting rocks apart and secreting organic acids that can dissolve minerals and increase rock porosity, making them more vulnerable to weathering (Lenton, 2001).

Another effect from changes in pO_2 on the plant community is the Warburg effect. Increases in O_2 concentrations can reduce the amount of biomass, particularly during ‘C_3’ photosynthesis. During C_3 photosynthesis O_2 and CO_2 compete for the enzyme Rubisco, which can act as either an oxygenase or carboxylase (Lenton and Watson, 2000b). Increases in the pO_2 content can therefore reduce net photosynthesis as O_2 is preferentially assimilated by the Rubisco enzyme rather than CO_2.

The ‘M8’ model involves adding feedbacks that use the O_2 mixing ratio to influence the vegetation abundance and net primary productivity on the land. This in turn alters the amount of P weathered and the amount of C buried.

The negative feedback works by increased pO_2 levels causing a decrease on the biomass and land vegetation, through a combination of the Warburg effect and

increased fire probability. A decrease in vegetation leads to a decline in larger vegetation that enhance P weathering, thus limiting the amount of P reaching the marine system by run off/riverine input. Less P to the marine system will also trigger a decrease in nitrate, primary production and thus C_{org} burial. The reduced P supply on the land is also thought to suppress organic production on the land, limiting the biomass further. Both of these effects reduce the amount of O_2 liberated to the atmosphere (Figure 3.3).

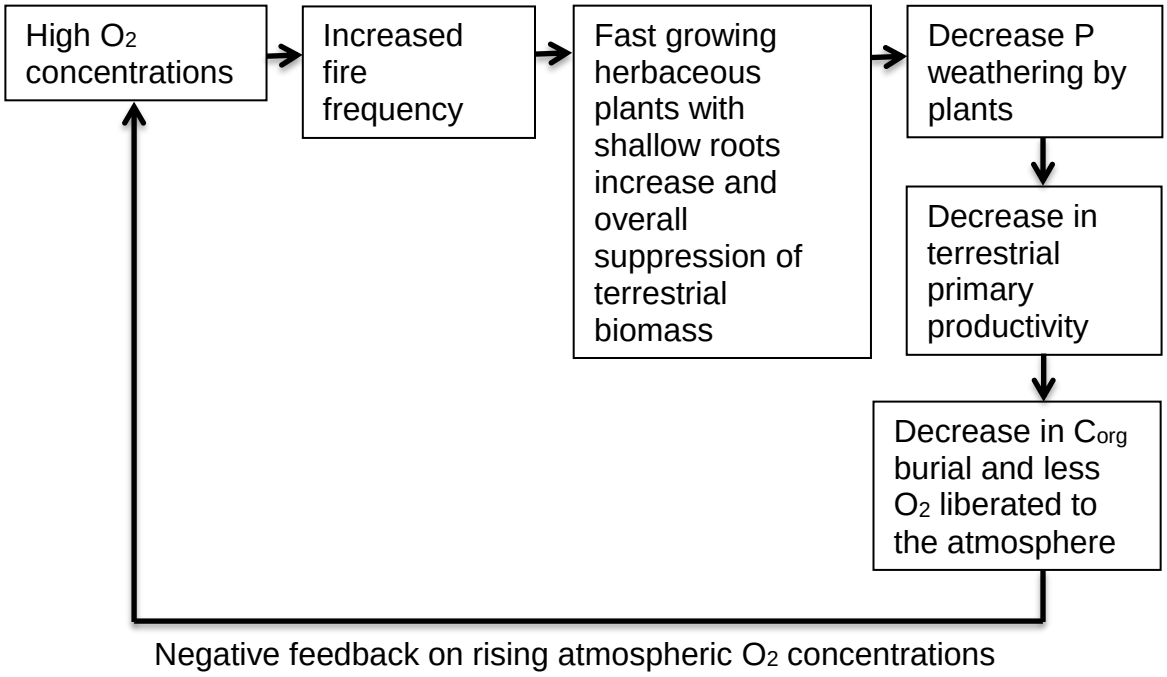

Figure 3.3 – Lenton and Watson (2000b) and Lenton (2001) atmospheric O_2 regulation feedback against rising atmospheric O_2.

Within the model, results indicated that this feedback was stronger, with only a 5% decline in biomass required to achieve a new steady state in the O_2 content of the atmosphere. A 50% increase in uplift resulted in a stabilization of pO_2 contents at 21.2% and decreased uplift rates of up to 50% stabilized O_2 concentrations at 16.3%.

A decrease in O_2 can also be stabilized by another feedback involving fire. In an atmosphere of 16.3% O_2, the probability of a wildfire is greatly reduced, thus a decrease in the amount of wildfires will enable vegetation to recover and thrive. The Warburg effect will also allow for increased C_3 photosynthesis and net production, as CO_2 is preferentially assimilated instead of O_2. Increased vegetation enhances P weathering and thus terrestrial and marine organic burial, increasing O_2 levels. The addition of these feedbacks to the original basic ocean model can be seen in Figure 3.4.

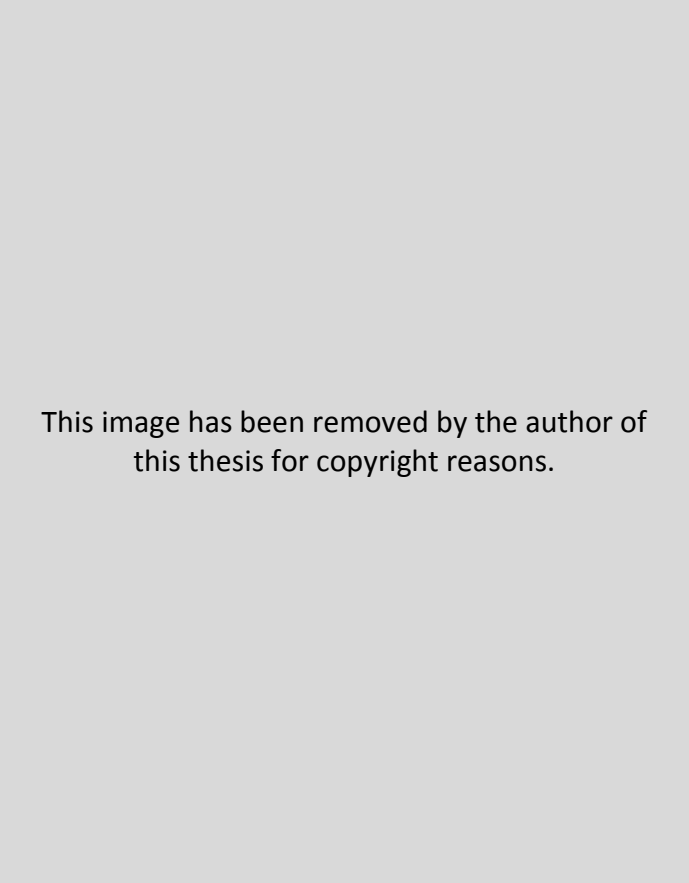

Figure 3.4 – Model 'M8'. An 'extended model' built on the 'basic ocean model (M1)' to include the effects of fire and suppression of terrestrial vegetation on the stabilization of pO_2 (Taken from Lenton and Watson, 2000b).

In 2001, Lenton (2001) suggested a further feedback, in which P is preferentially recycled from organic matter buried under anoxic conditions (Van Cappellen and Ingall, 1994; Lenton, 2013). This allows the increased availability of P in the marine system to fuel productivity in the surface waters. An increase in P supply is predicted to fuel marine primary productivity and therefore increase C_{org} burial, and pO_2. This feedback can be seen in Figure 3.5.

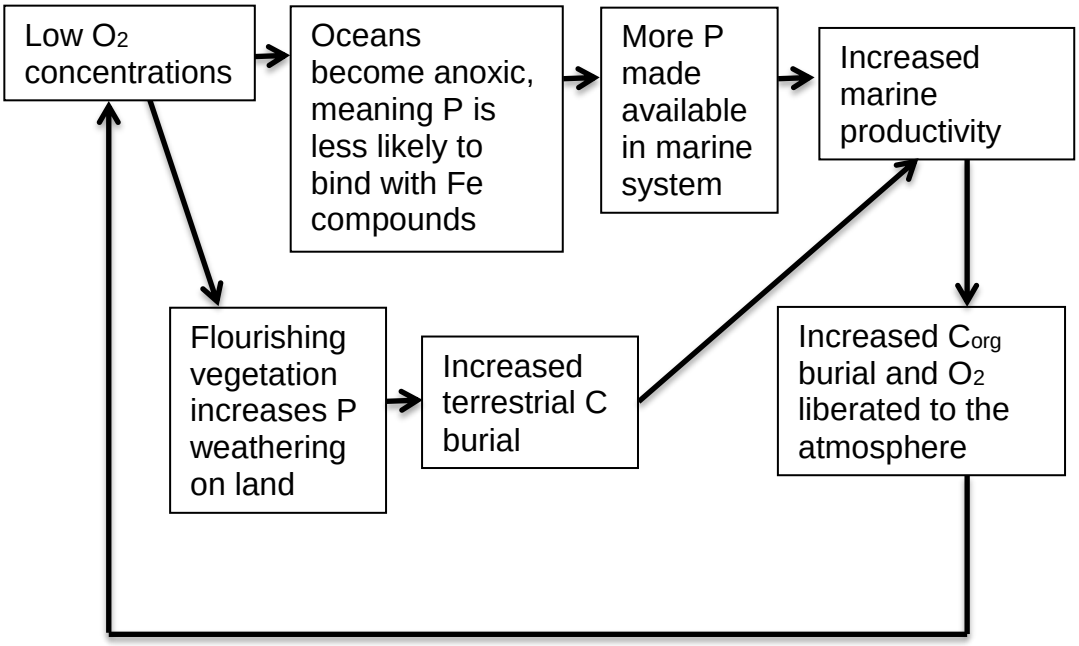

Figure 3.5 – Lenton and Watson (2000b) and Lenton (2001) atmospheric O_2 regulation feedback against declining atmospheric O_2

When these new feedbacks are tested against Berner and Canfield's (1989) rock abundance model, the influence of the additional feedbacks in constraining pO_2 become clear (Figure 3.6).

Figure 3.6 – Predicted atmospheric O_2 concentrations over the last 550 Myrs from Berner and Canfield's (1989) rock abundance model (thin line) compared with the inclusion of negative feedbacks proposed by Lenton and Watson (2000b) and Lenton (2001) involving the weathering of phosphorous. Symbols: Ɛ=Cambrian; O-Ordovician; S-Silurian; D-Devonian; C-Carboniferous; P-Permian; TR-Triassic; J- Jurassic; K-Cretaceous; T-Tertiary (taken from Lenton, 2001, p. 623).

The negative feedbacks involving the enhancement and supression of P weathering, and its control on the source of O_2 (C_{org} burial), appear strong, reducing the upper limit of pO_2 predicted by Berner and Canfield's model. This is particularly apparent during the Cambiran to Devonian period where low pO_2 concentrations are estimated until the rise of land plants and thus the start of enhanced P weathering causes a sharp increase in pO_2 estimated during the Late Silurian - Early Carboniferous (Lenton, 2001).

Although the extended model (M8) has proved to be effective in modeling the last ~400 Myrs of pO_2 concentrations, there are some variables that the model is unable to account for; for example changing climate and its effect on the moisture content of land vegetation. This could mean that in past climates where the moisture content of the vegetation was higher than 20%, fire probability may not have increased by as much as the model suggests at just 20% moisture content. Another limitation with Lenton and Watson's (2000b) model, is that by not incorporating changes in CO_2, it is unable to account for any influences that rising/falling pCO_2 may have had on the terrestrial system. As the model feedbacks rely heavily on changes in terrestrial biomass fueling the weathering of P, changes in global CO_2 and their effects on biomass should be considered.

One model that does consider changes in CO_2 aswell as pO_2 is the GEOCARBSULF model (Berner et al., 2006), by combining mass balance isotope fractionation models with the GEOCARB model.

Mass Balance Calculations using Carbon and Sulphur Isotopes

C and S isotopes are used to determine Fbg (rate of burial of C_{org}), Fwg (rate of oxidative weathering of C_{org} + reduced C), Fbp (rate of pyrite (plus organic) S burial in sediments), and Fwp (rate of oxidative weathering of pyrite (plus organic) S plus reduced S) over geological time (Berner et al., 2003). Garrels and Lerman (1984) produced one of the first models using an isotope mass balance model, although the model has since been adapted to incorporate negative feedback processes such as the rapid recycling feedback (Berner and Canfield, 1989) and O_2 dependent C and S isotope fractionations (e.g. Berner, 2001) to help stabilize pO_2 predictions.

The model works by using the isotope record of C and S within sedimentary rocks to calculate rates of variations in the processes that affect pO_2, over time (e.g. weathering and burial fluxes).

Over time the isotopic composition of the oceans changes, reflecting variations in global photosynthesis and bacterial sulphate reduction. These changes are recorded in the calcium carbonate ($CaCO_3$) and calcium sulphate deposited within sedimentary rocks. The $^{13}C/^{12}C$ ratios largely reflect changes in global photosynthesis as the lighter ^{12}C is preferentially assimilated by primary producers, leaving an enrichment of ^{13}C, recording heavier $\delta^{13}C_{carbonate}$ signals in the oceans and sedimentary carbonate rocks. The $^{34}S/^{32}S$ ratios record variations in bacterial sulphate reduction to hydrogen sulphide (H_2S), which causes a depletion of ^{34}S in the sedimentary pyrite produced. Sulphate reducing bacteria flourish in low O_2, high organic matter environments, accounting for up to 50% of all organic matter mineralization in coastal and shelf ecosystems during anoxic periods (Jørgensen, 1982; Mudryk et al., 2000; Plugge et al., 2011). During anaerobic respiration the sulphate reducing bacteria mineralize the organic matter at the sea floor and reduce sulphate producing H_2S (Jørgensen, 1982; Mudryk et al., 2000). During the sulphate reduction process, studies have shown that the sulphide produced is depleted in ^{34}S by ~5%-46% compared to the normal isotopic composition of sulphate (depending on the rate of SO_4

reduction) (Habicht and Canfield, 1997), and can therefore change the $^{34}S/^{32}S$ composition of the seawater at the time.

Berner (2001) also suggests that "in the presence of O_2, sedimentary S undergoes increased isotope fractionation because of multiple cycles of sulphate reduction and sulphide oxidation accompanying the overturn of sediments near the sediment/seawater interface, due to bioturbation and wave and current stirring" (Berner, 2001, p. 686). Therefore as pO_2 concentrations increase, the amount of oxidation/reduction cycles increases, resulting in increased isotope fractionation (Berner, 2001). This isotopic composition is then incorporated into sediments. Therefore increased organic matter burial results in the removal of ^{12}C and ^{32}S resulting in heavier signals in $\delta^{34}S$ and $\delta^{13}C_{carbonate}$ in sedimentary rock.

The weathering of organic matter; pyrite, carbonates and sulphates, and the oxidation of reduced gases, involves little isotope fractionation. The isotopic composition of the sedimentary rocks therefore remain from the time that they were deposited at the ocean floor (Berner, 2001). Periods where the isotopic signals of $\delta^{34}S$ and $\delta^{13}C_{carbonate}$ are light are assumed to be periods where organic matter and pyrite sulphur rates declined, and weathering increased.

Therefore using mass balance calculations, the rates of weathering and burial of carbonates, C_{org}, pyrite, and sulphates can be determined over time by looking at changes in the total C, total S, ^{13}C and ^{34}S content (Figure 3.7). This is conducted by starting with present-day weathering, degassing and burial rates, and then comparing them with the isotopic composition of the sediments and the past rates calculated from the changes in composition (Berner et al., 2003).

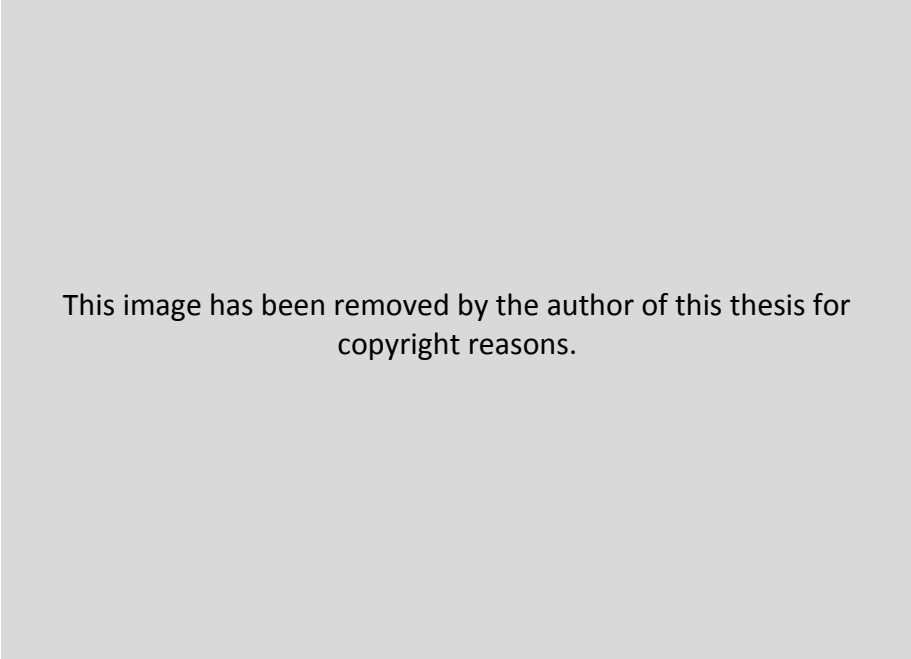

Figure 3.7 – Box model used for calculating variations in the fluxes affecting atmospheric O_2 using mass balance calculations. Each box represents total C and total S content along with their isotopic signature. Degassing is grouped with weathering, and the relative changes in O_2 are represented by either ($-O_2$) for O_2 subtractions or ($+O_2$) for O_2 additions to the atmosphere (taken from Berner et al., 2003, p. 109).

The results from the mass balance isotope model, such as the one conducted by Berner (2001) suggest little variation in palaeo-pO_2 predictions compared with Berner and Canfield's (1989) rock abundance model (Figure 3.8). However Berner (2001) concludes that the results suggest that pO_2 has "varied considerably over Phanerozoic time" (Berner, 2001, p. 693), but that "much more modelling is needed before one can say anything more definite about absolute past concentrations of O_2" (Berner, 2001, p. 693), illustrating the need for considerations of other feedback processes and their effect on pO_2 predictions to keep pO_2 within the limits of combustion. To address this, more 'comprehensive' models have been proposed that incorporate biological as well as more geological feedbacks.

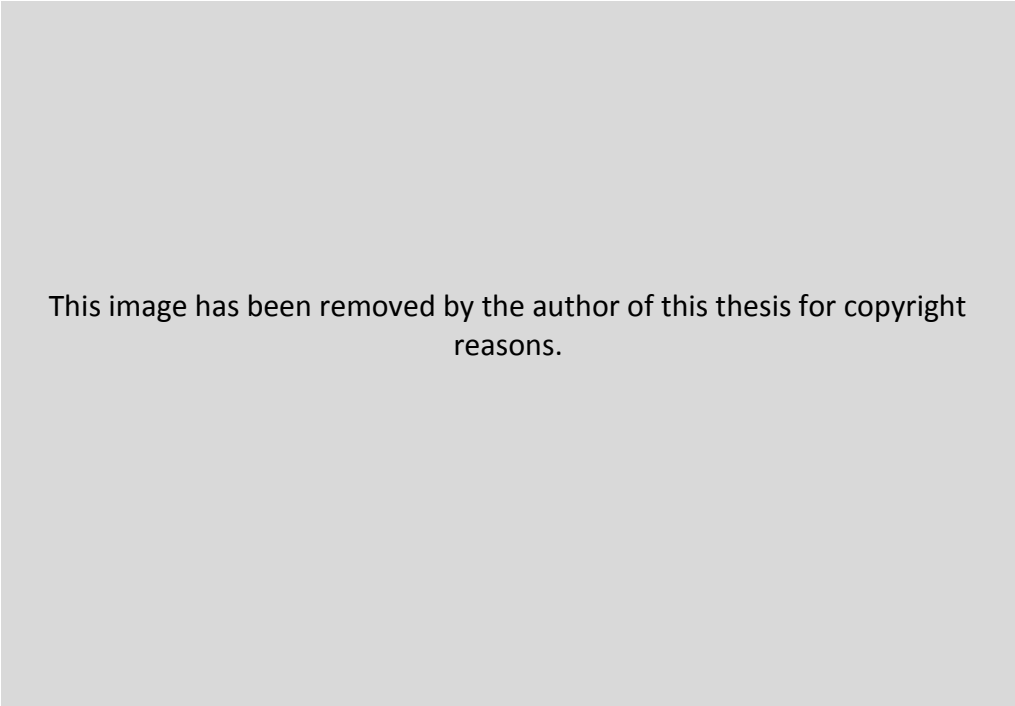

Figure 3.8 – Plot of palaeo-atmospheric O_2 predictions (%) over the Phanerozoic illustrating the comparison between Berner and Canfield's (1989) rock abundance model and the mass isotope balance model by Berner (2001). Canfield = Berner and Canfield (1989) rock abundance predictions; other lines illustrate the three 'best O_2 estimates' by Berner (2001) by varying the sensitivity of O_2 to sulphur isotope fractionation (where n is higher, there is more sensitivity of O_2 to fractionation); and to C isotope fractionation by photosynthesis ($\Delta_c(0)$). $\Delta_c(0)$ value is the value chosen for C isotope fractionation under PAL O_2. Taken from Berner, 2001, p. 693

The GEOCARB model (Berner, 1991)

The GEOCARB (box) model (Berner, 1991) was designed to better understand links between the global C cycle and climate over geological time (Mills, 2012). The model uses exchanges of C between reservoirs (Organic (reduced) C; Carbonate (oxidized) C and the ocean-atmosphere) to estimate the relative rates of removal and release of CO_2 to the ocean-atmosphere system by assuming that other elements of the global C cycle remain constant over geological timescales (>10^6 years) (Berner, 1997; Mills, 2012). Therefore the GEOCARB model works on intervals of 10 Myrs only (Berner and Kothavala, 2001).

To do this, the GEOCARB model uses three boxes which simulate the ocean-atmosphere reservoir, and crustal reservoirs organic C and carbonate C (Figure 3.9). By analyzing changes in isotope ratios and formulas to determine changes

in weathering and degassing relative to present day, fluxes between the reservoirs are calculated (Berner and Kothavala, 2001).

Figure 3.9 – Three box model used in the GEOCARB model, illustrating the movement of C between reservoirs. Organic and Carbonate C represent crustal reservoirs. Fbg = removal of CO_2 through photosynthesis and resulting burial of C_{org}; Fbc = Continental weathering allows reaction of CO_2 with calcium and magnesium silicates to form calcium and magnesium carbonates on ocean floor; Fwc and Fwg = release rate of C via weathering; Fmg and Fmc = degassing rate through thermal breakdown from metamorphism, diagenesis and volcanism. (Constructed from Berner and Kothavala, 2001; Mills, 2012).

The forcings used in the GEOCARB model include rates of uplift; degassing, and the depth of marine carbonate burial. Continental uplift rate is estimated using calculated changes in the $^{87}Sr/^{86}Sr$ signal of seawater for submarine volcanic-seawater reactions, without the Sr from terrestrial weathering. These are then compared to the actual Sr signal of seawater, and the difference used to determine the input from continental weathering (Berner and Kothvala, 2001).

The degassing rate is determined by calculating sea floor spreading rates using Gaffin's (1987) and Engebreston et al.'s (1992) sea level inversion method (Berner and Kothavala, 2001; Mills, 2012). From this global degassing rates are estimated (e.g. Franck and Bounama, 1997) (Mills, 2012).

The GEOCARB model (Berner, 1991) has since been adapted (e.g. COPSE) and revised numerous times (e.g. GEOCARB II by Berner (1994); GEOCARB III by Berner and Kothavala. (2001) and GEOCARBSULF by Berner (2006)), with the latest GEOCARBSULF adding the sulphur cycle.

COPSE (Carbon-Oxygen-Phosphorous-Sulfur-Evolution) model (Bergman et al., 2004)

The COPSE model created a new way of predicting past pO_2 levels by coupling biogeochemical feedbacks and adapting previous models, such as the GEOCARB model (Berner, 2001) and Lenton and Watson's (2000b) model.

Like the GEOCARB model, the COPSE model is also a box model for the Phanerozoic and analyses the movement between reservoirs (e.g. estimations of weathering, burial and degassing (Berner, 1991; 1997; 2006; Mills, 2012)) due to external forcings. However, the COPSE model adapts parts of the GEOCARB model by combining certain aspects (e.g. elements of the geological and geochemical Phanerozoic C cycle (Berner, 1991; 1997; Bergman et al., 2004) with Lenton and Watson's (2000b) model along with a simple sulfur model (based on Kump and Garrels, 1986).

The GEOCARB model is unable to "account for the effects of changing pO_2 levels on the productivity of terrestrial biota, which in turn affects weathering rates and organic C burial rates," (Bergman et al., 2004, p. 399) yet the Redfield Revisited model involving feedbacks that couple O_2 and ocean nutrients, does not account for changes in the C-cycle. The COPSE model aims to fill in the gaps left by previous models, by simulating the combined effect of both CO_2 and O_2 on the terrestrial biota (Bergman et al., 2004).

The model reservoirs used in COPSE include an atmosphere-ocean reservoir (O_2, CO_2, oceanic phosphate, nitrate, sulphate and calcium), and a crustal reservoir (including C_{org}, carbonate C, pyrite (reduced) sulphur and gypsum (oxidized) sulphur). Unlike other model adaptations such as the GEOCARBSULF model, the COPSE model does not use $\delta^{13}C$ and $\delta^{34}S$ isotope records as a forcing mechanism, therefore allowing the isotope records to be predicted (Bergman et al., 2004). Instead, the forcing mechanisms used include two geological forcings and four biological/evolutionary forcings. These are detailed in Table 3.1 below.

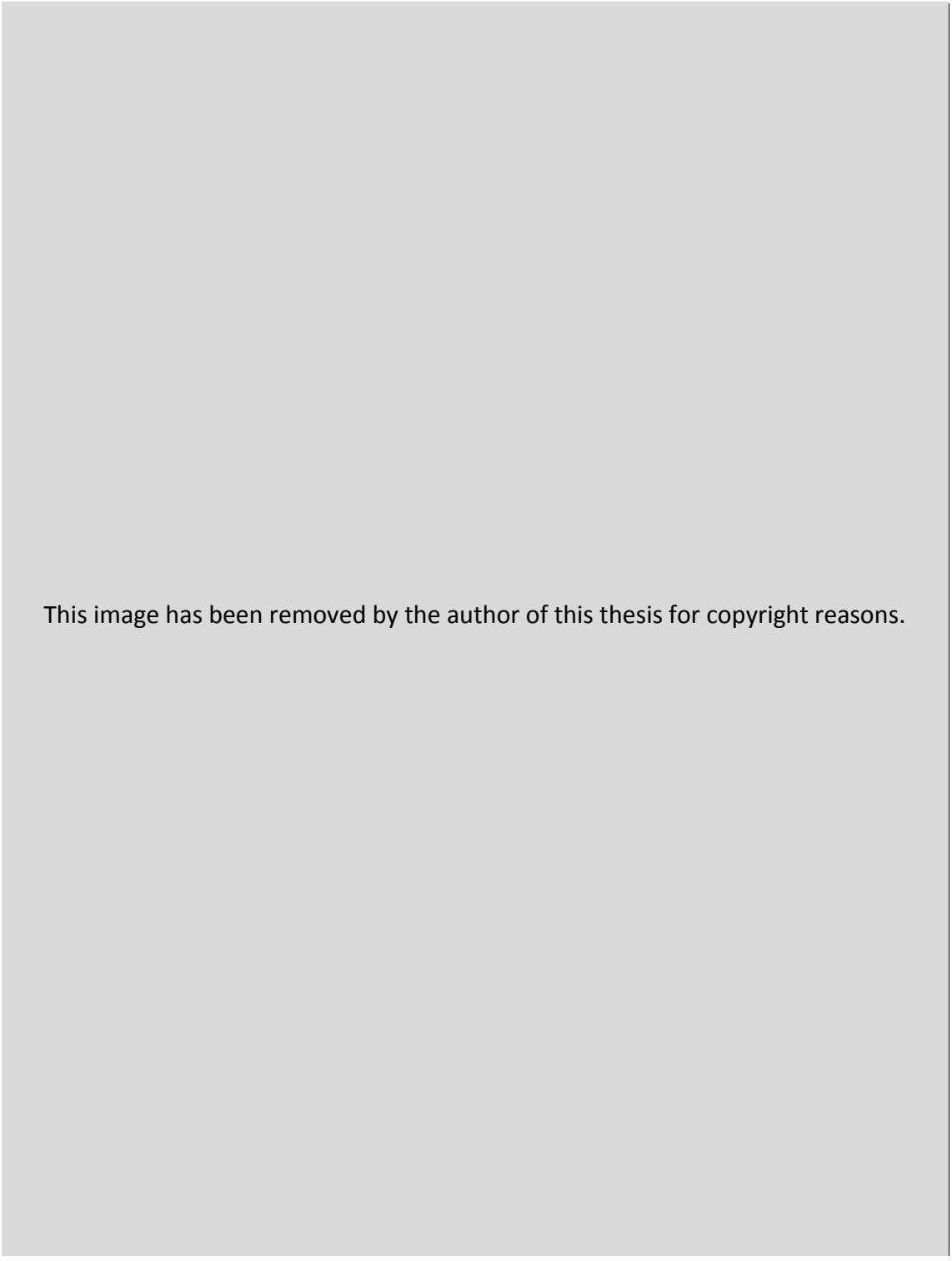

Table 3.1 – Outline of the forcing mechanisms used within the COPSE model (modified from Bergman et al., 2004).

The geological forcings in the COPSE model (***D, U***) are based on those used in the GEOCARB model for uplift and degassing, which are then "tied linearly to weathering rates" (Bergman et al., 2004, p. 408) following GEOCARB and

Redfield Revisited models. The evolutionary forcings (***E, W, B, I***) attempt to capture major events during the Phanerozoic (e.g. “the rise in carbonate degassing due to mid-Mesozoic rise of calcareous plankton, which are largely deposited in deep water” that are “thought to have increased carbonate susceptibility to subduction and thermal decompositions” (Bergman et al., 2004, p. 401); capturing key changes in the evolution and spread of vascular land plants particularly during the rise in the Silurian to the Carboniferous, and the rise of angiosperms in the Cretaceous). These in turn will affect other forcing parameters such as the weathering rate due to biological activity (as outlined in Lenton and Watson’s (2000b) model).

COPSE begins with present day reservoir sizes and pre-industrial levels, and is then run to simulate the past 350 Myrs using constant external forcings. Each model run removes/adds different feedback mechanisms, the results of which for the predicted O_2, CO_2, $\delta^{13}C$ and $\delta^{34}S$ and C_{org} burial, indicate which feedbacks have the most effect. Figure 3.10 illustrates the model schemes used in the COPSE model runs and different feedbacks associated with them.

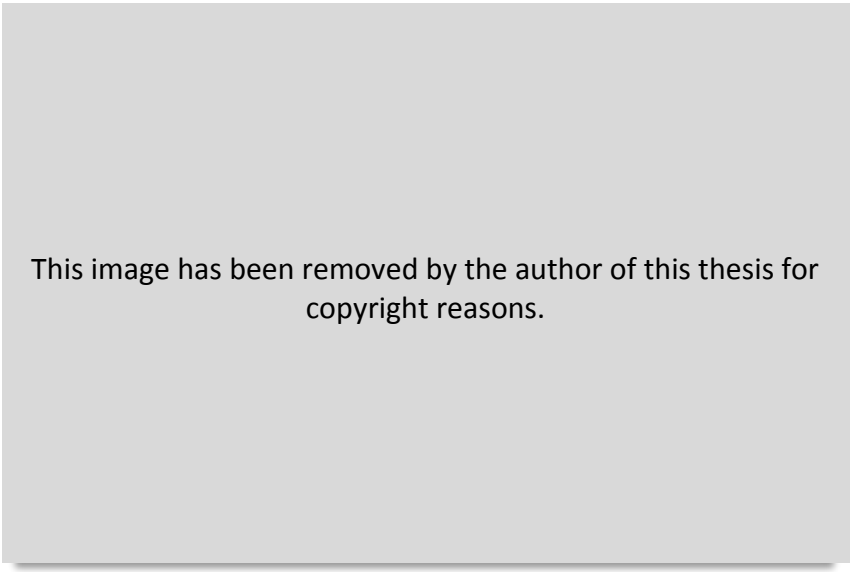


This image has been removed by the author of this thesis for copyright reasons.


This image has been removed by the author of this thesis for copyright reasons.


This image has been removed by the author of this thesis for copyright reasons.

Figure 3.10– Diagrams taken from Bergman et al. (2004) illustrating cycles and feedback schemes used within the COPSE model. For external forcings, refer to the table below.

A – Illustrates the P and N cycles
B – C_{org} and O_2 cycles (A-Atmosphere and Ocean CO_2, G-Crustal organic (reduced) C).
C – C-cycle and inorganic forcings
D – The sulphur cycle and calcium

Key
Circles represent fluxes and other model parameters; shaded ovals represent reservoirs; black rectangles represent external forcings; solid arrows indicate 'positive causality' and dashed arrows indicate 'negative causality'.
Reservoirs: P-Phosphate reservoir; N- Nitrate reservoir, O-Atmosphere and Ocean O_2, C-Crustal Carbonate (oxidised) carbon, S- Oceanic Sulfate, PYR- crustal pyrite (reduced) sulphur, GYP-Gypsum (oxidised) sulphur, CAL-Ocean calcium.
Fluxes and Parameters: *oxidw* – Oxidative weathering of organic carbon; *carbw* – weathering of carbonates, *silw* – weathering of silicates, *phosw* – weathering of phosphorous, *pland* - phosphorous flux to land, *psea* – phosphrous flux to the sea, d*enit* –denitrification, *nfix* – nitrogen fixation, *newp* – new production, *anox* – bottom water anoxia, *mocb* - marine burial flux of organic carbon, *mopb* – marine burial flux of phosphate, m*onb* – marine burial flux of nitrate, *capb* – marine burial flux, calcium bound, *fepb* – marine burial flux, iron sorbed, *V* – terrestrial vegetation, *locb* – organic carbon burial, *ocdeg* – degassing of organic carbon, c*cdeg* – degassing of carbonate carbon, *mccb* – marine carbonate carbon burial, *T* – temperature parameter, g*ypw* – weathering of gypsum, *pyrw* – weathering of pyrite, *mgsb* – marine burial of sulphur as gypsum, *mpsb* – marine burial of sulphur as pyrite.

The results of several runs of the COPSE model indicate that different feedback mechanisms have varying degrees of influence on the predictions of pO_2; CO_2, the C and sulfur isotope records and levels of C_{org} burial. For the purpose of this thesis, I will focus on the pO_2 predictions in particular. Each run of the model used in the prediction of Phanerozoic pO_2 concentrations is described briefly below (Table 3.2) (for full details with relevant equations, refer to Bergman et al., 2004).

Table 3.2 – Description and definitions of each of the COPSE model runs (modified from Bergman et al., 2004).

The results of the COPSE baseline run illustrated that there were two O_2 peaks of different magnitude when compared to Berner and Canfield's (1989) O_2 predictions (Figure 3.11).

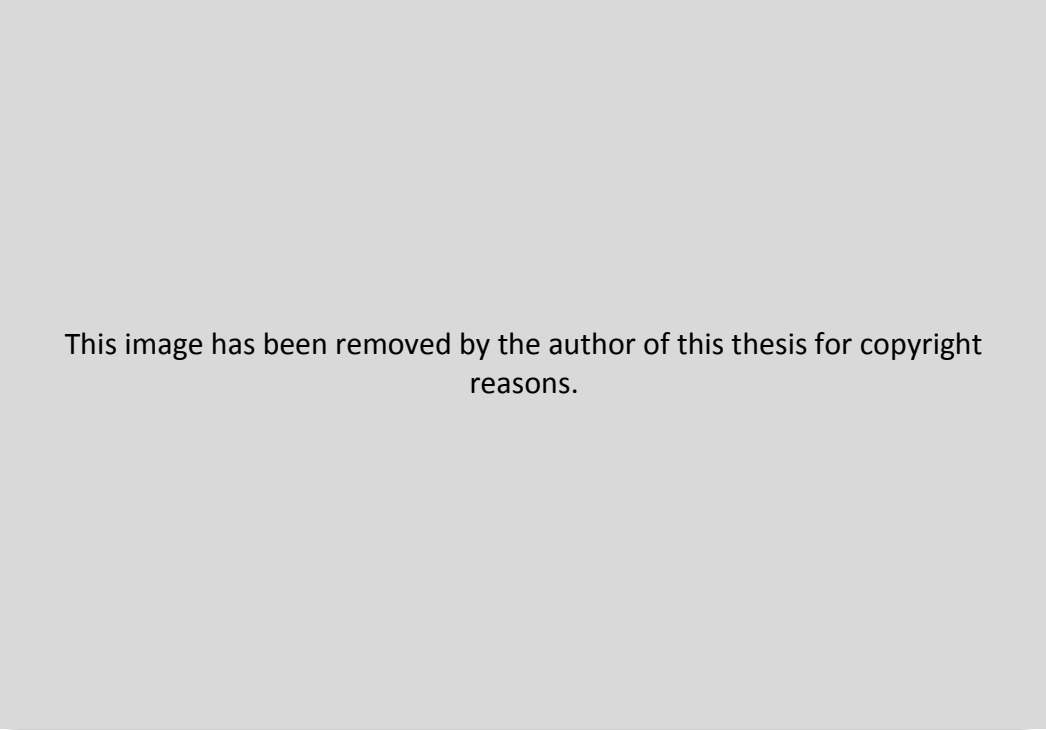

Figure 3.11 – Results from several COPSE model runs illustrating the strength of different feedbacks on pO_2 estimates. Notice in particular the strength of having fire as a feedback and the model's predicted O_2 concentrations compared with Berner and Canfield's (1989). (Berner and Canfield = B&C). Taken from Bergman et al. (2004).

The O_2 peak in the Permo-Carboniferous of ~1.4 PAL (lower than that predicted by Berner and Canfield (1989)) is explained as being due to the effects of land plant colonization, resulting in high burial rates of terrestrially derived C_{org}, pushing pO_2 concentrations up, although still being regulated to within the fire maximum range. The Cretaceous peak of ~1.55 PAL (slightly higher than Berner and Canfield (1989) predicted, is suggested to have been caused by high degassing rates and the evolution of angiosperms. The feedback and effects of these changes on pO_2 can be seen in Figure 3.12.

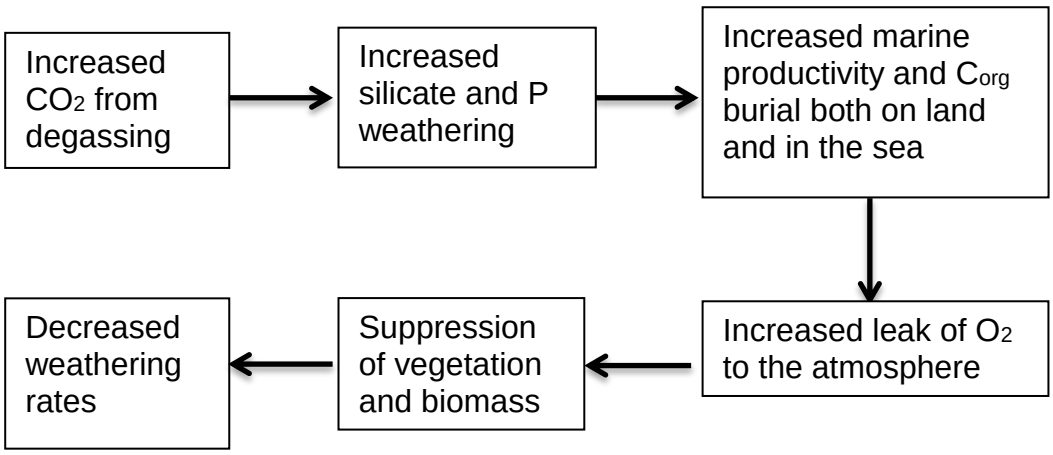

Figure 3.12 - Flow diagram illustrating a potential feedback mechanism operating due to high rates of CO_2 degassing.

When altering the strengths of some of the feedback mechanisms in the model, Bergman et al. (2004) concluded that feedbacks such as the sulphur cycle; the relationship between pyrite burial and pO_2 and the effects of fire as a feedback mechanism, were required to regulate pO_2 levels. In comparison, the VCI feedback was not important for O_2 regulation as it had little impact when removed from the model. However variations in O_2 and the relationship with oxidative weathering, and the effects of vegetation on both O_2 and CO_2 concentrations are important. The results and conclusions made by Bergman et al. (2004) for each of the feedbacks tested are outlined in Table 3.3 below.

This image has been removed by the author of this thesis for copyright reasons.

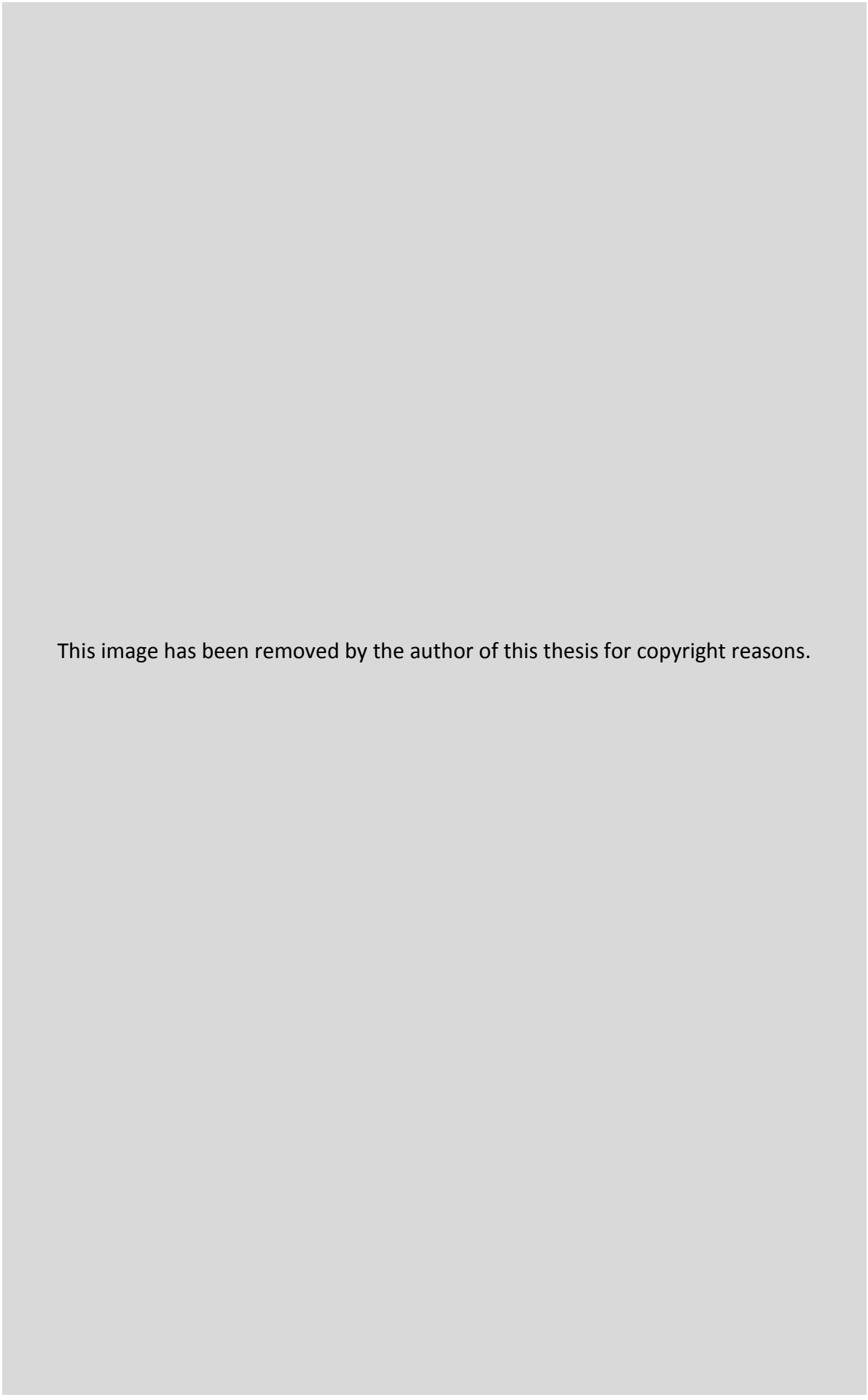
This image has been removed by the author of this thesis for copyright reasons.

Table 3.3 – The results and conclusions made by Bergman et al. (2004) for each of the feedbacks tested within respective model runs.

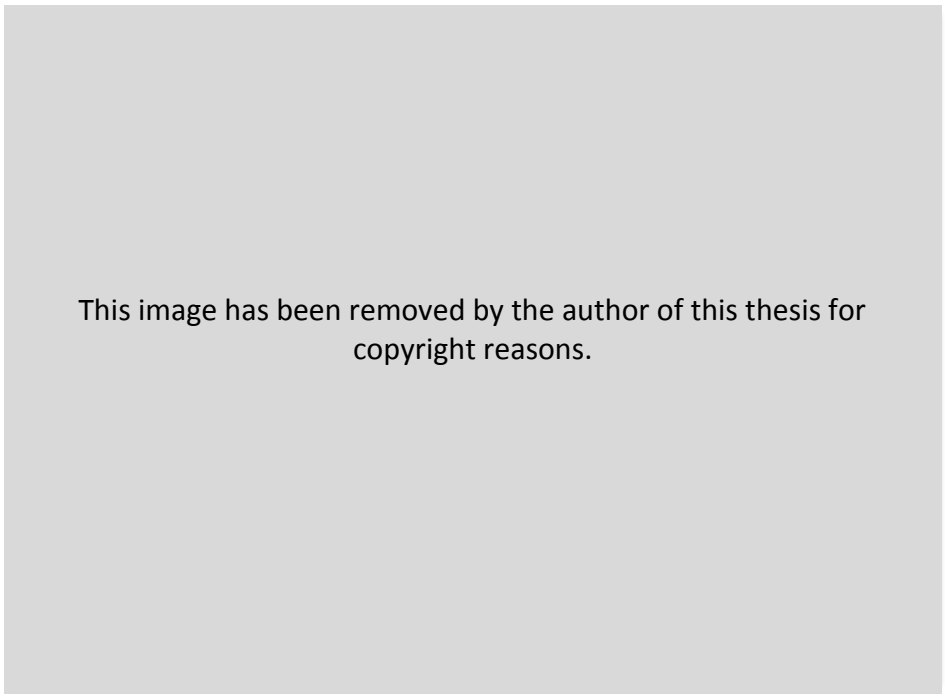

Figure 3.13 – Results from model runs including VCI feedback (run 2), no oxidative weathering (run 3) and no sulphur cycle (run 9) against the baseline model run (run 1) and Berner and Canfield's (1989) run (B&C). Taken from Bergman et al. (2004, p. 419).

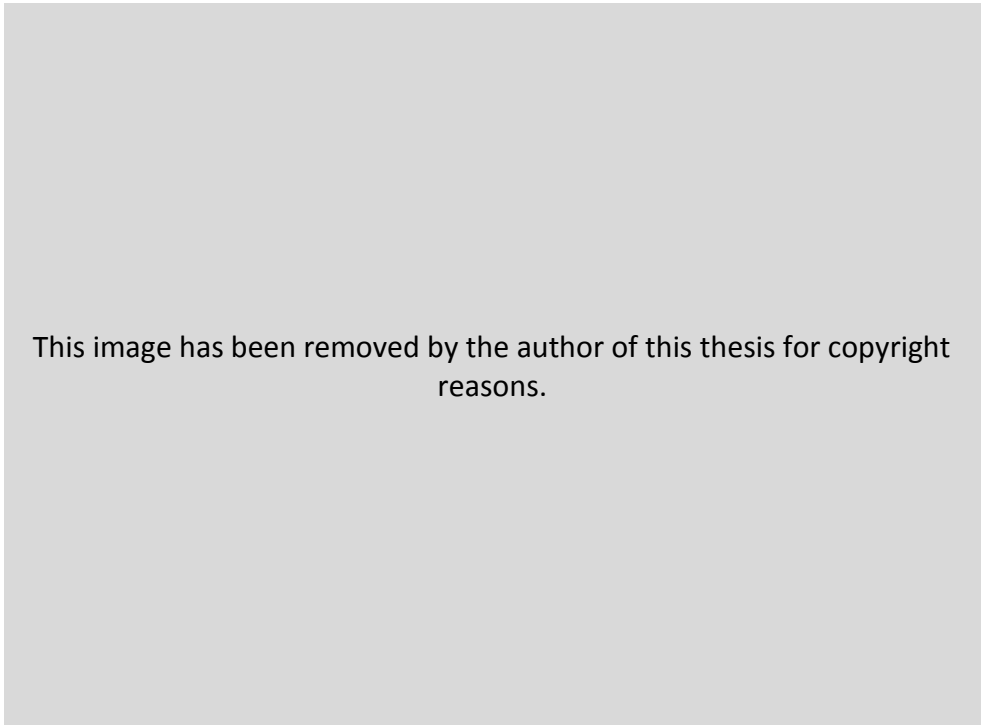

Figure 3.14 – Results from model runs including run 1 which 'uses the 'OCT' feedback for terrestrial vegetation V is compared to predictions using the full 'Friend' feedback (run 4) and the temperature independent (run 5). Charcoal record constraints are also illustrated for minimum and maximum pO_2. (Bergeman et al., 2004, p. 419).

The results from the COPSE model indicate that feedbacks from the GEOCARB (Berner, 1991) model, the Redfield Revisited models (Lenton and Watson, 2000b) and the sulfur cycles (based on Kump and Garrels, 1986) are required when modelling past pO_2 levels. However, the model does indicate that some feedbacks that were previously thought to be important in the regulation such as the 'VCI feedback' and the temperature dependent 'Friend feedback' do not have a significant impact on pO_2 predictions. Instead, the sulfur cycle, the effects of pyrite burial on O_2 and fire feedbacks are considered an essential factor, particularly for pO_2 regulation over the last 350 Myrs.

GEOCARBSULF

Similar to the COPSE model, the GEOCARBSULF model combines previous models. However, unlike the COPSE model, the GOECARBSULF model combines the GEOCARB III model with an isotope fractionation model, meaning that the model is unable to predict past isotopic signals (Mills, 2012).

The combination of these models enables GEOCARBSULF to predict past pO_2 and CO_2 levels, through combining the O_2 dependence of C and sulfur isotope fractionation and rapid recycling, with aspects of the GEOCARB model. The inclusion of "non-dimensional factors affecting weathering (e.g. mountain uplift and erosion) that have been applied to the GEOCARB model" are applied to the isotope mass balance model (Berner, 2006, p. 5654).

In order to predict past pO_2 concentrations, the model analyses variations in the input of O_2 from sources (C_{org} and pyrite-sulfur burial) comparing them to the output of O_2 sinks (e.g. weathering of C_{org} and pyrite sulphur in rocks, as well as the oxidation of reduced C and sulfur by volcanism/metamorphism) (Berner, 2006). The burial rates of C_{org} and pyrite sulphur are "calculated from the weathering and metamorphic/volcanic fluxes via isotope balance equations (Berner, 2001; 2004)", whilst the rates of degassing, like the GEOCARB model are estimated from changes in sea floor spreading rates (Berner, 2006, p. 5655). Calculations for GEOCARBSULF are conducted for every 1 Myrs, starting at 570Ma and run until the present. The results are then smoothed over every 10 Myrs, causing the model to miss any short-term events (Berner, 2006).

Within the model, two main negative feedbacks are used; the rapid recycling feedback (Berner and Canfield, 1989) and sulphur isotope fractionation (Berner,

2001). The sulfur isotope fractionation equation ($\alpha_s(‰) = 35(O_2/38)^n$) is based on the assumption that during higher pO_2 levels, there is a greater re-oxidation and cycling of sulfur by bioturbation and therefore a larger fractionation occurs. For the inclusion of the non-dimensional parameters (including variations in exposure of rocks by erosion due to high relief (this is suggested as being more important than weathering caused by variations in pO_2 content), changes in land area and changes in the amount of flushing of soils by river run-off), a weathering expression is provided, as in the original GEOCARB model (Equation 3.2) (Berner, 2006).

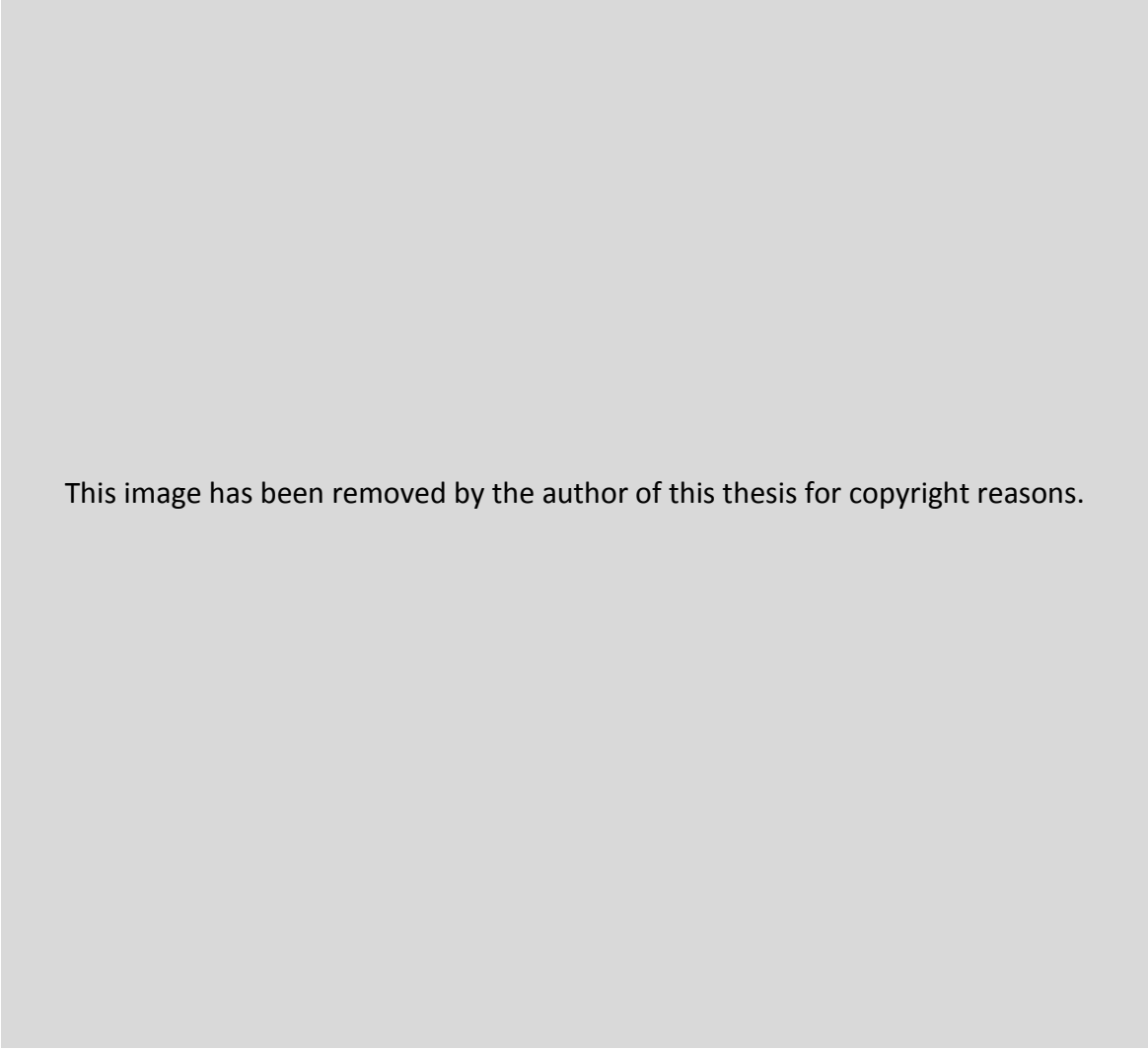

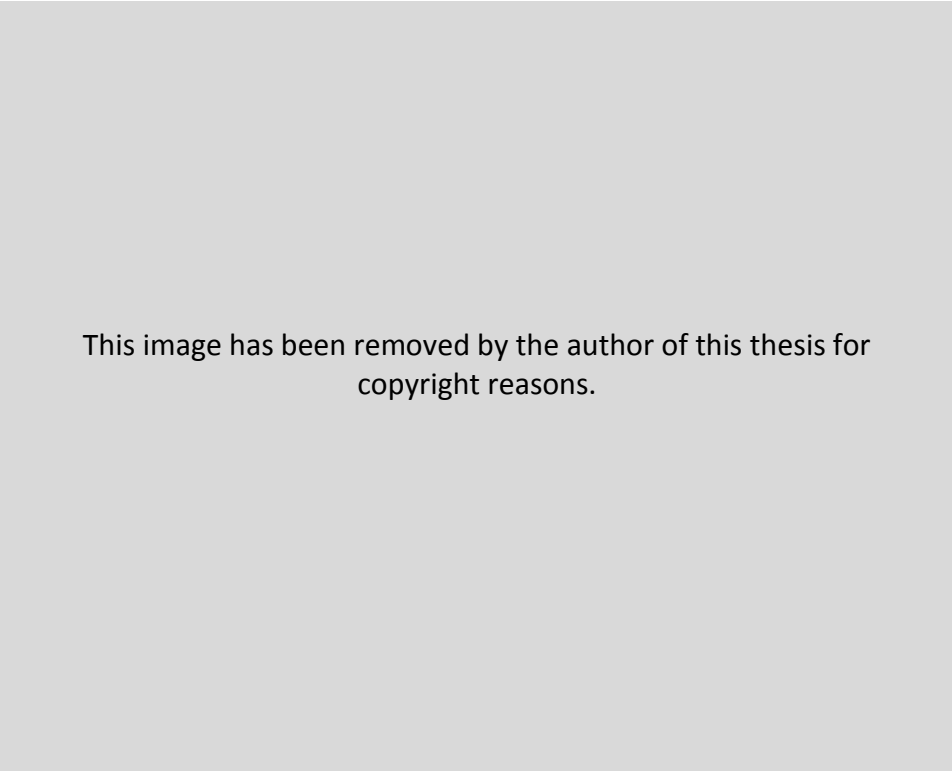

Figure 3.15 – Results from the GEOCARBSULF (2006) model illustrating palaeo-pO_2 predictions. Taken from Berner (2006).

The results from the GEOCARBSULF model (Figure 3.15) illustrate little variation from the original isotope mass balance models and Berner and Canfield's (1989) rock abundance model, with no real change from the predictions of the original GEOCARB model throughout the Phanerozoic. Berner (2006) suggests that from the results, it could be argued that the incorporation of non-dimensional weathering fluxes does not affect pO_2/CO_2 predictions. It is therefore concluded that the main control on pO_2 levels are the burial fluxes of C_{org}.

In 2009 the GEOCARBSULF model was further adapted to include new C isotope data that had been taken from ~2000 brachiopods from sediments spanning across the Permian and Carboniferous periods (Berner, 2009). Variations in the C isotopic composition of marine vs. terrestrial C is also incorporated in the new GEOCEARBSULF (2009) model, producing slightly different palaeo-pO_2 predictions for the last ~600 Myrs (Figure 3.16). The predictions from the revised GEOCARBSULF model are generally higher than those produced by the 2006 model, particularly over the last ~300 Ma. Furthermore, the new GEOCARBSULF (2009) results do not fall below 15% pO_2, which importantly sits within the 'fire

window', suggested by Belcher and McElwain (2008), meaning that these results are in agreement with the continuous charcoal record found (Scott and Glasspool, 2006).

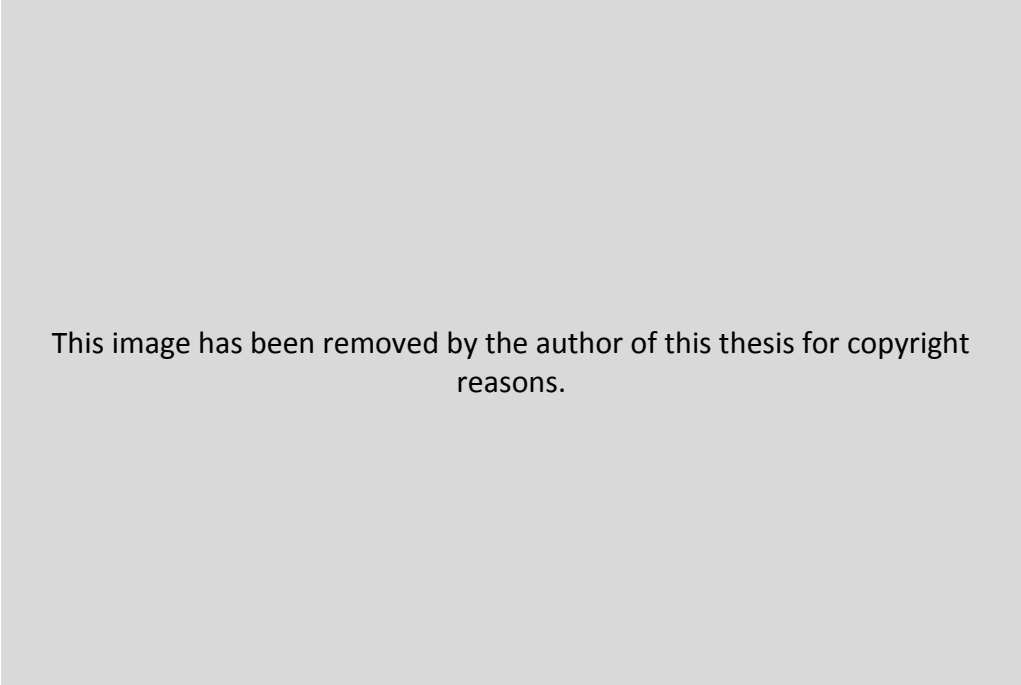

Figure 3.16 – Results from the GEOCARBSULF (2009) model (labelled O_2 revised) illustrating palaeo-atmospheric oxygen predictions compared to the GEOCARBSULF (2006) (labelled O_2 GEOCARBSULF) model. Taken from Berner (2009).

3.3 Summary

The product of wildfire, charcoal, appears to provide a good proxy for analysing variations in pO_2 due to its near continuous presence over the last >400 Myrs, and the fact that variations in its abundance appear to well track numerical model predictions of atmospheric O_2. The relationship between wildfire and pO_2, and the near continuous presence of fossil charcoal within the geological record, suggests that pO_2 concentrations have remained within combustion limits (~17 to 35% pO_2), and thus remained fairly stable throughout the last ~400 Myrs. This relationship has enabled the development of many biogeochemical feedbacks, many of which use wildfire as a key natural feedback component (e.g. Kump, 1988; Lenton and Watson, 2000b; Lenton, 2001; Bergman et al., 2004).

The advancement of numerical pO_2 models has illustrated the importance of biogeochemical cycles and the control over the source of O_2, C_{org} and reduced sulphur burial. Although oxidative weathering has been shown to have a weak negative feedback on rising pO_2 concentrations, model results indicate that the dominant control on long-term O_2 levels and their apparent stability through time, lies with the source of pO_2, C_{org} burial (Lenton, 2013).

3.4 OAEs and atmospheric O_2

During an OAE, increased burial and preservation of C_{org} and pyrite are recorded in the rock record (Jenkyns, 2010; Gill et al., 2011). Numerical biogeochemical models show that over millions of years, C_{org} and pyrite burial represents the net flux of O_2 to the planet, therefore exerting a significant control on global pO_2 concentrations.

The predicted long timescale of OAEs, often occurring over millions of years, matches the long, million year residence time of O_2 in the ocean-atmosphere system (Handoh and Letnon, 2003, Catling and Claire, 2005). It has therefore been hypothesized that global changes in pO_2 concentrations may have been possible during these events (Handoh and Lenton, 2003).

Handoh and Lenton's (2003) hypothesis began with the realization that Cretaceous OAEs appeared to occur at fairly frequent intervals of just a few million years apart (e.g. OAE 1a at ~120 million years ago (Ma); OAE 1b at ~112 Ma, OAE 1d at ~99 Ma, OAE 2 at ~91 Ma, and OAE 3 at ~87 Ma. This reoccurrence led Handoh and Lenton (2003) to propose a natural feedback mechanism that would allow for 'self-sustaining oscillations' in ocean anoxia and oxygenation, through the P and O_2 biogeochemical cycles.

Like Lenton and Watson (2000b), Handoh and Lenton's (2003) model uses positive and negative feedback mechanisms, driven by continental weathering and involving P availability and resulting changes in ocean productivity and bottom water oxygenation. A fast positive feedback and slower negative feedback mechanism is suggested to enable the self-sustaining oscillations observed between the Cretaceous OAEs (Handoh and Lenton, 2003).

Positive feedbacks involve the limiting nutrient P and its changing availability between anoxic and oxygenated bottom waters. Important also is the delivery of P to the marine system, which has been shown to enable the stability of pO_2 over the last ~350 Myrs (Lenton and Watson, 2000b). Thus the model also includes feedbacks involving fire frequency and the effects of O_2 on photosynthesis (as outlined in Lenton and Watson's model, 2000b). The feedbacks used in Handoh and Lenton's (2003) model are outlined in Figure 3.17

Figure 3.17 - Positive and negative feedback loops used in Handoh and Lenton's (2003) model. Black arrows indicate inverse relationships, whilst blue arrows indicate direct relationships. Taken from Handoh and Lenton (2003).

Here a rapid positive feedback is initiated by an increase in continental weathering (*W*) which increases P weathering and input into the oceans. This increases marine productivity leading to the depletion of O_2 in bottom waters. This enables increased efficiency of P recycling from the sediments (Van Cappellen and Ingall, 1994), and thus a decline in buried P_{org} and P_{Fe}, thus

allowing more P to be available to fuel productivity, which will eventually lead to an anoxic event.

Once an OAE has been initiated, a slower negative feedback occurs. During an OAE there is an increase in C_{org} burial due to the increase in productivity and preservation under anoxic conditions. The increase in C_{org} burial leads to an increase in O_2 that exceeds the O_2 sink caused by oxidative weathering on land. This leads to an increase in pO_2 and thus fire frequency, which acts to limit land vegetation. The decline in biomass causes a decline in P weathering, but not enough to stop the rise in pO_2. This eventually allows the rise in pO_2 to begin to remove anoxia from the oceans.

In order for another event to occur, once oxic, C_{org} burial cannot match oxidative weathering, so pO_2 declines until another OAE is triggered.

Using these feedbacks, Handoh and Lenton (2003) hypothesize that C_{org} burial should gradually increase prior to an OAE, then rapidly increase over thousands of years during the OAE, before declining at the end of the event. pO_2 concentrations are therefore predicted to gradually increase during the OAE with rising C_{org} burial, reaching a peak at the end of the OAE as high pO_2 concentrations terminate the event. The relationship between pO_2 and fire frequency suggest that the charcoal content of the sediments should track pO_2 changes, with sediments at the start of the OAE exhibiting lower charcoal abundances. Charcoal abundances should then gradually rise during the OAE, reaching a peak at the OAE termination. The model prediction of changes in oceanic phosphate, nitrate, O_2, anoxia, fire frequency and weathering across time are shown in Figure 3.18.

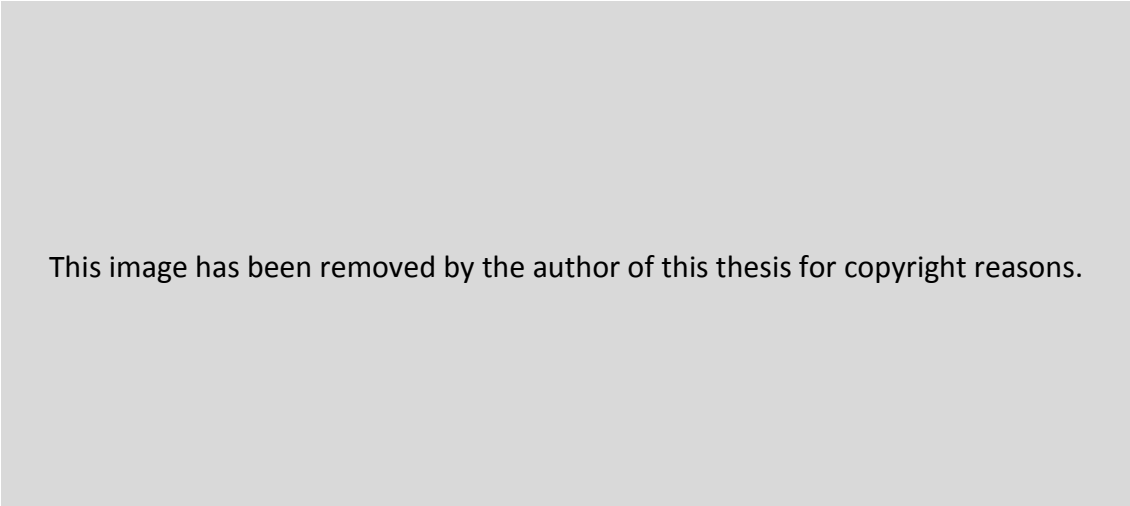

Figure 3.18 Modelled changes in pO_2 (O_2) and fire frequency (F) across an OAE, plotted against million year timescales, modified from Handoh and Lenton (2003). A = anoxic fraction (high during an OAE); W = continental weathering, PO_4 = oceanic phosphate, NO_3 = oceanic nitrate (fueling productivity and thus C_{org} burial).

OAEs therefore provide a perfect geological test bed for understanding the functioning of the Earth's biogeochemical cycles and regulation of its atmospheric content under extreme conditions. Furthermore the hypothesized change in wildfire activity during an OAE in response to predicted changes in atmospheric O_2 concentrations, makes charcoal the perfect proxy to test the fossil record for evidence of Handoh and Lenton's (2003) model, which until this point has only been predicted by numerical models, and never backed up with palaeontological evidence.

4. “Ocean oxygen depletion takes about a million years to recover naturally” (International Business Times, 2017)

The research presented in the following chapter has been published as:

Baker S.J., Hesselbo S.P., Lenton T.M., Duarte L.V., Belcher C.M. (2017). Charcoal evidence that rising atmospheric oxygen terminated Early Jurassic ocean anoxia. *Nature Communications*. DOI: 10.1038/ncomms15018

Refer to appendices A to C for extended detail on materials, methods and site stratigraphy.

4.1 Abstract

The Toarcian Oceanic Anoxic Event (T-OAE) was characterized by a major disturbance to the global carbon(C)-cycle, and depleted oxygen in Earth’s oceans resulting in marine mass extinction. Numerical models predict that increased organic carbon burial should drive a rise in atmospheric oxygen (pO_2) leading to termination of an OAE after ~1 Myr. Wildfire is highly responsive to changes in pO_2 implying that fire-activity should vary across OAEs. Here we test this hypothesis by tracing variations in the abundance of fossil charcoal across the T-OAE. We report a sustained ~800 kyr enhancement of fire-activity beginning ~1 Myr after the onset of the T-OAE and peaking during its termination. This major enhancement of fire occurred across the timescale of predicted pO_2 variations, and we argue this was primarily driven by increased pO_2. Our study provides the first fossil-based evidence suggesting that fire-feedbacks to rising pO_2 may have aided in terminating the T-OAE.

4.2 Introduction

It has been suggested that projections of anthropogenic C-emissions likely exceed levels that have initiated Oceanic Anoxic Events (OAEs) in Earth's past (Hoegh-Guldberg and Bruno, 2010; Barclay et al., 2010), implying that anthropogenic forcing of the Earth System may cause a future OAE, with implications for food security and for the oceans as a net C sink. OAEs are identified in the rock record by globally traceable organic-rich sediments and excursions within the $\delta^{13}C$ record (Hesselbo et al., 2007; Jenkyns, 2010) representing periods of major disturbance to the global C-cycle (Jenkyns, 2010). The study of OAEs therefore provides a geological test bed for understanding the functioning of global biogeochemical cycles under extreme conditions and rapid shifts in C-emissions. Burial of organic carbon (C_{org}) and reduced sulfur (pyrite) burial generate long-term build-up of oxygen to Earth's atmosphere (Garrels and Lerman, 1984; Kump, 1988; Berner, 1999; Lenton and Watson, 2000b; Berner, 2004; Canfield, 2005). It has thus been predicted that during an OAE, where increased burial of C_{org} and pyrite (Gill et al., 2011) occur, that pO_2 concentrations should have risen (Handoh and Lenton, 2003) (Figure 4.1). Wildfire responds strongly to pO_2 (Watson, 1978; Belcher and McElwain, 2008; Belcher et al., 2010b) and has been implicated in providing an essential long-term negative feedback, counteracting rising pO_2 throughout geological time (for example, see Kump, 1988; Handoh and Lenton, 2003; Lenton, 2013). We therefore hypothesize that fire-activity should track projected pO_2 changes across an OAE (Figure 4.1).

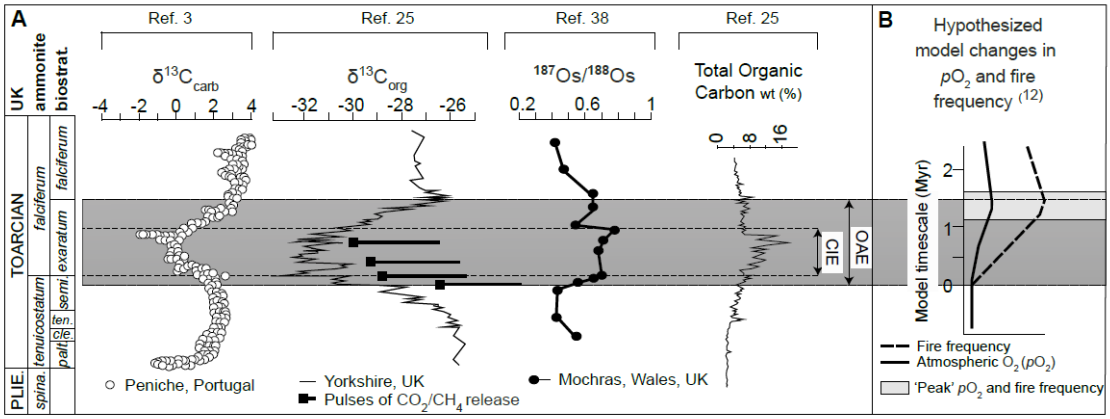

Figure 4.1 – Summary of published data collected across the early Toarcian oceanic anoxic event. (a) Carbonate carbon isotope profile from Peniche and the organic carbon isotope profile from Yorkshire illustrating the step-wise nature of the negative excursion, and postulated pulses of light carbon release from Kemp et al. (2011) plotted alongside are the osmium isotope profile from Mochras and total organic carbon content from the Yorkshire section. (b) Handoh and Lenton's (2003) hypothesized model changes in atmospheric oxygen and wildfire frequency across an oceanic anoxic event, with period of modelled peak oxygen and wildfire frequency highlighted.

Variation in the occurrence and abundance of charcoal throughout Earth history is taken to represent changes in fire activity and appears to correlate with broad trends in the abundance of pO_2 (Belcher and McElwain, 2008; Glasspool and Scott, 2010). A few studies have looked at the fossil-charcoal record within Devonian marine black shales and related them to changes in pO_2 and fire-feedbacks (Kaiho et al., 2013; Rimmer et al., 2015). However, fossil charcoal has not been studied across events such as OAEs in order to test the hypothesis that fire-feedbacks to pO_2 may have acted together to rebalance the Earth system during these events (Handoh and Lenton, 2003; Berner, 2004). Here we test this hypothesis by assessing the charcoal content of sediments from two sites deposited in the southern Laurasian Seaway, at Mochras in Wales, UK and Peniche, Portugal.

In this study, we find that charcoal abundances and therefore inferred wildfire-activity at both study locations are enhanced ~1 Myr after the onset of the T-OAE. The enhancement of fire activity is sustained for ~800 kyr and peaks during the OAE termination. Variations in pO_2 are anticipated to occur over Myr timescales (Lenton and Watson, 2000b; Catling and Claire, 2005; Lenton, 2013) due to the long residence time of oxygen within the ocean-atmosphere system

(Handoh and Lenton, 2003; Catlin and Claire, 2005). The major enhancement of fire-activity occurring ~1 Myr after the start of the T-OAE and lasting over ~800 kyr is strikingly similar to the Myr timescale required for predicted global pO_2 variations. Our findings therefore provide the first fossil-based evidence to support the postulation that OAEs are terminated by a rise in pO_2 levels.

4.3 Methods

4.3.1 Study locations

Two sites were studied that record the T-OAE, deposited within the southern Laurasian Seaway; Peniche in Portugal and Mochras in the UK (Figure 4.2).

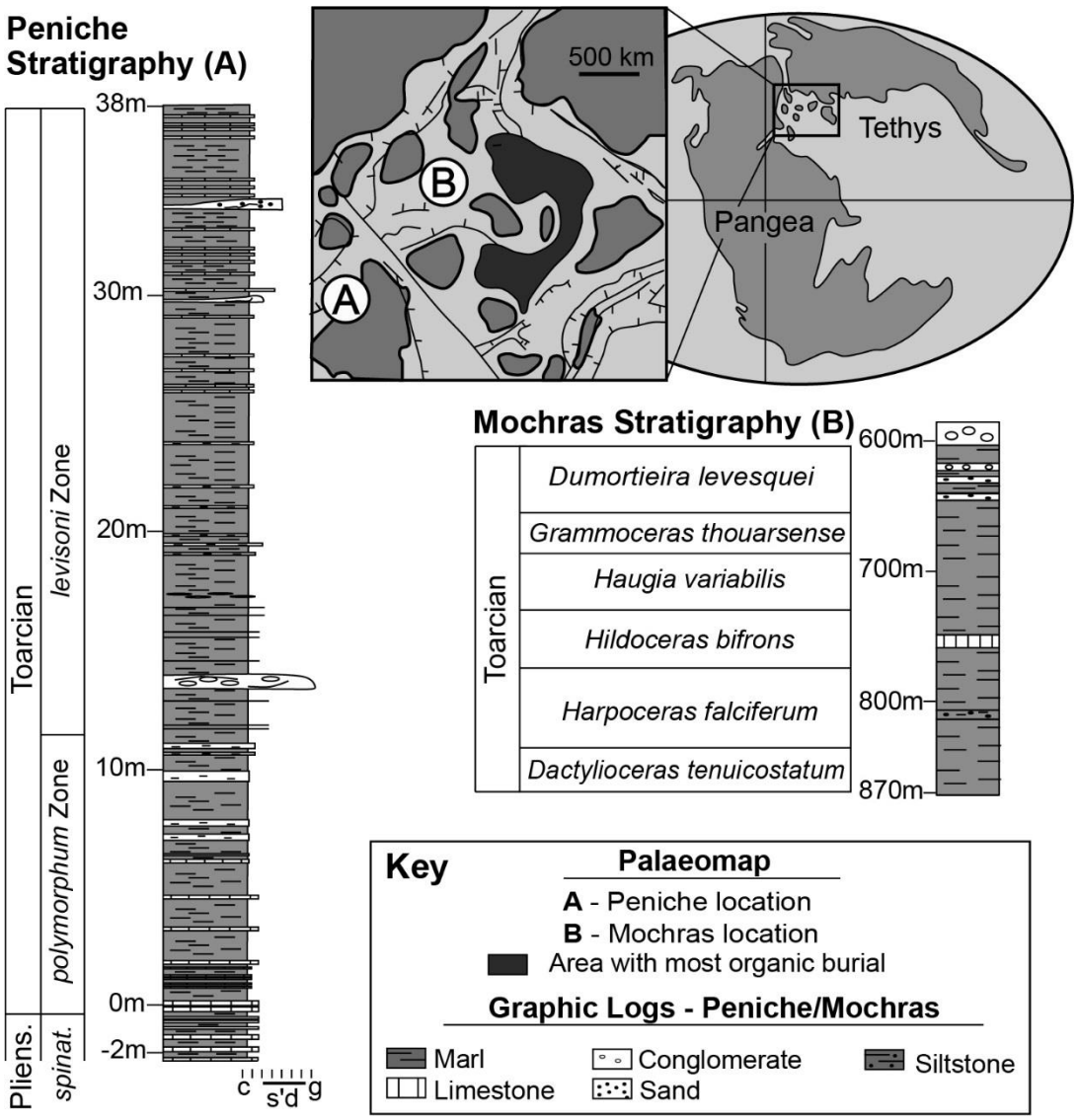

Figure 4.2 – Jurassic Palaeo-map of the sample localities and relative site stratigraphies for the Mochras and Peniche sections. Palaeo-map and Peniche log were edited from Hesselbo et al. (2007). Mochras log edited from Hesselbo et al. (2013).

At Peniche, the Pliensbachian-Toarcian carbonate ramp succession is particularly well exposed, including the Toarcian GSSP (for example, see Rocha et al., 2016). The deepest part of the ramp (~200 m), represented by the Praia do Abalo sample locality, was bounded by the high-relief Berlenga–Farilhões horst, which provided terrestrial material to the sample site (Duarte, 2007). The site is unlikely to be influenced by a rise in sea level, as the horst would not have become more distal from the depositional area (Hesselbo et al., 2007). In Wales, UK, the Llanbedr (Mochras Farm) core, referred to as Mochras, drilled in 1967–1969, provides a complete section of mostly Early

Jurassic sediments dating from the Late Rhaetian to Late Toarcian (Woodland, 1971; Dobson and Whittington, 1987). The sediments were deposited within a basinal marine setting, which became deeper during the initiation of the OAE, continuing throughout the falciferum zone into the bifrons zone (beyond the studied section) (Muller, 1990) influenced by nearby terrigenous sources around the Cardigan Bay area (Dobson and Whittington, 1987). Both sites are within the Laurasian Seaway (see Hesselbo and Pieńkowski (2011) and references therein), and are anticipated to capture regional signals of burning from the nearby emergent land.

4.3.2 Sample collection and processing

Rock samples were collected from the exposed cliff sections in Peniche, and from the Mochras core, stored at British Geological Survey, Keyworth. The samples were picked from marl units, characterized by minor lithological changes and are considered to have been deposited within relatively uniform palaeo-environments, minimizing the distortion of any fire-signals observed. Fossil charcoal was extracted from the Peniche and Mochras rock samples (48 samples in total were processed and analysed) using standard palynological acid maceration techniques. The remaining organic particles were sieved using a 125 µm mesh, where both size fractions were collected. The >125 µm size fractions were analysed using a binocular microscope, where all charcoal particles in each 20 g sample were quantified. The <125 µm fraction retained was quantified by evenly dispersing the organic particles in a known quantity of water. A known volume was then pipetted and made into slides using standard palynological techniques. Two transects of each slide were quantified, and scaled up to the known quantity of the <125 µm sample (Belcher et al., 2005). Selected particles were studied using a scanning electron microscope (SEM) to confirm their identification as charcoal (Figure 4.3). To ensure changes in fossil charcoal concentrations were not biased by a change in nature or abundance of terrestrial organic material, a palynofacies analysis of each sample was conducted, quantifying the abundance of pollen and spores; plant cuticle, amorphous organic matter and coalified particles (see appendix B).

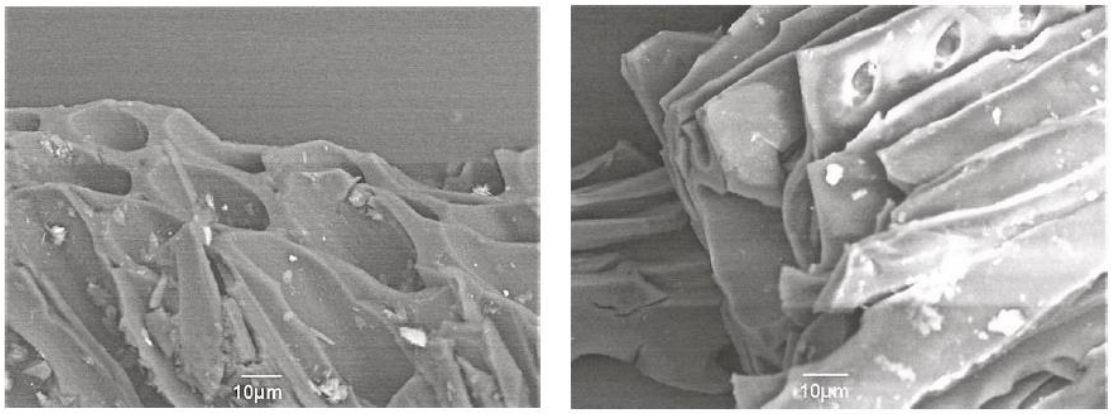

Figure 4.3 – SEM images of charcoal fragments from the Peniche section. The fragments show the preservation of cellular anatomy and fused/ homogenized cell walls—a key feature in charcoal identification.

4.4 Results

4.4.1 Palaeo-wildfire

We find background charcoal abundances range between 22,000 and 75,000 particles per 10 g rock at Mochras, and 37,000 and 122,000 at Peniche prior to the T-OAE. Charcoal abundance rises briefly above background levels during the onset of the T-OAE, evidenced by 950,000 particles at Peniche (10.4 m log height) and 133,000 at Mochras (842 m depth), the start of which is widely identified in the rock record by a shift towards negative $\delta^{13}C$ values at the culmination of a positive $\delta^{13}C$ trend (Hesselbo et al., 2007) (Figure 6.4). Charcoal abundances then decline to background values during the period of the negative carbon isotope excursion (CIE). Abundances remain at/below background levels until the final stages of the OAE (22.4 m at Peniche and 809 m at Mochras), where abundances increase to 293,000 particles at Peniche and 350,000 at Mochras. Although there appears to be variability within the charcoal abundance data, at both study locations abundances remain above background levels for ~9.6 m at Peniche (between log heights 22.4 m and 32 m); and 23 m at Mochras (between core depths 809 m and 786 m), with the exception of one point at 803 m at Mochras, where abundances decline to 45,000 particles per 10 g of rock. Once the T-OAE has terminated, identified by the $\delta^{13}C$ values returning to towards pre-excursion levels, abundances return to background levels as evidenced at Peniche from a mean of 411,000 particles

between log heights 22.20 m and 32 m to a mean of 62,000 particles between 32 m and 38.2 m; and at Mochras from a mean charcoal abundance of 307,000 particles between core depths 809–786 m to a mean of 113,000 particles between depths of 785 m and 771 m.

4.4.2 Palynofacies

The reported variations in charcoal abundance do not appear to be an artefact of preservation or changes in terrestrial organic delivery across the OAE, because variations in preserved phytoclasts (comprising terrestrial vegetal matter including charcoal, plant cuticles, pollen and spores and coalified material), show little correlation with the variations in charcoal abundance at either site (Figure 6.4). This is further statistically supported by higher than 0.05 P values of p = 0.384 for the Mochras section (where Pearsons R equalled 0.0186), and p = 0.195 for Peniche (where R equalled 0.2153), indicating that the correlation between charcoal abundance and phytoclast abundance throughout the sections is not significant.

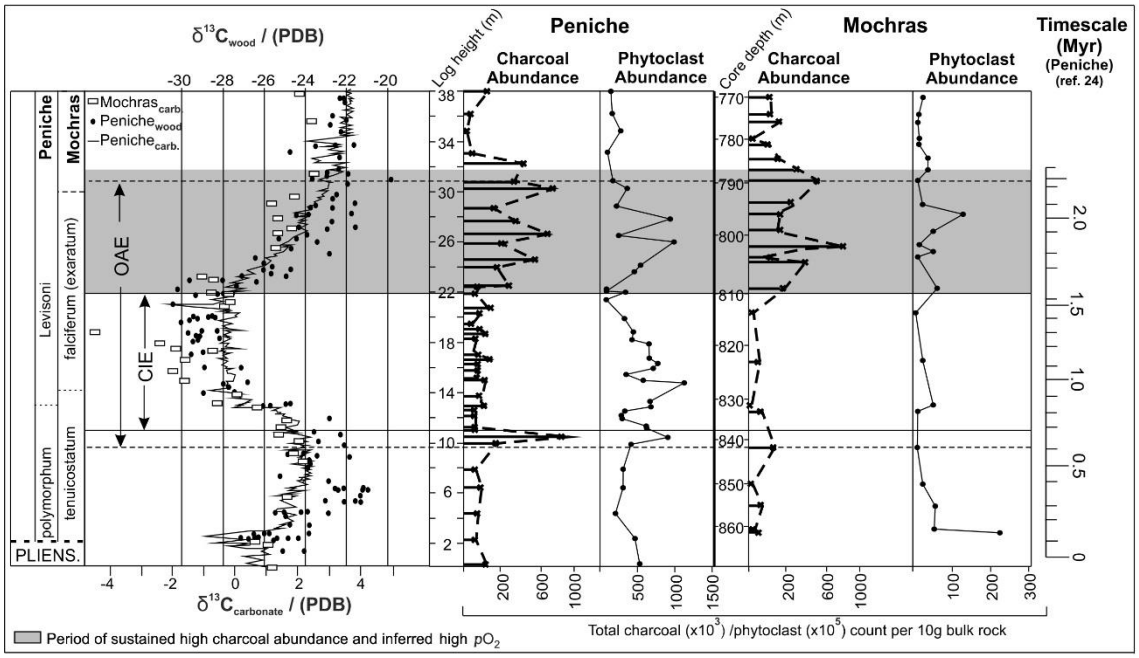

Figure 4.4 – Charcoal and phytoclast abundances across the T-OAE. Charcoal and phytoclast data collected in this study, plotted against published wood and carbonate carbon isotope profiles from Peniche and Mochras, and calculated cyclostratigraphic timescale from the Peniche section by Huang and Hesselbo (2014). $\delta^{13}C_{wood}$ and $\delta^{13}C_{carb}$ profiles for Peniche are from Hesselbo et al. (2007). The $\delta^{13}C_{carb}$ for Mochras is from Jenkyns and Calyton (1997) and correlated to the Peniche sequence using Pittet et al. (2014).

4.5 Discussion

Fluctuations in the abundance of terrestrial phytoclasts have been used to indicate shifts in proximal palaeo-shoreline distance from the depositional site, as well as changes in preservation, for example, due to a switch from anoxic to an oxic environment (El Beialy et al., 2016). At Mochras, the depositional site is anticipated to have gradually deepened, beginning at the OAE initiation and continuing throughout the falciferum ammonite zone into the bifrons ammonite zone beyond the studied section (Muller, 1990). Interestingly, phytoclast abundances do not appear to reflect this deepening trend, suggesting that the site may have continued to experience a similar influx of terrestrial material throughout the OAE and beyond. Therefore this deepening is unlikely to explain enhanced charcoal abundance towards the end of the OAE; if anything deepening might be expected to decrease the amount of charcoal reaching the depositional environment at this site. Furthermore the lack of correspondence between variations in phytoclast abundance and charcoal abundance, implies

that the enhanced number of fossil-charcoal particles that occur during the final stages of the OAE are unlikely to be due to a change in organic preservation, and therefore most likely reflect a real change in fire-activity. The charcoal is further unlikely to have been reworked up-section as there is no evidence of reworking in the biostratigraphic record of the sites, nor evidence for enhanced bioturbation at the onset of this phase of the OAE. Because charcoal abundance is limited below this point, reworking of the older sediments appears an unlikely source for the abundant charcoal that appears in the final phases of the OAE.

Published astronomically calibrated timescales for the Peniche section (Suan et al., 2008; Huang and Hesselbo, 2014) estimate a total duration of between ~900 kyrs and ~1.7 Myrs for the T-OAE, respectively. These timescales have previously been compared and correlated with Toarcian sediments exposed in Yorkshire, UK, which also illustrates a strong astronomical forcing within the $\delta^{13}C_{org}$ record (Kemp et al., 2011). The section we have studied at Mochras provides twice the thickness and is considered to be stratigraphically more complete than that exposed in Yorkshire (Hesselbo et al., 2013; Ruhl et al., 2016). For the purpose of this study, we have used the most up-to-date published correlation of the Peniche and Mochras section (Pittet et al., 2014) plotted alongside the most up-to-date published cyclostratigraphically calibrated timescale from the Peniche section (Huang and Hesselbo, 2014).

Using the published timescale, we estimate that background charcoal abundances persisted for the duration of ~600 kyrs (Huang and Hesselbo, 2014) prior to the initiation of the OAE. The sustained increase in charcoal abundances at 22.4 m at Peniche and 809 m at Mochras, occurs at an estimated ~1 Myrs after the OAE onset (Figure 4.4), remaining elevated for an estimated 800 kyrs–1 Myrs before declining towards background abundances after the OAE termination. The major change in inferred wildfire-activity estimated at ~1 Myrs after the OAE onset appears to corroborate the hypothesis of Handoh and Lenton (2003), suggesting that a rise in pO_2 may have assisted in terminating the T-OAE by ventilating the ocean. However, while Handoh and Lenton (2003) predict that pO_2 and thus fire-activity should be at a minimum at the start of the OAE and gradually rise throughout (Figure 4.1), our analysis reveals a brief rise in fire-activity during the T-OAE initiation at

both study sites, although albeit a much smaller rise in abundances at the Mochras site. Calculation of the *Z scores* for this brief rise in charcoal abundances (Z = 10.43 at Peniche and Z = 3.39 at Mochras) indicates that this increase in charcoal abundance at the onset, is statistically significant (larger than the critical Z value of 1.645) when compared to the background counts at both study sites. While, this observation is based on only one data-point in each section and requires corroboration, the brief rise in charcoal abundance occurs at the culmination of a positive $\delta^{13}C$ trend. This could imply that the positive $\delta^{13}C$ trend is indicative of an earlier prolonged increase in C_{org} burial, and therefore that pO_2 began rising before the OAE.

Fire responses to rising pO_2 are non-linear (see Fig. 4 in Belcher et al., 2010b); therefore, depending on the timing of the onset of C_{org} burial and the abundance of pO_2 prior to the OAE, the fire responses could be variable throughout the OAE (Belcher et al., 2010b). The pO_2 estimates for 183 Ma range between 16 and 21% (Glasspool and Scott, 2010). If background pO_2 were ~19%, and the onset of C_{org} burial were capable of leading to a rapid 1% rise in pO_2 by the start of the OAE, there would be a rapid rise in fire-activity as pO_2 transitioned between 19 and 21% (Belcher et al., 2010b). Beyond 21% the fire response would slow but still continue to rise throughout the OAE with rising C_{org} burial and pO_2, reaching a peak towards the end. However, most models estimate baseline pO_2 at ~20% (Bergman et al., 2004; Lenton, 2013), which would generate a slower fire response at the onset of enhanced C_{org} burial, with fire-activity gradually rising throughout and peaking at the end of the OAE. Therefore the initial peak in fire-activity would require a different explanation.

A study by McElwain et al. (2005) on a T-OAE section at Bornholm, Denmark, reveals that during the initiation, significant climatic changes occurred. Although, this sequence (McElwain et al., 2005) preserves only the lower part of the negative CIE, and was conducted at a higher resolution than that captured here, a rise in global temperatures and drying of the regional climate is inferred due to increased abundance of thermophilic plant taxa immediately before the first negative $\delta^{13}C$ shift. Past Mesozoic global warming events have been shown to enhance fire activity (Belcher et al., 2010) and warm, dry periods are commonly linked with increased fire probability and large fire events (Clark, 1990; Dale et al., 2001), which tend to be enhanced when dry periods succeed

wetter periods that are favourable to fuel accumulation. Thus the brief enhancement of fire-activity may have been influenced by climatic changes occurring over timescales of a few hundred to thousand years close to the onset of the OAE; either driven directly by the climate change or from a resulting change in vegetation, the fuel for fires. Following the brief rise in fire-activity, charcoal diminishes to near background levels, rather than rising gradually throughout the OAE. During the negative CIE, pulses of isotopically light C suggest enhanced input of CO_2 into the atmosphere from volcanic sources (Kemp et al., 2011) leading to increased global temperatures (Korte et al., 2015), sufficient to provoke methane (CH_4)-hydrate dissociation (Hesselbo et al., 2007). This combined with an increase in terrestrial methanogenesis and a potential positive feedback associated with the decomposition of plant litter enabling further release of CO_2 and CH_4 from terrestrial sources (for example, Pieńkowski et al., 2016; Them et al., 2017), thus created the large negative CIE and enhanced CH_4 driven global warming. Coupled ocean-atmosphere models suggest an increase in global precipitation rates of+9 cm per year driven by the subsequent rises in CO_2 (Dera and Donnadieu, 2016). Increased continental weathering rates of up to ~3 times larger than before the excursion (Percival et al., 2016), have also been suggested based on a positive excursion in $^{187}Os/^{188}Os$ within the Jet Rock beds of Yorkshire and at Mochras (Percival et al., 2016) (Figure 4.1). These imply a warmer but wetter world; an expected feedback response to greenhouse induced warming (McElwain et al., 2005). Hence suppression of the rise in fire-activity throughout the negative CIE may be due to a significantly wetter climate, damping any pO_2-fire response. Of significance however, is the ability of fire-activity to continue at background levels, which may indicate rising pO_2 enabling fuels with higher moisture contents to continue to burn at a similar level to before the event Watson, 1978; Belcher et al., 2008; Belcher et al., 2010a).

Towards the end of the T-OAE the $\delta^{13}C$ record rises to more positive values again. At the same time, charcoal abundances at both sites increase, and remain elevated until the point of the T-OAE's termination. This synchronous rise begins at an estimated ~1 Myr (Huang and Hesselbo, 2014) after the start of anoxia, with charcoal abundances remaining elevated for an inferred ~800

kyr (Huang and Hesselbo, 2014), before returning to near background values (Figure 4.4).

Following the negative CIE, palaeoclimatic conditions are hypothesized to have gradually cooled and dried, continuing well beyond the point of the T-OAE termination (Dera et al., 2009; Korte et al., 2016). Climatic drying will have likely aided any pO_2 driven enhancement of fire-activity, removing the suppression of fire under the wetter conditions of the CIE. Importantly however, beyond the OAE termination, charcoal abundances no longer track the inferred climate changes and instead decline despite the hypothesized climate continuing to dry and cool. Instead, after an inferred ~800 kyr (Huang and Hesselbo, 2014) of enhanced fire-activity the system appears to return to near background functioning, evidenced by the decline in charcoal at Peniche between 33.2 m and 38.2 m, and at Mochras between 785 m and 771 m.

Variations in pO_2 are anticipated to occur over Myr timescales (Lenton and Watson, 2000b; Catling and Claire, 2005; Lenton, 2013), due to the long residence time of oxygen within the ocean-atmosphere system (Handoh and Lenton, 2003; Catling and Claire, 2005), which is set by the large reservoir of oxygen in the atmosphere, ~ 3.7 x 10^{19} mol (Catling and Claire, 2005), divided by the relatively small flux of oxygen from C_{org} burial ~18 x 10^{12} mol oxygen yr^{-1} (Catling and Claire, 2005; Hoegh-Guldberg and Bruno, 2010). The major enhancement of fire-activity for ~800 kyr is strikingly similar to the Myr timescale required for hypothesized global pO_2 reservoir variations (Handoh and Lenton, 2003; Catling and Claire, 2005). In the model of Handoh and Lenton (2003), increased C_{org} burial across the OAE should lead to a gradual rise in pO_2 and an increase in fire-activity, which leads to suppression of vegetation and a decline in chemical weathering rate (particularly of phosphorous) towards the end of the OAE (Handoh and Lenton, 2003). The latter prediction appears to be supported by the rapidly declining $^{187}Os/^{186}Os$ towards the end of the T-OAE (Cohen et al., 2004; Percival et al., 2016). Some Earth system models (for example, COPSE (Bergman et al., 2004) depend on the sensitivity of fires to pO_2 and the impact that fires have on vegetation biomass (Bergman et al., 2004; Lenton, 2013) to regulate pO_2. Fire is estimated to suppress Earth's present day vegetation biomass by 50% (Woodward et al., 2001) at pO_2 ~21%, yet fire cannot be sustained (and therefore cannot suppress vegetation) below

pO_2 ~15–17% (Belcher and McElwain, 2008). Even a modest increase in pO_2 driven by enhanced C_{org} burial during the T-OAE, from, for example, the base level of pO_2 (~20%) estimated for the Jurassic (Bergman et al., 2004; Lenton et al., 2013) to 21%, could have led to a 5% increase in burn probability due to the rapid response of fire to pO_2 around this baseline level (Belcher and McElwain, 2008). This in turn could have significantly enhanced the suppression of vegetation by fire (Lenton, 2013) by the end of the T-OAE. The resulting fire suppression of plant-driven phosphorus weathering may have assisted in terminating the T-OAE by reducing the input of phosphorus to the ocean and therefore productivity and oxygen demand in the water column. This effect would have combined with the direct effect of rising pO_2 re-oxygenating the ocean and in turn causing phosphorus to be more efficiently removed to sediments (Handoh and Lenton, 2003). Specifically, as the ocean starts to re-oxygenate this is predicted (Handoh and Lenton, 2003) to increase the removal of phosphorus adsorbed to iron oxide minerals (Fe–P)) (Colman and Holland, 2000) and that preserved in organic matter (Org-P) (Van Cappellen and Ingall, 1994; 1996), lowering the ocean PO_4 concentration and thus lowering oxygen demand in the water column—a strong positive feedback amplifying the re-oxygenation of the ocean. The data presented here provides the first fossil evidence that pO_2 driven fire-feedbacks may have played a significant role in terminating ocean anoxia. We note that further work at additional study site(s) away from the Tethys region would be required to provide evidence that this fire response to rising pO_2 was global in extent.

4.6 Conclusion

In conclusion, the observed increase in abundance of fossil charcoal, taken as a proxy for fire-activity occurring towards the end of the T-OAE is hypothesized to be primarily driven by increased pO_2, providing the first fossil-based evidence to support the postulation that OAEs are terminated by a rise in pO_2 levels. Thus the response of fire to Earth system perturbations across the T-OAE appears to capture a geologically rapid enhancement of pO_2 implying that relatively small but significant changes in this key atmospheric gas may be possible over the timescale of an OAE. Such rapid C-cycle driven changes to pO_2 suggest that new higher time-resolution models of pO_2 over Earth's history may be required to explore the relationship between changes in C-cycling and Earth system functioning. This is critical because it appears that oxygen-fire feedbacks have the ability to regulate key processes that help re-oxygenate the ocean during perturbations to C-cycling and return the Earth system to background functioning. Given that that modern ocean is 'on the edge of anoxia' (Handoh and Lenton, 2003) and observations that the Earth system may take millions of years to regain background function if the ocean is tipped into an anoxic state, it will be critical to manage anthropogenic disruption to the C-cycle and maintain the natural functioning of wildfire-activity in order to regulate the Earth system within habitable bounds.

5. Climate change drivers and fire history across Cretaceous OAE 2

5.1 Introduction

Periods of ocean anoxia were common throughout the Cretaceous, evidenced in the geological record by common occurrences of widespread black shales (Jarvis et al., 2011) (e.g. Weissert Event; Faraoni Event, Selli Event, Paquier Event, Breistroffer Event; OAE 2 and OAE 3). Oceanic Anoxic Event II (OAE 2) is considered to be the "most widespread and best defined OAE of the mid-Cretaceous" (Turgeon and Creaser, 2008, p. 323) and occurred ~93.5 Ma across the Cenomanian-Turonian boundary (Turgeon and Creaser, 2008; Barclay et al., 2010).

In the previous chapter, an increase in total charcoal abundance during the final stages of the T-OAE, were hypothesized to be indicative of increases in atmospheric pO_2 concentrations, driven by enhanced burial of C_{org} during the OAE. However, OAE 2 occurs during a period of estimated already high atmospheric pO_2 concentrations, of between 23% vol. and 27% vol. (Lenton, 2013, Mills et al., 2016). These are values that are significantly higher than the 20% to 21% vol. estimated for the Jurassic period (Lenton, 2013). Between pO_2 concentrations of 23% and 27% vol. laboratory experiments show that probability of ignition and fire spread (defined as burn probability by Belcher et al., 2010) becomes much less sensitive to changes in O_2 (Belcher et al., 2010). Thus, any changes in pO_2 driven by C_{org} burial during OAE 2, are likely to be much less important in terms of driving major changes in fire. This suggests that variations in fire and the associated abundance of charcoal in the fossil record, might be more likely to be driven by other factors superimposed upon the general high fire activity assumed throughout much of the Cretaceous (Glasspool and Scott, 2010; Belcher and Hudspith, 2016). This potentially makes OAE 2 a strong candidate for assessing the possibility of shorter time scale climate responses to Earth system perturbations across OAEs, which might be evidenced by the fossil record of fire.

Despite the major change in fire activity across the T-OAE, attributed to C_{org} burial driven enhancement of pO_2, Baker et al. (2017) hypothesized that the geologically short-lived increase in charcoal abundance during the initiation of the T-OAE was likely driven by CO_2/CH_4 induced climate change. Similarly, the onset of OAE 2 has been linked to climatic changes (e.g. Jarvis et al., 2011). OAE 2 is hypothesized to have been triggered by an influx of volcanically derived CO_2, driving increases in global temperatures, enhancing the hydrological cycle and increasing continental weathering rates (Du Vivier et al., 2015; Jenkyns et al., 2017). These changes coupled with rising sea level appear to have enabled a flux of otherwise limiting nutrients to the marine system, enhancing primary production and C_{org} burial (Mort et al., 2007; Pogge von Strandmann et al., 2013; Du Vivier et al., 2014, 2015).

Support for this idea comes from high-resolution stomatal pCO_2 proxy analysis conducted for the initiation of OAE 2, and into the early stages of anoxia. This method has identified two distinct periods of CO_2 release followed by CO_2 drawdown (Barclay et al., 2010). Barclay et al. (2010) estimated that CO_2 levels began to rise gradually prior to the start of the OAE, reaching a peak of $\sim 500^{+400}/_{-180}$ ppm within the OAE 2 interval (Figure 5.1). However, this overall rise in pCO_2 is interrupted by two inferred rapid phases of CO_2 drawdown, which also appear to be expressed in the global $\delta^{13}C_{org}$ record as small positive excursions (Barclay et al., 2010). These rapid changes in pCO_2 are hypothesized to have led to significant climatic changes, causing large shifts in northern hemisphere temperatures and the hydrological cycle (Jenkyns et al., 2017).

The study of the charcoal fossil record during the early stages of OAE 2 could therefore provide key information regarding the relationship between rapid changes in the C-cycle, climate, and wildfire activity occurring over medium (hundreds of thousands of years) timescales.

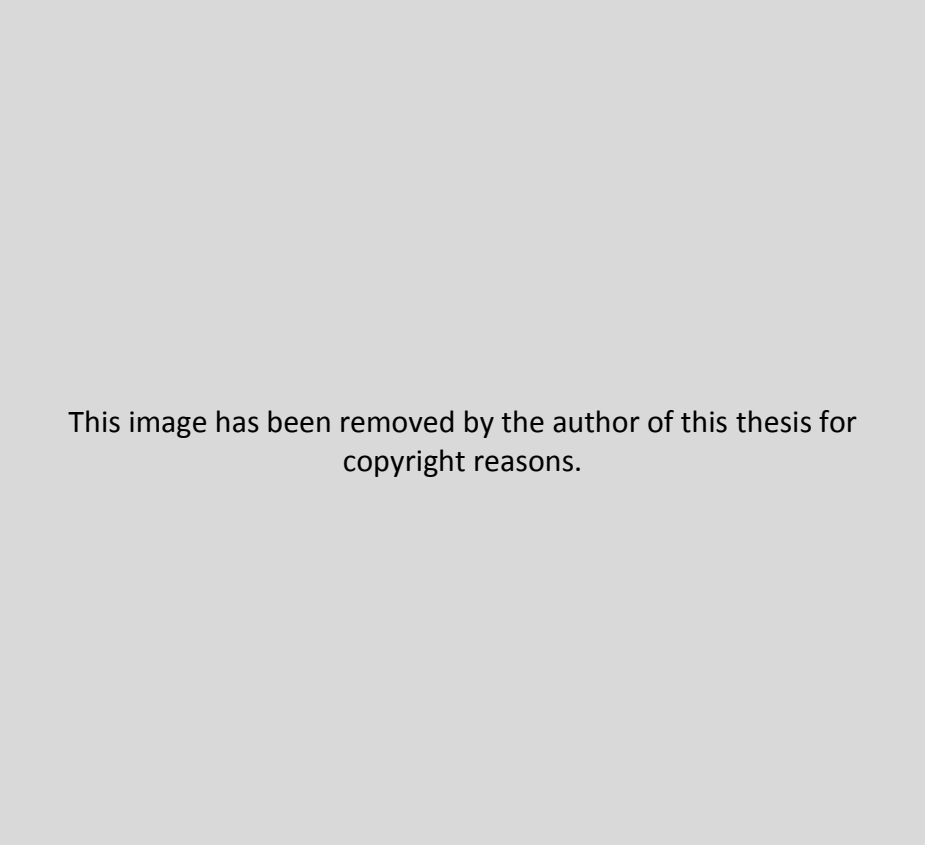

Figure 5.1 – Collected data across OAE 2, taken from Barclay et al. (2010), showing the composite stratigraphic section; terrestrial $\delta^{13}C_{org}$ curve, stomatal index and estimated CO_2 changes across OAE 2 within the Dakota Fm, Utah, U.S.A.

5.2 OAE 2

The mid-Cretaceous period (123-93 Ma) is believed to have experienced high seafloor spreading rates and periods of extensive volcanic activity, resulting in high pCO_2 levels and increased global temperatures (Jarvis et al., 2011 and references therein). Mean average global temperatures during the Cretaceous are suggested to have been between 2°C to 5°C higher than present day, with a low temperature gradient between tropical and polar regions (Barron et al., 1995; Schouten et al., 2003; Jenkyns et al., 2004; Laurin and Sageman, 2007; Zhou et al., 2012).

During the OAE, deposition of organic rich shales occurs and coincides with a shift towards positive $\delta^{13}C$ isotope values in both bulk organic matter (up to 6‰), and carbonates (of up to 3‰) (Figure 5.2) (Scholle and Arthur, 1980; Turgeon and Creaser, 2008; Barclay et al., 2010; Robinson et al., 2017) and

lasts from ~430 kyr to ~1 Myr (Barclay et al., 2010; Pogge von Strandmann et al., 2013).

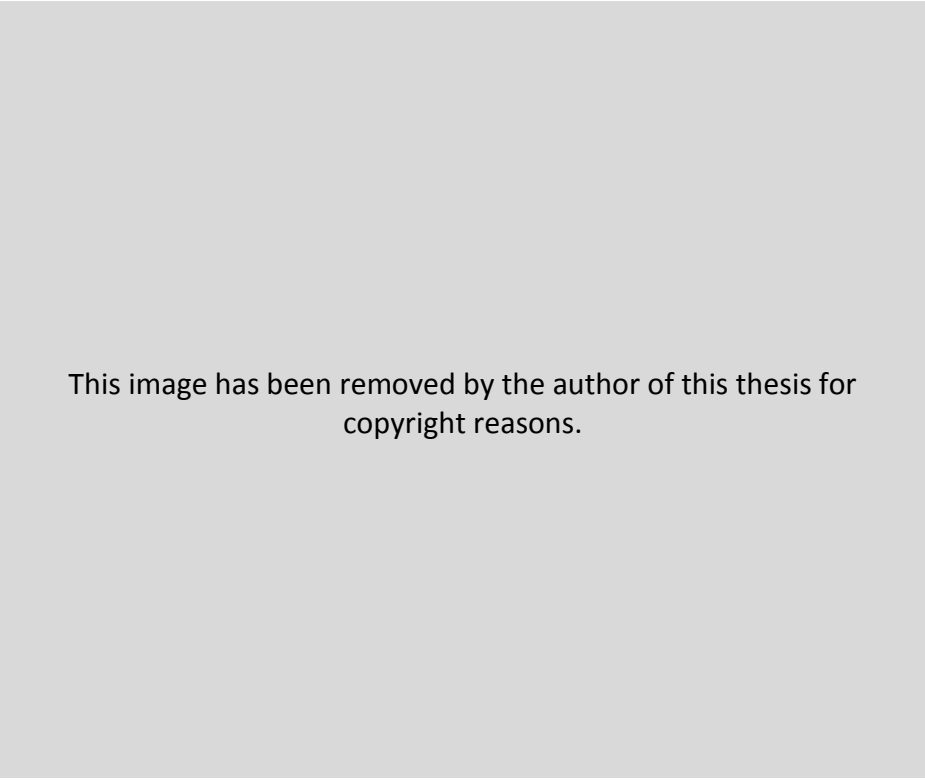

Figure 5.2 –Summary of Cretaceous OAE occurrences, illustrating a positive excursion in the bulk carbonate C isotope ($\delta^{13}C_{carb}$) record at the start of OAE 2 (modified from Robinson et al., 2017). $\delta^{13}C_{carb}$ data collected from: (5) Weissert et al. (1998); (6) Erbacher et al. (1996); (7) Jenkyns et al. (1994); (8) Jarvis et al. (2002); (9) Abramovich et al. (2003).

OAE 2 sediment deposits can be found across the globe (Figure 5.3), with notable records present in Europe, North and South America and just off the west coast of Africa (Jarvis et al., 2011). The global stratotype section and point (GSSP) for the C-T boundary is located at Pueblo (Colorado, U.S.A), and provides a near complete record across OAE 2 generally, and the C-T boundary in particular (Keller et al., 2004).

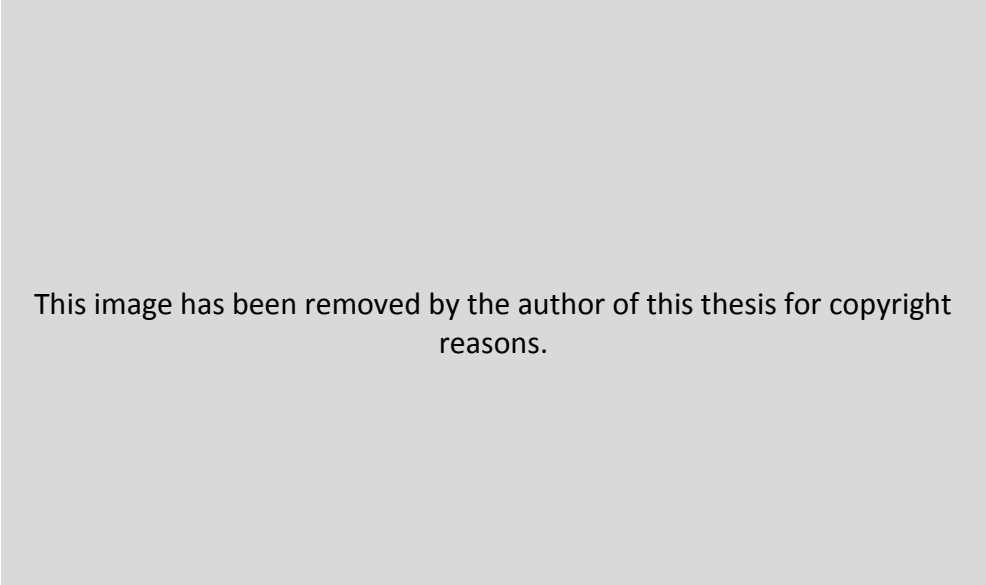

Figure 5.3 – Palaeo-map of the Cretaceous (~95 Ma), illustrating localities across the globe that present black shales/sediments with more than 1% total organic carbon, deposited during OAE 2 (taken from Robinson et al., 2017). “Plate reconstructions are from the Ocean Drilling Stratigraphic Network (http://www.odsn.de),”where localities are based upon Schlanger et al. (1987); Takashima et al. (2006) and Dickson et al. (2016) (Robinson et al, 2017, p. 7).

5.3 Materials and Methods

5.3.1 The Study Site

OAE 2 deposits can be found well exposed within the Dakota Formation, in southern Utah, located ~500 km west of Pueblo (Figure 5.4).

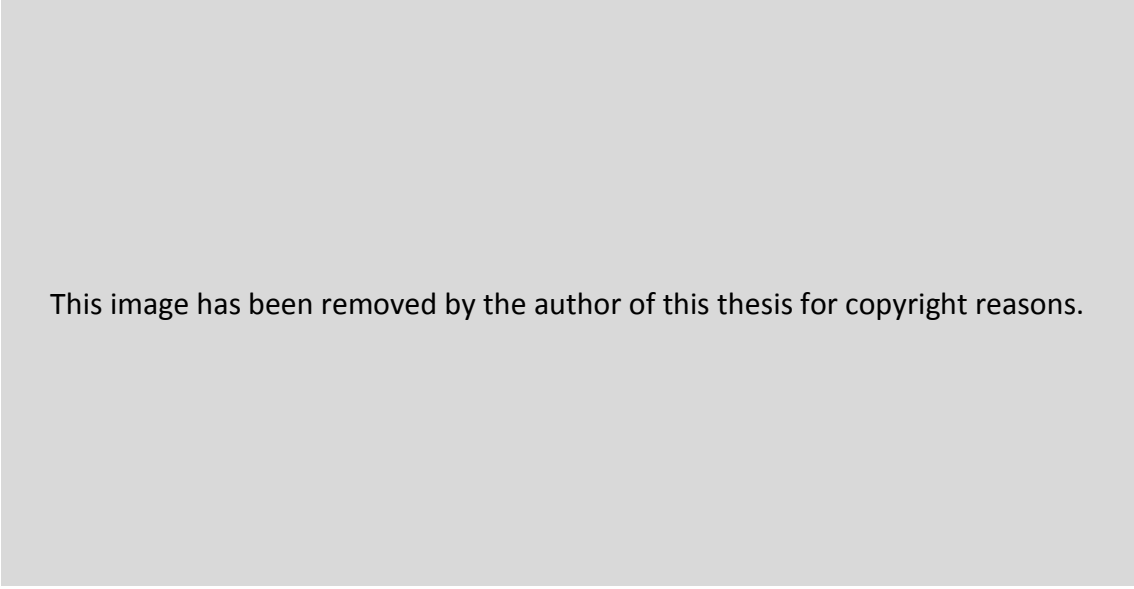

Figure 5.4 – Palaeomap of the Cretaceous, illustrating GSSP Pueblo (P) and the study locations across Utah and Colorado (adapted from Barclay et al., 2010). Study areas include Cedar Canyon (CC) (where 'Big Hill' samples were collected from), Kanarra Mountains (KM), Cottonwood Canyon (CWC), Wahweap Creek (WC). Blake Nose (B), Demerara Rise (D), Eastbourne (E), Gubbio (G), Pueblo (P) and Tarfaya (T) represent areas with relatively well studied OAE 2 sedimentary records.

At the Utah localities, the high rates of tectonic subsidence, coupled with high rates of sediment input, provide a stratigraphically expanded and detailed record of the OAE (Laurin and Sageman, 2007). A "high resolution biostratigraphic and bentonite-stratigraphic framework" is also available (e.g. Elder, 1985, 1991; Elder and Kirkland, 1985, Elder et al., 1994) (Laurin and Sageman, 2007, p. 731). During the Cretaceous, this site would have been located on the western margin of the Western Interior Seaway (WIS) situated within the Kaiparowits Basin (Uličný, 1999). The samples used in this study, kindly provided by R.S Barclay, were previously collected by Uličný, (1999) and Laurin and Sageman (2007) and used in Barclay et al. (2010). Samples were collected from numerous outcrops exposed between the Kanarra Mountains and the north-west margin of Lake Powell (labelled '3' and '4' respectively, Figure 5.5) that make up a composite log of the mid-Cretaceous sediments (Figures 5.6; 5.7).

The high sedimentation rate of these near-shore depositional sites, provides an expanded study section recording the early stages of OAE 2 (Laurin and Sageman, 2007), enabling the capture of potential small-scale variations in

wildfire activity, and allowing a detailed comparison with the associated pulses in CO_2 previously recorded by Barclay et al. (2010) (Figure 5.1).

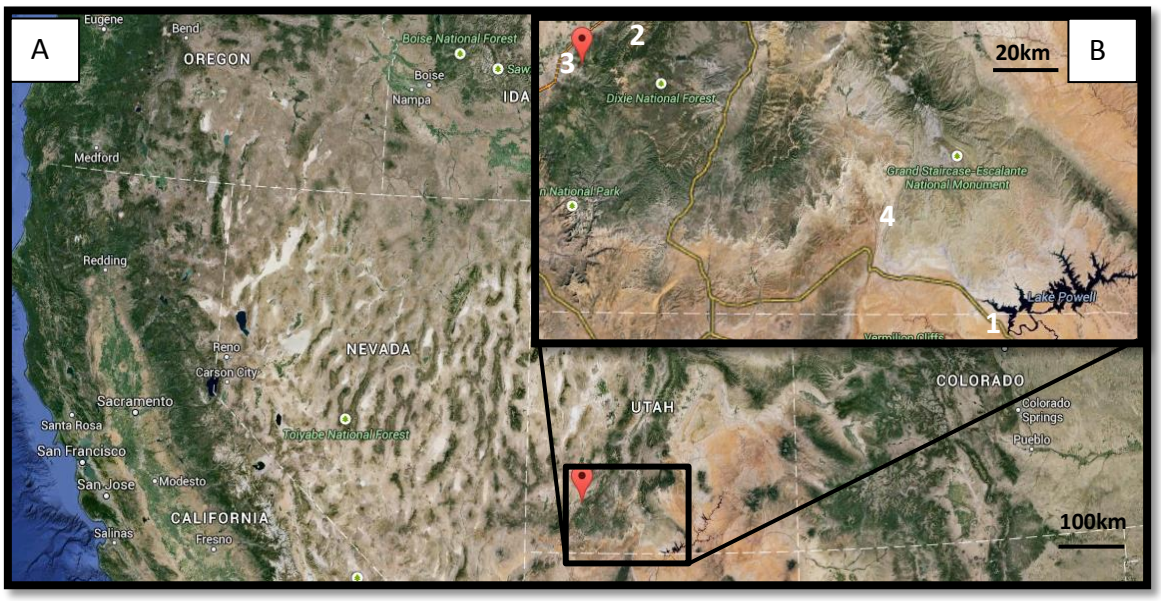

Figure 5.5 – A – Satellite image of Utah, United States of America. **B –** Satellite image illustrating where the sites are located for exposures of deposits across the Cretaceous OAE 2, within Southern Utah. Exposures were found and samples collected at Wahweap Creek (1), Big Hill (2), Kanarra Mountains (3) and Cottonwood Canyon (4). Satellite images courtesy of Google Earth.

5.3.2 Depositional Setting

The Middle and Upper members of the Dakota Formation have been extensively studied at high resolution by Uličný, (1999), and Laurin and Sageman (2007), with Uličný (1999) providing details on the Middle Dakota Formation, leading up to the beginning of OAE 2, whilst Laurin and Sageman (2007) provide details on the Upper Dakota Formation, following on from Uličný's (1999) study.

The sediments deposited during the OAE change significantly, displaying a range of depositional environments indicative of sea level fluctuations; these include sandstone, claystone and coal beds deposited within back barrier; fluvial and floodplain, lagoonal and peat swamp, shore-face, tide-influenced estuarine environments and semi-enclosed bays (Figures 5.8; 5.9) (Laurin and Sageman, 2007; Barclay et al., 2010). Transgressive and regressive phases during deposition can also be inferred from the sections (Uličný, 1999; Laurin

and Sageman, 2007). All sections have been extensively studied, with detailed accounts given by Uličný, (1999) and Laurin and Sageman (2007).

The middle member of the Dakota Fm is largely composed of non-marine sandstones; mudstones, organic rich claystones, coal horizons and carbonaceous mudstones, with any occasional marine strata representative of "short-lived marine incursions" (Barclay et al., 2015, p. 215). The upper Dakota member is characterized by "marginal marine sandstones, mudstones and shale" with an occasional organic rich claystone (Barclay et al., 2015, p. 216).

Samples for this thesis were from the middle and upper Dakota Fm and were chosen from two distinct lithologies across the OAE; organic-rich claystones and mudstones (with the exception of one siltstone). Sampling from predominantly just two lithologies, is intended to minimise any influence on charcoal abundances from the varying depositional environment, although the changes in inferred depositional environment are taken into account.

5.3.3 Methods

Bulk rock samples were kindly collected by R.S. Barclay, taken from organic mudstones and claystones across the OAE initiation (Figure 5.6; 5.7). For this study, the >125µm charcoal content was quantified (Appendices A and B) to capture a local-regional scale representation of palaeo-wildfire activity (Tinner et al., 2006). Due to the variations in depositional setting (Figures 5.8 and 5.9) and thus to ensure that charcoal abundances were not biased due to overall changes in the flux of organic material to the sites, the total organic matter (TOM) content left after acid maceration was weighed. Charcoal counts were then expressed as per gram of organic matter (g/TOM) (Figure 5.10).

Charcoal abundance expressed per 10g bulk rock, is also provided (Figure 5.10). The similar pattern of variations in charcoal abundances observed between the two graphs (charcoal count vs. charcoal abundance per g/TOM) corroborates the calculated abundance per g/TOM data, indicating that despite potential erosional surfaces and hiatuses between sampled intervals, the abundance per g/TOM data provides a good reflection of variations in charcoal across the OAE initiation.

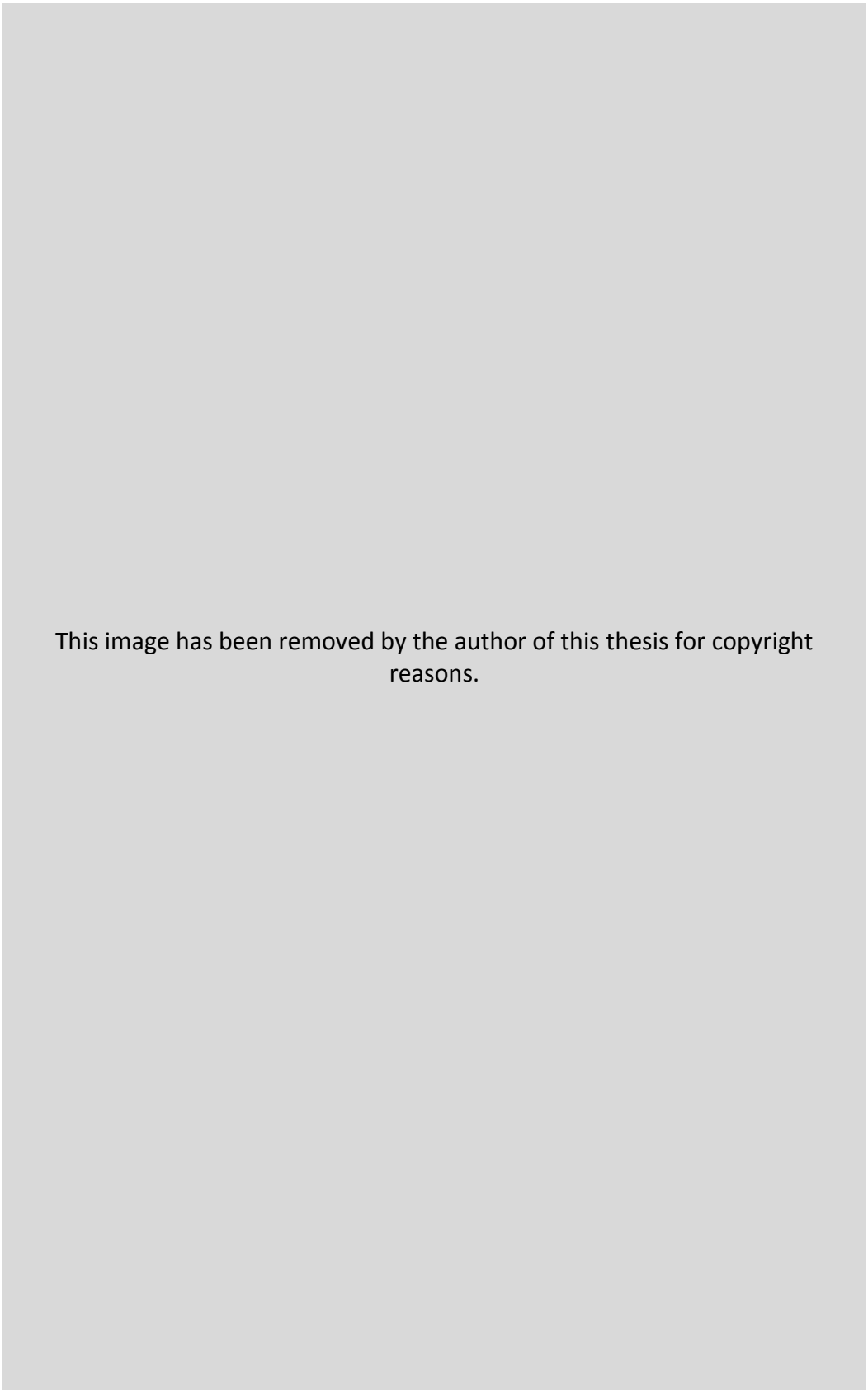

Figure 5.6 – Stratigraphic logs and respective $\delta^{13}C_{organic}$ values taken from bulk rock samples within the Dakota Fm, used to create the composite charcoal record. Location of samples used in this thesis (shown in red), and the positioning of Cretaceous OAE 2 is also shown. Logs and $\delta^{13}C_{organic}$ data modified from Barclay et al. (2010) according to R.Barclay *pers.comms.*

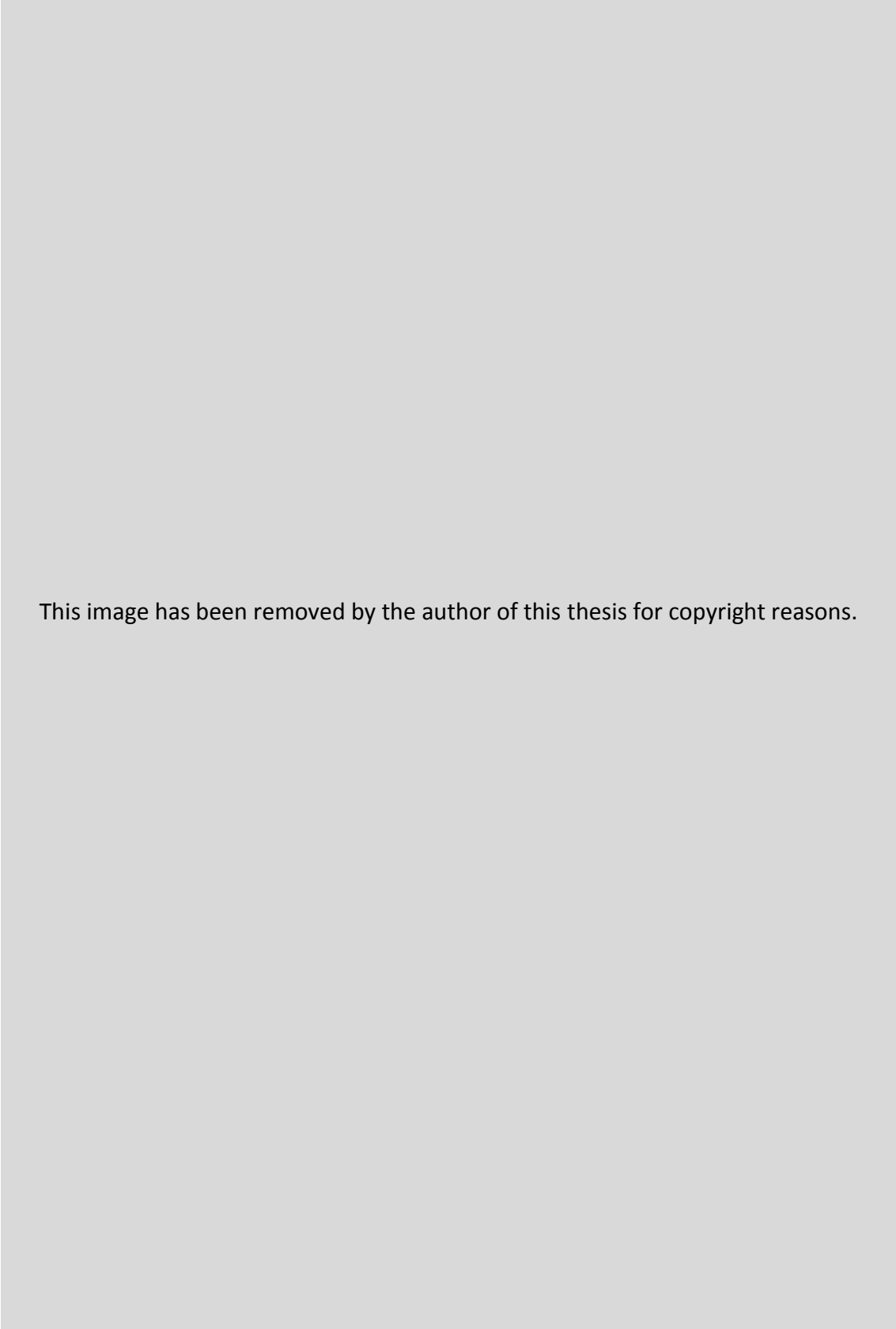

Figure 5.7 – Sedimentary logs for each study collection site detailing where samples were collected from. Logs modified from Barclay et al. (2010).

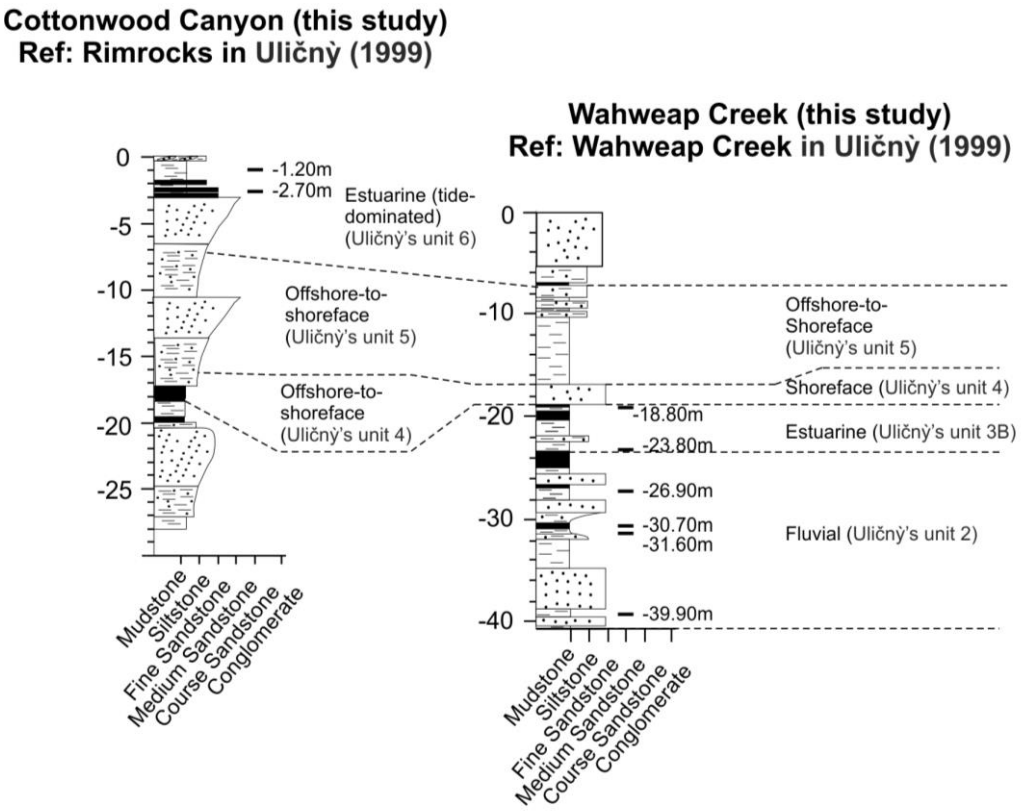

Figure 5.8 – Inferred depositional environment for Cottonwood Canyon and Wahweap Creek sections studied in this thesis, from correlations to the equivalent sections published in Uličný (1999). Correlations taken from those made in Barclay et al. (2010) (SI) according to R.Barclay *pers.comms.*

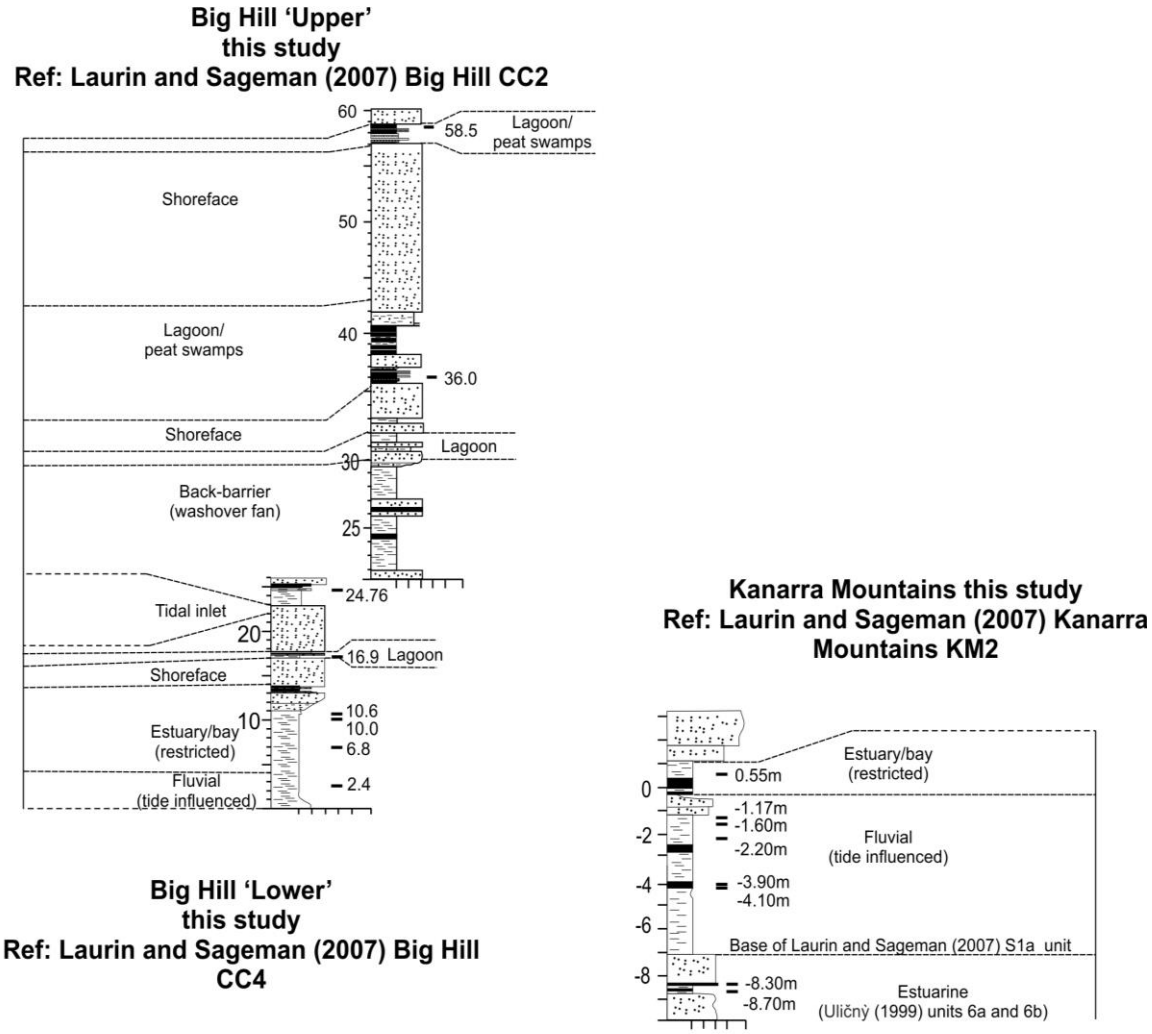

Figure 5.9 – Inferred depositional environment for Big Hill 'Upper', Big Hill 'Lower' and Kanarra Mountain sections from correlations to the equivalent sections published in Laurin and Sageman (2007). Correlations taken from those made in Barclay et al. (2010) (SI) according to R.Barclay *pers.comms.*

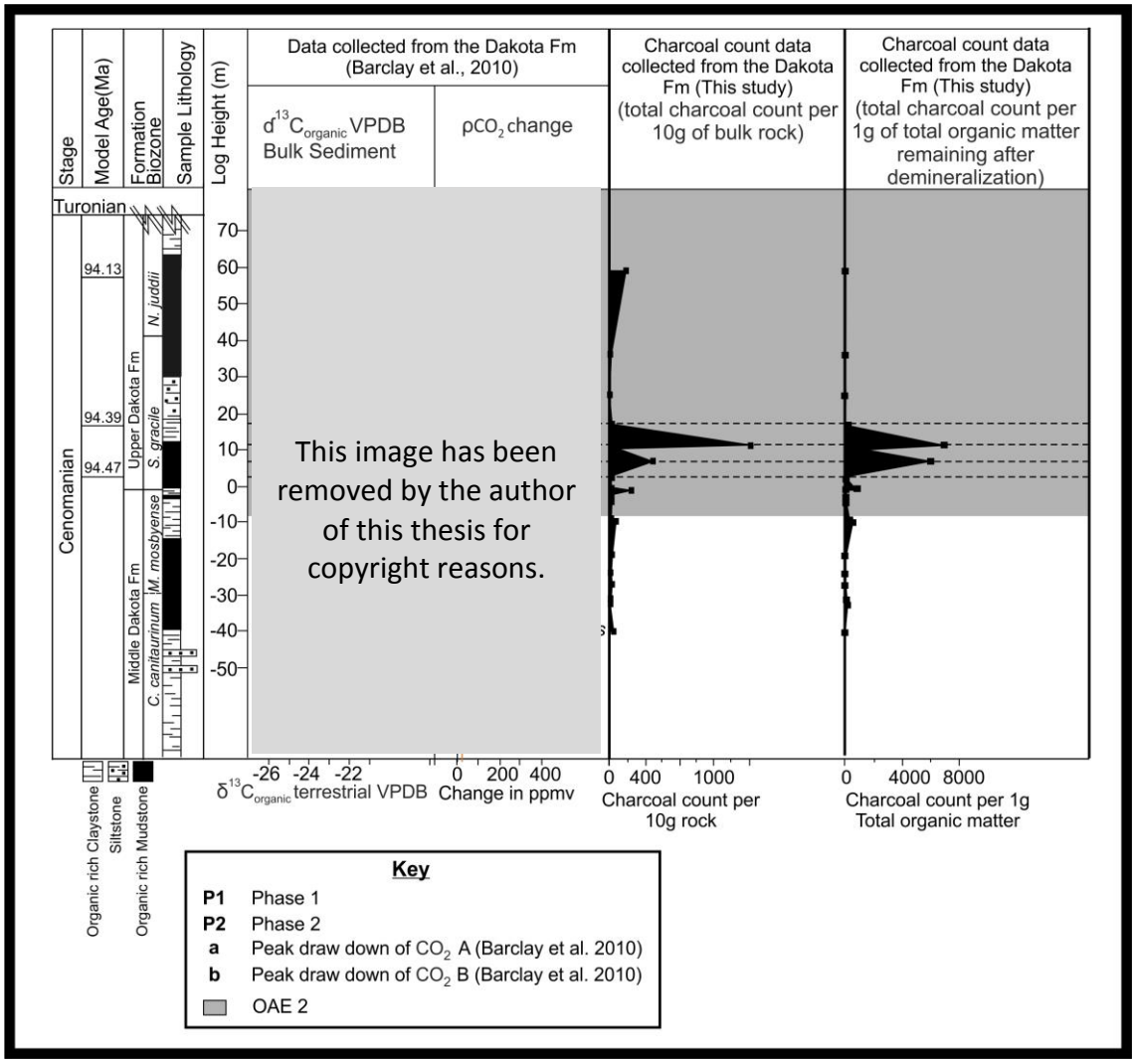

Figure 5.10 – Charcoal data from this study analysed from within the Dakota Fm across the initiation of OAE 2, displayed as total charcoal counts per 10g bulk rock, and total charcoal counted per 1g of total organic matter remaining after demineralization. Note the change in scale between the counted charcoal and the calculated abundance per g/TOM.

5.4 Results

The abundance of charcoal per g/TOM to the study site was found to be generally low prior to the OAE, up until log height +6.8 m (Figure 5.11), averaging 189 particles per g/TOM. An increase in charcoal abundance to 5965 particles per g/TOM occurs at +6.8 m log height. The charcoal abundance then declines briefly, although remaining above background at +10.0 m to 1446 particles, before increasing again at +10.6 m to 6947 particles per g/TOM. At +16.9 m charcoal abundance declines to just 186 particles, and remains below 35 particles per g/TOM throughout the rest of the studied OAE section.

Whilst the increase in charcoal abundance is based on only two data-points and therefore would require further study at a coeval section to corroborate this trend, importantly, variations in charcoal abundance do not correlate with any total organic matter variations (Figure 5.12), nor any change in the sample collection site (Figure 5.13), nor any variation in sample lithology (Figure 5.12). We therefore suggest that these factors are unlikely to be influencing the charcoal record. However, a change in the inferred depositional environment from predominantly estuarine and fluvial-floodplain deposits to an interpreted ‘semi-enclosed bay’ (Figure 5.9) (as suggested by Laurin and Sageman, 2007) must be taken into account.

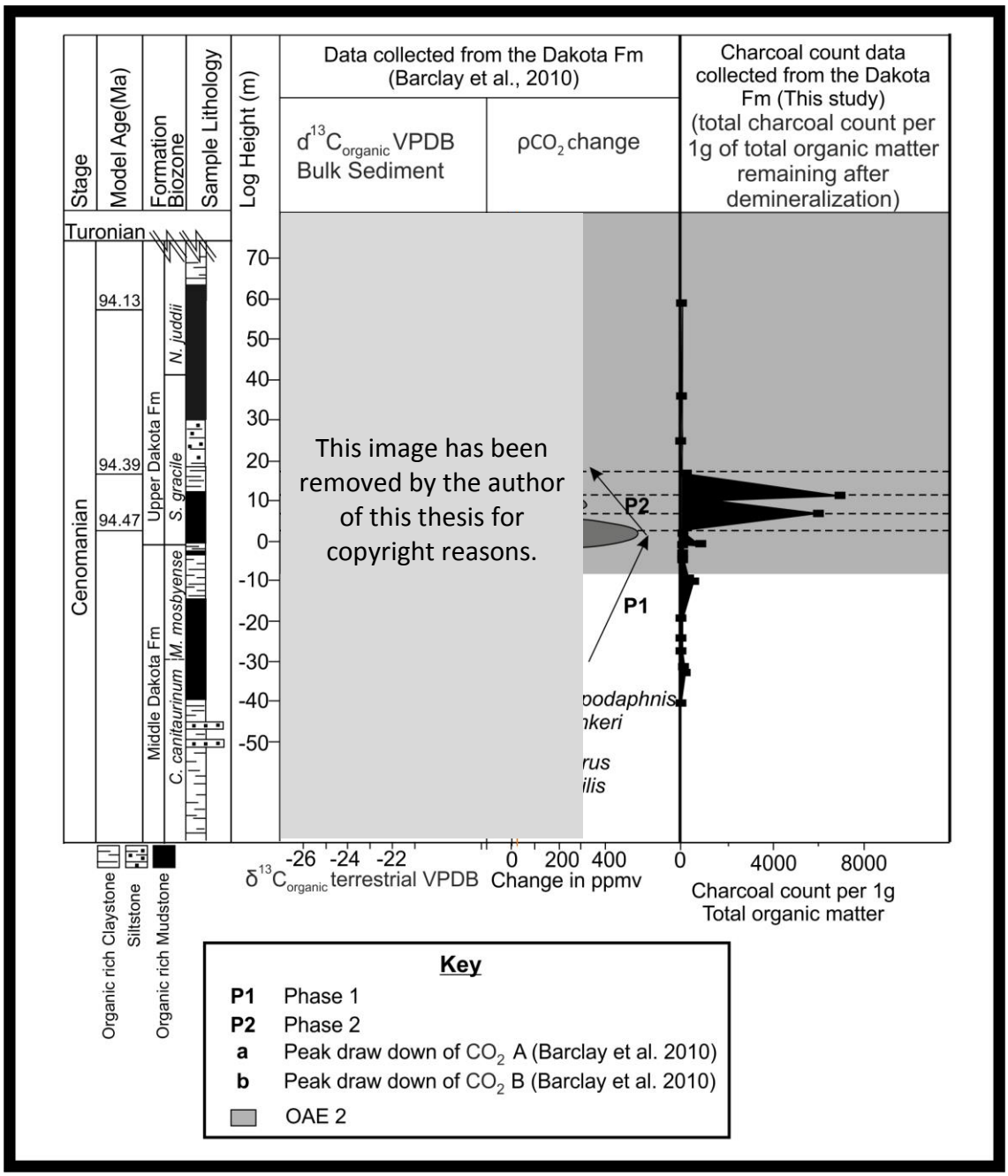

Figure 5.11 – Charcoal count per 1g of total organic matter variations across the early stages of OAE 2, plotted against $\delta^{13}C_{organic}$ curve and estimated changes in CO_2 from Barclay et al. (2010).

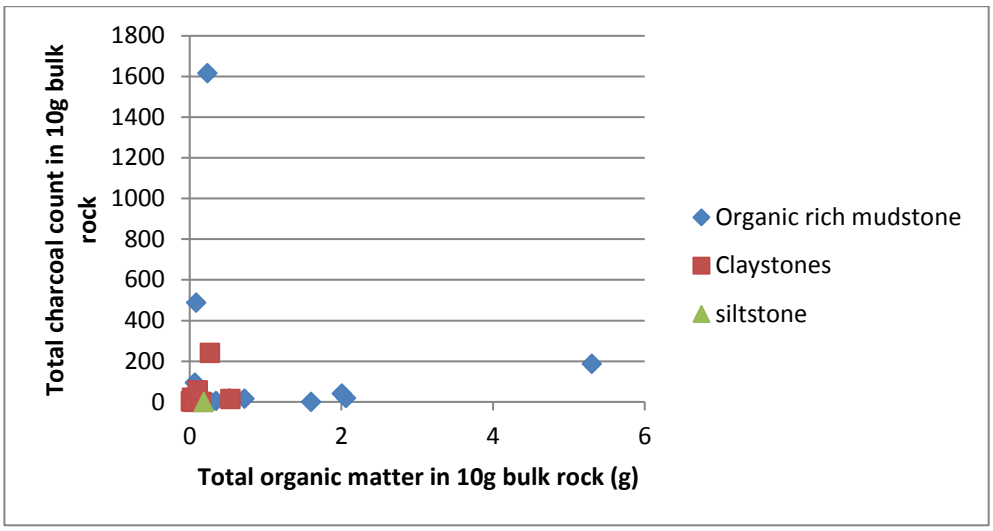

Figure 5.12 – Cross-plot of total >125µm charcoal abundance counted per 10g against total organic matter in 10g sample, illustrating no correlation between char abundances and total organic matter, nor within different facies.

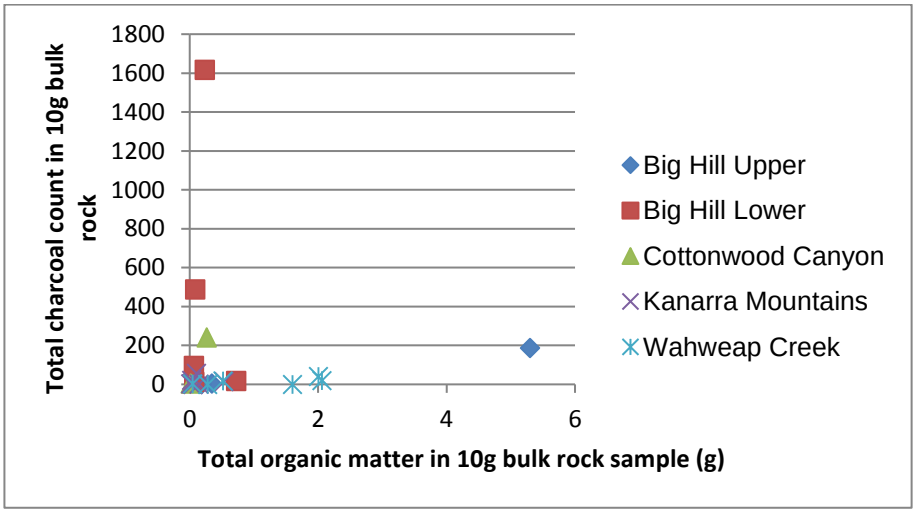

Figure 5.13 – Cross-plot of total >125µm charcoal abundance counted per 10g against total organic matter in 10g sample at the different sample locations, illustrating no correlation between char abundances and total organic matter found at different localities.

5.5 Discussion

5.5.1 Can the variations in charcoal abundance be driven by changes in depositional environment?

The changing depositional environments suggested to have occurred throughout the middle and upper members of the Dakota Fm (Uličný, 1999, Laurin and Sageman, 2007) could be considered to have influenced the charcoal signal preserved in these sediments. Below ~4.00 m log height, the depositional environment of the studied sections varies between fluvial (~-40.00 m to ~22.00m log height (Uličný, 1999)), tidally influenced estuarine (samples collected between ~-22.0 m to -19.5 m log height in Wahweap Creek; samples collected between 0.0 m and -3.0 m at Cottonwood Canyon, and samples collected between -10.0 m and -6.0 m at Kanarra Mountians) (Uličný, 1999; Laurin and Sageman, 2007)), and fluvial-floodplain deposits (~-6.00 m to ~-0.50 m at Kanarra mountians, and 0.0 m and ~+4.0 m at the Big Hill 'Lower' section (Laurin and Sageman, 2007)) (refer to Figures 5.8 and 5.9). The sample collected at -0.55 m in the Kanarra mountain section and the higher charcoal abundances found at 6.80 m; 10.00 m and 10.60 m within the Big Hill Lower section occur within sediments hypothesized to have been deposited within a semi-enclosed bay (Laurin and Sageman, 2007). The depositional environment then changes again to an interpreted tide-dominated estuary for the samples collected at 24.76 m log height, to a back barrier for the sample collected at 24.76 m (Laurin and Sageman, 2007), to lagoon/peat swamps for the samples collected at 36.00 m and 58.50 m log height (Laurin and Sageman, 2007).

Peat swamps, flood plain and lagoon settings are ideal catchment areas for charcoal produced by local fires, often constituting the basis for many Quaternary based charcoal studies (e.g. D'Costa et al., 1993; Ribeiro et al., 2016; Mackenzie and Moss, 2017). Fluvial environments may act to transport charcoal and other terrigenous material away to nearshore, shallow marine settings (Nichols, 2000; Forbes et al., 2006), such that, shallow marine settings and mouths of major rivers often receive the highest concentration of sediment transported by riverine and run-off processes (Nichols, 2000). Hence, a higher abundance of charcoal may be expected within the samples collected from the

inferred semi-enclosed bay environment (Laurin and Sageman, 2006), when compared with the samples collected from interpreted fluvial deposits. This could be suggested to explain the higher abundance observed for the samples collected at log heights 6.80 m, 10.00 m and 10.60 m, and the lower charcoal abundance found deposited within inferred fluvial environments at log heights -26.90 m to -39.90 m and -1.17 m and – 4.10 m. However, this would not seem to explain the low charcoal abundance found within the inferred lagoon/peat swamp environments, nor the sample collected at -0.55 m, interpreted by Laurin and Sageman (2007) to have also been deposited within a semi-enclosed bay. Furthermore the charcoal abundance observed between log heights 6.80 m and 10.60 m varies, yet the depositional environment remains constant. Hence another hypothesis for the observed changes in charcoal abundance in this section must be suggested.

Fluvial, estuarine and enclosed bay sediments would be expected to record charcoal abundances variably, due to time averaging and each individual sediment package representing different amounts of geological time. For example 10cm of mudrock does not usually represent the same amount of time as 10cm of sandstone, where sedimentation rates between rock types are highly variable. Furthermore, different sediment types typically also preserve organic material differently, where mudrocks typically better preserve organic material than sandstones (both wind and waterlain) (Gautier et al., 1985; Cai et al., 2007). Therefore, this difference would also be anticipated to introduce bias to the preservation of charcoal between the variable sedimentary units in this study. In order to account for this the charcoal counts have been expressed as per unit of organic matter.

The higher charcoal abundance in the enclosed bay sediments are therefore even more surprising because even allowing for consideration of charcoal abundance according to both organic content and sedimentation the bay deposits still contain considerably more charcoal than the fluvial deposits. This correction ought to be in favour of enhancing the charcoal abundance in coarser grained organic lean sediments and diminishing charcoal abundance in finer grained more organic rich sediments. Moreover, the sediments within the section that contain the highest organic content are the peaty lagoonal facies at

the top of the section, which sees a large decline in charcoal abundance expressed per unit of organics. Figure 5.10 shows how this adjustment to the raw charcoal abundance alters the patterns of charcoal throughout the section, highlighting that correcting for overall organic preservation does indeed decrease charcoal abundance comparatively (e.g. see log height +60m (peaty facies)). This also highlights that whilst, the peaks in charcoal abundance are decreased they still host charcoal contents way above the 'corrected' background for the site. This therefore argues that the inferred variations in fire activity are driven by factors outside of key depositional controls.

5.5.2. Climatic forcings on fire across OAE 2

Within the Dakota Fm, two distinct phases in estimated pCO_2 concentrations (Barclay et al., 2010) can be recognised: 1) is set against an overall rising trend in pCO_2 between ~-30 m log height and +2.5 m that is characterised by generally low charcoal abundances, and interrupted by a distinctive drawdown phase of pCO_2 labelled 'a'. 2) A second phase is set against an overall declining trend in pCO_2 from +2.5 m log height and marked by a major drawdown in pCO_2 phase labelled 'b' at ~+16.5 m log height (see Figure 5.11) (Barclay et al., 2010). The charcoal abundances quantified in this second phase are elevated during this period of estimated declining pCO_2 between log heights +6.8 m and +10.6 m (Barclay et al., 2010), and interestingly they appear to vary according to smaller variations in pCO_2 set against this falling trend.

5.5.2.1 Phase 1 (P1): Pre-OAE environmental changes

OAE 2 is hypothesized to have been triggered by a large magmatic episode, occurring ~ 80 kyr prior to anoxic initiation (Turgeon and Creaser, 2008; Barclay et al., 2010; Du Vivier et al., 2014; 2015; Jenkyns et al., 2017). During this time, a negative shift of osmium-isotope ($^{187}Os/^{188}Os$) data to un-radiogenic values (Turgeon and Creaser, 2008; Du Vivier et al., 2014) coupled with shifts in lithium (δ^7Li from carbonates) (Pogge von Strandmann et al., 2013), strontium ($^{87}Sr/^{86}Sr$ from marine shells and fragments) (Frijia and Parente, 2008) and lead (Pb ($^{206}Pb/^{204}Pb$; $^{207}Pb/^{204}Pb$; $^{208}Pb/^{204}Pb$) from clay-rich sediment samples) (Kuroda et al., 2007) isotopes are observed.

This negative movement of $^{187}Os/^{188}Os$ and $^{87}Sr/^{86}Sr$ isotope values across the OAE onset suggests mafic influence, whilst the coeval decline in δ^7Li indicates the weathering of sub-aqueous/sub-aerial mafic material. This is because the $^{87}Sr/^{86}Sr$ of seawater (measured from the shells and fragments) is predominantly controlled by riverine/run-off fluxes delivering terrigenous Sr that has been mobilized by continental weathering (which deliver an average isotopic ratio of ~0.710 to the oceans), and ocean hydrothermal processes, which delivers Sr mobilized from geothermal processes, often occurring along mid-ocean ridges, which supply a Sr isotopic ratio of ~0.703 (Hess et al., 1991; Frijia and Parente, 2008). Thus, variations in the $^{87}Sr/\ ^{86}Sr$ of the ocean through time can be used to provide information on climatic and geodynamic processes that control these fluxes, where positive shifts in marine $^{87}Sr/^{86}Sr$ ratios are commonly interpreted to represent periods of increased chemical weathering driven by climate and tectonic changes (e.g. Hodell et al., 1989). In contrast, negative shifts in $^{87}Sr/^{86}Sr$ are commonly related to increased submarine volcanism (e.g. Jones and Jenkyns, 2001). Similarly, $^{187}Os/^{188}Os$ isotope ratios are predominantly controlled by weathered continental crust (giving average ratio values of ~1.4), and submarine volcanism (values of ~0.13) (Du Vivier et al., 2014).

Lithium isotope fractions are further useful as “Li is almost totally situated in silicate and silicate secondary minerals so that, even in carbonate-rich catchments, Li is entirely dominated by weathering of silicate rocks (Kisakürek et al., 2005; Millot et al., 2010)” (Pogge von Strandmann et al., 2013, p. 668). The δ^7Li signal from ‘primary silicate rocks’ sits between ~0 – 5˚/₀₀ with basalt averaging ~2 – 5˚/₀₀ and continental crust averaging ~0˚/₀₀ (Pogge von Strandmann et al., 2013). In contrast, the δ^7Li signal in modern rivers is highly variable, exhibiting between 6 – 42˚/₀₀ (Pogge von Strandmann et al., 2013). This is hypothesized to be due to the preferential uptake of ^6Li by secondary clay minerals (Pogge von Strandmann et al., 2013), hence riverine δ^7Li signal represents sources from primary silicate rocks as well as secondary mineral formation (Pogge von Strandmann et al., 2013). Therefore a high δ^7Li riverine flux can be used as an indicator of high silicate weathering rates, whilst a low δ^7Li signal can be used as an indicator for high chemical weathering intensity (representative of the ratio of weathered material supplied to the oceans relative

to the amount retained by 'secondary mineral formation') (Pogge von Strandmann et al., 2013).

The shift in Pb isotopes towards "characteristic values of volcanic rocks from contemporaneous LIPs (Caribbean and Madagascar flood basalts)" (Kuroda et al., 2007, p. 211), found within the silicate sediment fraction in the Bonarelli section (Italy), provides further evidence for sub-aerial volcanism, where large releases of volcanic CO_2 and particulate minerals into the atmosphere enabled shifts in isotopic compositions found in European sections (Kuroda et al., 2007). Hence, a large magmatic/mafic influence, likely from LIP eruptions from the Ontong Java Plateau, Caribbean and Arctic Plateau and the Madagascar Flood Basalts, have been suggested as the likely trigger for OAE 2, coupled with increased sea floor spreading rates (Jenkyns et al., 2017 and references there in). The influence of this magmatic episode appears to link with the timing of rising CO_2 concentrations in the section studied here and by Barclay et al. (2010). The CO_2 rise begins well before the onset of anoxia - as evidenced by the first movement of $\delta^{13}C_{org}$ to positive values and stomatal estimates of pCO_2 (Barclay et al., 2010, Jenkyns et al., 2017). Rising pCO_2 concentrations, starting at ~-30 m log height (Figure 5.11), continue throughout the early stages of the OAE, peaking at an estimated $500^{+400}/_{-180}$ ppm at ~+2.4 m log height (Barclay et al., 2010).

Throughout this period, the charcoal abundances at the study site are generally low, rising a little at the onset of the OAE from 10 charcoal particles per g/TOM to 555 at -8.70 m although quickly returning back to 10 particles at 8.30 m. Increasing CO_2 concentrations have been associated with rising global temperatures and enhancements of the hydrological cycle (Weissert et al., 1985; Bazzaz, 1990; McElwain et al., 2005; Gedney et al., 2006; Steinthorsdottir et al., 2012), the latter might be anticipated to suppress fire activity by increasing fuel moisture. Temperature proxy data for sea surface temperatures (SST) from the TEX_{86} method and $\delta^{18}O$ also supports the idea that global temperatures rose in the lead up to OAE 2 (Forster et al. 2007; Sinninghe Damsté et al. 2008; Jarvis et al. 2011). Both proxies, taken from European sites and TEX_{86} from ODP sites at (equatorial) Demerara Rise and around the Newfoundland Basin (proto-North Atlantic, ODP 2176, ~30°N palaeo-latitude), indicate a warming trend in the lead up to anoxia. At high resolution, a short-term excursion towards higher $^{87}Sr/^{86}Sr$ isotope values has

also been observed across the onset of the OAE, coeval to the warming of sea waters, before the return to an overall negative $^{87}Sr/^{86}Sr$ trend (Frijia and Parente, 2008). This small, positive excursion is suggested to be a result of enhanced rates of continental weathering, driven by global warming induced hydrological changes, during the very early stages of ocean anoxia, that were capable of overriding any mafic influence on the $^{87}Sr/^{86}Sr$ signal (Frijia and Parente, 2008; Jenkyns et al., 2017). These changes, coupled with rising sea level are hypothesized to have enabled a flux of key, limiting nutrients to the marine system, driving increases in primary production and burial of C_{org} initiating ocean anoxia (Mort et al., 2007; Pogge von Strandmann et al., 2013; Du Vivier et al., 2014, 2015) and may have facilitated in the small flux of charcoal to the study site observed at -8.70 m.

Following rising pCO_2 concentrations, Barclay et al. (2010) note a brief decline in estimated concentrations at ~-4.6 m (labeled 'a' Figure 5.11). However, SST calculations using TEX_{86} in the Newfoundland Basin, offshore Canada (Forster et al., 2007) and the Bass River borehole, New Jersey (van Helmond et al., 2013), situated ~65 to 70 km east of our study site, suggest SST remained high, peaking at ~36.5°C at the Bass River site (van Helmond et al., 2013). Here, humid and potentially fire suppressing, 'greenhouse conditions' are thought to have prevailed despite the decline in CO_2 (van Helmond et al., 2013). Jenkyns et al. (2017) therefore postulate that the pCO_2 drawdown cannot "have outpaced any volcanogenic supply" as proxy data indicate temperatures were able to remain elevated (Jenkyns et al., 2017, p. 38).

During this period of inferred CO_2 decline ('a'), δ^7Li (from carbonates) (Pogge von Strandmann et al., 2013) and calcium ($\delta^{44/42}Ca$ (from carbonates)) (Blättler et al., 2011) isotope values recorded in European sections Eastbourne and Raia del Pedale continue to decline (Jenkyns et al., 2017).

As indicated with the δ^7Li, Ca isotopes can also be used as a proxy to identify changes in weathering (Jenkyns et al., 2017). This is because the marine Ca cycle constitutes inputs from mid-ocean ridges and riverine influx carrying Ca from continental weathering, and outputs via seafloor $CaCO_3$ deposition (Blättler et al., 2011). Fractionation of the Ca isotopes occurs during the precipitation of isotopically light $CaCO_3$ (Blätler et al., 2011), and this signature can alter due to

imbalances in input/output fluxes, such that changes in the Ca ratio can depict changes in climate (and thus global weathering).

Thus, the CO_2 drawdown observed close to the OAE onset is hypothesized to have been predominantly caused by the increased weathering of silicates (Jarvis et al., 2011, Jenkyns et al., 2017) occurring under an enhanced hydrological cycle (Frijia and Parente, 2008). This is coupled with increased C_{org} burial, evidenced by the movement of $\delta^{13}C$ towards positive values (Jenkyns et al., 2017). The decline in pCO_2 concentrations appears short lived, as stomatal estimates show rising CO_2 levels before a second, prolonged decline begins at +2.4 m log height, reaching minimum pCO_2 values at ~ +16.9 m ('b' Figure 5.11) (Barclay et al., 2010). Throughout the interval between -30 m and +2.4 m, charcoal abundances per g/TOM at the site remained consistently lower, ranging between 0 and 916 particles per g/TOM since prior to and during the early phases of the OAE (Figure 5.11). Irrespective of the depositional environment, this is perhaps surprising, as the Cretaceous period is considered by most to be a period of high pO_2 concentrations (e.g. Berner et al., 2003; Bergman et al., 2004; Mills et al., 2016).

At high atmospheric pO_2 concentrations (>23%) changes in fuel moisture become the more important driver of variations in fire activity (Watson, 1978; Watson and Lovelock, 2013) because changes in pO_2 alone above 23% vol. lead to little variation in burn probability (see Figure 4 in Belcher et al., 2010/ Figure 1.10 in Chapter 1 herein). However as pO_2 rises, increasingly wet fuel is able to carry a fire because the moisture of extinction (the point at which a fire can no longer spread) is raised. Belcher and Hudspith, (2016) modelled the differences in surface fire behaviour for different fuel types in both current ambient and in 'super ambient' 26% O_2 (Figure 5.14a).

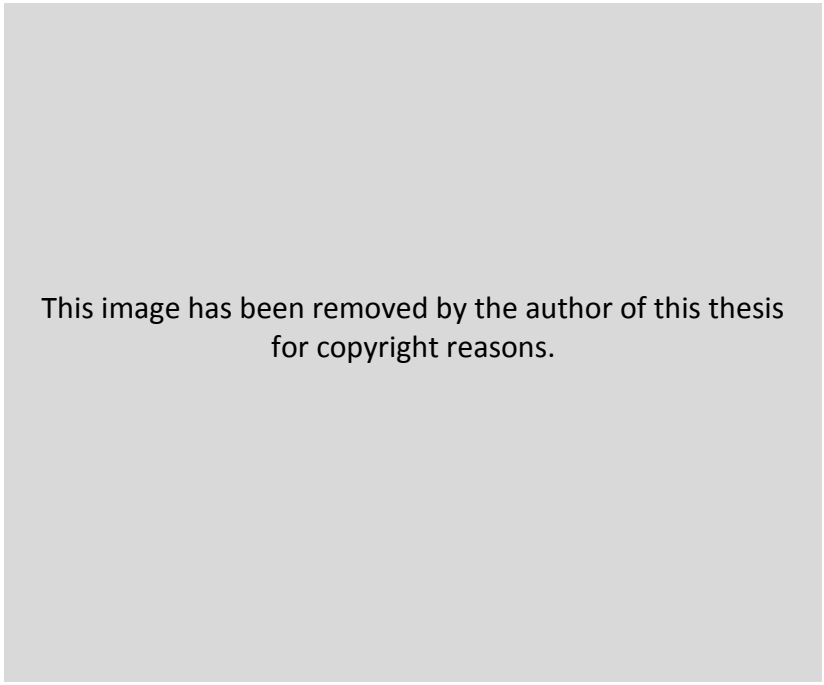

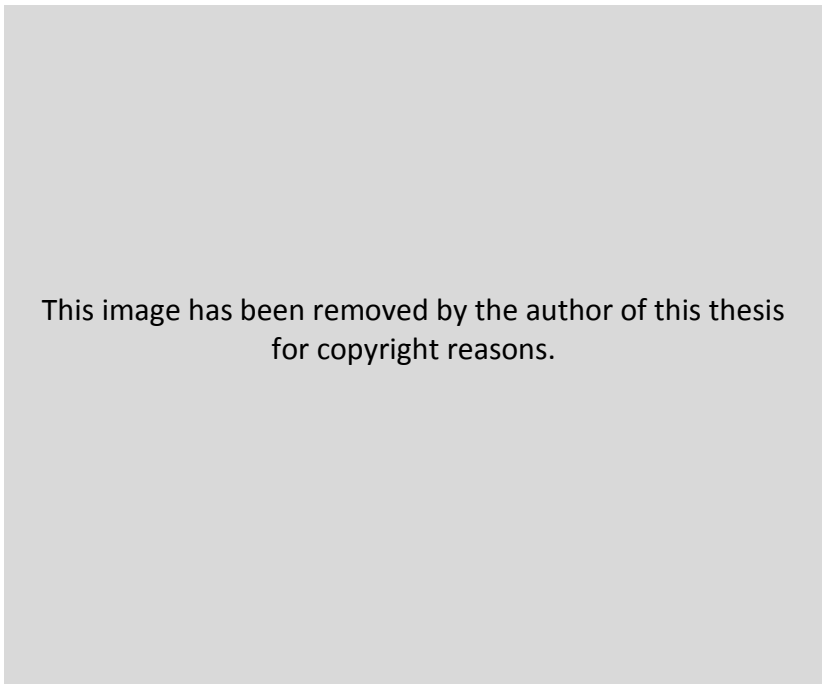

Figure 5.14 (a) Plots illustrating the estimated fire behaviour (modified from Belcher and Hudspith, 2016) showing different rates of fire spread in dead fuels with varying moisture content for four Cretaceous fuel models. CL – conifer litter; WUn – weed-dominated understory; SUn – shrub-dominated understory; FUn – Fern understory. Red lines and circles indicate model outputs for ambient O_2, whilst dashed black lines with grey circles indicate model outputs for super ambient O_2 (26%). Note that at ambient O_2, model estimates for all fuel types
end at a moisture of extinction of 39%.
(b) Extended (dotted) lines show rate of fire spread under super ambient O_2 (26%) up to a dead fuel moisture of 80%. This is based on the calculated moisture of extinction for super ambient O_2 equalling 80% for all fuel types (ref. Table S2, Belcher and Hudspith, 2016).

It can be seen that increasing pO_2 enables fires to continue to spread above 39% (modern day) moisture of extinction and that spread rate is also increased. However, there are limits to fire spread even at high pO_2, with Belcher and Hudspith (2016, Table S2) estimating the moisture of extinction to be ~80% at 26% pO_2 (Figure 5.14b). Belcher and Hudspith, (2016) used the equation $M_{ex} = 8O_2–128$ (Watson & Lovelock, 2013) to estimate moisture of extinction in their models. By assuming that pO_2 was between 25% and 27% during the period leading up to OAE 2 (Mills et al., 2016) then the moisture of extinction would be between 77% and 88%. If Belcher and Hudspith's (2016) surface fire spread data for different fuel types is extended across this range, a rise of just 10% fuel moisture would likely cease fire spread in their low fuel load models (their CL2 and WUn2 models) and halve the spread rate in higher fuel load models (their SUn2 and FUn2 models) (Figure 5.14b).

Furthermore, the intensity of surface fires (see Figure 3C in Belcher and Hudspith, 2016), would also fall significantly by ~2/3 from approximately 900 kWm^{-1} to 300 kWm^{-1} as fuel moisture increased. Most surface fires are started in dead and drier surface fuels. These surface fires then have to be able to dry the overstory canopy fuels below the required moisture of extinction before significant crown fires can be ignited and carried (note: most live fuel is >100% in its moisture content (Pollet and Brown, 2007)). This is significant because fireline intensity relates to flame heights and the ability of heat energy from surface fires, to scorch the forest canopy and transition to crown fires (see Belcher and Hudspith, 2016). Here, lowering of fireline intensity leads to lower flame heights and which therefore limits the ability of surface fires to dry, scorch and ignite the canopy. Therefore, the potential enhancement of the hydrological cycle, even leading to just a 10% rise in fuel moisture, in the phases leading up to onset of the OAE would be anticipated to have a strong negative influence on large fire potential, despite estimated high pO_2, and likely explains the relatively low abundances of charcoal to the study area.

5.5.2.2 Phase 2 (P2): During OAE environmental changes

Phase P2 starts from ~ +2.3 m log height and runs through to +16.9 m. It begins with the period of peak pCO_2 recorded in the section as estimated using the stomatal proxy method (Barclay et al., 2010), and ends at CO_2 minimum

labelled ‘b’ (Figure 5.11). The pCO_2 trend throughout this period is that of overall decline set with a brief enhancement of pCO_2 at ~+10.0 m log height. During this period the abundance of charcoal per g/TOM suddenly increases to 5965 particles per g/TOM/year at +6.8 m log height. Abundances appear to decline briefly at ~+10.0 m to 1446 particles g/TOM coincident with the brief rise in pCO_2, rise again peaking at 6947 particles g/TOM at +10.6 m log height, before falling to just 186 particles g/TOM at +16.9 m (Figure 5.11).

Sea surface temperature (SST) estimates using TEX_{86} data from the Bass River borehole, New Jersey, suggest that immediately after the first positive shift in $\delta^{13}C_{org}$ representing the onset of the OAE, SSTs began to rapidly decline, dropping by an estimated ~2.5°C (van Helmond et al., 2013). Data from onshore and offshore sections, including TEX_{86} data from the Newfoundland Basin (Sinninghe Damsté et al., 2010) and $\delta^{18}O$ data from the Gröben, Northern Germany (Voight et al., 2006), also show a sudden switch in global temperature trends to a period of cooling (Jarvis et al., 2011). This cooling is hypothesized to have resulted from the drawdown of pCO_2, where peak cooling occurs during minimum pCO_2 concentrations (Jarvis et al., 2011). Jarvis et al. (2011) tentatively link this period of ‘peak cooling’ to the Plenus Cold Event, identified in many European sections (including Eastbourne, UK and northern French sections) by an influx of boreal marine fauna (e.g. the belemnite *Praeactinocamax plenus*) (see Jarvis et al., 2011).

The overall decline in pCO_2 concentrations observed at the study site between log heights +2.3 m and +16.9 m, has been attributed to increased C-sequestration by primary production that were capable of drawing down twice the magnitude of CO_2 compared to the first CO_2 drawdown (labelled ‘a’) (Barclay et al., 2010). When correlated by Jarvis et al. (2011) using C-isotope stratigraphy and biostratigraphy to European section Pont d’Issole, this large drawdown of estimated CO_2 observed in the WIS, was found to be coeval with the period of SST cooling, where ‘b’ corresponds with minimum SST estimates. During the cooling phase, van Helmond et al. (2013) noted an increase in terrestrial to marine (T/M) ratios in the Bass River borehole, where saccate gymnosperm species in the pollen and spore assemblages were dominant. As their modern relatives, pine and spruce “are generally associated with relatively dry conditions (Willis et al., 1998)” (van Helmond et al., 2013, p. 125), van Helmond et al. (2013) interpret their sudden dominance to be indicative of drier

climate conditions. This is coupled with rising Ti/Al ratios, interpreted to be due to an increase in dust transported by the wind as “Ti concentrates in heavy minerals are mainly transported by wind” (van Helmond et al., 2013, p. 125). Van Helmond et al. (2013) therefore suggest that the drawdown of pCO_2, may have led not only to global cooling but also a drying of the climate. Interestingly Jenkyns et al. (2017) also find that at Eastbourne, as SST estimates show cooling, the δ^7Li isotope trend switches towards higher values of δ^7Li. This contrasts with the decreasing δ^7Li trend found during the onset of anoxia, postulated to be due to increased weathering of mafic material under rising pCO_2 concentrations (Jenkyns et al., 2017). Jenkyns et al. (2017) interpret this sudden switch in δ^7Li trends, as a decline in the weathering and degradation of silicate minerals under the cooler, climatic conditions occurring during a period of decreasing CO_2 concentrations.

Drier climate conditions can lead to a rise in wildfire activity by reducing the moisture content of fuels (Viegas et al., 1992; Collins et al., 2006). A decline in the moisture content of vegetation, below the required moisture of extinction, would enable and increase the rate of fire spread, fire intensity and also increase the likelihood that a surface fire would transition to a crown fire (Belcher and Hudspith, 2016). For example, a decrease in fuel moisture by 20% from a moisture of extinction of 80% at 26% vol. pO_2, would enable flame heights in surface fires carried in fern and/or shrub-dominated understories to reach ~1.6 m and ~1.7 m respectively (Belcher and Hudspith, 2016). These flame heights would likely enable the drying and scorching of the canopy vegetation up to around 10 m into the canopy and therefore likely increase the chance of ignition. Fuel moistures lower than the 60% inferred here could further enhance fire. It could therefore be suggested that during this period of CO_2 drawdown, climate conditions became more favourable to wildfire activity, enabling fire to spread more easily under the hypothesized drier climate and leading to a larger abundance of charcoal to the inferred semi-enclosed bay depositional site.

A brief decline in charcoal per g/TOM is observed to occur during phase P2 at +10.0 m log height, coeval with evidence for a small pulse in CO_2 (Figure 5.11). A small, swift reversal in the cooling and ‘drying’ trend during this phase can be observed in SST estimates and T/M ratios at the Bass River borehole, New

Jersey, before estimates rapidly return to reach peak cooling (see Figure 2, van Helmond et al., 2013). If found to be coeval with the estimated pulse in CO_2 at +10.0 m log height (Barclay et al., 2010), the geologically brief switch in SST and climate proxy data (van Helmond et al., 2013) could thus explain the brief decline in fire activity. However, further study involving higher resolution sampling at coeval study sites would be required to support this hypothesis.

As pCO_2 concentrations reach a minimum at 'b' (Figure 5.11), charcoal abundances decline to just 186 particle g/TOM, and remain low throughout the rest of the studied anoxic section. At the point of minimum CO_2 estimates ('b'), proxy estimate for SST also reach minimum values, estimated at ~28°C compared with ~33°C at the onset of anoxia (Jarvis et al., 2011), and begin to switch towards warmer estimates (Jarvis et al., 2011; van Helmond et al., 2013). Terrestrial/marine (T/M) ratios and Ti/Al ratios at the New Jersey site also shift towards values observed during the onset of the OAE (van Helmond et al., 2013).

Previously, the coupled increase in T/M and Ti/Al ratios were hypothesized by van Helmond et al. (2013) to be representative of drying of the climate. This was due to a dominance of saccate gymnosperm species within the T/M ratios – postulated to be reflective of relatively dry conditions, and the high Ti/Al ratios – interpreted to be due to an increase in dust transported by the wind (van Helmond et al., 2013). Hence, in contrast, declining T/M ratios and Ti/Al ratios are interpreted by van Helmond et al. (2013) to likely reflect a climatic shift towards more humid conditions and increased run-off rates.

Furthermore, at the European Eastbourne section, δ^7Li isotope values begin to once again increase, suggesting an enhancement of silicate weathering, before δ^7Li isotopes return towards pre-excursion values in the final stages of the OAE (Jenkyns et al., 2017). These conditions are anticipated to have prevailed for the remainder of the OAE (Jarvis et al., 2011; van Helmond et al., 2013). It could therefore be hypothesized that the return to low charcoal abundances, is due to the return to warm, humid conditions, where high fuel moistures once again supressed wildfire activity. This may explain the consistently low charcoal abundance found at log heights 36.00 m and 58.50 m which are inferred to have been deposited within lagoon/peat swamp environments.

5.6 Conclusion

Throughout the early stages of OAE 2, fluctuations in volcanically derived CO_2 are hypothesized to have led to significant changes in the global climate. The influx of CO_2 from LIPs during this time, was punctuated by two distinct drawdown periods that have been associated with increased C sequestration by primary producers (Barclay et al., 2010) and silicate weathering (Jenkyns et al., 2017). Here, we find that the first CO_2 decline close to the OAE initiation, where recent proxy data suggests increased silicate weathering may have aided in the drawdown of CO_2 concentrations (e.g. Jenkyns et al., 2017) (alongside C sequestration), appears to have had little influence on the climate and inferred wildfire activity. However, the second, longer period of CO_2 decline has a significant impact on wildfire activity at the Western Interior Seaway site. Published proxy data indicate that during this draw down of CO_2, global cooling and possibly drying of the climate occurred (van Helmond et al., 2013; Jenkyns et al., 2017). δ^7Li isotope values indicate a brief period during the OAE where silicate weathering declined, and C sequestration by primary producers became the dominant drawdown mechanism of volcanic CO_2 (Barclay et al., 2010; Jenkyns et al., 2017). During this period, inferred wildfire activity appears to have suddenly increased, evidenced by a high charcoal abundance that remains elevated until minimum CO_2 concentrations were reached.

Although variations in depositional environment occur, fluctuations in charcoal abundance do not appear to link with changes in the depositional environment. Thus, the higher charcoal abundances may likely have been driven by an inferred drier climate during CO_2 drawdown, occurring during the early stages of anoxia. Our data illustrates that climate driven changes in wildfire activity may be observed even under the modelled high pO_2 concentrations of the Cretaceous period, and also illustrates how irrespective of changing depositional environment, hypothesized changes in the hydrological cycle, and likely moisture content of fuel, appear to be the dominant control on wildfire activity. Our charcoal data provides further support for significant and geologically rapid climate shifts occurring during the early stages of OAE 2 associated with fluxes in volcanically derived pCO_2 concentrations.

6. Background rhythms of Earth System changes: The Milankovitch cycles

6.1 Introduction to the Milankovitch cycles

The Earth's climate is continuously changing. As the Earth orbits around the sun, the amount of solar energy the Earth's surface receives changes resulting in natural, cyclic variations in climate both regionally, between the northern and southern hemispheres, and globally (Berger et al., 1992). These natural variations in solar radiation are caused by changes in the shape of the orbit and positioning of the Earth on its axis around the sun, referred to as 'Milankovitch cycles' that currently occur over timescales of ~23 kyr, ~41 kyr, ~100 kyr and ~400 kyr (House, 1995). As the sun is considered "by far the most important driving force of the climate system" (Beer et al., 2000, p. 403), these orbital cycles are thought to be responsible for driving periodic and prominent changes in climate, some of which have included the pacing of widespread glaciations (Berger, 1988; Bennett, 1990; Imbrie et al., 1992; Ruddiman 2006), as well as the pacing of increased burial of organic carbon (C_{org}) in the oceans over longer timescales (e.g. Martinez and Dera, 2015). Understanding and identifying these periodic changes in solar insolation is therefore deemed crucial, particularly in respect to "the ongoing evolution of climate" (Martinez and Dera, 2015, p. 12604), with or without the influence of man.

The theory that fluctuations in solar energy may force significant changes in climate was first proposed by Jospeh Adhémar in the late 1800's, but was later developed by James Croll (1875; 1885) who hypothesized that the occurrence of ice ages must have something to do with the astronomical control on the amount of sunlight the Earth received during winter months (Bowen et al., 1986; Loutre, 2003). However, it was in 1924 with a publication by Milutin Milanković using a mathematical theory, which really developed the astronomical

hypothesis for the Pleistocene ice ages. Milanković's calculation of orbitally induced changes in solar insolation and climate enabled the production of radiation curves, illustrating high northern hemisphere insolation changes (Loutre, 2003). These orbital forcings comprised precession, obliquity and eccentricity cycles, each of which have a different periodicity and can interact with one another to amplify or weaken the forcing effect (Martinez and Dera, 2015).

6.1.1 The Precession Cycle

The shortest orbital cycle, the precessional cycle, is produced by a 'wobble' of the Earth as it spins (Figure 6.1) and has a current periodicity of ~23 kyrs (Looney, 2011). During periods of minimum precession index, for the southern hemisphere, and thus maximum precession index for the northern hemisphere, solar insolation in the northern hemisphere is at its highest during the summer months (summer solstice coincides with perihelion (closest point in the Earth's orbit to the sun)), thus making northern hemisphere summers generally warmer (Tuenter et al., 2003; Daniau et al., 2013), and winters cooler, as the winter solstice coincides with aphelion (furthest point away from the sun) (Figure 6.2). This results in high seasonal contrast in the northern hemisphere and low seasonal contrast in the southern hemisphere. The opposite is true for maximum precession index in the southern hemisphere (Tuenter et al., 2003). The precession cycle can therefore exert a control over the strength of the seasons in one hemisphere compared to the other, although its effects are dominant in tropical regions and low-latitude continental climate belts (Sha et al., 2015; Martinez and Dera, 2015).

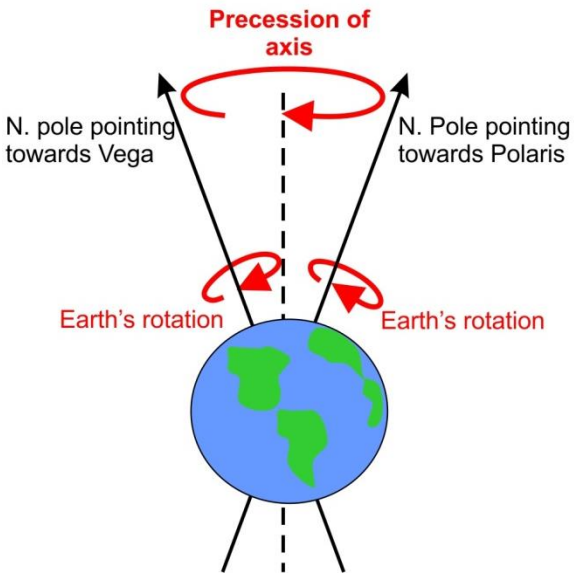

Figure 6.1 – Illustration of the movement of the Earth during a precessional cycle

The magnitude of the precession cycle is determined by the eccentricity of the Earth's orbit, thus the precession index is defined as $e\sin\tilde{\omega}$ where '*e*' is the orbital eccentricity and '$\tilde{\omega}$' refers to the longitude of perihelion (point at which the Earth is closest to the sun during its orbit) (Figure 6.2) (Tuenter et al., 2003).

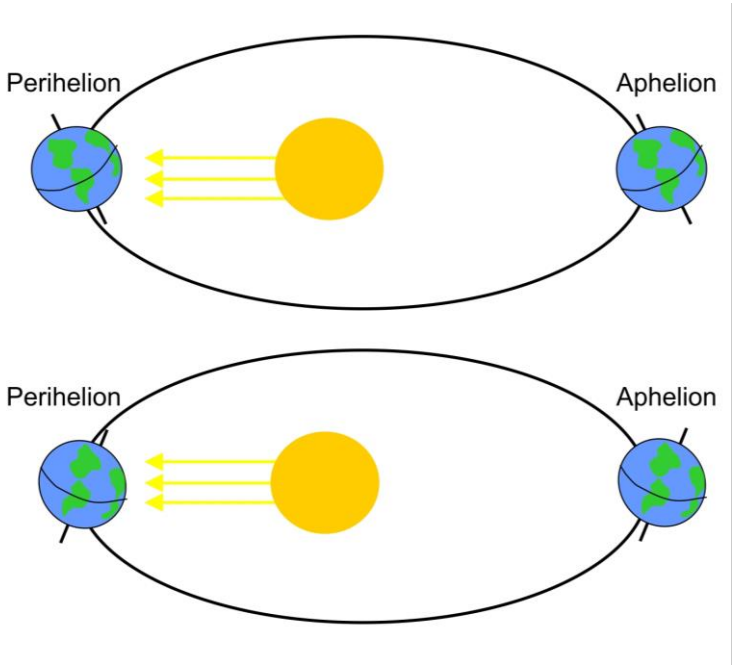

Figure 6.2 – Illustration of the movement of the Earth during a precessional cycle. **A:** Maximum solar insolation (represented by the yellow arrows) in the southern hemisphere, creating greatest seasonal contrast when perihelion coincides with southern hemisphere summer solstice. Northern hemisphere's winter solstice coincides with perihelion creating low seasonal contrast. **B:** Maximum solar insolation in northern hemisphere, when coinciding with northern hemisphere summer solstice. Southern hemisphere winter solstice coincides with perihelion, thus creating low seasonal contrast.

Precession-driven changes in summer solar radiation are postulated to be capable of driving changes in temperature (Tuenter et al., 2003), and precipitation patterns through the movement of the inter-tropical convergence zone (ITCZ) (a narrow zone close to the equator where south-east trade winds and north-east trade winds converge, presenting a "tropical belt of deep convective clouds" and high rainfall (Schneider et al., 2014, p. 45). Over long timescales, the ITCZ is suggested to migrate towards a "differentially warming hemisphere" Schneider et al., 2014, p. 45), such that during high summer solar insolation in the Southern hemisphere, the ITCZ will migrate southwards (McGee et al., 2014; Schneider et al., 2014) (e.g. Kutzbach, 1994; Valdes et al., 1995; Daniau et al., 2013; Woillez et al., 2016). A key example of this can be seen in a South African Quaternary section covering the last ~170 kyr, where periods of maximum precession index (high summer insolation in the

southern hemisphere) are anticipated to lead to increased precipitation by reinforcing “the convection associated with the ITCZ” (Daniau et al., 2013, p. 5070) over the last ~170 kyr. This hypothesis appears to be supported by variations in pollen abundances (e.g. forest expansion of *Podocarpus* pollen – indicative of humid periods during maximum precession index (Daniau et al., 2013). During minimum precession index; the ITCZ is predicted to migrate northwards, causing a reduction in rainfall in southern Africa (Daniau et al., 2013).

6.1.2 Obliquity Cycle

The obliquity cycle has a current ~41 kyr periodicity and is produced by changes in the axial tilt of the Earth between 21.5° and 24.5° with respect to the perpendicular to the plane of the orbit (Figure 6.3) (Looney, 2011). With reduced axial tilt, the radiation from the sun is more evenly distributed across winter and summer months. With increasing obliquity, the amount of solar radiation reaching high latitudes increases during the summer, whilst during the winter, insolation decreases. Obliquity therefore predominantly affects high latitudes (beyond ~35°N/S) (Collman et al., 1995), as the effect of changing solar radiation decreases towards the equator (Sha et al., 2015). Hence, changes in obliquity can determine the strength of the temperature gradient between latitudes, and the strength of the seasons in low latitude regions.

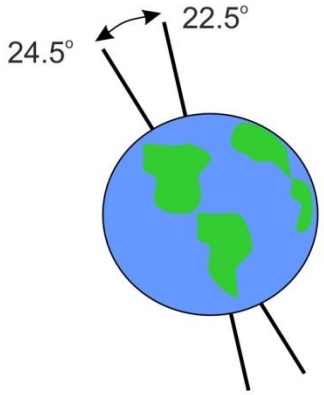

Figure 6.3 – Illustration of the Obliquity cycle. During this ~41 kyr cycle, the Earth tilts between 24.5° and 22.5° relative to the axial plane of the orbit.

The effects of obliquity on climate have been less extensively studied, after many authors theorised that eccentricity and precession likely dominated the pacing of the Pleistocene glacial-interglacial cycles, over the last ~1 Myr (Huybers and Wunsch, 2005). However, early Pleistocene glacial cycles (between 1 to 2 Ma) have been found to occur over a similar timescale to that of obliquity (~40 kyr) (e.g. Raymo and Nisancoiglu, 2003; Huybers, 2006), with 33 out of 36 significant de-glaciations occurring during periods of anomalously large obliquity (Huybers, 2007). Huybers (2007) postulates that obliquity is therefore the main forcing component behind the glacial-interglacial cycles during the Early Pleistocene, arguing that the ~100 kyr forcing of insolation variations caused by eccentricity, are “too small to directly cause the glacial cycles” (Huybers, 2007, p. 52).

6.1.3 Eccentricity Cycle

The longest cycle, eccentricity, refers to the shape of Earth’s orbit around the sun, and occurs over medium timescales ~100 kyr (short-eccentricity) and ~400 kyr (long-eccentricity), as well as longer timescales of millions of years, termed ‘grand orbital cycles’ (e.g. ~9 Myr) (Martinez and Dera, 2015). Fluctuations between more and less elliptical orbits alter the distance between the Earth and the sun and thus the amount of insolation received at the Earth’s surface globally (Figure 6.4). At high eccentricity, the shape of the Earth’s orbit is more

elliptical, compared to low eccentricity when its orbit is nearly circular. Currently, eccentricity is fairly low (~0.0607) (Berger, 2001) as there is only a 3% difference in solar insolation between the closest approach between the Earth and Sun as it orbits (perihelion) (around the 3rd January) and the furthest departure (aphelion) (around the 4th July) (Graham, 2000). At high eccentricity, the amount of solar radiation and thus insolation received at the Earth's surface is anticipated to be ~20% to 30% higher at perihelion than at aphelion (Graham, 2000).

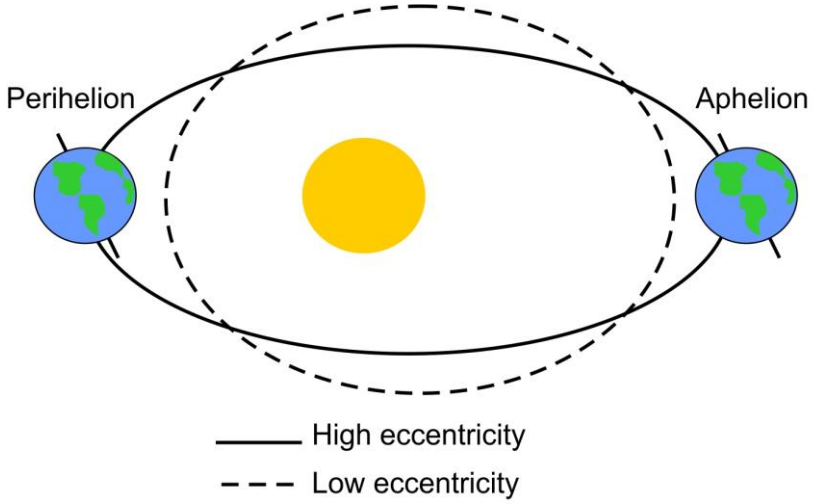

Figure 6.4 – Illustration of the Milankovitch eccentricity cycle.

The eccentricity of the Earth's orbit is hypothesized to indirectly cause prominent changes in climate (Cowan et al., 2012). In particular, the short ~100 kyr cycle has been classed as the main driver in Quaternary glacial-interglacial cycles occurring over the last ~1 million years (Myr) through the modulation of the strength of the precession cycle (Hays et al., 1976; Clemens and Tiedemann, 1997; Sigman and Boyle, 2000; Lisiecki, 2010). This is because direct changes in solar insolation from the eccentricity cycle are only capable of altering radiation intensity by ~3 to 4% (Kingston, 2005; Huybers et al., 2007; Lisiecki, 2010; Abe-Ouchi et al., 2013), thus the small change in radiation is too small to directly cause prominent climate changes such as glacial-interglacial cycles (Huybers et al., 2007). The long eccentricity cycle (~400 kyr) is postulated to be capable of indirectly pacing continental weathering intensity, riverine nutrient inputs and oceanic fertilization (Ma et al., 2011; Martinez and

Dera, 2015, p 12607), also through the modulation of the precession cycle; whilst the long multi-million 'grand' eccentricity cycle has recently been postulated to be capable of pacing C_{org} burial (e.g. Martinez and Dera, 2015).

The periodicities of the cycles described above, change slowly with time (Beer et al., 2000). This is because the oscillations in the Earth's orbit and tilt change with the gravitational forces from other planets, (Berger et al., 1992; Beer et al., 2000). The precession and obliquity cycle periodicities are strongly influenced the "character of the Earth-Moon system" (House, 1995, p. 12). Here, previous calculations suggest a shortening of the distance between the Earth and the moon, and the length of the day going back in time, that are thought to have "induced a shortening of the fundamental periods for the obliquity and climatic precession" (Berger et al., 1992, p. 560). Thus for example, during the Early Jurassic period, the length of the precession cycle is postulated to have been ~20-to-21 kyrs (Bonis et al., 2010; Ruhl et al., 2016) compared with the 23 kyr periodicity of today. An example of how precession and obliquity periodicities change over geological time is given in Figure 6.5. The eccentricity cycle however, is calculated to have remained fairly constant over geological time (Berger et al., 1992).

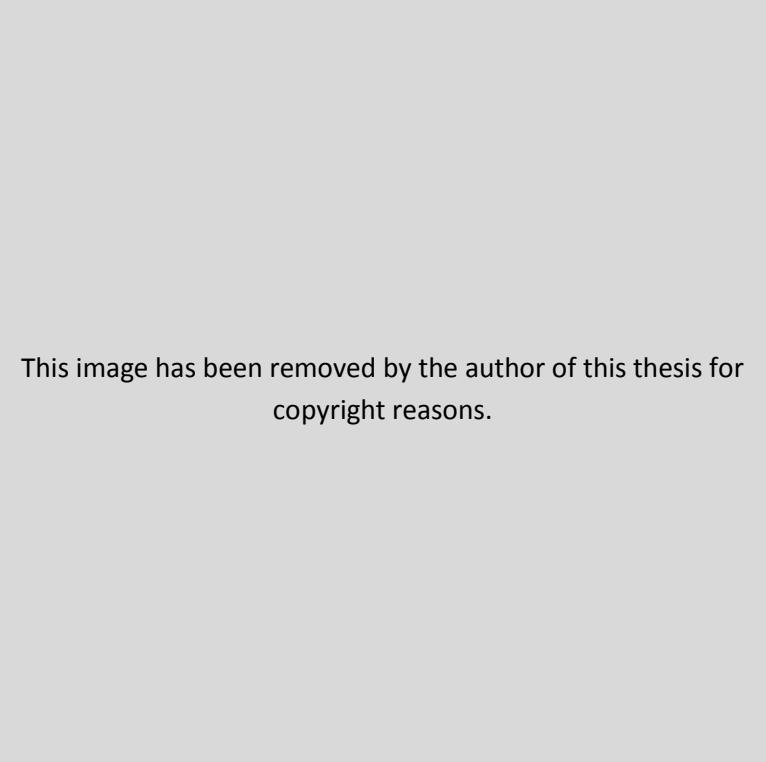

Figure 6.5 – Graph taken from House (1995) illustrating the changing periodicity of the precession and obliquity cycle through geological time (based on Berger et al, 1989).

6.2 Summary

The Milankovitch cycles refer to natural changes in the amount of solar radiation received geographically and/or globally at the Earth's surface driven by cyclic changes in the Earth's orbit and positioning around the sun. They occur over varying timescales, divided into precession, obliquity and eccentricity, with the shortest 'precession' cycle currently occurring over ~23 kyr, whilst the longest 'eccentricity' cycle can occur over timescales of between ~100 kyr up to ~9 Myr. Precession cycles likely force changes in the strength of hemisphere-specific seasonality. Changes in obliquity can determine the strength of the temperature gradient between latitudes, as well as seasonal strength in low-latitude regions. Eccentricity has been hypothesized to have driven the pacing of Quaternary glacial-interglacial cycles occurring over the last 1 million years, through the modulation of the strength of the precession cycle.

7. Fire responds to Milankovitch scale climate changes

7.1 Introduction

The relationship between fire, climate and the environment is a growing concern with respect to future climate change (Woillez et al., 2016). Fire's potential influence on ecosystems, human societies and the atmosphere "through the release of aerosols, reactive trace gases, and greenhouse gases" (Forkel et al., 2016, p.1) has led to an increase in the number of studies trying to understand the environmental drivers and effects of wildfire, particularly when it comes to anthropogenic climate change (Mortiz et al., 2012). An example of this can be seen in the latest two IPCC reports (IPCC, 2007; IPCC, 2014), which heavily feature the effects of future climate change on wildfire activity with the "IPCC AR4 chapter on ecosystem impacts focussing almost exclusively on projected increases in fire" (Mortiz et al., 2012, p.1).

As our climate changes, rising temperatures and shifts in precipitation patterns are anticipated to increase the risk of fire in many regions across the world (Lui et al., 2010; Rocca et al., 2014), whilst other areas are predicted to experience a decrease in wildfire activity (Scholze et al., 2006). As climate can influence wildfire in a number of ways (for example, control over fuel loads through biomass changes; ignition sources through the frequency of lightning strikes; and controlling conditions conducive for fire spread e.g. fuel moisture etc.), predicting the effects that future climate change may have on wildfire activity is challenging (Mortiz et al., 2012; Guyette et al., 2014). To aid in the analysis of changing patterns in wildfire activity, many models compare their predicted fluctuations in climate-driven fire activity, to 'long-term' historical averages/patterns (e.g. Pechony and Shindell, 2010; Mortiz et al., 2012), some of which have been compiled directly from the sedimentary charcoal record (e.g. Marlon et al., 2009). Commonly, these 'long-term' fluctuations are in the

range of between tens of years up to ~2000 years (Marlon et al., 2009; Mortiz et al., 2012).

Comparisons of 'newly discovered' fire patterns with longer-term trends in wildfire activity are important as they enable disentangling of the charcoal record across time, separating background signals from charcoal peaks (Clark and Royal, 1996; Iglesias et al., 2015), and thus "allowing a more sophisticated reconstruction of the fire history" (Iglesias et al., 2015, p.5). Yet there appear to be few studies that have analysed medium timescale fire trends occurring over tens to hundreds of thousands of years, within the geological record. Instead many studies appear to either focus on significant geological events (e.g. Collinson et al. (2003) studying wildfire and vegetation shifts across the Paleocene-Eocene thermal maximum; Belcher et al. (2010); van de Schootbrugge (2010) and Peterson and Lindström, (2012) studying changes in wildfire across the Triassic-Jurassic boundary, during a period of high volcanic CO_2 emissions, and floral turnover; Belcher et al. (2003); Belcher, (2009); Belcher et al. (2009); Morgan et al. (2013) studying for evidence of wildfires during the Chicxulub impact at the Cretaceous-Paleogene boundary), or on wildfire trends occurring over many millions of years (e.g. Glasspool and Scott, 2010; Baker et al., 2017). For wildfire patterns occurring over timescales of tens to hundreds of thousands of years, information is only provided from studies that focus on the Quaternary period (~2.5 Ma to present), in particular, over the last ~110 kyrs (e.g. Haberle et al., 2001; Paduano et al., 2003; Briles et al., 2005; Markgraf et al., 2007; Power et al., 2008; Jiménez-Moreno, 2011; Daniau et al., 2013; Fischer et al., 2015).

Analysis of sedimentary charcoal across these timescales in the Quaternary (e.g. Jiménez-Moreno, 2011; Daniau et al., 2013; Power, 2013), have led to the identification of a natural oscillation in inferred wildfire activity, illustrating 'cyclic' variations in charcoal abundance over the last ~170 kyr. These 'cyclic' oscillations are interpreted to have been driven by orbitally forced climate and vegetation changes associated with Milankovitch cycles (Jiménez-Moreno, 2011; Danaiu et al., 2013).

Milankovitch cycles can often be found expressed in the geological record by the rhythmic deposition of carbonate-rich beds, alternating amongst darker,

organic carbon-rich beds, coupled with small variations in the $\delta^{13}C$ record (Brown et al., 2009; Soua, 2010; Hinnov, 2013) (e.g. the Jurassic Belemnite Marls, Dorset (Weedon and Jenkyns, 1990; Weedon and Jenkyns, 1999)). In particular, orbital forcings have been extensively documented within Early Jurassic deposits (e.g. Mochras Farm (Llanbedr) borehole, Wales, UK (Ruhl et al., 2016); Yorkshire, UK (Kemp et al., 2011); Dorset, UK (Weedon and Jenkyns, 1990; 1999); Peniche, Portugal (Huang and Hesselbo, 2014); Newark Basin, north-eastern U.S.A (Olsen and Kent, 1999); Junggar Basin, Western China (Sha et al., 2015).

The Mochras Farm (Llanbedr) borehole (herein referred to as Mochras) provides a ~1300 m record which "uniquely combines stratigraphic expansion and biostratigraphic completeness" (Hesselbo, *pers. comms*). The sediments preserved in the Mochras core were deposited at a palaeolatitude of ~30°N (Hesselbo et al., 2007), and are described as being at a palaeogeographically "critical latitude, influenced by both subtropical and mid-latitude climate and oceanography, and thus very susceptible to astronomical forcing (Bjerrum et al., 2001; Ruhl et al., 2010)" (Hesselbo et al., 2013, p.88). An extensive high-resolution analysis of element concentration data of the sediments in the Mochras core, presented by Ruhl et al. (2016, p.150), enables the identification of Ca-rich – organic-rich bed and bundle alternations, occurring over the timescales of Milankovitch precession and eccentricity cycles. These high-resolution, astronomically calibrated sediments make Mochras an ideal section to analyse wildfire changes across naturally occurring and well-defined lithological cycles, during a time period that does not coincide with major global C-cycle perturbations/internal Earth system forcing events (e.g. volcanism etc).

Analysis of palaeo-wildfire activity across Milankovitch cycles could therefore provide key information on the natural 'background' signal of wildfire across medium timescales, thus providing a reference for future wildfire studies carried out during the Early Jurassic period within the northwestern Tethys region. Due to the strong relationship between climate and wildfire (e.g. Swetnam and Betancourt, 1990; Marlon et al., 2008; Aldersley et al., 2011; Mortiz et al., 2012), the analysis of wildfire may also provide further information on how changes in the Earth's orbit may have influenced the Early Jurassic climate, providing fossil evidence in support of global circulation model predictions of

orbital forced climate changes during the Jurassic period (e.g. Kutzbach, 1994; Vollmer et al., 2008).

7.2 Materials and Methods

7.2.1 The Study Site

The study sediments are from the Mochras Farm (Llanbedr) Borehole, drilled in west Wales in the UK in 1967-1970. The now existing core slabs provide a near complete section of Lower Jurassic strata dating from the Late Sinemurian through to the Late Toarcian (Woodland, 1971). The studied sediments were deposited during the *subnodosus to gibbosus* subzones of the *A. margaritatus* ammonite Zone, during the Pliensbachian, Early Jurassic, and comprise ~10 m of the core, between core depths ~934 m to ~944 m (see Figure 4d in Ruhl et al., 2016).

7.2.2 Depositional Setting

During the Early Jurassic, the Earth's climate is hypothesized to have been fairly equable and warm compared to present day (Hallam, 1994), where Jurassic poles were likely devoid of permanent ice (Frakes, 1978; Hallam, 1994), and some northern and southern regions never experienced temperatures below 0°C (Vakhrameev, 1991). The Pliensbachian is hypothesized to have been one of the cooler periods of the Early Jurassic, with annual temperature fluctuation estimates (taken from $\delta^{18}O$ marine calcite) ranging between ~7°C and ~20°C (Korte et al., 2015).

Using ferns whose living relatives are known to be intolerant of hard frosts, it was identified that during the Early Jurassic, northern and southern floral zones likely existed (Hallam, 1994). These zones encompassed Greenland, Siberia, Japan and northern and central Europe in the northern zone, and parts of Mexico, the Middle East and southern China in the southern zone (Hallam, 1994). In particular, between palaeo-latitudes of ~30°N and ~30°S, fossil faunal distributions of Jurassic corals suggest the presence of a 'tropical belt' (Hallam, 1984; 1994), where periods of intense monsoon rainfall are predicted. The high rainfall rates associated with the monsoons are postulated to have originated

over the Tethys area (Chandler et al., 1992), and the distribution of the Pangean landmass, divided equally across the two hemispheres, is thought to have made conditions ideal for maximising monsoonal circulation, creating 'mega-monsoons' (Kutzbach and Gallimore, 1989; Dubiel et al., 1991; Parrish, 1993; 1995). The postulated relative distributions of biomes (i.e. the floral assemblages) and the climate belts that they relate to for the Early Jurassic are illustrated in figure 7.1.

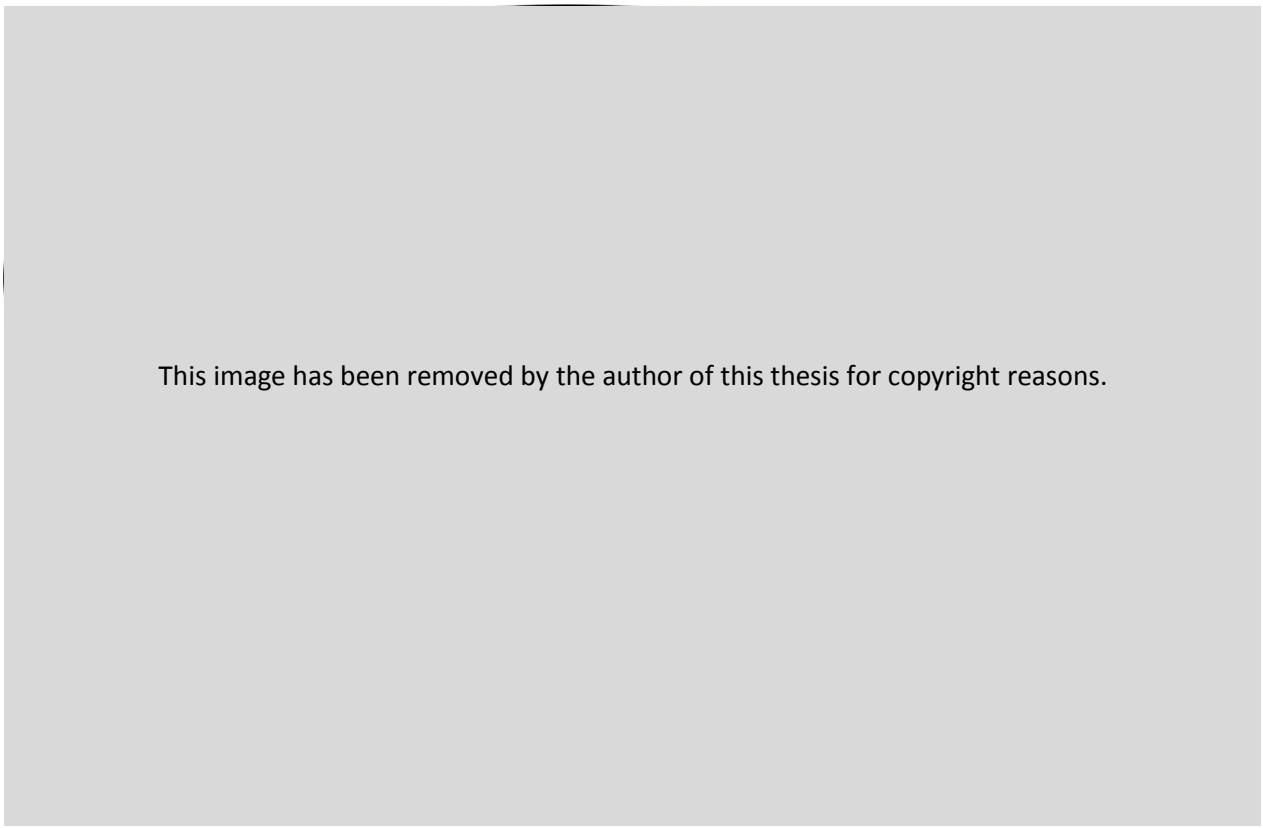

Figure 7.1 – Early Jurassic Palaeomap illustrating predicted biome/climate zone. (Re-drawn from Rees et al., 2000).

As Milankovitch cycles are known to influence present day monsoon patterns (e.g. Daniau et al., 2013), the location of Mochras in the Early Jurassic under the likely influence of an intense monsoon cycle, presents an ideal study location for analysing the effects of Milankovitch forcing on Early Jurassic climate. As the study site was located at a palaeo-latitude of ~ 30°N (Hesselbo et al., 2007), the sediments illustrate a strong precession and eccentricity

component (Ruhl et al., 2016). The obliquity cycle is most prominent in high latitude regions beyond ~35°N which may explain why it is not clearly observed within the sediments studied (Ruhl et al., 2016). Thus this study focusses on changes in palaeo-wildfire activity occurring over the eccentricity and precession cycles defined (Ruhl et al., 2016). The sediments studied here were deposited within a basinal marine setting with influence from nearby terrigenous sources around the Cardigan Bay area (Dobson and Whittington, 1987).

7.2.2 Methods

Rock samples were kindly collected and provided by M. Ruhl, W. Xu and M. Storm from the Llanbedr core, stored at British Geological Survey, Keyworth. Samples were collected at between 0.10 m and 0.43 m intervals from a 6.17 m length of core, between core depths 934.00 m and 940.30 m, taken within the *subnodosus-gibbosus* subzones of the *margaritatus* ammonite Zone in the Pleinsbachian, (appendix E) where no significant isotopic excursions/climatic changes are present. The sampling resolution of ~33 cm intervals was determined by X-ray fluorescence (XRF) analysis of the core conducted by M. Rhul, whose variations in 'detrended' calcium percentage, revealed Milankovitch cycles of precession, and long and short eccentricity (~100 kyr and ~400 kyr cycles) (refer to Ruhl et al., 2016 for details). The sampled section covers ~6 precession cycles and ~1.3 100 kyr eccentricity cycles (Ruhl et al., 2016).

Fossil charcoal was extracted from the Mochras rock samples (18 samples in total were processed and analysed from the core) by demineralizing ~20 g of rock in cold hydrochloric acid (10% HCl), followed by 32% HCl, for 48 hours to remove carbonate followed by cold hydrofluoric acid (40% HF) for 72 hours to remove any silicate present. A second treatment of 32% HCl over 24 hours was given to remove any calcium fluoride precipitates, before being rinsed with distilled water until a neutral pH was reached. The organics were sieved using a 125 µm mesh to separate charcoal into two size fractions thought to reflect local and regional signals of burning (Mooney and Tinner, 2011). The >125 µm size fractions were analysed using a binocular microscope where all charcoal particles in each 20 g sample were quantified. The <125 µm fraction was

pipetted onto slides, suspended in a known volume of water. Two transects were quantified and then scaled-up to the known quantity of the sample (Belcher et al., 2005). The palynofacies analysis was also conducted in this way. To ensure that changes in fossil charcoal concentrations were not biased by a change in nature or abundance of terrestrial organic material, a palynofacies analysis of each sample was conducted, quantifying the abundance of pollen and spores; plant cuticle, amorphous organic matter (AOM) and coalified particles.

7.3 Results

The Early Jurassic section of the Mochras core consists of alternating beds of highly bioturbated calcareous mudstone (calcium carbonate ($CaCO_3$) contents ~10 to 65% - expressed at Ca percentages (%Ca) in Figure 7.2 and 7.3)) with darker, millimetre laminated organic rich mudstone beds (total organic carbon (TOC) contents ~0.9 to 1.2%) (Ruhl et al., 2016). Within the Mochras core, one alternation from a carbonate-rich bed to a carbonate-poor bed is defined as a 'couplet' (Ruhl et al., 2016) (as marked on Figures 7.2 and 7.3). These couplets however are not evenly spaced within the Mochras core, and furthermore successively vary in their characteristics, such that some couplets contain beds of higher %Ca compared with other couplets. For example, the couplet comprising the carbonate-rich bed sitting between core depths of 935.2 m and 936.2 m (Figure 7.2) and the carbonate-poor bed sitting between core depths of 935.2 m and 934.8 m, consists of a higher %Ca when compared with the couplet consisting of a carbonate-poor bed sitting between 937.5 m and 938.0 m and the carbonate-rich bed sitting between 936.8 m and 937.5 m (Figure 7.2).

These varying couplet characteristics form what is defined as a 'bundle' (Ruhl et al., 2016) (as marked on Figures 7.2 and 7.3). Here, one alternation between a couplet consisting of higher %Ca with a couplet consisting of generally lower %Ca defines one bundle. One bundle therefore consists of 4 – 5 bed-scale changes in carbonate, evident as bed scale variations in %Ca. These are indicated in Figures 7.2 and 7.3 as 'high Ca' and 'low Ca' contained within bundle-scale Ca changes.

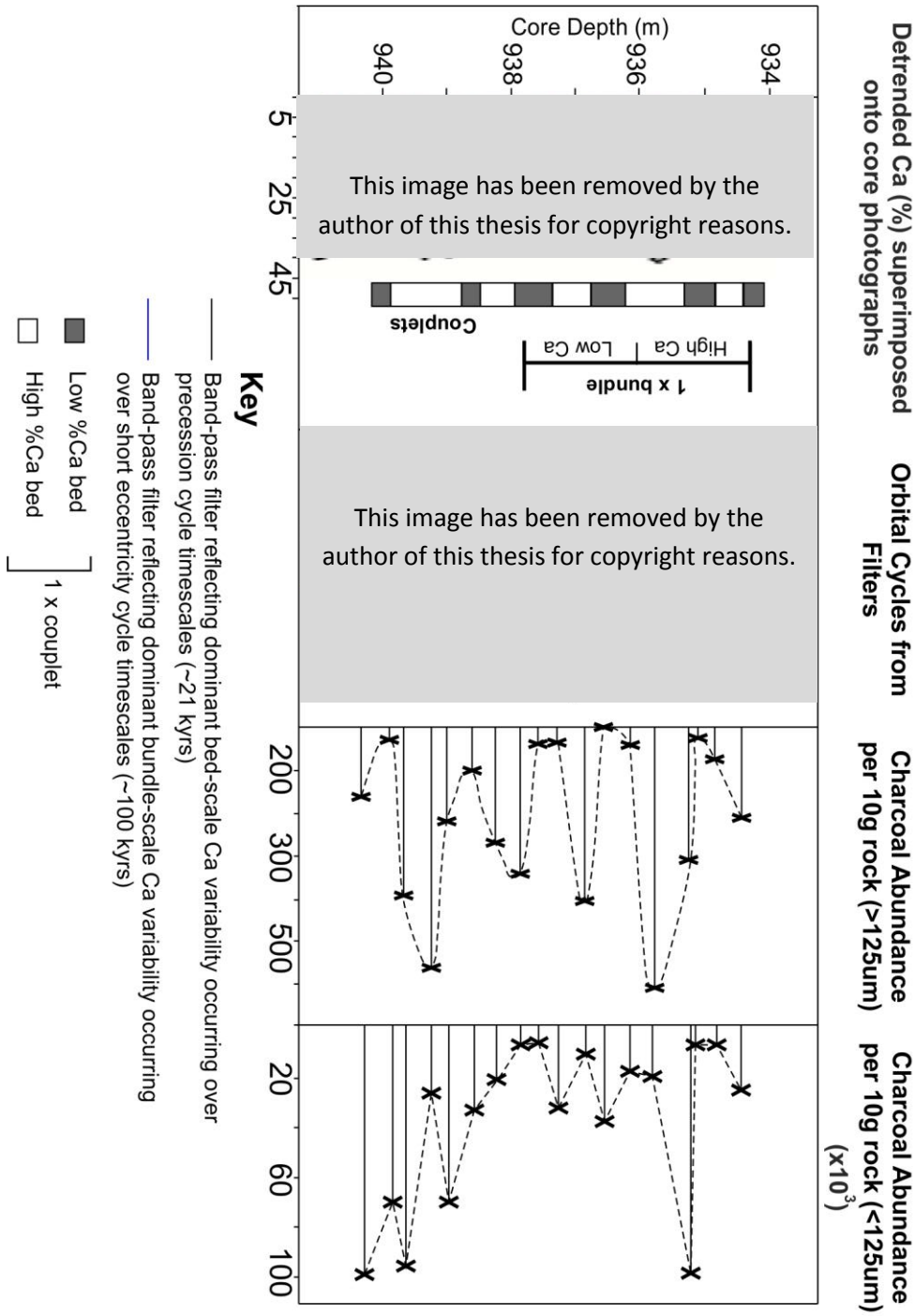

Figure 7.2 – Variations in charcoal abundances across 6 bed-scale variations in Ca content occurring across precessional cycle timescales (depicted by the black line in 'band-pass filters', and bundle scale variability in Ca content occurring across timescales of short (100 kyr) eccentricity, depicted by the blue line in band-pass filters. De-trended Ca percentages, core photographs and band-pass filters are taken from Ruhl et al. (2016). One couplet refers to one high %Ca and one low %Ca bed.

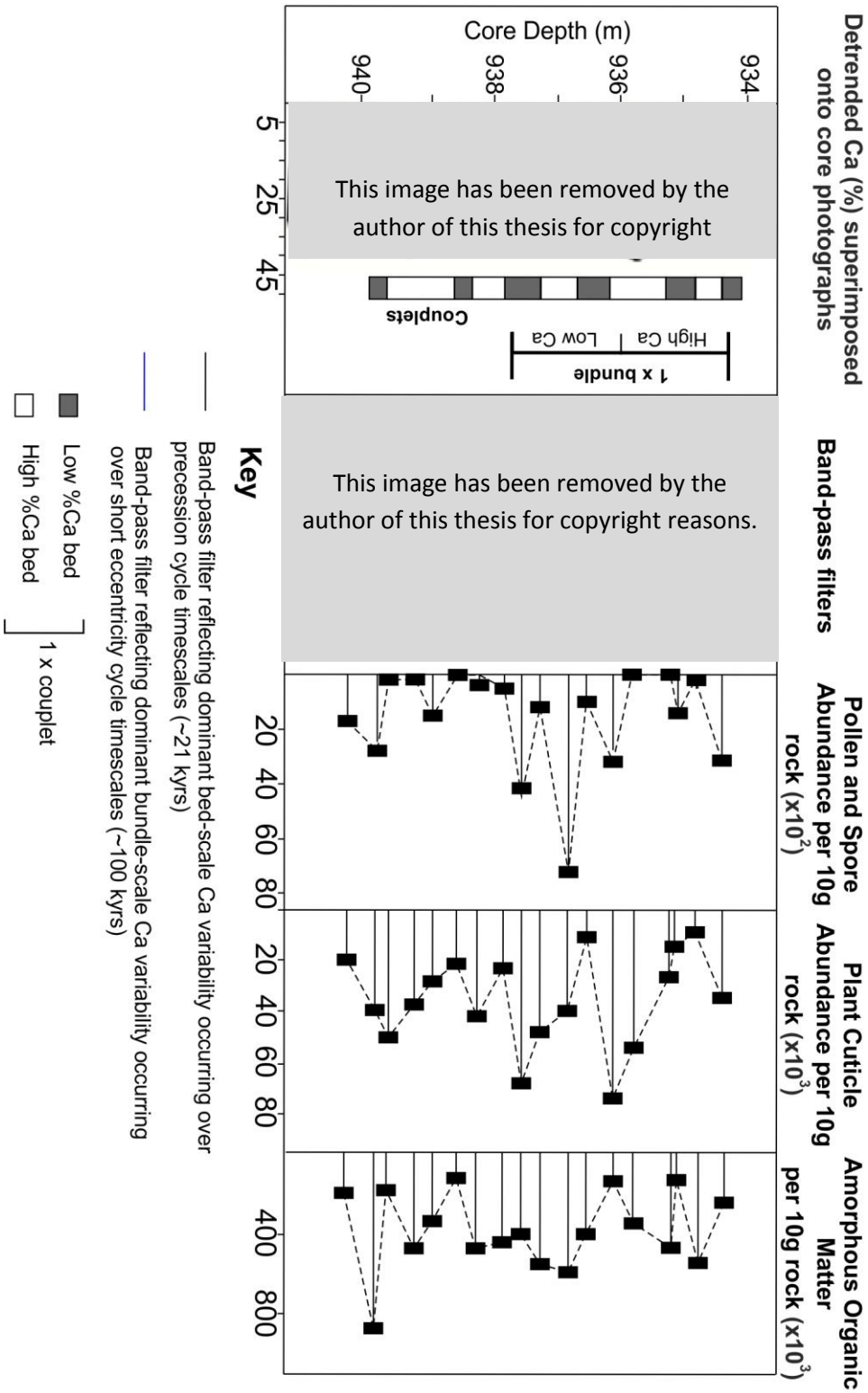

Figure 7.3 – Variations in total pollen and spore; plant cuticle and amorphous organic matter (AOM) abundances across 6 bed-scale variability in Ca content occurring across precessional cycle timescales (depicted by the black line in 'band-pass filters', and bundle scale variability in Ca content occurring across timescales of short (100 kyr) eccentricity, depicted by the blue line in band-pass filters. De-trended Ca percentages, core photographs and band-pass filters are taken from Ruhl et al. (2016).

Figure 7.2 illustrates the changes in >125 μm and <125 μm charcoal abundances counted in this study, plotted across the published %Ca changes (Ruhl et al., 2016), whilst Figure 7.3 illustrates changes in observed pollen and spore abundance; plant cuticles and amorphous organic matter (AOM) (this study) plotted against the published %Ca variations (Ruhl et al., 2016).

Throughout the section, variations in charcoal abundances in the Mochras core tightly correspond to variations in couplet-scale and/or bundle-scale Ca content variations (Figure 7.2). The greatest abundance of >125 μm charcoal particles at Mochras are found in beds containing high Ca percentages, with abundances ranging between 341 and 609 particles per 10 g of sediment (e.g. core depths of 935.8 m; 936.8 m, 937.8 m and 939.2 m). In contrast, lower >125 μm charcoal abundances ranging between 1 and 101 particles per 10 g are found in beds containing low percentages of Ca. This tight correlation between >125 μm charcoal abundances and changes in Ca percentage is supported by *Pearson's correlation* where *R* equalled 0.524 and *P* equalled 0.026 indicating a significant correlation ($P = <0.05$).

Interestingly within the single lithological 'bundle' (Ruhl et al., 2016), where couplets containing low carbonate contents occur (between core depths of 936.00 m to 937.80 m), the >125μm charcoal abundances, although still vary in accordance with the bed-scale changes in Ca content, also appear broadly lower, with highest abundances reaching 341 and 405 particles per 10g, and lowest abundance of just 1 particle (Figure 7.2). This compares with the higher %Ca observed between core depths of 934.40 m to 936.00 m and between 937.80m and 940.33 m where the >125μm charcoal abundances appear generally higher, where highest >125 μm abundances reach 605 and 562 particles per 10 g, and lowest abundances reach 27 and 30 particles per 10 g respectively. The relationship between >125 μm char abundances with %Ca is further demonstrated in Figure 7.4, which illustrates a positive relationship between increasing %Ca and increasing >125 μm char abundances.

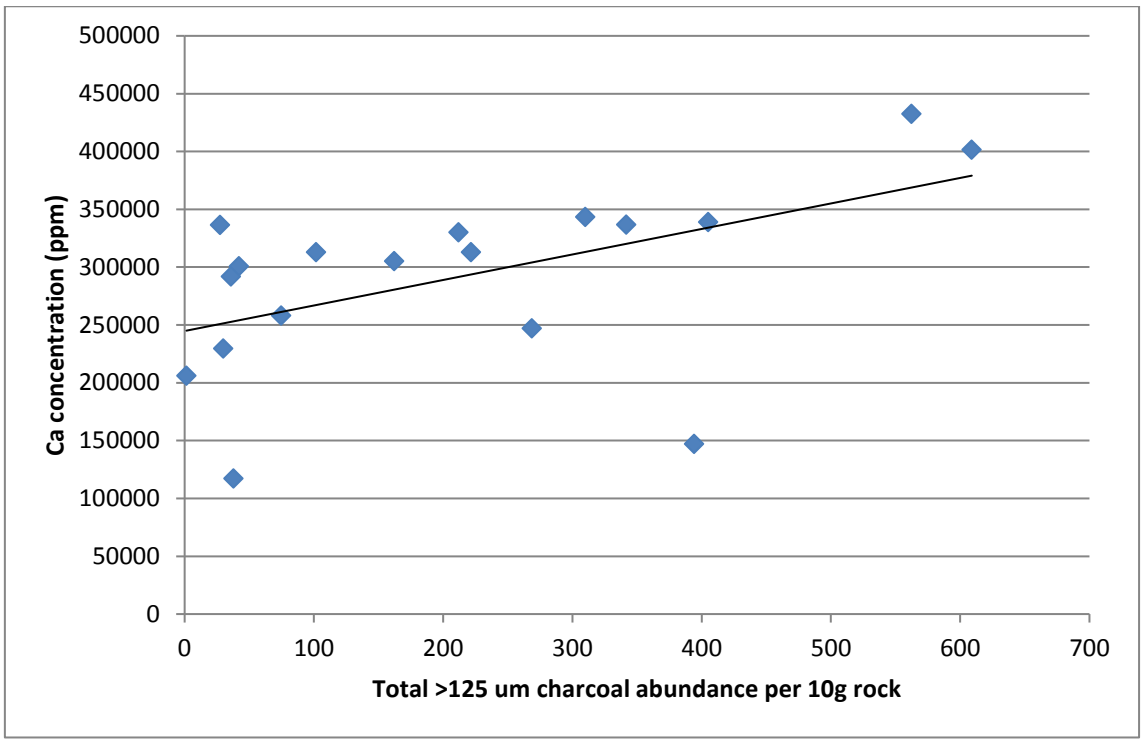

Figure 7.4 – Cross-plot illustrating increased >125 µm charcoal abundances occurring within beds containing higher Ca (ppm). (Ca measurements taken from Ruhl et al., 2016).

In contrast, the <125 µm charcoal abundances do not appear to vary in accordance with the Ca rich/Ca poor bed scale changes (a *P* value of 0.56 confirms the correlation is not significant) (Figure 7.5).

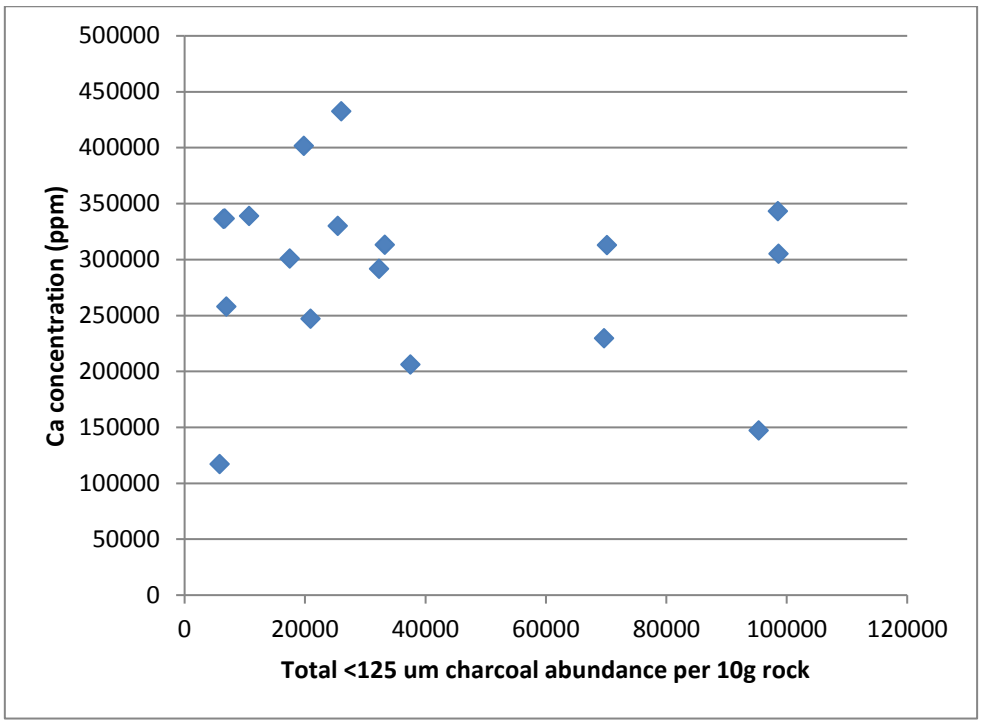

Figure 7.5 – Cross-plot illustrating no trend between increased <125 µm charcoal abundances and beds containing higher Ca (ppm) (Ca measurements taken from Ruhl et al., 2016 (SI)).

However abundances do appear to vary across the 'bundle' changes in Ca percentage. Here <125 µm charcoal abundances are elevated averaging 52,553 particles per 10g between core depths 937.80 m and 940.33 m; and 31,409 particles between core depths 934.40 m and 936.00 m within couplets of generally higher %Ca percentages. In contrast within couplets exhibiting generally lower %Ca between core depths 936.00 m and 937.80 m, <125 µm charcoal abundances average 20,727 particles per 10 g.

The palynofacies analysis (Figure. 7.3), indicates that total pollen and spore abundances appear to vary, but like the <125 µm charcoal fraction, do not correspond to variations in individual bed variations in %Ca, yet instead appear to coincide with the bundle-scale changes in %Ca. Here, the highest pollen and spore abundances correspond with lower percentages in Ca, with an average abundance of 16,341 between core depth 936.00 m and 937.80 m. This compares with higher Ca percentages observed between core depths 934.40 m to 936.00 m and between 937.80 m and 940.33 m where average abundance reach 4,463 and 6,708 per 10 g respectively. When compared with variations in

charcoal abundance, higher pollen and spore counts do not correlate with higher >125 µm not <125 µm charcoal counts (Figures 7.6, 7.7).

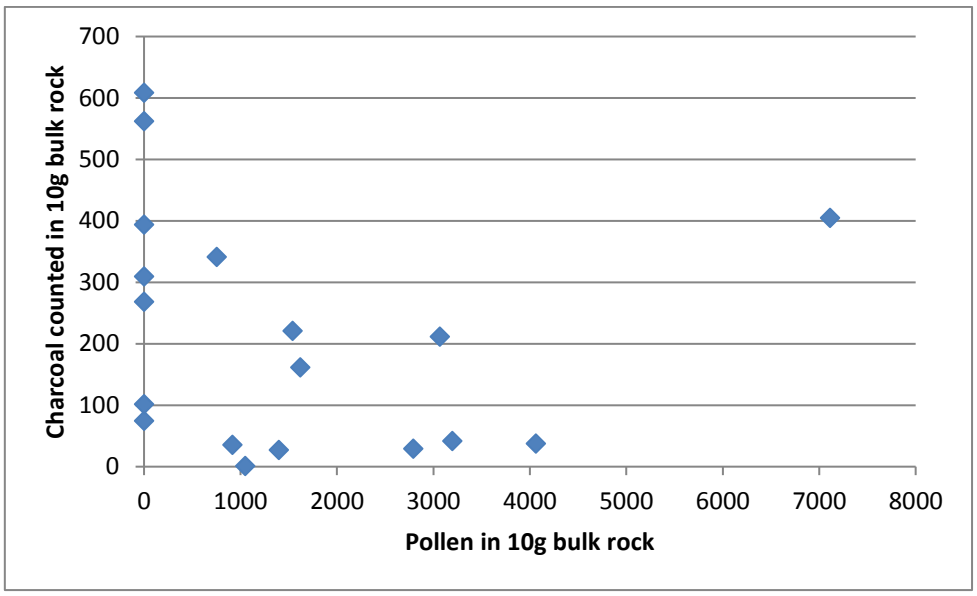

Figure 7.6 – Cross-plot illustrating a lack of trend between increased >125 µm charcoal abundances and increased pollen and spore abundances.

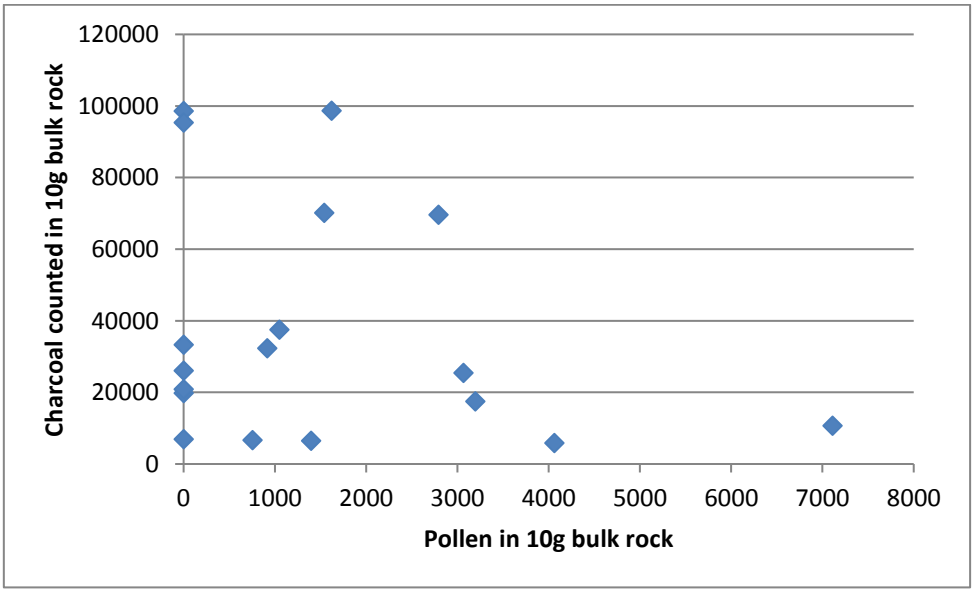

Figure 7.7 – Cross-plot illustrating a lack of trend between increased <125 µm charcoal abundances and increased pollen and spore abundances.

Total plant cuticle abundances are similar to the >125 µm charcoal fraction and vary accordingly with individual bed scale changes in %Ca, although they appear to slightly precede peak %Ca contents. Here, we see generally high plant cuticle abundances just before peak %Ca, and lower abundances just after high %Ca throughout the majority of the studied core section (Figure. 7.3). This pattern continues until core depth 937.50 m where plant cuticle abundances and the individual bed %Ca appear to be overridden by the bundle-scale changes in Ca, such that high cuticle abundances occur during minimum %Ca of close to ~10% (Figure 7.3). Therefore, it is maybe not surprising that when compared with the >125 µm charcoal counts that there appears to be a weak correlation between higher plant cuticle abundances and higher charcoal abundances (Figure 7.8). However, as high plant cuticle abundances slightly precede peak bed scale %Ca whilst the high >125 µm char abundances do not, it is not unexpected to see that a P value of 0.55 indicates that the correlation between >125 µm charcoal and plant cuticle abundances are not significant. Plant cuticle abundances do not have any correlation with the <125 µm charcoal size fraction (Figure 7.9). The AOM does not appear to be influenced by changes in either bed scale or bundle-scale Ca content, and does not have any correlation with variations in charcoal abundances of either size fraction (Figures 7.10, 7.11).

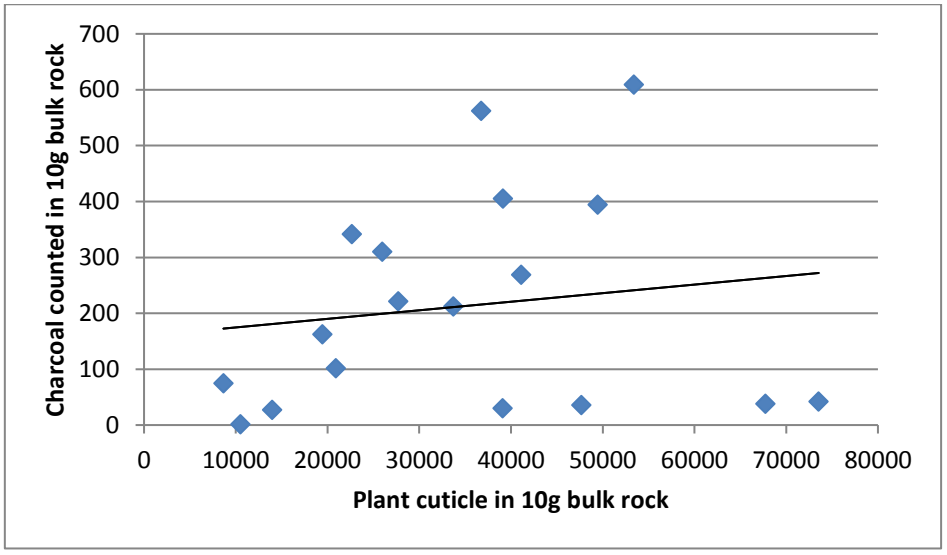

Figure 7.8 – Cross-plot illustrating a lack of trend between increased >125 µm charcoal abundances and increased plant cuticle abundances.

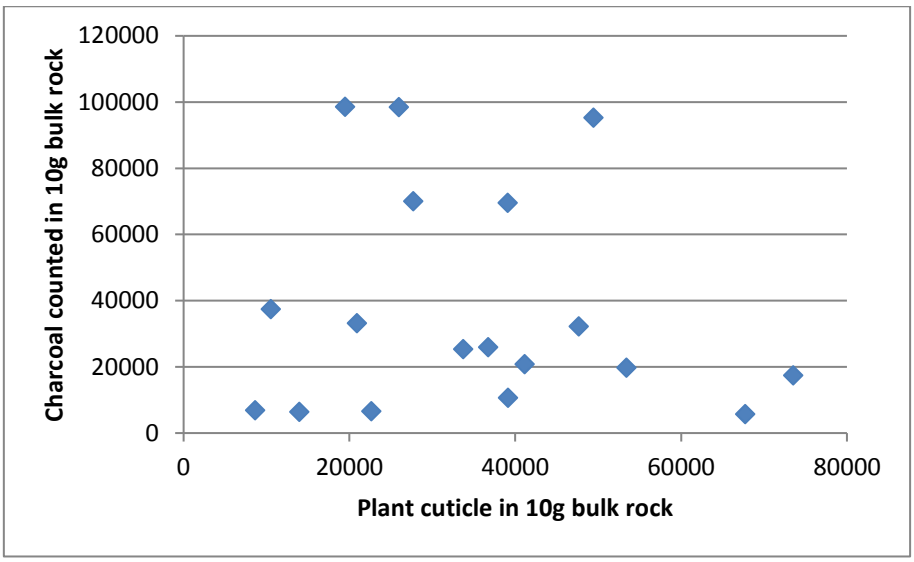

Figure 7.9 – Cross-plot illustrating a lack of trend between increased <125 µm charcoal abundances and increased plant cuticle abundances.

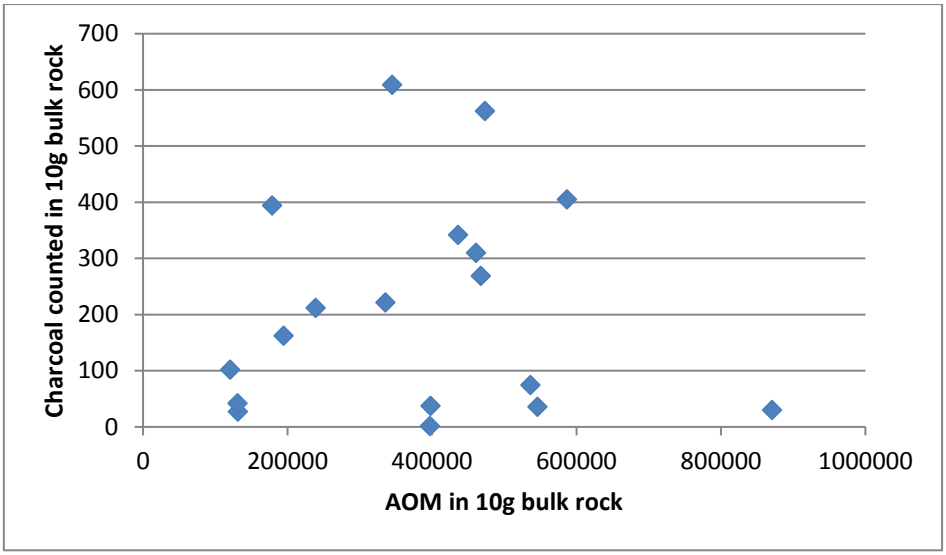

Figure 7.10 – Cross-plot illustrating a lack of trend between increased >125 µm charcoal abundances and increased AOM abundances.

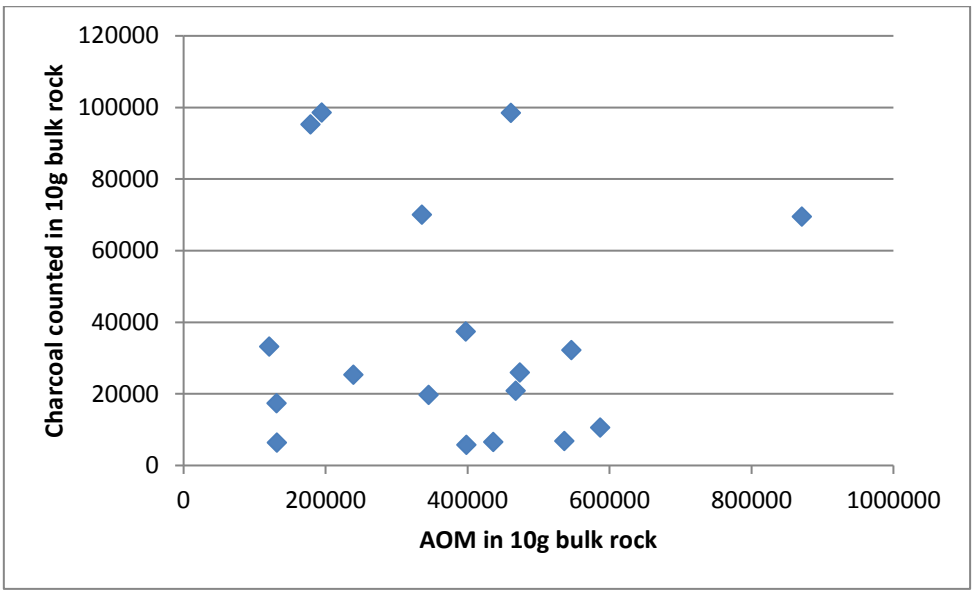

Figure 7.11 – Cross-plot illustrating a lack of trend between increased <125 µm charcoal abundances and increased AOM abundances.

7.4 Discussion

Precession Cycle forced variations in palaeo-wildfire activity

Precession cycles have been shown to force changes in precipitation patterns (e.g. Kutzbach, 1994; Popescu et al., 2006; Daniau et al., 2013). For example, Kutzbach (1994) used a climate model to simulate the effects of Milankovitch cycles on southern hemisphere Pangean climate during the Early Jurassic. Within the simulation Kutzbach (1994) found that the variations in solar insolation, caused by changes in the Earth's precession, were strong enough to influence monsoonal activity. Thus rainfall and run-off over much of the Pangean (sub)tropics would undergo cyclic changes in phase with the precession cycle (Bonis et al., 2010). In particular, the Tethys coastline was found to experience the largest amount of monsoon precipitation during the maximum of the precession index, where summer monsoon precipitation was simulated to exceed 8 mm/day (Kutzbach, 1994). This compares with west equatorial Pangea where rainfall was estimated to have exceeded 2 mm/day (Kutzbach, 1994). Vollmer et al. (2008) used Kutzbach's (1994) model and 'transferred' the results to the northern hemisphere by "inverting the precession signal" (Vollmer et al., 2008, p. 3). Thus periods of low precession index for the

southern hemisphere, become high precession index for the northern hemisphere. Vollmer et al. (2008) found that periods of high precession, and thus times of maximum solar insolation in the northern hemisphere, coincided with times of maximum monsoon intensity for the Early Jurassic. This is anticipated to be due to the high summer temperatures causing increased evaporation of Tethyan seawaters, transporting moisture northwards and over nearby continents (Vollmer et al., 2008). In contrast, during periods of low summer solar insolation in the northern hemisphere (minima precession index, and when summer solar insolation is highest in the southern hemisphere), a decrease in evaporation occurs enabling seasonal drying (Vollmer et al., 2008).

Vollmer et al.'s (2008) analysis of sedimentary facies changes across a precession cycle, deposited at ~30°N in a series of playa cycles, supported this hypothesis, illustrating that high precession and solar insolation in the northern hemisphere likely led to hot, wet summers with maximum monsoonal rainfall, resulting in the deposition of stratified mudstones. In contrast during lowest precession, minimum monsoon precipitation occurred, resulting in the deposition of red, oxidized mudstones that likely formed during cold dry summers (Vollmer et al., 2008). Evidence for changes in the intensity of the monsoon during the precession cycle at a palaeo-latitude of ~30°N can also be observed in pollen data. For example, Bonis et al. (2010) found that within Triassic sediments of St. Audrie's Bay, changes in peaks in spore abundance could be related to precession-induced variations in monsoon strength (maximum monsoon during maximum precession index coincided with a peak in spores), whilst increased palynomorph concentrations could be linked with periods of increased run-off corresponding to the eccentricity cycle.

Are Shifts in fire activity related to changes in seasonality and monsoonal shifts?

Within the Mochras core, the alternations in carbonate rich-to-organic rich beds, determined by hand-held X-ray fluorescence (XRF) (see Ruhl et al., 2016 for more details) are interpreted by Ruhl et al. (2016) to likely represent ~21 kyr precession cycles, following the interpretation of the carbonate rich – organic

rich couplets in the coeval Belemnite Marl section in Dorset (interpreted to represent the ~21 kyr precession cycles (Weedon and Jenkyns, 1999)).

High carbonate production (evidenced by the high Ca content in figures 7.2 and 7.3) is commonly associated with minima precession index, and thus (hemisphere specific) solar insolation minima (e.g. Hilgen et al., 1995; Aziz et al., 2003; 2004; Abels et al., 2005; Natalicchio et al., 2012; Yang and Lehrmann, 2014; Hilgen et al., 2015). During precession index minima, a decline in seasonal contrast weakens monsoonal intensities causing a decline in summer precipitation (Vollmer et al., 2008). As carbonate precipitation has been observed to be facilitated in warmer, shallow seawater (James, 1977; Nelson, 1988) and/or under a low dilution of terrigenous sediment (Chave, 1967; Nelson, 1988), the reduced seasonality during precession index minima is hypothesized to enable carbonate deposition/precipitation under the reduced rainfall and the generally year-round warmer climate (Yang and Lehrmann, 2014). In contrast, the carbonate-poor, organic-rich mudstones are commonly associated with periods of high precession index, and thus solar insolation maxima, where high summer rainfall is suggested to have led to an increased flux of terrigenous material to the shallow marine system, diluting carbonate production (Yang and Lehrmann, 2014; Ruhl et al., 2016). It could therefore be suggested that the carbonate beds with high Ca content within the Mochras core may have been deposited during minimum precession index, whilst the organic-rich, Ca-poor beds may have been deposited during maximum precession index. However it should be noted that little is known about how the astronomical signal is transferred and recorded to the rock record. Furthermore, the influence of Milankovitch cycles on the deposition of sediments is also strongly dependent on the palaeo-latitude at which the sediments are deposited (Ruhl *pers. comms*.). Therefore a link between bed and bundle Ca percentages with precession index and eccentricity maxima/minima remains tentative throughout this study.

Our >125 μm charcoal abundances, located at a palaeo-latitude of ~30°N, display a cyclic pattern of increasing and declining abundances in phase with the Ca-content at the bed scale, where high abundances occur within beds

containing high Ca contents, and low within beds containing low Ca contents and high organic contents (Figure 7.3; 7.4). Assuming that these changes in Ca content are a response to Milankovitch cyclical changes, and represent precession index maxima and minima, then it would appear that the flux of >125 μm charcoal to the study site and/or inferred wildfire activity during the Early Jurassic was strongly influenced by changes in the precession cycle, where high >125 μm abundances appear to occur during precession index minima.

If interpreted as reflecting changes in wildfire activity, the pattern of high charcoal abundances during hypothesized minimum precession index may conform to expectations. During precession index minima, a decline in summer solar insolation is anticipated to lead to a decline in monsoon intensities, resulting in a decline in summer precipitation at ~30°N palaeo-latitude, during the Early Jurassic (Vollmer et al., 2008). During the winter months Vollmer et al. (2008) postulate seasonal drying, but where winters are predicted as being generally warmer (possibly warm enough to cause evaporation of playa systems leading to them drying out (Vollmer et al., 2008)). This compares with maximum precession index, where hotter summers (particularly when summer solstice coincides with perihelion) are anticipated to intensify the monsoon, leading to higher precipitation rates, and where the winters are anticipated to have been much colder. Vollmer et al. (2008) hypothesised that the winters were cold enough that water was unable to evaporate from the playa system studied. Thus a smaller seasonal variation occurs compared with maximum precession index. The Vollmer et al. (2008) hypothesis for seasonal contrasts/interannual variability occurring during the Early Jurassic across a precesional cycle is shown in Figure 7.12.

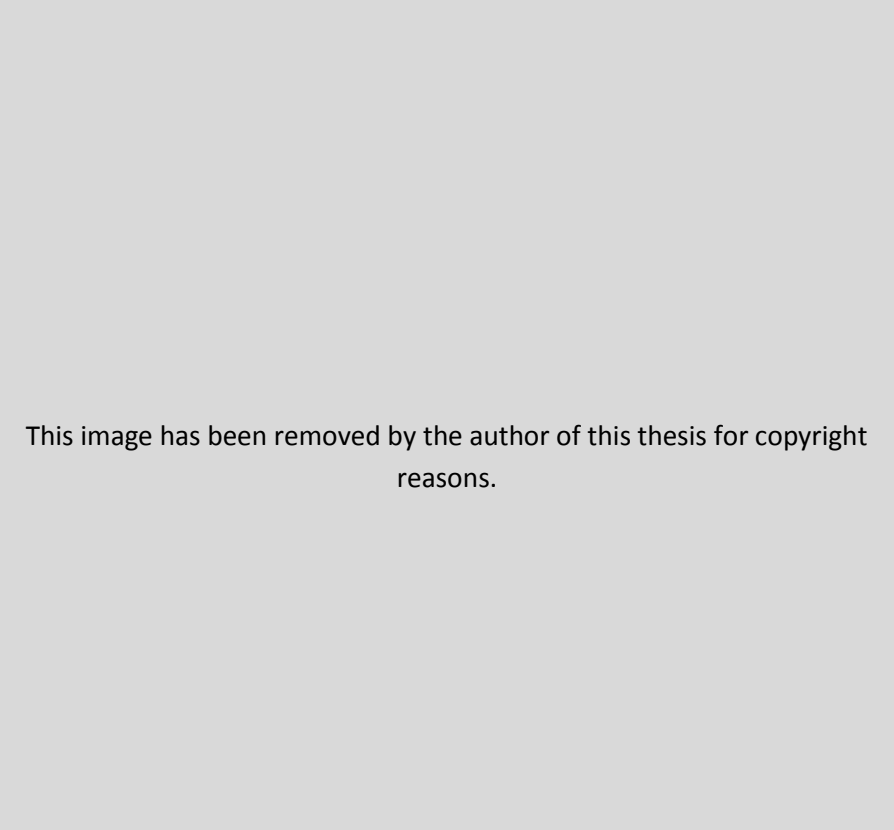

Figure 7.12 – Illustration of changes in inter-annual climate during the course of one precession cycle, at ~30°N during the Early Jurassic (R-annual run-off, Precip – summer precipitation T- temperature) From Vollmer et al. (2008).

Decreased seasonality during minima precession index may have made conditions conducive for extensive burning due to the drying of fuels, enabled by the presence of milder winters, and summers experiencing a less intensified monsoon period (Vollmer et al., 2008). This would increase the susceptibility of fuel to burning, as fuel moisture contents are decreased, and thus the amount of energy required to heat and dry fuels before they can be ignited (probability of ignition and spread) is reduced (Cochrane and Ryan, 2009). The increased ability for fires to spread would ultimately enable increased burning of vegetation and an increased production of charcoal transported to the study site.

Did coupled climate and fuel driven changes influence fire activity?

Another hypothesis for the increase in >125 µm charcoal occurring over the timescale of a precession cycle could be a vegetation change. Shifts in biomass and vegetation dominance across the timescale of a precession cycle are not uncommon, and have been found in both a modern day (Quaternary) section (e.g. Daniau et al., 2013), as well as a deep time (Jurassic) section (e.g. Bonis et al., 2010). Within this section spanning the Late Triassic period through to the Early Jurassic at St Audrie's Bay, Bonis et al. (2010) note a switch in dominant palynomorph taxa across the timescale of a precession cycle, using a principle components analysis (PCA) on "the relative pollen and spore abundance data. By relating the palynomorph taxa with their botanical affinity" Bonis et al. (2010, p. 878) "revealed temperature and humidity gradients in the data" (see Figure 7 in Bonis et al., 2010), where moisture loving, spore producing plants such as lycophytes (e.g. *Heliosporites reissingeri*) and ferns (e.g. *Deltoidospora* spp.) (Srivastava, 2011), are compared with taxa which are linked with cooler, drier conditions such as *Classopollis meyeriana* – a cheirolepidaceous conifer (Bonis et al., 2010; Bonis and Kürschner, 2012). Within the study, periods of increased spore abundance were inferred to reflect wetter phases, which Bonis et al. (2010, p. 883) note "may be related to intensified monsoon activity on the precessional scale", and are thus 'tentatively assigned' to maximum precessional index and the precession cycle. In comparison less humid phases (tentatively linked with precession index minima and minimum summer insolation and monsoon intensity (Vollmer et al., 2008; Bonis et al., 2010) were found to correspond to a decline in spore abundance and spore producing taxa, and an increase in conifer pollen (Bonis et al., 2010).

The taxa observed by Bonis et al. (2010) are also common throughout the Early Jurassic (Gradstein and Kerp, 2012) and although these phase changes in dominant plant taxa were described for the latest Triassic, and in sediments located ~120 km south of the Mochras core site, it is likely that similar cyclic phases in vegetation occurred on the land close to Mochras in response to orbital shifts.

A similar set of cyclic changes in dominant vegetation type from ferns to conifers could explain the observed variations in the abundance of >125 µm

charcoal particles, where high charcoal abundances would be anticipated to occur during the less humid, precession index minima periods, associated with a decline in spore producing fern vegetation (moisture loving plants), and a rise in dominance of conifer pollen (better adapted to lower moisture) (e.g. as in Bonis et al., 2010). Interestingly, conifers also have a high quantity of terpenes (Ormeño et al., 2009; Belcher, 2013). Terpenes have a high heating value, meaning that they have the potential for larger heat release during combustion (Zhao et al., 2012; Belcher, 2013; Simpson et al., 2016), which could aid fire propagation by heating and drying fuels ahead of the fire (Núñez-Regueira et al., 2005; Ormeño et al., 2009; Zhao et al., 2012; Belcher, 2013; Simpson et al., 2016).

It could therefore be suggested that a combination of summer solar insolation forced changes in precipitation (e.g. Vollmer et al., 2008) and climate-driven floral change (e.g. Bonis et al., 2010) which together may have interacted over the course of the ~21 kyr precession cycle timescales to influence fire activity. Further study is therefore required to assess whether any shifts in vegetation occur across precessional cycles during the Pliensbachian, and high-resolution palynological studies are therefore worthy of study in the future within the Mochras core.

Potential evidence for climate and vegetation forcings on preservation and run-off

Unlike the >125 µm charcoal record, relative variations in plant cuticle abundances and <125 µm charcoal across the Ca-rich – Ca-poor lithological changes at Mochras appear less straight forward, and instead, variations in plant cuticle abundances may seem at odds to the notion that Ca-rich beds may be deposited during a period of low precession (e.g. as suggested by Hilgen et al., 1995; Aziz et al., 2003; 2004; Abels et al., 2005; Natalicchio et al., 2012, and Yang and Lehrmann, 2014). Within the studied section, total plant cuticle abundances, although slightly precede maximum %Ca (and hypothesized precession index minima), do appear higher compared with the organic rich beds containing lower %Ca (Figure 7.3). The <125µm charcoal appears uninfluenced by the bed-scale changes in Ca content (Figure 7.2).

Changes in plant cuticle abundances could be indicative of variations in terrestrial plant biomass and/or the amount of influx of material to the study site and/or changes in the preservation potential at the site of deposition (Gorin and Steffan, 1990). Enhanced seasonality, particularly rainfall seasonality, is described as producing “the ideal situation for increasing fuel load” and vegetation biomass (Daniau et al., 2010, p. 5071). Therefore plant cuticle deposition may be expected to increase during periods of enhanced seasonality and monsoonal intensity (with the more organic-rich (low Ca content) beds), as opposed to a period of equable all-year round climate with little seasonality. Tentatively linking the Ca-poor beds with precession index maxima means that an alternative hypothesis of variations in the amount of terrestrial material from run-off, delivering phytoclasts (including charcoal) to the study site, appears unlikely.

Charcoal deposited in the shallow marine environment is commonly transported via fluvial and/or aeolian processes (Patterson et al., 1987). Following a fire, charcoal particles have been found to either fall to the surrounding burn area where they are held in soils and later transported to the marine setting via fluvial processes (run-off and riverine transport), or are transported almost immediately via atmospheric processes to the marine environment (Griffen and Goldberg, 1975). Smaller fragments have been shown to be more susceptible to being carried large distances by the wind, compared with larger fragments that tend to be deposited closer to the burn site (Radtke et al., 1991). Therefore if this hypothesis were correct, the larger >125 μm size fraction of charcoal, coupled with the increased plant cuticle abundances, would be expected to reflect periods of enhanced run-off driven by maximum precession index (Vollmer et al., 2008), enabling a flux of terrestrial phytoclasts to the depositional study site.

These hypotheses could suggest that the low carbonate beds, with higher abundances of charcoal and plant cuticles should be occurring during maximum precession index, not minima. However, Ruhl et al. (2016) identify that iron (Fe) and titanium (Ti) concentrations taken from the Mochras core fluctuate across the Ca rich-Ca poor lithological cycles, but in opposition to Ca contents, such that high Fe and Ti concentrations occur during low Ca percentages and *vice versa*. Ruhl et al. (2016) interpret the high Fe and Ti concentrations during the

high TOC and low Ca beds to suggest carbonate dilution, supported by relative fluctuations in the hydrogen index (HI) where low HI values, indicative of high terrigenous influence (Fahl and Stein, 1997), corresponding with low Ca percentages (Ruhl et al., 2016). A similar interpretation can be found in the Huang et al. (2015) study whereby low carbonate content beds occurring during an interglacial phase and found in a core taken from the South China sea, were hypothesized to reflect a high terrigenous input causing dilution of carbonate percentages. This finding would correspond well with a period of high precession index relating to the low carbonate beds, where an intensification of the monsoon during the Jurassic has been modelled and predicted (Vollmer et al., 2008). Therefore a period of increased delivery of terrigenous material including charcoal to the study site during the deposition of the Ca-rich beds is unlikely, and therefore provides support to the tentative link between the depositions of Ca-rich beds during precession index minima.

It may also be possible that plant cuticle was variably preserved during different phases of the precessional cycle. However this appears unlikely, as wet conditions are known to preferentially preserve plant cuticles from aerobic decay (Retallack et al., 1999; Gorin and Steffan, 1991). Hence a larger proportion of charcoal would be expected to have been preserved under the increased precipitation postulated during maximum precession index. Furthermore, thin section analysis conducted by Ruhl et al. (2016, p. 4) indicate “evidence for early diagenetic processes, such as calcite replacement and cementations, possibly resulting from the degradation of organic matter and the associated reduction of sulphate” within the Ca rich beds. Hence, it is unlikely that higher abundances of >125 μm charcoal and plant cuticles within the high %Ca content beds are reflective of changes in terrigenous supply and/or preservation and may instead reflect true climate/vegetation induced changes.

Eccentricity cycle related changes in fire activity

Within the studied section of the Mochras core, the 'bundles' of carbonate rich vs carbonate poor beds are interpreted as likely representing the short eccentricity cycle (~100 kyrs) (Ruhl et al., 2016). As eccentricity is thought to modulate the precession cycle, the sedimentary signal is suggested to be similar to that produced during a precession cycle where carbonate percentages are generally higher during minimum (short) eccentricity (Wu et al., 2013).

In comparison to the bed scale %Ca changes occurring over a precessional cycle timescale (Ruhl et al., 2016), variations in the bundle Ca content occurring over the timescale of a short eccentricity cycle (Ruhl et al., 2016), appear coeval with variations in all phytoclast abundances analysed (with the exception of AOM). Here, pollen and spore abundances appear higher averaging ~16,341 between core depths 936.00 m and 937.80 m where 'bundle' Ca contents appear lower (Figure 7.3). This compares with averages of ~4,463 between core depths 934.20 m and 936.00 m, and ~6,708 between core depths 937.80 m and 939.80 m where bundle Ca contents appear generally higher. In contrast, the <125 µm charcoal abundances are lower, in line with the lower 'bundle' Ca percentages (Figure 7.2).

The >125 µm charcoal fraction, which I have shown varies with bed scale %Ca content variations occurring over the timescales of a precession cycle, also appears to relate to 'bundle' Ca changes occurring over the timescale of a short eccentricity cycle, exhibiting generally lower abundances during lower bundle %Ca, compared with higher %Ca bundles (Figure 7.2). A similar pattern of change is observed within the plant cuticle abundances, which follow changes in bed scale Ca content changes occurring across precession cycle timescales, until de-trended %Ca reach minimum values at 937.5 m, where plant cuticle abundances are high despite the low bed (and bundle) Ca content (Figure 7.3).

Changes in the eccentricity of the Earth's orbit can control the magnitude of the precession cycle, and thus precession driven climate changes (Tuenter et al., 2003; Vollmer et al., 2008; Martinez and Dera, 2015). Hence it is not surprising that changes in bundle Ca contents occurring over the timescale of a short eccentricity cycle (Ruhl et al., 2016) appear to have an over-riding effect on >125 µm charcoal, plant cuticle and bed-scale %Ca in the Mochras core. Yet, it

is surprising that the <125 μm charcoal abundances, and pollen and spore abundances vary across the bundle scale %Ca variations occurring over a short eccentricity cycle timescale, yet do not vary across the couplet scale %Ca occurring over a precession cycle timescale. Further work should therefore look to analyse variations in phytoclasts, including charcoal at high resolution, over a longer timespan to test whether a precession scale signal in the <125 μm charcoal and pollen and spore, and plant cuticles can be observed elsewhere within the Mochras core, and assess whether the observed variations represent a true signal.

Eccentricity changes are hypothesized to have led to abrupt and potentially larger magnitude changes in seasonality and monsoonal activity during the Early Jurassic period (Bonis et al., 2010; Martinez and Dera, 2015), and may even have been capable of indirectly pacing continental weathering rates and riverine inputs over long multi-million year timescales (Martinez and Dera, 2015).

Maximum eccentricity in the Mesozoic is often associated with high seasonality, experiencing “annually dry climates disturbed by short periods of intensive rainfalls and storms, alternating between the Northern and Southern Hemispheres (Ma et al., 2011; Sprovieri et al., 2013)” (Martinez and Dera, 2015, p 12607). The high seasonal contrast during eccentricity maxima is suggested to have led to the development of intensified monsoons (also termed mega-monsoons) during the wet seasons (precession index maxima), enabling increased run-off rates and the increased transportation of material from the terrestrial to the marine realm (Bonis et al., 2010; Martinez and Dera, 2015). Interestingly at the nearby Triassic section at St Audrie’s Bay, Bonis et al. (2010) observe an increase in terrestrial palynomorph concentrations occurring over the timescale of a short eccentricity cycle, which Bonis et al. (2010, p. 884) also interpret to likely reflect enhanced monsoon activity “and more run-off during eccentricity maxima”. The increase in terrestrial palynomorph concentrations were found to occur during the deposition of organic carbon rich black shale beds, which Bonis et al. (2010) note support the interpretation that the high terrestrial palynomorph concentrations were occurring during eccentricity maxima. Based on this, the low Ca-content, high organic content couplets found in the Mochras core, occurring over the timescale of

approximately half a short eccentricity cycle, could also be tentatively linked with periods of high eccentricity. It is within this low carbonate part of the bundle, that our pollen and spore abundances and plant cuticle abundances appear high (Figure 7.3), whilst both >125 μm and <125 μm charcoal abundances appear generally lower (Figure 7.2).

One interpretation could be that during eccentricity maxima, conditions become conducive for phytoclast preservation (particularly during precession maxima), allowing for an increase in the abundance of pollen and plant cuticles to be preserved in the studied Mochras sediments. However, this would not explain the low charcoal abundances observed during this period. Another interpretation could be that the high plant cuticle and pollen abundances are reflecting a period of increased terrestrial biomass and/or the delivery of terrestrial material to the study site during eccentricity maxima. This could support the Bonis et al. (2010, p. 884) hypothesis that during 'high eccentricity' periods "an intensified monsoon system may induce extension of the climate belts. Because moisture penetrated further into the hinterland, vegetation such as Cheirolepidiaceae and other gymnosperms could cover a larger area, and enhanced seasonal runoff would transport a relatively large amount of pollen, as is reflected in the low spore abundance during eccentricity maxima". Although further study would need to be conducted identifying the species of pollen preserved across these timescales in the Mochras core. However, if this were true, the lower charcoal abundances found during eccentricity maxima at Mochras, are unlikely to have been caused by a decline in the delivery of charcoal to the study site. Hence we hypothesize that the lower <125 μm and >125 μm charcoal abundances occurring during these periods, suggests suppression of wildfire activity, despite the hypothesized expansion of vegetation and thus potential fuel loads, and increased terrestrial run-off (Bonis et al., 2010).

The expansion of climate belts and 'moisture penetration' into hinterlands away from coastal regions during eccentricity maxima (Bonis et al., 2010) may likely have increased fuel moisture, meaning that the probability of ignition and fire spread becomes lower, and potentially over a larger area of the land surface, particularly during precession maxima (Bonis et al., 2010). During combined eccentricity maxima and precession minima, a decline in summer precipitation

is hypothesized, leading to a warmer, drier annual climate (Vollmer et al., 2008; Bonis et al., 2010; Martinez and Dera, 2015). During this period our >125 μm char abundances still increase during precession index minima, although appear slightly lower when compared with periods when inferred precession minima coincides with inferred eccentricity minima (e.g. core depths ~935.80m and ~939.20 m) (Figure 7.2). It could therefore be hypothesized that during periods of precession minima and eccentricity maxima, the annually drier conditions may be more conducive for burning due to the likely decline in fuel moisture as previously discussed, and may therefore explain the continued observed variation in >125 μm charcoal abundances across the precessional cycle. In comparison, the <125 μm char abundances appear consistently low throughout the inferred eccentricity maxima period, irrespective of changes in precession index. Charcoal particle sizes of <125 μm have typically been attributed to a regional signal of burning (Conedera et al., 2009), thus a larger, extended area experiencing increased seasonal rainfall during eccentricity maxima, may explain the reduced abundances of the <125μm size fraction of charcoal reaching the study site.

In contrast during eccentricity minima, a decline in monsoonal intensities and the development of moderate seasonal contrasts in both hemispheres is hypothesized (Martinez and Dera, 2015). It could therefore be suggested that during eccentricity minima, a reduction in climate belt extent (Bonis et al., 2010) may have enabled a reduction in vegetation moisture content, making vegetation more susceptible to burning. This coupled with the predicted potential of a larger, more extensive fuel source covering areas further in-land (Bonis et al., 2010) may have led to a larger burn area, where the development of Cheirolepidiaceae and other gymnosperms could further aid in fire spread and propagation (as previously discussed). It may be this more extensive ‘regional’ fuel source that is being translated into the charcoal record through the increase in the smaller <125 μm abundances.

7.5 Conclusion

Our charcoal and palynofacies data taken across well-defined high and low carbonate content beds and couplets occurring across the timescale of precession and short eccentricity cycles within the Early Jurassic Mochras core - indicate that palaeo-wildfire activity is very sensitive to orbitally driven changes in climate and possibly vegetation. Here, variations in the larger >125 μm fraction of charcoal and plant cuticle abundances observed across bed-scale variations in Ca-content occurring over the timescale of a precession cycle, may be reflective of vegetation shifts similar to those postulated by Bonis et al. (2010) across such timescales, where a shift from spore to conifer pollen abundances during a transition from hypothesized maximum precession index (modelled to drive an intensified monsoonal period across Tethys) to minima precession index (modelled to experience a weakening of the monsoonal period enabling drier conditions to prevail) appear to match our shift from low charcoal and plant cuticle abundances to high charcoal and plant cuticle abundances, if Ca-rich beds are tentatively linked with precession index minima. Across bundle scale Ca changes, occurring across the timescale of a short eccentricity cycle, all analysed phytoclasts (except AOM) appear to vary in accordance with the changes in Ca content. Changes in eccentricity modulate the magnitude of the precession cycle, hence it is surprising that the <125 μm charcoal abundances, and pollen and spore abundances vary across the bundle scale %Ca variations occurring over a short eccentricity cycle timescale, yet do not vary across the couplet scale %Ca occurring over a precession cycle timescale.

Bonis et al. (2010) postulate that short (100 kyr) eccentricity cycles may have enabled the expansion of climate belts during eccentricity maxima, which could have allowed for the expansion of vegetation in-land within the Tethys region during the Early Jurassic period. Our variations in both the smaller <125 μm and larger >125 μm fractions of charcoal across these eccentricity timescales may provide support for the Bonis et al. (2010) hypothesis as a larger, regional scale expansion of vegetation could provide a larger fuel source for fires. As the <125 μm fraction is commonly linked with regional scale signals of burning, the variations in the <125 μm could be reflective of the larger, more extensive fuel source postulated by Bonis et al. (2010). However, future work should look to

test whether a precession scale signal in the <125 μm charcoal and pollen and spore, and plant cuticles can be observed elsewhere within the Mochras core to corroborate these findings.

Our data illustrate that natural variations in charcoal abundance are possible over intermediate timescales within the geological record, and thus suggest a need to take into consideration and incorporate 'natural background' fluctuations in fire activity occurring over medium timescales, when analysing and predicting past and future climate change patterns. This is particularly important when analysing charcoal from sediments that are likely to have been influenced by monsoons during deposition.

8. Discussion and Synthesis

8.1 Introduction

This chapter summarises and discusses the research presented in this thesis; how each of the aims set out in section 1.4 have been addressed, the key findings and contribution of the findings to the field of research, and the potential for future research.

8.2 The role of fire as a feedback process in ending significant, global C-cycle perturbation events (OAEs) over long timescales, and testing model hypotheses that OAEs were terminated due to a rise in atmospheric O_2.

8.2.1 Summary of research and key findings

As outlined in Chapter 3, burial of C_{org} and reduced sulfur (pyrite) generate long-term build-up of O_2 in Earth's atmosphere (Garrels and Lerman, 1984; Kump, 1988; Berner, 1999; Lenton and Watson, 2000b; Berner, 2004; Canfield, 2005). It has thus been predicted that during an OAE, where increased burial of C_{org} and pyrite (Gill et al., 2011) occur, that atmospheric O_2 concentrations should have risen (Handoh and Lenton, 2003). Within Handoh and Lenton's (2003) model (Figure 3.18), atmospheric O_2 is predicted to rise gradually throughout the OAE, starting from the onset of the OAE and C_{org} burial, and should peak during its termination where the high atmospheric O_2 concentrations aid in the termination of the event. However, this has never been tested in the geological record.

Wildfire has been shown to respond strongly to changes in atmospheric O_2 (Watson, 1978; Belcher and McElwain, 2008; Belcher et al., 2010b) and has been implicated in providing an essential long-term negative feedback, counteracting rising atmospheric O_2 throughout geological time (for example, see Kump, 1988; Handoh and Lenton, 2003; Lenton, 2013). Hence, wildfire activity provides a

suitable proxy to test Handoh and Lenton's hypothesis, that should track projected atmospheric O_2 changes across an OAE (e.g. see Figure 4a in Handoh and Lenton, 2003 or figure 3.18, Chapter 3 herein). The findings presented in Chapter 4, and published in Baker et al. (2017), test this hypothesis and contribute the first fossil based evidence in support of these model predictions (Handoh and Lenton, 2003).

Chapter 4 presents an analysis of the wildfire record in the form of fossil charcoal abundances, taken across the Toarcian OAE. Here, increased abundances of total charcoal occur during the final stages of the T-OAE, appearing coeval in two separate study sites that were located at a palaeo-latitude of ~30°N. The coeval rise in charcoal abundances when compared with the most up-to-date published calibrated cyclostratigraphic timescale (Huang and Hesselbo, 2014), appear to occur over the ~1 million year timescale predicted for atmospheric O_2 variations (Lenton and Watson, 2000b; Handoh and Lenton, 2003; Catling and Clare, 2005; Lenton, 2013). Charcoal abundances were found to begin to rise ~1 Myrs after the onset of the OAE, and remain elevated for ~800 kyr until the OAE has been terminated. Thus the observed variations in charcoal abundances are hypothesized to have been driven by changes in atmospheric O_2. The results presented in this thesis corroborate the previous model based hypothesis postulated by Handoh and Lenton (2003) that a rise in atmospheric O_2 concentrations, driven by the increase in C_{org} burial, is capable over the timescale of an OAE, and may have led to its termination.

As wildfire has been implicated in providing an essential long-term negative feedback, counteracting rising atmospheric O_2 throughout geological time (e.g. Kump, 1988; Lenton and Watson, 2000b; Handoh and Lenton, 2003; Lenton, 2013), the hypothesized rise in atmospheric O_2 driven fire activity may have played an essential feedback role during the final stages of the OAE. The increase in wildfire activity ought to have significantly enhanced the suppression of vegetation (Lenton, 2013) assisting in terminating the T-OAE by causing a decline the weathering of P, due to the removal of large land plants, with deep roots under high fire frequencies which would decrease the amount of P delivered to the oceans. This should cause ocean primary productivity and the demand for O_2 in the water column to decline. This fire-driven suppression of vegetation

leading to alterations to ocean P coupled with rising atmospheric O_2, may have combined to aid in the re-oxygenation of the Jurassic oceans, which in turn, would enable more P to be efficiently removed to sediments (Handoh and Lenton, 2003). As the ocean starts to re-oxygenate this is predicted (Handoh and Lenton, 2003) to increase the removal of P adsorbed to iron oxide minerals (Fe–P)) (Colman and Holland, 2000) and P preserved in organic matter (Org-P) (Van Cappellen and Ingall, 1994; 1996), lowering the ocean PO_4 concentration. This would therefore lower the O_2 demand in the water column, creating a strong positive feedback strengthening the re-oxygenation of the ocean. The increased abundance of charcoal, taken as a proxy for a rise in wildfire activity presented in Chapter 4 supports this hypothesis indicating that O_2 driven fire feedbacks occurring over the long Myr timescale, may have played a significant role in terminating Jurassic anoxia.

8.2.2 Contributions to the research field

The results presented in Chapter 4 and published in Baker et al. (2017) are important as they capture a geologically rapid rise in fire activity that we postulate to be a result of enhancement of atmospheric O_2 occurring over the short timescale of the Toarcian OAE. This implies that small but significant changes in O_2 may be possible over the timescale of OAEs, and as such, these rapid C-cycle driven changes to atmospheric O_2 suggest that new higher time-resolution models of O_2 over Earth's history may be required to explore the relationship between changes in C-cycling and the functioning of the Earth system. This is particularly significant for numerical O_2 prediction models that use multi-million year 'time-steps' such as the GEOCARB model (time-steps of ~10 Myrs) (Berner and Kothavala, 2001); the rock abundance model (time-steps of ~9 Myrs) (Berner and Canfield, 1989) and the GEOCARBSULF model, (which although is conducted every 1 Myrs, is smoothed over every 10 Myrs) (Berner, 2006), which will miss these significant, geologically short term events.

The importance of fire as a feedback mechanism in the natural world, and in regulating atmospheric O_2 concentrations within the 'fire window' have been explored by some Earth system models (for example COPSE (Bergman et al., 2004)), that depend on the sensitivity of fires to atmospheric O_2 and the impact

that fires have on vegetation biomass (Bergman et al., 2004; Lenton, 2013) to regulate atmospheric O_2 (as discussed in Chapter 3). For example, Bergman et al. (2004) illustrated that without the effect of increased O_2-driven fire activity suppressing vegetation, atmospheric O_2 concentrations become poorly regulated, where estimates rise to nearly 1.7 times PAL (~35.7% vol.) during the Cretaceous period (~100 Ma), and where PAL do not decline enough to reach their current measured levels of 21% vol. (see Chapter 3, Figure 3.11). The key role that fire plays as a feedback process via a control over P weathering/distribution to the marine system has been illustrated by Kump (1988) and Lenton (2013), where debate remains as to whether fires aid in the redistribution of P from the land to the oceans (e.g. Kump, 1988) or whether fires act to limit P weathering through the suppression of land vegetation (e.g. Lenton and Watson, 2000b; Bergman et al., 2004). It has been shown that removing the influence of fires on P re-distribution (e.g. Kump, 1988) appears to have little effect on modelled atmospheric O_2 changes compared with the effect of fire on P weathering (e.g. Bergman et al., 2004), with one exception at ~300 Ma (Figure 8.1), suggesting that the feedback is weak. Furthermore, Inghall and Jahnke (1994) and Lenton and Watson (2000b) also found Kump's (1988) P re-distribution feedback to be too weak in stabilizing atmospheric O_2 estimates (Lenton, 2001). Thus the effect of fires on P weathering through the suppression of land vegetation is postulated to present the most significant feedback (e.g. Lenton and Watson, 2000b; Lenton, 2001; Handoh and Lenton, 2003; Lenton, 2013).

In Lenton (2013), P weathering by plants is separated from the silicate continental weathering forcing function used in the 2004 COPSE model (Bergman et al., 2004). Instead Lenton (2013, p. 303) assumes that "P weathering depends linearly on the uplift of land during mountain building, is halved under abiotic conditions, and the half that is under biological control depends on vegetation biomass and hence fires." This separation (and new formulation) allows for the analysis of the role of fire in the distribution and weathering of P to the marine system (and subsequent C_{org} burial and O_2 concentrations) even during periods of expected higher continental weathering rates e.g. due to continental uplift/degassing. Lenton (2013) found that this separation instantly resulted in a "striking stabilization of atmospheric oxygen" where peaks in O_2 occurring during

the Permian period reached 23% vol. and lowest O_2 concentrations reached 20.6% vol. during the Middle Triassic (Lenton, 2013, p. 303). This is important, as Lenton's (2013) study indicates that this remarkable stabilization from the effect of fires on the weathering of P can occur even during times of high degassing and thus high silicate weathering rates, which forces C_{org} burial and atmospheric O_2 concentrations up – something that is often observed during OAEs. An example of this can be observed for the Cretaceous period, which is often associated with high rates of degassing (Li et al., 2016). Here, switching off the feedback of fire on P weathering produces peak O_2 estimates of up to ~27% vol. during the Cretaceous period, whilst including the suppression of vegetation and thus P weathering by an increase in fire activity, brings O_2 estimates down to ~22% vol. (Figure 8.1), demonstrating the significant role that fire plays as a feedback process.

The results presented in Chapter 4, illustrating a sustained period of high charcoal abundances and thus inferred wildfire activity towards the end of the OAE, therefore provides the first fossil evidence that fire feedbacks may have aided in the termination of ocean anoxia, enabling the return of oxygenated waters. This is important as it appears that O_2-fire-O_2 feedbacks may have the ability to regulate key processes that help in re-oxygenating the ocean, returning the Earth system to background functioning after a significant perturbation to the C-cycle. Hence, maintaining the natural functioning of wildfire in the modern world may be key to aid in the continued regulation of the Earth system.

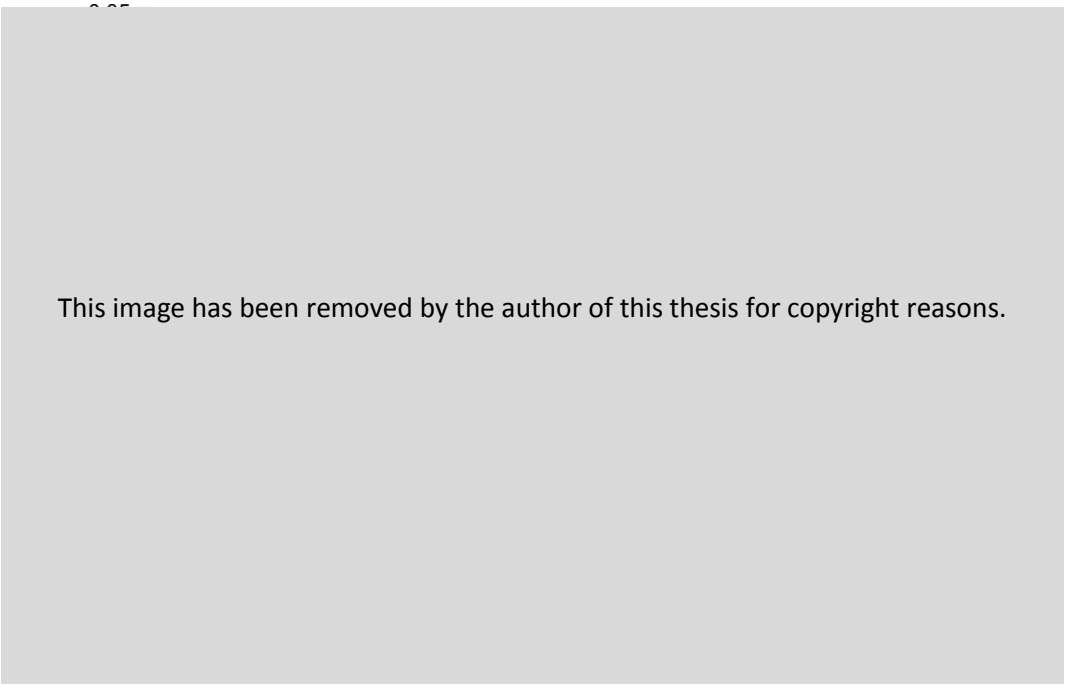

Figure 8.1 – Modelled variations in atmospheric O_2 for the last ~350 Myrs, using Lenton's (2013) "new formulation of fire feedback on phosphorus weathering (dashed line), and the effect of removing fire feedback on phosphorus redistribution from this (dot-dash line)." The solid line represents the baseline model run. (Taken from Lenton, 2013, p. 304).

8.2.2.1 Could this 'natural mechanism' of rising atmospheric O_2 also be true for other OAEs?

The re-occurrence of Cretaceous OAEs (1a, 1b, 1d, OAE 2 and OAE 3) is hypothesized to be due to a shift in the Earth system towards a "self-sustaining oscillation" involving switches between an oxic and anoxic ocean (Handoh and Lenton, 2003). Here, fast positive feedbacks between P concentrations, primary productivity and ocean anoxia are counteracted by slower negative feedbacks involving the gradual rise in atmospheric O_2 that is hypothesized to eventually end ocean anoxia (Handoh and Lenton, 2003).

In Chapter 4, the record of fossil charcoal taken across the T-OAE provided the first fossil based evidence in support of Handoh and Lenton's (2003) hypothesis, that rising atmospheric O_2 concentrations and resultant fire feedbacks may have acted together to 'naturally' terminate the T-OAE. Based on this fossil evidence, it could therefore be hypothesized that rising atmospheric O_2 should also be observed towards the termination point for all other anoxic events, in particular

those found during the Cretaceous period for which Handoh and Lenton's (2003) model hypothesis was based upon.

As outlined in Chapter 5, testing this hypothesis using the record of wildfire for the Cretaceous period is problematic due to the estimated high atmospheric O_2 during the Cretaceous of between 23% vol. and 27% vol. (Lenton, 2013, Mills et al., 2016), and the resulting decline in sensitivity of ignition probability and fire spread to O_2 changes around these high O_2 estimates (Belcher et al., 2010). However there may be other geological clues that could provide support for this hypothesis.

In 2006 Hu et al. (2006, p. 182) identified Cretaceous Oceanic Red Bed (CORBs) deposits, occurring approximately the same number of times to that of the Cretaceous OAEs, and "mostly reoccurring alternately" to the OAE beds. Of particular interest are the two globally extensive CORBs that can be found following the globally widespread organic rich deposits of OAEs 1a and 2 (e.g. Hu et al., 2006; Xi et al., 2007; Wagreich et al., 2009; Wang et al., 2011; Neuhuber and Wagreich, 2011; Hu et al., 2012) (Figure 8.2, 8.3). Oceanic red beds (ORBs) form in the marine environment under highly oxic bottom water conditions (Hu et al., 2005; Wang et al., 2011; Neuhuber and Wagreich, 2011) presented as red shales and/or marls (Xi et al., 2007). Detailed mineralogical studies indicate that the origin of the CORB's red colouration is predominantly due to the presence of hematite (or iron oxide), that form under oxic conditions and provide the sediments with their distinct red colouration (Hu et al., 2012). The presence of these beds has therefore been used as an indicator for changes in bottom water oxygenation (Wang et al., 2011).

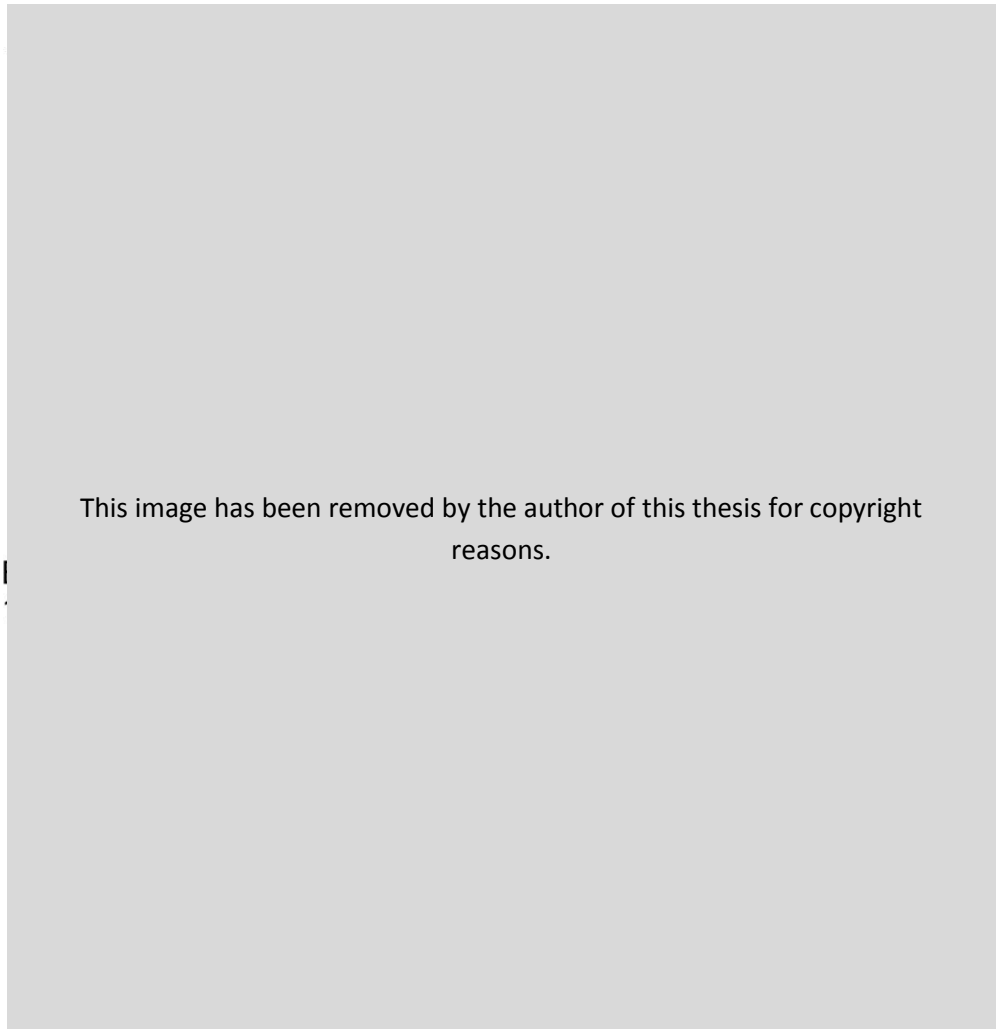

Figure 8.2 – Palaeogeographic map illustrating the widespread deposition of OAE 1a deposits ~120 Myrs ago **(A)** and CORB deposits at 105 Myrs ago **(B)** compiled from published literature by Wang et al. (2011). Black circles represent deposits exhibiting all three OAE deposit characteristics including a high organic matter content, excursion in the $\delta^{13}C$ record and deposition of back shales; half black, half white circles represent deposits exhibiting two out of the three OAE deposit characteristics, and white circles represent deposits exhibiting just one out of the three OAE deposit characteristics.

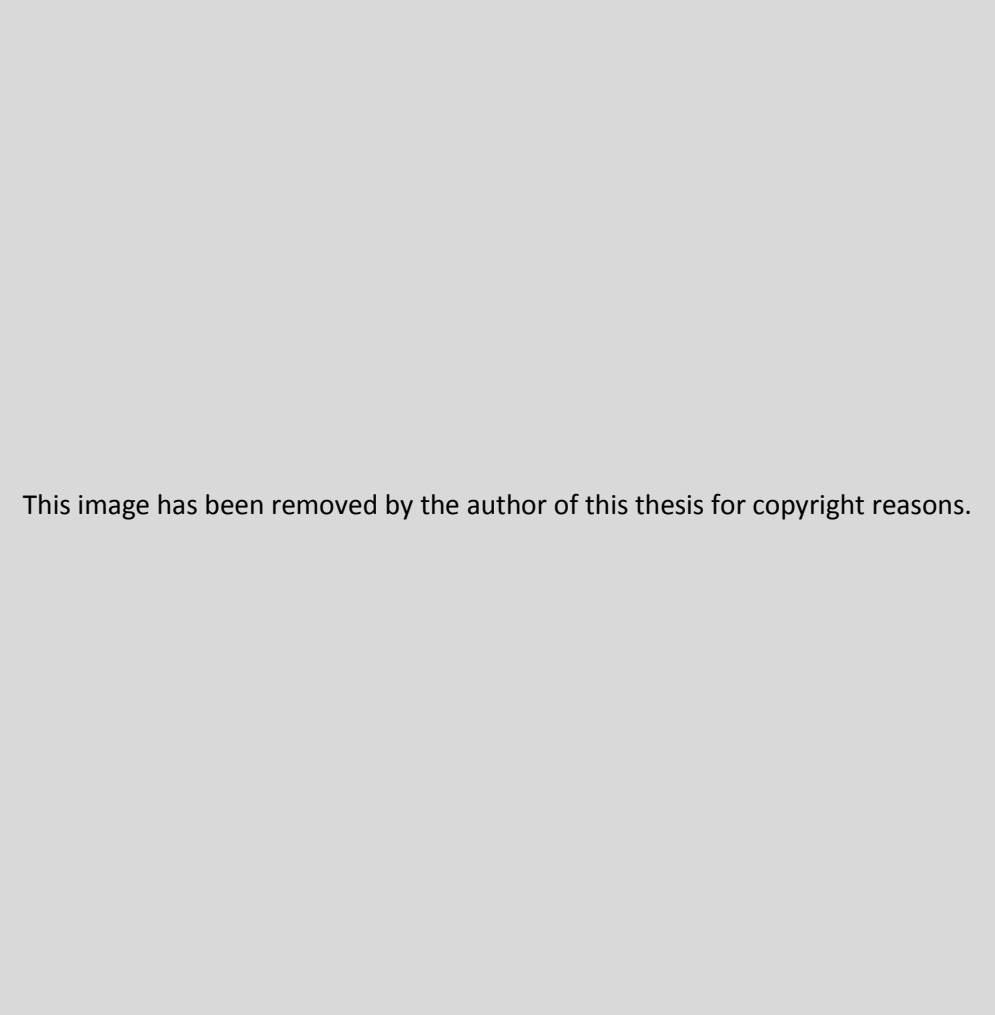

Figure 8.3 – Palaeogeographic map illustrating the widespread deposition of OAE 2 deposits ~93 Myrs ago **(A)** and CORB deposits at 80 Myrs ago **(B)** compiled from published literature by Wang et al. (2011). Black circles represent deposits exhibiting all three OAE deposit characteristics including a high organic matter content, excursion in the $\delta^{13}C$ record and deposition of back shales; half black, half white circles represent deposits exhibiting two out of the three OAE deposit characteristics, and white circles represent deposits exhibiting just one out of the three OAE deposit characteristics.

The formation of CORBs has often been associated with the presence of cold, O_2-rich bottom waters, likely forming due to a change in global climate and/or alteration in ocean circulation (e.g. Xi et al., 2007; Wagreich, 2009; Wang et al., 2011; Hu et al., 2012). In recent years, this has been linked to the occurrence of OAEs where rapid drawdown of CO_2 by primary producers and increased amounts of C_{org} and pyrite burial during an OAE, is suggested to have initiated global cooling and resulting enhanced formation of cold deep water which has a higher dissolved O_2 content and thus a higher "oxidising capacity" (Hu et al., 2012, p. 244). Figure 8.4 illustrates this simplified feedback process hypothesized

by Wang et al. (2011) leading to a well oxygenated ocean and lower surface productivity.

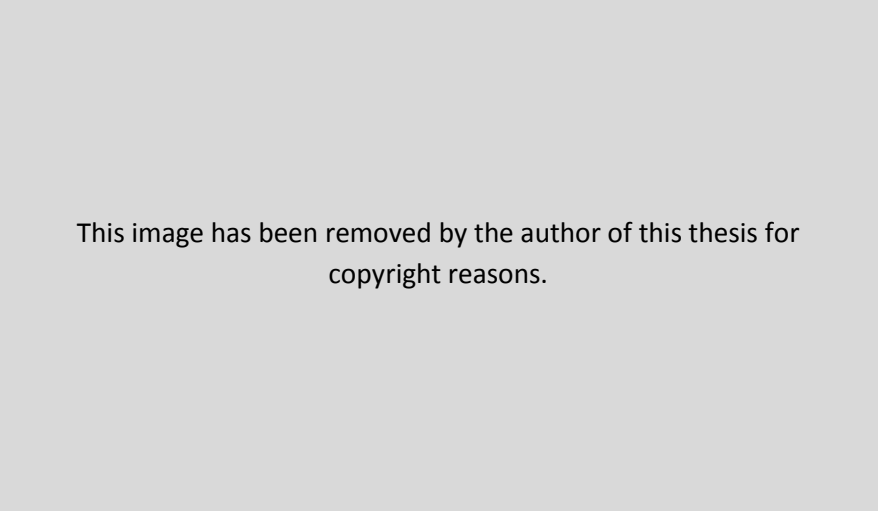

Figure 8.4 – Simplified model hypothesized by Wang et al. (2011, p. 35) "for the transition from Cretaceous OAEs to CORBs"

Wang et al. (2011, p.35) and Hu et al. (2012) further briefly suggest that the enhancement of C_{org} burial during an OAE could have resulted in "an equal addition of O_2 to the atmospheric oxygen reservoir, assuming a CO_2-to-O_2 photosynthetic ratio of 1:1 (Arthur et al., 1988, p. 716)", however the main focus appears to remain on the switch to a cooler climate (e.g. Xi et al., 2007; Wang et al., 2011; Hu et al., 2012).

The apparent global nature of the CORBs, and their coeval deposition within the deep ocean (e.g. North Atlantic) and in basinal and slope environments (e.g. Tethys) suggests that like OAEs, these CORB deposits may "indicate a widespread or even global change in the climate-ocean system" (Hu et al., 2012, p. 238) (see also Wagreich et al., 2009 and Wang et al., 2011). This is particularly the case for CORBs following OAE 2 deposits, where Wagreich et al. (2009, p. 84) hypothesize that "a widespread or even global change in the climate-ocean system" was "the primary cause for the end of global OAE 2" where, "geochemical and isotope evidence from the Ultrahelvetic Buchberg section suggests that palaeo-oceanographic conditions changed gradually from anoxic during the latest Cenomanian OAE 2 to oxic during the Early to Middle Turonian".

The ‘transition time’ between the Cretaceous OAE 1a and OAE 2 deposits and the deposition of CORBs is found to occur over Myr timescales (Wang et al., 2011), with transition times of ~0.95 Myrs between the end of OAE 1a and a the beginning of CORB 1 in the Gorgo a Cerbara section in Italy (Hu et al., 2012), and ~1.3 Myrs between the end of OAE 1a and the beginning of CORB 1 in the Yenicesihlar section in Turkey (Hu et al., 2012). This Myr timescale is also observed between the deposition of OAE 2 deposits and CORB deposits, where in the Umbria–Marche section in Italy, ~1.5 Myrs is estimated for the transition time (Hu et al., 2012), and ~1.1 Myrs to 1.5 Myrs for the transition observed in the Buchberg section in Austria (Hu et al., 2012).

These transition times are of particular interest as, if taken from the start of the OAE, the ‘transition time’ between the start of OAE 1a and the start of CORB 1 is estimated at ~1.65 Myrs, whilst for OAE 2, the transition time is also estimated at ~2 Myrs (assuming a duration of ~500 kyr for OAE 2) (Hu et al., 2012). Furthermore the first ‘red bed’ occurrence following the start of OAE 2 occurs ~1.1 Myrs after anoxic initiation (assuming a ~500 kyr duration) in the Italian section; ~1.2 Myrs after anoxic initiation in the Austrian section, and ~1.17 Myrs within an Eastern Atlantic section (Wang et al., 2011).

Within the studied T-OAE section presented in Chapter 4, rising charcoal abundances, hypothesized to have been primarily driven by rising atmospheric O_2 concentrations (Baker et al., 2017), appears to occur ~1 Myrs after anoxic initiation, remaining elevated until the termination of the OAE ~1.8 Myrs after C_{org} burial begun. At the termination point, peak atmospheric O_2 concentrations are predicted (Handoh and Lenton, 2003). The timings estimated between the beginning of OAE 1a and OAE 2 deposits and the beginning of CORB deposits of ~ 1 Myrs between OAE initiation and the occurrence of the first CORB, and ~1.65 Myrs to ~2 Myrs between OAE initiation and extensive CORB deposition (Wang et al., 2011; Hue et al., 2012) appear strikingly similar to the timescale over which changes in charcoal abundances were found during the T-OAE, and the Myr timescales required for atmospheric O_2 changes (Lenton and Watson, 2000b; Catling and Claire, 2005; Lenton, 2013). The results presented in Chapter 4, may therefore provide support for the hypothesis that the deposition of CORBs may have been aided by an increase in atmospheric O_2 concentrations driven by enhanced C_{org} burial during OAEs 1a and 2, coupled with a decline in global

temperatures, as postulated by Wang et al. (2011) and Hu et al. (2012). Fire-O_2 proxies across the T-OAE (Chapter 4 this thesis; Baker et al., 2017) coupled with the observation that Cretaceous CORB deposition appears to operate on a similar timescale, suggests that C_{org} burial during OAEs is capable of driving ~1 Myr changes in atmospheric O_2. Future research should seek to consider the significance of C_{org} burial to drive changes in atmospheric O_2 within a million years because whilst OAEs have been a focus of major study on their impacts on marine biota, it is now clear that shorter-term changes in atmospheric O_2 may have implications for extinction and evolution in terrestrial biota's.

8.2.2.2 What can this information tell us about the hypothesis for biomass burning and the negative C-isotope excursion?

The driving mechanism behind the release of isotopically light C into the ocean-atmosphere system, recorded during the Toarcian OAE by a negative shift in $\delta^{13}C$, remains a subject of debate (Jenkyns, 2010). Currently, multiple mechanisms have been postulated including large volcanic events (e.g. Mahoney et al., 1993; Storey et al., 1995; Tejada et al., 1996; Sinton and Duncan, 1997; Torsvik et al., 1998; Kerr, 1998; Larson and Erba, 1999; Tejada et al., 2000; Snow et al., 2005; Wignall 2005); CH_4 hydrate dissociation (Dickens et al., 1995; 1997; 2000; Gröcke et al., 1999; Hesselbo et al., 2000; Jahren et al., 2001; Kemp et al., 2005; Pearce et al., 2008; Zeebe et al., 2009); thermogenic CH_4 release from the intrusion of mantle derived melts into C-rich strata (e.g. McElwain et al., 2005; Svensen et al., 2007; Retallack and Jahren, 2008; Ganino and Arndt, 2009; Flögel et al., 2011) and biomass burning (e.g. Finkelstein et al., 2006).

One hypothesis of particular interest is that suggested by Finkelstein et al. (2006) involving the occurrence of wildfires and extensive biomass burning. Here Finkelstein et al. (2006) hypothesize that combustion of peat; organic matter, vegetation and/or soil sustained over ~1000 years could be capable of nearly doubling atmospheric CO_2 concentrations from PAL. According to Finkelstein et al. (2006, p. 501), this doubling of CO_2 could be capable of producing a "pronounced negative $\delta^{13}C$ excursion in the atmosphere (up to approximately -2.4‰)". Finkelstein et al.'s (2006) hypothesis therefore implies that an increase in biomass burning could be evident in the fossil record during negative CIE shifts.

The results presented in Chapter 4 could aid in constraining the potential mechanisms responsible for the T-OAE negative CIE. Here, charcoal abundances remain at/below 'background' abundances throughout the duration of the negative C-isotope excursion during the T-OAE, increasing only as the recorded $\delta^{13}C$ values rise ~1 Myrs after the start of the anoxic event (see Figure 4.4, Chapter 4). This pattern of low charcoal abundances is observed at both study sites. As Finkelstein et al.'s (2006) biomass burning mechanism would imply that there should be an increase in fossil evidence of wildfires observed during this period, our results do not appear to support Finkelstein's hypothesis, suggesting that increased biomass burning was an unlikely source of light C released during this period. However, further study should look to further test Finkelstein et al.'s (2006) hypothesis of increased biomass burning during the negative CIE of the T-OAE, by looking at the pattern of wildfire activity in other study locations, in particular, areas thought to have been peat-dominated.

8.3 What can the record of wildfire tell us about Earth system changes occurring over medium timescales during the early stages of an OAE?

8.3.1 Summary of research and key findings

In Chapter 5 variations in charcoal abundances, taken to represent changes in fire activity, across the initiation and into the 'early stages' of Cretaceous OAE 2 were analysed. OAE 2 occurred during a period in Earth's history considered to have experienced high atmospheric O_2 concentrations of between 23% vol. and 27% vol. (Lenton, 2013; Mills et al., 2016). Hence, any major variations in inferred wildfire activity are unlikely to have been primarily driven by atmospheric O_2 changes due to the decline in sensitivity of burn probability and fire spread to O_2 changes (Belcher et al., 2010). This enables drivers such as changes in climate that may be responding to Earth system changes, to become more significant in shaping wildfire activity and thus the history of fire preserved as fossil charcoal. In particular, at high atmospheric O_2 concentrations, variations in fuel moisture become the more important driver (Watson, 1978; Watson and Lovelock, 2013).

Significant climate changes are hypothesized to have occurred during the early stages of OAE 2, driven by the changes in CO_2 determined by the release of volcanically derived CO_2 source and C-sequestration by primary producers (e.g. Barclay et al., 2010; Jarvis et al., 2011; van Helmond et al., 2013; Jenkyns et al., 2017). Here, rising CO_2 concentrations in the lead up to the OAE (beginning ~80 kyr prior to its initiation) are hypothesized to have led to increased global temperatures (evidenced by SST proxies TEX_{86} and $\delta^{18}O$ (Forster et al., 2007; Sinninghe Damsté et al. 2008; Jarvis et al. 2011)), an enhanced hydrological cycle and enhanced continental weathering rates (evidenced by a brief movement in Sr isotope record towards positive values (Frijia and Parente, 2008)). Following the rise in CO_2 concentrations, Barclay et al. (2010) note a brief decline in estimated CO_2 concentrations, yet published SST estimates from TEX_{86} proxy data in nearby study sites remain high, suggesting that humid, 'greenhouse conditions' prevailed despite a brief period of CO_2 drawdown (van Helmond et al., 2013).

Throughout this period, charcoal abundances within the Dakota Fm were found to be consistently low, despite the high atmospheric O_2 concentrations estimated (e.g. Mills et al., 2016). If atmospheric O_2 is taken to have been between ~25% and ~27% (e.g. Mills et al., 2017), then moisture of extinction can be estimated to have been between 77% and 88% (following Watson and Lovelock, 2013). If a 10% rise in fuel moisture is assumed based on the proposal that the hydrological cycle was enhanced leading to humid greenhouse conditions, then this ought to have an impact on fire behaviour. Following Belcher and Hudspith's (2016) fire behaviour modelling outputs in high O_2, a 10% rise in fuel moisture could be capable of ceasing fire spread in low fuel load models such as conifer litter and in weedy/herbaceous dominated understories, and would halve spread rates in higher fuel load models such as fern understory and shrub-dominated understory (Belcher and Hudspith, 2016 and see Fig 5.7 in this thesis). Furthermore, the estimated decline in the intensity of surface fires due to increased fuel moisture would reduce the ability of surface fires to dry and scorch canopy foliage, which would otherwise enable a fire to ignite and spread to the canopy (Belcher and Hudspith, 2016). It is therefore likely that although atmospheric O_2 concentrations for the Cretaceous period are estimated to have been much higher than PAL than those estimated for the Jurassic, an increase in fuel moisture of just 10%, driven by rising volcanically derived CO_2 and an enhancement in the hydrological cycle over the relatively short timescale of OAE 2, could have had a significant negative impact on fire activity and fire behaviour, including the ability of fires to spread, during this period.

Following this phase of rising CO_2 concentrations, a period of CO_2 drawdown is hypothesized, evidenced using the stomatal proxy method (Figure 5.6) (Barclay et al., 2010). During this period (labelled phase 2 / 'P2'), there is a sustained rise in charcoal abundances occurring within the Dakota Fm, coeval with published stomatal proxy method estimates of declining CO_2 concentrations and hypothesized C–sequestration (Barclay et al., 2010). The drawdown of CO_2 during this phase is hypothesized to have initiated global cooling, where SST estimates drop by ~2.5°C at the nearby Bass River borehole site, New Jersey (van Helmond et al., 2013). Furthermore, the climate is suggested to have become drier, inferred from the dominance of gymnosperm species in the pollen and spore assemblages during this phase at the New Jersey site (van Helmond

et al., 2013). Thus it is hypothesized that a decline in fuel moisture during this cooler, drier phase may have made conditions more favourable to fire, enabling an increase in fire activity and fire spread (under the modelled higher background O_2), resulting in the observed rise in charcoal abundances coeval with a period of CO_2 drawdown.

8.3.2 Contributions to the research field

This study contributes what is believed to be the first analysis of wildfire activity conducted across the initiation of OAE 2. This study illustrates that CO_2 – climate – driven wildfire changes can be observed over medium timescales during these significant C-cycle perturbation anoxic events, even under modelled high atmospheric O_2 concentrations. The data presented in Chapter 5 provides support for previous hypotheses of geologically rapid CO_2 driven climate shifts occurring during the early stages of OAE 2 (e.g. Barclay et al., 2010; Jarvis et al., 2011; van Helmond et al., 2013; Jenkyns et al., 2017), and indicates that changes in fuel moisture are likely the dominant driving factor behind medium-timescale fire changes during the Cretaceous superambient O_2 world. This study demonstrates that the record of wildfire in the form of fossil char can be used to identify significant climatic changes occurring over medium timescales during the early stages of Cretaceous OAE 2, where increases in fuel moisture can be tentatively attributed to a decline in wildfire activity over tens to hundreds of thousands of years, whilst drier climate conditions appear to result in increased charcoal abundances and inferred fire activity.

8.4 Comparing variations in wildfire across the Jurassic T-OAE and Cretaceous OAE 2

The T-OAE and Cretaceous OAE 2 occur during very different periods of Earth's history. The T-OAE is hypothesized to have occurred during a time when global temperatures were fairly equable compared with present day, and where estimated atmospheric O_2 concentrations were ~20% vol. (Lenton, 2013). In comparison, OAE 2 occurred during a time when global temperatures were much warmer (estimated SSTs of up to ~3-5°C warmer than today) (Wilson and Norris, 2001), and where atmospheric O_2 concentrations estimates were much higher, ranging between ~23% vol. and 27% vol. (Lenton, 2013, Mills et al., 2016).

The charcoal record, at first glance, similarly appears to evidence contrasting trends between the T-OAE and OAE 2. The T-OAE reveals higher charcoal abundances occurring in the final stages of the OAE, during a period of increasingly positive $\delta^{13}C$ values hypothesized to have been driven by an increase in atmospheric O_2 (Baker et al., 2017). In contrast this overall rise in charcoal abundance towards the end of OAE 2 in the Dakota Fm is not apparent potentially owing to high background pO_2 throughout the duration of this event, or the lack of preservation of the upper portion of the OAE at this study site, for which this composite section preserves only ~540 kyrs of sediment deposits following that start of the OAE (Barclay et al., 2010). Whilst, interestingly there is strong evidence of climatically driven variations in charcoal abundance during the early stages of OAE 2 that appear to correspond with periods of rising CO_2 during a period dominated by negative $\delta^{13}C$ values. These high-resolution variations in fire activity during the early stages of the T-OAE at Peniche and Mochras do not appear as obvious.

However, there are also some similarities between the two charcoal records. During the early stages of OAE 2, rising CO_2 concentrations are suggested to have led to rising global temperatures and an enhancement of the hydrological cycle (Barclay et al., 2010; Jenkyns et al., 2017). This rising CO_2 trend was punctuated by a brief CO_2 drawdown (labelled 'a', Figure 5.10) (Barclay et al., 2010), yet SST proxies indicate global temperatures remained high and greenhouse conditions prevailed (Forster et al., 2007; Van Helmond et al., 2013).

Following this phase of rising CO_2 concentrations (labelled 'P1' Figure 5.10) stomatal proxy estimates indicate a declining CO_2 trend, that appears to coincide with increased C-sequestration during the OAE, falling global temperatures, and a likely decline in humid greenhouse conditions. McElwain et al. (2005) conducted a similarly high resolution study of the early stages of the T-OAE at the Bornholm locality in Denmark and describe a similar pattern of climatic changes, based on the study of fossil plants, to that observed during the early stages of OAE 2. McElwain et al. (2005), whom also use the stomatal proxy method, identify a gradual rising CO_2 trend immediately prior to the OAE coeval with an estimated ~2°C temperature rise. A decline in CO_2 is then identified from the stomatal proxy results, coincident with the onset of organic rich strata, marking the T-OAE initiation and suggesting C-sequestration (McElwain et al., 2005). This is then followed by an abrupt increase in CO_2 (estimated at ~1200 p.p.m.v) and a ~6.5°C temperature rise coincident with the beginning of the negative CIE (McElwain et al., 2005). McElwain et al.'s (2005) analysis of thermophilic plant taxa during these early stages infers that the climate was relatively dry, becoming wetter as CO_2 fluxes increase, and greenhouse conditions prevail during the negative CIE (McElwain et al., 2005).

Interestingly, the charcoal record analysed across the initiation of the T-OAE at Peniche and Mochras and that of OAE 2 at Utah appear to respond similarly with respect to inferred changes in CO_2 and climate. For example, the charcoal record across the initiation of the T-OAE, at both Peniche and Mochras reveals a 'spike' in charcoal abundances at the culmination of the early positive $\delta^{13}C$ trend, coinciding with the period where McElwain et al.'s (2005) stomatal index proxy from Bornholm suggests a brief drawdown of CO_2, and where a dry climate is inferred from thermophilic plant taxa (Figure 8.5) (McElwain et al., 2005).

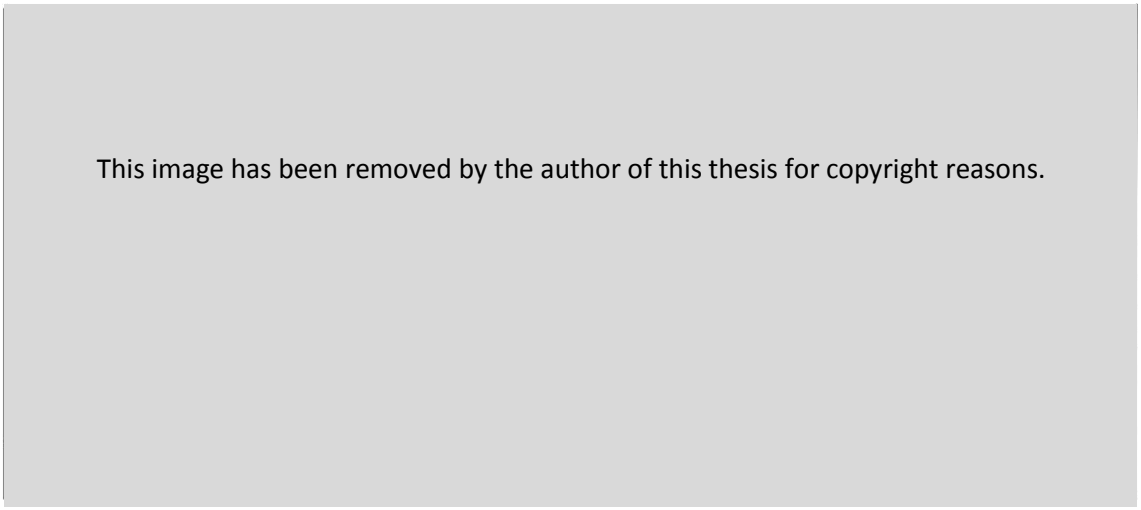

Figure 8.5 - $\delta^{13}C_{carbonate}$ curve of Peniche and Mochras, $\delta^{13}C_{organic}$ from Yorkshire, and the $\delta^{13}C_{wood}$ from Peniche and Bornholm plotted alongside McElwain et al.'s (2005) coniferale abundances; pCO_2 changes and inferred climatic phases during the early stages of the T-OAE at the Bornholm site.

Charcoal abundances in the two sections studied here then rapidly decline during the negative CIE, a period where McElwain et al. (2005) suggest a large pulse of CO_2 and infer a much wetter climate based on changes to abundant wet loving plant taxa. Similarly during the early stages of OAE 2 in the Dakota Fm, the charcoal record appears to respond similarly, with consistently low abundances during the period of hypothesized rising CO_2 concentrations in the run up to the OAE (Barclay et al., 2010), and increased abundances during an inferred CO_2 drawdown period. This is particularly interesting, because it suggests that CO_2 induced climate changes may have been the primary driving force behind variations in palaeo-fire activity during the initiation and early stages of an OAE, irrespective of the different 'background' atmospheric O_2 concentrations, giving rise to a geologically short-lived 'spike' in charcoal abundances close to/during the initiation of both the Toarcian and the Cretaceous anoxic events. Whilst, the early parts of the T-OAE studied here show some hints of similarity with OAE 2, future work might seek to study the onset of the T-OAE at the Mochras and Peniche sections at a resolution matching that of OAE 2, as this may reveal similar pulses-drawdown phases of CO_2, fire and climate change.

Another hypothesis for the rise in charcoal abundances during the initiation of these OAEs, could be an increased flux of charcoal to the study sites associated with a rise in sea level (e.g. Muller, 1999; Laurin and Sageman, 2007; Barclay et

al., 2010). Here, a rise in sea level may have enabled removal of charcoal from the newly flooded land surface providing a 'spike' in charcoal abundances during the initiation of both OAEs. However, Hesselbo et al. (2007) suggest that the Peniche study site is unlikely to have been influenced by a rise in sea level as the emergent horst block from which phytoclast material was likely primarily derived from "would not have become more distal from the depositional area" (Baker et al., 2017, p. 6; Hesselbo et al., 2007). Furthermore, there is no coeval 'spike' in phytoclast material observed at the studied Mochras site (see Chapter 4, Figure 4.4), which would be expected with increased leaching and removal of material into the study site. It is therefore proposed that the increase in charcoal during the initiation of the T-OAE may reflect a true wildfire signal (Baker et al., 2017), with the changes driven by atmospheric-climate variations.

8.4.1 What are the implications of increased wildfire activity across the initiation of an OAE?

The initiation of an OAE is often associated with an influx of nutrients from the land to the oceans, in particular P, that fuels primary productivity in surface waters and increases the amount of C_{org} buried. During the initiation of the T-OAE and OAE 2, geochemical sediment analyses indicate a noticeable flux of P entering the marine system. For example, P measurements ($P_{detritic}$ + $P_{reactive}$) increase from ~500 µg/g to over 1000 µg/g immediately prior to the negative CIE in the nearby T-OAE section of the Posidonia Shale, in the Swiss Mountains (Montero-Serrano et al., 2015) (Figure 8.6), and for the Pueblo GSSP section for OAE 2, all P species measured (P_{Fe}; $P_{authigenic}$, $P_{detritic}$, P_{org}) reach peak values at the onset of the OAE (from 0.10 to 0.20 (P_{Fe}); 0.50 to 5.00 (P_{auth}), 0.25 to 0.50 (P_{det}) and from 0.08 to 0.20 (P_{org})) (Mort et al., 2007) (Figure 8.7).

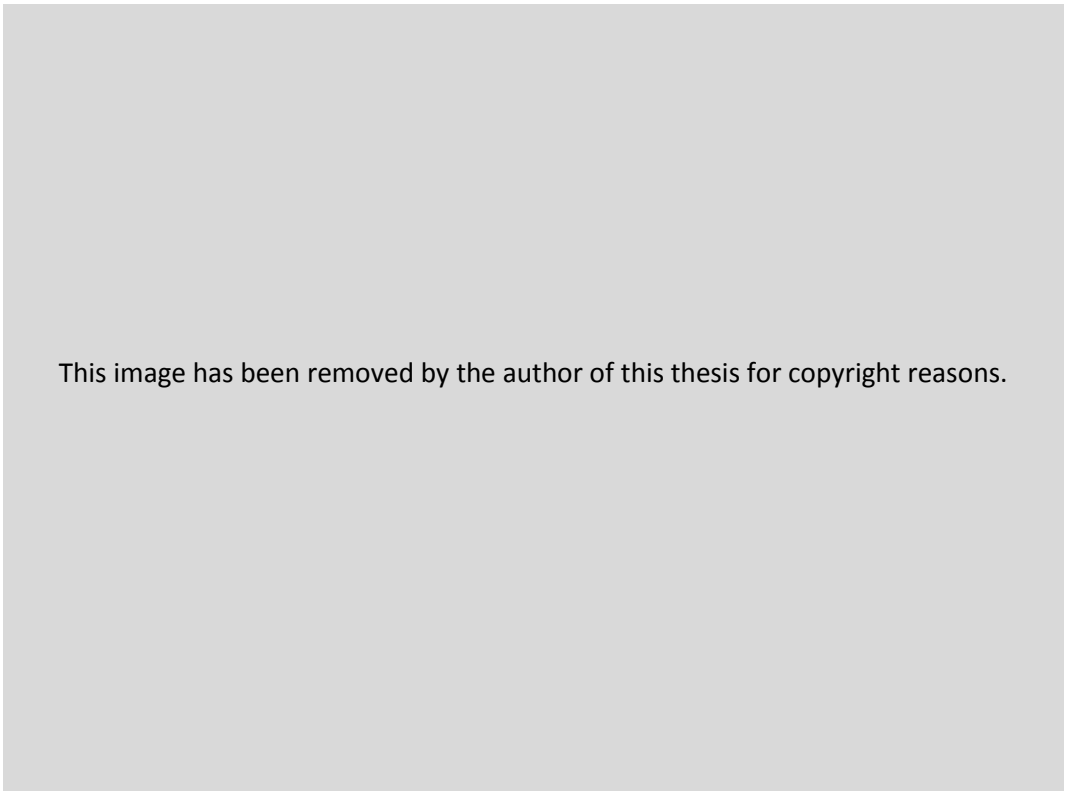

Figure 8.6 – Variations in organics, including P across the T-OAE from the Posidonia Shale, Swiss Mountains. Modified from Montero-Serrano et al. (2015). Grey shaded area indicates the negative CIE during the T-OAE. Box denotes the flux in P observed during the initiation of the OAE.

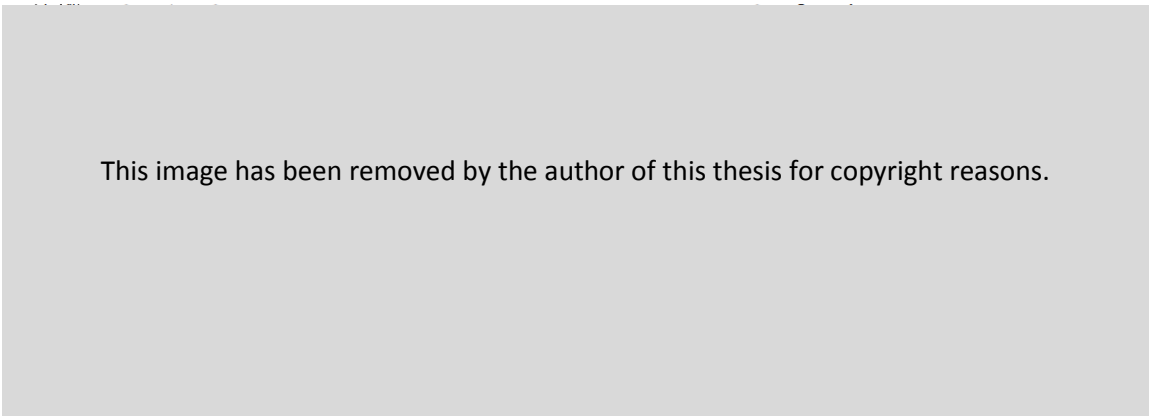

Figure 8.7 – Variations in P speciation across the initiation of OAE 2 from the Pueblo section, USA. Modified from Mort et al. (2007). Grey shaded area indicates the negative CIE during the T-OAE. The onset of OAE 2 occurs at the 'peak' in P_{authi} and continues up beyond the section shown.

As previously indicated in section 8.2.2 (this thesis), a debate remains as to whether fires act to limit P weathering (e.g. Lenton and Watson, 2000b; Handoh

and Lenton, 2003; Lenton, 2013) or instead aid in its redistribution to the marine system (e.g. Kump, 1988) (Lenton, 2013). When tested by Lenton (2013), it was found that a decline in P weathering through the suppression of land vegetation by fires had a greater influence in stabilizing atmospheric O_2, bringing peak O_2 estimates down from 27% vol. to 22% vol. whilst removing the effect of P redistribution following a fire, produced a higher peak O_2 estimate of ~25% vol. (Figure 8.1). However, over much shorter timescales, studies have shown that following a fire, the concentration of P in nearby streams increases significantly, suggesting that in the modern day, fire can actually aid in the redistribution of P from the land to nearby streams which feed into the marine environment. For example, Spencer and Hauer (1991) found that P concentrations in nearby streams increased from 3µg-P/L pre-fire to 135µg-P/L within 24 hours post-fire. Similarly Taylor et al. (1993) found an increase in P from 0.05 mg/L pre-fire and flood to 0.10 g/L post-fire and flood. Although it is likely that the flux in P observed during the initiation of the T-OAE and OAE 2 may be predominantly driven by increased continental weathering and a rising sea level, it is interesting that coinciding with the flux of P found at nearby study sites, and the OAE initiation, there is also evidence for an increase in wildfire activity at the three study locations, from two different anoxic events. Hence, future work may want to consider to what effect an increase in wildfire activity could have in aiding the delivery of limiting nutrients such as P during the initiation of such events.

8.5 What are the wider implications of studying fire feedbacks across OAEs?

The research presented in Chapters 4 and 5 illustrate that the record of wildfire is sensitive to climatic changes occurring across medium timescales, as well as to atmospheric O_2 changes occurring across long timescales. Both studies contribute important geological evidence for changes occurring during times of significant C-cycle perturbations that occurred many millions of years ago in Earth's past.

Current research indicates that the 'global' OAEs (T-OAE, OAE 1a and OAE 2) were triggered during periods of warm global temperatures, "induced by rapid influx of CO_2 into the atmosphere from volcanogenic and/or methanogenic sources" (Jenkyns, 2010, p. 1) (e.g. Jarvis et al, 2011; Bottini et al., 2012; Percival et al., 2016; Jenkyns et al., 2017). Here, rising CO_2 concentrations, large outpourings from LIP eruptions and an enhancement of the hydrological cycle are hypothesized to have led to an increase in continental weathering rates, enabling an increased supply of limiting nutrients, including P, to the marine system. This increased supply of nutrients, observed tens of thousands of years prior to the initiation of OAE 2 (Mort et al., 2007), likely fuelled primary productivity in surface waters, triggering an anoxic event that is capable of lasting hundreds of thousands of years to millions of years.

Present day records from the Mauna Loa Observatory illustrate that atmospheric CO_2 concentrations have continuously increased over the last 50 years, from concentrations of ~ <320 ppm in 1958 to over 400 ppm this year (NOAA, 2017). "Each of the last three decades has been successively warmer at the Earth's surface than any preceding decade since 1850" where "warming in the climate system is unequivocal, with many of the observed changes unprecedented over decades to millennia: warming of the atmosphere and the ocean, diminishing snow and ice, rising sea levels and increasing concentrations of greenhouse gases" (IPCC, 2013, p. 5).

Throughout this time, O_2 concentrations in the modern oceans have declined (Stramer et al., 2008; Watson, 2016; Schmidtko et al., 2017), with new research

indicating that the global oceanic O_2 content has decreased by more than 2% since 1960 (Schmidtko et al., 2017). Ocean O_2 depletion can now be observed in a variety of locations across the world, where an estimated quadrupling of the volume of oceanic water devoid of O_2 has occurred since 1960 (Gilbert, 2017), leading to an increase in the number and expanse of 'dead zones' (Schmidtko et al., 2017) (Figure 8.8).

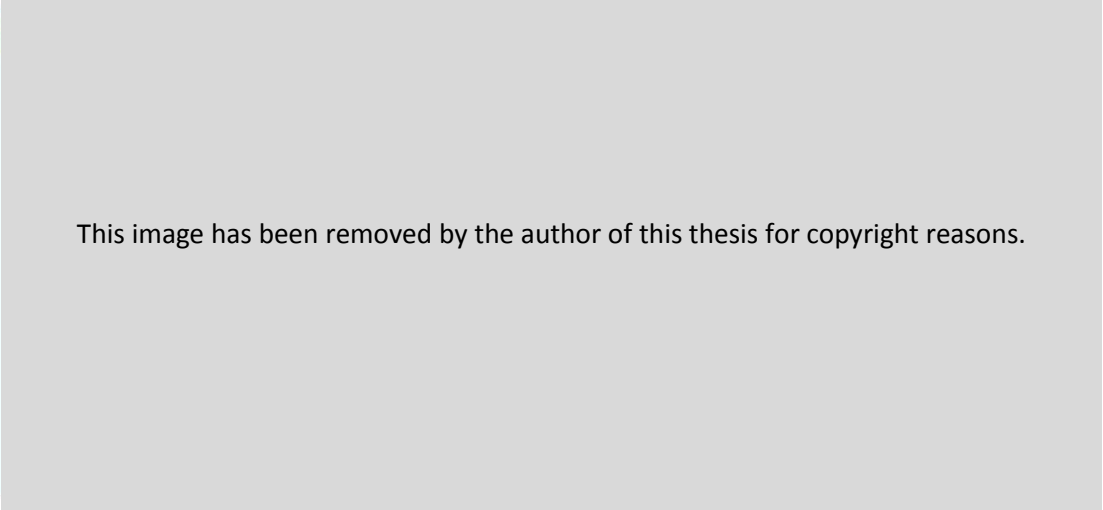

Figure 8.8 – Global map illustrating location of known 'dead zones' in 2008. (Map taken from Diaz and Rosenberg, 2008).

"Since the industrial revolution, land-use changes, agricultural run-off, and sewage discharges have more than doubled the amount of phosphorus entering the ocean via rivers (Mackenzie et al., 2002)" (Watson, 2016, p. 1529). As a result of this increased nutrient run-off (e.g. Diaz and Rosenburg, 2008) (Watson, 2016), an increase in the number of low O_2 zones have appeared around coastal areas and inland seas (Diaz and Rosenburg, 2008). Here, a prime example of the effects of increased nutrient delivery on the levels of hypoxia in the oceans can be seen in the northern Gulf of Mexico, where the extent of the dead zone is very much linked with the discharge of freshwater from the Mississippi River (Diaz and Rosenburg, 2008). Here Diaz and Rosenburg (2008) (referencing Rabalais et al., 2007) indicate that during years with little river flow to the Gulf of Mexico, the area of hypoxia is ~<5000 km^2, yet when the river flow is high, delivering large quantities of nutrients from agricultural activities in the U.S., the area of hypoxia extends to over 15,000 km^2.

Although, many of these low O_2 coastal zones are postulated to be driven by increased nutrient run-off (e.g. Diaz and Rosenburg, 2008) (Watson, 2016), Schmidtko et al. (2017, p. 335) indicate that in "some cases (these) may have been affected by the larger-scale oxygen changes", with ~15% of the O_2 depletion observed since 1960 hypothesized to have been caused by warming of the oceans and the resulting decline in solubility (Schmidtko et al., 2017). Hence, it is maybe not surprising that the modern ocean has been increasingly referred to as being 'on the edge of anoxia' (e.g. Lenton and Watson, 2000b; Handoh and Lenton, 2003; Watson, 2016), with "some of today's processes reminiscent of those thought to have promoted OAEs in the distant past" (Watson, 2016, p. 1529).

Watson (2016, p. 1530) indicates that the increase in observed nutrient influx from human activities would "need to be sustained for at least a thousand years to produce a change in phosphate levels sufficient to bring on a full-scale OAE", implying that that a globally widespread anoxic event is not imminent. However, the re-occurrence of such events in Earth's past, and the increasing development of hypoxic zones across the globe indicates that our knowledge and understanding of these events and how they come to an end may be crucial for our future, as an OAE would have both extensive economic and societal implications.

8.6 What is the natural 'background rhythm' of wildfire across medium timescales?

8.6.1 Summary of research and key findings

Chapter 7 presents an analysis of variations in charcoal abundances, taken from sediments deposited during part of the Early Jurassic (Pliensbachian) at the Mochras core site. Here, variations in charcoal abundances of both size fractions (>125 µm and <125 µm), were found to occur across bundle scale variations in Ca percentage which are tentatively linked with changes in the short (100 kyr) eccentricity cycle (Ruhl et al., 2016). This was also observed in the palynofacies analysis, where variations in pollen and spore abundances and plant cuticle abundances appeared to coincide with bundle scale variations in Ca content. In contrast, only the >125µm charcoal fraction was found to vary across bed scale Ca content changes - which had been tentatively attributed to changes in the ~21 kyr precession cycle (Bonis et al., 2010; Ruhl et al., 2016).

The variations in charcoal abundances appear to evidence that palaeo-wildfire activity was very sensitive to orbital scale forcing across medium timescales. Orbital driven changes in climate and vegetation have been observed during the Early Jurassic (e.g. Vollmer et al., 2008; Bonis et al., 2010), as well as in recent (Quaternary) sections (e.g. Daniau et al., 2013). Thus, as hypothesized in Chapter 7, variations in charcoal abundances observed across these timescales were likely driven by climate and/or resulting vegetational shifts occurring across orbital timescales of precession and short eccentricity.

8.6.2 Contributions to the research field

Chapter 7 contributes what is believed to be the first analysis of charcoal abundances and thus inferred wildfire activity, across natural orbital cycles in deep time. The variations in charcoal abundances appear to be influenced across both precession (~21 kyr) and short eccentricity (~100 kyr) timescales - hence it appears that the record of wildfire is sensitive to orbital forcings occurring over medium timescales. This dataset not only provides information on the natural background rhythm of wildfire for the Early Jurassic, indicating that future studies conducted on changes in wildfire activity should consider variations in charcoal

abundances occurring over orbital timescales, but also illustrates, for what is believed to be the first time, that orbital driven changes in wildfire can be observed in deep time as well as 'modern day' (Quaternary) sediments (e.g. Daniau et al., 2013). This is particularly important as this dataset indicates the need to consider these 'background' variations occurring across medium timescales when analysing and disentangling the charcoal record as evidence of ancient fire activity.

8.6.3 Linking the Milankovitch cycles with OAEs

As outlined in Chapter 6 and 7, the short Milankovitch cycles (~21 kyr precession and ~100 kyr eccentricity) have been implicated in pacing regional-to-hemispherical climate changes via oscillations in solar insolation resulting in strong-to-weak seasonal contrast. However, the discovery of cyclic variations in the $\delta^{13}C$ record occurring over a periodicity of ~9 Myrs throughout the Jurassic and Early Cretaceous (Figure 8.9) by Martinez and Dera (2015), led to the postulation of a long multi-million year eccentricity cycle, that could be capable of indirectly controlling the C-cycle (Martinez and Dera, 2015).

Long, million year orbital cycles have been implicated in pacing long-term processes such as continental weathering rates through the modulation of the shorter orbital cycles that are linked with seasonal contrast (e.g. Martinez and Dera, 2015). By controlling continental weathering and run-off rates, these long eccentricity cycles may be capable of indirectly pacing C_{org} burial (e.g. Martinez and Dera, 2015) and thus the timings of OAE occurrences (e.g. Mitchell et al., 2008; Kemp et al., 2011; Martinez and Dera, 2015).

In particular, Martinez and Dera (2015) hypothesize that periods of long eccentricity minima could lead to a decline in seasonal contrast, which may have enabled year-round wetter conditions, capable of supplying more nutrients to the oceans via an increase in continental weathering and run-off, and a constant fluvial influx from the land to oceans. This is suggested to have fuelled primary productivity in the photic zone, enhancing C_{org} burial and leading to the formation of persistent anoxic waters (Figure 8.10) (Martinez and Dera, 2015).

A similar theory can be seen in Mitchell et al.'s (2008) study where the timing of Cretaceous OAE 2 is suggested to have occurred during periods of "unusually low insolation variations, owing to simultaneous nodes in all orbital parameters" observed within the Scaglia Bianca Formation in the Umbria-Marches region, Italy (Mitchell et al., 2008, p. 1). Mitchell et al. (2008, p. 1) further indicate that other OAEs such as the mid Cenomanian Event and OAE 1d, similarly coincide with insolation nodes and dampened seasonality.

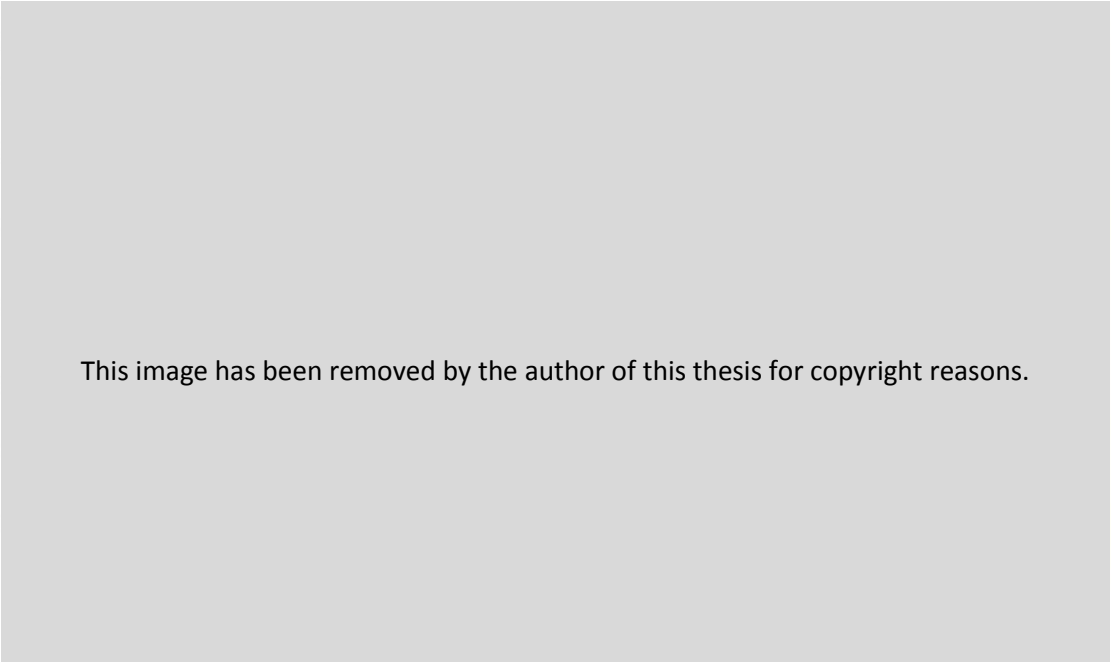

Figure 8.9 – Illustration of ~9 Myr C-cycle variations throughout the Jurassic and Early Cretaceous period, hypothesized to have been forced by a ~9 Myr eccentricity cycle (Martinez and Dera, 2015).

During eccentricity maxima, where increased seasonality is postulated, a similar scenario is hypothesized to occur during the wet season, where prolonged periods of 'megamonsoons' likely enable increased transfer of organic matter to the marine system, by accelerating continental run-off rates and fluvial discharge (Martinez and Dera, 2015). This period of enhanced run-off is anticipated to have enabled the transfer of nutrients to the oceans, and thus promote primary productivity "producing seasonal productivity blooms", which over these long timespans could "tip the system into anoxia" (Martinez and Dera, 2015, p. 12608). However, enhanced C_{org} burial is short-lived as during the dry season, terrestrial vegetation is limited by a decline in precipitation, causing a decrease in organic matter transported to the marine system (Martinez and Dera, 2015). Wildfire

activity is also hypothesized to increase during this time (Figure 8.10). Here, a decline in the delivery of organic matter and nutrients to the marine system is postulated, enabling the "recovery of oxic conditions during the cool season, degrading the organic particles" (Martinez and Dera, 2015, p.12608).

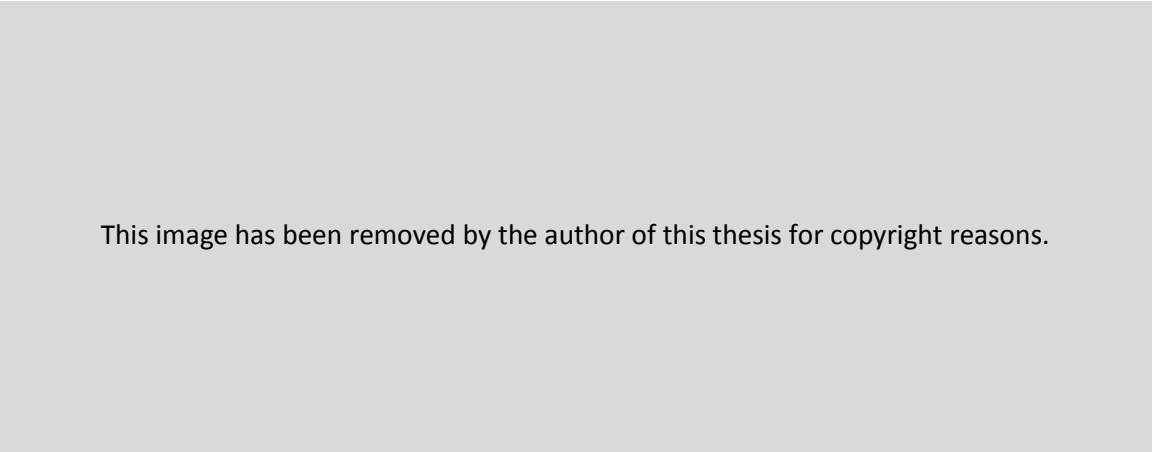

Figure 8.10 – Martinez and Dera's (2015) illustration of 'long' eccentricity maxima versus 'long' eccentricity minima and the hypothesized effects on primary productivity and resulting C_{org} burial in the oceans.

Martinez and Dera's (2015) study is particularly interesting, as not only does it link ocean anoxia with orbital forcing, but also indicates that a coeval increase in the occurrence of wildfires and a decline in terrestrial vegetation during periods of long eccentricity maxima, may play an important role in controlling the amount of organic material reaching the marine system, returning periods of anoxia to 'oxic' states.

Although over these longer multi-million year timespans, the hypothesized lithological signal appears in opposition to that recorded and hypothesized for the shorter ~100 kyr eccentricity cycle studied in Chapter 7 herein, the results presented in Chapter 7 illustrate that variations in inferred wildfire activity are apparent over orbital cycles, albeit only over the short eccentricity cycles during the Early Jurassic. It could therefore be hypothesized that this wildfire signal could also be observed over the longer multi-million year eccentricity cycle postulated by Martinez and Dera (2015), and thus presents an opportunity to study longer-time wildfire changes that may be apparent within the geological record.

Furthermore, the results presented in Chapter 4 indicate that increased wildfire activity is apparent towards the end of the Toarcian period of anoxia, and may have played an important role in aiding the return of oxic waters, through the likely suppression of vegetation and resulting decline in P weathering. Although this is not postulated by Martinez and Dera (2015), this key feedback process may further aid in the recovery of the ocean system, in support of Martiez and Dera's hypothesis of a decline in C_{org} burial during periods of higher wildfire activity. Hence, the apparent natural oscillations in inferred wildfire activity found to occur over the shorter Jurassic Milankovitch cycles presented in Chapter 7, if found to occur over the longer eccentricity cycles as well, imply that fire-feedbacks may be crucial in helping maintain the natural functioning of the Earth system, providing a buffer and possibly preventing the system (at least on a local-regional scale) from tipping into anoxic states more regularly. Future work should look to test this hypothesis to see whether variations in wildfire activity are possible over these longer multi-million year timescales.

8.6.4 Could the observed charcoal variations occurring during the Jurassic OAE (T-OAE) section also be reflective of Milankovitch cycle changes?

With the knowledge that changes in charcoal abundances can be observed over Milankovitch cycle timescales within the Jurassic, and that Kemp et al. (2011) hypothesize a strong orbital forcing during the T-OAE within the Peniche section, it is relevant to consider whether some of the smaller time-scale variations in char abundance observed within the T-OAE section could be reflective of Milankovitch scale forcing. However, it is important to note that the observed period of increased charcoal abundances occurring across a ~800 kyr time does not correspond with the length of any of the Milankovitch cycles. Furthermore, all charcoal abundances remain above 'background' values throughout this period, indicating that orbital forcing alone is unlikely to be driving force behind the sustained charcoal abundances across this ~800 kyr time period. Hence the hypothesis discussed in Chapter 4 and published in Baker et al. (2017) for increased atmospheric O_2 concentrations driving the observed rise in charcoal abundances, remains.

The Early Jurassic of the Mochras core has been extensively studied with published Milankovitch timescale calibrations (see Ruhl et al., 2016). However, there is as yet no Milankovitch cycle calibration for the T-OAE section of the Mochras core. Thus comparing the variations in char abundances observed during the Pliensbachian of the Mochras core with the variations observed across the T-OAE in the Mochras core is challenging. However, Milankovitch cycles have been studied for the Peniche section of the T-OAE (e.g. Suan et al., 2008; Huang and Hesselbo, 2014). Here, Huang and Hesselbo (2014, p. 1348) indicate that "the Peniche 405 kyr tuned series indicates that pre-and post-CIE intervals experienced strong precession-eccentricity-forced climate change, whereas the CIE interval is marked by dominant obliquity forcing".

The 'detrended' filter published by Huang and Hesselbo (2014) for the Peniche T-OAE section is shown plotted alongside the charcoal data collected in this thesis in Figure 8.11. The filters are expressed as representing long (405 kyr) and short (100 kyr) eccentricity cycles, corresponding to ~5.8 m and ~1.50 m within the Peniche section (Huang and Hesselbo, 2014). It should be noted that sampling resolution for the entire Peniche section is not high enough to pick up shorter Milankovitch cycles such as the precession cycle, nor for every short eccentricity cycle proposed.

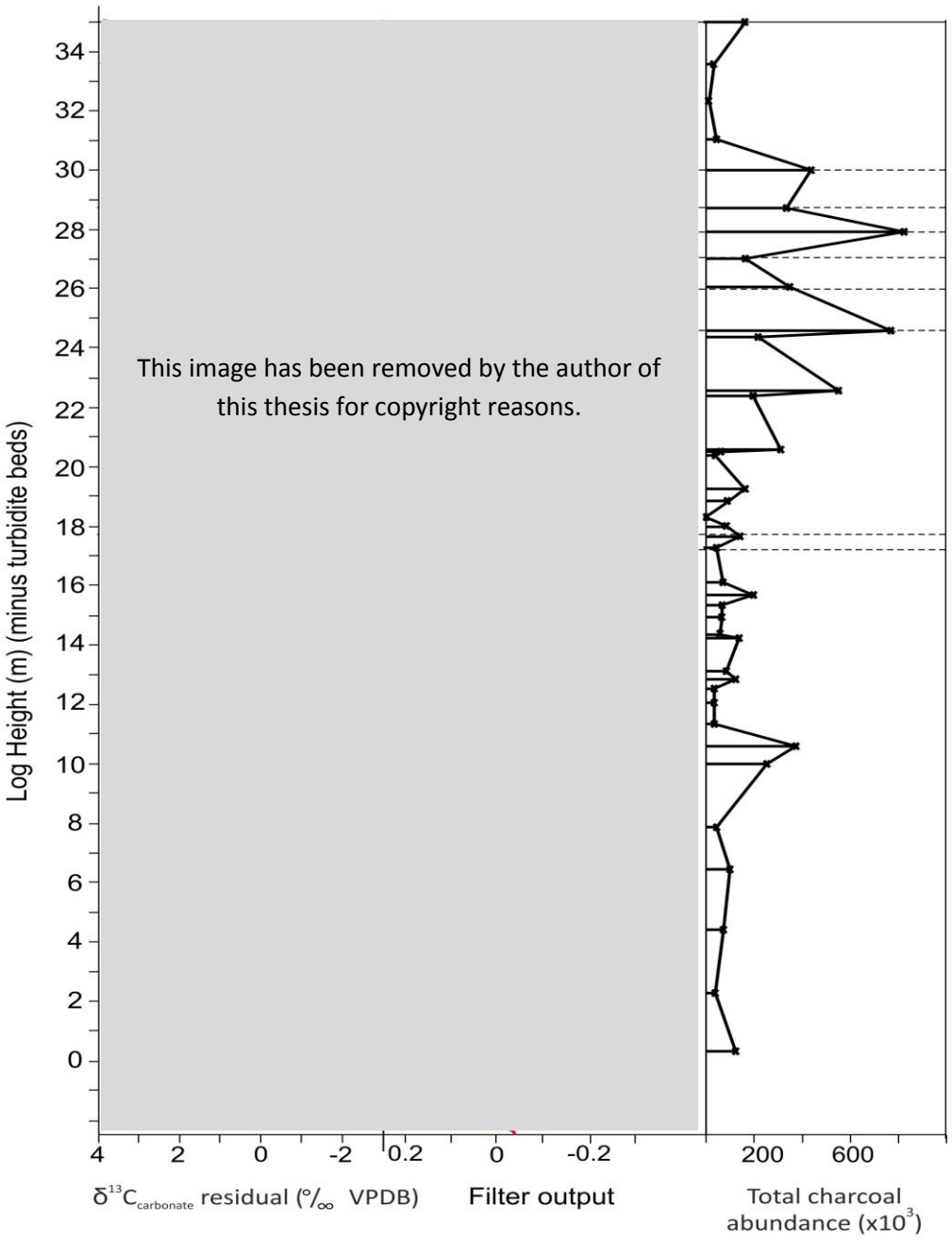

Figure 8.11 - Variations in total charcoal abundances (in 10 g bulk rock) from this thesis, across the T-OAE from a turbidite free Peniche section, plotted against Huang and Hesselbo's (2014) turbidite-free $\delta^{13}C_{carb}$ data and 'bandpass filtered series' illustrating 405 kyr, 5.8 m cycles (blue) and 100 kyr, 1.5 m cycles (red).

At first glance, it appears that the charcoal abundances, within the upper portion of the Peniche section display a cyclic pattern (Figure 8.11). Within the 'upper' OAE section (20.29 m to 30.98 m log height) 'peaks' in charcoal abundances occur every ~2.0 m (within the edited turbidite-free log), with the exception of a 3.34 m gap between peak charcoal abundances at 24.56 m and 27.90 m log height. Similarly the 'lower' charcoal abundances occur every ~2.0 m (with the

exception of 2.74 m between low abundances found at 27.10 m and 24.36 m log height). Although this pattern is only displayed in four data points, and thus corroboration would be required, this regular cyclicity of total charcoal abundances occurring every ~2.0 m is precisely equal to the mean of the two hypothesized cycle lengths for the short eccentricity cycle within this section of the T-OAE at Peniche of ~1.50 m (Huang and Hesselbo, 2014) and ~2.73 m (Suan et al., 2008). Both studies hypothesize a likely dominant eccentricity cycle during this portion of the OAE. Hence, it could be hypothesized that the apparent charcoal abundance 'cyclicity' observed within the 'upper portion' of the OAE may also, in part, be reflective of Milankovitch scale cycles, where smaller scale fluctuations are present within the larger O_2 driven fire activity peak.

Additionally, although maximum and minimum eccentricity index is not defined by Huang and Hesselbo (2014), it appears that between ~24.50 m log height and 30.00 m log height, that high charcoal abundances occur either just before, of just after a minimum in the 100 kyr band pass filter, whilst low charcoal abundances occur close to the maximum values in the 100 kyr band pass filter (with an exception at ~26.10 m where higher charcoal abundances occur close to a maxima in band pass filter output). Interestingly the opposite appears to be true during the negative CIE, where two charcoal abundance samples occur over the hypothesized timescale of the 100 kyr eccentricity (Huang and Hesselbo, 2014), where a higher charcoal abundance occurs at ~17.80 m log height, coeval with high bandpass filter output, and low abundances at ~17.20 m log height, coeval with low bandpass filter output. Although this is based on just two data points, and would therefore require corroboration, it is interesting that during the negative CIE, where the precession - 100 kyr eccentricity forced climate change is hypothesized to have weakened, and where obliquity becomes the dominant forcing (Huang and Hesselbo, 2014) that the charcoal abundance data appears to no longer 'track' the bandpass filter outputs, indicative of the 100 kyr eccentricity cycle.

Although further work involving higher resolution sampling would be required to test the hypotheses stated above, should they prove to be correct, the sustained higher than background abundances throughout the 'upper' portion of the OAE may indicate that changes in charcoal abundances are capable of picking up medium timescale, Milankovitch-driven variations even under the higher

atmospheric O_2 conditions proposed for this period (Baker et al., 2017) (although it should be noted that by how much atmospheric O_2 may have risen towards the end of the T-OAE is unknown). Furthermore, the apparent de-coupling of variations in char abundance with the 100 kyr eccentricity band-pass filter during the negative CIE, a period hypothesized to have been dominated by obliquity forcing compared with pre and post-CIE precession-eccentricity forcing (Huang and Hesselbo, 2014), suggests that variations in charcoal abundances may also be sensitive to obliquity forcing, much like the precession and eccentricity forcing demonstrated in Chapter 7. Future work should look to test this hypothesis.

8.6.5 Could the observed charcoal variations occurring during the Cretaceous OAE 2 section also be reflective of Milankovitch cycle changes?

The influence of Milankovitch cycles on the sedimentary record has also been documented for deposits occurring during the mid-Cretaceous (e.g. Elder and Kirkland, 1985; Gilbert, 1985; Kauffman, 1995; Keller et al., 2004; Eldrett et al., 2015a,b).

At the GSSP in Pueblo, the onset of OAE 2 is marked by a major sea level transgression, resulting in the deposition of the Bridge Creek Limestone Member of the Greenhorn Formation, Colorado (Elder and Kirkland, 1985; Kauffman, 1995; Keller et al., 2004). Within this member, deposits of rhythmically inter-bedded marl-limestone sequences are observed (Figure 8.12) (Eldrett et al., 2015a). Identification of these rhythmically inter-bedded sequences, within Cretaceous Western Interior Seaway (KWIS) deposits of the Cenomanian Bridge Creek Member, were first hypothesized to represent a sedimentological expression of climate cycles by Gilbert et al. (1985) (Eldrett et al., 2015a). These rhythmically deposited beds have since been related to Milankovitch cycles where “spectral analyses of geochemical, lithological and palaeobiological data have provided quantitative evidence for the existence of the primary astronomic forcing signal observed in Cenomanian and Turonian sequences of the KWIS, suggesting that, despite warm equitable climates of the greenhouse world during that time, climate responded to changes in solar insolation driven by Milankovitch

cycles (Sageman et al., 1997, 1998; Meyers et al., 2001)" (Eldrett et al, 2015a, p. 99).

Sageman et al. (1997; 1998) and Meyers et al. (2001) suggest that a combination of the Milankovitch cycles provided the driving force behind limestone-marl alternations observed within the Bridge Creek Member, with (eccentricity modulated) obliquity hypothesized to have influenced 'high-latitude precipitation', enabling the dilution of carbonate sediments, and (eccentricity modulated) precession hypothesized to have influenced evaporation and upwelling (Eldrett et al., 2015a). Interestingly, similarly to that hypothesized for central portion of the T-OAE, obliquity forcing is hypothesized to have the "most persistent high amplitude signal" (when not 'muted' by precession index minima) (Eldrett et al., 2015a).

The (short) eccentricity signal identified within the Mustang-1 core, Iona-1 core and the USGS Portland Core-1, as well as at the GSSP Pueblo site by Eldrett et al. (2015b) is shown in Figure 8.12. Within Eldrett et al.'s (2015b) study, there is approximately one complete short eccentricity cycle occurring between the onset of the OAE (defined by Eldrett et al., (2015b) as the '1st build up') and the first bentonite bed 'A' (Figure 8.12).

Barclay et al. (2010) use the presence of bentonite beds as well as ammonite and bivalve index fossils (first used to correlate the section to GSSP Pueblo by Elder et al. (1994)), to correlate the Dakota Fm study with the GSSP Pueblo (Figure 8.13). This published correlation enables the 'start' of the OAE and bentonite 'A' bed identified at Pueblo, to be correlated with the start of the OAE and bentonite 'A' bed identified within the Dakota Fm studied in this thesis (Bentonite 'A' identified at ~34m log height within coeval 'Big Water' section (Barclay R.S. *pers. comms*.)). Although the 'low resolution' correlation between the onset of the OAE and bentonite bed 'A' presented in Barclay et al. (2010) (Figure 8.13), means an accurate correlation between the hypothesized short eccentricity cycles (Eldrett et al., 2015b) and the studied charcoal abundance found within Dakota Fm is problematic, and therefore that the influence of the short eccentricity cycle on the charcoal abundances cannot be accurately defined, an inference can be made.

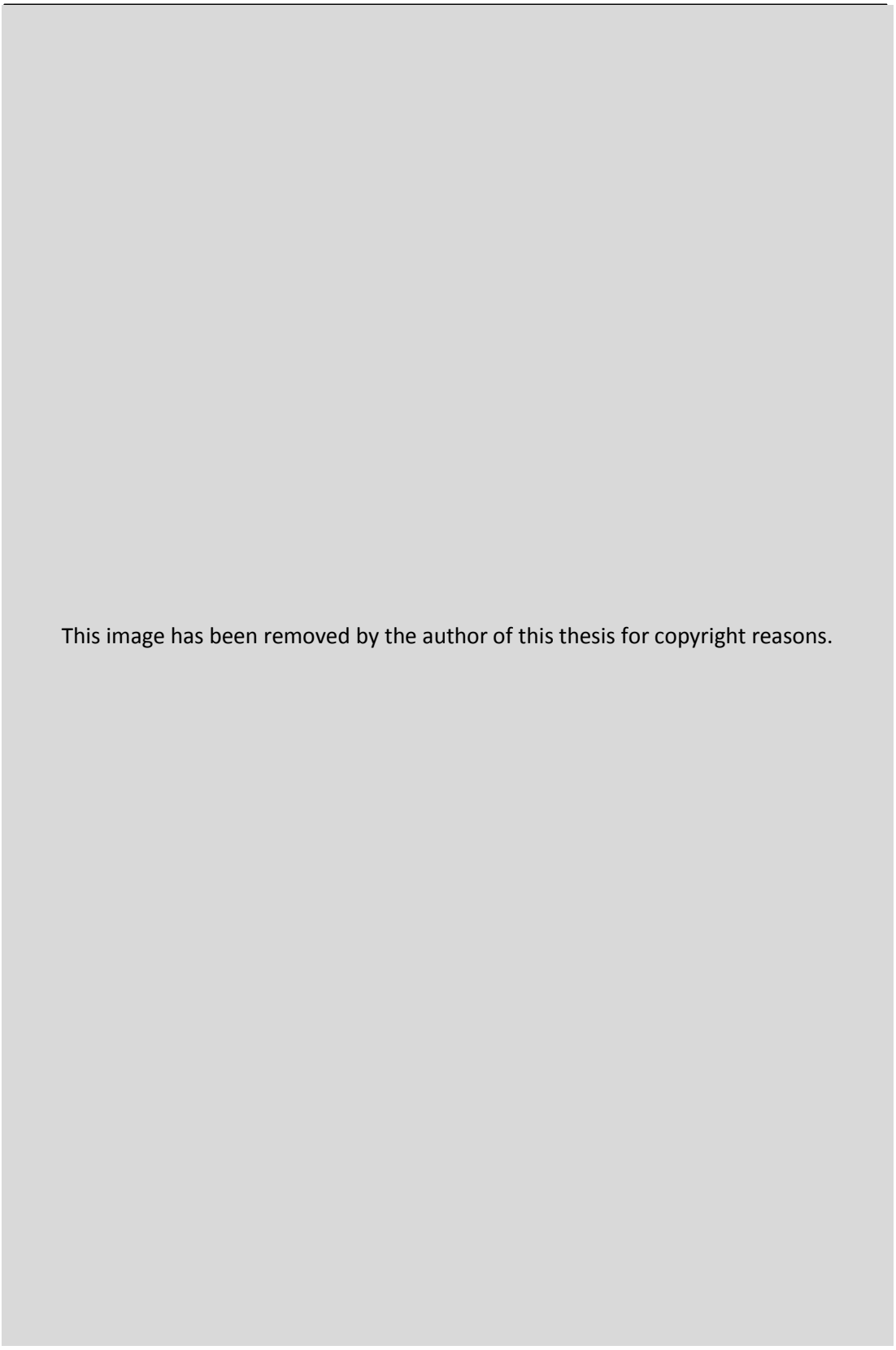

Figure 8.12 – Illustration of proposed short eccentricity cycles within the Iona-1 core, and correlated to the Mustang-1 core; the USGS Portland Cre-1 and GSSP Pueblo. Bentonite 'A' bed labelled as "A" in each section, and 'start' of OAE taken from the beginning of the '1st build up' (taken from Eldrett et al., 2015b).

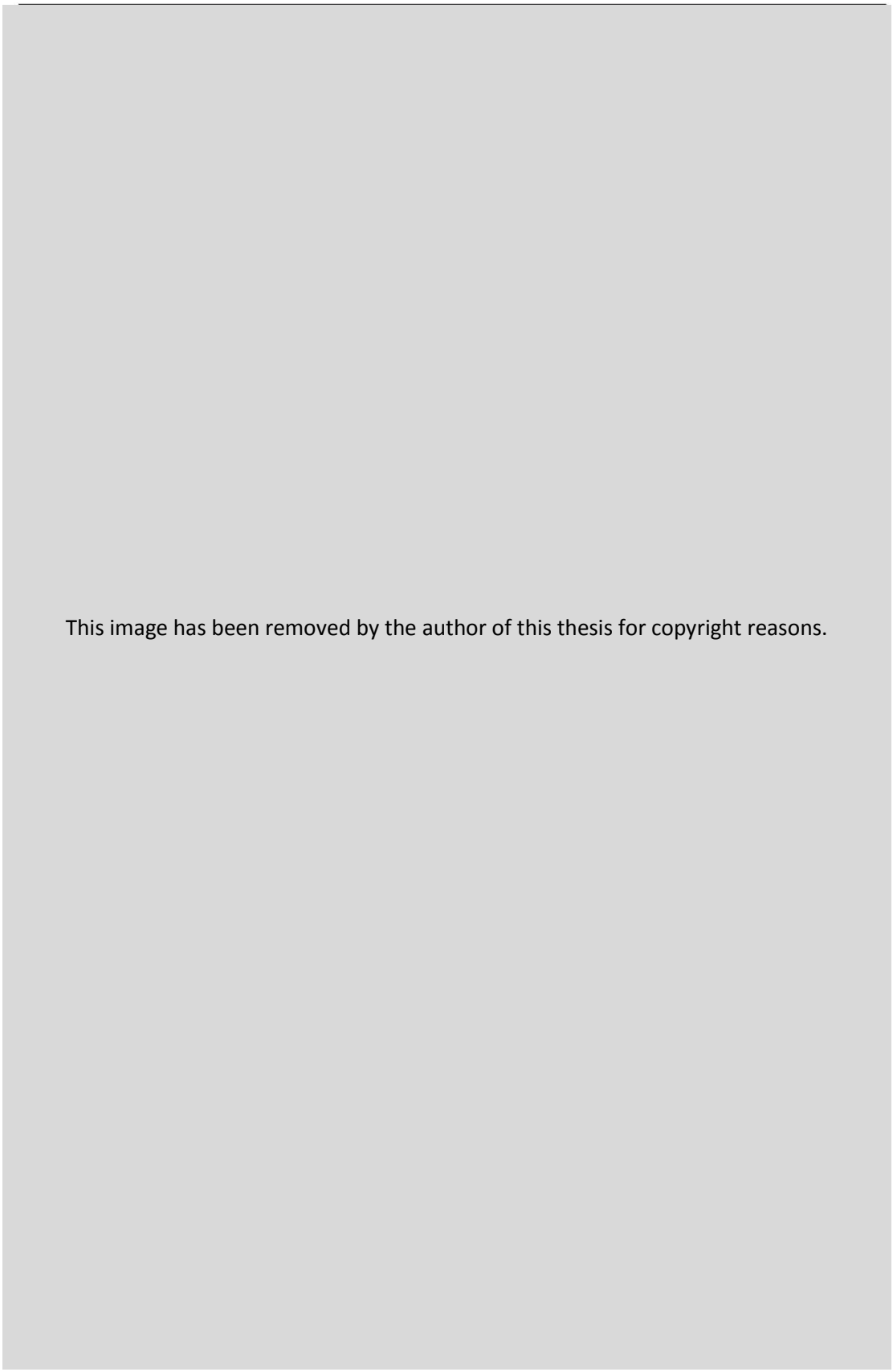

Figure 8.13 – Taken from Barclay et al.'s (2010 (SI)) - correlation of the Dakota Fm (studied in this thesis) with the Pueblo section published in Sageman et al., (2006), identifying the 'start' of the OAE and the location of bentonite beds 'A', 'B' and 'C'.

The three samples exhibiting a higher charcoal flux within the Dakota Fm (this thesis) were collected from the same organic mudstone bed, situated within the 'Big Hill Lower' section (see appendix). These three samples span an estimated ~22 kyr (according to J.Laurin's age model (see appendix)). This is similar to the present day periodicity of the precession cycle of ~21 kyr. Hence, it could be hypothesized that the increase in charcoal flux observed in the Dakota Fm during the early stages of OAE, may also have been influenced by Milankovitch forcings.

However, charcoal abundances prior to and after the increase observed between log heights of 6.8m and 10.6m (Figure 5.10, Chapter 5) remain low throughout the studied section. Although possible, it appears highly unlikely that Milankovitch cycle driven changes in wildfire activity throughout the rest of the studied interval were missed.

Furthermore, the hypothesized climate changes occurring during the early stages of the OAE driven by the inferred influxes of volcanically derived CO_2 and resulting drawdown by primary producers (e.g. Barclay et al., 2010), may override/mask any smaller Milankovitch driven climate changes. As discussed in Chapter 5, the observed charcoal abundance variations during the early stages of OAE 2, within the Dakota Fm, appear coeval with the hypothesized climate changes driven by the volcanically derived CO_2. As these inferred CO_2 changes, calculated from stomatal abundances, were collected from the same sections as that analysed for the changes in char abundance, it is likely that the variations in charcoal are strongly linked to the inferred CO_2 driven climate changes, rather than primarily by any Milankovitch forcings, or that the volcanogenic CO_2 climatic influence overrides any Milankovitch scale forcing.

8.6 Limitations and opportunity for future work

Interpreting the record of palaeo-wildfire through the use of sedimentary charcoal is also not straightforward, due to the number of influential factors that can distort the charcoal record (Iglesias et al., 2015; Leys et al., 2015). These can include direct fire-induced bias in charcoal formation (Hudspith and Belcher, 2017) as well as the more commonly considered pre-depositional and post-depositional re-working (Figure 8.14).

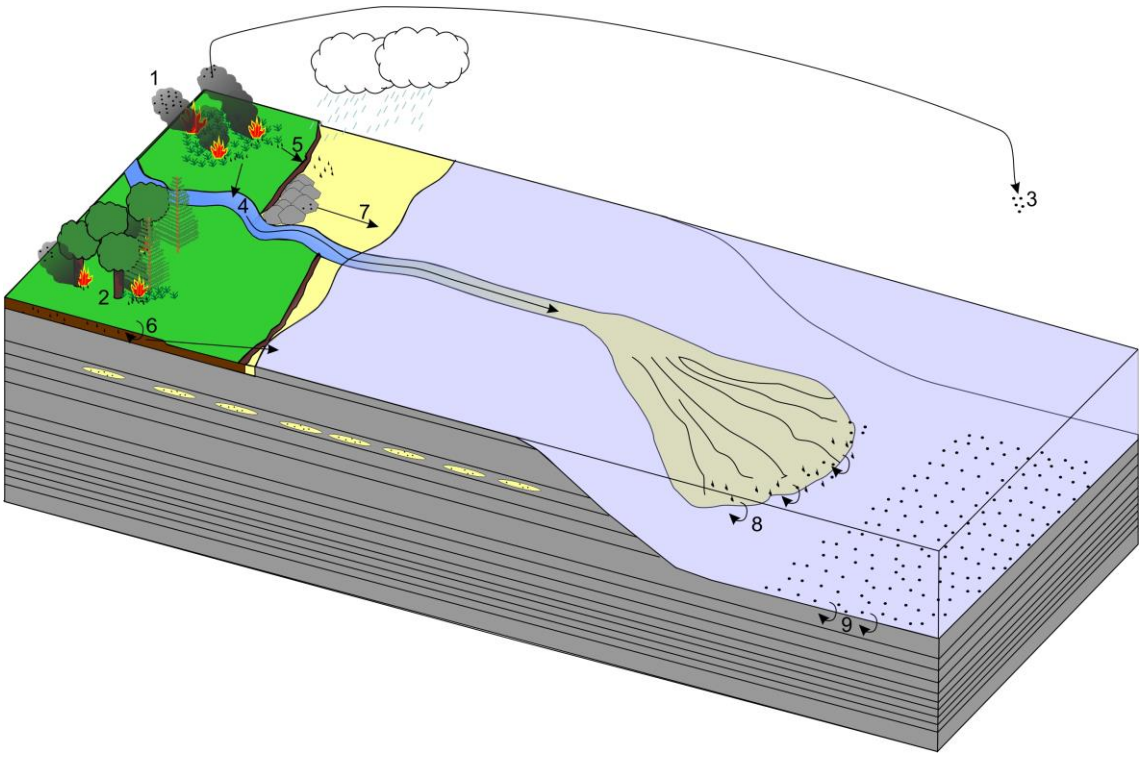

Figure 8.14 – Diagram illustrating pathways of charcoal formation and deposition in a marine setting. Fire, vegetation type and charcoal formation: 1 – More vigorous fires can produce greater amounts of ash particles compared to smaller, less vigorous fires (Schaefer, 1974). Burned area can also influence the amount of char produced as fires burning a larger surface area can produce more char (Leys et al., 2015). 2 – Some vegetation types can produce different char amounts (Hudspith and Belcher, 2017). Charcoal transport mechanisms: 3 – Smaller charcoal particles (commonly <125 µm can get transported by air almost geologically instantly from the burn site to the deep ocean. 4 - Charcoal particles of all sizes may also get transported by fluvial mechanisms away from the burn site to the shallow marine environment, or to deeper marine environments through a sub-marine fan. These water transported particles can take up to 1500 years to be deposited from the burn site to the final site of deposition in the deep ocean (Frueh and Lancaster, 2014). 5 – Particles may be transported following a fire by surface water run-off. This is common if precipitation follows a fire. Re-working and re-deposition of charcoal particles: 6 – If the charcoal particles are not transported away from the fire, they can become incorporated into soil layers, where bioturbation can cause the charcoal particles to sink to lower soil layers. These layers may later be eroded and washed into the marine environment up to hundreds to thousands of years later than initial char deposition (Personius, 1993). 7 – Charcoal particles within rock formations may also be weathered and eroded away over time, leading to the charcoal particles being washed into the marine system and re-deposited many years after their original formation. 8 – Re-working of charcoal particles may occur in turbidite environments, where recently deposited char can get mixed with previously deposited charcoal in lower sedimentary layers. 9 – Re-working of charcoal between sea bed layers can also occur through bioturbation in both shallow and deep marine environments.

Stratigraphic variations and sampling intervals should also be considered such as “uneven sampling over time” – where some equally spaced samples may represent larger portions of depositional time compared to others and where changes in depositional setting and subsequent variations in taphonomy (Iglesias et al., 2015, p. 2), as well as challenges in interpreting what a change in charcoal abundance is reflecting. For example some vegetation types can produce more charcoal fragments than others (Hudspith and Belcher, 2017) e.g. herbaceous/grass fires tend to produce a larger number of smaller charcoal fragments than forest fires (Patterson et al., 1987; Leys et al., 2015). Furthermore the nature of a fire may also be important in controlling the amount of charcoal produced (Patterson et al., 1987), where for example, more ‘vigorous’ fires produce larger amounts of small ash particles (Schaefer, 1974), and where changes in burned area can also be related to changes in charcoal abundances (Leys et al., 2015). Hence, it is imperative that fire reconstructions from the charcoal record are coupled with modelled/known climate; vegetation, environmental and sedimentological changes that could influence its interpretation. More critically, experimental research is required to link charcoal production to fire dynamics both in laboratory-controlled conditions (e.g. Hudspith and Belcher, 2017) and in field-scale wildfires. Some aspects of charcoal inventories from wildfires have been addressed by Santín et al. (2015) in regards to consideration of C-cycling in modern fires, however, such field approaches need to be considered in terms of the fossil record as this may yield important contributions in regards to the contribution of variations in charcoal abundances to short and long-term carbon stores throughout Earth history.

Throughout this thesis, each of the points discussed above have been carefully considered to try to minimise any misrepresentation of the charcoal record. For example, where possible, samples were collected from similar depositional strata, such as mudstones, which are likely to have a similar rate of deposition to minimise any un-evenness in the depositional time analysed. Samples from the Mochras and Peniche sections were also compared and correlated with published time-scales. To minimise any misrepresentation of changes in char abundances due to significant increases or decreases in organic flux to the OAE 2 depositional sites, or due to significant changes in organic preservation, non-charred organic material for each sample and study site were quantified/weighed.

Finally, pre and post-depositional re-working was also considered. Pre-depositional re-working is particularly important to consider for the marine study sites (Mochras and Peniche), as charcoal can be transported to the marine system by fluvial mechanisms, such as run-off or rivers, or via aerial mechanisms such as wind. These mechanisms therefore allow for potentially differential deposition of charcoal fragments within the marine environment. Aerially deposited charcoal fragments are more likely transported and deposited almost instantaneously (e.g. <125μm sized particles can be lofted by fires from the land to ocean basins (Horn and Underwood, 2014), fluvial derived charcoal can either be deposited close to the time of the fire (e.g. deposited within a few years), or could be deposited many hundreds-to-thousands of years later as recycled charcoal from erosion of previously deposited char in soil layers (Personius, 1993). An example of this can be seen in Frueh and Lancaster's (2014, p. 110) study which demonstrated that 'mean inherited ages' (inherited age defined as "the difference between times of carbon fixation in a material and deposition of that material within sediments") of charcoal found within sediments deposited as debris-flow deposits, fluvial gravels and fines within southern Oregon Coast Range, USA, could be up to 1500 yrs old, indicating a lapse in time between char formation and char deposition. Furthermore, bioturbation in sediments can cause the movement of charcoal fragments whereby fragments become emplaced within sediments after deposition (e.g. Bull, 2007).

The variations in the >125μm fraction and the <125μm fraction were studied across the T-OAE from the Mochras and Peniche study sites, as well as the Milankovitch cycles in the Mochras core. The difference between the >125μm fraction and the <125μm fraction in this study could therefore potentially be due to differential transport regimes between different size fractions of char, where according to Frueh and Lancaster (2014), the larger fraction could be up to 1500 years older than the <125μm fraction found within the same sample. As the shortest timescale variations in charcoal abundance was across ~23 kyr (Milankovitch precession cycle timescale), the ~1500 year delay in deposition is unlikely to influence the pattern of charcoal enough to de-couple the >125μm and <125μm trends observed at inferred maxima and minima cycle indexes, however

for samples collected in between, this lapse in time should be considered. Furthermore, the samples collected from the Peniche section constituted ~3 cm strata thickness, which when compared with Huang and Hesselbo's (2014) calibrated cyclostratigraphy, is found to equate to ~2000 years' worth of deposition (assuming constant deposition rate and without turbidite/re-deposited beds). Hence the thickness of sample collected for these sites is unlikely to have been significantly influenced by the delay (if any) between deposition of the larger >125μm fraction and deposition of the smaller <125μm fraction. However despite this, and although sediments that display evidence of re-working/re-deposition (e.g. a prime example being the turbidite beds within the Peniche T-OAE section) were avoided, pre-depositional re-working of charcoal in the source area, like with many proxies, is difficult to completely rule out.

Post-depositional reworking, for example, charcoal weathered out of rocks on the continents and shed to the ocean may further influence the charcoal signal, particularly for studies conducted over long timescales, and where there is evidence for increased continental weathering, such as during the negative CIE of the T-OAE.

During the negative CIE, as discussed in Chapter 4, ocean-atmosphere models and geological osmium isotope data indicate a period of enhanced continental weathering. If post-depositional re-working occurred, it would be during this time that one would anticipate any 'extra' charcoal to be weathered out of the rocks or from the land and deposited to the marine system, where both of the study depositional sites are located. However, throughout the duration of the negative CIE, the consistently low abundances in both the Mochras and Peniche study sites suggest that it is unlikely that post-depositional re-working of charcoal occurred.

Furthermore, the analysis of organics quantified/weighed within the OAE 2 sections, and the Mochras Milankovitch study section illustrates that there were no significant changes in organics present and thus variations in charcoal abundances are unlikely to be due to significant changes in organic preservation and/or delivery of organics from the terrestrial to the marine realm.

Despite these caveats and considerations, the presence and abundance of fossil charcoal has been extensively utilized, to provide information on both short and

long-term fire trends, from the analysis of the number wildfire episodes (e.g. Scott, 2000; Scott et al., 2000; Belcher et al., 2005; Scott and Glasspool, 2006; Belcher et al., 2010; Higuera et al., 2010; Danaiu et al., 2013; Chipman et al., 2015; Ribeiro et al., 2016; Baker et al., 2017), through to 'reconstructing' atmospheric O_2 concentrations for the last 400 Myrs (e.g. Glasspool and Scott, 2010). It is clear that when carefully considered, changes in charcoal abundance as a proxy for fire activity provide a unique tool that unequivocally argues for the presence of fires in Earth's ancient past. Having indicated in this thesis that charcoal abundances/fire histories have varied across a large range of timescales in Earth's deep past, relating to variations in atmospheric oxygen, climate and orbital cycles, it is clear that this strength should now be built on to develop our understanding beyond fossil charcoal 'fire frequency' considerations, to better consider fire feedbacks to the Earth system.

Studies should seek to consider to what extent charcoals can provide quantitative data, for example, in terms of atmospheric O_2 (e.g. Glasspool and Scott, 2010) or perhaps whether abundance and form might relate to fuel type or even fire behaviour (Daniau et al., 2013; Crawford et al., 2017 (in review)). For example, within Glasspool and Scott's (2010) study, abundances of charcoal in coals (described as inertinite) are analysed, and grouped into 10 Myr time periods. From the knowledge that laboratory experiments demonstrate that combustion cannot occur below O_2 levels of <15%, and therefore charcoal will not be present, an inertinite percentage of 0% is assigned (although later considered as 0.2% in Glasspool and Scott, 2010). At PAL of 21% vol. O_2, a 4.3% inertinite is calculated based on the abundance of charcoal found in differing peats from across the globe. For the upper limit of O_2 (suggested to be between 25% to 35%), a maximum inertinite percentage of 44.4% is calculated from published abundances observed during the Permian – a period modelled to have experienced high atmospheric O_2, where the Inert% of 44.4% corresponds to the mean of the upper O_2 estimates of ~30% (Scott and Glasspool, 2010). From these estimates, a calibration of atmospheric O_2 is calculated, enabling the percentages of inertinite found for the last ~400 Myrs of Earth's history to be used to estimate relative atmospheric O_2 concentrations. Here they make two assumptions; firstly that the upper limit for fires is 30% O_2, for which there is little data than that

inferred by Watson (1978), and 2) that fires and hence charcoal abundance in coals would increase linearly with atmospheric O_2.

Belcher et al. (2010) illustrate that burn probability is non-linearly related to atmospheric O_2 (see Figure 1.10 herein) and that beyond O_2 concentrations of ~23% burn probabilities reach close to ~100% in fuels of equal moisture. Whilst, Watson and Lovelock (2013) indicate that at higher O_2 variations in fuel moisture and thus the influence on the moisture of extinction become the more important factor. These imply that changes in wildfire activity (i.e. frequency alone) driven by variations in atmospheric O_2 beyond ~23% vol. are less likely to be sensitive and may not be easily observable within the fossil charcoal record (Lenton, 2013).

Moreover, Belcher and Hudspith (2016) highlight that fuel and O_2 driven changes in fire behaviour as opposed to 'frequency,' are likely the more important aspect of fire regime, and as yet, little is known about how variations in fire behaviour influence the formation of charcoal. Hudspith and Belcher (2017) have speculated that at least for analogue Cretaceous fuels, different fuel types containing different flower morphologies that burn at different intensities, influence the abundance and nature of charcoal that remains following fires, before it may even reach the depositional environment. Hence, charcoal's utility as a direct quantitative "palaeo-O_2 proxy" as proposed by Glasspool and Scott (2010) is not yet possible, particularly at high atmospheric O_2 (>23%) where the upper limit of the fire window is ill defined, and the link to fuel moisture-O_2 effects not yet well explored.

Therefore, whilst variations in charcoal abundance are able to qualitatively infer significant variations in fire activity, the future should look towards estimating major shifts in fire behaviour, and the likely upper limits of O_2 and its influence on fire, before fire activity would be considered incompatible with the existence of large land plants on Earth, and before a quantitative charcoal based O_2-proxy can be developed.

9. Thesis Conclusions

The research presented in this thesis contributes to our understanding of the fossil record of fire across medium and long timescale, what the record of fire can tell us and how fire may play an essential role in regulating the Earth system and re-equilibrating the Earth system following a significant carbon-cycle perturbation.

Firstly, the research presented in this thesis contributes what is believed to be the first fossil evidence in support of a model based theory (Handoh and Lenton, 2003) that rising atmospheric O_2, driven by the increased organic carbon burial during the OAE, led to the Toarcian OAE's natural termination ~1.8 Myrs after it began (Baker et al., 2017). The sustained rise in charcoal abundances, occurring during the final ~800 kyr stage of the T-OAE suggests that fire feedbacks may have played a key role in aiding in the termination of the event by suppressing land vegetation and thus the weathering of the limiting nutrient phosphorus, which may have aided in reducing the amount of organic carbon buried, and returning the Earth system towards background functioning.

The results presented capture a geologically rapid enhancement of atmospheric O_2 occurring over the short timescale of the Toarcian OAE, implying that small but significant changes in O_2 may be possible over the timescale of OAEs. As such, new higher time-resolution models of O_2 over Earth's history may be required to explore the relationship between changes in C-cycling and the functioning of the Earth system.

Secondly, the research presented in this thesis indicates that significant CO_2 – climate driven changes in wildfire activity can be observed even under the modelled high atmospheric O_2 concentrations of the Cretaceous period, supporting previous hypotheses for significant and geologically rapid CO_2 driven climate shifts, occurring during the early stages of ocean anoxia and perturbation to the global C-cycle. These results suggest that climate driven changes in the moisture content of fuel were likely the dominant control on wildfire activity during this 'high O_2 period'.

Thirdly, this thesis presents an analysis of charcoal abundance variations occurring across natural, orbitally forced cycles, termed the Milankovitch cycles. The results presented illustrate that natural variations in charcoal abundance are possible over intermediate timescales within the geological record, and therefore suggests a need to take into consideration and incorporate ‘natural background’ fluctuations in fire activity occurring over medium timescales, when analysing and predicting past and future climate change - fire patterns.

As such this research demonstrates how combustion in the natural world may play an essential role in re-equilibrating and regulating the Earth system and maintaining it within habitable bounds prior to human arrival and should stand as a baseline point within which we must set against own impact on managing fire and ignitions into the future.

Appendices

Appendix A. Identifying Palaeo-wildfire

Products of combustion

Combustion generates a number of solid, particulate and gaseous products (Scott, 2000). These products include char, ash and partially charred material, soot, tar, polycyclic aromatic hydrocarbons (PAHs) and other carbonaceous aerosols such as organic and black carbon (Clark et al., 1997; Scott, 2000). The temperature reached during pyrolysis determines the proportions of the products produced, such that higher proportions of char and tar are generated under low temperatures (up to 600°C), whilst higher proportions of flammable volatiles and pyrogenic PAHs are produced under high temperatures (up to 900°C) (Scott, 2000; Denis et al., 2012).

If sufficient time and O_2 are provided, all of the fuel is combusted, leaving little residual products, commonly in the form of ash (Glasspool and Scott, 2013). Although, "these conditions are often not met and a pyrolysis residue (charcoal) will remain" (Glasspool and Scott, 2013, p. 180), the process of diagenesis and oxidation means that many of the products of combustion do not survive to be incorporated within the fossil record. This can include incompletely charred material that can be broken down on decadal timescales if deposited in well-aerated soils (Bird et al., 1999). However, completely charred material in the form of charcoal is highly resistant to decomposition and degradation, even in highly oxic environments (Verado, 1997; Matthewman et al., 2012). Furthermore, Verado (1997) indicates that experiments conducted on microbial decomposition of charcoal (e.g. Schneour, 1966) illustrated that no decomposition occurred on the charcoal by the microbes. This is likely due to microbes failing to attach to the charcoal (Alexander, 1981; Verado, 1997). The

charring process therefore allows the evidence of wildfire to be preserved within sediments over 350 Myrs old in the geological record (Scott, 2000; Mooney and Tinner, 2011). As charcoal can only be formed by the combustion of plant matter by a fire, the presence of charcoal "can be regarded as direct evidence for the occurrence of wildfires during the geological past" (Uhl et al., 2014, p. 101), outside of volcanically influenced sediments (e.g. pyroclastic flow deposits and tephra deposits). Furthermore, the preservation of charcoal particles over a few microns in size also enables taxonomic identification (Scott and Glasspool, 2006), making the study of fossil charcoal in the geological record a suitable palaeo-wildfire proxy.

The process of Charcoalification

Charcoal is formed naturally from the incomplete combustion of plant material during the process of pyrolysis (Chaloner, 1989; Scott, 2010). The charring process involves the burning of plant material in the absence of O_2 (Beaumont, 1985; Scott and Jones, 1991). During the process of pyrolysis, the plant is 'subjected to rapid high temperature heating' (Scott, 2010, p. 14) (particularly as many wildfires are initiated by lightning strikes). This heating causes the cellulose in the plant tissues to break down, producing carbon monoxide (CO), CO_2 and CH_4, which then mixes with O_2 and burns creating heat (Pyne et al., 1996). The heat of the fire penetrates the plant tissue where there is little/no O_2, creating a charring front. It has been suggested that at temperatures of >325°C cell walls fuse which has been suggested as a key feature in the identification of charcoal (Scott, 2010). However, recent research indicates that this just a phase of charcoalification and that cell walls may become separated again and fragment following longer periods of heating (Hudspith and Belcher, 2017; Crawford, Baker and Belcher, in review). However, as no other known process is capable of generating fused cell walls, finding this in fossil charcoals does imply that it may help in identifying fossil charcoal, but that it is not a required feature.

The Fusain Debate

In the Collins English Dictionary, fusain is defined as "a dull black brittle form of carbon resembling charcoal, found in certain coals". However, throughout much of the early literature, a debate existed as to whether fossil fusain was actually

fossil charcoal or the product of something else (Harris 1958, Harris, 1981; Sander and Gee, 1990; Scott and Damblon, 2010). As Scott and Glasspool (2007) and Scott and Damblon (2010) indicate, one of the most problematic areas of charcoal study is the different use of terminology when describing it. Throughout the literature, charcoal may be referred to as many, if not all of the inertinite macreals (e.g. fusinite, semifusinite, inertodertrinite, macrinite and funginite and secretinite), all of which are deemed to have acquired physical and optical characteristics through increased temperatures (Scott and Glasspool, 2007), and could all therefore be termed as charcoal.

Initial studies considered fusain as being a product of wet decay (e.g. Stützer, 1929, Stützer and Noe, 1989), or of biogeochemical origin (e.g. Schopf, 1975). However, due to many similarities identified between fossil charcoal and fusain, for example its appearance under a light microscope (e.g. Harris, 1958) and a scanning electron microscope (SEM) (e.g. Cope, 1980), fusain is now widely recognised as being fossil charcoal (e.g. Harris, 1981; Cope, 1980; Cope and Chaloner, 1985; Chaloner, 1989; Scott, 1989; Jones and Chaloner, 1991) and will therefore not be differentiated within this thesis.

Charcoal Identification

Macro and Microscopic Charcoal

Macro-charcoal fragments often refer to particles larger than 100µm, whilst micro-charcoal refers to particles smaller than 100µm (Mooney and Tinner, 2011). Macroscopic charcoal is often separated from sediments through wet sieving (e.g. Clark, 1990; Tinner et al., 2006), after petrographic thin section analysis became unpopular due to the preparation time (Mooney and Tinner, 2011), however both micro- and macrochar are commonly analysed using a microscope.

Charcoal identification under light microscopy has been the centre of debate for many years (e.g. Patterson et al., 1987 and Clark, 1988), with some attempting to classify charcoal into different genus/species levels (e.g. Hutchinson and Goulden, 1966). However, recently charcoal identification features have been in agreement with many adding to the list of the defining features present.

Initial studies describe microscopic charcoal as presenting jet black, opaque, angular particles, separating them from “clear or brown amorphous weakly

structured particles" that represent vegetal matter (Patterson et al., 1987, p. 9) (see also Swain, 1973; Clark, 1982; Clark, 1988). This progressed to include having a distinct fibrous appearance, and breaking with a "rectilinear fracture" compared to coalified particles that were deemed structure-less and breaking with conchoidal fracture (Cope, 1980, p. 664). By 1990, the defining features of charcoal had been extended to include a silky lustre, high reflectance, cell wall homogenisation (under a Scanning electron microscope (SEM)) and/or occasionally a cuboid shape (Sander and Gee, 1990) (Figure A1). It was also suggested that most charcoal shows a distinct cleavage along the "radial plane of the wood fracture" (Sander and Gee, 1990, p. 273). Since Sander and Gee's (1990) study, many authors have described charcoal fragments similarly (e.g. Jones and Chaloner, 1991; Thevenon et al., 2003; Daniau et al., 2007; Duffin et al., 2008; Conedera et al., 2009), with the addition of a 'graphite like sheen' and a 3D needle like shape (Belcher et al., 2005). These characteristics make charcoal clearly and easily identifiable under both light and scanning electron microscopes.

When prepared for palynological thin section analysis, charcoal is often described as being "translucent grey-brown structured particles or as black fibrous grains sometimes exhibiting cellular structure"' and can therefore be easily distinguished from "coalified material which will be typically dark orange-brown in colour with irregular shape" (Belcher, 2005, p 30) (Figure A2 and A3).

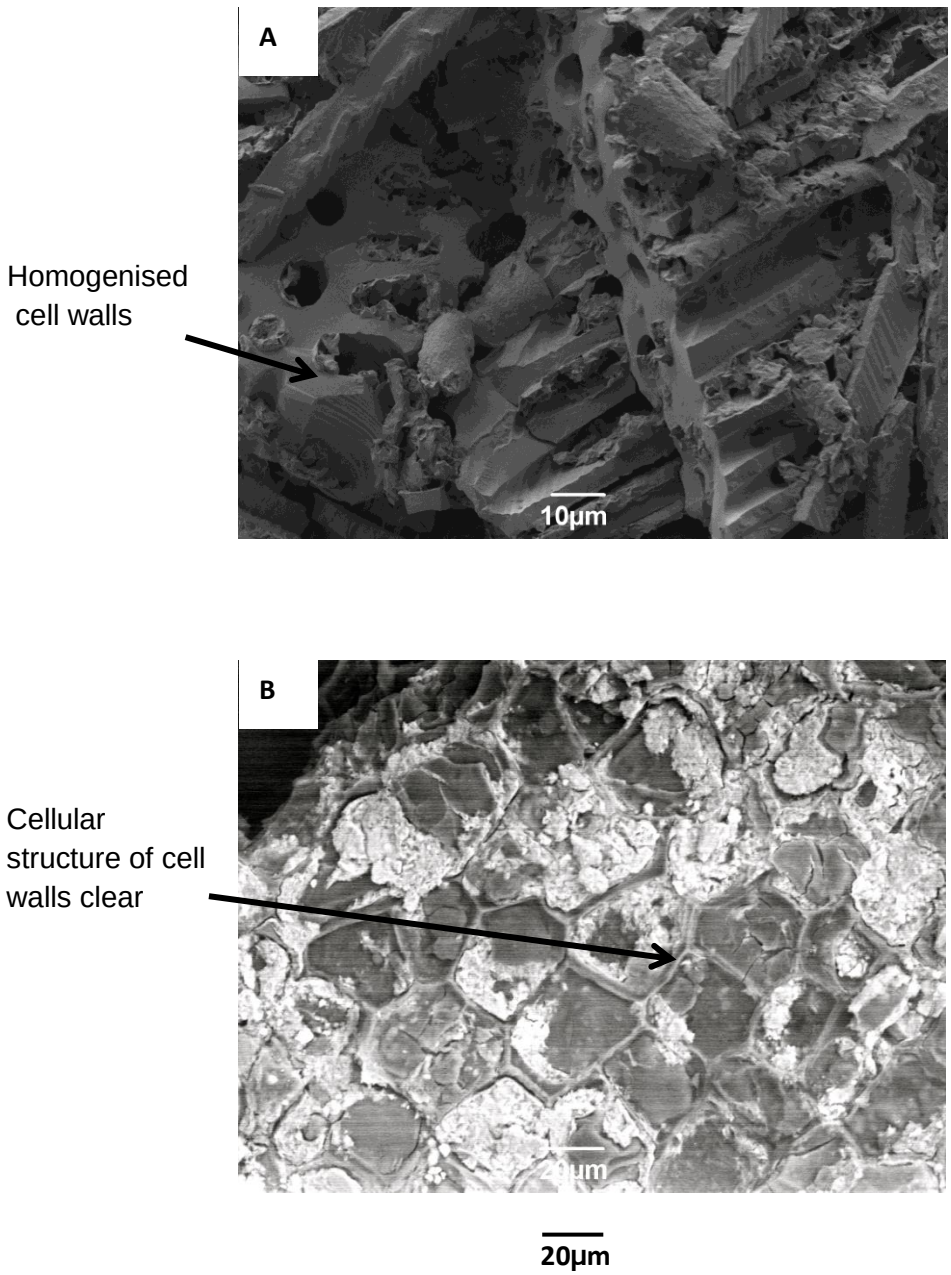

Figure A1 – **(A)** Photograph taken under an SEM illustrating the homogenisation of the cell wall in a charcoal fragment, compared with the lack of cell wall homogenisation of a non-charred particle under an SEM **(B)**.

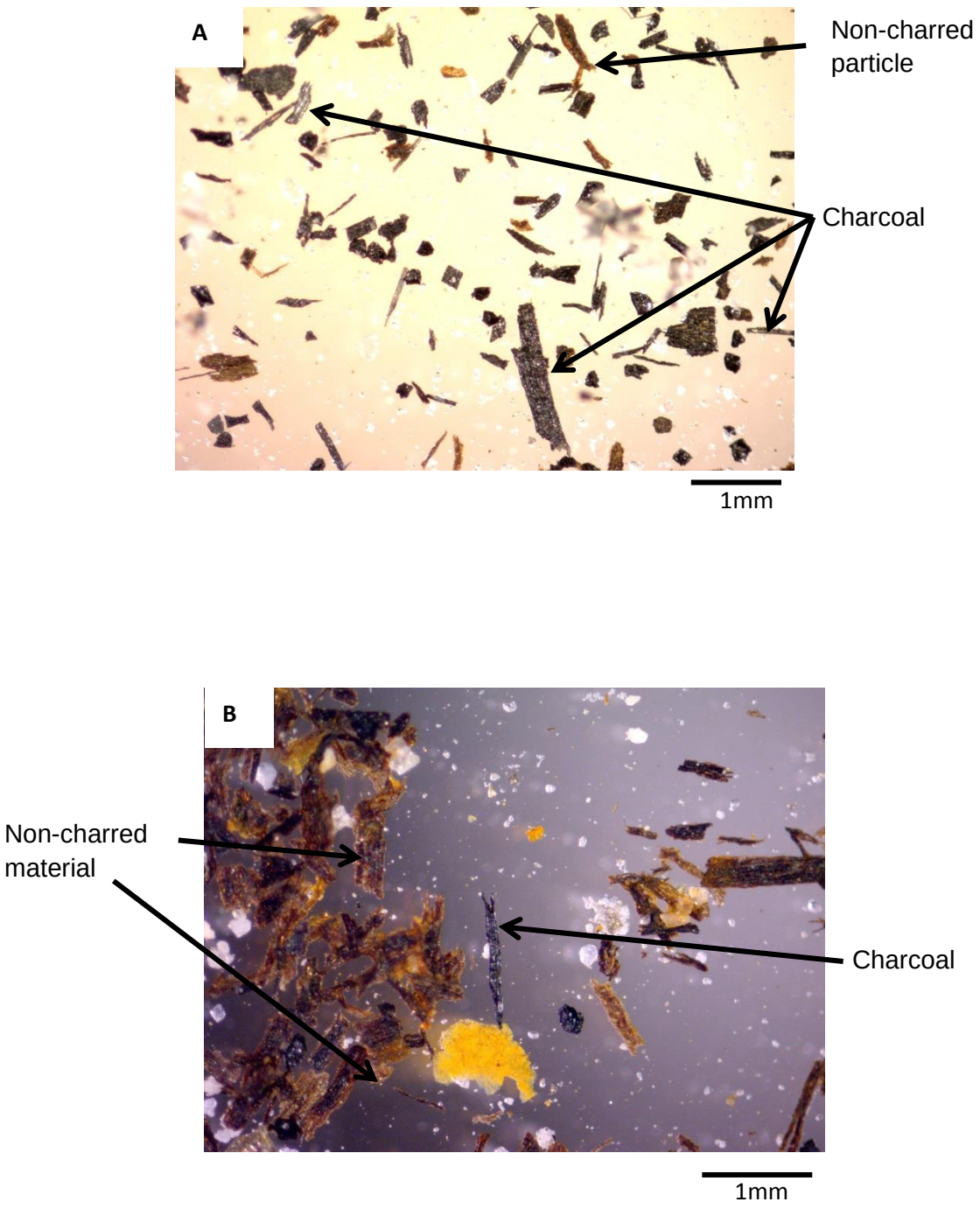

Figure A2 – **(A)** Image taken of charcoal fragments illustrating graphite like, silvery sheen under bright field illumination, compared with orange-brown un-charred material. Image taken from T-OAE Mochras sample 2805'11'', >125µm.

(B) Image taken of charcoal under dark field illumination. Charcoal particles illustrate graphite-like sheen compared with varying shades of brown uncharred vegetal matter. Image taken from T-OAE Mochras sample 2637'9'', >125µm.

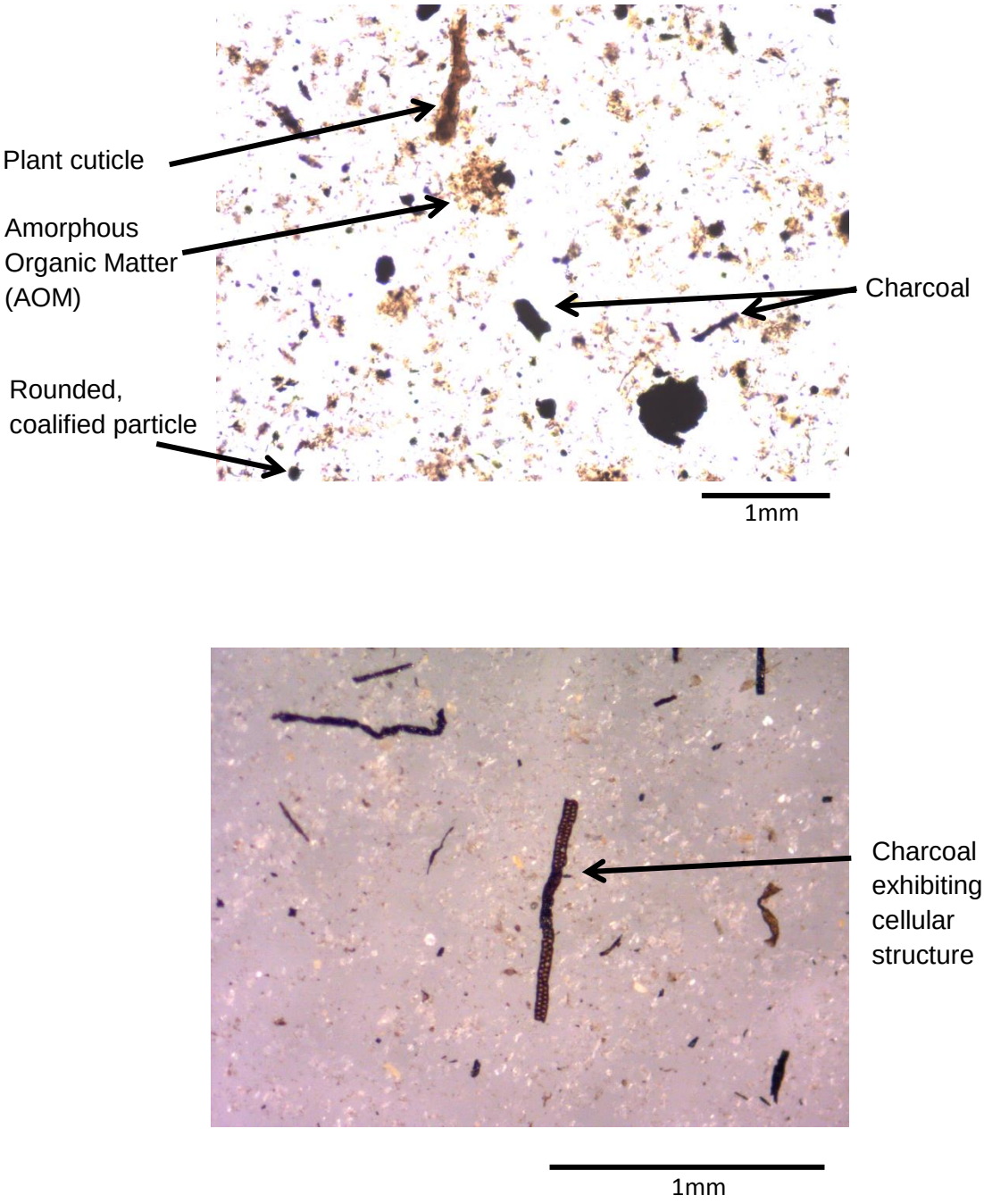

Figure A3 – Charcoal particles in a palynology slide, under a low powered transmitted light microscope. Charcoal particles appear as black, opaque, fibrous particles, compared with structureless or rounded coalified particles, and brownish hues of vegetal matter **(A)**. Image from T-OAE Peniche sample pp 20.20. Charred particles can also illustrate cellular structure **(B)**. Image from T-OAE Peniche sample Penpal 8, under transmitted light microscope.

Quantifying Fossil Charcoal

When quantifying fossil charcoal, there are a number of methods that have been used, including the use of pollen slides; a density separation, software imaging and palynofacies analysis.

Pollen Slide Method

The pollen slide method is thought to be the most popular method for charcoal identification (Rhodes, 1995; Carcaillet et al., 2001) and is regularly used throughout the literature (e.g. Durne and McVeen, 1959; Tsukada and Deevey, 1967; Swain, 1978; Tinner et al., 1998 and Carcaillet et al., 2001). Prior to preparing 'pollen slides' samples are demineralized and sieved, where this process enables the more resistant organic fragments (including charcoal) to be easily identified. The method of demineralization is described below and is taken from Moore et al. (1991); and was used in Belcher et al. (2005) and Belcher (2005). To demineralize, each sample is immersed in hydrochloric acid (HCl) (10% conc.) for approximately 72 hours, until any obvious reactions cease, to remove any carbonates present. The sample is then treated with hydrofluoric acid (HF) (30-40% conc.) for approximately 72 hours to remove any silicates present. Another treatment with HCl ensures the removal of any calcium fluoride precipitates, before being washed with distilled water until a neutral pH is reached.

After sieving to divide the micro-charcoal from the macro-charcoal, both size fractions are dispersed in a known quantity of distilled water (Belcher, 2005). Approximately 50µl – 100µl of the solution containing micro-charcoal is then pipetted onto a cover slip and mixed with two droplets of Polyvinyl alcohol before being dried. The cover slips are then mounted onto slides using petroproxy resin 154 (Belcher, 2005). Once this procedure has been conducted, the analysis of microcharcoal can be undertaken in a number of ways under a transmitted light microscope. For example, Belcher (2005) and Belcher et al. (2005) count the number of charcoal particles present across two transects of the slide. These are then expressed as charcoal per gram of sediment (Belcher, 2005; Belcher et al., 2005). Other methods however include the 'point-count' method, 'absolute particle abundance method' and 'size class method' (Rhodes, 1998; Mooney and Tinner, 2011). For the macro-charcoal, the sieved fraction

can be decanted into a petri dish and quantified under a dissecting microscope, where all particles are counted and again their abundance expressed as per gram of rock dissolved.

Microchar counting methods

Point-Count Method

The point-count method was first introduced by Clark (1982) and has since been used by many authors when quantifying micro-charcoal (e.g. Duffin et al., 2008 and references therein). The point-count method measures charcoal abundance by recording the number of charcoal particles 'hit' by a standard number of points on an eyepiece reticle during scans on a pre-determined area of slide (Rhodes, 1998) or the ratio of the number of points intersecting a phase to the total number of points applied being proportional to the area of that phase (Clark, 1982; Mooney and Tinner, 2011). Within Duffin et al.'s (2008) study, micro-charcoal was counted using a Nikon Eclipse 400 microscope at 400 x magnification. To ensure 'statistical significance' at least 200 *lycopodium* spores and 100 charcoal particles were counted (also used within Finsinger and Tinner, 2005).

'Absolute Particle Abundance Method'

All charcoal particles are counted and recorded regardless of their size, giving a total number of charcoal particles on one slide. This method has been used by Iversen, (1941) and Davis (1967) (Rhodes, 1998).

'Size-class method'

Charcoal pieces are recorded based on the particle length or surface area using the eyepiece grid. Charcoal pieces are expressed as area of charcoal within individual size classes "or as a total area of charcoal encountered in a sample by summing the areas of the individual size classes (e.g. Waddington, 1969; Swain, 1973)" (Rhodes, 1998, p. 113).

Limitations to the pollen slide method

Although extensively used, much of the literature also indicates restrictions associated with the use of pollen slides. Clark (1988) for example, indicated that one of the disadvantages associated with charcoal identification on pollen slides

was the small size of the fragments ranging between 5μm and 8μm long. This is problematic because charcoal is usually counted at a lower magnification and could therefore be missed. This problem has also been highlighted by Patterson et al. (1987) and Rhodes (1998) indicating that very small particles make charcoal pieces more difficult to identify (Mooney and Tinner, 2011).

However, Tinner and Hu (2003) found the pollen slide method to be accurate yet time consuming. Their study, which aimed to assess and determine the relationship between the charcoal area and number of charcoal particles, indicated that the measuring of charcoal area on pollen slides, although accurate, was 'unnecessary'. Instead, Tinner and Hu (2003) suggest that the counting of charcoal fragments was more than adequate to provide accurate results.

Software Imaging

The use of imaging software as a way of detecting and counting charcoal is rarely referred to throughout the literature. Few studies that use imaging as a way of analysing charcoal include studies by Clark (1984); Beaufort et al. (2003); Thevenon et al. (2003) and Daniau et al. (2007). Thevenon et al. (2003) conducted their imaging analysis through the use of a transmitting light microscope and a digital camera driven by SYRACO software (SYstéme de Reconnasissance Automatique de COccolites. Automated measurements on selected dark particles were then performed by Scion Image analysis software, the results of which are given as an area (mm^2) per gram of sediment (occupied by the dark particles) (Thevenon et al., 2003). Morphological parameters were then calculated on medium sized particles (63-150μm) to determine the charcoal shape variability. This included perimeter, length and width measurements.

Daniau et al. (2007) used a similar method to Thevenon et al. (2003), citing that previous authors had found the preparation method successful (e.g. Bird and Gröcke, 1997). Within Daniau et al.'s (2007) study, slides were scanned using an automated Leica DMRBE microscope in transmitted light (Daniau et al., 2007) in 100 fields of view. These were then analysed using an "adapted program of image analysis written in Scion Image software" (Daniau et al., 2007, p. 1373) that allowed for easy charcoal recognition. Daniau et al. (2007)

do not suggest any limitations to the use of imaging as a method for charcoal analysis, due to the combined use of petrographic thin sections as well as image analysis. Conedera et al. (2009) however do identify restrictions to this method briefly, describing that commonly when using a digital camera every pixel represents about 0.2µm x 0.2µm, which allows the quantification of very fine particles. The disadvantage to which however is that as finer particles are quantified, there is an increased risk of including other opaque minerals or soot particles. However, as discussed in Thevenon et al.'s (2003) paper prior to Conedera et al. (2009), the samples are treated with three acid treatments including hydrochloric acid, nitric acid and hydrogen peroxide that act to digest any organic material, carbonate or pyrite that could otherwise make the identification of charcoal more ambiguous. Other preparation acids can include Potassium hydroxide, acetolysis and hydrogen fluoride (Moss and Kershaw, 2000). Beaufort et al. (2003) does however indicate that it is not possible to be certain that some of the black, opaque particles left after using acids are not minerals that were not completely dissolved. Daniau et al. (2007) attempted to solve this ambiguity by removing any particles less than 15 pixels on their imaging software. This therefore eliminated the risk of non-charcoal particles being quantified. Although this method does not appear popular throughout the charcoal literature, it is suggested to have a low percentage error of just 1% (Beaufort et al., 2003) and could therefore be deemed as a more accurate, reliable method in comparison to other methods used. However, there is considerable ongoing debate about the use of image analysis to quantify charcoals and what parameters should be included (e.g. Crawford and Belcher, 2015). In all cases image analysis takes a significant time to acquire data, and in particular, becomes problematic for ancient sediments because as yet automated techniques are unable to distinguish charcoalified particles from coalified particles making these approaches more challenging and potentially less accurate than traditional human based counting approaches (Belcher et al., 2013b)

Palynofacies analysis

Palynofacies is the analysis of sedimentary organic matter using microscopy as an aid in the identification of different facies. From this, predictions in variations

in palaeoenvironment, basin analysis and also fossil fuel exploration can be made (Mendonça Filho et al., 2012).

Initial studies (e.g. by Combaz, 1964) described palynofacies as “the total assemblage of microscopic organic constituents present in a rock that remain after maceration in HCL and HF” (Mendonça Filho et al., 2012, p. 219). These are observed under transmitted light microscopes after mounting on slides using palynological preparation procedures. Palynofacies analysis is now also defined as including the determination of kerogen types and their abundance (Mendonça Filho et al., 2012). Kerogen types include; Type I (mainly derived from fresh water algae or amorphous organic matter (AOM)); Kerogen Type II (comprising pollen grains; spores, cuticles and marine organic matter); Kerogen Type III (commonly derived from terrestrial plants) and Kerogen Type IV (secondary type of kerogen and includes only aromatic components e.g. carbonized organic matter such as charcoal) (Mendonça Filho et al., 2012) (Figure A4).

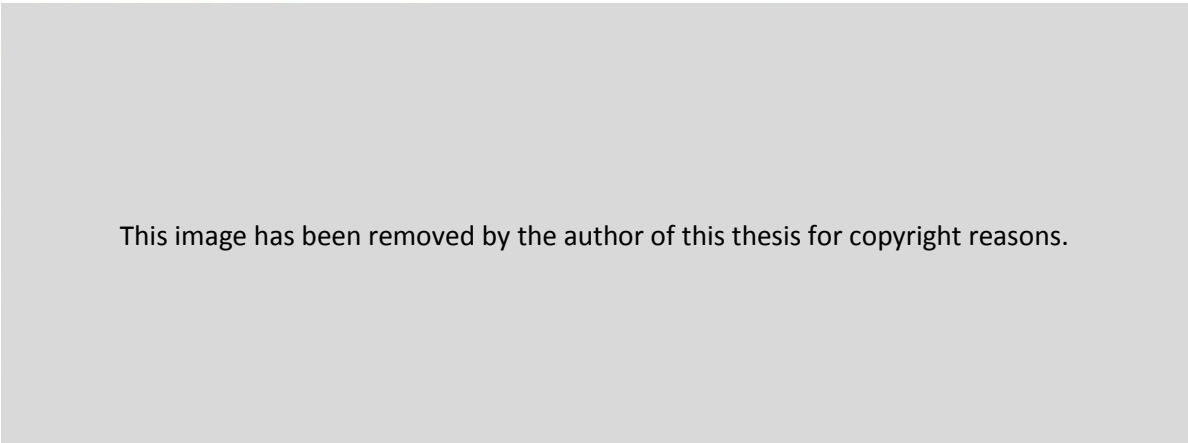

Figure A4 – Plates illustrating the different Types of Kerogen analysed during palynofacies analysis (Taken from Mendonça Filho et al., 2012)
Plate 1 – AOM and fresh water algae related to Kerogen Type I
Plate 2 – AOM, pollen Grain, Cuticle, Prasinophyte Algae, Acritarchae and Dinocysts, related to Kerogen Type II
Plate 3 – Wood tissues (non-opaque phytoclasts), related to Kerogen Type III
Plate 4 – Carbonized wood tissure (opaque phytoclasts) related to Kerogen Type IV

Palynofacies analysis can therefore be used to provide information on any changes in terrestrial vegetation that may have influenced fire activity and behaviour and the charcoal record, as well as changes in the degree of terrigenous supply to the depositional environment.

Reconstructing fire history

Introduction

When reconstructing fire history the products of combustion become a useful tool. Here, most common methods use either charcoal counts from the sedimentary record, or tree-ring scar analysis (Denis et al., 2012). Tree ring scar analysis provide precise information on short-term fire events, however it requires a substantial population of trees in order to obtain all fire events and the time is limited to the life-span of the tree (Denis et al., 2012). PAHs have also been used as indicators of past fires in the geological record, often alongside charcoal records (e.g. Marynowski and Simoneit, 2009; Belcher et al., 2009), however Denis et al. (2012) indicate that there is no validation of PAHs as an indicator for past fire events. Furthermore there is a limit on the detection of PAHs produced by past fire events using instruments, as PAHs are commonly studied in much higher concentrations as pollutants than that produced by a natural forest fire (Denis et al., 2012). In contrast, variations in charcoal abundance have been extensively used as a proxy in reconstructing fire events and the analysis of long-term variations in fire frequency (e.g. Patterson et al., 1987; MacDonald et al., 1991; Whitlock and Anderson, 2003; Glasspool and Scott, 2009) (Whitlock and Larsen, 2001; Higuera et al., 2011).

Here, isolated peaks in charcoal abundance within the sedimentary record are linked to ‘fire episodes’ (Higuera et al., 2011), which can be attributed to periods of large fires, and/or increased occurrence of fires with high severity, and/or periods of high fire re-occurrence, occurring during the time spanned by the peak in charcoal (Clark, 1988; Whitlock and Larsen, 2001; Millspaugh et al., 2003; Marlon et al., 2009; Higuera et al., 2011). Linking high charcoal abundances with ‘fire episodes’ or ‘fire activity’ aims to avoid misrepresentation of charcoal peaks in the sedimentary record, which in the past have been complicated with number, frequency and/or intensity of fires (Iglesias et al., 2015).

The use of charcoal peaks for reconstructing fire history was first demonstrated by Swain (1973, 1978), who tallied microscopic charcoal (<100µm) fragments as part of a routine pollen analysis (Millspaugh et al., 2003). From this a fire reconstruction was made based on the ratio of charcoal-to-pollen accumulation in lake sediments in Wisconsin. Since, the use of microscopic charcoal for fire

reconstruction has since been extensively used (e.g. Patterson et al., 1987; Smith and Anderson, 1992; Reasoner and Huber, 1999; Innes and Simmons, 2000; Carcaillet et al., 2001) (Millspaugh et al., 2003). An example of this method can be seen in Figure A5 whereby the charcoal concentration and calculated accumulation rate correlates well with known fire frequency.

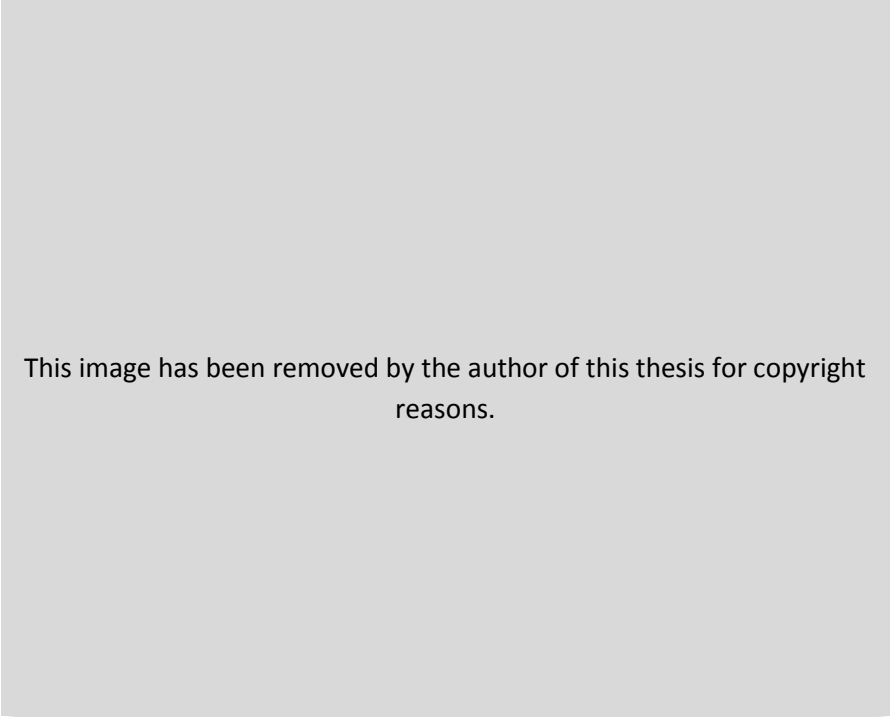

Figure A5 – Diagram illustrating known fire frequency and its correlation with charcoal accumulation rate and concentration taken from sediments in the Cygnet Lake, Yellowstone National Park. (Millspaugh et al., 2003, p.482).

Micro-charcoal analysis within sediments is a well-established method used in the reconstruction of local, regional and global records of wildfires (Carcaillet et al., 2001; Conedera et al., 2009, Turner et al., 2010). “Fire events produce a pulse in charcoal that is rapidly transported away from the fire site through airborne and fluvial transport mechanisms” and accumulate in nearby catchment areas such as lakes or nearshore settings (Turner et al., 2010, p. 374). Identifying these pulses within the sedimentary record enables the reconstruction of periods of increased fire events (Turner et al., 2010).

As the accumulation of charcoal within sediments can occur over longer periods of time due to varying transportation processes, when studying the record of wildfires within sediments, it is important to understand the taphonomic

implications, in order to understand what type of palaeo-fire record is being analysed (e.g. local versus distal).

Charcoal Taphonomy

The term ‘taphonomy’ was first used in 1940 by Efremov, who used it to refer to all the processes occurring after the death of an organism (Parisot et al., 2010). The term has since been adapted, and is now defined as describing “the processes acting upon an object from the point at which it is produced to the point where it is finally sampled” (Patterson et al., 1987, p. 4). Distances and methods of charcoal transportation both during and after fire events have been widely discussed throughout the literature with particular attention on the factors influencing its dispersal (e.g. Patterson et al. 1987; Clark, 1990; Clark and Royall, 1995; Whitlock and Millspaugh, 1996; Scott, 2000; Nichols et al., 2000; Ohlson and Tryterud, 2000; Gardner and Whitlock, 2001; Whitlock and Larsen, 2001; Whitlock and Anderson, 2003; Enache and Cumming, 2006; 2007 and many more).

The rate at which charcoal accumulates within a catchment area is dependent on the fire characteristics e.g. the rate of fuel consumption, efficiency of combustion and how much charcoal is produced (although relatively little is known about this) and the processes transporting and depositing the charcoal to a site (Whitlock and Larsen, 2001; Gardner and Whitlock, 2001). Many studies on charcoal accumulation are focused on lakes as the main catchment area (e.g. Whitlock and Millspaugh, 1996; Gardner and Whitlock, 2001; Whitlock and Larsen, 2001; Whitlock and Anderson, 2003), with fewer focusing on marine sediments, yet charcoal deposited within marine sediments has the potential to provide both a regional and global wildfire signal (Suman et al., 1997) across geological timescales.

Figure A6 illustrates the sources of charcoal in a watershed. “Primary charcoal refers to the material introduced during or shortly after a fire event” (Whitlock and Larsen, 2001, p. 2), and is therefore deposited almost instantaneously. Secondary charcoal refers to material that is deposited after fire events, e.g. during non-fire years. This is introduced to the watershed through processes such as surface run-off and lake-sediment mixing (Whitlock and Larsen, 2001). As charcoal particles are easily transported, the source of the charcoal (and

original fire) can vary between local (e.g. within the watershed area); extra-local (nearby the watershed) and regional (distal).

Figure A6 – diagram illustrating sources of charcoal in a watershed (taken from Whitlock and Larsen, 2001).

Defining size-class and distance travelled

The relationship between charcoal particle size and distance travelled from the source area has been heavily debated throughout the literature (e.g. Patterson et al., 1987; Clark, 1988; 1990; Whitlock and Millspaugh, 1996; Gardner and Whitlock, 2001). Patterson et al.'s (1987) study suggested that charcoal particles of less than (<) 100µm in size could be carried to great heights (Radtke et al., 1991) and large distances away from the source area by the wind, therefore leaving macroscopic fragments to be deposited close to the source. Thus over short timescales (days to years), wind speed and direction are hypothesized to play a pivitol role in how and where charcoal is dispersed (Patterson et al., 1987; Clark, 1990; Gélinas et al., 2001; Thevenon et al., 2003;

Tinner et al., 2006, Conedera et al., 2009). It was therefore predicted that macroscopic charcoal represented a local signal and microscopic charcoal a regional signal. However, other studies (e.g. MacDonald et al., 1991; Clark and Royall, 1996; Ohlson and Tryterud's, 2000) found that microscopic charcoal particles did not always coincide with longer distances from the fire source, but in fact could indicate fires occurring at short distances from the point of deposition. Likewise larger charcoal fragments could travel further than anticipated. One suggestion for this was due to varying densities of charcoal and its formation. Sander and Gee (1980) noted that freshly made charcoal had a low density, and hypothesized that because of this, recent specimens, if in water, should float for up to several days depending on charring conditions, and could therefore be transported longer distances. This is due to the internal wood structure; the degree of air-filled spaces open to the atmosphere, and the presence of "open cell lumina which remain open during charring" (Sander and Gee, 1990, p. 273) (see also Nichols et al., 2000; Scott, 2010).

Furthermore a study conducted by Vaughan and Nichols (1995) indicated that different charring temperatures could lead to variations in the brittleness of charcoal and therefore its porosity characteristics. It was illustrated that temperatures of up to 300°C result in the fusion of the cell walls which would inhibit water penetration and therefore slow the time of waterlogging and settling (Vaughan and Nichols, 1995; Enache and Cumming, 2006, 2007, Scott, 2009, and McParland et al., 2009). Nichols et al. (2000) also indicate that different material illustrates different hydrodynamic behaviour, for example leafy shoots and flowers could take longer to become waterlogged when compared to woody tissue. This may result in separation and sorting of charred materials during transportation.

Other studies (e.g. Clark et al., 1998; Pisaric, 2002) focused on variations in fire characteristics and their effects on the charcoal dispersal through convection columns. Clark et al. (1998) studied the upward convection of particles conducted on experimental crown fires in boreal Canada. Within the study Clark et al. (1998) found that particles of smaller size (10 μm) could be 'lofted' to low heights and/or great heights from the burn area, concluding that particle-size distribution does not necessarily distinguish between nearby sources and distant sources, as first suggested (e.g. by Patterson et al., 1987; Clark, 1988). This has since been further supported by conclusions made by Pisaric (2002)

whose study of fallout from a small-medium size forest fire in Montana, indicated that certain macroscopic plant remains had been transported up to 20km from the burn area. Pisaric (2002) suggested that this was due to severe convection and vortices associated with intense forest fires and therefore stress that it is difficult to distinguish between local and regional derived charcoal.

Although it has been found to be problematic when applying particle size to distance transported from the burn area, microscopic charcoal provides a good indicator for regional fire history that may also reflect fire that occurred in the local environment (Mooney and Tinner, 2011).

Deposition within Lake Sediments

Charcoal deposition within lakes can provide high-resolution records of local-regional scale burning, due to rapid settling of charcoal particles within lake sediments (Oris et al., 2014). However, when re-constructing short term, high-resolution fire histories caution must be taken. For example, Larsen and MacDonald (1993) discovered that lake characteristics could influence sediment mixing and therefore the resulting deposition pattern of charcoal observed within them. Their results showed that the degree of sediment mixing likely to occur in a small lake is directly related to the depth and surface area of the lake. This was later supported by Whitlock and Millspaugh (1996), within which it is stressed that several assumptions are made during the interpretation of charcoal within lakes, including the source area of the charcoal; timing of the charcoal introduction, and the patterns of its accumulation within the lake. Eight lakes were sampled over five years to analyse the pattern of charcoal accumulation at different areas away from the burn area. Five of the lakes had watersheds within the burn area and three located outside the burn area. Initial sampling revealed that all lakes received charcoal during and shortly after the fire. Much of the material was also blown offshore to the littoral zone. Furthermore, their results showed that within subsequent years, deeper lakes exhibited higher charcoal abundances. This was deemed to be a result of re-suspension and re-deposition of littoral and sub-littoral charcoal as well as charcoal that had been subsequently washed down from nearby burned slopes.

Up to four years after the initial burn, deep-water lakes within the burn area exhibited a higher percentage of charcoal abundance in comparison to the lakes located in the unburned sites. Whitlock and Millspaugh (1996) therefore

suggest that there may be a lag of up to a few years between the occurrence of a fire and the resulting charcoal accumulation in lakes. This suggestion has since been confirmed by a similar study by Whitlock et al. (1997) who also indicated that lakes in burned and unburned watersheds initially received charcoal from fall-out and that after the fifth year the burned watersheds illustrated an increased accumulation of charcoal in deep water in comparison to those in the unburned region.

Deposition within Marine Sediments

Prior to reaching the marine environment, fluxes of charcoal are transported via fluvial or atmospheric mechanisms (Griffin and Goldberg, 1975; Forbes et. al., 2006), enabling the charcoal found to provide both regional and global information on biomass burning and changes in wildfire activity (Suman et al., 1997).

Rivers are estimated to be able to transport up to 12.2Tg of black carbon per year to the ocean, most of which “disperses and settles as river plumes depart continental shelves” (Masiello and Druffel, 1998, p. 1912) (see also Suman et al., 1997). These water depths are usually less than 200m (Suman et al., 1997), and as Masiello and Druffel (1998) indicate, many studies have found evidence suggesting that river-borne soil does not reach deeper, more remote ocean sediments (e.g. Hedges and Mann, 1979).

Within a shallow marine setting, if the area lies next to an uplifted continental region with a drainage pattern of rivers, rivers feed the coast and shallow marine system dominating shallow marine sedimentation with terrigenous sediments (Nichols, 2000; Forbes et al., 2006). The highest concentration of sediment is found at the mouth of major rivers as well as the adjacent coastal regions due to longshore transport (Nichols, 2000). Deeper marine settings can also be influenced by riverine-like deposition through the development of submarine fans. At the edge of continental shelves where there is a natural “break between shallow and deep marine environments” (Nichols, 2000, p. 194) or a fault induced break, canyons form, altering a gently sloping sea floor to a steep escarpment. Submarine canyons commonly form, localizing the flow of water down the escarpment and creating a series of points for which the flow spreads out (Figure A7). Submarine fan sediments are commonly dominated by

turbidity flows, indicating periods of rapid mass flow down the feeder canyon from the shelf (Nichols, 2000).

The amount of charcoal reaching continental margins can vary due to the concentration and flux being delivered to the area, for example, changes in climate (e.g. increased rainfall and runoff or increased frequency of storms, could increase the amount of sediment reaching rivers and being transported to the marine environment (Swenson et al., 2005), tectonics (e.g. regional uplift and changes in the sediment supply), and biological and physical mixing (Mitra et al., 2014). An example of this can be seen in studies on the deposition of black carbon within the deep ocean which indicate that the black carbon incorporated within deep ocean sediments is ancient and can be up to 2,000 to 5,500 years older than the C_{org} in the same sediments (Boyd, 2014). This is due to some fragments remaining trapped in 'intermediate reservoir pools' such as oceanic dissolved C_{org} and/or terrestrial soils before run-off and erosion eventually transport the sediment to the marine environment (Masiello and Druffel, 1998; Boyd, 2014).

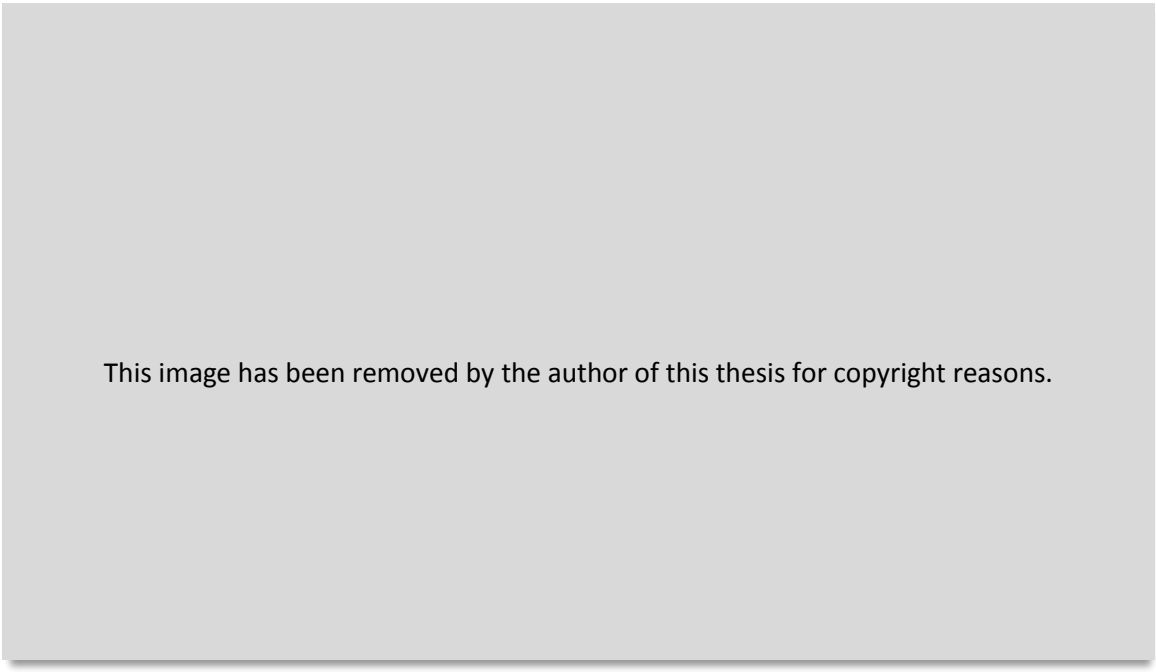

Figure A7 - Diagram illustrating a continental margin with a submarine canyon and submarine fan. (Taken from: http://kids.britannica.com/comptons/art-126157/A-submarine-canyon-is-a-deep-narrow-underwater-valley-cut).

Charcoal transported via atmospheric mechanisms however, such as by the wind, are deposited within the marine environment almost instantly. The deep

ocean receives larger amounts of microscopic charcoal, transported by air currents compared to that transported by run-off and erosion (Forbes et al., 2006), with an estimated 6.9Tg per year travelling via the wind to the surface ocean (Suman et al., 1997). ~52 - 99% of black carbon reaching the deep ocean is <10 μm, and is in the form of aerosol black carbon (Clark et al., 2006; Suman et al., 1997), therefore the size fraction of charcoal studied is commonly <100 μm (Paterson et al., 1987).

Studies on charcoal deposition within deep-sea settings, commonly identify regional-global histories of wildfire activity within deep-sea cores, over hundreds to thousands of years (e.g. Smith et al., 1973; Herring, 1985; Verardo and Ruddiman, 1996; Daniau et al., 2013), making them the perfect setting for analysing changes in biomass burning across medium and long-term timescales such as glacial-interglacial cycles (e.g. Verardo and Ruddiman, 1996; Daniau et al., 2013). In contrast, charcoal deposited to the shallow marine environment (e.g. Nichols and Jones, 1992; Falcon-Lang, 1998; Rimmer, 2015) preserves larger size fractions of charcoal (>500μm) and thus can also record variations in local-regional scale burning. Here, charcoal transported by both wind and water can provide information of terrestrial burning where little/no terrestrial records exist (e.g. Rimmer et al., 2015). One example of this can be found in Rimmer et al. (2015) whereby the study conducted on charcoal deposited within a shallow marine setting in Kentucky, enabled the identification of biomass burning during the Frasnian (Devonian) which prior to this identification was expressed as being a ‘charcoal gap’ (Scott and Glasspool, 2006). Rimmer et al. (2015, p. 6) therefore suggests that shallow marine settings, such as those recorded in black shale strata, may provide a “more continuous record of fire than is possible in many terrestrial systems”, and a more detailed record over shorter timespans compared with the deep ocean.

Summary

Literature suggests that may be a strong relationship between the distances travelled by charcoal from its source/burn area, and the size of the charcoal particle (e.g. Patterson et al., 1987, Clark, 1988, 1990). It was initially suggested that macroscopic charcoal (sizes larger than approximately 100 μm) would only

travel up to one kilometre away from the source area (Clark 1990). Microscopic particles (commonly defined as anything below 100 µm) can be transported by the wind up to hundreds of thousands of kilometres away (Clark, 1988) and were therefore deemed as illustrating a regional fire history within lacustrine environments (Patterson et al., 1987, Clark, 1988, 1990). Subsequent literature, (e.g. MacDonald et al., 1991, Clark and Royal, 1996) found that microscopic charcoal could be responding to both local and regional fire signals, and thus may not determine a regional signal alone. However they did conclude that there was a correlation between macroscopic particles (of sizes 40,000 µm) and local fires. It is therefore argued that sediments comprising of both macroscopic and microscopic charcoals can represent a local fire event, and that when studying microscopic size fractions, both regional and local fire signals can be captured (Innnes and Simmons, 2000; Belcher et al., 2005).

Within the shallow marine environment, charcoal is commonly transported and deposited on continental shelves via riverine transportation. Within the deeper ocean, microscopic charcoal accumulates within ocean sediments, transported from the original burn area by the wind. These particles are therefore commonly <10µm in size (Clark et al., 2006; Suman et al., 1997). The shallow marine record of charcoal provides an important repository for wildfire history for local and regional signals, and provides information on terrestrial burning where little/no terrestrial records exist, whilst charcoal deposited in lake sediments provides charcoal records over shorter timescales.

Appendix B. Materials and Methods

Introduction

The processing methods used for each of the sections studied in this thesis are identical, and thus will be discussed within this chapter. The field methods for sample collection across the initiation of OAE-2 and across Milankovitch cycles within the Mochas core are discussed within their relevant chapters (e.g. study sites and stratigraphy for OAE 2 will be outlined in Chapter 5, and the Mochras Milankovitch sample collection is detailed in Chapter 7). The field methods used for the collection of samples across the T-OAE from Peniche, Portugal and from the Mochras core is detailed below.

Field Methods

At the Peniche locality, samples were hammered/chiseled out of an exposed cliff face section, collecting ~40g+ of bulk rock sample, and placed into labeled plastic bags. Eleven of the Peniche samples used were kindly provided by S.Hesselbo. S.J. Baker collected the remaining 32 samples in May 2014 with the assistance of L.V. Duarte. The Mochras OAE samples were collected by S.J.Baker in July 2014 from the core, currently stored at the British Geological Society core store in Keyworth, Nottingham.

Laboratory Methods

Preparation and Demineralization of bulk rock samples

Prior to the analysis of charcoal, bulk sediment samples commonly go through a chemical and physical processing technique, similar to palynological techniques (Conedera et al., 2009). Early charcoal studies originated from studies focusing on pollen analysis within which charcoal fragments existed, and can be dated back to the work of Iversen in 1941 (Patterson et al. 1987; Whitlock and Larsen, 2001; Conedera et al., 2009). Pollen slide analysis is regularly used throughout the literature (e.g. Durne and McVeen, 1959; Tsukada and Deevey, 1967; Swain, 1973; Tinner et al., 1998 and Carcaillet et al., 2001) and is thought to be

the most popular method for charcoal identification (Rhodes, 1995; Carcaillet et al., 2001). This method is taken from Moore et al. (1991), and the same method used in this thesis.

The process involves the demineralization of the sample in order to reveal the more resistant organic fragments (including charcoal). 20g of each rock sample was immersed in hydrochloric acid (HCL) (10% concentration at room temperature) for ~24hours until any obvious reactions cease. This process removes any carbonates present. The sample is then topped up with water, and left for another 24 hours. This was found to make the samples easier to decante, as well as aiding in neutralising the HCl acid, before hydrofluoric (HF) acid is added, resulting in less calcium fluoride precipitates. The samples are then treated with HF (30-40% concentration at room temperature). To enable efficient mixing of the samples, samples were placed onto a biological shaker, which swills the samples continuously. Samples were left supervised on the shaker for 1 hour, before being removed and left for 72 hours (Figure B1). This process removes silicates from the rock samples. The samples were then topped up with water and left to settle. Once settled, the samples were carefully decanted into a waste bottle, before a second treatment of HCl. The addition of the HCl acid at this stage removes any calcium fluoride precipitates present. The samples were then again topped up with water, and left to settle before the rinsing process begins. The rinsing process involves continuous decanting and topping up with stilled water until a neutral pH is reached.

The process of de-mineralising took a minimum of 2 weeks of lab work to process 6 samples. The shorter time duration of 2 weeks for processing was achieved through the quick settling and neutralisation of certain samples, where 2 rinses with distilled water could be conducted twice a day, and only 8 rinses were required to obtain a neutral pH. Other samples required two treatments of HF, extending de-mineralising time, whilst other samples did not settle during the rinsing stages. This meant that some had to be sieved in the fume hood, using a 10μm mesh, before further rinses could be conducted. The sieving of one sample in the fume hood took on average, one hour to complete, due to the slow movement of the sample through the mesh. In total approximately 34 weeks were spent de-mineralising the samples, ready for charcoal analysis.

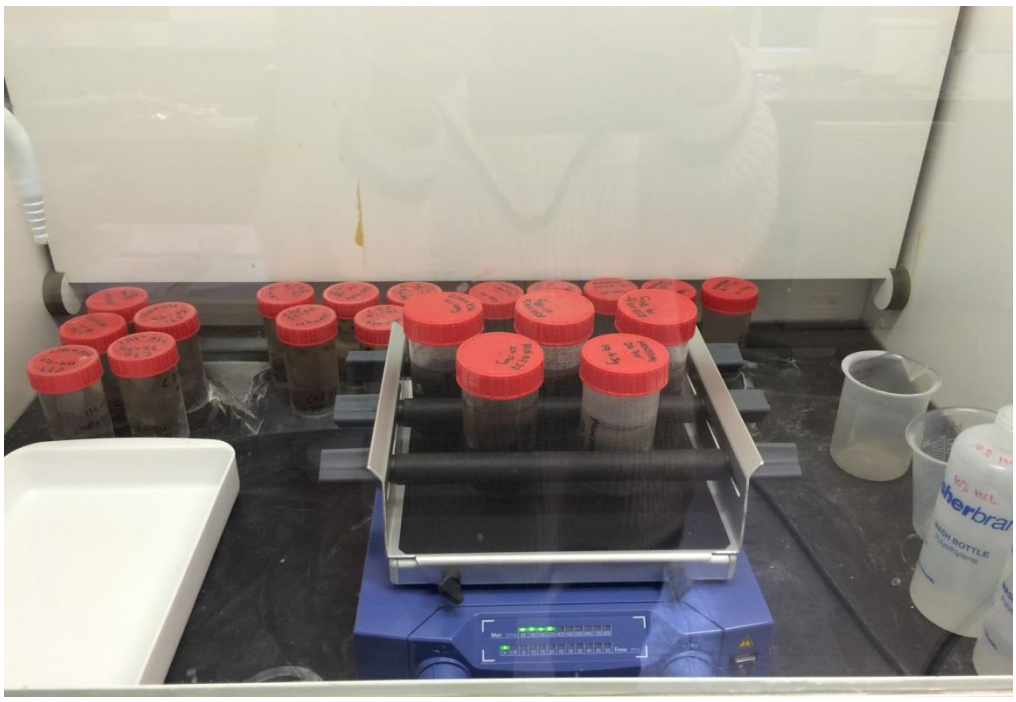

Figure B1 – Photograph taken of some of the Mochras T-OAE samples mixing with HF on the biological shaker within the fume hood.

Each sample was then carefully sieved using a 125µm mesh separating the organics into two size fractions: larger than 125µm, and less than 125µm. This method has been frequently used in the reconstruction of fire histories (Whitlock and Larson, 2001) (e.g. MacDonald et al., 1991; Millspaugh and Whitlock, 1995; Tinner et al., 1998, Thevenon et al., 2003). The remaining organics from each size fraction were then placed into separate labelled pots, dispersed in deionised water.

Quantification of Macro and Micro Fossil Charcoal

Macro-fossil charcoal

The identification of the >125µm fraction of charcoal was conducted using a Zeiss low power binocular light microscope, with the ability for dark field illumination. Each sample was carefully tipped into a gridded petri dish, with 1cm^2 grid squares, ensuring that particles were floating, not overlapping and that the grid squares could be easily identified (Figure B2). If a sample was particularly abundant in organics, a smaller proportion of the sample was used to reduce the risk of particles being counted more than once. Particle counts of

microsfossil charcoal were conducted following the procedures of Tinner and Hu (2003), where the total number of charcoal particles within the sample was recorded. The counted material was then carefully transferred into a new pot and the process repeated until the entire sample had been counted. Counting charcoal from different size fractions in a known quantity of sediment is a common method for analysing periods of fire events (e.g. Millspaugh and Whitlock, 1995) (Whitlock and Larsen, 2001). This method has been described as being fast and inexpensive when compared to other methods such as image analysis (Whitlock and Larsen, 2001). Results from the charcoal counts are expressed by gram of weight.

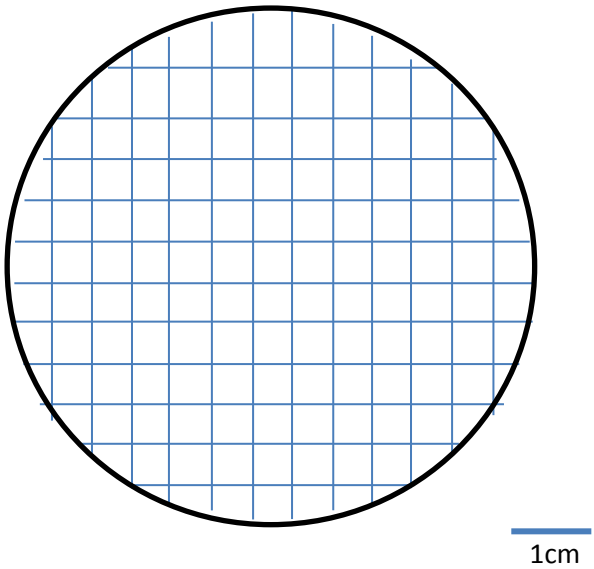

Figure B2 – Diagram of the gridded petri dish used for the quantification of charcoal.

Charcoal fragments were identified using key features described throughout the literature. These include being opaque, occasionally cuboid or angular in shape, deep black/greyish black or dark grey colour in contrast to brownish hues of vegetal matter (Patterson et al., 1987; Sander and Gee, 1990, Jones and Chaloner, 1991; Rhodes, 1998; Scott, 2010).

As the process of charcoalification causes homogenisation of layers within the cell wall (Scott, 2000) visible only under an SEM, a range of particles from two separate sections (one Jurassic and one Cretaceous) were selected at random, and analysed uncoated using Joel JSM 6390 LV SEM. The particles were carefully picked using a fine paintbrush, photographed under the light

microscope and placed onto SEM stubs to be analysed (Figure B3, B4). This confirmed their identity as charcoal.

Micro-fossil charcoal identification

The identification of the smaller <125 μm fraction of charcoal was conducted using a biological transmitted light microscope. Quantification of the <125 μm fraction was conducted by evenly dispersing all of the <125 μm organic particles in a known volume of water. To ensure that the same volume of water was in each sample, the samples were dried in a drying oven set at 22°C for 48 hours, until all of the water had been evaporated. A volume of 33.38 cm^3 of water was then added to each sample, and gently swilled until the particles were evenly dispersed. A known volume was then pipetted (using a clean pipette for each sample) and carefully placed onto the centre of a slide. A small wedge of glycerine jelly is then gently dropped into the centre of the sample drop. The slide was then placed onto a hot plate where it is left with half of the slide off, until the glycerine jelly has melted (taking care not to boil). The slide was then removed and using a clean teasing probe/instrument, the sample on the slide is mixed thoroughly.

Once mixed the slide was placed back onto the hot plate for a few seconds to re-heat the jelly, ready for the cover slip to be applied. The slide was then removed from the hot plate and a cover slip carefully applied. The slide can be placed back onto the hot plate to get the glycerine to spread out under the cover slip. The cover slip was then sealed with nail varnish around the edges.

Two transects of each slide were quantified for charcoal, and recorded and converted to particles per gram. This was calculated through knowing the area of one transect; the total slide area and volume, and the total sample volume (e.g. Belcher, 2005). This procedure has been successfully used in Belcher (2005) and De Vernal et al. (2010).

Palynofacies Preparation

Once each size fraction had been quantified for charcoal, the samples were re-mixed combining both the <125 µm and the >125 µm fractions. The samples then underwent the same procedure as that conducted for quantifying the <125µm charcoal pieces and dispersing the organic particles in a known quantity of water. Once well dispersed, a known volume was pipetted and made into palynofacies slides.

The same technique was also used in quantifying the ratio of vegetal matter to charcoal in each sample, where two transects of each slide were counted. Notes were taken of the number of pollen and spores; plant cuticular material, non-charred coalified plant remains, woody particles and amorphous organic matter (AOM), before being scaled up to the known quantity of sample.

Two transects were quantified as opposed to adding a *lycopodium* spore tablet as it has been noted that depending on the viscosity of the glycerine jelly during mounting, some palynomorphs can be distributed selectively on the slide with larger organics culminating at the edge or centre of the cover slip (De Vernal et al., 2010). Therefore to avoid bias, two transects are randomly selected and quantified on each slide. This method allows the analysis of the amount of organic material in each sample, without the influence of precipitate and/or pyrite minerals that may alter the measured weight of the remaining organics.

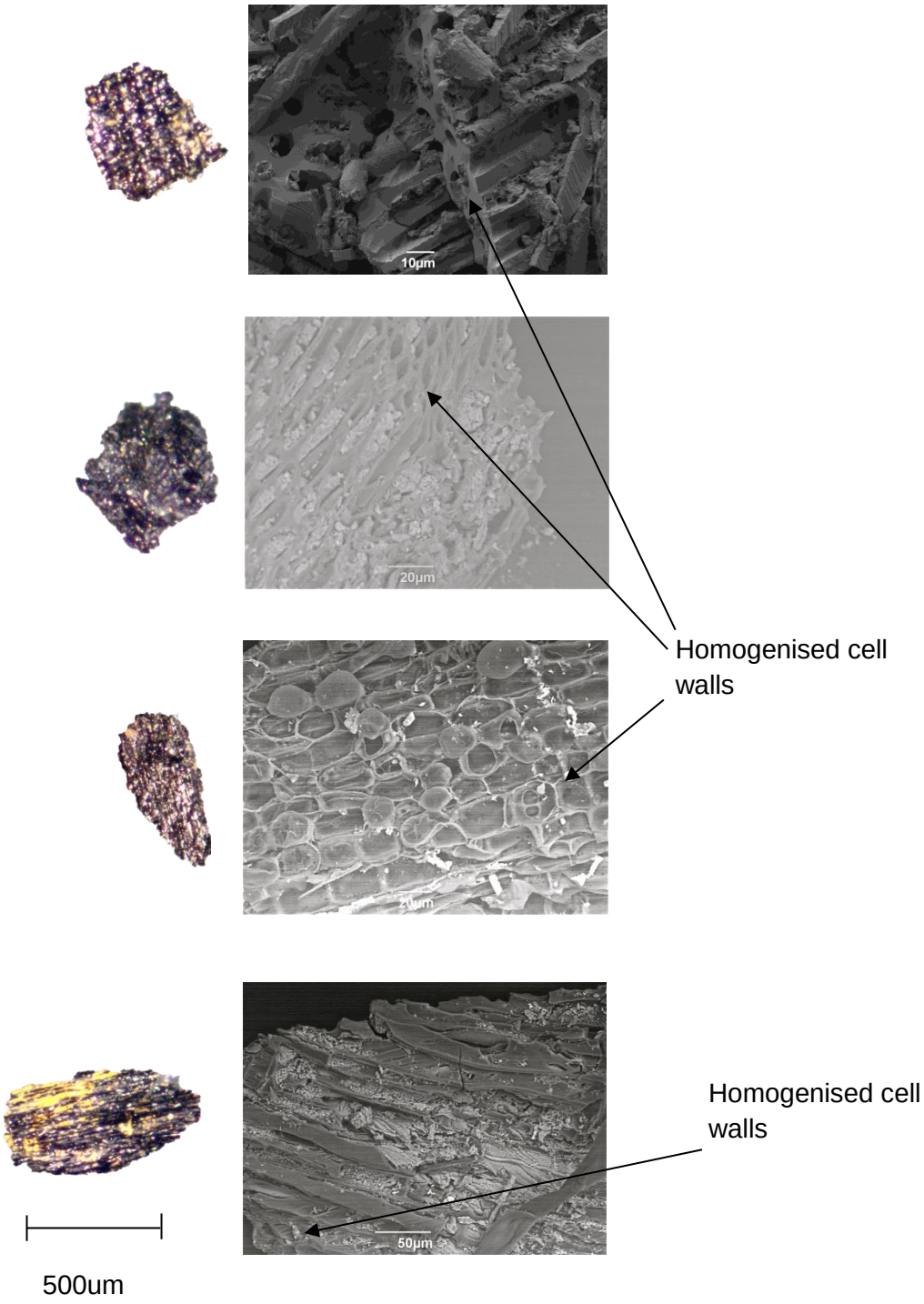

Figure B3 Cretaceous **c**harcoal images taken using a Zeiss binocular light microscope at 5 x magnification. SEM images were taken using a Joel JSM 6390 LV.

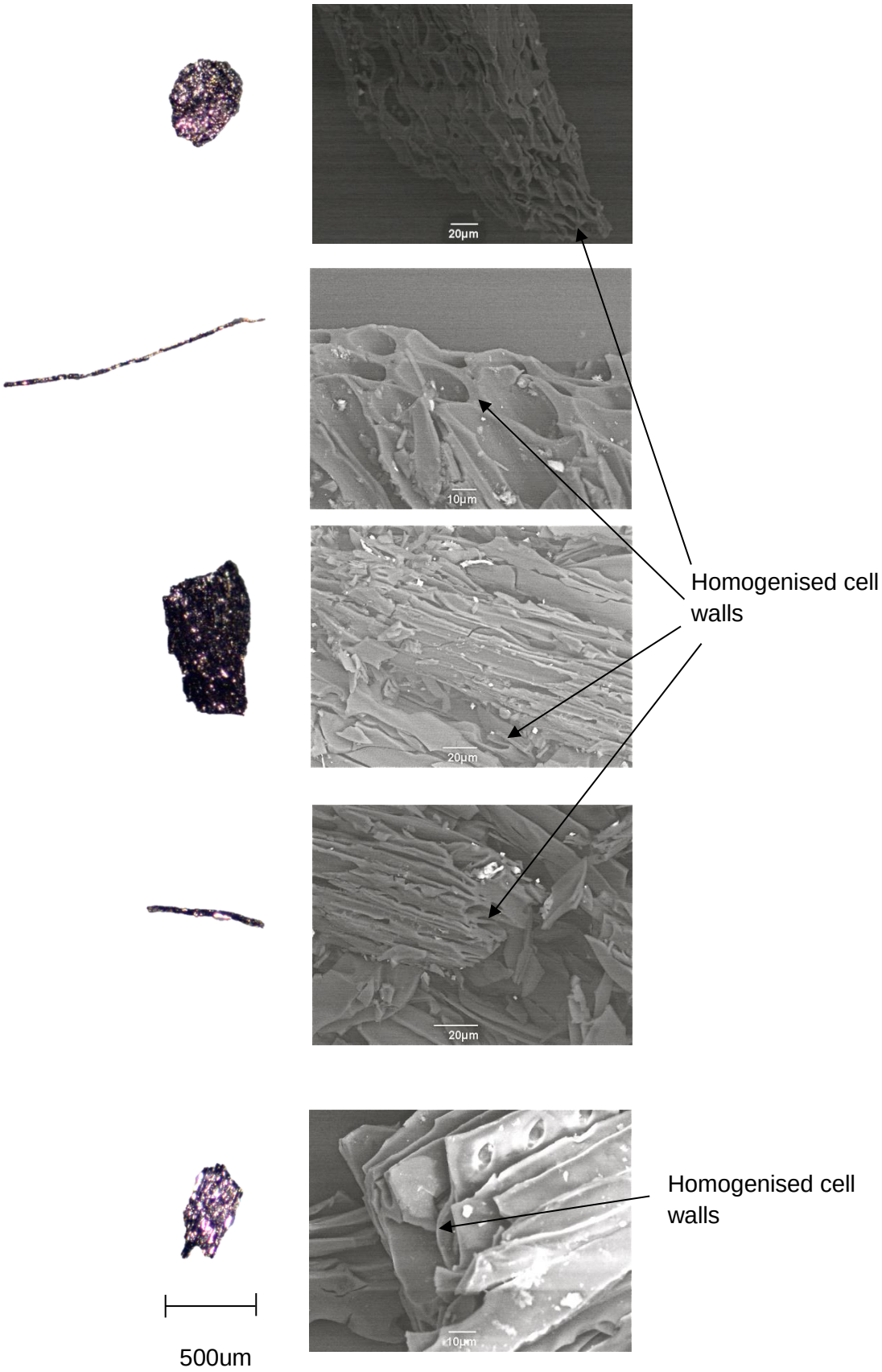

Figure B4 Jurassic **c**harcoal images taken using a Zeiss binocular light microscope at 5 x magnification. SEM images were taken using a Joel JSM 6390 LV.

Appendix C. T-OAE study sites and stratigraphy

Selection of study sites

Sediments deposited during the T-OAE can be largely found within European sections (Figure C1). Some of the well-known sections include Peniche, Portugal; Bornholm, Denmark; Mochras, Wales; Yorkshire, UK; Dotternhausen, SW Germany and the Marche-Umbria, Italy (van de Schootbrugge et al., 2005; Hesselbo et al., 2007).

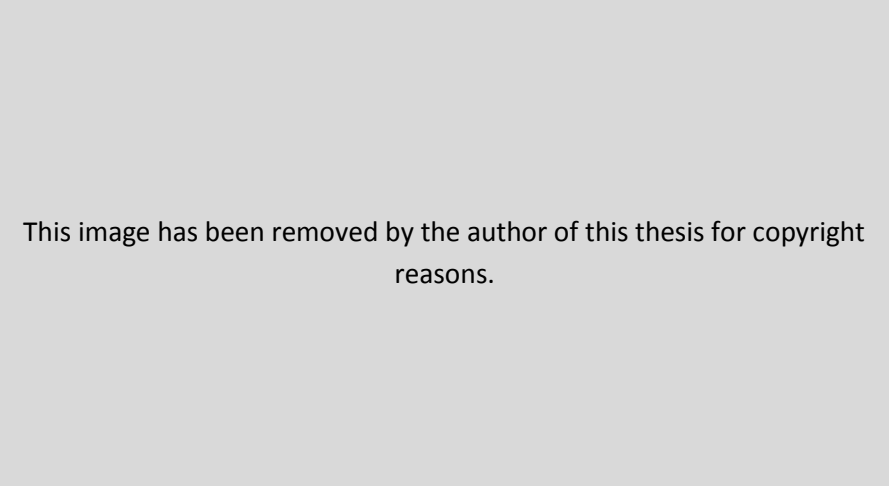

Figure C1- global distribution of black shales associated with the Toarcian OAE (taken from Jenkyns et al., 2001).

The T-OAE sediments exposed within the European sections were deposited ~30°N palaeo-latitude within the Laurasian Seaway, Tethys region during the Early Jurassic (Hesselbo et al., 2007). During the Early Jurassic, the Laurasian seaway was characterised by small islands surrounded by broad, shallow epi-continental seas (Hesselbo et al., 2007). Due to the continued subduction of the seafloor, much of the ocean sediments deposited prior to the Middle Jurassic (~165 Ma) have disappeared, leaving only sediments deposited within shallow marine palaeo-settings that were surrounded by shallow epi-continental seas to expose the Early Jurassic T-OAE (Meyers, 2014). Coupled with an extensive

array of published literature (e.g. Jenkyns and Clayton, 1986; van de Schootbrugge et al., 2005; McElwain et al., 2005; Hesselbo et al., 2007; Mattioli et al., 2009; Percival et al., 2016 and many more), the T-OAE sediments preserved within the European sections provide a good selection of locations for the study of wildfire activity across the T-OAE, from which the two study locations of Peniche and Mochras were chosen (Figure C2).

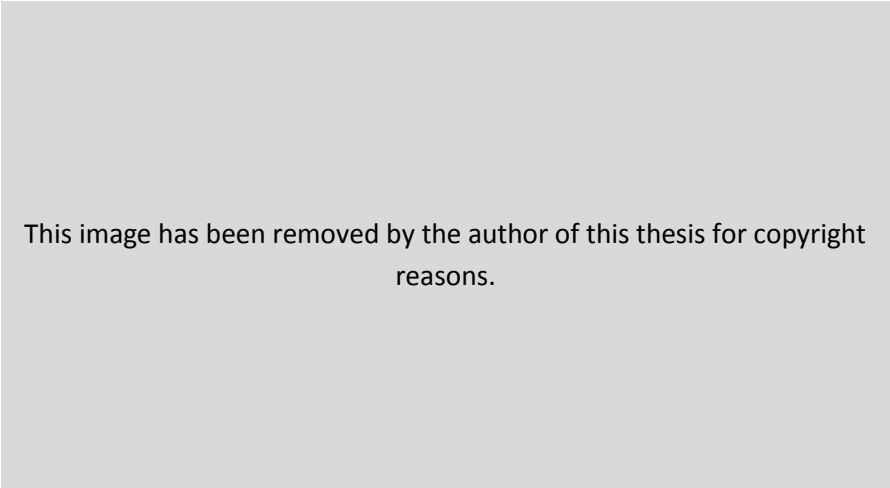

Figure C2 - Early Jurassic palaeo-map of the sample localities (edited from Hesselbo et al., 2007, and published in Baker et al., 2017). **A** – Peniche location, **B** – Mochras location.

Peniche, Portugal

Peniche outcrops provide a near continuous record of hemi-pelagic sediments deposited during the Early Pliensbachian through to the Middle Toarcian (Elmi, 2006; Suan et al., 2008). The section is well dated due to the presence of an extensive ammonite biostratigraphy (as expressed by Rocha et al., 1996; Reolid and Duarte, 2013), and has recently been established as a GSSP (Global Boundary Stratotype Section) due to its exceptional exposure of the Pliensbachian-Toarcian (P-T) boundary (Barrón et al., 2013). The site benefits from high resolution carbonate and wood carbon isotope profiles throughout the section as well as a cyclostratigraphic timescale (e.g. Suan et al., 2008; Huang and Hesselbo, 2014).

Location of Site and Exposure

The Pliensbachian-Toarcian sediments of the Cabo Carvoeiro and Lemede Formations (and the samples collected for this thesis) can be found exposed within the coastal cliffs and foreshore around Vista da Ponta do Torrão and Praia do Abalo area, situated ~95km north of Lisbon, Western Portugal (Elmi, 2007; Hesselbo et al., 2007) (Figure C3).

Figure C3 - Satellite image illustrating the field location of Ponta do Trovão, Peniche, Portugal (Courtesy of Google Earth).

Depositional Setting

The Early Jurassic sediments of Peniche were deposited on a north-west-facing carbonate ramp within the extensional Lusitanian Basin (Duarte, 2007; Hesselbo et al., 2007; Suan et al., 2008; Duarte et al., 2010; Pittet et al., 2014) (Figure C4). The deepest settings (suggested as being no more than 200 m deep (Bjerrum et al., 2001)) of the ramp were located on the north-western side

of the basin, bounded by a “steep, granitic-migmatitic structural high (the Berlenga-Farilhões horst), surrounded by a shallow carbonate platform” (Figure C4) (Pittet et al., 2014, p. 3).

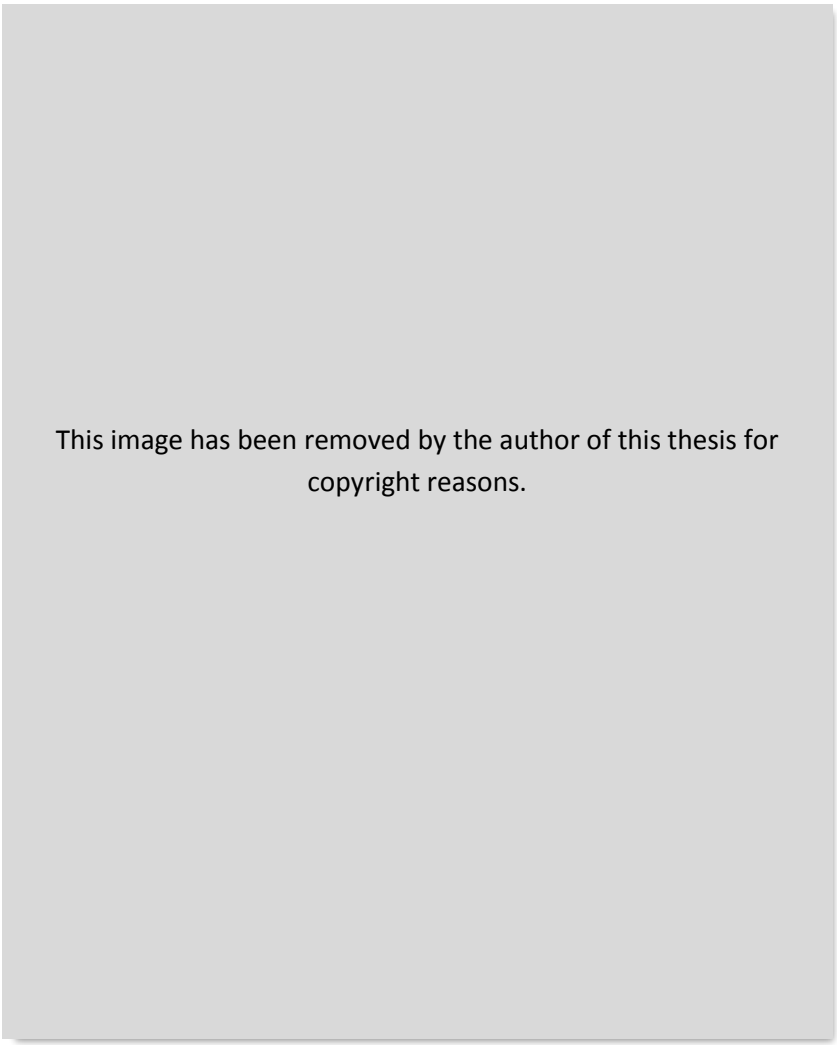

Figure C4 – Diagram illustrating the depositional setting for the Lusitanian Basin. (Taken from Pittet et al., 2014). Red circles indicate the Peniche study site location.

The Lower Jurassic record is dominated by regular hemi-pelagic marl-limestone alternations (Duarte, 2007; Hesselbo et al., 2007; Hermoso et al., 2009) (see Figure C5 for stratigraphic log). Towards the top of the *polymorphum* zone and throughout the *levisoni* zone, the sediments become more argillaceous, with the presence of turbidite beds with a sandy-silty matrix (Suan et al., 2008; Hermoso et al., 2009). The occurrence of a more argillaceous lithology has been interpreted as being due to large changes in sea level; tectonic activity and/or

hydrological cycling that pre-date the T-OAE, although the casual mechanism is poorly constrained (Pittet et al., 2014).

Variations in sea level could have a profound impact on sediment supply to the site, particularly in near-shore areas with a shallow gradient. However, as the Peniche study site is located within the deepest part of the basin, ~50 km (31 miles) away from the shallowest part of the basin, Hesselbo et al. (2007) argue that the high relief horst block would not have become closer/more distal from the area of sediment deposition during relative sea level rise/fall, and therefore the only changes in sediment supply at the site are likely to be due to weathering and erosion on land caused by climatic changes. Furthermore spectral analysis on the Peniche sediments conducted by Suan et al. (2008b) and Huang and Hesselbo (2014) indicate that sedimentation accumulation rates were fairly constant throughout the OAE interval. Samples were therefore collected from this depositional site, at the deepest part of the basin.

Within the Peniche section, the organic matter present is expressed as consisting mostly of terrestrial components, likely originating from the near-by exposed horst block (Duarte, 2007; Hermoso et al., 2009), with little marine C_{org} (<1%), with the exception of an 8cm thick bed within the *levisoni* zone (Hesselbo et al., 2007; Hermoso et al., 2009).

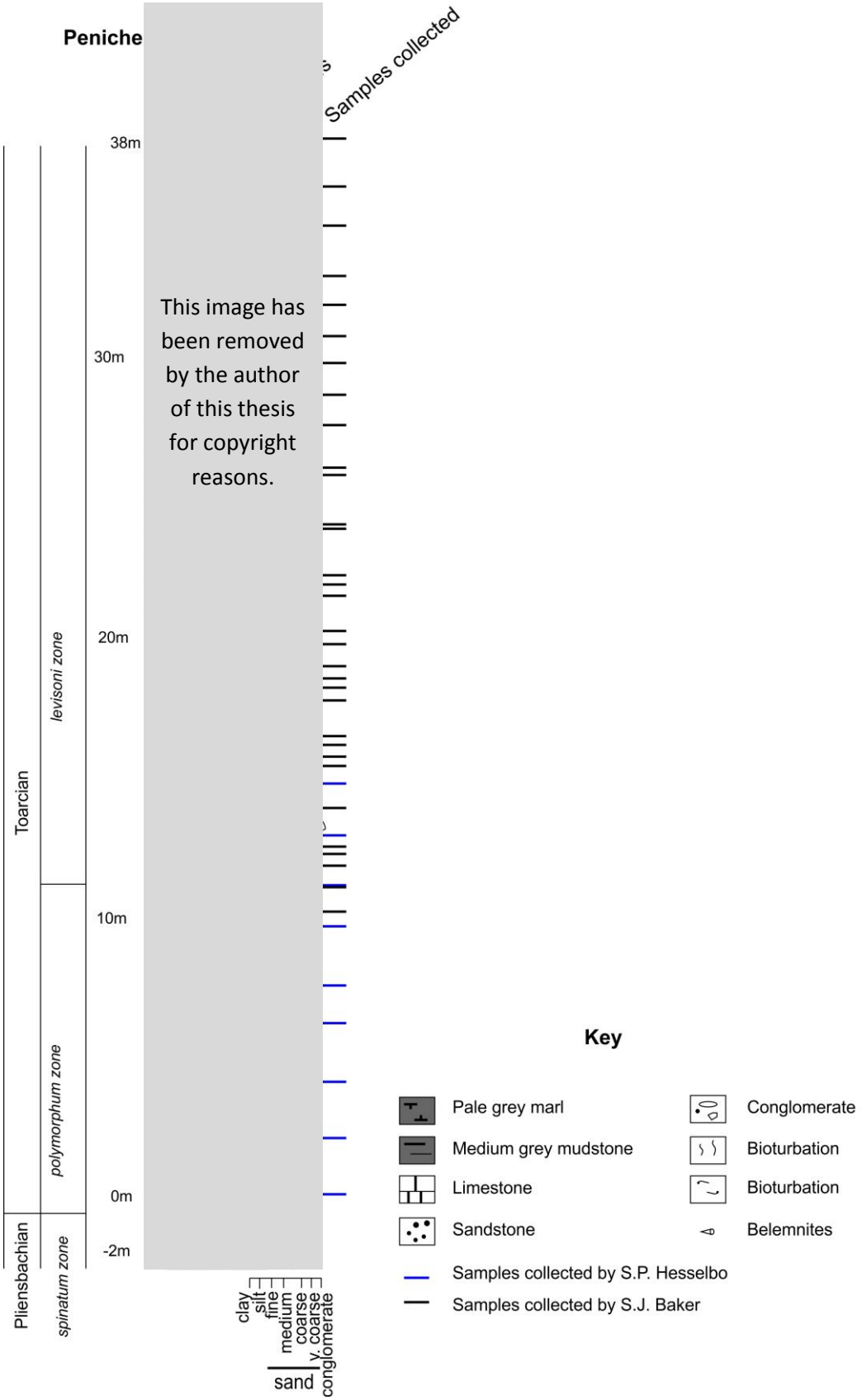

Figure C5 – Sedimentary log of the Peniche section across the T-OAE, illustrating where samples were collected from for this thesis. (Log modified from Hesselbo et al., 2007).

Palaeo-vegetation

A study conducted by Barrón et al. (2013) indicates that the past vegetation in Peniche consisted predominantly of conifers. Pollen species such as *Spheripollenites, Classopollis, Inaperturopollenites, Cerebropollenites, Arauconiacites, Alisporites,* and *Perincpollenites* were all found within the Pliensbachian-Toarcian sediments, along with one species of fern pollen, *Cycadophyta* (Barrón et al., 2013). The relative abundances of these species throughout the Upper Pliensbachian and into the Early Toarcian can be seen in Figure C6. The pollen grain *Spheripollenites* sp. part of the *Cheirolepidiaceae* conifer family (Wade-Murphy et al., 2006) is characteristic of seasonally dry, warm periods and can therefore also be used to indicate a change in climate from a cooler climate to a warmer climate where there is a dominance of this conifer species (Wade-Murphy et al., 2006).

Figure C6 – Diagram illustrating the abundance of pollen grains alongside vascular cryptograms and aquatic palynomorphs throughout the Upper Pliensbachian and into the Early Toarcian, in Peniche, Portugal. Modified from Barrón et al. (2013).

Field Collection of Samples

Collection of sediments from below, during and after the Toarcian-OAE were recorded and collected (Figure C5). At the Peniche locality, bulk rock samples were hammered/chiselled out of exposed sections, collecting approximately 20 g rock and placed into labelled plastic bags. Samples were carefully chosen from marl units, and where possible at 20 cm intervals, to ensure high resolution sampling. Identification of the anoxic event within the rock strata was based

upon published data and where required revised field data (e.g. re-construction of sedimentary logs to ensure accuracy). 11 of the Peniche samples were kindly provided by S.P.Hesselbo. The remaining samples were collected by S.J. Baker (May 2014) kindly assisted by L.V. Duarte.

The Mochras Farm (Llanbedr) Borehole, Wales

Location of the Site and Exposure

The Mochras Farm (Llanbedr) borehole was drilled between 1967 and 1969 on the West coast of Wales (Hesselbo et al., 2013) (Figure C7). The sediments retrieved constitute Early Jurassic sediments dating from the Late Sinemurian through to the Late Toarcian, providing a biostratigraphically complete section of nearly all of the Lower Jurassic, constituting marine mudstones (Ruhl et al., 2016) and providing "the thickest Lower Jurassic succession yet encountered in the British Isles" (Simms, 2004, p. 19). The core itself is ~1300m thick and was taken between 600-1900m below the surface (Hesselbo et al., 2013). This borehole provides a stratigraphically more complete section of the Early Jurassic than the equivalent section exposed in Yorkshire (Hesselbo et al., 2013; Ruhl et al., 2016), allowing for high-resolution sampling. Access to the borehole for sample collection was kindly provided by the British Geological Survey Keyworth core store in Nottingham during the summer of 2014.

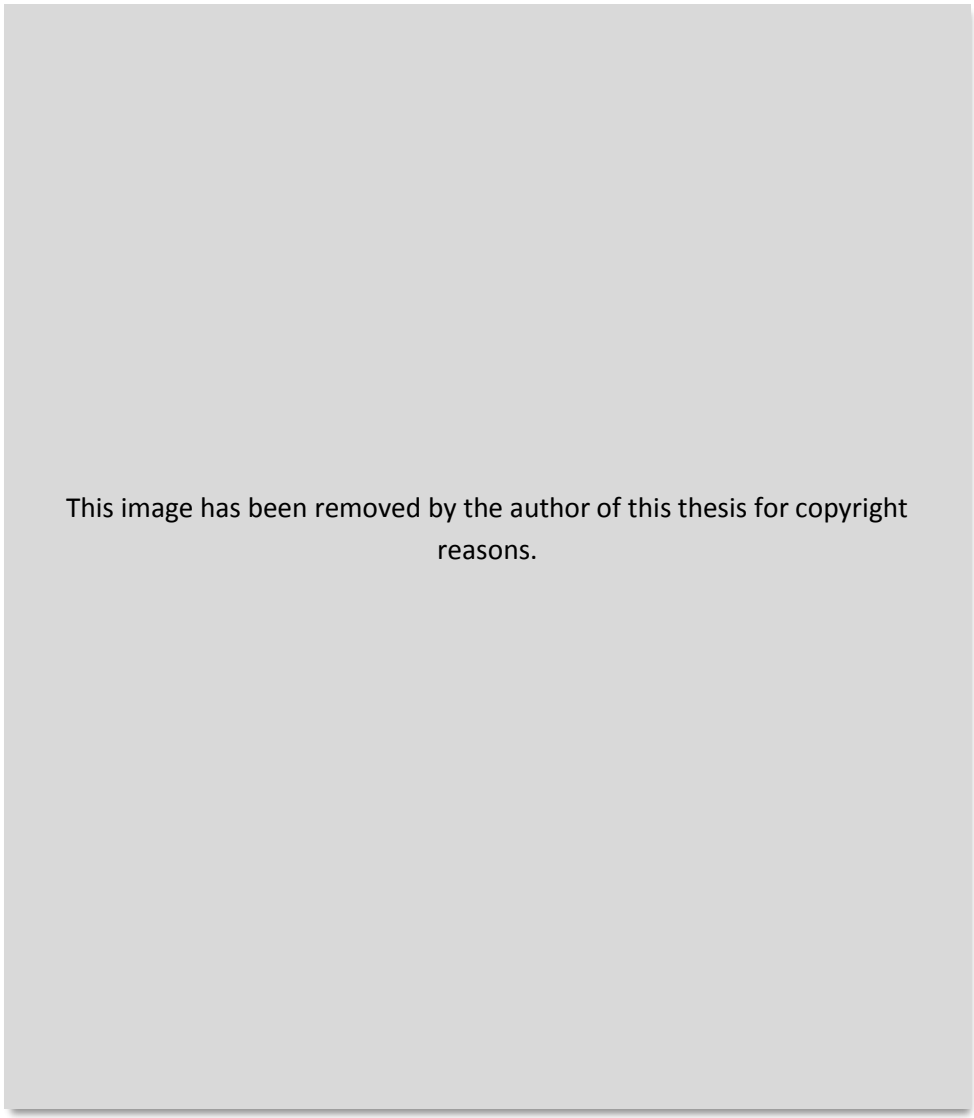

Figure C7- Geological map illustrating the location of the Mochras borehole within the Cardigan Basin, west coast of Wales. Taken from Hesselbo et al. (2013).

Depositional Setting

The Early Jurassic sediments found within the Mochras borehole can be found deposited on the edge of Cardigan Bay in North Wales (Hesselbo et al., 2013). Within the Mochras section, sedimentation rates are hypothesized to have been able to keep up with basin subsidence rates up until the Toarcian whereby a rapid transgressive period coincides with a period of slow sedimentation, and the generation of a deeper marine environment (Dobson and Whittington, 1987). The depositional environment is interpreted as being that of basinal marine which became deeper during the initiation of the OAE, continuing throughout the OAE and beyond the section studied (Muller, 1990). The site is

anticipated to have been influenced by nearby terrigenous sources around the Cardigan Bay area, apparent throughout the Early Jurassic section due to the presence of “large quantities of carbonaceous (mostly plant) material” (Dobson and Whittington, 1987, p. 343).

Palaeo-vegetation

The Jurassic palaeo-vegetation is often referred to as illustrating a diverse fossil flora, where at Red Cliff in Yorkshire, over 90 different species have been identified (Ingrouille, 1995). The palaeo-vegetation and pollen analysis for the Jurassic period in the Mochras Core section, is currently still being undertaken (Hesselbo et al., 2013, p. 87), however floral analysis of the Yorkshire section has already been well documented (e.g. Harris, 1961; Harris, 1980; Riding, 1984, Tidwell and Ash, 1994).

Throughout the Early to Middle Jurassic, the Yorkshire Ravenscar (Blea Wyke) section, gymnosperm pollen is documented as the dominant palynomorph group (Riding, 1984). This includes *Alisporites, Cerebropollenites mesozoicus, Perinopollenites elatoides, Callialasporites spp, Classopollis classoides* and *Araucariacites australis* (Riding, 1984). Spore presence is suggested to be indicative of European microfloras including, *Cyathidites australis, Duplexisporites problematicus, Gleicheniidites senonicus, Ischyosporites spp, Leptoledpidites spp., Lycopodiumporites austroclavatidites,* and *L. semimuris* (Riding, 1984, p. 112), thus expressing very similar vegetation types to the Peniche section of predominantly ferns and conifers (Vajda et al., 2016).

Collection of Samples

Samples from the Mochras borehole, taken from below, during and after the T-OAE were collected (Figure C8) by S.J.Baker (July 2014) from the BGS core store, Keyworth, Nottingham with the assistance of S.P. Hesselbo., J.B. Riding, W. Xu., M.Ruhl and H.C. Jenkyns.

Figure C8 – Summary stratigraphy and lithology of the Mochras core and illustration of where samples were collected from for this thesis.

Appendix D. Additional Mochras Milankovitch data

Collection of samples across the Milankovitch cycles from the Mochras core is fully described within Chapter 7.

Figure D1 illustrates where within the core, samples were collected from in relation to the Early Jurassic, Pliensbachian.

Figure D1 – Mochras Farm borehole with XRF-derived calcium and titanium record (taken from Ruhl et al., 2016), illustrating core position of samples analysed in this thesis.

Appendix E. Raw Data

PENICHE PALYNOFACIES DATA							
	COUNTS TAKEN ACROSS SLIDE TRANSECT					Total Phytoclasts	
Log height (cm)	Pollen and Spore Count	Charcoal Count (micro)	Amorphous Organic Matter (AOM)	Plant Cuticles and Phytoclasts	Coalified Material	In transect = pollen + spore +charcoal + Plant cut. + coal	Total Phytoclasts for <125µm
37	10	107	141	30	0	147	529×10^5
235	6	36	144	65	0	107	471×10^5
440	3	30	86	21	0	54	205×10^5
643	3	44	91	23	0	70	308×10^5
781	3	51	175	38	0	92	307×10^5
991	2	95	54	35	0	132	422×10^5
1040	1	192	288	33	0	226	905×10^5
1120	1	80	174	61	0	142	625×10^5
1133	47	50	66	41	0	138	608×10^5
1200	1	43	121	61	0	105	294×10^5
1240	2	52	224	21	0	75	330×10^5
1280	3	84	213	68	0	155	682×10^5
1308	6	69	180	97	0	172	688×10^5
1480	1	108	14	144	0	253	1114×10^5
1501	32	61	98	59	0	152	586×10^5
1560	2	65	305	72	0	139	347×10^5
1600	4	147	232	109	0	260	719×10^5
1640	5	83	112	116	0	204	776×10^5

PENICHE PALYNOFACIES DATA							
	COUNTS TAKEN ACROSS SLIDE TRANSECT					Total Phytoclasts	
Log height (cm)	Pollen and Spore Count	Charcoal Count (micro)	Amorphous Organic Matter (AOM)	Plant Cuticles and Phytoclasts	Coalified Material	In transect = pollen + spore +charcoal + Plant cut. + coal	Total Phytoclasts for <125µm
1680	0	65	91	107	0	172	654×10^5
1800	2	64	193	81	3	150	660×10^5
1840	2	79	65	55	0	136	435×10^5
1880	0	22	65	82	6	110	440×10^5
2000	0	35	149	66	0	101	323×10^5
2160	7	15	42	7	0	29	69×10^5
2200	2	50	153	56	2	110	346×10^5
2220	0	38	67	9	0	47	90×10^5
2400	0	111	404	53	0	164	459×10^5
2420	4	91	263	47	0	142	540×10^5
2600	13	69	257	40		122	983×10^5
2620	0	59	82	22	0	81	243×10^5
2780	1	117	291	85	0	203	935×10^5
2880	0	69	424	41		110	216×10^5
3020	4	101	153	24	0	129	361×10^5
3100	1	19	323	20	9	49	166×10^5
3320	5	18	110	18	0	41	98×10^5
3500	1	39	180	20	8	68	272×10^5

PENICHE PALYNOFACIES DATA							
	COUNTS TAKEN ACROSS SLIDE TRANSECT					Total Phytoclasts	
Log height (cm)	**Pollen and Spore Count**	**Charcoal Count (micro)**	**Amorphous Organic Matter (AOM)**	**Plant Cuticles and Phytoclasts**	**Coalified Material**	**In transect = pollen + spore +charcoal + Plant cut. + coal**	**Total Phytoclasts for <125µm**
3640	0	18	291	19	0	37	163×10^5
3820	2	29	61	22	0	53	155×10^5

PENICHE TOTAL CHARCOAL ABUNDANCES					
Log height (cm)	**Total >125µm charcoal abundance in rock processed**	**Total <125µm charcoal Abundance calculated from transects counted**	**Total charcoal (<125µm + >125µm)**	**Total rock (g) processed**	**Total charcoal counted per 10 g of rock ((charcoal total/total rock processed) x 10 g)**
37	117	245×10^3	245353	19.87	123×10^3
235	8	75×10^3	75694	20.10	37×10^3
440	43	135×10^3	135886	19.68	69×10^3
643	46	183×10^3	183973	19.30	95×10^3
781	52	81×10^3	81797	19.83	41×10^3
991	474	507×10^3	507985	19.71	257×10^3
1040	233	747×10^3	747931	20.01	373×10^3
1120	85	66×10^3	66271	20.00	33×10^3
1133	13	74×10^3	74946	20.89	35×10^3
1200	44	66×10^3	66927	20.08	33×10^3
1240	63	66×10^3	66946	20.05	33×10^3
1280	36	241×10^3	241247	20.04	120×10^3
1308	14	163×10^3	163505	20.01	81×10^3
1480	57	274×10^3	275019	19.98	137×10^3
1501	31	120×10^3	120410	20.60	58×10^3
1560	39	133×10^3	133804	20.07	66×10^3
1600	17	136×10^3	136259	20.10	67×10^3
1640	99	393×10^3	393720	19.96	197×10^3
1680	52	142×10^3	142487	20.06	71×10^3

PENICHE TOTAL CHARCOAL ABUNDANCES					
Log height (cm)	**Total >125µm charcoal abundance in rock processed**	**Total <125µm charcoal Abundance calculated from transects counted**	**Total charcoal (<125µm + >125µm)**	**Total rock (g) processed**	**Total charcoal counted per 10 g of rock ((charcoal total/total rock processed) x 10 g)**
1800	36	86×10^3	86736	20.01	43×10^3
1840	63	279×10^3	279360	20.01	139×10^3
1880	4	163×10^3	163495	20.00	81×10^3
1923	0	0	0	19.70	0
2000	52	176×10^3	176548	20.00	88×10^3
2040	235	326×10^3	327217	20.05	163×10^3
2160	293	79×10^3	79561	20.02	39×10^3
2200	188	123×10^3	123735	20.07	61×10^3
2220	262	626×10^3	627252	20.09	312×10^3
2400	310	392×10^3	392366	19.96	196×10^3
2420	71	578×10^3	578866	10.48	552×10^3
2600	1114	294×10^3	296066	13.56	218×10^3
2620	190	1483×10^3	1483870	19.28	769×10^3
2780	205	633×10^3	634009	18.23	347×10^3
2880	308	393×10^3	394240	23.35	168×10^3
3020	108	1192×10^3	1192530	14.55	819×10^3
3100	114	480×10^3	481015	14.42	333×10^3
3220	503	787×10^3	788232	18.05	436×10^3
3320	375	87×10^3	87768	19.98	43×10^3

PENICHE TOTAL CHARCOAL ABUNDANCES					
Log height (cm)	**Total >125µm charcoal abundance in rock processed**	**Total <125µm charcoal Abundance calculated from transects counted**	**Total charcoal (<125µm + >125µm)**	**Total rock (g) processed**	**Total charcoal counted per 10 g of rock ((charcoal total/total rock processed) x 10 g)**
3500	5	25×10^3	25495	21.55	11×10^3
3640	11	63×10^3	63735	19.30	33×10^3
3820	147	291×10^3	291587	18.15	160×10^3

PENICHE <125µm CHARCOAL DATA							
Total <125µm charcoal abundance in 2 slide transects	**Area of slide counted (mm^2)**	**100% of slide area (mm^2)**	**Calculated charcoal for 100% of slide**	**100% slide area is equal to 0.11 (ml)**	**Total volume of sample (cm^3)**	**As 1ml is equal to 1cm3 (total sample volume (cm^3)/0.11 (ml)**	**Total Charcoal for <125µm**
44	19.60	360	808	0.11	33.38	303.45	245×10^3
14	18.13	323	249	0.11	33.38	303.45	75×10^3
25	15.19	272	448	0.11	33.38	303.45	135×10^3
33	17.64	324	606	0.11	33.38	303.45	183×10^3
11	23.52	576	269	0.11	33.38	303.45	81×10^3
84	20.09	400	1672	0.11	33.38	303.45	507×10^3
176	31.50	441	2464	0.11	33.38	303.45	747×10^3
19	23.52	270	218	0.11	33.38	303.45	66×10^3
11	23.52	528	247	0.11	33.38	303.45	74×10^3
9	23.52	576	220	0.11	33.38	303.45	66×10^3
9	23.52	576	220	0.11	33.38	303.45	66×10^3
41	23.52	456	795	0.11	33.38	303.45	241×10^3
22	21.56	528	539	0.11	33.38	303.45	163×10^3
37	18.62	456	906	0.11	33.38	303.45	274×10^3
21	19.11	361	397	0.11	33.38	303.45	120×10^3
18	23.52	576	441	0.11	33.38	303.45	133×10^3
22	19.60	400	449	0.11	33.38	303.45	136×10^3
37	13.72	481	1297	0.11	33.38	303.45	393×10^3
23	19.60	400	469	0.11	33.38	303.45	142×10^3

PENICHE <125µm CHARCOAL DATA							
Total <125µm charcoal abundance in 2 slide transects	**Area of slide counted (mm^2)**	**100% of slide area (mm^2)**	**Calculated charcoal for 100% of slide**	**100% slide area is equal to 0.11 (ml)**	**Total volume of sample (cm^3)**	**As 1ml is equal to 1cm3 (total sample volume (cm^3)/0.11 (ml)**	**Total Charcoal for <125µm**
14	17.64	360	286	0.11	33.38	303.45	86×10^3
41	23.52	528	920	0.11	33.38	303.45	279×10^3
22	23.52	576	539	0.11	33.38	303.45	163×10^3
0	0.00	0	0	0.11	33.38	303.45	0
38	10.78	165	582	0.11	33.38	303.45	176×10^3
44	22.54	552	1078	0.11	33.38	303.45	326×10^3
16	14.70	240	261	0.11	33.38	303.45	79×10^3
21	23.52	456	407	0.11	33.38	303.45	123×10^3
134	13.23	204	2066	0.11	33.38	303.45	626×10^3
102	33.00	418	1292	0.11	33.38	303.45	392×10^3
154	14.21	176	1907	0.11	33.38	303.45	578×10^3
81	30.00	360	972	0.11	33.38	303.45	294×10^3
242	19.60	396	4889	0.11	33.38	303.45	1483×10^3
241	36.00	312	2089	0.11	33.38	303.45	633×10^3
102	33.00	420	1298	0.11	33.38	303.45	393×10^3
156	17.15	432	3930	0.11	33.38	303.45	1192×10^3
225	69.00	486	1585	0.11	33.38	303.45	480×10^3
159	23.52	384	2596	0.11	33.38	303.45	787×10^3
24	16.50	198	288	0.11	33.38	303.45	87×10^3

PENICHE <125µm CHARCOAL DATA							
Total <125µm charcoal abundance in 2 slide transects	**Area of slide counted (mm^2)**	**100% of slide area (mm^2)**	**Calculated charcoal for 100% of slide**	**100% slide area is equal to 0.11 (ml)**	**Total volume of sample (cm^3)**	**As 1ml is equal to 1cm3 (total sample volume (cm^3)/0.11 (ml)**	**Total Charcoal for <125µm**
21	82.50	330	84	0.11	33.38	303.45	25×10^3
15	31.50	441	210	0.11	33.38	303.45	63×10^3
41	22.54	528	960	0.11	33.38	303.45	291×10^3

PENICHE PALYNOFACIES DATA													
	COUNTS TAKEN ACROSS SLIDE TRANSECT					Total Phytoclasts In transect = pollen + spore +charcoal + Plant cut. + coal	Area of slide counted (mm^2)	100% of slide area (mm^2)	Calculated phytoclasts for 100% of slide	100% slide area is equal to 0.11 (ml)	Total volume of sample (cm^3)	Number of 0.11ml in total sample volume (total sample volume (cm^3)/0.11 (ml))	Total Phytoclasts for <125µm
Log height (cm)	Pollen and Spore Count	Charcoal Count (micro)	Amorphous Organic Matter (AOM)	Plant Cuticles and Phytoclasts	Coalified Material								
37	10	107	141	30	0	147	33	396	1764	0.11	3337.94	30041.45	529×10^5
235	6	36	144	65	0	107	33	484	1569	0.11	3337.94	30041.45	471×10^5
440	3	30	86	21	0	54	19.5	247	684	0.11	3337.94	30041.45	205×10^5
643	3	44	91	23	0	70	22.5	330	1027	0.11	3337.94	30041.45	308×10^5
781	3	51	175	38	0	92	21	234	1025	0.11	3337.94	30041.45	307×10^5
991	2	95	54	35	0	132	33	352	1408	0.11	3337.94	30041.45	422×10^5
1040	1	192	288	33	0	226	30	400	3013	0.11	3337.94	30041.45	905×10^5
1120	1	80	174	61	0	142	33	484	2083	0.11	3337.94	30041.45	625×10^5
1133	47	50	66	41	0	138	33	484	2024	0.11	3337.94	30041.45	608×10^5
1200	1	43	121	61	0	105	33	308	980	0.11	3337.94	30041.45	294×10^5
1240	2	52	224	21	0	75	33	484	1100	0.11	3337.94	30041.45	330×10^5
1280	3	84	213	68	0	155	33	484	2273	0.11	3337.94	30041.45	682×10^5
1308	6	69	180	97	0	172	22.5	300	2293	0.11	3337.94	30041.45	688×10^5

PENICHE PALYNOFACIES DATA													
	COUNTS TAKEN ACROSS SLIDE TRANSECT					Total Phytoclasts In transect = pollen + spore +charcoal + Plant cut. + coal	Area of slide counted (mm^2)	100% of slide area (mm^2)	Calculated phytoclasts for 100% of slide	100% slide area is equal to 0.11 (ml)	Total volume of sample (cm^3)	Number of 0.11ml in total sample volume (total sample volume (cm^3)/0.11 (ml))	Total Phytoclasts for <125µm
Log height (cm)	Pollen and Spore Count	Charcoal Count (micro)	Amorphous Organic Matter (AOM)	Plant Cuticles and Phytoclasts	Coalified Material								
1480	1	108	14	144	0	253	33	484	3711	0.11	3337.94	30041.45	1114×10^5
1501	32	61	98	59	0	152	24	308	1951	0.11	3337.94	30041.45	586×10^5
1560	2	65	305	72	0	139	18	150	1158	0.11	3337.94	30041.45	347×10^5
1600	4	147	232	109	0	260	33	304	2395	0.11	3337.94	30041.45	719×10^5
1640	5	83	112	116	0	204	33	418	2584	0.11	3337.94	30041.45	776×10^5
1680	0	65	91	107	0	172	33	418	2179	0.11	3337.94	30041.45	654×10^5
1800	2	64	193	81	3	150	33	484	2200	0.11	3337.94	30041.45	660×10^5
1840	2	79	65	55	0	136	24	256	1451	0.11	3337.94	30041.45	435×10^5
1880	0	22	65	82	6	110	33	440	1467	0.11	3337.94	30041.45	440×10^5
2000	0	35	149	66	0	101	33	352	1077	0.11	3337.94	30041.45	323×10^5
2160	7	15	42	7	0	29	21	168	232	0.11	3337.94	30041.45	69×10^5
2200	2	50	153	56	2	110	27	283	1153	0.11	3337.94	30041.45	346×10^5
2220	0	38	67	9	0	47	24	153	300	0.11	3337.94	30041.45	90×10^5

PENICHE PALYNOFACIES DATA													
	COUNTS TAKEN ACROSS SLIDE TRANSECT					Total Phytoclasts In transect = pollen + spore +charcoal + Plant cut. + coal	Area of slide counted (mm^2)	100% of slide area (mm^2)	Calculated phytoclasts for 100% of slide	100% slide area is equal to 0.11 (ml)	Total volume of sample (cm^3)	Number of 0.11ml in total sample volume (total sample volume (cm^3)/0.11 (ml))	Total Phytoclasts for <125µm
Log height (cm)	Pollen and Spore Count	Charcoal Count (micro)	Amorphous Organic Matter (AOM)	Plant Cuticles and Phytoclasts	Coalified Material								
2400	0	111	404	53	0	164	45	420	1531	0.11	3337.94	30041.45	459×10^5
2420	4	91	263	47	0	142	24	304	1799	0.11	3337.94	30041.45	540×10^5
2600	13	69	257	40		122	30	805	3274	0.11	3337.94	30041.45	983×10^5
2620	0	59	82	22	0	81	18	180	810	0.11	3337.94	30041.45	243×10^5
2780	1	117	291	85	0	203	42	644	3113	0.11	3337.94	30041.45	935×10^5
2880	0	69	424	41		110	49.5	324	720	0.11	3337.94	30041.45	216×10^5
3020	4	101	153	24	0	129	21	196	1204	0.11	3337.94	30041.45	361×10^5
3100	1	19	323	20	9	49	63	714	555	0.11	3337.94	30041.45	166×10^5
3320	5	18	110	18	0	41	40.5	324	328	0.11	3337.94	30041.45	98×10^5
3500	1	39	180	20	8	68	63	840	907	0.11	3337.94	30041.45	272×10^5
3640	0	18	291	19	0	37	49.5	726	543	0.11	3337.94	30041.45	163×10^5
3820	2	29	61	22	0	53	18	176	518	0.11	3337.94	30041.45	155×10^5

MOCHRAS TOTAL CHARCOAL ABUNDANCES						
Sample name	**Core depth (m)**	**Total >125µm charcoal abundance**	**Total <125µm charcoal abundance**	**Total charcoal (<125µm + >125µm)**	**Total rock (g) processed**	**Total charcoal counted per 10 g of rock ((charcoal total/total rock processed) x 10 g)**
Mochras 2529'8''	771.04	19	48×10^3	48486	4.04	120×10^3
Mochras 2541'10''	774.75	17	41×10^3	41875	3.36	124×10^3
Mochras 2548'6''	776.78	15	163×10^3	163040	9.52	171×10^3
Mochras 2566'5''	780.36	32	12×10^3	12658	11.16	11×10^3
Mochras 2578'	782.24	68	64×10^3	64757	6.48	99×10^3
Mochras 2582'8''	785.77	26	214×10^3	214608	14.05	152×10^3
Mochras 2592'7"	786.99	296	469×10^3	469311	15.98	293×10^3
Mochras 2560'3''	790.21	36	534×10^3	534106	10.46	510×10^3
Mochras 2606'10''	794.56	30	424×10^3	424902	18.06	235×10^3
Mochras 2611'9''	796.06	132	379×10^3	379929	21.67	175×10^3
Mochras 2621'8''	799.08	163	418×10^3	418741	25.28	165×10^3
Mochras 2631'4''	802.03	149	957×10^3	957210	11.98	799×10^3

MOCHRAS TOTAL CHARCOAL ABUNDANCES						
Sample name	**Core depth (m)**	**Total >125µm charcoal abundance**	**Total <125µm charcoal abundance**	**Total charcoal (<125µm + >125µm)**	**Total rock (g) processed**	**Total charcoal counted per 10 g of rock ((charcoal total/total rock processed) x 10 g)**
Mochras 2637'9''	803.99	146	98×10^3	98241	21.74	45×10^3
Mochras 2641'8''	804.97	125	341×10^3	341335	9.71	351×10^3
Mochras 2654'4''	809.04	68	291×10^3	291816	15.90	183×10^3
Mochras 2670'	813.82	0	0	0	19.63	0
Mochras 2701'6''	823.42	5	74×10^3	74189	17.18	43×10^3
Mochras 2729'2''	831.85	0	24×10^3	24188	20.47	11×10^3
Mochras 2733'7''	833.20	29	151×10^3	151156	21.85	69×10^3
Mochras 2765'4''	842.87	218	137×10^3	137550	10.36	132×10^3
Mochras 2790'1''	850.39	314	21×10^3	21736	10.08	21×10^3
Mochras 2805'11''	854.96	305	78×10^3	78781	10.54	74×10^3
Mochras 2824'7''	860.75	242	52×10^3	52661	15.55	33×10^3
Mochras 2826'7''	861.54	14	52×10^3	52433	8.25	63×10^3

Mochras <125 µm charcoal counts						
Area of slide counted (mm^2)	**100% of slide area (mm^2)**	**Calculated charcoal for 100% of slide**	**100% slide area is equal to 0.11 (ml)**	**Total volume of sample (cm^3)**	**As 1ml is equal to $1cm^3$ (total sample volume (cm^3)/0.11 (ml)**	**Total Charcoal for <125µm**
33.00	484	161	0.11	3337.94	30041.45	48×10^5
33.00	484	139	0.11	3337.94	30041.45	41×10^5
33.00	484	543	0.11	3337.94	30041.45	163×10^5
43.50	551	215	0.11	3337.94	30041.45	64×10^5
6.86	196	714	0.11	3337.94	30041.45	214×10^5
11.76	216	1561	0.11	3337.94	30041.45	469×10^5
27.00	600	1778	0.11	3337.94	30041.45	534×10^5
69.00	580	42	0.11	3337.94	30041.45	12×10^5
14.70	330	1414	0.11	3337.94	30041.45	424×10^5
82.50	700	1264	0.11	3337.94	30041.45	379×10^5
39.00	494	1393	0.11	3337.94	30041.45	418×10^5
30.00	937	3186	0.11	3337.94	30041.45	957×10^5
16.17	121	359	0.11	3337.94	30041.45	107×10^5
18.13	396	1136	0.11	3337.94	30041.45	341×10^5
10.78	361	971	0.11	3337.94	30041.45	291×10^5
10.78	484	0	0.11	3337.94	30041.45	0
21.56	484	247	0.11	3337.94	30041.45	74×10^5
93.00	576	81	0.11	3337.94	30041.45	24×10^5
16.66	289	503	0.11	3337.94	30041.45	151×10^5
21.56	352	457	0.11	3337.94	30041.45	137×10^5

Mochras <125 µm charcoal counts						
Area of slide counted (mm^2)	**100% of slide area (mm^2)**	**Calculated charcoal for 100% of slide**	**100% slide area is equal to 0.11 (ml)**	**Total volume of sample (cm^3)**	**As 1ml is equal to $1cm^3$ (total sample volume (cm^3)/0.11 (ml)**	**Total Charcoal for <125µm**
16.66	396	71	0.11	3337.94	30041.45	21×10^5
18.62	304	261	0.11	3337.94	30041.45	78×10^5
15.68	304	174	0.11	3337.94	30041.45	52×10^5
33.00	484	176	0.11	3337.94	30041.45	52×10^5

MOCHRAS PALYNOFACIES DATA														
		COUNTS TAKEN ACROSS SLIDE TRANSECT					Total Phytoclasts In transect = pollen + spore + charcoal + Plant cut. + coal	Area of slide counted (mm^2) -	100% of slide area (mm^2)	Calculated phytoclasts for 100% of slide	100% slide area is equal to 0.11 (ml)	Total volume of sample (cm^3)	Number of 0.11ml in total sample volume (total sample volume (cm^3)/0.11 (ml))	Total Phytoclasts for <125µm
Sample name	Log height (m)	Pollen and Spore Count	Charcoal Count (micro)	Amorphous Organic Matter (AOM)	Plant Cuticles and Phytoclasts	Coalified Material								
Mochras 2529'8''	771.04	5	20	488	21	21	67	40.5	486	804	0.11	3337.94	30041.45	241×10^5
Mochras 2541'10''	774.75	5	6	236	15	33	59	42.0	308	433	0.11	3337.94	30041.45	129×10^5
Mochras 2548'6''	776.78	4	5	236	16	0	25	36.0	408	283	0.11	3337.94	30041.45	85×10^5
Mochras 2566'5''	780.36	2	12	355	7	7	28	42.0	712	475	0.11	3337.94	30041.45	142×10^5
Mochras 2578'	782.24	16	8	879	23	4	51	48.0	384	408	0.11	3337.94	30041.45	122×10^5
Mochras 2582'8''	785.77	10	18	203	23	39	90	45.0	600	1200	0.11	3337.94	30041.45	360×10^5
Mochras 2592'7"	786.99	1	41	66	53	0	95	33.0	418	1203	0.11	3337.94	30041.45	361×10^5
Mochras 2560'3''	790.21	3	12	324	14	2	31	54.0	540	310	0.11	3337.94	30041.45	93×10^5
Mochras 2606'10''	794.56	2	46	92	23	9	80	18.0	165	733	0.11	3337.94	30041.45	220×10^5

MOCHRAS PALYNOFACIES DATA														
		COUNTS TAKEN ACROSS SLIDE TRANSECT					Total Phytoclasts In transect = pollen + spore + charcoal + Plant cut. + coal	Area of slide counted (mm^2) -	100% of slide area (mm^2)	Calculated phytoclasts for 100% of slide	100% slide area is equal to 0.11 (ml)	Total volume of sample (cm^3)	Number of 0.11ml in total sample volume (total sample volume (cm^3)/0.11 (ml))	Total Phytoclasts for <125µm
Sample name	Log height (m)	Pollen and Spore Count	Charcoal Count (micro)	Amorphous Organic Matter (AOM)	Plant Cuticles and Phytoclasts	Coalified Material								
Mochras 2611'9''	796.06	8	68	771	207	90	373	73.5	833	4227	0.11	3337.94	30041.45	1269×10^5
Mochras 2621'8''	799.08	0	62	305	72	0	134	48.0	608	1697	0.11	3337.94	30041.45	509×10^5
Mochras 2631'4''	802.03	0	15	139	18	2	35	33.0	425	451	0.11	3337.94	30041.45	135×10^5
Mochras 2637'9''	803.99	2	39	96	87	10	138	18.0	216	1656	0.11	3337.94	30041.45	497×10^5
Mochras 2641'8''	804.97	0	10	68	28	0	38	25.5	170	253	0.11	3337.94	30041.45	76×10^5
Mochras 2654'4''	809.04	3	24	73	114	0	141	33.0	484	2068	0.11	3337.94	30041.45	621×10^5
Mochras 2670'	813.82	0	9	63	0	0	9	33.0	484	132	0.11	3337.94	30041.45	39×10^5
Mochras 2701'6''	823.42	0	19	29	92	4	115	27.0	198	843	0.11	3337.94	30041.45	253×10^5
Mochras 2729'2''	831.85	2	31	296	101	3	137	60.0	720	1644	0.11	3337.94	30041.45	493×10^5

MOCHRAS PALYNOFACIES DATA														
		COUNTS TAKEN ACROSS SLIDE TRANSECT					Total Phytoclasts In transect = pollen + spore + charcoal + Plant cut. + coal	Area of slide counted (mm^2) -	100% of slide area (mm^2)	Calculated phytoclasts for 100% of slide	100% slide area is equal to 0.11 (ml)	Total volume of sample (cm^3)	Number of 0.11ml in total sample volume (total sample volume (cm^3)/0.11 (ml))	Total Phytoclasts for <125µm
Sample name	Log height (m)	Pollen and Spore Count	Charcoal Count (micro)	Amorphous Organic Matter (AOM)	Plant Cuticles and Phytoclasts	Coalified Material								
Mochras 2733'7''	833.20	2	17	137	6	0	25	33.0	484	367	0.11	3337.94	30041.45	110×10^5
Mochras 2765'4''	842.87	0	2	75	19	0	21	19.5	264	284	0.11	3337.94	30041.45	85×10^5
Mochras 2790'1''	850.39	1	26	137	36	0	63	33.0	396	756	0.11	3337.94	30041.45	227×10^5
Mochras 2805'11''	854.96	2	85	71	60	0	147	33.0	418	1862	0.11	3337.94	30041.45	559×10^5
Mochras 2824'7''	860.75	1	49	102	77	0	127	33.0	484	1863	0.11	3337.94	30041.45	559×10^5
Mochras 2826'7''	861.54	2	392	7	1	0	395	30.0	570	7505	0.11	3337.94	30041.45	2254×10^5

DAKOTA FM CHARCOAL AND TOTAL ORGANIC MATTER DATA COLLECTED					
Collection site	**Log height (m)**	**Total Sample Charcoal count**	**Charcoal count per 10g**	**Total Organic Content remaining (g)**	**Charcoal count per 1g of TOC**
BIG HILL UPPER	58.50	291	188	8.22	35
BIG HILL UPPER	36.00	7	5	0.47	15
BIG HILL LOWER	24.76	3	1	0.37	8
BIG HILL LOWER	16.90	26	13	0.14	186
BIG HILL LOWER	10.60	3265	1617	0.47	6947
BIG HILL LOWER	10.00	188	96	0.13	1446
BIG HILL LOWER	6.80	1014	489	0.17	5965
BIG HILL LOWER	2.40	28	17	1.16	24
KANARRA MOUNTIANS	-0.55	45	22	0.06	750
COTTONWOOD	-1.20	458	242	0.50	916
KANARRA MOUNTIANS	-1.17	7	3	0.03	233
KANARRA MOUNTIANS	-1.60	9	4	0.07	129
KANARRA MOUNTIANS	-2.20	10	5	0.07	143
COTTONWOOD	-2.70	8	4	0.03	267
KANARRA MOUNTIANS	-3.90	1	0	0.11	9
KANARRA MOUNTIANS	-4.10	32	15	1.12	29
KANARRA MOUNTIANS	-8.30	3	1	0.29	10
KANARRA MOUNTIANS	-8.70	122	58	0.22	555
WAHWEEP	-18.80	41	20	4.15	10
WAHWEEP	-23.80	1	1	3.16	0
WAHWEEP	-26.90	23	19	0.64	36
WAHWEEP	-30.70	0	0	0.47	0
WAHWEEP	-31.60	6	4	0.07	86

DAKOTA FM CHARCOAL AND TOTAL ORGANIC MATTER DATA COLLECTED					
Collection site	**Log height (m)**	**Total Sample Charcoal count**	**Charcoal count per 10g**	**Total Organic Content remaining (g)**	**Charcoal count per 1g of TOC**
WAHWEEP	-39.90	47	42	2.26	21

MOCHRAS MILANKOVITCH <125 µm CHARCOAL DATA										
Sample name	**Log height (m)**	**Sample Count <125um in 2 trans**	**Area of 2 transects counted (mm^2)**	**100% of slide area (mm^2)**	**charcoal for 100% slide**	**100% slide equal to 0.11 ml**	**Total volume of sample (cm3)**	**As 1ml is equal to 1cm3 (total sample volume (cm3)/0.11 (ml)**	**Total calculated char for <125**	**Calculated char per 10g**
3065'8''	934.41	15	66	462	105	0.11	33.37	300.41	31543.53	25×10^3
3067'	934.82	3	66	440	20	0.11	33.37	300.41	6008.291	6×10^3
3068'	935.13	7	66	340	36	0.11	33.37	300.41	10833.13	6×10^3
3068'04''	935.23	26	66	462	182	0.11	33.37	300.41	54675.45	98×10^3
3070'3''	935.81	7	153	1122	51	0.11	33.37	300.41	15421.28	19×10^3
3071'4''	936.14	12	66	440	80	0.11	33.37	300.41	24033.16	17×10^3
3072'8''	936.55	25	118	841	178	0.11	33.37	300.41	53527.25	37×10^3
3073'8''	936.85	12	75	275	44	0.11	33.37	300.41	13218.24	10×10^3
3075'1''	937.28	32	84	616	235	0.11	33.37	300.41	70497.28	32×10^3
3076'1''	937.59	3	72	480	20	0.11	33.37	300.41	6008.291	5×10^3
3077'	937.87	12	66	242	44	0.11	33.37	300.41	13218.24	6×10^3
3078'4''	938.27	6	66	484	44	0.11	33.37	300.41	13218.24	20×10^3
3079'5''	938.61	31	84	336	124	0.11	33.37	300.41	37251.4	33×10^3
3080'8''	938.99	10	63	1122	178	0.11	33.37	300.41	53502.4	70×10^3
3081'7''	939.27	11	66	484	81	0.11	33.37	300.41	24233.44	26×10^3
3082'11''	939.67	41	54	440	334	0.11	33.37	300.41	100360.7	95×10^3
3083'8''	939.90	17	153	1122	125	0.11	33.37	300.41	37451.68	69×10^3
3085'1''	940.33	38	105	840	304	0.11	33.37	300.41	91326.02	98×10^3

MOCHRAS MILANKOVITCH >125 µm CHARCOAL COUNTS					
Sample name	**log height (m)**	**Sample Count**	**Starting sample weight (g)**	**Total weight of rock counted for charcoal**	**Charcoal count per 10g**
3065'8''	934.41	263	12.41	12.41	212
3067'	934.82	65	8.7	8.7	75
3068'	935.13	46	16.82	16.82	27
3068'04''	935.23	172	5.55	5.55	310
3070'3''	935.81	475	7.8	7.8	609
3071'4''	936.14	58	13.78	13.78	42
3072'8''	936.55	2	14.29	14.29	1
3073'8''	936.85	502	12.39	12.39	405
3075'1''	937.29	78	21.85	21.85	36
3076'1''	937.59	39	10.35	10.35	38
3077'	937.87	680	19.9	19.9	342
3078'4''	938.28	170	6.33	6.33	269
3079'5''	938.61	114	11.21	11.21	102
3080'8''	938.99	169	7.63	7.63	221
3081'7''	939.27	524	9.32	9.32	562
3082'11''	939.67	415	10.53	10.53	394
3083'8''	939.90	16	5.38	5.38	30
3085'1''	940.33	150	9.26	9.26	162

TOTAL CHARCOAL ABUNDANCE FOR MOCHRAS MILANKOVITCH ANALYSIS			
log height (m)	**Total >125um char in 10g**	**Total char for <125 per 10g**	**Total charcoal count**
934.4152	211	25417	25629
934.8216	74	6906	6980
935.1264	27	6440	6467
935.228	309	98514	98824
935.8122	608	19770	20379
936.1424	42	17440	17482
936.5488	1	37457	37459
936.8536	405	10668	11073
937.2854	35	32264	32299
937.5902	37	5805	5842
937.8696	341	6642	6984
938.276	268	20881	21150
938.6062	101	33230	33332
938.9872	221	70121	70342
939.2666	562	26001	26563
939.673	394	95309	95703
939.9016	29	69612	69642
940.3334	161	98624	98786

MOCHRAS MILANKOVITCH PALYNOFACIES DATA										
Sample name	**Log height (m)**	**Pollen sample count in 2 trans**	**Area of 2 transects counted (mm^2)**	**100% of slide area (mm^2)**	**Pollen for 100% slide**	**100% slide equal to 0.11 ml**	**Total volume of sample (cm3)**	**As 1ml is equal to 1cm3 (total sample volume (cm3)/0.11 (ml)**	**Total calculated pollen**	**Calculated pollen per 10g**
3065'8''	934.41	1	30	380	13	0.11	33.37	300.41	3805	3066
3067'	934.82	0	25.5	213	0	0.11	33.37	300.41	0	0
3068'	935.13	1	22.5	176	8	0.11	33.37	300.41	2350	1397
3068'04''	935.23	0	19.5	234	0	0.11	33.37	300.41	0	0
3070'3''	935.81	0	33	352	0	0.11	33.37	300.41	0	0
3071'4''	936.14	1	33	484	15	0.11	33.37	300.41	4406	3197
3072'8''	936.55	1	33	330	5	0.11	33.37	300.41	1502	1051
3073'8''	936.85	2	33	484	29	0.11	33.37	300.41	8812	7112
3075'1''	937.28	1	28.5	380	7	0.11	33.37	300.41	2003	917
3076'1''	937.59	2	27	252	14	0.11	33.37	300.41	4206	4064
3077'	937.87	1	33	330	5	0.11	33.37	300.41	1502	755
3078'4''	938.27	0	24	260	0	0.11	33.37	300.41	0	0
3079'5''	938.61	0	19.5	169	0	0.11	33.37	300.41	0	0
3080'8''	938.99	1	22.5	176	4	0.11	33.37	300.41	1175	1540
3081'7''	939.27	0	22.5	285	0	0.11	33.37	300.41	0	0
3082'11''	939.67	0	22.5	300	0	0.11	33.37	300.41	0	0
3083'8''	939.90	1	30	300	5	0.11	33.37	300.41	1502	2792
3085'1''	940.33	1	27	270	5	0.11	33.37	300.41	1502	1622

MOCHRAS MILANKOVITCH PALYNOFACIES DATA										
Sample name	**Log height (m)**	**Amorphous organic matter sample count in 2 trans**	**Area of 2 transects counted (mm^2)**	**100% of slide area (mm^2)**	**AOM for 100% slide**	**100% slide equal to 0.11 ml**	**Total volume of sample (cm3)**	**As 1ml is equal to 1cm3 (total sample volume (cm3)/0.11 (ml)**	**Total calculated AOM**	**Calculated AOM per 10g**
3065'8''	934.41	78	30	380	988	0.11	33.37	300.41	296810	239170
3067'	934.82	186	25.5	213	1554	0.11	33.37	300.41	466738	536481
3068'	935.13	94	22.5	176	735	0.11	33.37	300.41	220891	131327
3068'04''	935.23	71	19.5	234	852	0.11	33.37	300.41	255953	461177
3070'3''	935.81	84	33	352	896	0.11	33.37	300.41	269171	345092
3071'4''	936.14	41	33	484	601	0.11	33.37	300.41	180649	131095
3072'8''	936.55	189	33	330	1890	0.11	33.37	300.41	567783	397329
3073'8''	936.85	165	33	484	2420	0.11	33.37	300.41	727003	586766
3075'1''	937.28	298	28.5	380	3973	0.11	33.37	300.41	1193647	546292
3076'1''	937.59	147	27	252	1372	0.11	33.37	300.41	412169	398231
3077'	937.87	289	33	330	2890	0.11	33.37	300.41	868198	436280
3078'4''	938.27	91	24	260	986	0.11	33.37	300.41	296159	467865
3079'5''	938.61	52	19.5	169	451	0.11	33.37	300.41	135387	120773
3080'8''	938.99	109	22.5	176	853	0.11	33.37	300.41	256140	335701
3081'7''	939.27	116	22.5	285	1469	0.11	33.37	300.41	441409	473615
3082'11''	939.67	47	22.5	300	627	0.11	33.37	300.41	188260	178784
3083'8''	939.90	156	30	300	1560	0.11	33.37	300.41	468647	871090
3085'1''	940.33	60	27	270	600	0.11	33.37	300.41	180249	194653

MOCHRAS MILANKOVITCH PALYNOFACIES DATA										
Sample name	**Log height (m)**	**Plant cuticle sample count in 2 trans**	**Area of 2 transects counted (mm^2)**	**100% of slide area (mm^2)**	**Plant cuticle for 100% slide**	**100% slide equal to 0.11 ml**	**Total volume of sample (cm3)**	**As 1ml is equal to 1cm3 (total sample volume (cm3)/0.11 (ml)**	**Total calculated plant cuticle**	**Calculated plant cuticle per 10g**
3065'8''	934.41	11	30	380	139	0.11	33.37	300.41	41858	33729
3067'	934.82	3	25.5	213	25	0.11	33.37	300.41	7528	8653
3068'	935.13	10	22.5	176	78	0.11	33.37	300.41	23499	13971
3068'04''	935.23	4	19.5	234	48	0.11	33.37	300.41	14420	25982
3070'3''	935.81	13	33	352	139	0.11	33.37	300.41	41657	53407
3071'4''	936.14	23	33	484	337	0.11	33.37	300.41	101340	73541
3072'8''	936.55	5	33	330	50	0.11	33.37	300.41	15021	10511
3073'8''	936.85	11	33	484	161	0.11	33.37	300.41	48467	39118
3075'1''	937.28	26	28.5	380	347	0.11	33.37	300.41	104144	47663
3076'1''	937.59	25	27	252	233	0.11	33.37	300.41	70097	67726
3077'	937.87	15	33	330	150	0.11	33.37	300.41	45062	22644
3078'4''	938.27	8	24	260	87	0.11	33.37	300.41	26036	41131
3079'5''	938.61	9	19.5	169	78	0.11	33.37	300.41	23432	20903
3080'8''	938.99	9	22.5	176	70	0.11	33.37	300.41	21149	27718
3081'7''	939.27	9	22.5	285	114	0.11	33.37	300.41	34247	36746
3082'11''	939.67	13	22.5	300	173	0.11	33.37	300.41	52072	49451
3083'8''	939.90	7	30	300	70	0.11	33.37	300.41	21029	39087
3085'1''	940.33	6	27	270	60	0.11	33.37	300.41	18025	19465

10. References

Abatzoglou, J.T., Williams, A.P. (2016). Impact of anthropogenic climate change on wildfire across western US forests. *Proceedings of the National Academy of Science of the United States of America, 113,* 1770 – 11775.

Abe-Ouchi, A., Saito, F., Kawamura, K., Raymo, M.E., Okuno, J., Takahashi, K., Blatter, H. (2013). Insolation-driven 100,000-year glacial cycles and hysteresis of ice-sheet volume, *Nature, 500,* 190-195

Abels, H.A., Hilgen, F.J., Krijgsman, W., Kruk, R.W., Raffi, I., Turco, E., Zachariasse, W.J. (2005). Long-period orbital control on middle Miocene global cooling: Integrated stratigraphy and astronomical tuning of the Blue Clay Formation on Malta. *Paleoceanography. 20*, 1-17. doi:10.1029/2004PA001129

Abramovich, S., Keller, G., Stüben, D. and Berner, Z. (2003). Characterization of late Campanian and Maastrichtian planktonic foraminiferal depth habitats and vital activities based on stable isotopes. *Palaeogeography, Palaeoclimatology, Palaeoecology*, *202*, 1–29.

Adams, D.D., Hurtgen, M.T., Sageman, B.B. (2010). Volcanic triggering of a biogeochemical cascade during Oceanic Anoxic Event 2, *Letters to Nature Geoscience, 3,* 201-204

Alberta Government. (2012). How different tree species impact the spread of wildfire. Retrieved on 10 January 2017 from http://www1.agric.gov.ab.ca/$department/deptdocs.nsf/all/formain15737/$file/BraggCreek-DifferentTreeSpecicesImpactWildfire-Aug03-2012.pdf?OpenElement

Aldersley, A., Murray, S.J., Cornell, S.E. (2011). Global and regional analysis of climate and human drivers of wildfire. *Science of the Total Environment. 409,* 3472-3481

Alexander, M. (1981). Biodegradation of chemicals of environmental concern. *Science. 211,* 132-138

Algeo, T.J., Berner, R.A., Maynard, J.B., Scheckler, S.E., (1995). Late Devonian Oceanic Anoxic Events and biotic crises: rooted in the evolution of vascular land plants*? GSA Today, 5,* 64-66

Anderson, W.R., Catchpole, E.A., Butler, B.W. (2010). Convective heat transfer in fire spread through fine fuel beds, *International Journal of Wildland Fire*, *19,* 284-298

Anthenien, R.A., Tse, S.D., Fernansez-Pello, A.C. (2006). On the trajectories of embers initially elevated or lofted by small scale ground fire plumes in high winds, *Fire Safety Journal, 41,* 349-363

Arthur, M.A., Dean, W., Pratt, L.M. (1988). Geochemical and climatic effects of increased marine organic carbon burial at the Cenomanian/Turonian boundary. *Nature. 335*,714–717.

Arthur, M.A., Dean, W.E., Schlanger, S.O. (1985). Variations in the global carbon cycle during the Cretaceous related to climate, volcanism, and changes in atmospheric CO_2, In: Sunquist E.T., Broecker W.S. (Eds.), The Carbon Cycle and Atmospheric CO_2 : Natural Variations Archean to Present*,* *Geophysical Monograph Series, 32,* 504-529

Arthur, M.A., Sageman, B.B. (1994). Marine Black Shales: Depositional Mechanisms and Environments of Ancient Deposits, *Annual Review Earth and Planetary Science, 22,* 499-551

Arthur, M.A., Schlanger, S.O. (1979). Cretaceous “Oceanic Anoxic Events” as Causal Factors in Development of Reef-Reservoired Giant Oil Fields, *The American Association of Petroleum Geologists Bulletin, 63(6),* 870-885

Aziz, H.A., van Dam, J., Hilgen, F.J., Krijgsman, W. (2004). Astronomical forcing in Upper Miocene continental sequences: implications for the Geomagnetic Polarity Time Scale. *Earth and Planetary Science Letters. 222,* 243-258. doi:10.1016/j.epsl.2004.02.018

Aziz, H.A., Krijgsman, W., Hilgen, F.J., Wilson, D.S., Calvo, J.P. (2003). An astronomical polarity timescale for the late middle Miocene based on cyclic continental sequences. *Journal of Geophysical Research. 108,* 1 – 16 doi: 10.1029/2002JB001818

Bains, S., Corfield, R.M., Norris, R.D. (1999). Mechanisms of climate warming at the end of the Paleocene, *Science*, *285,* 724-727

Barber, T.M. (2002). Phosphate adsorption by mixed and reduced iron phases in static and dynamic systems, *Thesis submitted to the department of Geology of Stanford University for the degree of master of science,* retrieved on 9th July 2014 from http://soils.stanford.edu/theses/Theresa_Barber.pdf

Barclay, R.S., McElwain, J.C., Sageman, B.B. (2010). Carbon sequestration activate by a volcanic CO_2 pulse during Ocean Anoxic Event 2, *Nature Geoscience, 3,* 205-208

Barclay, R.S., Rioux, M., Meyer, L.B., Bowring, S.A., Johnson, K.R., Miller, I.M. (2015). High precision UePb zircon geochronology for Cenomanian Dakota Formation floras in Utah, *Cretaceous Research. 52,* 213-237

Barker, S., Ridgwell, A. (2012). Ocean Acidification, *Nature Education Knowledge, 3(10),* 21

Barrón, E., Comas-Rengifo, M.J., Duarte, L.V. (2013). Palynomorph succession of the Upper Pliensbachian–Lower Toarcian of the Peniche section (Portugal). Comunicações Geológicas. *100,* 55-61

Barron, E.J., Fawcett, P.J., Peterson, W.H. (1995). A “simulation” of mid-Cretaceous climate, *Palaeoceanography, 10,* 953-962

Bartolini, A., Baumgartner, P.O., Hunziker, J. (1996). Middle and Late Jurassic carbon stable-isotope stratigraphy and radiolarite sedimentation of the Umbria-Marche Basin (Central Italy)., *Eclogae Geol. Helv., 89*, 811 844

Bartolini, A., Baumgartner, P.O., Hunziker, J. (1996). Middle and Late Jurassic carbon stable-isotope stratigraphy and radiolarite sedimentation of the Umbria-Marche Basin (Central Italy)., *Eclogae Geol. Helv*., *89,* 811 844

Bazzaz, F.A. (1990). The Response of Natural Ecosystems to the Rising Global CO_2 Levels, *Annual Review of Ecology and Systematics. 21,* 167-196

Beaufort, L., de Garidel-Thoron, T., Linsley, B., Oppo, D., Buchet, N. (2003). Biomass burning and oceanic primary production estimates in the Sulu Sea area over the last 380 kyr and the East Asian monsoon dynamics. *Marine Geology. 201,* 53-65

Beaumont, E. (Ed.), (1985). Industrial Charcoal Making. FAO Forestry Paper, *Food and Agricultural Organization of the United Nations, Romme*(63)

Beer, T. (1991). The interaction of wind and fire, *Boundary-Layer Meteorology*, *54,* 287-308

Beer, J., Mende, W., Stellmacher, R. (2000). The role of the sun in climate forcing, *Quaternary Science Reviews, 19,* 403-415

Beerling, D.J., Lomas, M.R., Gröcke, D.R. (2002). On the nature of methane gas-hydrate dissociation during the Toarcian and Aptian Oceanic Anoxic Events, *American Journal of Science*, *302,* 28-49

Belcher, C. M. (2009). Reigniting the Cretaceous-Palaeogene firestorm debate, *Geology*, *37,* 1147–1148, doi:10.1130/focus122009.1.

Belcher, C. M. (2013). *Fire Phenomena and the Earth System: An Interdisciplinary Guide to Fire Science.* Chichester: John Wiley and Sons, Ltd.

Belcher, C.M. (2014). Earth, air and fire: Claire Belcher at TEDxExeter

Belcher, C.M., Collinson, M.E., Scott, A.C. (2005). Constraints on the thermal energy released from the Chicxulub impactor: new evidence from multi-method charcoal analysis, *Journal of the Geological Society*, *162,* 591-602, doi:10.1144/0016-764904-104

Belcher, C.M., Collinson, M.E., Scott, A.C, (2013a). A 450-Million-Year History of Fire, in Belcher C.M., (pp. 229-249). *Fire Phenomena and the Earth System,* West Sussex: John Wiley and Sons

Belcher, C.M., Punyasena, S.W., Sivaguru, M. (2013b). Novel Application of Confocal Laser Scanning Microscopy and 3D Volume Rendering toward Improving the Resolution of the Fossil Record of Charcoal. *PLoS ONE. 8(8),* e72265

Belcher, C. M., Collinson, M. E. & Scott, A. C. (2005). Constraints on the thermal energy released from the Chicxulub impactor: new evidence from multi-method charcoal analysis. *Journal of the Geological Society of London. 162,* 591–602

Belcher, C. M., Collinson, M.E., Sweet, A. R. Hildebrand, A.R., Scott A.C., (2003). Fireball passes and nothing burns – The role of thermal radiation in

the Cretaceous–Tertiary event: Evidence from the charcoal record of North America, *Geology, 31,* 1061–1064, doi:10.1130/G19989.1.

Belcher, C. M., P. Finch, M. E. Collinson, A. C. Scott, and N. V. Grassineau. (2009). Geochemical evidence for combustion of hydrocarbons during the K-T impact event, *Proceedings of the National Academy of Sciences*, *106,* 4112–4117, doi:10.1073/ pnas.0813117106.

Belcher, C.M., Hudspith, V.A. (2016). Changes to Cretaceous surface fire behavior influenced the spread of the early angiosperms, *New Phytologist, 213***,** 1521-1532

Belcher, C.M., Mander, L., Rein, G., Jervis, X., Haworth, M., Hesselbo, S.P., Glasspool, I.J., McElwain, J.C. (2010b). Increased fire activity at the Triassic/Jurassic boundary in Greenland due to climate-driven floral change. *Nature Geoscience. 3,* 426-429

Belcher, C.M., McElwain, J.C. (2008). Limits for Combustion in Low O_2 Redefine Paleoatmospheric Predictions for the Mesozoic, *Science, 321*, 1197-1200, doi: 10.1126/science.1160978

Belcher, C.M., Yearsley, J.M., Hadden, R.M., McElwain, J.C., Rein G, (2010a). Baseline intrinsic flammability of Earth's ecosystems estimated from paleoatmospheric oxygen over the past 350 million years, *PNAS, 1-6*, doi/10.1073/pnas.1011974107

Belcher, C.M., Hudsptih, V.A. (2017). Changes to Cretaceous surface fire behaviour influenced the spread of the early angiosperms. *New Phytologist. 213,* 1521 – 1532.

Bennett, K.D. (1990). Milankovitch Cycles and Their Effects on Species in Ecological and Evolutionary Time. *Paleobiology. 16,* 11-21

Berger, A. (2001). Where astronomy meets geology: from Ice Ages to global warming, retrieved on 28th February 2017 from: http://www.igpp.ucla.edu/colloquia/lectures/berger/

Berger, A., Imbrie, J., Hays, G., Kukla, G. & Saetzman, B. (1989). Pre-Quaternary Milankovitch frequencies. *Nature*, *323,* 133

Berger, A., Loutre, M.F., Laskar, J. (1992). Stability of the Astronomical Frequencies Over the Earth's History for Paleoclimate Studies. *Science. 255.* 560-566

Berger, A., Loutre, M.F., Laskar, M.F. (1992). Stability of the Astronomical Frequencies over the Earth's History for Paleoclimate Studies, *Science, 255*, 560

Bergman, N.M. (2003). COPSE: A New Biogeochemcial Model for the Phanerozoic, *School of Environmental Sciences, Norwich University of East Anglia*, 197

Bergman, N.M., Lenton, T.M., Watson, A.J. (2004). COPSE: a new model of biogeochemical cycling over Phanerozoic time, *American Journal of Science, 304*, 397-437

Berner, R.A. (1991). A model for atmospheric CO_2 over Phanerozoic time, *American Journal of Science*, *291*, 339-376

Berner, R.A. (1997). The rise of plants and their effect on weathering and atmospheric CO_2, *Science*, *276,* 54-546

Berner, R. A. (1999). Atmospheric oxygen over Phanerozoic time. *Proceedings of the National Academy of Science. 96,* 10955–10957

Berner, R. A. (2004). *The Phanerozoic Carbon Cycle: CO_2 and O_2. 150,* Oxford University Press

Berner, R.A. (2006). GEOCARBSULF: A combined model for Phanerozoic atmospheric O_2 and CO_2, *Geochemica et Cosmochimica Acta, 70*, 5653-5664

Berner, R.A. (2001). Modeling atmospheric O2 over Phanerozoic time, *Geochimica et Cosmochimica Acta*, *65(5*), 685-694

Berner, R.A., Beerling, D.J., Dudley, R., Robinson, J.M., Wildman, Jr, R.A. (2003). Phanerozoic Atmospheric Oxygen. *Earth and Planetary Science Letters. 31,* 105-134

Berner, R.A., Canfield, D.E. (1989). A New Model for Atmospheric Oxygen over Phanerozoic Time, *American Journal of Science, 289,* 333-361

Berner R.A., Kothavala Z. (2001). Geocarb III: A Revised Model of Atmospheric CO_2 over Phanerozoic Time, *American Journal of Science, 301(2*), 182-204, doi:10.2475/ajs.301.2.182

Bianucci, L., Fennel, K., Denman, K.L. (2012). Role of sediment denitrification in water column oxygen dynamics: comparison of the North American East and West Coasts. *Biogeosciences. 9,* 2673-2682

Bird, M.I., Gröcke D.R. (1997). Determination of the abundance and carbon isotope composition of elemental carbon in sediments. *Geochimica et Cosmochimica Acta, 61,* 3413-3423

Bird, M.I., Moyo, C., Veenendaal, E.M., Lloyd, J., Frost, P. (1999). Stability of elemental carbon in a savanna soil. *Global Biogeochemical Cycles 13,* 923e932.

Bjerrum, C. J., Surlyk, F., Callomon, J. H., and Slingerland, R. L. (2001). Numerical Paleoceanographic study of the Early Jurassic transcontinental Laurasian Seaway, *Paleoceanography*,*16***,** 390– 404

Blättler, C.L., Jenkyns, H.C., Reynard, L.M., Henerson, G.M. (2011). Significant increases in global weathering during Oceanic Anoxic Events 1a and 2 indicated by calcium isotopes. *Earth and Planetary Science Letters. 309,* 77-88

Bond, W. J. (2008). What limits trees in C4 grasslands and savannas? *Annual Review of Ecology, Evolution, and Systematics. 39,* 641–59. doi: 10.1146/annurev.ecolsys.39.110707.173411

Bonis, N.R. and Kürschner, W.M. (2012). Vegetation history, diversity patterns, and climate change across the Triassic/Jurassic boundary, *Paleobiology 38,* 240-264.

Bonis, N.R., Ruhl M., Kürschner, W.M. (2010). Milankovitch-scale palynological turnover across the Triassic-Jurassic transition at St. Audrie's Bay, SW UK, *Journal of the Geological Society, London, 167,* 877-888

Bornemann, A., Pross, J., Reichelt, K., Herrle, J.O., Hemleben, C., Mutterlose, J. (2005). Reconstruction of short-term Palaeoceanographic changes during the formation of the Late Albian 'Niveau Breistroffer' black shales (Oceanic Anoxic Event 1d, SE France, *Journal of the Geological Society, 162*, 623-639

Bottini, C., Cohen, A.S., Erba, E., Jenkyns, H.C., Coe, A.L. (2012). Osmium-isotope evidence for volcanism, weathering, and ocean mixing during the early Aptian OAE 1a. *Geology. 40,* 583, doi:10.1130/G33140.

Bougeault, C., Pellenard, P., Deconinck, J-F., Hesselbo, S.P., Dommergues, J-L., Bruneau, L., Cocquerez, T., Laffont, R., Huret, E., Thibault, N. (2017). Climatic and palaeoceanographic changes during the Pliensbachian (Early Jurassic) 2 inferred from clay mineralogy and stable isotope (C-O) geochemistry (NW Europe), *Global and Planetary Change,* doi: 10.1016/j.gloplacha.2017.01.005

Bowen, D.Q., Rose, J., McCabe, A.M., Sutherland, D.G. (1986). Correlation of Quaternary glaciaitions in England, Ireland, Scotland and Wales. *Quaternary Science Reviews. 5,* 299-340, doi: 10.1016/0277-3791(86)90194-0

Bowman, D.M.J.S., Balch, J.K., Artaxo, P., Bond, W.J., Carlson, J.M., '…' Pyne S.J. (2009). Fire in the Earth System. *Science. 324,* 481 – 487. doi: 10.1126/science.1163886 (2009).

Boyd, J. (2014). Analysis finds that more than half of black carbon never reaches bottom, Study:Black carbon is ancient by the time it reaches the seafloor, RICE University News and Media, retrieved on 7th April 2014 from http://news.rice.edu/2014/04/07/study-black-carbon-is-ancient-by-the-time-it-reaches-seafloor/

Bralower, T.J. (2008). Volcanic cause of catastrophe, *Nature*, *454*, 285-287

Breugel, Y.van. (2006). Causes for negative carbon isotope anomalies in Mesozoic marine sediments: Constraints from modern and ancient anoxic settings, *Geologica Ultraiectina*, 258

Brice, K.L., Bralower, T.J., Duncan, R.A., Huber, B.T., Leckie, R.M., Sageman, B.B. (2002). Cretaceous climate-Ocean Dynamics: Future Directions for IODP, A JOI/USSSP And NSF Sponsored Workshop, retrieved on 22 October 2014 from http://www.whoi.edu/ccod/CCOD_report.html

Briles, C.E., Whitlock, C., Bartlein, P.J. (2005). Postglacial vegetation, fire, and climate history of the Siskiyou Mountains, Oregon, USA, *Quaternary Research, 64***,** 44-56

Brockway, D.G., Lewis, C.E. (1997). Long-term effects of dormant-season prescribed fire on plant community diversity, structure and productivity in a longleaf pine wiregrass ecosystem. *Forest Ecology and Management. 96,* 167-183, doi.org/10.1016/S0378-1127(96)03939-4

Broecker, W.S. (2000). Abrupt climate change: casual constraints provided by the paleoclimate record, *Earth-Science Reviews, 51,* 137-154

Brown, R.E., Koeberl, C., Montanari, A., Bice, D.M. (2009). Evidence for a change in Milankovitch forcing caused by extraterrestrial events at Massignano, Italy, Eocene-Oligocene boundary GSSP.In C. Koeberl., A. Montanari (Eds.). *The Late Eocene Earth—Hothouse, Icehouse, and Impacts.* doi:10.1130/2009.2452(08)

Bull, W.B. (2007). 3.3 Fault Segmentation of Mountain Fronts – 3.3.1 Different Ways to Study Active Faults, Tectonic Geomorphology of Mountains, *A New Approach to Paleoseismology*. (pp. 101). Blackwell Publishing, Oxford, UK

Burke, W.H., Denison, R.E., Hetherington, E.A., Koepnick, R.B., Nelson, H.F., Otto, J.B. (1982). Variation of seawater $^{87}Sr/^{86}Sr$ throughout Phanerozoic time, *Geology*, 10:516-519

Cai, J., Bao, Y., Yang, S., Wang, X., Fan D., Xu J., Wang A. (2007). Research on preservation and enrichment mechanisms of organic matter in muddy sediment and mudstone, *Science in China Series D: Earth Sciences, 50,* 765-775

Caldeira, K., Kasting, J.F. (1992). The life span of the biosphere revisited, *Nature*. *360,* 721-723

Canfield, D.E. (1994). Factors influencing organic carbon preservation in marine sediments, *Chemical Geology, 114*, 315-329

Canfield, D. E. (2005). The early history of atmospheric oxygen: homage to Robert M. Garrels. *Earth and Planetary Science Letters. 33,* 1–36.

Carcaillet, C., Bergeron, Y., Richard, P.J.H., Frechette, B., Gauthier, S. & Prairie, Y.T. (2001). Change of fire frequency in the eastern Canadian boreal

forests during the Holocene: Does vegetation composition or climate trigger the fire regime? *Journal of Ecology, 89*, 930–946

Caswell, B.A., Coe, A.L. (2012). A high-resolution shallow marine record of the Toarcian (Early Jurassic) Oceanic anoxic Event from the East Midlands Shelf, UK, *Palaeogeography, Palaeoclimatology, Palaeoecology, 365*,124-135
Catling, D. C. & Claire, M. W. (2005). How Earth's atmosphere evolved to an oxic state: a status report. *Earth and Planetary Science Letters. 237,* 1–20

Chaloner, W.G. (1989). Fossil charcoal as an indicator of palaeoatmospheric oxygen level, *Journal of the Geological Society, 146*, 171-174

Chandler, M.A., Rind D., Ruedy R. (1992). Pangaean climate during the Early Jurassic: GCM simulations and the sedimentary record of paleoclimate, *Geological Society of America Bulletin, 104,* 543-559

Chanton, J.P., Rutowski, C.M., Schwartz, C.C., Ward, D.E., Boring, L. (2000). Factors influencing the stable carbon isotopic signature of methane from combustion and biomass burning. *Journal of Geophysical Research. 105,* 1867-1877

Chave, K.E. (1967). Recent carbonate sediments: an unconventional view. *Council on Education in the Geological Sciences. 15*, 200 204.

Chipman, M.L., Hudspith, V.A., Higuera, P.E., Duffy, P.A., Kelly, R., Oswald, W.W., Hu, F.S. (2015). Spatiotemporal patterns of tundra fires: late-Quaternary charcoal records from Alaska. *Biogeosciences. 12,* 4017-4027

Clark, R.L. (1982). Point count estimation of charcoal in pollen preparations and thin sections of sediments, *Pollen et Spores*, *24*, 523-535

Clark, J. S. (1990). Fire and climate change during the last 750 Yr in Northwestern Minnesota. *Ecological Monographs. 60,* 135–159

Clark, J.S., Cachier H., Goldammer J.G., Stocks B. (Ed). (1997). *Sediment Records of Biomass Burning and Global Change. NATO ASI Series, Vol.1 51*. Springer-Verlag Berlin Heidelberg

Clark, J.S., Lynch, J., Stocks, B.J., Goldammer, J.G. (1998). Relationships between charcoal particles in air and sediments in west-central Siberia, *The Holocene*, *8,1*, 19-29

Clark, A.D., Owens, S.R., Zhou, J.C. (2006). An ultrafine sea-salt from breaking waves: implications for cloud condensation nuclei in the remote marine atmosphere, *Journal of Geophysical Research Atmosphere, 111,* doi:10.1029/2005JD006565

Clark, J.S., Royall, P.D. (1996). Local and Regional Sediment Charcoal Evidence for Fire Regimes in Presettlement North-Eastern North America, *Journal of Ecology*, *84,* 365-382

Clark, F.R.S., Russell, D.A. (1981). Fossil charcoal and the palaeoatmosphere, *Nature, 290*, 428

Clemens, S.C., Tiedemann, R. (1997). Eccentricity forcing of Pliocene-Early Pleistocene climate revealed in a marine oxygen-isotope record, *Letters to Nature, 385***,** 801-804

Cochrane, M.A., Ryan, K.C. (2009). Fire and fire ecology: concepts and principles. In M.A. Cochrane (Ed.), *Tropical Fire Ecology: Climate Change, Land Use and Ecosystem, Dynamics.* (pp. 24 – 62). Berlin:Springer

Cohen, A. S., Coe, A. L., Harding, S. M. & Schwark, L. (2004). Osmium isotope evidence for the regulation of atmospheric CO_2 by continental weathering. *Geology 32*, 157–160.

Cohen, A.S., Coe, A.L., Kemp, D.B. (2007). The Late Palaeocene-Early Eocene and Toarcian (Early Jurassic) carbon isotope excursions: a

comparison of their time scales, associated environmental changes, causes and consequences, *Journal of the Geological Society*, *164,* 1093-1108

Collins, B.M., Kelly, M., van Wagtendonk, J.W., Stephens, S.L. (2006). Spatial patterns of large natural fires in Sierra Nevada wilderness areas*. Landscape Ecology. 22,* 545– 557. doi:10.1007/s10980-006-9047-5.

Collinson, ME., Hooker, J.J., Gröcke, D.R. (2003). Cobham Lignite Bed and penecontemporaneous macrofloras of southern England: A record of vegetation and fire across the Paleocene-Eocene Thermal Maximum, Wing S.L., Gingerich P.D., Schmitz B. (Eds)., *Causes and Consequences of Globally Warm Climates in the Early Paleogene: Boulder, Colorado, Geological Society of America Special Paper, 369,* 333-349

Colman, A. S. & Holland, H. D. (2000). In C.R. Glenn, L. Prévôt, & P. Lucas, (Eds.). *Marine Authigenesis: from global to microbial, Chapter: The global diagenetic flux of phosphorus from marine sediments to the oceans: redox sensitivity and the control of atmospheric oxygen levels* (pp 53–75) Society for Sedimentary Geology.

Colman, S.M., Peck, J.A., Karabanov, E.B., Carter, S.J., Bradbury, J.P., King, J.W., Williams, D.F. (1995). Continental climate response to orbital forcing from biogenic silica records in Lake Baikal, *Letters to Nature, 378***,** 769-771

Condie, K.C. (2004). Supercontinents and superplume events: distinguishing signals in the geologic record, *Physics of the Earth and Planetary Interiors, 146*, 319-332

Condie, K.C., Des Marais, D.J., Abbott, D. (2001). Precambrian superplumes and supercontinents:a record in black shales, carbon isotopes, and paleoclimates? *Precambrian Research, 106*, 239-260

Conedera M., Tinner W., Neff C., Meurer M., Dickens A.F., Krebs P. (2009), Reconstructing past fire regimes: methods, applications, and relevance to fire management and conservation, *Quaternary Science Reviews, 28*, 555- 576

Cope, M.J. (1980). Physical and chemical properties of coalified and charcoalified phytoclasts from some British Mesozoic sediments: *An organic geochemical approach to palaeobotany, Physics and Chemistry of the Earth*, *12*, 663-677

Cope, M.J., Chaloner, W.G. (1980). Fossil charcoal as evidence of past atmospheric composition, *Nature, 283,* 647-649

Cowan, N.B., Voigt, A., Abbot, D.S. (2012). Thermal phases of Earth-like planets: estimating inertia from eccentricity, obliquity, and diurnal forcing, *The Astrophysical Journal, 757*, 1-13

Coward, H.F., Jones, G.W. (1952). Limits of flammability of gases and vapours. *Bulletin 503 Bureau of Mines*

Crawford, A.J., Baker, S.J., Belcher, C.M. (2017). Fossil charcoals from the Lower Jurassic challenge assumptions on charcoal morphology and identification. *Palaeontology* (in press).

Crawford, A.J., Belcher, C.M (2015). Area–volume relationships for fossil charcoal and their relevance for fire history reconstruction. *The Holocene. 26,* 822-826

Croll, J. (1875). *Climate and Time and their Geological Relations.* Daldy, Isbister and Co., London

Croll, J. (1885). *Climate and Cosmology.* Adam and Charles Black, Edinburgh.

Cui, Y., Kump, L.R., Ridgwell, A.J., Charles, A.J., Junium, C.K., Diefendorf, A.F., Freeman, K.H., Urban, N.M., Harding, I.C. (2011). Slow release of fossil carbon during the Palaeocene-Eocene Thermal Maximum, *Nature Geoscience*, *4*, 481-485

Cwynar, L.C. (1987). Fire and the forest history of the North Cascade Range, *Ecology*. *68,* 791-802

D'Costa D.M., Grindrod J., Ogden R. (1993). Preliminary environmental reconstructions fromlate Quaternary pollen and mollusc assemblage at Egg Lagoon, King Island, Bass Strait. *Austral Ecology. 18.* 351-366

Dale, V. H., Joyce, L.A., McNulty, S., Neilson, R.P., Ayres, M.P., Flannigan, M.D., Hanson, P.J. '…' Wotton, M. (2001). Climate change and forest disturbances. *Bioscience 51,* 723–73

Dale, V.H., Joyce, L.A., McNulty, S., Neilson, R.P., Ayres, M.P., Flannigan, M.D., '...' Wotton B.M. (2001), *Climate Change and Forest Disturbances, Bioscience*, *51*, 723-734

Daniau, A.L., Sanchez Goni, M.F., Beaufort, D., Laggoun-Défarge, F., Loutre, M.F., Duprat, J. (2007). Dansgaard-Oeschger climatic variability revealed by fire emissions in southwestern Iberia. *Quaternary Science Reviews. 26,* 1369-1383

Daniau, A.L., Sanchez Goni, M.F., Martinez, P., Urrego, D.H., Bout-Roumazeilles, V., Desprat, S., Marlon, J.R. (2013). Orbital-scale climate forcing of grassland burning in southern Africa. *PNAS. 26,* 5069-5073

Davis, R.B. (1967). Pollen studies of near-surface sediments in Maine lakes. In Cushing, E.J. and Wright, H.E., (Eds.) *Quaternary palaeoecology*, (pp. 143-174). New Haven: Yale University Press

DeBano, L.F. (1990). The effect of fire on soil properties. *SOLO, Paper presented at the Symposium on Management and Productivity of Western-Montane Forest Soils, Boise.* Retrieved on 5th August 2016 from https://forest.moscowfsl.wsu.edu/smp/solo/documents/GTRs/INT_280/DeBano_INT-280.php

Denis, E.H., Toney, J.L., Tarozo, R., Anderson, R.S., Roach,L.D., Huang, Y. (2012). Polycyclic aromatic hydrocarbons (PAHs) in lake sediments record historic fire events: Validation using HPLC-fluorescence detection. *Organic Geochemistry. 45,* 7-17

Dera, G, Brijaud, B., Monna, F., Laffont, R., Pucéat, E., Deconinck, J-F., Pellenard, P., Joachimski, E., Durlet, C. (2011) Climatic ups and downs in a disturbed Jurassic world. *Geology 39*, 215–218.

Dera, G. & Donnadieu, Y. (2016). Modeling evidence for global warming, Arctic seawater freshening, and sluggish oceanic circulation during the Early Toarcian anoxic event. *Paleoceanography 27,* 1–15.

Dera, G., Pellenar, P., Neige, P., Deconinck, J-F., Pucéat, E., Dommergues, J-L. (2009). Distribution of clay minerals in Early Jurassic Peritethyan seas: palaeoclimatic significance inferred from multiproxy comparisons. *Palaeogeography, Palaeoclimatology, Palaeoecology. 271,* 39–51

Demaison, G.J., Moore, G.T. (1980), Anoxic environments and oil source bed genesis, *Organic Geochemistry, 2,* 9-31

De Vernal, A., Bilodeau, G., and Henry, M. (2010). Micropaleontological Preparation Techniques and Analyses. *Cahier du Geotop n°3*

Diaz, R.J., Rosenburg, R. (2008). Spreading Dead Zones and Consequences for Marine Ecosystems, *Science, 321,* 926-929

Dickens, G.R. (2000). Methane oxidation during the late Palaeocene thermal maximum, *Societe Geologique de France, 171*, 37-49

Dickens, G.R., Castillo, M.M., Walker, J.C.G. (1997). A blast of gas in the latest Paleocene: Simulating first-order effects of massive dissociation of oceanic methane hydrate, *Geology*, *25*, 259-262

Dickens, G.R., O'Neil, J.R., Rea, D.K., Owen, R.M. (1995). Dissociation of oceanic methane hydrate as a cause of the carbon isotope excursion at the end of the Paleocene, *Paleoceanography*, *10,* 965-971

Dickson, A.J., Jenkyns, H.C., Porcelli, D., van den Boorn, S. and Idiz, E. (2016). Basin-scale controls on the molybdenum-isotope composition of seawater during Oceanic Anoxic Event 2 (Late Cretaceous). *Geochimica, Cosmochimica Acta*, *178,* 291–306.

Dobson, M. R. & Whittington, R. J. (1987). The geology of Cardigan Bay. *Proceedings of the Geological Association. 98,* 331–353

Duarte, L. V. (2007). In R.B., Rocha, (Ed.) *The Peniche Section (Portugal). Contributions to the definition of the Toarcian GSSP* (pp17–23) International Subcommission of Jurassic Stratigraphy

Duarte, L.V., Silva, R.L., Oliveira, L.C.V., Comas-Rengifo, M.J., Silva, F. (2010). Organic-Rich facies in the Sinemurian and Pliensbachian of the Lusitanian Basin, Portugal: Total organic carbon distribution and relation to transgressive-regressive facies cycles, *Geologica Acta. 8(3),* 325-340

Dubiel, R.F., Parrish, J.T., Parrish, J.M., Good, S.C. (1991). The Pangean Megamonsoon-Evidence from the Upper Triassic Chinle Formaiton, Colorado Plateau, *USGS Staff—Published Research, Paper 218*

Duffin, K.I., Gillson, L., Willis, K.J. (2008). Testing the sensitivity of charcoal as an indicator of fire events in savannah environments: quantitative predictions of fire proximity, area and intensity, *The Holocene*, *18,2*, 279-291

Durne, S.E., McVean, D.N. (1959). Forest History of the Beinn Eighe Nature Reserve, *New Phytologist, 58(2),* 228-236

Du Vivier, A.D.C., Jacobson, A.D., Lehn, G.O., Selby, D., Hurtgen, M.T., Sageman, B.B. (2015). Ca isotope stratigraphy across the Cenomanian–Turonian OAE 2: Links between volcanism, seawater geochemistry, and the carbonate fractionation factor. *Earth and Planetary Science Letters. 416,* 121-131.

Du Vivier, A.D.C., Selby, D., Sageman, B.B., Jarvis, I., Gröcke, D.R., Voigt, S. (2014). Marine $^{187}Os/^{188}Os$ isotope stratigraphy reveals the interaction of volcanism and ocean circulation during Oceanic Anoxic Event 2. *Earth and Planetary Science Letters. 389,* 23-33

El Beialy, S. Y., Zobaa, M. K. & Taha, A. A. (2016) Depositional palaeoenvironment and hydrocarbon source potential of the Oligocene Dabaa Formation, north Western Desert, Egypt: a palynofacies approach. *Geosphere 12,* 346–353

Elder, W.P. (1985). Biotic patters across the Cenomanian–Turonian extinction boundary near Pueblo, Colorado, in Pratt, L.M., Kauffman, E.G., and Zelt, .B., (Eds)., *Fine-Grained Deposits and Biofacies of the Cretaceous Western Interior Seaway:Evidence of Cyclic Sedimentary Processes: SEPM, Field Trip Guidebook 4*, 157–169.

Elder, W.P., (1991), Molluscan paleoecology and sedimentation patterns of the Cenomanian–Turonian extinction interval in the southern Colorado plateau region, in Nations, J.D., and Eaton, J.G., (Eds)., Stratigraphy, Depositional Environments, and Sedimentary Tectonics of the Western Margin, Cretaceous Western Interior Seaway: *Geological Society of America, Special Paper 260*, 113–137

Elder, W.P., Gustason, E.R., Sageman, B.B. (1994). Correlation of basinal carbonate cycles to nearshore parasequences in the Late Cretaceous Greenhorn Seaway, Western Interior, U.S.: Geological Society of America, Bulletin, *106*, 892–902.

Elder, W.P., Kirkland, J.I. (1985). Stratigraphy and Depostional Enviornments of the Bridge creek Limestone Member of the Greenhorn Limestone at Rock Canyon Anticline near Pueblo, Colorado. In: Pratt, L.A., Kauffman, E.G., Zelt, F.B. (Eds.), *Fine Grained Deposits and Biofacies of the Cretaceous Western Interior Seaway: Evidence of Cyclic Sedimentary Processes. Field Trip Guidebook*, *vol. 4.* (pp. 122 – 134). Society of Economic Paleontologists and Mineralogists, Tulsa

Eldrett J.S., Ma C., Bergman S.C., Ozkan A., Minisini D., Lutz B., Jackett S-J., Macaulay C., Kelly A.E. (2015a). Origin of limestone–marlstone cycles: Astronomic forcing of organic-rich sedimentary rocks from the Cenomanian to early Coniacian of the Cretaceous Western Interior Seaway, USA, *Earth and Planetary Science Letters, 423***,** 98-113

Eldrett, J.S., Ma, C., Bergman, S.C., Lutz, B., Gregory, F.J., Dodsworth, P. '…' Kelly, A.E. (2015b). An astronomically calibrated stratigraphy of the Cenomanian, Turonian and earliest Coniacian from the Cretaceous Western Interior Seaway, USA: Implications for global chronostratigraphy, *Cretaceous Research. 56,* 316-344

Elmi, S., (2007). Pliensbachian/Toarcian boundary: the proposed GSSP of Peniche (Portugal), *Volumina Jurassica, 4*, 5-16

Elmi, S., (2006), Pliensbachian/Toarcian boundary: The proposed GSSP of Peniche (Portugal), *Volumina Jurassica IV*, 5-16

Enache M.D., Cumming B.F., (2006). Tracking recorded fires using charcoal morphology from the sedimentary sequence of Prosser Lake, British Columbia (Canada), *Quaternary Research, 65*, 282-292

Enache, M.D., Cumming, B.F., (2007). Charcoal morphotypes in lake sediments from British Columbia (Canada): an assessment of their utility for the reconstruction of past fire and precipitation, *Journal of Paleolimnology, 38(3)*, 347-363

Engebreston, D.C., Kelley, K.P., Cashman, H.J., Richards, M.A., (1992). 180 million years of subduction, *GSA Today*, *2*, 93-100

Erba, E., Bartolini, A., Larson, R.L. (2004). Valanginian Weissert oceanic anoxic event. *Geology. 32,* 149-152, doi: https://doi.org/10.1130/Go20008.1

Erbacher, J., (1994). Entwicklung und Palaiozeanographie mittel- kretazischer Radiolarien der estlichen Tethys (Italien) und des Nordatlantiks. *Tabinger Mikropal~iontol. Mitt. 12*, 120

Erbacher J., Thurow J., (1998). Mid Cretaceous Radiolarian Zonation, Cramp A., (Eds.), *Geological Evolution of Ocean Basin: Results from the Ocean Drilling Program,* 71 -81

Erbacher J., Thurlow J., Littke R., (1996). Evolution patterns of radiolarian and organic matter variations: A new approach to identify sea-level changes in Mid-Cretaceous pelagic environments*, Geology, 24*, 499-502

Fabry, V.J., Seibel, B.A., Feely, R.A., Orr, J.C., (2008). Impacts of ocean acidification on marine fauna and ecosystem processes, *ICES Journal of Marine Science, 65*(3), 414-432 doi: 10.1093/icesjms/fsn048

Fahl, K., Stein, R. (1997). Modern organic carbon deposition in the Laptev Sea and the adjacent continental slope: surface water productivity vs. terrigenous input. *Organic Geochemistry. 26*, 379-390

Falcon-Lang, H.J., (1998). The impact of wildfire on an Early Carboniferous coastal environment, North Mayo, Ireland. *Palaeogeography, Palaeoclimatology, Palaeoecology.139*,121-138.

Falkowski, P., Katz, M., Milligan, M., Fennel, K., Cramer, B., Aubry, M.P., Berner, R.A., Zapol, W.M., (2005). The rise of atmospheric oxygen levels over the past 205 million years and the evolution of large placental mammals, *Science, 309*, 2202-2204

Fernandes, P.M., Rego, F.C. (1998). A New Method to Estimate Fuel Surface Area-to-Volume Ratio Using Water Immersion. *International Journal of Wildland Fire. 8(3),* 121-128

Ferrio J.P., Voltas J., Araus J.L. (2003). Use of carbon isotope composition in monitoring environmental changes, *Management of Environmental Quality, 14*,82-98

Finkelstein D.B., Pratt L.M., Brassell S.C., (2006). Can biomass burning produce a globally significant carbon-isotope excursion in the sedimentary record?, *Earth and Planetary Science Letters*, *250*, 501-510

Fischer H., Schüpbach S., Gfeller G., Bigler M., Röthlisberger R., Erhardt T., Stocker T.F., Mulvaney R., Wol E.W. (2015). Millennial changes in North American wildfire and soil activity over the last glacial cycle, *Nature Geoscience, 8,* 723-728

Flannigan, M.D., Krawchuk, M.A., de Groot, W.J. Wotton, B.M., Gowman, L.M. (2009). Implications of changing climate for global wildland fire. *International Journal of Wildland Fire. 18,* 483 – 507. doi: 10.1071/WF08187

Flannigan, M.D., Wotton, B.M. (1990). Lightning-ignited forest fires in northwestern Ontario. *Canadian Journal of Forest Research. 21,* 277-287

Flannigan, M.D., Stocks, B.J., Wotton, B.M. (2000). Climate change and forest fires. *The Science of the Total Environment. 262,* 221-229

Flannigan, M.D., Stocks, B.J., Turetsky, M.R., Wotton, B.M. (2009). Impact of climate change on fire activity and fire management in the circumboreal forest. *Global Change Biology. 15,* 549–560. doi:10.1111/j.1365-2486.2008.01660.x

Flannigan, M.D., Wotton, B.M. (2001). Climate, weather, and area burned. In: Johnson, E.A., Miyanishi, K. (Eds) *Forest fires behavior and ecological effects*. (pp 351–373). Academic, New York

Flögel S., Wallmann K., Poulsen C.J., Zhou J., Oschlies A., Voigt S., Kuhnt W., (2011). Simulating the biogeochemical effects of volcanic CO2 degassing on the oxygen-state of the deep ocean during the Cenomanian/Turonian Anoxic Event (OAE2), *Earth and Planetary Science Letters*, *305*, 371-384

Föllmi, K.B. (1996). The phosphorus cycle, phosphogenesis and marine phosphate-rich deposits. *Earth-Science Reviews. 40,* 55-124

Föllmi, K.B., Bôle, M., Jammet, N., Froidevaux, P., Godet, A., Bodin, S., Adatte, T., Matera, V., Fleitmann, D., Spangenberg, J.E., (2012). Bridging the Faraoni and Selli oceanic anoxic events: late Hauterivian to early Aptian dysaerobic to anaerobic phases in the Tethys, *Climate of the Past, 8*, 171-189

Forbes, M.S., Raison, R.J., Skjemstad, J.O., (2006). Formation, transformation and transport of black carbon (charcoal) in terrestrial and aquatic ecosystems, *Science of the Total Environment. 370*, 190-206

Forest Service. (2015). The rising cost of wildfire operations: Effects on the Forest Service's Non-Fire Work. *United States Department of Agriculture.* 1-16

Forkel M., Dorigo W., Lasslop G., Teubner I., Chuvieco E., Thonicke K. (2016). Identifying required model structures to predict global fire activity from satellite and climate data, *Geoscientific Model Development Discussions*, 1-35, doi:10.5194/gmd-2016-301

Forster, A., Schouten, S., Moriya, K., Wilson, P.A., Sinninghe Damsté, J.S. (2007). Tropical warming and intermittent cooling during the Cenomanian/Turonian oceanic anoxic event 2: Sea surface temperature records from the equatorial Atlantic. *Paleoceanography. 22,* doi: 10.1029/2006PA001349

Frakes, L.A. (1978). *Climates Throughout Geologic Time, Elsevier Scientific Publishing Company*, Amsterdam-Oxford-New York:160-178

Frijia G., Parente M. (2008). Strontium isotope stratigraphy in the upper Cenomanian shallow-water carbonates of the southern Apennines: Short-term perturbations of marine $^{87}Sr/^{86}Sr$ during the oceanic anoxic event 2, *Palaeogeography, Palaeoclimatology, Palaecology, 261,* 15-29

Froelich P.N., Klinkhammer G.P., Bender M.L., Luedke N.A., Heath G.R., Cullen D., Dauphin P. (1979). Early oxidation of organic matter in pelagic sediments of the eastern equatorial Atlantic: suboxic diagenesis, *Geochemica et Cosmochimica Acta, 43*, 1075-1090

Frueh, W.T., Lancaster, S.T. (2014). Correction of deposit ages for inherited ages of charcoal: implications for sediment dynamics inferred from random sampling of deposits on headwater valley floors, *Quaternary Science Reviews. 88*, 110-124

Fuquay, D.M., Baughman, R.G., Latham, D.J. (1979). A model for predicting lightning fire ignition in wildland fuel. *USDA Forest Service. Intermountain Forest and Range Experiment Station, Research Paper INT-217*, Ogden, UT

Gaffin, S., (1987). Ridge volume dependence on seafloor generation rate and inversion using long term sealevel change, *American Journal of Science*, *287*, 596-611

Gale A.S., Christensen W.K. (1996). Occurrence of the belemnite Actinocamax plenus in the Cenomanian of SE France and its significance, *Bulletin go the Geological Society of Denmark*, *43,* 68-77

Gale A.S., Jenkyns H.C., Kennedy W.J., Corfield R.M. (1993). Chemostratigraphy versus biostratigraphy: data from around the Cenomanian-Turonian boundary., *Journal of the Geological Society London, 150*, 29-32

Gallagher, R.V., Beaumont, L.J., Hughes, L., Leishman, M.R. (2010). Evidence for climatic niche and biome shifts between native and novel ranges in plant species introduced to Australia. *Journal of Ecology. 98,* 1-10. doi: 10.1111/j.1365-2745.2010.01677.x

Ganino C., Arndt N.T., (2009). Climate changes caused by degassing of sediments during the emplacement of large igneous provinces, *Geology, 37*, 323-326, doi: 1130/G25325A.1

Gardner, J.J., Whitlock, C., (2001). Charcoal accumulation following a recent fire in the Cascade Range, Northwestern USA, and its relevance for fire history studies, *The Holocene, 11,5*, 541-549

Garrels, R. & Lerman, A. (1984). Coupling of the sedimentary sulfur and carbon-cycles-an improved model. *American Journal of Science. 284,* 989–1007

Gautier, D.L., Kharaka, Y.K., Surdam, R.C. (1985). Relationships of organic matter and mineral diagenesis, *SEPM.* Retrieved on 1st June 2017 from http://scnotes.sepmonline.org/content/sepscrel/1/local/front-matter.pdf

Gedney N., Cox P.M., Betts R.A., Boucher O., Huntingford C., Stott P.A. (2006). Detection of a direct carbon dioxide effect in continental river runoff records, *Nature, 439,* 835-838

Gélinas, Y., Prentice, K.M., Baldock, J.A., Hedges, J.I., (2001). An improved thermal oxidation method for the quantification of soot/graphitic black carbon in sediments and soils, *Journal of Environmental Science and Technology 35(7)*, 3519 – 3525.

Gibbons, P., Bommel, L.V., Gill, A.M., Cary, G.J., Driscoll, D.A., Bradstock, R.A., Knight, E., Mortiz, M.A., Stephens, S.L., Lindenmayer, D.B. (2012). Land Management Practices Associated with House Loss in Wildfires. *PLOS one. 7,* 1 – 7, doi: 10.1371/journal.pone.0029212

Gilbert, G.K. (1895). Sedimentary measurement of geologic time. *The Journal of Geology. 3,* 121–127.

Gilbert, D. (2017). Oceans lose oxygen, *Nature. 542,* p. 303-304

Gill, B. C., Lyons, T. W. & Jenkyns, H. C. (2011). A global perturbation to the sulfur cycle during the Toarcian Oceanic Anoxic Event. *Earth and Planetary Science Letters. 312,* 484–496

Glasspool, I. J., Edwards, D., Axe, L. (2004). Charcoal in the Silurian as evidence for the earliest wildfire. *Geology 32,* 381–383. Doi:10.1130/G20363.1

Glasspool, I.J., Scott, A.C., (2010). Phanerozoic concentrations of atmospheric oxygen constructed from sedimentary charcoal, *Nature Geoscience. 3,* 627 – 630, doi:10.1038/NGEO923

Glasspool, I.J., Scott, A.C. (2013). Identifying Past Fire Events. In C.M. Belcher (Ed.). *Fire Phenomena and the Earth System, An Interdisciplinary Guide to Fire Science.* (pp. 179 – 207). West Sussex: John Wiley and Sons

Glasspool, I.J., Scott, A.C., Waltham, D., Pronina, N., Shao, L. (2015). The impact of fire on the Late Paleozoic Earth System. *Frontiers in Plant Science. 6,* 1-13. doi: 10.3389/fpls.2015.00756

Gorin G.E., Steffan D. (1991). Organic facies as a tool for recording eustatic variatiosn in marine fine-grained carbonates – example of the Berriasian stratotype at Berrias (Ardèche, SE France), *Palaeograography, Palaeoclimatology, Palaeoecology*, *85,* 303-320, DOI: 0031-0182/91/$03.50

Gradstein S.R., Kerp H. (2012). 12. A Brief History of Plants on Earth. Gradstein F.M., Ogg J.G., Schmitz M., Ogg M.G. (Eds.). *The Geologic Time Scale 2012. Volume 1*. Elsevier. Oxford.

Graham S. (2000). Milutin Milankovitch (1879-1958), NASA Earth Observatory, retrieved on 28th February 2017 from http://earthobservatory.nasa.gov/Features/Milankovitch/

Greisman, A., Gaillard, M-J. (2009). The role of climate variability and fire in early and mid Holocene forest dynamics of southern Sweden. *Journal of Quaternary Science. 24,* 593-611

Griffin J.J., Goldberg E.D. (1975). The fluxes of elemental carbon in coastal marine sediments, *Limnology and Oceanography, 20,* 456-463, doi: 10.4319/lo.1975.20.3.0456

Grissino-Mayer, H.D., Swetnam, T.W. (2000). Century-scale climate forcing of fire regimes in the American Southwest. *The Holocene. 10,2.* 213-220

Gröcke, D.R., Hesselbo, S.P., Jenkyns, H.C., (1999). Carbon-isotope composition of Lower Cretaceous fossil wood: Ocean-atmosphere chemistry and relation to sea-level change, *Geology*, *27*, 155-158

Gröcke, D.R., Price, G.D., Barabochkin, E., Mutterlose, J., Ruffell, A.H., (2003). The Valanginian terrestrial carbon-isotope record, *Geophysical Research Abstracts*, 5, EAE03-A-13644

Gu, B., Alexander V. (1996). Stable Carbon Isotope Evidence for Atmospheric CO2 Uptake by Cyanobacterial Surface Scums in a Eutrophic Lake, *Applied and Environmental Microbiology*, 1803-1804

Guo, H., Du Y., Kah L.C., Huang J., Hu C., Huang H., Yu W., (2013). Isotopic composition of organic and inorganic carbon from the Mesoproterozoic Jixian Group, North China: Implications for biological and oceanic evolution, *Precambrian Research, 224*, 169-183

Guyette, R.P., Thompson F.R., Whittier J., Stambaugh M.C., Dey D.C. (2014). Future Fire Probability Modeling with Climate Change Data and Physical Chemistry, *Forest Ecology, 60,* 862-870

Habicht, K.S., Canfield, D.E., (1997). Sulfur isotope fractionation during bacterial sulfate reduction in organic-rich sediments, *Geochemica et Cosmochimica Acta, 61(24*), 5351-5361

Hallam, A. (1994). Chapter 10. Jurassic climate as inferred form the sedimentary and fossil record, *Palaeoclimates and their modelling, With special reference to the Mesozoic era, Springer Netherlands,* 79-88

Hallam, A. (1982). Chapter 17. The Jurassic Climate, *Climate in Earth History: Studies in Geophysics, Studies in Geophysics,* 150-198

Hallam, A., (1984). Distribution of fossil marine invertebrates in relation to climate, P.J. Brenchley, (Ed)., *Fossils and Climate*, (pp. 107-125) Wiley, London

Hallam, A., Cohen J.M. (1989). The Case for Sea-Level Change as a Dominant Casual Factor in Mass Extinction of Marine Invertebrates (and Discussion), *Philosophical Transactions of the Royal Society B, 325,* 437-455

Handoh, I.C., Lenton, T.M., (2003). Periodic-Mid Cretaceous Oceanic anoxic events linked by oscillations of the phosphorous and oxygen biogeochemical cycles. *Global Biogeochemical Cycles. 17,* 1 – 11.

Harberle S.G., Hope G.S., van der Kaars S. (2001). Biomass burning in Indonesia and Papua New Guinea: natural and human induced fire events in the fossil record, *Palaeogeography, Palaeoclimatology, Palaeoecology, 171*, 259-268

Harberle, S.G., Ledru, M-P. (2001). Correlations among Charcoal Records of Fires from the Past 16,000 Years in Indonesia, Papua New Guinea, and Central and South America. *Quaternary Research. 55,* 97-104

Harris, T.M., (1981). Burnt ferns from the English Wealden, *Proceedings of the Geological Association*, *92*, 47-58

Harris, T.M., (1958). Forest Fire in the Mesozoic, *Journal of Ecology*, *46(2*), 447-453

Harris, T.M., (1961). The Yorkshire Jurassic Flora. I. Thallophyta-Pteridophyta, British Museum (Natural History) London

Harris, T.M., (1980). The Yorkshire Jurassic fern Phlebopteris braunii (Geoppert) and its reference to Matonia R. Br., Bulletin of the British Museum (Natural History). *Geology, 33*, 295-311

Harvey L.D.D. (1989). Milankovitch Forcing, Vegetation Feedback, and North Atlantic Deep-Water Formation, *Journal of Climate, 2,* 800-815

Hasegawa, T., Pratt, L.M., Maeda, H., Shigeta, Y., Okamoto, T., Kase, T., Uemura, K., (2003). Upper Cretaceous stable carbon isotope stratigraphy of terrestrial organic matter from Sakhalin, Russian Far East: A proxy for the isotopic composition of paleoatmospheric CO_2: *Palaeogeography, Palaeoclimatology, Palaeoecology, 189*, 97-115

Hayes J.M. (1993). Factors controlling 13C contents of sedimentary organic compounds: Principles and evidence, *Marine Geology, 113*, 111-125

Hays J.D., Imbrie J., Shackleton N.J. (1976). Variations in the Earth's Orbit: Pacemaker of the Ice Ages, *Science, 194*, 1121-1132

He, T., Pausas, J.G., Belcher, C.M., Schwilk, D.W., Lamont, B.B. (2012). Fire-adapted traits of Pinus arose in the fiery Cretaceous. *New Phytologist. 194,* 751-759, doi: 10.1111/j.1469-8137.2012.04079.x

Hedges, J.I., Mann, D.C. (1979). The lignin geochemistry of marine sediments from the southern Washington coast, *Geochemica et Cosmochemica Acta, 43*, 1809-1818

Heilman, W.E., Bian, X., (2010). Turbulent kinetic energy during wildfires in the north central and north-eastern US, *International Journal of Wildland Fire. 19*, 346-363

Hély, C., Flannigan, M., Bergeron, Y., McRae D. (2001). Role of vegetation and weather on fire behavior in the Canadian mixed wood boreal forest using two fire behavior prediction systems, *Canadian Journal of Forest Research Reviews. 31,* 430-441

Herbert-Smith, M. (1979). The age of the Tertiary deposits of the Llanbedr (Mochras Farm) borehole as determined from palynological studies, *The Tertiary rocks at the Llanbedr (Mochras Farm) Borehole, Report of the Institute of Geological Sciences, 78/24*, 15-29

Hermoso, M., Le Callonnec, L., Minoletti, F., Renard, M., Hesselbo, S.P., (2009). Expression of the Early Toarcian negative carbon-isotope excursion in separated carbonate microfractions (Jurassic, Paris Basin), *Earth and Planetary Science Letters, 277*, 194-203

Herrle J.O., Kößler P., Friedrich O., Erlenkeuser H., Hemleben C., (2004). High-resolution carbon isotope records of the Aptian to Lower Albian from SE France and the Mazagan Plateau (DSDP Site 545): a stratigraphic tool for paleoceanographic and paleobiologic reconstruction, *Earth and Planetary Science Letters, 218*, 149-161

Hesselbo, S. P. Bjerrum, C., Hinnov, L., MacNiocaill, C., Miller, K., Riding, J., Van de Schootbrugge, B. (2013). Mochras borehole revisited: a new global standard for Early Jurassic earth history. *Scientific Drilling, 16***,** 81-91 doi:10.5194/sd-16-81-2013

Hesselbo S.P., Gröcke D.R., Jenkyns H.C., Bjerrum C.J., Farrimand P., Morgans Bell H.S., Green O.R., (2000). Massive dissociation of gas-hydrate during a Jurassic oceanic anoxic event, *Letters to Nature*, *406*, 392-395

Hesselbo, S. P., Jenkyns, H. C., Duarte, L. V. & Oliveira, L. C. V. (2007). Carbon-isotope record of the Early Jurassic (Toarcian) Oceanic Anoxic Event from fossil wood and marine carbonate (Lusitanian Basin, Portugal). *Earth and Planetary Science Letters 253,* 455–470

Hesselbo, S. P. & Pieńkowski, G. (2011). Stepwise atmospheric carbon-isotope excursion during the Toarcian Oceanic Anoxic Event (Early Jurassic, Polish Basin). *Earth and Planetary Science Letters. 301,* 365–372

Higgins, J.A., Schrag, D.P. (2006). Beyond methane: Towards a theory for the Paleocene-Eocene Thermal Maximum, *Earth and Planetary Science Letters*, *245*, 523-537

Higuera, P.E., Gavin, D.G., Bartlein, P.J., Hallett, D.J. (2011). Peak detection in sediment–charcoal records: impacts of alternative data analysis methods on fire-history interpretations, *International Journal of Wildland Fire. 19,* 996-1014

Hilgen, F., Hinnov, L.A., Aziz, A., Abels, A., Batenburg, S., Bosmans, S., '...' Zeeden, C. (2015). Stratigraphic continuity and fragmentary sedimentation: the success of cyclostratigraphy as part of integrated stratigraphy. In. D.G. Smith., R.J. Bailey., P.M. Burgess., A.J. Fraser, (Eds.)., Strata and Time: Probing the Gaps in Our Understanding. (pp 157-197). *The Geological Society of London, Special Publications. 404,* Oxford

Hilgen, F.J., Krijgsman, W., Langereis, C.G., Lourens, L.J., Santarelli, A., Zachariasse W.J. (1995). Extending the astronomical (polarity) time scale into the Miocene. *Earth and Planetary Science Letters. 136*, 495-510. doi.org/10.1016/0012-821X(95)00207-S

Hinnov L.A. (2013). Cyclostratigraphy and its revolutionizing applications in the earth and planetary sciences, *Geological Society of America Bulletin, 125,* 1703-1734

Hirota, M., Holmgren, M., Van Nes, E.H., Scheffer, M. (2011). Global Resilience of Tropical Forest and Savanna to Critical Transitions. *Science. 334,* 232-235, doi: 10.1126/science.1210465

Hodell, D.A., Mueller, P.A., McKenzie, J.A., Mead, G.A., (1989). Strontium isotope stratigraphy and geochemistry of the late Neogene ocean, *Earth and Planetary Science Letters. 92,* 165-178

Hoegh-Guldberg, O. & Bruno, J. F. (2010). The impact of climate change on the World's marine ecosystems. *Science. 328,* 1523–1528

Hoffmann, W.A., Jaconis, S., McKinley, K.L., Geiger, E.L., Gotsch, S.G., Franco, A.C. (2012). Fuels of microclimate? Understanding the drivers of fire feedbacks at savannah-forest boundaries, *Austral Ecology, 37,* 634-643

Holford S.P., Green P.F., Turner J.P. (2005). Palaeothermal and compaction studies in the Mochras borehole (NW Wales) reveal early Cretaceous and Neogene exhumation and argue against regional Palaeogene uplift in the southern Irish Sea, *Journal of the Geological Society, 162*, 829-840

Holland, H.D., (1984). The Chemical Evolution of the Atmosphere and Oceans, Princeton Series in Geochemistry, Princetown University Press, New Jersey

Horn, S.P., Underwood, C.A. (2014). Methods for the study of soil charcoal as an indicator of fire and forest history in the Appalachian region, U.S.A. In. T.A. Waldrop, (Ed.). *Proceedings, Wildland Fire in the Appalachians: Discussions among managers and Scientists*. (pp 104-110). Asheville, NC: U.S. Department of Agriculture Forest Service, Southern Research Station.

Hotinski R.M., Bice K.L., Kump L.R., Najjar R.G., Arthur M.A., (2001). Ocean stagnation and end-Permian anoxia, *Geology, 29*, 7-10

House M.R. (1995). Orbital forcing timescales: an introduction, *Geological Society of London Special Publications, 85,* 1-18

Hu, X., Jansa, L., Wang, C., Sarti, M., Bak, K., Wagreich, M., Michalik, J., Soták J. (2005). Upper Cretaceous oceanic red beds (CORBs) in the Tethys: occurrences, lithofacies, age, and environments, *Cretaceous Research, 26*,3-20

Hu, X., Scott, R.W., Cai, Y., Wang, C., Melinte-Dobrinescu, M.C. (2012). Cretaceous oceanic red beds (CORBs): Different time scales and models of origin, *Earth Science Reviews, 115,* 217-248

Huang E., Tian J., Qiao P., Wan S., Xie X., Yang W. (2015). Early interglacial carbonate-dilution events in the South China Sea: Implications for strengthened typhoon activities over subtropical East Asia. *Quaternary Science Reviews. 125*. 61-77

Huang, C. & Hesselbo, S. P. (2014). Pacing of the Toarcian Oceanic Anoxic Event (Early Jurassic) from astronomical correlation of marine sections. *Gondwana Research. 25,* 1–8

Hudspith, V.A., Belcher, C.M. (2017). Fire biases the production of charred flowers: Implications for the Cretaceous fossil record. *Geology,* doi: 10.1130/G39093.1

Hudspith, V.A., Belcher, C.M., Kelly, R., Hu, F.S. (2015). Charcoal Reflectance Reveals Early Holocene Boreal Deciduous Forests Burned at High Intensities. *Plos One.* 1-11, doi:10.1371/journal.pone.0120835

Hunt, J.M., (1979). Origin and Migration, How Gas Forms. *Petroleum Geochemistry and Geology*, W.H. Freeman and Company, 150-186

Hutchinson G.E., Goulden C.E., (1966). The history of Laguna de Petenxil; The plant microfossils, *Memoirs of the Connecticut Academy of Arts and Science, 17*, 67-73

Huybers P. (2007). Glacial variability over the last two million years: an extended depth-derived agemodel, continuous obliquity pacing, and the Pleistocene progression, *Quaternary Science Reviews, 26,* 37-55

Huybers, P., and C. Wunsch (2005). Obliquity pacing of late Pleistocene glacial terminations, *Nature. 434,* 491 – 494.

Iglesias V., Yospin G.I., Whitlock C. (2015). Reconstruction of fire regimes through intergrates paleoecological proxy data and ecological modelling, *Frontiers in Plant Science*, *5*, 1-12

Imbrie, J., Berger, A., Boyle, E.A., Clemens, S.C., Duffy, A., Howard, W.R., '...'Toggweiler, J.R. (1993). On the structure and origin of major glaciation cycles 2. The 100,000-year cycle. *Paleoceanography. 8,* 699-735

Ingrouille, M. (1995). 1.7 The Jurassic, The fossil flora: 440 million to 14 thousand years ago. In: M. Ingrouille. *Historical Ecology of the British Flora.* (pp. 31-36). Springer, Surrey

Innes, J.B., Simmons, I.G. (2000). Mid-Holocene charcoal stratigraphy, fire history and palaeoecology at North Gill, North York Moors, UK. *Palaeogeography, Palaeoclimatology, Palaeoecology. 164,* 151-165

IPCC, (2007). Climate Change 2007: Synthesis Report. Contribution of Working Groups I, II and III to the Fourth Assessment Report of the Intergovernmental Panel on Climate Change [Core Writing Team, Pachauri, R.K and Reisinger, A. (Eds.)]. IPCC, Geneva, Switzerland, 104

IPCC, (2013). Climate Change 2013: The Physical Science Basis. Contribution of Working Group I to the Fifth Assessment Report of the Intergovernmental Panel on Climate Change [Stocker, T.F., D. Qin, G.-K. Plattner, M. Tignor, S.K. Allen, J. Boschung, A. Nauels, Y. Xia, V. Bex and P.M. Midgley (Eds.). *Cambridge University Press*, Cambridge, United Kingdom and New York, NY, USA, 1535

IPCC, (2014). *Climate Change 2014: Synthesis Report*. *Contribution of Working Groups I, II and III to the Fifth Assessment Report of the Intergovernmental Panel on Climate Change* [Core Writing Team, R.K. Pachauri and L.A. Meyer (eds.)]. IPCC, Geneva, Switzerland, 151

Iversen. J. (1941). Land occupation in Denmark's Stone Age . *Danmarks Geologiske Undersogelse II. 66,* 1-68

Ivimey-Cook H.C. (1971). Stratigraphical palaeontology of the Lower Jurassic of the Llanbehr (Mochras Farm) Borehole, Woodland A.W. (Ed)., *The*

Llanbehr (Mochras Farm) Borehole, Institute of Geological Sciences U.K., *71*, 87-92

Jahren A.H., (2002). The biogeochemical consequence of the mid-Cretaceous superplume*, Journal of Geodynamics*, *34*, 177-191

Jahren A.H., Arens N.C., Sarmiento G., Gurrero J., Amundson R., (2001). Terrestrial record of methane hydrate dissociation in the Early Cretaceous, *Geology*, *29*, 159-162

James, N.P. (1977). Facies Models 7. Introduction to carbonate facies models. *Geoscience Canada. 4,* 123-125.

Jarvis I., Lignum J.S., Gröcke D.R., Jenkyns H.C. (2011). Black shale deposition, atmospheric CO_2 drawdown, and cooling during the Cenomanian-Turonian Oceanic Anoxic Event, *Paleoceanography, 26***,** 1-17

Jarvis, I., Mabrouk, A., Moody, R.T.J. and Cabrera, S.D. (2002). Late Cretaceous (Campanian) carbon isotope events, sea-level change and correlation of the Tethyan and Boreal realms. *Palaeogeography, Palaeoclimatology, Palaeoecology*. *188*, 215–248.

Jenkyns H.C., (2003). Evidence for rapid climate change in the Mesozoic-Paleogene greenhouse world., *Philosophical Transactions of the Royal Society of London Series a-Mathematical Physical and Engineering Sciences, 361*, 1885-1916

Jenkyns H.C., (1980). Cretaceous anoxic events; from continents to oceans, *Journal of the Geological Society, 137*,171-188
Jenkyns H.C., (2010). Geochemistry of organic anoxic events, *Geochemistry Geophysics Geosystems, 11*,1-30

Jenkyns H.C., Clayton C.J., (1986). Black shales and carbon isotopes in pelagic sediments from the Tethyan Lower Jurassic, *Sedimentology, 33*, 87-106

Jenkyns H. C., Clayton, C. J. (1997). Lower Jurassic epicontinental carbonates and mudstones from England and Wales: chemostratigraphic signals and the early Toarcian anoxic event. *Sedimentology 44*, 687–706.

Jenkyns H.C., Dickson A.J., Ruhl M., Van Den Boorn S.H.J.M. (2017). Basalt-seawater interaction, the Plenus Cold Event, enhanced weathering and geochemical change: deconstructing Oceanic weathering and geochemical change: deconstructing Oceanic Anoxic Event 2 (Cenomanian-Turonian, Late Cretaceous), *Sedimentology, 64,* 16-43

Jenkyns, H.C., Forster, A., Schouten, S., Sinninghe Damsté, J.S. (2004). High temperatures in the Late Cretaceous Arctic Ocean. *Nature. 432,* 888-892. doi:10.1038/nature03143

Jenkyns, H.C., Gale, A.S. and Corfield, R.M. (1994). Carbon- and oxygen-isotope stratigraphy of the English chalk and Italian Scaglia and its paleoclimatic significance. *Geological Magazine*, *131,* 1–34.

Jiménez-Moreno, G., Anderson, R. S., Atudorei, V., & Toney, J. L. (2011). A high-resolution record of climate, vegetation, and fire in the mixed Conifer forest of Northern Colorado, USA, *Bulletin of the Geological Society of America*, *123*, 240-254. DOI: 10.1130/B30240.1

Jolly, M.W., Cochrane, M.A., Freeborn, P.H., Holden, Z.A., Brown, T.J., Williamson, G.J., Bowman, D.M.J.S. (2015). Climate-induced variations in global wildfire danger from 1979 to 2013, *Nature Communications. 6,*1-11. doi:10.1038/ncomms8537

Jones, T.P., Chaloner, W.G., (1991). Fossil charcoal, its recognition and palaeoatmospheric significance, *Palaeogeography, Palaeoclimatology, Palaeoecology (Global Change Section). 97,* 39 – 50.

Jørgensen B. B., (1982). Mineralization of organic matter in the sea bed – the role of sulfate reduction, *Nature, 296*, 643–645.

Kah L.C., Sherman A.G., Narbonne G.M., Knoll A.H., Kaufman A.J., (1999). $\delta^{13}C$ stratigraphy of the Proterozoic Bylot Supergroup, Baffin Island, Canada: implications for regional lithostratigraphic correlations*, Canadian Journal of Earth Sciences, 36*, 313-332

Kaiho, K. Yatsu, S., Oba, M., Gorjan, P., Casier, J-G., Ikeda, M. (2013). A forest fire and soil erosion event during the Late Devonian mass extinction. *Palaeogeography, Palaeoclimatology, Palaeoecology. 392,* 272–280

Katz, M.E., Cramer, B.S., Mountain, G.S., Katz, S., Miller, K.G., (2001). Uncorking the bottle: What triggered the Paleocene/Eoceen thermal maximum methane release?, *Paleoceanography, 16*, 549-562

Kauffman, E.G. (1995). Global Change Leading to Biodiversity Crisis in a Greenhouse World: The Cenomanian-Turonian (Cretaceous) Mass Extinction. In: *National Research Council, Effects of Past Global Change on Life. The National Academies* (pp. 47-72)

Keeling, R.F., Shertz, S.R. (1992). Seasonal and interannual variations in atmospheric oxygen and implications for the global carbon cycle, *Letters to Nature, 358*, 723-727

Keller, G., Berner, Z., Adatte, T., Stueben, D. (2004). Cenomanian–Turonian and δ13C, and δ18O, sea level and salinity variations at Pueblo, Colorado. *Palaeogeography, Palaeoclimatology, Palaeoecology. 211,* 19-43

Kemp D.B., Coe A.S., Cohen A.S., Schwark L., (2005). Astronomical pacing of methane release in the Early Jurassic period*, Letters to Nature, 437*, 396-400

Kemp D.B., Coe A.L., Cohen A.S., Weedon G.P. (2011). Astronomical forcing and chronology of the early Toarcian (Early Jurassic) oceanic anoxic event in Yorkshire, UK, *Paleoceanography,* 26(4): 1-17, DOI: 10.1029/2011PA002122

Kennett, J.P., Cannariato, K.G., Hendy, I.L., Behl, R.J., (2000). Carbon Isotopic Evidence for Methane Hydrate Instability During Quaternary Interstadials, *Science, 288,* 128-133

Kerr A.C., (1998). Oceanic plateau formation: a cause of mass extinction and black shale deposition around the Cenomanian-Turonian boundary?, *Journal of the Geological Society, 155,* 619-626

Kingston, J.D. (2005). Orbital controls on seasonality. In D.K. Brockman., C.P. van Schaik. (Eds.). *Seasonality in Primates: Studies of Living and Extinct Human and Non-Human Primates.* (pp 521-543). Cambridge University Press

Korte, C., Hesselbo, S.P., Ullmann, C.V., Dietl, G., Ruhl, M., Schweigert, G., Thibault, N. (2015). Jurassic climate mode governed by ocean gateway. *Nature Communications. 6,* 1–7

Kozlova, E.A., Manning, A.C., Kisilyakhov, Y., Seifert, T., Heimann, M. (2008). Seasonal, synoptic, and diurnal-scale variability of biogeochemical trace gases and O2 from a 300-m tall tower in central Siberia. *Global Biogeochemical Cycles. 22,* doi:10.1029/2008GB003209

Kuhnt, W., F. Luderer, S. Nederbragt, J. Thurow, Wagner, T. (2005). Orbital-scale record of the late Cenomanian-Turonian oceanic anoxic event (OAE-2) in the Tarfaya Basin (Morocco*), International Journal of Earth Science, 94,*147–159, doi:10.1007/s00531-004-0440-5.

Kump, L.R., (1988). Terrestrial feedback in atmospheric oxygen regulation by fire and phosphorous. *Nature. 335,* 152 – 154.

Kump L.R., Arthur M.A., (1999). Interpreting carbon-isotope excursions: carbonates and organic matter, *Chemical Geology, 161*, 181-198

Kump, L.R., Garrels, R.M., (1986). Modelling atmospheric O_2 in the global sedimentary redox cycle, *American Journal of Science*, 286:337-360

Kump, L.R., Kasting, J.F., Crane, R.G., (2014). *The Earth System*, Third Edition, Pearson Education Inc., United States of America

Kuroda, J., Ogawa, N.O., Tanimizu, M., Coffin, M.F., Tokuyama, H., Kitazato, H., Ohkouchi, N. (2007). Contemporaneous massive subaerial volcanism and late cretaceous Oceanic Anoxic Event 2. *Earth and Planetary Science Letters. 256,* 211-223

Kutzbach, J.E., (1994). Idealized Pangean climates: sensitivity to orbital change. Pangea: paleoclimate, tectonics, and sedimentation during accretion, zenith, and breakup of a supercontinent. In: Klein, G.D. (Ed.), *GSA Special Paper. Geological Society of America*, Inc., Boulder, CO:41–55.

Kutzbach, J.E., Gallimore, R.G., (1989). Pangean Climates: Megamonsoons of the Megacontinent, *Journal of Geophysical Research Atmospheres. 94(D3),* 3341-3357

Larsen, C.P.S., MacDonald, G.M., (1993). Lake Morphometry, sediment mixing and the selection of sites for fine resolution palaeoecological studies, *Quaternary Science Reviews, 12*, 781-792

Larson R.L., Erba E., (1999). Onset of the Mid-Cretaceous greenhouse in the Barremian-Aptian: Igneous events and the biological, sedimentary, and geochemical responses, *Paleoceanography, 14*, 663-678

Lasaga, A. C., Ohmoto, H. (2002). The oxygen geochemical cycle: Dynamics and stability. *Geochimica et Cosmochimica Acta. 66,* 361-381

Laurin, J., Sageman, B.B. (2007). Cenomanian-Turonian Coastal Record in SW Utah, U.S.A: Orbital-scale trangressive-regressive events during Oceanic Anoxic Event II, *Journal of Sedimentary Research. 77,* 731-756

Leckie R.M., Bralower T.J., Cashman R., (2002). Oceanic anoxic events and plankton evolution: Biotic response to tectonic forcing during the Mid Cretaceous, *Palaeooceanography, 17*,1-29

Lenton T.M., (2013). Fire Feedbacks on Atmospheric Oxygen. In. C.M. Belcher (Ed). *Fire Phenomena and the Earth System*, (pp. 289-308) Wiley-Blackwell Press

Lenton T.M., (2001). The role of land plants, phosphorus weathering and fire in the rise and regulation of atmospheric oxygen*, Global Change Biology, 7*, 613-629

Lenton, T.M, Watson, A.J., (2000a). Redfield revisited 1. Regulation of nitrate, phosphate, and oxygen in the ocean. *Global Biogeochemical Cycles. 14,* 225 – 248.

Lenton, T.M., Watson, A.J., (2000b). Redfield revisited 2: What regulates the oxygen content of the atmosphere? *Global Biogeochemical Cycles. 14*, 249 – 268.

Levis, F.L., Ward, D.S. (2013). Quantifying the role of fire in the Earth system – Part 1: Improved global fire modelling in the Community Earth System Model (CESM1). *Biogeosciences. 10,* 2293 – 2314, doi:10.5194/bg-10-2293-2013

Leys, B.A., Brewer, S.C., McConaghy, S., Mueller, J., McLauchlan, K.K.. (2015). Fire history reconstruction in grassland ecosystems: amount of charcoal reflects local area burned. *Environmental Research Letters. 10*

Lhermitte, S., Verbesselt J., Verstraeten W.W., Veraverbeke S., Coppin P. (2011). Assessing inter-annual vegetation regrowth after fire using the pixel based regeneration index. *ISPRS Journal of Photogrammetry and Remote Sensing. 66,* 17-27, doi.org/10.1016/j.isprsjprs.2010.08.004

Li, M., Black, B., Zhong, S., Manga, M., Rudolph, M.L., Olson, P. (2016). Quantifying melt production and degassing rate at mid-ocean ridges from global mantle convection models with plate motion history*, Geochemistry, Geophysics, Geosystems*, 1-21, dio: 10.1002/2016GC006439

Li F., B. Bond-Lamberty, and S. Levis, (2014). Quantifying the role of fire in the Earth system Part 2: Impact on the net carbon balance of global terrestrial ecosystems for the 20th century. *Biogeosciences. 11,* 1345–1360, doi:10.5194/bg-11–1345-2014.

Lisiecki L.E. (2010). Links between eccentricity forcing and the 100,000-year glacial cycle, *Nature Geoscience, 3***,** 349-352

Liu Y., Lo L., Shi Z., Wei K-Y., Chou C-J., Chen T-C., Chuang C-K., Wu C-C., Mii H-S., Peng Z., Amakawa H., Burr G.S., Lee S-Y., DeLong K.L., Elderfield H., Shen C-C. (2015). Obliquity pacing of the western Pacific Intertropical Convergence Zone over the past 282,000 years, *Nature Communications, 6,* doi:10.1038/ncomms10018

Liu Y., Stanturf J., Goodrick S. (2010). Trends in global wildfire potential in a changing climate, *Forest Ecology and Management, 259,* 685-697
Looney C.G., (2011), 2.14 Interactions of Climate Factors, *Climate Change and the Emergence of Civilization, Global Warming, Great Floods and Ice Ages,* Xilbris Corporation, ISBN: 978-1-4568-6692-1

Lonero, A. (2008). How Are Methane Hydrates Formed, Preserved, and Released? *Geology 340 Term Paper*, University of Hawaii at Hilo, Hilo, 53-58.

Loutre M.F., (2003). Ice ages (Milankovitch theory), *Elsevier Science Ltd,* retrieve*d* on 28th February 2017 from http://curry.eas.gatech.edu/Courses/6140/ency/Chapter10/Ency_Atmos/Ice_age.pdf

Ma W., Tian J., Li Q., Wang P., (2011). Simulation of long eccentricity (400-kyr) cycle in ocean carbon reservoir during the Miocene Climate Optimum: Weathering and nutrient response to orbital change, *Geophysical Research Letters, 38,* L10701.

MacDonald, G.M., Larsen, C.P.S., Szeicz, J.m., Moser, K.A., (1991). The Reconstruction of Boreal Forest Fire History from Lake Sediments: A Comparison of Charcoal, Pollen, Sedimentological, and Geochemical Indicies, *Quaternary Science Reviews, 10*, 53-71

Mackenzie L., Moss P. (2017). Late Quaternary record of vegetation and climate change from Hazards Lagoon, eastern Tasmania. *Quaternary International. 432.* 58-65

Mackenzie, F.T., Ver, L.M., Lerman, A., (2002). Century-scale nitrogen and phosphorus controls of the carbon cycle*, Chemical Geology, 190*, 13-32

Mahoney J.J., Storey M., Duncan R.A., Spenser K.J., Pringle M.S., (1993). Geochemistry and geochronology of Leg 130 Basement Lavas: Nature and Origin of the Ontong Java Plateau, Berger W.H., Kroenke L.W., Mayer L.A. et al. (Eds.), *Proceedings of the Ocean Drilling Program, Scientific Results, 130,* 3-22

Markgraf, V., Whitlock, C., Haberle, S. (2007). Vegetation and fire history during the last 18,000 cal. Yr B.P. in Southern Paragonia: M Mallín Pollux,

Coyhaique, Province Aisén (45°41′30″ S, 71°50′30″ W, 640 m elevation), *Palaeogeography, Palaeoclimatology, Palaeoecology, 254,* 492-507

Marlon J.R., Bartlein P.J., Carcaillet C., Gavin D.G., Harrison S.P., Higuera P.E., Joos F., Power M.J., Prentice I.C. (2009). Climate and human influences on global biomass burning over the past two millennia, *Nature Geoscience, 1*, 687-702

Martinez M., Dera G. (2015). Orbital pacing of carbon fluxes by a ~9-My eccentricity cycle during the Mesozoic, *Proceedings of the National Academy of Sciences, 112*, 12604-12609

Matthewman, R., Cotton, L.J., Martins, Z., Sephton, M.A. (2012). Organic geochemistry of late Jurassic paleosols (Dirt Beds) of Dorset, UK, *Marine and Petroleum Geology. 37,* 41-52

Matthewman, R., Cotton, L.J., Martins, Z., Sephton, M.A. (2012). Organic geochemistry of late Jurassic paleosols (Dirt Beds) of Dorset, UK. *Marine and Petroleum Geology. 37,* 41-52

Mattioli, E., Pittet, B., Petitpierre, L., Mailliot, S. (2009). Dramatic decrease of pelagic carbonate production by nannoplankton across the Early Toarcian anoxic event (T-OAE). *Global and Planetary Change. 65.* 134-145

Marynowsji, L., Simoneit, B.R.T. (2009). Widespread upper Triassic to lower Jurassic wildfire records from Poland: evidence from charcoal and pyrolytic polycyclic aromatic hydrocarbons. *Palaios. 24,* 785-798

Masiello, C.A., Druffel, E.R.M., (1998). Black Carbon in Deep-Sea Sediments, *Science. 280*, 1911-1913

Mayorga, E., Aufdenkampe, A.K., Masiello, C.A., Krusche, A.V., Hedges, J.I., Quay, P.D., Richey, J.E., Brown, T.A., (2005). Young organic matter as a

source of carbon dioxide outgassing from Amazonian rivers, *Letters to Nature, 436*, 538-541, doi:10.1038/nature03880

McArthur J.M., Howarth R.J., Bailey T.R., (2001). Strontium isotope stratigraphy: LOWESS version 3: best fit to the marine Sr-isotope curve for 0-509 Ma and accompanying look-up table for deriving numerical age, *Journal of Geology, 109,* 155-170

McElwain, J. C., Wade-Murphy, J. & Hesselbo, S. P. (2005). Changes in carbon dioxide during an oceanic anoxic event linked to intrusion into Gondwana Coals. *Letters to Nature. 35,* 479–482.

McGee, D., Donohoe, A., Marshall, J., Ferreira, D. (2014). Changes in ITCZ location and cross-equatorial heat transport at the Last Glacial Maximum, Heinrich Stadial 1, and the mid-Holocene. *Earth and Planetary Science Letters. 390,* 69-79

Mendonça Filho, J.G., Menezes, T.R., Oliveira Mendonça, J., Donizeti de Oliveira, A., Freitas da Silva, T., Rondon, N.F., & Sobrinho da Silva, F. (2012). *Organic facies: palynofacies and organic geochemistry approaches*. In: Panagiotaras D. (Ed.), *Geochemistry - Earth's System Processes*. Editions InTech, (pp. 211-248).

Menegatti A.P., Weissert H., Brown R.S., Tyson R.V., Farrimond P., Strasser A., Caron M., (1998). High-resolution $\delta^{13}C$ stratigraphy through the early Aptian “Livello Selli” of the Alpine Tethys., *Palaeoceanography, 13*, 530-545

Met Office (2015). Research-Foundation Science-Parametrizations-The Atmospheric Boundary Layer. Retrieved on 22nd April 2017 from http://www.metoffice.gov.uk/research/foundation/parametrizations/boundary-layer

Meyers, P.A. (2014). Why are the $\delta^{13}C_{org}$ values in Phanerozoic black shales more negative than in modern marine organic matter?. *Geochemistry, Geophysics, Geosystems. 15.* 3085-3106, doi: 10.1002/2014GC005305

Meyers, S.R., Sageman, B., Hinnov, L. (2001). Integrated quantitative stratigraphy of the Cenomanian–Turonian Bridge Creek Limestone Member using Evolutive Harmonic Analysis and stratigraphic modeling. *Journal of Sedimentary Research*. *71,* 627–643.

Miller K.G., Sugarman P.J., Browning J.V., Kominz M.A., Hernández J.C., Olsson R.K., Wright J.D., Feigenson M.D., Van Sickel W. (2003). Late Cretaceous chronology of large, rapid sea-level changes: Glacioeustasy during the greenhouse world, *Geology, 31*, 585-588

Mills B., (2012). Weathering pathways and limitations in biogeochemical models: Application to Earth system evolution, *A thesis submitted to the School of Environmental Sciences of the University of East Anglia in partial fulfilment of the requirements for the degree of Doctor of Philosophy*

Mills B.J.W., Belcher C.M., Lenton T.M., Newton R.J. (2016). A modelling case for high atmospheric oxygen concentrations during the Mesozoic and Cenozoic, *Geology*, doi: 10.1130/G38231.1

Millspaugh, S.H., Whitlock, C., Bartlein, P.J., (2003). Variations in fire frequency and climate over the past 17 000 yr in central Yellowstone National Park, *Geology, 28*(3), 211-214

Mitchell, R.N., Bice, D.M., Montanari, A., Cleaveland, L.C., Christianson, K.T., Coccioni, R., and Hinnov, L.A. (2008). Oceanic anoxic events? Orbital prelude to the Bonarelli Level (OAE 2). *Earth and Planetary Science Letters. 267* 1–16, doi:10.1016/j.epsl.2007.11.026

Mitra S., Zimmerman A.R., Hunsinger G., Woerner W.R., (2014). Black carbon in coastal and large river systems, In: T.S. Bianchi., M.A. Alison., W-J.

Cai. (Eds.), *Biogeochemical Dynamics at Major River-Coastal Interfaces-Linkages with Climate Change*. (pp. 200-234). Cambridge University Press, New York

Montero-Serrano J-C., Föllmi K.B., Adatte T., Spangenberg J.E., Tribovillard N., Fantasia A., Suan G. (2015). Continental weathering and redox conditions during the early Toarcian Oceanic Anoxic Event in the northwestern Tethys: Insight from the Posidonia Shale section in the Swiss Jura Mountains. *Palaeogeography, Palaeoclimatology, Palaeoecology. 429.* 83-99

Mooney, S. D., Harrison, S. P., Bartlein, P. J., Daniau, A.-L., Stevenson, J., Brownlie, K. C., '...' Black, M. (2011). Late Quaternary fire regimes of Australasia. *Quaternary Science Reviews. 30,* 28–46, doi: 10.1016/j.quascirev.2010.10.010

Mooney, S.D., Tinner, W. (2011). The analysis of charcoal in peat and organic sediments. *Mires and Peat. 7,* 1-18

Moore, R. C., (1949). Divisions of the Pennsylvanian System in Kansas, *Kansas Geological Survey, Bulletin. 83*, 203

Moore P.D., Webb J.A., Collinson M.E., (1991). The Treatment of Samples, Pollen Analysis, *Blackwell Science Ltd, 45*

Morandini, F., Santoni, P.A., Balbi, J.H. (2001). The contribution of radiant heat transfer to laboratory-scale fire spread under the influences of wind and slope, *Fire Safety Journal, 36,* 519-543

Morberly R., Larsen R.L., (1975). Mesozoic Magnetic Anomalies, Oceanic Plateaus and Seamount Chains in the Northwestern Pacific Ocean, in Larsen R.L., Moberly R., et al., *Initial Reports of the Deep Sea Drilling Project, 32*, 945-957

Morgan J., Artemieva N., Goldin T. (2013). Revisiting wildfires at the K-Pg boundary, *Journal of Geophysical Research: Biosciences, 118,* 1508-1520 doi:10.1002/2013JG002428

Mort, H.P., Adatte, T., Föllmi, K.B., Keller, G., Steinmann, P., Matera, V., Berner, Z., Stüben, D. (2007). Phosphorus and the roles of productivity and nutrient recycling during oceanic anoxic event 2. *The Geological Society of America. 35,* 483-486

Mortiz, M.A., Parisien, M-A., Batllori, E., Krawchuk, M.A., Dorn, J.V., Ganz, D.J., Hayhoe, K. (2012). Climate change and disruption to global fire activity. *Ecosphere. 3,* 1 – 22.

Moss, P.T, Kershaw, A.P. (2000). The last glacial cycle from the humid tropics of northeastern Australia: comparison of a terrestrial and a marine record. *Palaeogeography, Palaeoclimatology and Palaeoecology 155*, 155–76.

Mudryk, Z.J., Podgórska, B., Bolalek, J., (2000). The occurrence and activity of sulphate-reducing bacteria in the bottom sediments of the Gulf of Gdańsk, *Oceanologia, 42(1),* 105-117

Muller, F. L. (1990). *The Paleoecology of the Liassic Benthic Foraminifera of Great Britain* (PhD. dissertation, Rutgers University).

Murray J.W., Stewart K., Kassakian S., Krynytzky M., DiJulio D., (2005). Oxic, Suboxic and Anoxic Conditions in the Black Sea, in Gilbert A., Yanko-Hombach V., Panin N. (Eds.)., *Climate Change and Coastline Migration as Factors in Human Adaptation to the Circum-Pontic Region*: From Past to Forecast, Kluwer Publishers:1-26

NASA. (2005). NASA – What's the Difference Between Weather and Climate? Retrieved on 10th January 2017 from https://www.nasa.gov/mission_pages/noaa-n/climate/climate_weather.html

Natalicchino, M., Birgel, D., Pierre, F.D., Martire, L., Clari, P., Spötl, C., Peckmann, J. (2012). Polyphasic carbonate precipitation in the shallow subsurface: Insights from microbially-formed authigenic carbonate beds in upper Miocene sediments of the Tertiary Piedmont Basin (NW Italy). Palaeogeography, *Palaeoclimatology, Palaeoecology. 329-330*, 158-172. doi.org/10.1016/j.palaeo.2012.02.026

Nelson, C.S. (1988). An introductory perspective on non-tropical shelf carbonates. *Sedimentary Geology. 60*, 3-12

Nepstad, D., Carvalho, G., Barros, A.C., Alencar, A., Capobianco, P., Bishop, J. '...' Lopes, U. (2001). Road paving, fire regime feedbacks, and the future of Amazon forests, *Forest Ecology and Management. 154,* 395-407

Nepstad, D., Lefebvre, P., Silva, U.L.D., Tomasella, J., Schlesinger, P., Solórzano, L. '...' Benito, C. (2004). Amazon drought and its implications for forest flammability and tree growth: a basin-wide analysis. *Global Change Biology. 10,* 704-717, doi: 10.1111/j.1529-8817.2003.00772.x

Neuhuber, S., Wagreich, M., Wendler, I., Spötl, C., (2007). Turonian Oceanic Red Beds in the Eastern Alps: concepts for palaeoceanographic changes in the Mediterranean Tethys, *Palaeogeography, Palaeoclimatology, Palaeoecology. 251,* 222-238

Nichols, G.J., Cripps, J.A., Collinson, M.E., Scott, A.C., (2000). Experiments in waterlogging and sedimentology of charcoal: results and implications, *Palaeogeography, Palaeoclimatology, Palaeoecology, 164*, 43-56

Nichols, G., and Jones, T.P. (1992). Fusain in Carboniferous shallow marine sediments, Donegal, Ireland: the sedimentological effects of wildfire. *Sedimentology. 39,* 487- 502.

Nixon, M.F., Grozix, J.L.H., (2007). Submarine slope failure due to gas hydrate dissociation: a preliminary quantification*, Canadian Geotechnical Journal, 44(3),* 314-325

NOAA. (2017). Trends in Atmospheric Carbon Dioxide, Earth System Research Laboratory, Global Monitoring Division. Retrieved June 23, 2017 from https://www.esrl.noaa.gov/gmd/ccgg/trends/full.html

Novakov, T., Penner, J.E. (1993). Large contribution of organic aerosols to cloud-condensation-nuclei concentrations. *Nature. 365*, 823-826

Núñez-Regueira, L., Rodriguez-Anon, J.A., Proupin, J., Mourino, B., Artiaga-Diaz, R. (2005). Energetic study of residual forest biomass using calorimetry and thermal analysis. *Journal of Thermal Analysis and Calorimetry*, *80,* 457-464

Ohlson, M., Tryterud, E., (2000). Interpretation of the charcoal record in forest soils: forest fires and their production and deposition of macroscopic charcoal, *The Holocene, 10,4*, 519- 525

Olsen P.E., Kent D.V. (1999). Long-period Milankovitch cycles from the Late Triassic and Early Jurassic of eastern North America and their implications for the calibration of the Early Mesozoic time-scale and the long-term behaviour of the planets, *Philosophical Transactions of the Royal Society of London, 357***,** 1761-1786

Oris, F., Ali, A.A., Asselin, H., Paradis, L., Bergeron, Y., Finsinger, W. (2014). Charcoal dispersion and deposition in boreal lakes from 3 years of monitoring: Differences between local and regional fires. *Geophysical Research Letters. 41,* 6743–6752, doi:10.1002/2014GL060984.

Ormeño, E., Céspedes, B., Sánchez, I.A., Velasco-García, A., Moreno, J.M., Fernandez, C., Baldy, V. (2009). The relationship between terpenes and flammability of leaf litter. *Forest Ecology and Management. 257,* 471-482

O'Sullivan K.N., (1979). The sedimentology, geochemistry, and conditions of deposition of the Tertiary rocks of the Llanbedr (Mochras Farm) borehole, *The Tertiary rocks at the Llanbedr (Mochras Farm) Borehole,* Report of the Institute of Geological Sciences, *78/24*, 1-13

Paduano G.M., Bush M.B., Baker P.A., Fritz S.C., Seltzer G.O. (2003). A vegetation and fire history of Lake Titicaca since the Last Glacial Maximum, *Palaeogeography, Palaeoclimatology, Palaeoecology, 194,* 259-279

Pälike H., Norris R.D., Herrle J.O., Wilson P.A., Coxall H.K., Lear C.H. (2006). The Heartbeat of the Oligocene Climate System, *Science, 314,* 1894-1898, doi: 10.1126/science.1133822

Parisot I.T., Chabel L., Chrzavzez J., (2010), Anthracology and taphonomy from wood gathering to charcoal analysis. Areview of the taphonomic processes modifying charcoal assemblages, in archaeological contexts, *Palaeogeography, Palaeoclimatology, Palaeoecology, 291,* 142-153

Parrish, J.T. (1993). Climate of the Supercontinent Pangea, *The Journal of Geology 101*, 100th Anniversary Symposium: Evolution of the Earth's Surface, 215-233

Parrish, J.T., (1995). Geologic Evidence of Permian Climate, *The Permian of Northern Pangea*, 53-61

Patterson W.A., Edwards K.J., Maguire D.J. (1987). Microscopic charcoal as a fossil indicator of fire, *Quaternary Science Reviews, 6,* 3-23

Pausas, J .G., (2004). Changes in fire and climate in the eastern Iberian peninsula (Mediterranean basin). *Climate Change. 63,* 337–50

Pearce C.R., Cohen A.S., Coe A.L., Burton K.W., (2008). Molybdenum isotope evidence for global ocean anoxia coupled with perturbation to the

carbon cycle during the Early Jurassic, Geology, *36*, 231-234, doi: 10.1130/G24446A.1

Pechony, O., Shindell D.T. (2010). Driving forces of global wildfires over the past millennium and the forthcoming century, *Proceedings of the National Academy of Sciences of the United States of America. 107*, 19167-19170

Pedersen T.F., Calvert S.E., (1990). Anoxia vs. Productivity: What Controls the Formation of Organic-Carbon-Rich Sediments and Sedimentary Rocks? (1), *AAPG Bulletin, 74*, 454-466

Percival, L. M. E., Cohen, A.S., Davies, M.K., Dickson, A.J., Hesselbo, S.P., Jenkyns, H.C., Leng, M.J., Mather, T.A., Storm, M.S., Xu, W. (2016). Osmium isotope evidence for two pulses of increased continental weathering linked to Early Jurassic volcanism and climate change. *Geology. 44,* 759–762

Personius, S.F. (1993). Age and Origin of Fluvial Terraces in the Central Coast Range, Western Oregon. U.S. Geological Survey Bulletin 2038, United States Geovernment Printing Office, Washington

Peterson H.I., Lindström S. (2012). Synchronous Wildfire Activity Rise and Mire Deforestation at the Triassic-Jurassic Boundary, *PLOS ONE, 7,*1-15

Peterson, D.W., Reich, P.B. (2008). Fire frequency and tree canopy structure influence plant species diversity in a forest-grassland ecotone. *Plant Ecology. 194,* 5-16, doi:10.1007/s11258-007-9270-4

Petsch S.T., (2003). The Global Oxygen Cycle, *Treatise on Geochemistry, 8*, 515-555

Pieńkowski, G., Hodbod, M. & Ullmann, C. V. (2016). Fungal decomposition of terrestrial organic matter accelerated Early Jurassic climate warming. *Science Reports. 6,* 31930.

Pittet, B., Suan, G., Lenoir, F., Duarte, L. V. & Mattioli, E. (2014). Carbon isotope evidence for sedimentary discontinuities in the lower Toarcian of the Lusitanian Basin (Portugal): Sea level change at the onset of the Oceanic Anoxic Event. *Journal of Sedimentary Geology. 303,* 1–14

Pisaric, M.F.J., (2002). Long-distance transport of terrestrial plant material by convection resulting from forest fires, *Journal of Paleolimnology, 28*, 349-354

Planas E., Pastor E., (2013). Wildfire Behaviour and Danger, Belcher C.M. (Ed)., *Fire Phenomena and the Earth System, An Interdisciplinary Guide to Fire Science*. (pp. 53 – 75). West Sussex: John Wiley and Sons

Plugge C.M., Zhang W., Scholten J.C., Stams A.J.M., (2011). Metabolic Flexibility of Sulfate-Reducing Bacteria, *Frontiers in Microbiology,* 2, retrieved on 23rd July 2014 from http://www.ncbi.nlm.nih.gov/pmc/articles/PMC3119409/

Pogge von Strandmann P.A.E., Jenkyns H.C., Woodfine R.G. (2013). Lithium isotope evidence for enhanced weathering during Oceanic Anoxic Event 2, *Nature Geoscience, 6*, 668-672

Pollet J., Brown A. (2007). Bureau of Land Management, Utah State Office, Salt Lake City, Utah, retrieved on 23rd February 2017 from http://www.wfas.net/nfmd/references/fmg.pdf

Popescu S-M., Suc J-P., Loutre M-F. (2006). Early Pliocene vegetation changes by eccentricity-precession. Example from Southwestern Romaina, *Palaeogeography, Palaeoclimatology, Palaeoecology*, *238*, 340-348

Pompeckj, J.F. (1901). Der Jura zwischen Regensburg und Regenstauf, *Geognostische Jahreshefte. 14,* 139-220

Porterie, B., Zekri, N., Clerc, J-P., Loraud, J-C. (2007). Modelling forest fire spread and spotting process with small world networks, *Combustion and Flame. 149,* 63-78

Power M.J. (2013). 10. A 21,000-Year History of Fire, *Fire Phenomena and the Earth System, An Interdisciplinary Guide to Fire Science,* Belcher C.M. (Ed.)., WileyBlackwell:207-229

Power M.J., Marlon J., Ortiz N., Bartlein P.J., Harrison S.P., Mayle F.E., Ballouche A., Bradshaw R.H.W., Carcaillet C. et al., (2008). Changes in fire regiemes since the Last Glacial Maximum: an assessment based on a global synthesis and analysis of charcoal data, *Climate Dynamics, 30*, 887-907

Pratt L.M. (1984). Influence of Paleoenvironmental Factors on Preservation of Organic Matter in Middle Cretaceous Greenhorn Formation, Pueblo, Colorado, *AAPG Bulletin, 68*,1146- 1159

Pyne, S.J., Andrews, P.L., Laven, R.D., (1996). Introduction to Wildfire, Wiley and Sons, New York.

Rabalais, N.N., Turner, R.E., Sen Gupta, B.K., Boesch, D.F., Chapman, P., Murrell, M.C. (2007). Hypoxia in the Northern Gulf of Mexico: Does the Science Support the Plan to Reduce, Mitigate, and Control Hypoxia?, *Estuaries and Coasts, 30*(5), 753-772

Radtke, L. F., D. A. Hegg, P. V. Hobbs, J. D. Nance, J. H. Lyons, K. K. Laursen, R. E. Weiss, P. J.Riggan & D. E. Ward, (1991). Particulate and trace gas emissions from large biomass fires in North America. In J.S. Levine, (Ed.) *Global Biomass Burning: Atmospheric, Climatic, and Biospheric Implications*. (pp 209-224). MIT Press, Cambridge

Ramathan, V., Crutzen, P.J., Kiehl, J.T., Rosenfeld, D. (2001). Aerosols, Climate, and the Hydrological Cycle. *Science. 294.* 2119-2124

Randall, P.J., Hayes, J.E., Hocking, P.J., Richardson, A.E. (2001). Root Exudates in Phosphorus Acquisition by Plants. *Plant Nutrient Acquisition.* 71-100

Randerson, J.T., Liu, H., Flanner, M.G., Chambers, S.D., Jin, Y., Hess, P.G., '...' Zender, C.S. (2006). The Impact of Boreal Forest Fire on Climate Warming. *Science. 314,* 1130-1132

Raymo. M, E., Nisancioglu, K.H. (2003). The 41 kyr world: Milankovitch's other unsolved mystery. *Paleoceanography. 18,* 1-6, doi: 10.1029/2002PA000791

Raymo, M.E. (1997). The timing of major climate terminations, P*aleoceanography, 12,* 577-585

Reasoner, M. A. & U. M. Huber, (1999). Postglacial palaeoenvironments of the upper Bow Valley, Banff National Park, Alberta, Canada. *Quaternary Science Reviews. 18*, 475–492.

Reilly, M.J., Wimberly, M.C., Newell, C.L. (2006). Wildfire effects on plant species richness at multiple spatial scales in forest communities of the southern Appalachians. *Journal of Ecology. 94,* 118-130

Reilly, M.J., Wimberly, M.C., Newell, C.L. (2006). Wildfire effects on plant species richness at multiple spatial scales in forest communities of the southern Appalachians. *Journal of Ecology. 94,* 118-130

Rein, G. (2013). Smouldering Fires and Natural Fuels. In. Belcher C.M. (Ed.), *Fire Phenomena and the Earth System, An Interdisciplinary Guide to Fire Science.* (pp. 15 – 35). West Sussex: John Wiley and Sons

Retallack G.J., Bestland E.A., Fremd T.J. (1999). *Eocene and Oligocene Paleosols of Central Oregon, Special Paper 344,* Geological Society of America, Inc., Colorado*,* 11

Retallack G.J., Jahren A.H., (2008). Methane Release from Igneous Intrusion of Coal during Late Permian Extinction Events, *The Journal of Geology, 116*, doi: 10.1086/524120

Reolid M., Duarte L.V. (2013). Sponge-microbialite buildups from the Toarcian of the Coimbra region (Northern Lusitanian Basin, Portugal): paleoecological and paleoenvironmental significance, *Facies*, doi: 10.1007/s10347-013-0389-6

Rhodes A.N., (1998). A method for the preparation and quantification of microscopic charcoal from terrestrial and lacustrine sediment cores, *The Holocene*, *8,1*, 113-117

Ribeiro, V., Guerra-Sommer, M., Gruber, N.L.S., Jasper, A., Barboza, E.G., Menegat, R., Manzolli, R.P. (2016). Charcoal Peaks in The Quaternary of Southern Brazil: Climate, Men and Fire. *Gravel. 14,* 11-22

Rimmer, S. M., Hawkins, S. J., Scott, A. C. & Cressler, W. L. (2015). III The rise of fire: fossil charcoal in late Devonian marine shales as an indicator of expanding terrestrial ecosystems, fire, and atmospheric change. *American Journal of Science, 315,* 713–733.

Robinson, S., Heimhofer, U., Hesselbo, S.P., Petrizzo, M.P. (2017). Mesozoic climates and oceans – a tribute to Hugh Jenkyns and Helmut Weissert. *Sedimentology. 64,* 1-15

Rocca M.E., Brown P.M., MacDonald L.H., Carrico C.M. (2014). Climate change impacts on fire regimes and key ecosystem services in Rocky Mountain forests, *Forest Ecology and Management, 327***,** 290-305

Rocha, R. B. (Coord.), Marques, B., Kullberg, J. C., Caetano, P., Lopes, C., Soares, A. F., Duarte, L. V., Marques, J., Gomes, C. (1996). The 1st and 2nd rifting phases of the Lusitanian Basin: stratigraphy, sequence analysis and

sedimentary evolution. C. E. C. Project MILUPOBAS, Contract nº JOU2-CT94-0348 (unpublished report), *Lisboa, 4 vols.*

Rocha, R. B., Mattioli, E., Duarte, L.V., Pittet, B., Elmi, S., Mouterde, R. '…' Suan, G.. (2016). Toarcian Stage of Lower Jurassic defined by the Global Boundary Stratotype Section and Point (GSSP) at the Peniche section (Portugal). *Episodes 39*, 460–481

Ronov, A.B. (1976). Global carbon geochemistry, volcanism, carbonate accumulation, and life. *Geochemistry International (translation of Geokhimiya). 13,* 172-195

Rothermel, R.C. (1972). A mathematical model for predicting fire spread in wildland fuels. *Research Paper INT-115. USDA Forest Service, Intermountain Forest and Range Experiment Station, Ogden, UT, USA.*

Ruddiman W.F. (2006). Orbital changes and climate, *Quaternary Science Reviews, 25***,** 3092-3112

Ruhl M., Deenen M.H.L., Abels H.A., Bonis N.R., Krijgsman W., Kürschner W.M. (2010). Astronomical constraints on the duration of the early Jurassic Hettangian stage and recovery rates following the end-Triassic mass extinction (St Audrie's Bay/East Quantoxhead, UK), *Earth and Planetary Science Letters, 295,* 262-276

Ruhl, M., Hesselbo, S.P., Hinnov, L., Jenkyns, H.C., Xu, W., Riding, J.B., Storm, M. '…' Leng, M.J. (2016). Astronomical constraints on the duration of the Early Jurassic Pliensbachian Stage and global climatic fluctuations. *Earth and Planetary Science Letters. 455,* 149–165

Rushforth S.R. (1971). A flora from the Dakota Sandstone Formation (Cenomanian) near Westwater, Grand Country, Utah, *Brigham Young University Science Bulletin xiv, 3*, 1-43

Sageman, B.B., Meyers, S.R., Arthur, M.A. (2006). Orbital time scale and new C-isotope record for Cenomanian- Turonian boundary stratotype. *Geological Society of America. 34,* 125-128

Sageman, B.B., Rich, J., Arthur, M.A., Birchfield, G.E., Dean, W.E. (1997). Evidence for Milankovitch periodicities in Cenomanian–Turonian lithologic and geochemical cycles, Western Interior U.S. *Journal of Sedimentary Research*. *67*, 285–301.

Sageman, B., Rich, J., Savrda, C.E., Bralower, T., Arthur, M.A., Dean, W.E., (1998). Multiple Milankovitch cycles in the Bridge Creek Limestone (Cenomanian–Turonian), Western Interior basin. In: M.A. Arthur, W.E. Dean, (Eds.), *Stratigraphy and Paleoenvironments of the Cretaceous Western Interior Seaway, USA. In: Concepts in Sedimentology and Paleontology*, vol. 6. (pp. 153–171) Society of Sedimentary Geology.

Sander P.M., Gee C.T., (1990). Fossil Charcoal: Techniques and Applications, *Review of Palaeobotany and Palynology, 63*, 269-279

Santín, C., Doerr, S.H., Preston, C.M., González-Rodríguez, G. (2015). Pyrogenic organic matter production from wildfires: a missing sink in the global carbon cycle. *Global Change Biology. 21,* 1621-1633, doi: 10.1111/gcb.12800

Schaefer, V.J. (1974). Some physical relationships of fire particulate smoke. *Proceedings of the 13th annual Tall Timbers Fire Ecology Conference,* 303-307

Schaltegger, U., Guex, J., Bartolini, A., Schoene, B., Ovcharova, M. (2008). Precise U–Pb age constraints for end-Triassic mass extinction, its correlation to volcanism and Hettangian post-extinction recovery. *Earth and Planetary Science Letters. 267,* 266-275

Schlanger S.O., Arthur M.A., Jenkyns, H.C., Scholle P.A., (1987). The Cenomanian-Turonian Oceanic Anoxic Event, I. Stratigraphy and distribution of organic carbon-rich beds and the marine $\delta^{13}C$ excursion, *Geological Society Special Publications, 26*, 371-399

Schlanger, S.O., Jenkyns, H.C. (1976). Cretaceous Oceanic Anoxic Events: Causes and Consequences, *Geologie En Mijnbouw, 55,* 179-184

Schmidtko, S., Stramma, L., Visbeck, M. (2017). Decline in global oceanic oxygen content during the past five decades, *Nature. 542,* 335-339, doi:10.1038/nature21399

Schneider, T., Bischoff, T., Haug, G.H. (2014), Migrations and dynamics of the intertropical convergence zone, *Nature Review. 513,* 45-53

Schneour, E. (1966). Oxidation of graphite carbon in certain soils. *Science, 151,* 991-992

Scholze, M., Knorr, W., Arnell, N.W. & Prentice, I.C. (2006). A climate-change risk analysis for world ecosystems. *Proceedings of the National Academy of Sciences USA. 103,* 13116–13120.

Schouten S., Hopmans E.C., Forster A., van Breugel Y., Kuypers M.M.M., Sinninghe Damsté (2003). Extremely high sea-surface temperatures at low latitudes during the middle Cretaceous as revealed by archaeal membrane lipids, *Geological Society of America, 31,* 1069-1072

Schouten S., van Kaam-Peters M.E., Irene W., Rijstra C., Schoell M., Sinninghe Damste S., (2000). Effects of an oceanic anoxic event on the stable carbon isotopic composition of early Toarcian carbon, *American Journal of Science, 300,* 1-22

Scholle P.A., Arthur M.A., (1980). Carbon isotope fluctuations in Cretaceous pelagic limestone: potential stratigraphic and petroleum exploration tool, *AAPG Bulletin, 64*, 67-87

Schootbrugge van de, B., Quan, T.M., Lindström, S., Püttmann, W., Heunisch, C., Pross, J., Fiebig, J. '...'Falkowski, P.G. (2009). Floral changes across the Triassic/Jurassic boundary linked to flood basalt volcanism. *Nature Geoscience. 2,* 589-594

Schopf, J.M., (1975). Modes of fossil preservation. *Review of Palaeobotany and Palynology*., *20*, 27-53.

Schouten S., van Kaam-Peters M.E., Irene W., Rijstra C., Schoell M., Sinninghe Damste S., (2000). Effects of an oceanic anoxic event on the stable carbon isotopic composition of early Toarcian carbon, *American Journal of Science, 300*,1-22

Schuchert, C. (1910). Paleogeography of North America, *Geological Society of America Bulletin. 20,* 427-606

Schuur, E.A., Trumbore, S.E., Mack, M.C., Harden, J.W. (2003). Isotopic composition of carbon dioxide from a boreal forest fire:Inferring carbon loss from measurements and modelling. *Global Biogeochemical Cycles. 17,* 1-9, , doi:10.1029/2001GB001840,

Scott A.C., (2009). Forest Fire in the Fossil Record, In: A. Cerdà., P.R Robichaud (Eds.). *Fire Effects on Soils and Restoration Strategies*, (pp. 1-39) Science Publishers Inc., New Hampshire

Scott, A.C., (2000). The Pre-Quaternary history of fire, *Palaeogeography, Palaeoclimatology, Palaeoecology.* 164, 281 – 329.

Scott. A.C. (2010). Charcoal recognition, taphonomy and uses in palaeoenvironmental analysis, *Palaeogeography, Palaeoclimatology, Palaeoecology, 291,* 11-39

Scott, A.C., (1989). Observations on the nature and origin of fusain, *International Journal of Coal Geology*, *12,* 443-475

Scott, A. C., Bowman, D. J. M. S., Bond, W. J., Pyne, S. J., Alexander, M. (2014). *Fire on Earth: An Introduction.* Chichester: John Wiley and Sons.

Scott A.C., Damblon F., (2010). Charcoal: Taphonomy and significance in geology, botany and archaeology, *Palaeogeography, Palaeoclimatology, Palaeoecology*, *291*, 1-10

Scott, A.C., Glasspool, I.J. (2006). The diversification of Paleozoic fire systems and fluctuations in atmospheric oxygen concentration. *PNAS. 103,* 10861-10865

Scott, A.C., Jones, T.P., (1991). Microscopical observations of Recent and fossil charcoal, *Microscopy and Analysis, 25*, 13–15.

Scripps O_2 Programme (2016). Retrieved on 22 July 2016 from http://scrippso2.ucsd.edu

Selley R.C., (1990). Generation and Migration of Petroleum, in Elements of Petroleum Geology Second Edition, *Academic Press, United States of America*, 196

Sha J., Olsen P.E., Pan Y., Xu D., Wang Y., Zhang X., Yao X., Vajda V. (2015). Triassic–Jurassic climate in continental high-latitude Asia was dominated by obliquity-paced variations (Junggar Basin, Ürümqi, China), *Proceedings of the National Academy of Sciences, 112,* 3624-3629, doi/10.1073/pnas.1501137112

Sigman D.M., Boyle E.A. (2000). Glacial/interglacial variations in atmospheric carbon dioxide, *Nature Review Article, 407,* 859-869

Simpson, K.J., Ripley, B.S., Christin, P-A., Belcher, C.M., Lehmann, C.E.R., Thomas, G.H., Osborne, C.P. (2016). Determinants of flammability in savannah grass species. *Journal of Ecology. 104,* 138-148

Sinninghe Damsté J.S., van Bentum E.C., Reichart G-J., Pross J., Schouten S. (2008). A CO_2 decrease-driven cooling and increased latitudinal temperature gradient during the mid-Cretaceous Oceanic Anoxic Event 2, *Earth and Planetary Science Letters, 293***,** 97-103

Sinton C.W., Duncan R.A., (1997). Potential links between ocean plateau volcanism and global ocean anoxia at the Cenomanian-Turonian boundary, *Economic Geology*, *92(7-8*), 836-842

Smith, S.J., Anderson, R.S. (1992). Late Wisconsin Paleoecologic Record from Swamp Lake, Yosemite National Park, California. *Quaternary Research. 38,* 91-102

Snow L.J., Duncan R.A., Bralower T.J., (2005). Trace element abundances in the Rock Canyon Anticline, Pueblo, Colorado, marine sedimentary section and their relationship to Caribbean plateau construction and oxygen anoxic event 2, *Paleoceanography*, 20

Solomon, S., Qin, D., Manning, M., Chen, Z., Marquis, M., Averyt, K.B., Tignor, M., Miller, H.L. (2007). Technical summary, in Climate Change 2007: The Physical Science Basis—Contribution of Working Group I to the Fourth Assessment Report of the Intergovernmental Panel on Climate Change, edited by S. Solomon, D. Qin, M. Manning, Z. Chen, M. Marquis, K.B. Averyt, M. Tignor, H.L. Miller, (pp. 19–91), Cambridge Univ. Press, Cambridge, U. K.

Soua, M., (2010). Time series (Orbital cycles) analysis of the latest Cenomanian - Early Turonian sequence on the southern Tethyan margin using foraminifera. *Geologica carpathica. 61,* 11–120.

Spenser C.N., Hauer F.R. (1991). Phosphorus and Nitrogen Dynamics in Streams during a Wildfire. *Journal of the North American Benthological Society. 10(1).* 24-30

Sprovieri M., Sabatino N., Pelosi N., Batenburg S.J., Coccioni R., Lavarone M., Mazzola S., (2013). Late Cretaceous orbitally-paced carbon isotope stratigraphy from the Bottaccione Gorge (Italy), *Palaeogeography, Palaeoclimatology, Palaeoecology, 379–380***,** 81–94.

Srivastava S.K. (2011). Spore-pollen biostratigraphy of the English Jurassic. *Palaeontographica Abteilung B Band 285 Lieferung 4-6*, 113 - 201

Staver, A.C., Archibald, S., Levin, S.A. (2011). The Global Extent and Determinants of Savanna and Forest as Alternative Biome States. *Science. 334*, 230-232, doi: 10.1126/science.1210465

Stelzer, R.S., Scott, J.T., Bartsch, L.A., Parr, T.B., (2014). Particulate organic matter quality influences nitrate retention and dentrification in stream sediments: evidence from a carbon burial experiment, *Biogeochemistry, 119*, 387-402

Steinthorsdottir, M., Woodward, F.I., Surlyk, F., McElwain, J.C. (2012). Deep-time evidence of a link between elevated CO_2 concentrations and perturbations in the hydrological cycle via drop in plant transpiration. *Geology. 40,* 815-818, doi: https://doi.org/10.1130/G33334.1

Stephens, S.L., Agee, J.K., Fule, P.Z., North, M.P., Romme, W.H., Swetnam, T.W., Turner, M.G. (2013). Managing Forests and Fire in Changing Climates, *Science. 342,* 41 – 42. doi: 10.1126/science.1240294

Stopler, M., Bender, M.L., Dreyfus, G.B., Higgins, J.A. (2016). A Pleistocene ice core record of atmospheric O_2 concentrations. *Science. 353,* 1427-1430

Storey M., Mahoney J.J., Saunders A.D., Duncan R.A., Kelly S.P., Coffin M.F., (1995). Timing of hot-spot related volcanism and the breakup of Madagascar and India, *Science*, *267*, 852-855

Stramer, L., Johnson, G.C., Sprintall, J., Mohrholz, V. (2008). Expanding Oxygen-Minimum Zones in the Tropical Oceans. *Science. 320,* 655-658, doi: 10.1126/science.1153847

Stringer, J. (2009). Wildfire and Woodlands: Assessing and Reducing Risks, Kentucky Woodlands Magazine Online, Forestry Extension Office, Department of Forestry, *University of Kentucky and the Kentucky Division of Forestry, 4,* 2-4

Stützer O. (Ed). (1929). 'Fusit', Vorkommen, Engstehung und praktische Bedeutung der Faser-kohle, *Schr. Brennstoffgeol.,* 2

Stützer O., Noe A.C., (1940). *The Geology of Coal,* by Stützer O., reviewed by Noe A.C., University of Chicago Press

Suan, G., Pittet, B., Bour, I., Mattioli, E., Duarte, L.V., Mailliot, S. (2008). Duration for the Early Toarcian carbon isotope excursion deduced from spectral analysis: consequence for its possible causes. *Earth and Planetary Science Letters. 267*, 666–679

Sullivan, A.L., Ball, R. (2012). Thermal decomposition and combustion of cellulosic biomass, *Atmospheric Environment, 47,* 133-141

Suman, D.O., Kuhlbusch, T.A.J., Lim, B., (1997). Marine Sediments: A reservoir for Black Carbon and their Use as Spatial and Temporal Records of Combustion*, Sediment Records of Biomass Burning and Global Change, 51,* 271-293

Svensen, H., Planke, S., (2008). The North Atlnatic volcanic province (NAVP) and the Paleocene-Eocen Thermal Maximum (PETM), *Large Igneous Province Commission,* retrieved on 28th April 2014 from http://www.largeigneousprovinces.org/08aug

Svensen, H., Planke, S., Chevallier, L., Malthe-SØrenssen, A., Corfu, F., Jamtveit, B., (2007). Hydrothermal venting of greenhouse gases triggering Early Jurassic global warming, *Earth and Planetary Science Letters*, *256*, 554-566

Svensen, H., Planke, S., Malthe-Sorenssen, A., Jamtveit, B., Myklebust, R., Eidem, T.R., Rey, S.S., (2004). Release of methane from a volcanic basin as a mechanism for initial Eocene global warming, *Nature, 429*, 7-47

Swain, A.M., (1973). A history of fire and vegetation in northeastern Minnesota as recorded in lake sediment, *Quaternary Research*, *3*, 383-396

Swanson, F.J., (1981). Fire and geomorphic processes. In: Mooney, H.A., Bonnicksen, T.M., Christiansen, N.L., Lotan, J.E., Reiners, W.A. (Eds.), *Fire Regime and Ecosystem Properties, United States Department of Agriculture, Forest Service, General Technical Report WO vol. 26*. (pp 401-421) United States Government Planning Office, Washington, DC

Swenson, J.B., Paola, C., Pratson, L., Voller, V.R., Murrau, A.B. (2005). Fluvial and marine controls on combined subaerial and subaqueous delta progradation: Morphodynamic modelling of compound-clinoform development, *Journal of Geophysical Research: Earth Surface, 110*(F2), doi: 10.1029/2004JF000265

Swetnam, T.W., Betancourt, J.L. (1990). Fire-southern oscillation relations in the southwestern United States. *Science. 31,* 1017-1020

Tachajapong, W., Lozano, J., Mahalingam, S., Zhou X., Weise, D.R. (2008). An investigation of crown fuel bulk density effects on the dynamics of crown fire initiation in shrublands, *Combustion Science and Technology. 180,* 593-615

Takashima, R., Nishi, H., Yamanaka, T., Tomosugi, T., Fernando, A.G., Tanabe, K., Moriya, K., Kawabe, F. and Hayashi, K. (2011). Prevailing oxic environments in the Pacific Ocean during the mid-Cretaceous Oceanic anoxic event 2. *Nature Communications*, *2*, 234. doi: 10.1038/ncomms1233.

Tappert, R., McKeller, R.C., Wolfe, A.P., Tappert, M.C., Ortega-Blanco, J., Muehlenbachs, K. (2013). Stable carbon isotopes of C3 plant resins and ambers record changes in atmospheric oxygen since the Triassic. *Geochimica et Cosmochimica. 121,* 240-262

Tappin D.R., Chadwick R.A., Jackson A.A., Wingfield R.T.R., Smith N.J.P., (1994). The Geology of Cardigan Bay and the Bristol Channel, *HMSO for the British Geological Survey, London*

Taylor MJ., Shay J.M., Hamlin S.N. (1993). Changes in water-quality conditions in Lexington reservoir, Santa Clara County, California, following a large fire in 1985 and flood in 1986. *U.S. Geological Survey. Water-Resources Investigations Report 92-4172.* 1-23

Taylor, S.W., Wotton, B.M., Alexander, M.E., Dalrymple, G.N. (2004). Variation in wind and crown fire behaviour in a northern jack pine-black spruce forest, *Canadian Journal of Forest Research, 34,* 1561-1576

Tejada M.L.G., Mahoney J.J., Duncan R.A., Hawkins M.P., (1996). Age and geochemistry of basement and alkali rocks of Malatia and Santa Isabel, Solomon Islands, southern margin of Ontong Java Plateau, *Journal of Petrology*, *37*, 361-394

Tejada M.L.G., Mahoney J.J., Neal C.R., Duncan R.A., Petterson M.G., (2002). Basement geochemistry and geochronology of Central Malatia, Solomon Islands, with implications for the origin and evolution of the Ontong Java Plateau, *Journal of Petrology*, *43*, 449-484

Them, T. R., Gill, B.C., Caruthers, A.H., Gröcke, D.R., Tulsky, E.T., Martindale, R.C., '…' Smith, P.L. (2017). High-resolution carbon isotope records of the Toarcian Oceanic Anoxic Event (Early Jurassic) from North America and implications for the global drivers of the Toarcian carbon cycle. *Earth and Planetary Science Letters. 459,* 118–126

Thevenon, F., Williamson D., Vincens A., Taieb M., Merdaci O., Decobert M., Buchet G. (2003). A late-Holocene charcoal record from Lake Masoko, SW Tanzania: climatic and anthropologic implications, *The Holocene*, *13,5:*, 85-792

Thomas, D.J., Zachos, J.C., Bralower, T.J., Thomas, E., Bohaty, W., (2002). Warming the fuel for the fire evidence for the thermal dissociation of methane hydrate during the Paleocene-Eocene thermal maximum, *Geology. 30,* 1067-1070

Thonicke, K., Rolinski, S., von Bloh, W., Walz, A., Rammig, A. (2013). Role of fire in biome-boundary shifts in Europe. Talk presented at EGU General Assembly Conference, Vienna, Austria, 7th - 12th April

Tidwell, W.D., Ash, S.R. (1994). A Review of Selected Triassic to Early Cretaceous Ferns, *Journal of Plant Research, 107*, 417-442

Tinner, W., Conedera, M., Ammann, B., Gaggeler, H.W., Gedye, S., Jones, R., Sagesser, B., (1998). Pollen and charcoal in lake sediments compared with historically documented forest fires in southwestern Switzerland since AD 1920, *The Holocene*, *8,1*, 31-42

Tinner, W., Hu, F.S., Beer, R., Kaltenrieder, P., Scheurer, B., Krähenbühl, U. (2006). Postglacial vegetational and fire history: pollen, plant macrofossil and charcoal records from two Alaskan lakes, *Vegetation History and Archaeobotany, 15*, 279-293

Torero, J.L. (2013). 1. An Introduction to Combustion in Organic Materials. In Belcher C.M. (Ed.), *Fire Phenomena and the Earth System: An Interdisciplinary Guide to Fire Science.* (pp. 3 – 15). West Sussex:John Wiley and Sons, Ltd

Torsvik T.H., Tucker R.D., Ashwal L.D., Eide E.A., Ratotosolofo N.A., de Wit M.J., (1998). Late Cretaceous magmatism in Madagascar: palaeomagnetic evidence for a stationary Marion hotspot, *Earth and Planetary Science Letters*, *164*, 221-232

Tourtelot, H.A. (1979). Black shale – its deposition and diagenesis, *Clays and Clay Minerals. 27,* 313-321

Tsikos, H., Jenkyns, H.C., Walsworth-Bell, B., Petrizzo, M.R., Forster, A., Kolonic, S., Erba, E., Premoli Silva, I., Baas, M., Wagner, T., Sinninghe Damsté, J.S., (2004). Carbon-isotope stratigraphy recorded by the Cenomanian-Turonian Oceanic Anoxic Event: correlation and implications based on three key localities*, Journal of the Geological Society, 161*, 711-719

Tsukada M., Deevey E.S., Jr. (1967). Pollen analysis from four lakes in the southern Maya area of Guatemala and El Salvador., Cushing E.J., Wright H.E., Jr (Eds.)., *Quaternary Paleocology,* 303-331

Turgeon, S.C., Creaser, R.A. (2008). Cretaceous oceanic anoxic event 2 triggered by a massive magmatic episode, *Nature. 454,* 323-326

Tuenter E., Weber S.L., Hilgen F.J., Lourens L.J. (2003). The response of the African summer monsoon to remote and local forcing due to precession and obliquity, *Global and Planetary Change, 36,* 219-235

Turner, R., Roberts, N., Eastwood, W.J., Jenkins, E., Rosen, A., (2010). Fire, climate and the origins of agriculture: micro-charcoal records of biomass burning during the last glacial-interglacial transition in Southwest Asia, *Journal of Quaternary Science, 25(3)*, 371-386

Turquety, S. (2013). Evaluating the Atmospheric Impact of Wildfires. In. Belcher C.M. (Ed.), *Fire Phenomena and the Earth System, An Interdisciplinary Guide to Fire Science.* (pp. 253 – 273). West Sussex: John Wiley and Sons

Twenhofel, W.H. (1915). Notes on black shale in the making. *American Journal of Science. 4,* 272-280

Twenhofel, W.H. (1939). Environments of origin of black shales. *American Association of Petroleum Geology Bulletin. 23,* 1178-1198

Tyler, S.C., Blake, D.R., Rowland, F.S., (2012). $^{13}C/^{12}C$ ratio in methane from the flooded Amazon forest, *Journal of Geophysical Research: Atmospheres, 92(D1)*, 1044-1048, doi: 10.1029/JD092iD01p01044

Tyrell, T., (1999). The relative influences of nitrogen and phosphorus on oceanic primary production, *Nature, 400,* 525-531

Uhl, D., Dolezych, M., Böhme, M., (2014). Taxodioxylon-like charcoal from the Late Miocene of western Bulgaria, *Acta Palaeobotanica, 54(1),* 101-111

Uličný, D. (1999). Sequence stratigraphy of the Dakota Formation (Cenomanian), southern Utah: interplay of eustasy and tectonics in a foreland basin, *Sedimentology. 46,* 807-836. Doi: 10.1046/j.1365-3091.1999.00252.x

Vadja, V., Linderson, H., McLouchlin, S. (2016). Disrupted vegetation as a response to Jurassic volcanism in southern Sweden. In: B.P. Kear., J. Lindgren., J.H. Hurum., J. Milàn., V. Vajda. (Eds). *Mesozoic Biotas of*

Scandinavia and its Arctic Territories, Geological Society of America, London, Special Publications, 434

Vakhrameev, V.A. (1991). *Jurassic and Cretaceous Floras and Climates of the Earth*, Cambridge University Press

Valdes, P.J., Sellwood, B.W., Price, G.D. (1995). Modelling Late Jurassic Milankovitch climate variations. *Geological Society of London Special publications. 85,* 115-132

Van Breugel, Y., (2006). Causes for negative carbon isotope anomalies in Mesozoic marine sediments: constraints from modern and ancient anoxic settings. *Geologica Ultraiectina*, *258,* 9-18.

Van Breugel, Y., Schouten, S., Tsikos, H., Erba, E., Price, G.D., Sinninghe Damsté, J.S. (2007). Synchronous negative carbon isotope shifts in marine and terrestrial biomarkers at the onset of the early Aptian oceanic anoxic event 1a: Evidence for the release of ^{13}C-depleted carbon into the atmosphere. *Paleoceanography. 22,* 1-13, doi:10.1029/2006PA001341

Van Cappellen, P. & Ingall, E. D. (1994). Benthic phosphorus regeneration, net primary production, and ocean anoxia: a model of the coupled marine biogeochemical cycles of carbon and phosphorus. *Paleoceanography 9,* 677–692

Van Cappellen, P. & Ingall, E. D. (1996). Redox stabilization of the atmosphere and oceans by phosphorus- limited marine productivity. *Science 271*, 493–496

Van de Schootbrugge (2010). Palaeoclimate: A fiery start to the Jurassic, *Nature Geoscience, 3***,** 381-382

Van de Schhotbrugge, B., McArthur, J.M., Bailey, T.R., Rosenthal, Y., Wright, J.D., Miller, K.G. (2005). Toarcian oceanic anoxic event: An assessment of

global causes using belemnite C isotope records. *Paleoceanography. 20,* doi: 10.1029/2004PA001102

Van der Werf, G. R., J. T. Randerson, L. Giglio, N. Gobron, and A. J. Dolman (2008). Climate controls on the variability of fires in the tropics and subtropics, *Global Biogeochemical Cycles, 22,* 1-13, doi:10.1029/2007GB00312

Van Helmond N.A.G.M., Sluijs A., Reichart G-J., Sinninghe Damsté J.S., Slomp C.P., Brinkhuis H. (2013). A perturbed hydrological cycle during Oceanic Anoxic Event 2, *Geology, 42*, 123-126

Vaughan, A., Nichols, G., (1995). Controls on the deposition of charcoal; implications for sedimentary accumulation of fusain, *Journal of Sedimentary Research, 65*, 129-135

Verado, D.J. (1997). Charcoal analysis in marine sediments, *Limnology and Oceanography. 42,* 192-197

Viegas, D.X., Viegas, M.T.S.P., Ferreira, A.D. (1992). Moisture Content of Fine Forest Fuels and Fire Occurrence in Central Portugal. *International Journal of Wildland Fire. 2,* 69-86

Vincent E., Berger W.H., (1985). Carbon dioxide and polar cooling in the Miocene: the Montery Hypothesis, Sundquist E.T.S., Broecker W.S., (Eds.), The Carbon Cycle and Atmospheric CO_2: Natural Variation Archean to the Present, *Geophysical Monograph Series, 32*, 455- 468

Voigt, S., A. S. Gale, Voigt, T. (2006). Sea- level change, carbon cycling and palaeoclimate during the Late Cenomanian of northwest Europe; an integrated palaeoenvironmental analysis, Cretaceous Res., 27, 836–858, doi:10.1016/j.cretres.2006.04.005.

Voiland, A. (2015). Study: Fire seasons getting longer, more frequent. Retrieved on 12 January 2017 from https://climate.nasa.gov/news/2315/study-fire-seasons-getting-longer-more-frequent/

Vollmer T., Werner R., Weber M., Tougiannidis N., Röhling H-G., Hambach U. (2008). Orbital control on Upper Triassic Playa cycles of the Steinmergel-Keuper (Norian): A new concept for ancient playa cycles, *Palaeogeography, Palaeoclimatology, Palaeoecology, 267***,** 1-16

Waddington, J.C.B. (1969). A stratigraphic record of the pollen influx to a lake in the Big Woods of Minnesota . *Geological Society of America Special Paper 123,* 263-282

Wade-Murphy, J., Kuerschner, W.M., Hesselbo, S.P., (2006). Abrupt and gradual vegetation changes associated with Toarcian global change inferred from high resolution palynological studies of the Korsodde section on Bornholm (DK*), Geophysical Research Abstracts, 8*

Wagreich, M., (2012). “OAE 3” – a low-to mid-latitude Atlantic oceanic event during the Coniacian-Santonian. *Climate of the Past, 8*, 1209-1227
Wagreich, M., Neuhuber, S., Egger, H., Wendler, I., Scott, R., Malata, E., Sanders, D. (2011). Cretaceous Oceanic red beds (CORBs) in the Austrian Eastern Alps: passive-margin vs. active-margin depositional setting. In X. Hu., C. Wang., R.W. Scott., M. Wagreich., L. Jansa. *Cretaceous Oceanic Red Beds: Stratigraphy, Composition, Origins, and Paleoceanographic and Paleoclimatic Significance.* (pp 73-91). Society for Sedimentary Geology, Oklahoma

Walker, J., Peet, R.K. (1984). Composition and species diversity of pine-wiregrass savannas of the Green Swamp, North Carolina. *Plant Ecology. 55,* 163-179

Wang, C., Hu, X., Huang, Y., Wagreich, M., Scott, R., Hay, W. (2011). Cretaceous oceanic red beds as possible consequence of oceanic anoxic events. *Sedimentary Geology. 235,* 27-37

Wang, X., Parisien, M-A., Taylor, S.W., Candau, J-N., Stralberg, D., Marshall, G.A. '…' Flannigan, M.D (2017). Projected changes in daily fire spread across Canada over the next century. *Environmental Research Letters. 12,* 1 – 12, doi:10.1088/1748-9326/aa5835

Waterhouse, H.K. (1999a). Orbital forcing of palynofacies in the Jurassic of France and the United Kingdom, *Geology*, *27,* 511–514.

Waterhouse, H.K. (1999b). Regular terrestrially derived palynofacies cycles in irregular marine sedimentary cycles, Lower Lias, Dorset, UK, *Journal of the Geological Society, London, 156***,** 1113–1124.

Watson, A.J. (1978). Consequences for the biosphere of forest and grassland fires. PhD thesis, Department of Engineering and Cybernetics, University of Reading

Watson, A.J. (2016). Oceans on the edge of anoxia. *Science. 354,* 1529-1530, doi: 10.1126/science.aaj2321

Watson, A.J., Lovelock, J.E. (2013). The Dependence of Flame Spread and probability of Ignition on Atmospheric Oxygen: an Experimental Investigation. In. Belcher C.M. (Ed.), *Fire Phenomena and the Earth System, An Interdisciplinary Guide to Fire Science.* (pp. 15 – 35). West Sussex: John Wiley and Sons

Watson, A.J., Lovelock, J.E., Margulis, L. (1978). Methanogenesis, fires and the regulation of atmospheric oxygen. *Biostems. 10,* 293-298

Weedon G.P., Jenkyns H.C. (1999). Cyclostratigraphy and the Early Jurassic timescale: Data from the Belemnite Marls, Dorset, southern England, *The Geological Soceity of America, 111*, 1823-1840

Weedon G.P., Jenkyns H.C. (1990). Regular and irregular climatic cycles and the Belmnite Marls (Pliensbachian, Lower Jurassic, Wessex Basin), *Journal of the Geological Society, 147***,** 915-918

Weissert, H., Bréhéret, J.G., (1991). A carbonate-carbon isotope record from Aptian-Albian sediments of the Vocontian Trough. *Bulletin de la Societe. Géologique de France., 162*, 1133-1140

Weissert H., Channel J.E.T., (1989). Tethyan Carbonate Carbon Isotope Stratigraphy across the Jurassic-Cretaceous Boundary: An indicator of Decelerated Global Carbon Cycling? *Palaeoceanography, 4*, 483-494

Weissert, H., Erba, E., (2004). Volcanism, CO_2 and palaeoclimate: a Late Jurassic-Early Cretaceous carbon and oxygen isotope record, *Journal of the Geologicla Society, 161*, 695-702, doi: 10.1144/0016-764903-087

Weissert, H., Lini, A., Föllmi, K.B. and Kuhn, O. (1998). Correlation of Early Cretaceous carbon isotope stratigraphy and platform drowning events: a possible link?. *Palaeogeography. Palaeoclimatology. Palaeoecology*, *137*, 189–203.

Weissert H.J., McKenzie J.A., Channell J.E.T., (1985). Natural Variations in the Carbon Cycle during the Early Cretaceous, Sundquist E.T.S., Broecker W.S., (Eds.), The Carbon Cycle and Atmospheric CO2: Natural Variation Archean to the Present, *Geophysical Monograph Series, 32*, 531-545

Weissert H., Mohr H., (1996). Late Jurassic climate and its impact on carbon cycling, *Palaeogeography,Palaeoclimatology, Palaeoecology, 122,* 27-43

Westrich J.T., Berner R.A., (1984). The role of sedimentary organic matter in bacterial sulfate reduction: The *G* model tested, *Association for the Sciences of Limnology and Oceanography, 29*, 236-249

Whitlock, C., Anderson, R.S., (2003). Fire History Reconstructions Based on Sediment Records from Lakes and Wetlands, In T.T. Veblen., G. Montenegro, W.L. Baker, T.W. Swetnam. (Eds.). *Fire and Climatic Change in Temperate Ecosystems of the Western Americas,* (pp. 3-31). Springer-Verlag New York.

Whitlock, C., Bradbury, J.P., Milspaugh, S.H., (1997). Controls on Charcoal Distribution in Lake Sediments: Case Studies from Yellowstone National Park and Northwestern Minnesota, Sediment Records of Biomass Burning and Global Change, *NATO ASI Series, 51*, 367-386

Whitlock, C., Larsen, C., (2001). Charcoal as a fire proxy, In: J.P. Smol., H.J.B. Birks., W.M. Last. (Eds.).*Tracking Environmental Change Using Lake Sediments*, *3*, (pp. 1-23). Springer, Netherlands

Whitlock, C.L., Millspaugh, S.H., (1996). Testing the assumptions of fire-history studies: an examination of modern charcoal accumulation in Yellowstone National Park, USA, *The Holocene, 6*,*1*, 7-15

Wignall, P.B. (2007). The end-Permian mass extinction – how bad did it get? *Geobiology 5*, 303–309.

Wignall P.B., (2005). The link between large igneous province eruptions and mass extinctions, *Elements, 1*, 293-297

Wignall P., (2004). Environmental and climatic impact of the eruption of large igneous provinces, Large Igneous Provinces Commission, *International Association of Volcanology and Chemistry of the Earth's Interior*, retrieved on 20th February 2014 from http://www.largeigneousprovinces.org/node/28

Wignall P.B., Sun Y., Bond D.P.G., Izon G., Newton R.J., Védrine S., Widdowson M., Ali J.R., Lai X., Jiang H., Cope H., Bottrell S.H., (2009). Volcanism, Mass Extinction, and Carbon Isotope Fluctuations in the Middle Permian of China, *Science*, *324*, 1179-1182

Wildman R.A., Hickey L.J., Dickinson M.B., Berner R.A., Robinson J.M., Dietrich M., Essenhigh R.H., Wildman C.B., (2004). Burning of forest materials under late Paleozoic high atmospheric oxygen levels, *Geology. 32*,457-460

Woillez, M.-N., Levavasseur, G., Daniau A.-L., Kageyama, M., Urrego, D.H., Sánchez-Goñi, M.-F., Hanquiez, V. (2014). Impact of precession on the climate, vegetation and fire activity in southern Africa during MIS4, *Climate of the Past, European Geosciences Union. 10,* 1165 – 1182.

Woodward, F. I., Lomas, M. R. & Lee, S. E. (2001). In J. Roy., B. Saugier, & H.A. Mooney (Eds.) *Terrestrial Global Productivity, Chapter: Predicting the Future Productivity and Distribution of Global Terrestrial Vegetation* (pp. 521–541) Academic Press.

Woodland, A. W. (1971). *The Llanbedr* (*Mochras Farm*) *Borehole*. Report No. 71/18 115*, Institute of Geological Sciences*.

Woolnough W.G., (1937). Sedimentation in Barred Basins, and Source Rocks of Oil, *AAPG Bulletin, 21*, 1101-1157

World Ocean Review 1, (2010). Climate change and methane hydrates, Ocean Chemistry, retrieved on 28th April 2014 from http://worldoceanreview.com/en/wor-1/ocean-chemistry/climate-change-and-methane-hydrates/

Wotton, B.M., Martell, D.L. (2005). A lightning fire occurrence model for Ontario, *Canadian Journal of Forest Research. 35,* 1389-1401

Wu, H., Zhang, S., Hinnov, L.A., Jiang, G., Feng, Q., Li, H., Yang, T. (2013). Time-calibrated Milankovitch cycles for the late Permian. *Nature Communications. 4,* 2452, doi:10.1038/ncomms3452

Xi, C., Wang, C., Xiumian, H., Yongjian, H., Pingkang, W., Jansa, L., Xuan, Z. (2007). Cretaceous Oceanic Red Beds: Distribution, Lithostratigraphy and Paleoenvironments. *Acta Geologica Sinica. 81,* 1070-1086

Yang, W., Lehrmann, D.J. (2014). Peritidal carbonate cycles induced by carbonate productivity variations: A conceptual model for an isolated Early Triassic greenhouse platform in South China. *Journal of Palaeogeography. 3(2)*, 115-126. DOI: 10.3724/SP.J.1261.2014.00047

Zachos, J.C., Wara, M.W., Bohaty, S., Delaney, M.L., Petrizzo, M.R., Brill, A., Bralower, T.J., Premoli-Silva, I., (2003). A transient rise in tropical sea surface temperature during the Paleocene-Eocene Thermal Maximum, *Science, 302*, 1551-1554

Zeebe R.E., Zachos J.C., Dickens G.R., (2009). Carbon dioxide forcing alone insufficient to explain Palaeocene-Eocene Thermal Maximum warming, *Letters to Nature Geoscience*, *2*: 576-580

Zhao, F.J., Shu, L.F., Wang, Q.H. (2012). Terpenoid emissions from heated needles of Pinus sylvestris and their potential influences on forest fires. *Acta Ecologica Sinica. 32,* 33-37

Zhou, J., Poulsen, C.J., Rosenbloom, N., Shields, C., Briegleb, B. (2012). Vegetation-climate interactions in the warm mid-Cretaceous. *Climate of the Past. 8,* 565-576